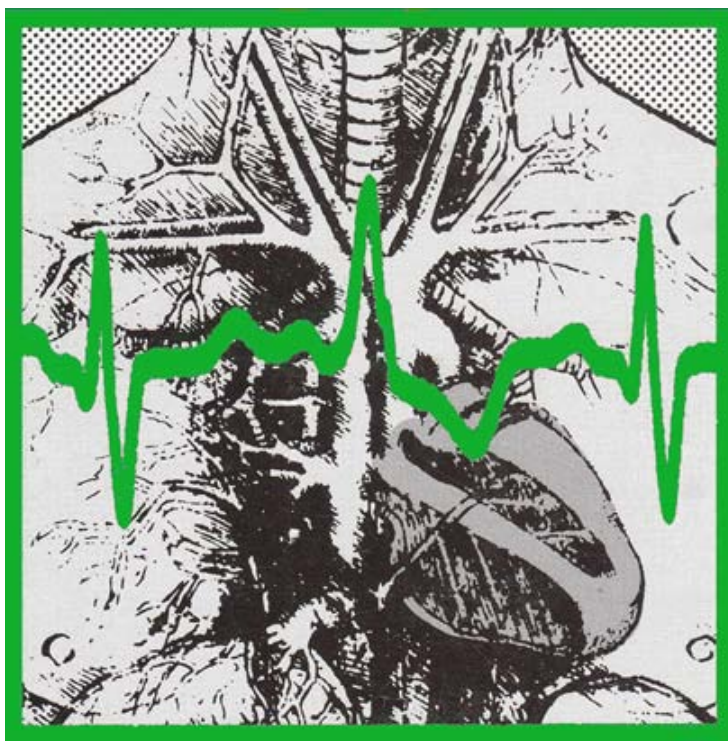


COMPUTING IN CARDIOLOGY

September 22-25, 2013
Zaragoza, Spain



COMPUTING

IN

CARDIOLOGY



**Welcome to Zaragoza,
Bienvenido a Zaragoza,**

Table of Contents

Sponsors.....	ii
Letter from the President	vii
Welcome to Zaragoza	ix
Map of the City Center.....	x
Map of the campus	x
Detailed maps of the conference rooms.....	xi
Hotels and Conference Venue	xiii
Transportation	xiii
Farewell party map	xv
Registration	xvi
Internet access.....	xvi
Meals.....	xvi
Accompanying Persons	xvii
Post conference and accompanying person tours	xvii
Useful numbers:.....	xvii
For Authors and Speakers.....	xvii
Oral Presentations	xvii
Poster Presentations.....	xviii
Rosanna Degani Young Investigator Award.....	xviii
PhysioNet / Computing in Cardiology Challenge 2013.....	xviii
Manuscripts.....	xix
Conference Overview	xx
Sunday Symposium	xx
Scientific Sessions	xxi
Monday Social Program.....	xxi
Monday Social Program Schedule	xxii
Tuesday Evening Reception	xxii
Wednesday farewell party.....	xxii
New Abstract Number Formatting	xxii
Scientific Sessions Program Overview.....	xxiii
Scientific Program	xxvi
Abstracts.....	1

Sponsors

We would like to thank our sponsors and those who have made generous donations:



**Universidad
Zaragoza**



Mortara



Instituto Universitario de Investigación
en Ingeniería de Aragón
Universidad Zaragoza

PHILIPS



Escuela de
Ingeniería y Arquitectura
Universidad Zaragoza



GE Healthcare
Life Sciences



Cardiolund

ciber-66n

Centro Investigación Biomédica en Red
Bioingeniería, Biomateriales y Nanomedicina

IOP Publishing

ZOLL.



Zaragoza
AYUNTAMIENTO

GTC

Communication
Technologies Group



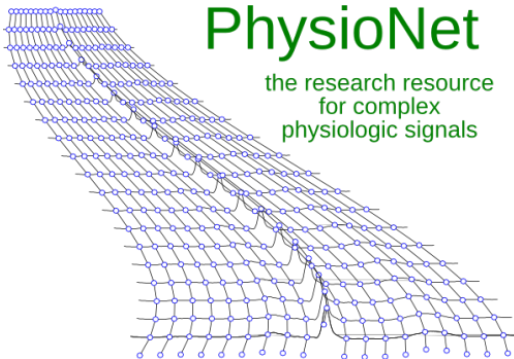
instituto de investigación
en ingeniería de Aragón
Universidad de Zaragoza

The 40th conference on Computing in Cardiology is hosted by:



**Universidad
Zaragoza**

The CinC 2013 Scientific Program is endorsed by:





The Engineering in Medicine and Biology Society of the IEEE advances the application of engineering sciences and technology to medicine and biology, promotes the profession, and provides global leadership for the benefit of its members and humanity by disseminating knowledge, setting standards, fostering professional development, and recognizing excellence.

The field of interest of the IEEE Engineering in Medicine and Biology Society is the application of the concepts and methods of the physical and engineering sciences in biology and medicine. This covers a very broad spectrum ranging from formalized mathematical theory through experimental science and technological development to practical clinical applications. It includes support of scientific, technological and educational activities.

Engineering in Medicine and Biology Society

445 Hoes Lane
Piscataway, New Jersey, USA 08854
Telephone: +1 732 981 3433
Facsimile: +1 732 465 6435
E-mail: emb-exec@ieee.org, www.embs.org

PUBLICATIONS

IEEE PULSE

Transactions on Biomedical Engineering/Transactions on Biomedical Engineering Letters
Transactions on Information Technology in Biomedicine
Transactions on Neural Systems and Rehabilitation Engineering
Transactions on Medical Imaging
Transactions on NanoBioscience
Transactions on Computational Biology and Bioinformatics
Transactions on Biomedical Circuits and Systems
Reviews on Biomedical Engineering

ELECTRONIC PRODUCTS

EMBS Electronic Resource

CONFERENCES

Annual International Conference of the IEEE Engineering in Medicine and Biology Society (EMBC)
IEEE EMBS Special Topic Conference on Neural Engineering (NER)
International Symposium on Biomedical Imaging (ISBI)
International Conference on Biomedical Robotics and Biomechanics (BIROB)
International Conference on Rehabilitation Robotics (ICORR) AMA/IEEE-EMBS Medical Technology Conference (MedTech)
Grand Challenges Conference Series (GCBE)

SUMMER SCHOOLS Sponsored by EMBS

International Summer School on Biomedical Imaging
International Summer School on Biomedical Signal Processing
International Summer School on Biocomplexity
International Summer School on Medical Devices and Biosensors
International Summer School on Information Technology in Biomedicine



Computing in Cardiology 2014

Cambridge, Massachusetts, USA

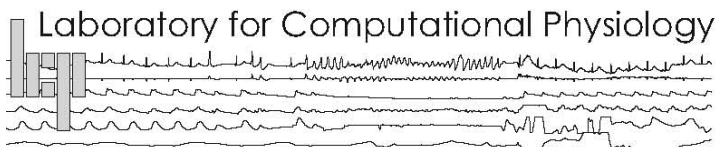
6-10 September 2014

We cordially invite you to attend the 41st annual scientific meeting of Computing in Cardiology, which returns to Cambridge, Massachusetts next September. Cambridge is the home of the Massachusetts Institute of Technology and of Harvard University. The conference will be hosted by MIT's Laboratory for Computational Physiology.

Situated on opposite banks of the scenic Charles River, Boston and Cambridge are lively, surprising, multicultural, eminently walkable cities with excellent modern public transportation, and nearly four centuries of history. Over 100 colleges and universities, with over 250,000 students, contribute to the cities' cultural life and diversity. Among the area's major attractions are the Boston Museum of Fine Arts, the Isabella Stuart Gardner Museum, the Boston Symphony Orchestra, the USS Constitution, and (for baseball fans) Fenway Park, as well as dozens of smaller but noteworthy landmarks, musical and theatrical performing groups, parks, museums, and the waterfront, harbor, and its islands. During the social program, attendees will sample some of these hidden gems.

Boston is easily reached by non-stop flights from Amsterdam, Dublin, Frankfurt, Lisbon, London, Madrid, Munich, Paris, Rome, Tokyo, Zurich, and many major cities in North America. The conference venue, the Royal Sonesta Hotel, is on the Cambridge bank of the Charles, three miles (five km) from Logan International Airport, within a mile of the MIT campus, and adjacent to Boston's Museum of Science and a variety of restaurants and shops; the hotel provides free shuttle service to other nearby attractions.

For further details, please refer to cinc.mit.edu/2014/.



Board of Directors and Local Committee

BOARD OF DIRECTORS

President

Peter Macfarlane, DSc
University of Glasgow
Glasgow, UK

Secretary

Leif Sörnmo, DSc
Lund University Lund, Sweden

Treasurer

Victor Mor-Avi, PhD
University of Chicago Chicago, IL, USA

Past President

Harold Ostrow, MSEE
Gaithersburg, MD, USA

Willem Dassen, PhD
Maastricht University Maastricht,
The Netherlands

Paul Kligfield, MD
Weill Cornell Medical School
New York, NY, USA

Pablo Laguna, PhD
University of Zaragoza
Zaragoza, Spain

George Moody
Massachusetts Institute of
Technology Cambridge, MA, USA

Dewar Finlay, PhD
University of Ulster
Belfast, UK

Sheryl Prucka, MSEE
Park City, UT, USA

Ex-Officio

ESC Representative
Marek Malik, MD, PhD University of
London, England

Editor, Proceedings

Alan Murray, PhD
Newcastle University
Newcastle upon Tyne, UK

LOCAL COMMITTEE

Pablo Laguna, PhD, Chair
Juan Pablo Martínez, PhD, co-Chair
Esther Pueyo PhD,
Raquel Bailón, PhD,
José Felix Rodríguez, Ph.D.
José García, PhD
Álvaro Alesanco, PhD
Eduardo Gil, Ph.D.
Violeta Monasterio, Ph.D.
Mariano Llamedo, Ph.D.
Daniel Romero, Ph.D.

CinC 2013 SECRETARIAT ADDRESS

Escuela de Ingeniería y Arquitectura.
Edif. Torres Quevedo
C/María de Luna, 3; 50018 –
ZARAGOZA, Spain

<http://eina.unizar.es>

Email: cinc2013@unizar.es

Web site: <http://cinc2013.org>

Letter from the President

Dear Participant,

Welcome to the 40th Computing in Cardiology conference. Since the first meeting of the group in 1974, Computing in Cardiology has met in Spain on only one previous occasion in 2006, in Valencia. The Board of Computing in Cardiology is therefore delighted that Pablo Laguna and colleagues from the University of Zaragoza volunteered to host this year's meeting in Spain where there is a lot of activity in the field of Biomedical Engineering. They have prepared an excellent meeting and social programme, which attracted the highest number of abstracts in recent years. It is pleasing to note that there is still a huge interest among engineers in particular for attending Computing in Cardiology.

With one eye on the future, if any of you would like to consider hosting a Computing in Cardiology meeting at some stage in the future, please do contact any member of the Board. There are a number of interested individuals willing to organise meetings over the next few years but advance planning is highly recommended so please step forward now if you think you would like to host a future meeting. In particular, if Computing in Cardiology has not been held in your country on a previous occasion, and there are quite a few European countries which have not hosted this meeting, then why not consider being the first person or group to arrange such a meeting locally?

I can advise that, next year, some members of the Board will be obliged to resign, having served their term of office and so the Board will require replacements. It is possible that a new approach to election of Board members will be instituted but plenty of notice will be given about whichever procedure is to be adopted.

As for the present, I hope you have a scientifically stimulating meeting which will send you home full of new ideas that will enable you to submit an abstract for consideration for presentation at next year's meeting in Boston, Massachusetts from 6th-10th September, 2014. Of course, I trust that you will also enjoy the

excellent social programme which has also been arranged in order to make your visit to Zaragoza even more enjoyable.

May I take this opportunity to thank Pablo Laguna and all of the Local Organising Committee for the tremendous amount of work they have done in preparing Computing in Cardiology 2013. I am sure it will be a great success.

Best wishes

Peter Macfarlane

President, Computing in Cardiology

Welcome to Zaragoza

Dear Colleague,

It is with great pleasure that we welcome you to the 40th Annual Scientific Conference of Computing in Cardiology, being held in Zaragoza, Spain from Sunday, 22nd to Wednesday, 25th September 2013.

Zaragoza is a modern and welcoming city, with more than 2000 years of history. Its Iberian, Roman, Muslim and Christian heritage has shaped during centuries a beautiful city, full of surprises. Capital city of the Kingdom of Aragón for six centuries, it has many cultural and historical landmarks, as well as a rich folklore and a renowned gastronomy. Zaragoza boasts a number of privileged natural spaces (Parks, river banks, groves, river meanders...) where water, and in particular the Ebro River, takes the central stage, giving the city a special type of energy and light.

Computing in Cardiology provides an international forum for scientists and professionals from the fields of medicine, physics, engineering and computer science, and has been held annually since 1974. We are particularly pleased that such an event takes place in our city for the first time.

The conference will begin on Sunday afternoon 22nd September at 13:00 hours with a special symposium of invited talks related to the topic of Electrophysiological Cardiac Modelling. A reception at Museum Ibercaja Camón Aznar will be offered at the end of the symposium. The scientific sessions include oral and poster presentations and will begin on Monday morning. In the afternoon, the traditional social program will take place, with a canoe trip on the Ebro river, visits to some of the most prominent monuments, such as the Aljafería Palace, the Basilica of El Pilar, La Seo Cathedral, La Lonja, and the Roman Walls, which are outstanding examples of Roman, Muslim, Jewish and Christian heritage, finishing with a spectacular gala dinner in the fabulous setting Finca Sansui. Sessions will continue on Tuesday, ending with a reception at the City Hall, and will be concluded on Wednesday afternoon, followed by a farewell party.

As the local organizer, the Engineering School of the University of Zaragoza has the pleasure and honor to be the host of Computing in Cardiology 2013. We warmly welcome delegates from around the world and hope that you will enjoy your visit to Zaragoza. The Local Organizing Committee will be glad to assist you in meeting your expectations.

We look forward to seeing you in Zaragoza, being our wish that your stay at the city results pleasant and profitable, from both scientific and personal perspectives. Thank you!

Sincerely,



Pablo Laguna,
Chair of the Local Organizing Committee

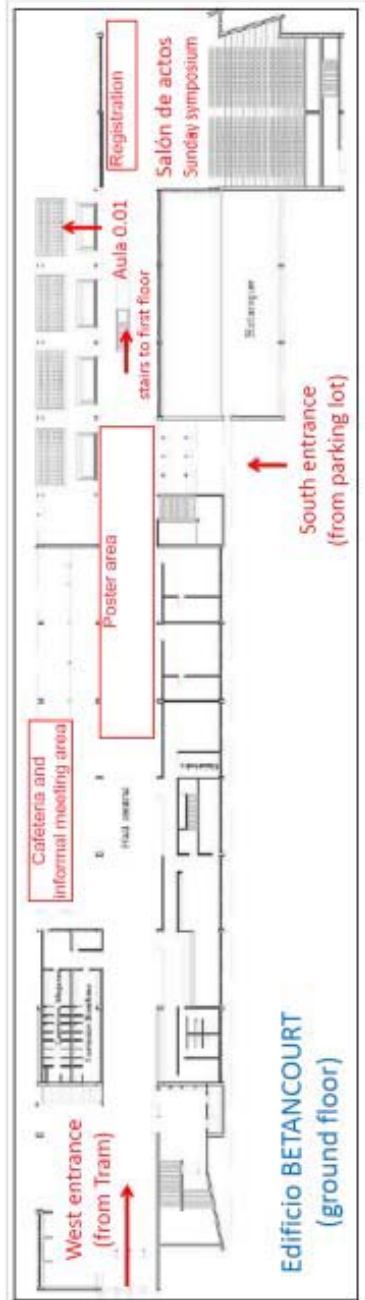
Map of the City Center

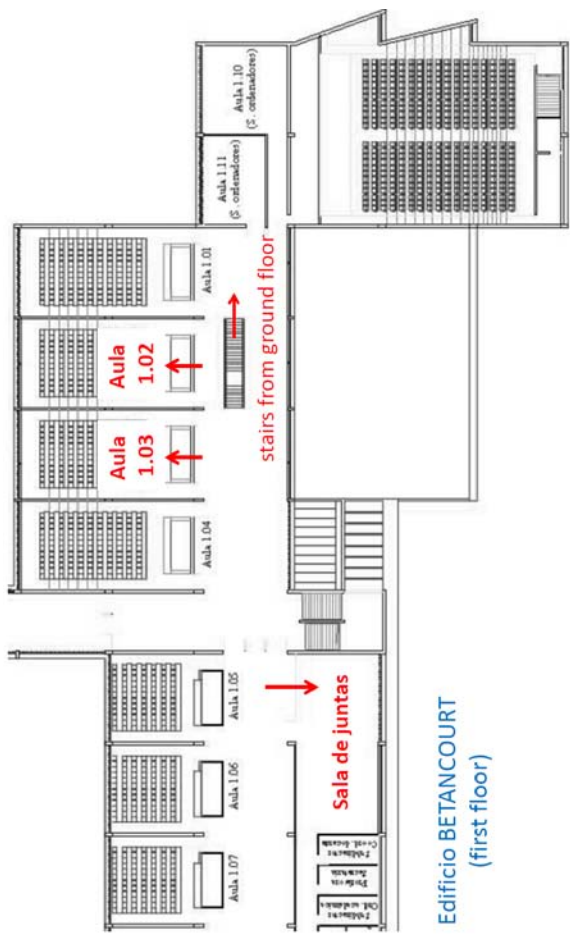


Map of the campus



Detailed maps of the conference rooms





Hotels and Conference Venue

A variety of accommodation options, ranging from a hostel to 5* hotels and fitting any budget, have been recommended to ensure your pleasant stay in Zaragoza. The Local Organizing Committee recommends that you book your room as early as possible to avoid disappointment.

The conference is being held in lecture rooms located at the Engineering School (Betancourt Building) of The University of Zaragoza as outlined below:

Sunday Symposium	“Salón de Actos” (Auditorium)
opening and closing ceremonies	“Salón de Actos” (Auditorium)
regular oral sessions	Ground floor “Salon de Actos” , Aula 0.01 First floor “Sala de Juntas” , Aulas 1.03, 1.02
poster sessions	Betancourt Building, ground floor, Hall

Please refer to the map of the Betancourt Building and to the detailed conference program to be sure you are in time for the sessions of your interest. The buildings and lecture rooms will be clearly marked with the Computing in Cardiology signs.

Transportation

The public tram is a convenient way to commute between the conference site and downtown hotel area, see the map below for tram line 1, between conference site and hotel area. Tickets can be bought at the tram stations, and can be used for transfer to the bus transportation system.

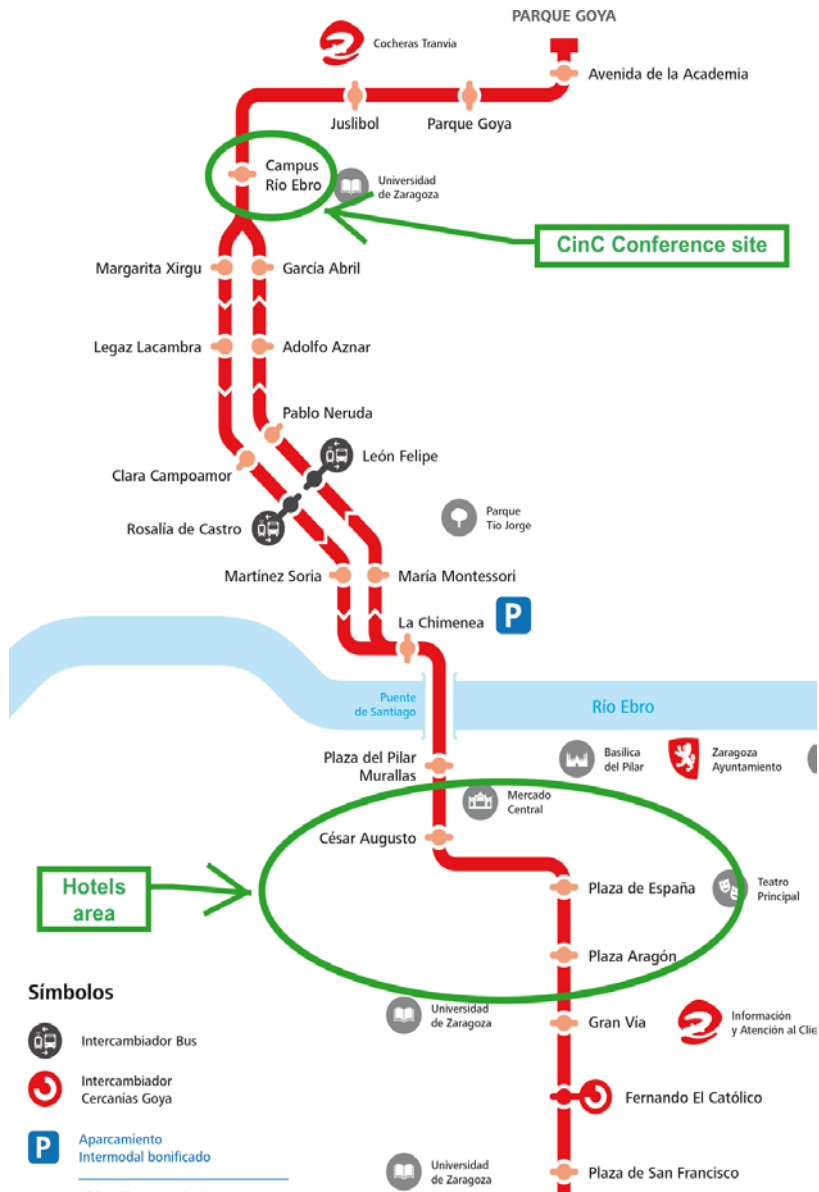
Transportation to the reception on Sunday (after the symposium end) and on Tuesday is NOT provided. The tram stop at "Plaza del Pilar" is the preferred stop for the Camón Aznar Museum (Espoz y Mina, 23) or "City Hall" (Plaza del Pilar 18) where the two receptions will take place. A few minutes by walk separate the stop from the sites.

For the Monday social event, bus transportation will be provided from the conference site to the different sites where the activities will take place. It is important that delegates are on time at the sites. Designated sites and schedule are provided in the Social Program section of this booklet.

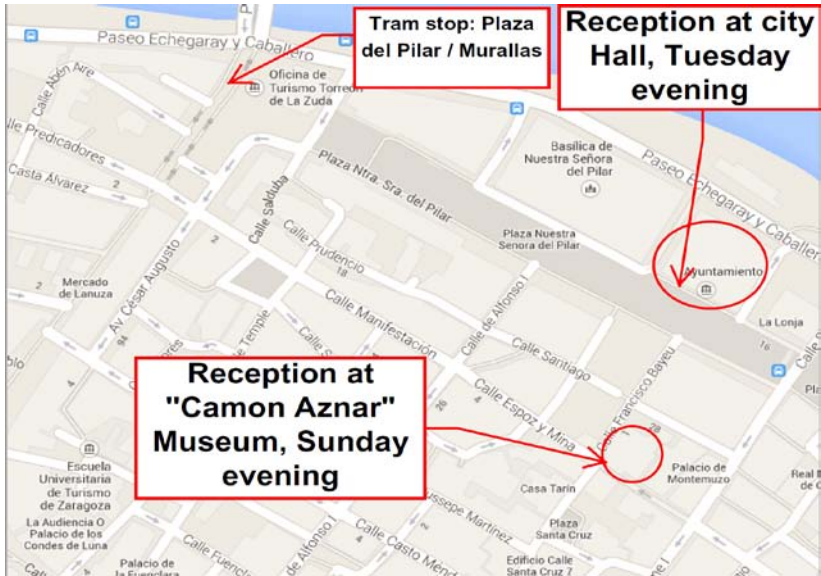
For the Wednesday farewell party at "Las playas" resort inside "Parque del Agua" (Avenida del Botánico, 8), 19:00 hours, you can go by taking the Ci2 bus. You can get off the tram three stop back from conference site, at the "Pablo Neruda" stop, and then take the Ci2 bus direction to the "Estación" getting off six stop ahead, at the "Parque" bus stop. See maps.

Hiring a taxi is easy everywhere and any driver will bring you to the Engineering campus or elsewhere. You may refer to the Betancourt building (conference site) inside the Engineering campus. Some drivers accept credit cards for payment but it is good to check in advance when taking the taxi. Just in case, two taxi companies phone numbers are: +34 976757575, +34 976424242

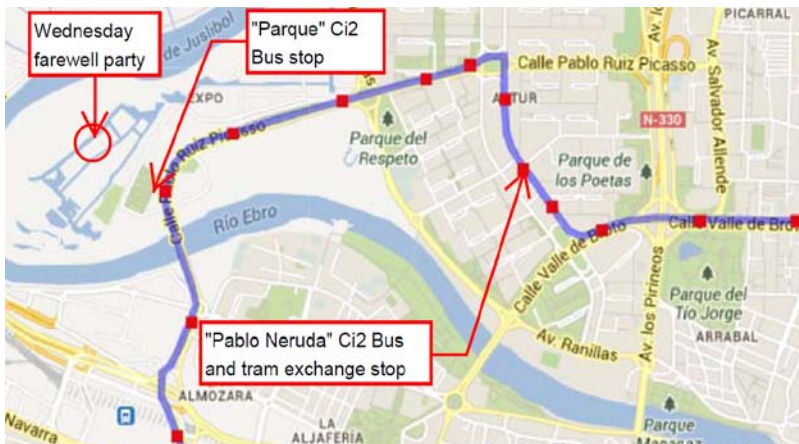
Tram map



Receptions map



Farewell party map



Registration

The conference registration and information desk will be located on ground floor of Betancourt building, just in front of the “**Salon de actos**” (Auditorium). The registration desk will be labeled with the CinC sign and will be open during the following hours:

Sunday, 22nd September	13:00 – 18:00
Monday, 23rd September	08:30 – 13:00
Tuesday, 24th September	08:30 – 18:00
Wednesday, 25th September	08:30 – 18:00

Internet access

Within the conference rooms, wireless network will be available free of charge. The network name is ‘**cinc2013**’ and the password is ‘CINC++cinc’. For those using **eduroam**, this network is available at the conference site. The only device you need is a WiFi-enabled laptop or smartphone. Should you need assistance in getting connected, please ask the nearest volunteer for help.

Meals

The delegates will not have to worry about meals. Just, in order to keep up the meeting timetable, the attendees are kindly asked to proceed quickly to the Restaurants or buffets immediately after the session finishes

- The **Sunday** symposium concludes with a visit to the “Camon Aznar” Museum where **reception light food** will be served, together with music entertainment.
- **Monday** sit down **lunch** will be served after the S2* sessions in the **University cafeteria** (ground floor) from 12:45 to 14:00
- **Monday** social event concludes with a **dinner** in a emblematic environment at the “Finca Sansui” restaurant close to Zaragoza,
- **Tuesday buffet lunch** will be provided after the S4* sessions and overlapping the **Posters session P5* in the Central Hall** (ground floor) from 12:45 to 13:45.
- After **Tuesday** sessions, participants are invited to travel by their own to the city hall (see map) where a Mayor House reception will be given accompanied by a **light refreshment**. For this evening, participants are encouraged to explore some of the Zaragoza restaurants, tapas bars, pubs, etc. on their own.
- **Wednesday buffet lunch** will be provided after the S9* sessions and overlapping the **Posters session PA* in the Central Hall** (ground floor) from 12:45 to 13:45. For the evening, a farewell party will be given after 19:00 at “Las playas” resort inside “Parque del Agua” (Avenida del Botánico, 8).

Regular coffee breaks with tea, coffee, soft drinks, cakes and fruits will be served at the conference breaks:

Accompanying Persons

The accompanying person registration allows the guest to attend:

- The visit and reception on Sunday evening to the Camón Aznar Museum
- The Monday social event starting at 13:00 with lunch, participation as an activist or passivist in the activities and in the gala dinner, to be held at the Finca Sansui Restaurant.
- The Tuesday reception at the City hall.
- The Wednesday farewell party after conference end.

Post conference and accompanying person tours

For tours outside the conference program, both during the conference for accompanying persons, and before/after the conference for all participants, you are directed to the conference travel agency “El Corte Inglés”. The travel agency will be happy to arrange personalized package tours to a variety of local and area historical, cultural and recreational sites. You can contact them at congresos_zaz@viajeseci.es or by phone (+34 976 469 628). To book a tour, please fill out and send a form at www.cinc2013.org to “El Corte Inglés” by fax (+34) 976 282 450 or email at congresos_zaz@viajeseci.es, before September 12th.

Useful numbers:

Emergency calls free of charge from mobile boxes:	112
Direct emergency numbers in Zaragoza:	
Police:	091 / 092
Ambulance:	061
<i>Computing in Cardiology</i> Registration Desk:	+34 976 762704

For Authors and Speakers

Oral Presentations

The time allocated for each oral presentation is 10 minutes, followed by 5 minutes for discussion (except in sessions S33 and S43. See below). Speakers are expected to adhere strictly to this schedule, which will be enforced by session chairpersons in order to finish sessions on time and to permit participants to move successfully from one parallel session to another.

All conference rooms will be equipped with a computer projection system (LCD projector and PC with Windows XP, PowerPoint 2003, Windows Media Player and Adobe Acrobat reader). Speakers are required to allow adequate time prior to their sessions to load and check their presentations

on the designated computer. A local staff member will be available for help. In addition, speakers are required to meet with their session chairpersons in the scheduled conference room at least 10 minutes before the beginning of the session. It is good idea to ensure that the chairperson knows how to correctly pronounce your name.

Poster Presentations

Poster sessions will take place in the **Betancourt Building Hall**, ground floor, on Tuesday, 24th September from 13:15, and on Wednesday, 25th September, from 13:15. The Exhibition Hall is located on the ground floor of the building, through the entrance lobby ahead. Authors are required to be present at their posters during their assigned session in order to discuss their work with other conference attendees.

Authors are welcome to visit the Exhibition area at least 30 minutes prior to the poster session and hang their posters at the location designated with the correct number. Posters may be hung:

- between 09:00 and 12:30 for the Tuesday session, and
- between 09:00 and 12:30 for the Wednesday session.

Subject areas for the poster sessions will be clearly marked and poster boards will be numbered with a card corresponding to the page number in this book. Mounting materials will be provided at the entrance. Authors are expected to remove their posters immediately after the end of the sessions to allow the timely cleaning of the Exhibition Room.

Rosanna Degani Young Investigator Award

Computing in Cardiology runs an annual competition to encourage young investigators and to provide a living memorial to Rosanna Degani. The competition for the 2013 Rosanna Degani Young Investigator Award was open to persons under 36 years of age and in "training status" at the submission deadline of May 1st, 2013. Finalists in the competition will present their work in session M1, at 9:15 on Monday, 23rd September in the "**Salon de Actos**" room. The name of the winner will be announced during the closing plenary session on Wednesday.

PhysioNet/Computing in Cardiology Challenge 2013

Since 2000, Computing in Cardiology has annually issued a PhysioNet Challenge in cooperation with PhysioNet, part of the NIH sponsored Research Resource for Complex Physiologic Signals. The aim of this year's challenge is "*Noninvasive Fetal ECG*". The challenge sessions are on Tuesday, September 24th:

- S33 09:15 - 10:45
- S43 11:15 - 12:45

The time allocated for each oral presentation in these sessions is 3 minutes; the remaining time will be allocated to panel discussions. The winners will be announced during the closing plenary session on

Wednesday.

Manuscripts

Computing in Cardiology will publish the conference proceedings containing the complete manuscripts of all presentations. The complete proceedings will be freely available via the CinC web site (<http://www.cinc.org>). Also they will be published by IEEE at their IEEEXplore digital library. For any questions about manuscripts, consult the CinC web site, www.cinc.org, or contact via email Alan Murray, the Editor of the proceedings: **Alan.Murray@ncl.ac.uk**

Conference Overview

The conference begins on the afternoon of Sunday 22nd with a special symposium entitled "Electrophysiological Cardiac Modelling". A reception at the "Camón Aznar" Museum starts at the end of the symposium. The scientific sessions of the conference begin on Monday morning. During the afternoon, the traditional social program will take place. Sessions will continue on Tuesday, ending with an evening reception at the city Hall, and Wednesday, ending with an evening farewell party at "Las Playas" resort in "Parque del Agua". Sessions include both oral presentations and poster sessions.

Sunday Symposium

The Sunday Symposium will be held in "Salon de Actos", Edificio Betancourt.

- | | |
|---------------|---|
| 13:00 - 13:45 | Registration |
| 13:45 - 14:00 | Official Addresses |
| 14:00 - 14:45 | Invited lecture: <i>Factors in calcium store stability - discussion of potential therapeutic targets</i> , Dr. Antonio Zaza (Università di Milano- Bicocca): |
| 14:45 - 15:30 | Invited lecture: <i>Ionic mechanisms behind cardiac arrhythmias</i> , Dr. Andras Varró (University of Szeged) |
| 15:30 - 16:00 | Coffee break |
| 16:00 - 16:45 | Invited lecture: <i>Multiscale modeling of cell electrophysiology: from ion-channel molecular structure to the action potential</i> , Dr. Yoram Rudy (Washington University, Saint Louis) |
| 16:45 - 17:30 | Invited lecture: <i>Mechanisms of persistent atrial fibrillation</i> , Dr. José Jalife (University of Michigan) |
| 17:30 - 18:15 | Invited lecture: <i>Computer simulation of the electric activity of the heart. From the cell to the ECG</i> , Dr. José F. Rodríguez (Universidad de Zaragoza) |
| 18:15 – 19:30 | <i>Transportation, on your own, to Museum "Camon Aznar", see maps for details</i> |
| 19:30 - 22:30 | Reception at Museum "Camón Aznar" with light food and music, |

Scientific Sessions

The opening ceremony of the scientific sessions begins on Monday, 23rd September at 09:00 in the “Salon de Actos”, Aula (ground floor) and is immediately followed by the Rosanna Degani Young Investigator Final beginning at 09:15. All regular sessions are held in lecture rooms “Salon de Actos”, 0.01, 1.03, “Sala de Juntas” and 1.02 (only for Wednesday evening sessions). The buildings and the rooms bear labels with the CinC sign. Please see the enclosed map of the Betancourt Buildings.

Monday Social Program

Each year at CinC, Monday afternoon is set aside to facilitate a social event. This is an important part of the conference program as it allows attendees to network and relax in a more informal setting away from the scientific sessions. Please consider the following remarks:

- All Social Program participants are required to wear the T-shirts or caps provided in a distinct color for each group, as well as their CinC badges.
- As the Social Program starts immediately after the sessions, the participants may consider comfortable informal dress for the whole day.
- Adhesive labels with name will be provided for participants wishing to leave their delegate kits in a safe storage room at the University until Tuesday morning. Please do NOT leave money, credit cards, documents, hotel keys or cameras, since you may need them during the afternoon.

The social program will commence at 13:00 on Monday with lunch at the **Conference Venue**. As it is traditional in the Computing In Cardiology Social Program, participants can choose between Activist or Passivist activities.

The activist program will start at 15:00. At that time buses will depart from the Conference Venue to the Ebro river bank, near the Expo area, where participants will receive the basic instructions for kayak paddling, and will enter the river for a nice kayaking tour. This will be an excellent opportunity to enjoy Zaragoza, its bridges and some of its main buildings from a very different perspective. After the kayaking tour, there will be some free time for refreshment or sightseeing on your own in the area of Basilica of El Pilar and La Seo. Then, the buses will take you to the Finca Sansui, “the Garden of the Water” for the Conference Dinner.

The passivist program will also start at 15:00. At this time, the buses will depart for the historical center of Zaragoza, where participants will have a chance to visit the main touristic attractions of Zaragoza accompanied by a city guide: The Basilica of Our Lady of the Pillar, the Seo Cathedral and walk by the historical center. They will also be taken by bus to visit the

Aljaferia Palace, a fortified medieval Islamic palace from the second half of the 11th century, later to become the royal residence of the Kings of Aragon, which currently hosts the Parliament of the Autonomous Community of Aragon. After the sightseeing tour, buses will take the participants to the Conference Dinner site “Finca Sansui”, also known as “the Garden of the Water”

Monday Social Program Schedule

All participants	13:00 - 15:00	Lunch at Conference Venue
	15:00	Buses will depart to the Activist/Passivist activities.
Activists	15:15 - 19:00	Kayaking tour down the Ebro river.
	19:00 – 20:00	Visit of the El Pilar and/or La Seo and free time.
Passivists	15:15 - 20:00	Sightseeing tour in the historical center and Aljaferia Palace.
All participants	20:00	Buses depart to Finca Sansui
	20:30	Gala dinner
	22:30	Aragon’s folklore music and dances
	23:30	Bus returns to Zaragoza

Tuesday Evening Reception

The City Hall House will give a reception to all conference participants, including accompanying persons. We will have the opportunity to visit the city hall building that correspond to a renacentist palace centered around an inner open “patio”. The reception will be accompanied by **light refreshments**.

Wednesday farewell party

For those remaining in Zaragoza after the conference ends, there will be an opportunity to join a farewell party after 19:00 at “Las playas” resort inside “Parque del Agua” (Avenida del Botánico, 8). You can take bus Ci2, get off at the tram “Pablo Neruda” stop, then take bus Ci2 (direction to the “Estacion”), get off at “Parque” bus stop and walk to “Las playas” resort. Here, we can just relax, taking some drinks and/or light food, in a nice environmental setting, typically in September with still very good weather, while listening to some music.

New Abstract Number Formatting

Please note that the numbering of abstracts in this book has changed this year. Abstracts are now numbered “xxx-yyy” where “xxx” represents the page number of the abstract in this book, and “yyy” represents the submission number of the abstract. We hope that this numbering system will make it easier for authors to utilize this abstract book.

Scientific Sessions Program Overview

Monday, September 23, 2013

9:00	Welcome to CinC 2013	Salón de Actos
9:15	M1: Rosanna Degani Young Investigator Finals	Salón de Actos
10:45	Coffee Break	
11:15	S21: Software Platforms	Sala de Juntas
	S22: Electrophysiological Modeling.....	Aula 1.03
	S23: Ventricular Repolarization	Aula 0.01
	S24: Heart Rate Variability: Fetal and Adult	Salón de Actos
12:45	Lunch	University Cafeteria
14:00	Social Event	

Tuesday, September 24, 2013

9:00	Display Posters.....	Central Hall
9:15	S31: Cardiorespiratory Coupling	Aula 0.01
	S32: Ventricular Arrhythmias and Cardiac Arrest	Aula 1.03
	S33: Challenge I.....	Salón de Actos
	S34: Novel Technologies I	Sala de Juntas
10:45	Coffee Break	
11:15	S41: Echocardiography	Aula 0.01
	S42: Mobile and Remote Monitoring	Sala de Juntas
	S43: Challenge II.....	Salón de Actos
	S44: Ventricular Modelling: From Cell to ECG	Aula 1.03
12:45	Lunch	Central Hall
13:15	P5: Poster Session	Central Hall
15:15	S61: Myocardial Ischemia	Salón de Actos
	S62: Clinical Electrophysiology	Aula 0.01
	S63: Cardiac MRI	Aula 1.03
	S64: Novel Techniques.....	Sala de Juntas
16:45	Coffee Break	
17:00	S71: Ischemia Modelling	Aula 0.01
	S72: Modelling Electrophysiology	Sala de Juntas
	S73: Atrial Fibrillation Detection and Prediction.....	Salón de Actos
	S74: Multivariate CV Signal Modelling & Analysis.....	Aula 1.03
19:30	Reception	City Hall

Wednesday, September 25, 2013

9:00	Display Posters.....	Central Hall
9:15	S81: ECG Measurement	Salón de Actos
	S82: Cardiac Mechanics	Sala de Juntas
	S83: Cardiac Computed Tomography	Aula 1.03
	S84: Ventricular Cell-Tissue Modelling	Aula 0.01
10:45	Coffee Break	
11:15	S91: Clinical Aspects of Electrocardiography.....	Salón de Actos

	S92: Vascular Mechanics.....	Sala de Juntas
	S93: 3D Atrial Modelling	Aula 0.01
	S94: Sensor Technology and Heart Rate Analysis	Aula 1.03
12:45	Lunch	Central Hall
13:15	PA: Poster Session	Central Hall
15:15	SB1: ECG Signal Processing.....	Aula 0.01
	SB2: Physiological Atrial Modelling	Aula 1.02
	SB3: Atrial Fibrillation Physiology.....	Aula 1.03
	SB4: Intravascular Imaging	Sala de Juntas
	SB5: Prediction of Hypotension and BP Variability	Salón de Actos
16:15	Coffee Break	
16:30	MC: Closing Plenary.....	Salón de Actos
17:30	CC: Conference Closing Ceremony(ending at 18:00)	Salón de Actos
19:00	Farewell Party.....	Las Playas Resort

Scientific Program

Monday, September 23, 2013, 09:15

M1: Rosanna Degani Young Investigator Finals

Room: Salón de Actos

Chair(s): Peter Macfarlane and Willem Dassen

- 1-52 **Fluid-structure Interaction Analysis of Representative Left Coronary Artery Models with Different Angulations**
Jingliang Dong*, Zhonghua Sun, Kiao Inthavong, Jiyuan Tu
- 2-410 **Improved Electrocardiographic Detection of Hyperacute Ischemia by Difference Vector Analysis**
C Cato ter Haar*, Arie C Maan, Martin J Schlij, Cees A Swenne
- 3-313 **Semi-automated Detection and Quantification of Aortic Atheromas from Three-Dimensional Transesophageal Echocardiography**
Concetta Piazzese*, Wendy Tsang, Miguel Sotaquira, Roberto M Lang, Enrico G Caiani
- 4-21 **Prediction of Sudden Cardiac Death in Chronic Heart Failure Patients by Analysis of Restitution Dispersion**
Julia Ramírez*, Ana Mincholé, Juan Bolea, Pablo Laguna, Esther Pueyo

Monday, September 23, 2013, 11:15

S21: Software Platforms

Room: Sala de Juntas

Chair(s): Jocelyne Fayn and Álvaro Alesanco

- 5-427 **LightWAVE: Waveform and Annotation Viewing and Editing in a Web Browser**
George Moody*
- 6-286 **Elab: A Web-based Platform to Perform HRV Analysis and Store Cardiac Signals**
Óscar Barquero-Pérez*, Teresa Quintanilla, José García-Muñoz, Cristina Soguero-Ruiz, Mark Wilby, José Luis Rojo-Álvarez, Arcadi García-Alberola, Manuel de la Rosa, Miguel Cabañas, Iván González, Roberto Bravo
- 7-112 **Seamless Integration of Watermarks in DICOM Images**
Óscar J Rubio*, Álvaro Alesanco, José García
- 8-159 **An Interactive Digital Platform for Arterial Wave Intensity Analysis**
John L Tassone*, Ashraf W Khir
- 9-309 **A Cardiovascular Patient Follow-up System using Twitter and HL7**
Jesús Daniel Trigo*, Aitor Eguzkiza, Miguel Martínez-Espronedca, Luis Serrano

Monday, September 23, 2013, 11:15

S22: Electrophysiological Modeling

Room: Aula 1.03

Chair(s): José Maria Ferrero and Antonio Zaza

- 10-299 **Computational Modeling of Human Fetal Normal Sinus Rhythm and Arrhythmia**
Alan Benson, Adam Bleakley, Arun Holden*, Nikki Pelech, Eleftheria Pervolaraki, Catherine Whitfield, Sam Hodgson
- 11-322 **HCN and SCN5A Channel Mutations: Implications for Impaired Atrioventricular Nodal Conduction in a Heterogeneous Computer Model of Whole Mouse Heart**
Simon Joseph Castro*, Michael Alan Colman, Henggui Zhang
- 12-329 **Modeling the Influence of High Fibroblast Level on Arrhythmia Development and Obstructed Depolarization Spread**
Sándor Miklós Szilágyi*, László Szilágyi, Béat Hirsbrunner
- 13-28 **Heterogeneous Electrical Remodeling of the Failing Heart Modulates the Arrhythmogenic Substrate**
Juan Fco Gomez*, Karen Cardona, Lucia Romero, Javier Saiz, Beatriz Trenor
- 14-421 **Kalman Filter Based Estimation of Ionic Concentrations and Gating Variables in a Cardiac Myocyte Model**
Laura Munoz*, Niels Otani
- 15-428 **Uncertainty Visualization in Forward and Inverse Cardiac Models**
Brett Burton*, Burak Erem, Kristin Potter, Paul Rosen, Chris Johnson, Dana Brooks, Rob Macleod

Monday, September 23, 2013, 11:15

S23: Ventricular Repolarization

Room: Aula 0.01

Chair(s): Roberto Sassi and Esther Pueyo

- 16-81 **Exploring QT Variability Dependence from Heart Rate in Coma and Brain Death on Pediatric Patients**
Rute Almeida*, Ana Paula Rocha, Marta João Silva
- 17-130 **Comparing the Relationship Between QT/RR Slope and Basal QTc in LQT1 Patients and Healthy Subjects**
Josef Halamek*, Jean-Philippe Couderc, Pavel Jurak
- 18-278 **Lack of Autonomic Influence on QT Interval Variability In Patients With Heart Failure**
Sachin Nayyar, Muhammad Hasan, Thomas Sullivan, Judith Hunt, Prashanthan Sanders, Kurt Roberts-Thomson, Mathias Baumert*
- 19-100 **QT Interval Analysis in Electrograms of Isolated Guinea Pig Hearts Treated with Haloperidol**
Petr Vesely*, Josef Halamek, Tibor Stracina, Lenka Krejčírova, Marie Novakova
- 20-146 **Comparative Analysis of Short-Term Variability of RR and QT Intervals for the Assessment of Autonomic Nerve Activity**
Yi Zhu*, Xiaolin Yang, Zhigang Wang, Yi Peng
- 21-306 **The Linear Dependence of Ventricular Repolarization Variability on Heart Rate Variability in Head-Down Bed Rest Studies**
Juan Bolea*, Enrico G Caiani, Pablo Laguna, Rute Almeida

Monday, September 23, 2013, 11:15

S24: Heart Rate Variability: Fetal and Adult

Room: Salón de Actos

Chair(s): Riccardo Barbieri and Andreas Voss

- 22-57 **Fetal Heart Rate Pattern in Prenatal Diagnosis**
Dirk Hoyer*, Uwe Schneider
- 23-414 **Subspace Detection of the Impulse Response Function
from Intrapartum Uterine Pressure and Fetal Heart Rate
Variability**
Philip Warrick*, Emily Hamilton
- 24-251 **Increased Instability of Heartbeat Dynamics in Parkinson's
Disease**
Riccardo Barbieri*, Gaetano Valenza, Luca Citi, Maria Guerrisi,
Stefano Orsolini, Carlo Tessa, Stefano Diciotti, Nicola Toschi
- 25-256 **Assessment of Fetal Development using Multiscale
Multifractal Analysis of Heart Rate Variability**
Jan Gierałtowski*, Dirk Hoyer, Uwe Schneider, Jan Żebrowski
- 26-426 **Time-series Network Analysis for Detecting Cardiac
Autonomic Neuropathy using RR Interval Data**
Chandan Karmakar*, Ahsan Khandoker, Herbert Jelinek, Marimuthu
Palaniswami

Tuesday, September 24, 2013, 09:15

S31: Cardiorespiratory Coupling

Room: Aula 0.01

Chair(s): Jean-Marc Vesin and Giandomenico Nollo

- 27-178 **Quantification of Cardiorespiratory Coupling in Acute Schizophrenia Applying High Resolution Joint Symbolic Dynamics**
Steffen Schulz, Karl-Juergen Baer, Andreas Voss*
- 28-114 **Analysis of Cardio-respiratory Dynamics during Mental Stress using (Partial) Time-Frequency Spectra**
Devy Widjaja*, Michele Orini, Elke Vlemincx, Sabine Van Huffel
- 29-150 **Cardiorespiratory Coherence Analysis of Abnormal Heart Rate Responses during Deep Breathing**
Urban Wiklund, Amir Kadkhodaei, Kennet Anderson*
- 30-226 **Information decomposition of Short-term Cardiovascular and Cardiorespiratory Variability**
Luca Faes*, Alessandro Montalto, Giandomenico Nollo, Daniele Marinazzo
- 31-305 **Influence of Respiration in the Very Low Frequency Modulation of QRS Slopes and Heart Rate Variability in Cardiomyopathy Patients**
David Hernando*, Alejandro Alcaide, Esther Pueyo, Pablo Laguna, Andrés Arcentales, Beatriz Giraldo, Andreas Voss, Antonio Bayés-Genís, Raquel Bailón
- 32-377 **Estimating Respiratory Frequency from Heart Rate Variability During Treadmill Exercise Testing**
Lina María Sepúlveda-Cano, Edgar Felipe Sierra-Alonso, Germán Castellanos-Domínguez, Raquel Bailón-Luesma*, Pablo Laguna

Tuesday, September 24, 2013, 09:15

S32: Ventricular Arrhythmias and Cardiac Arrest

Room: Aula 1.03

Chair(s): Juan Pablo Martínez and Cees Swenne

- 33-125 **Probabilistic Classification Approaches for Cardiac Arrest Rhythm Interpretation during Resuscitation**
Ali Bahrami Rad*, Trygve Eftestøl, Jan T Kvaløy, Unai Ayala, Jo Kramer-Johansen, Kjersti Engan
- 34-354 **A New Rhythm Analysis Algorithm for Chest Compression Intervals: Effect on Cardiopulmonary Resuscitation Delivery**

Unai Ayala*, Unai Irusta, Jesús Ruiz, Digna González-Otero, Erik Alonso, Jo Kramer-Johansen, Trygve Eftestøl
- 35-138 **Increase of QRS Duration as a Short-Term Predictor of Ventricular Arrhythmias During Coronary Artery Occlusion.**
Alba Martín-Yebra*, Marina Demidova, Pyotr Platonov, Pablo Laguna, Juan Pablo Martínez
- 36-96 **Dependency of T-Wave Alternans Predictive Power for the Occurrence of Ventricular Arrhythmias on Heart Rate**
Laura Burattini*, Sumche Man, Cees A Sweene
- 37-335 **Risk Stratification for Arrhythmic Sudden Cardiac Death in Heart Failure Patients using Machine Learning Techniques**
George Manis*, Stavros Nikolopoulos, Petros Arsenos, Konstantinos Gatzoulis, Polychronis Dilaveris, Christodoulos Stefanadis
- 38-338 **Deceleration Capacity Alterations before Non Sustained Ventricular Tachycardia in Post Myocardial Infraction Patients**
Petros Arsenos, George Manis*, Stavros Nikolopoulos, Konstantinos Gatzoulis, Polychronis Dilaveris, Christodoulos Stefanadis

Tuesday, September 24, 2013, 09:15

S33: Challenge I

Room: Salón de Actos

Chair(s): Roger Mark and Joachim Behar

- 39-347 **Noninvasive Fetal ECG: the PhysioNet/Computing in Cardiology Challenge 2013**
Ikaro Silva*, Joachim Behar, Gari D Clifford, George B Moody
- 40-26 **Cancellation of the Maternal and Extraction of the Fetal ECG in Noninvasive Recordings**
Ivaylo Christov*, Iana Simova, Roger Abächerli
- 41-101 **Extracting R-wave Position from an FECG Record using Recognition of its Multi-channel Shapes**
Filip Plešinger*, Josef Halánek, Pavel Jurák
- 42-166 **Advanced Maternal ECG Removal and Noise Reduction for Application of Fetal QRS Detection**
Jukka A Lipponen*, Mika P Tarvainen
- 43-279 **A Novel Algorithm for Fetal QRS Detection in Abdominal ECG Recordings**
Andrea Fanelli*, Giovanni Magenes, Maria Gabriella Signorini
- 44-332 **Fetal QRS Detection and RR Interval Measurement in Noninvasively Registered Abdominal ECGs**
Christoph Maier*, Hartmut Dickhaus
- 45-184 **Noninvasive Fetal QRS Detection Using Linear Combination of Abdomen ECG Signals**
Or Perlman*, Amos Katz, Yaniv Zigel
- 46-216 **Fetal ECG Extraction From Abdominal Recordings using Array Signal Processing**
Masoumeh Haghpanahi*, David A Borkholder

Tuesday, September 24, 2013, 09:15

- 47-87 **Advanced Signal Processing Techniques for Fetal ECG Analysis**
Jakub Kuzilek*, Lenka Lhotska
- 48-432 **Fetal QRS Complex Detection using Semi-blind Source Separation Framework**
Fatemeh Razavipour*, Reza sameni, Marzieh Fatemi
- 49-121 **Fetal QRS Complex Detection Based on Three-Way Tensor Decomposition**
Mohammad Niknazar*, Bertrand Rivet, Christian Jutten
- 50-236 **Fetal Electrocardiogram R-peak Detection using Robust Tensor Decomposition and Extended Kalman Filtering**
Mahsa Akhbari, Mohammad Niknazar*, Christian Jutten, Mohammad B Shamsollahi, Bertrand Rivet
- 51-196 **Maternal Signal Estimation by Kalman Filtering and Template Adaptation for Fetal Heart Rate Extraction**
Fernando Andreotti*, Maik Riedl, Tilo Himmelsbach, Daniel Wedekind, Sebastian Zauneder, Niels Wessel, Hagen Malberg
- 52-399 **The Physionet / Computing in Cardiology Challenge 2013: Detection of fetal heart-rate and fetal RR interval from Fetal Electrocardiogram signals**
Srinivasan Vairavan*, Syed Haider, Eric Carlson, Minnan Xu, Saeed Babaeizadeh
- 53-315 **A Sequential Multiscale Bayesian Tracker for Maternal ECG Removal in Non-invasive Fetal ECG Recordings**
Guojun Li*, Xiaoping Zeng, Xiaona Zhou
- 54-275 **2013 PhysioNet Challenge: A Markov Chain Monte Carlo Approach to Locating Features in Noninvasive Fetal ECG Signals**
Tom Pollard*, Jack Carlyle, Jamie Jasinski, Alice Foster, Matthew Hills, Kirthika Narasimhan, Emma Gale, David Williams

Tuesday, September 24, 2013, 09:15

- 55-358 **Fetal Electrocardiogram QRS Detection Using Ensemble Empirical Mode Decomposition and Normalized Correlation Coefficient**
Paschalis Bizopoulos*, Evaggelos Karvounis, Dimitrios Tsalikakis, Dimitrios Koutsouris, Dimitrios Fotiadis
- 56-415 **A Robust Framework for Noninvasive Extraction of Fetal Electrocardiogram Signal**
Marzieh Fatemi*, Sajad Niknam, Fatemeh Razavipour, Reza Sameni
- 57-355 **Noninvasive Fetal QRS Detection using Echo State Network**
Mantas Lukoševičius*, Vaidotas Marozas

Tuesday, September 24, 2013, 09:15

S34: Novel Technologies I

Room: Sala de Juntas

Chair(s): Luca Mainardi and Sheri Prucka

- 58-269 **Peripheral Blood Volume Changes in Response to Ventricular Premature Beats During Dialysis**
Eglé Grigonytė*, Eduardo Gil, Pablo Laguna, Leif Sörnmo
- 59-323 **Probabilistic Modeling of the Oxygen Saturation Pattern for the Detection of Anomalies During Clinical Interventions**
Diego Martín-Martínez*, Pablo Casaseca-De-la-Higuera, Marcos Martín-Fernández, Carlos Alberola-López
- 60-281 **Determining Heart Activity Present in the Pressure Sensors of a Dialysis Machine**
Mattias Holmer*, Eglé Grigonytė, Frida Sandberg, Kristian Solem, Bo Olde, Leif Sörnmo
- 61-71 **Empirical Mode Decomposition Based Real-Time Blood Pressure Delineation and Quality Assessment**
Vladimir Ostojic, Tatjana Loncar-Turukalo*, Dragana Bajic
- 62-175 **Detection of Glaucoma based on the Analysis of Cardiovascular Signals**
Andreas Voss*, Katharina Witt, Eva Koch, Matthias Fuest, Niklas Plange
- 63-240 **Waving at the Heart: Implementation of a Kinect based Real-time Interactive Control System for Viewing Cineangiogram Loops During Cardiac Catheterization Procedures**
Bart Suelze, Robin Agten, Philippe B Bertrand, Thijs Vandenryt, Peter Dedrij, Ronald Thoelen, Pieter Vandervoort, Lars Grieten*

Tuesday, September 24, 2013, 11:15

S41: Echocardiography

Room: Aula 0.01

Chair(s): Enrico Caiani and Alfredo Hernandez

- 64-321 **Quantitative Characterization of Mitral Annulus and Leaflets from Transesophageal 3D Echocardiography**
Miguel Sotaquira*, Laura Fusini, Mauro Pepi, Roberto M Lang, Enrico G Caiani
- 65-320 **Dynamic Registration of Multiple-view US and MRI for the Characterization of Hypertrophic Cardiomyopathy**
Julián Betancur*, Antoine Simon, Frédéric Schnell, François Tavard, Erwan Donal, Alfredo I Hernández, Mireille Garreau
- 66-290 **3D Evaluation of Tricuspid Annulus Morphology in Patients with Pulmonary Hypertension**
Federico Veronesi*, Karima Addetia, Claudio Lamberti, Roberto Lang, Victor Mor-Avi
- 67-382 **Evaluation of Computed Tomography to Ultrasound 2D Image Registration for Atrial Fibrillation Treatment**
Zulma Sandoval*, Jean-Louis Dillenseger
- 68-218 **Early Detection of Cardiotoxicity in Chemotherapy-Treated Patients from Real-time 3D Echocardiography**
Cinzia Lorenzini, Cristiana Corsi*, Michele Aquilina, Alberto Farolfi, Andrea Rocca, Luca Frassinetti, Emanuela Scarpi, Dino Amadori, Claudio Lamberti
- 69-91 **Comparison of 2D and 3D Echocardiographic Measurement of Mitral-Aortic Angle**
Federico Veronesi*, Enrico Caiani, Cristiana Corsi, Claudio Lamberti

Tuesday, September 24, 2013, 11:15

S42: Mobile and Remote Monitoring

Room: Sala de Juntas

Chair(s): Enno van der Velde and José García

- 70-325 **An Evidence Based Android OSA Screening Application**
Joachim Behar*, Aoife Roebuck, Mohammed Shahid, Jonathan Daly, Niclas Palmius, Andre Hallack Miranda Pureza, Gari D. Clifford
- 71-363 **Long-term Effect of Telecare on Patients with Heart Failure and High Blood Pressure**
Masatsugu Tsuji*, Yuji Akematsu
- 72-41 **Remote Monitoring of Respiratory Rate in Critical Environments**
Kian Davoudi, Moein Shayegannia, Bozena Kaminska*
- 73-98 **Technical Verification of Applying Wearable Physiological Sensors in Ubiquitous Health Monitoring**
Eliasz Kańtoch*
- 74-181 **Proposal of Real-Time Echocardiogram Transmission based on Visualization Modes with WiMAX Access**
Eva Caveró*, Alvaro Alesanco, Ljiljana Trajkovic, Constantinos Pattichis, Jose Garcia
- 75-436 **Context-aware Cardiac Monitoring System for Early Detection of Heart Diseases**
Abdur Rahim Mohammad Forkan*, Ibrahim Khalil, Zahir Tari

Tuesday, September 24, 2013, 11:15

S43: Challenge II

Room: Sal3n de Actos

Chair(s): Gari Clifford and Ikaro Silva

- 76-128 **A multi-step Approach for Non-invasive Fetal ECG Analysis**
Maurizio Varanini, Gennaro Tartarisco*, Lucia Billeci, Alberto Macerata, Giovanni Pioggia, Rita Balocchi
- 77-30 **Noninvasive Fetal ECG Estimation based on linear transformations**
Mariano Llamedo*, Alba Mart3n-Yebra, Pablo Laguna, Juan Pablo Mart3nez
- 78-142 **A Wavelet-Based Method for Assessing Fetal Cardiac Rhythms from Abdominal ECGs**
Rute Almeida*, Hern3ni Gonalves, Ana Paula Rocha, Jo3o Bernardes
- 79-277 **PhysioNet/CinC Challenge 2013: A Novel Noninvasive Technique to Recognize the Fetal QRS Complexes from Noninvasive Fetal Electrocardiogram Signals**
Ali Ghaffari, Seyyed Abbas Atyabi*, Mohammad Javad Mollakazemi, Maryam Niknami, Ali Soleimani
- 80-72 **Non Invasive FECG Extraction From a Set of Abdominal Sensors**
Joachim Behar*, Julien Oster, Gari D Clifford
- 81-153 **Multi Stage Principal Component Analysis Based Method for Detection of Fetal Heart Beats in Abdominal ECG**
Robertas Petrolis, Algimantas Krisciukaitis*
- 82-173 **An Algorithm for the Analysis of Foetal ECG from 4-channel Non-invasive Abdominal Recordings**
Costanzo Di Maria, Wenfeng Duan, Marjan Bojarnejad, Fan Pan, Susan King, Dingchang Zheng, Alan Murray, Philip Langley*

Tuesday, September 24, 2013, 11:15

- 83-194 **Systematic Methods for Fetal Electrocardiographic Analysis: Determining the Fetal Heart Rate, RR Interval and QT Interval**
Chengyu Liu*, Peng Li
- 84-429 **Comparison of Three Methods for Fetal QRS detection**
Aruna Deogire*, Satish Hamde
- 85-172 **A Robust Algorithm for Fetal QRS Detection using the Non-invasive Maternal Abdomen ECG**
Martin Kropf*, Günter Schreier, Robert Modre-Osprian, Dieter Hayn
- 86-230 **Noninvasive Fetal ECG Detection from Maternal Abdominal Recording: the Physionet/CINC Challenge 2013**
Vito Starc*
- 87-271 **Fetal QRS Detection using Maternal Template Matching and Modified Pan Tompkins Algorithms**
Akshay Dhawan*
- 88-343 **Identification of Fetal QRS Complexes in Low Density Non-Invasive Biopotential Recordings**
Alessia Dessì*, Danilo Pani, Luigi Raffo
- 89-79 **Fetal ECG Detection in Abdominal Recordings: a Method for QRS Location**
Rui Rodrigues*
- 90-191 **Noninvasive Fetal ECG Extraction Using Temporal Frequency Analysis**
Joseph McBride*, Brent McFerrin, Craig Towers, Xiaopeng Zhao
- 91-135 **Multichannel Foetal Heartbeat Detection by Combining Source Cancellation with Expectation-weighted Estimation of Fiducial Points**
Luigi Yuri Di Marco*, Alberto Marzo, Alejandro Frangi

Tuesday, September 24, 2013, 11:15

92-179 **Fetal Heart Rate Discovery (FHRD) Algorithm for Detection of Fetal Heart Rate from Noisy, Noninvasive Fetal ECG Recordings**

Piotr Podziemski*, Jan Gierałtowski

Tuesday, September 24, 2013, 11:15

S44: Ventricular Modelling: From Cell to ECG

Room: Aula 1.03

Chair(s): Johannes Struijk and Olaf Dössel

- 93-349 **Validation of the V-index through Finite Element 2D Simulations**
Roberto Sassi*, Luca T Mainardi, Pablo Laguna, Jose F Rodriguez
- 94-102 **Repolarization Variability Mechanisms and its Relation with Cardiac Arrhythmogenesis**
Jose F Rodriguez*, Roberto Sassi, Esther Pueyo, Luca Mainardi
- 95-356 **Evaluating the Differences of Simulated Long-QT Syndromes in Body Surface ECGs**
Gunnar Seemann*, Maider Alvarez de Eulate, Niko Konrad, Julian Maier, Mathias Wilhelms, David Keller, Olaf Dössel, Eberhard Scholz
- 96-143 **Simulation of KCNJ2-linked Short QT Syndrome in Human Ventricular Tissue**
Cunjin Luo, Yongfeng Yuan, Kuanquan Wang*, Henggui Zhang, Yongfeng Yuan
- 97-170 **Electrocardiographic T-wave Flattening and Action Potential Triangulation before TdP Onset**
Tanveer A Bhuiyan*, Claus Graff, Morten B Thomsen, Johannes J Struijk
- 98-291 **Computational Analysis of Head-Down Bed-Rest Effects on Cardiac Action Potential Duration**
Elisa Passini*, Alessandro Pellegrini, Enrico G Caiani, Stefano Severi

Tuesday, September 24, 2013, 13:15

P51: Electrophysiological Modelling Techniques

Room: Central Hall

- 99-212 **Computer Simulation of the Rabbit Purkinje Fibre Action Potential in Heart Failure**
Jue Li*, Sunil Jit Logantha, Joseph Yanni-Gerges, Xue Cai, Halina Dobrzynski, George Hart, Mark Boyett
- 100-327 **Simulation of Arrhythmia using Adaptive Spatio-temporal Resolution**
Sándor Miklós Szilágyi*, László Szilágyi, Béat Hirsbrunner
- 101-366 **Coherent Structures and Nonlinear Control of Cardiac Tissue**
Roman Grigoriev*, Christopher Marcotte
- 102-165 **Inverse Reconstruction of Epicardial Potentials Improves by Vectorcardiography and Realistic Potentials**
Matthijs JM Cluitmans*, Pietro Bonizzi, Joël MH Karel, Paul GA Volders, Ralf LM Peeters, Ronald L Westra
- 103-167 **Automatic Parametrization Strategy for Cardiac Electrophysiology Simulations**
Caroline Mendonça Costa*, Elena Hoetzel, Bernardo Martins Rocha, Anton Prassl, Gernot Plank
- 104-43 **Cardiac Spiral Waves Drifting Due to Spatial Tissue Temperature Gradients**
Guy Malki*, Sharon Zlochiver

Tuesday, September 24, 2013, 13:15

P52: Ventricular Modelling

Room: Central Hall

- 105-35 **Realistic 3D Bidomain Model of Whole Heart Electrical Activity and ECG Generation**
Siniša Sovilj*, Ratko Magjarević, Nigel H. Lovell, Socrates Dokos
- 106-94 **Effects of Species-dependent Differences in Action Potential Shape in Setting β -adrenergic-stimulation Induced Current**
Luca Sala*, Chiara Bartolucci, Claudia Altomare, Marcella Rocchetti, Marcella Rocchetti, Gaspare Mostacciolo, Stefano Severi, Norbert Szentandrassy, Peter P Nanasi, Antonio Zaza
- 107-123 **A Comparison of Two Models of Human Ventricular Tissue: Simulated Ischaemia and Re-entry**
Mitra Abbasi*, Richard Clayton
- 108-202 **Modelling the Integrated Regulation Role of β -adrenergic Signaling and CaMKII in Human Myocyte Electrophysiological Properties**
Ling Dai, Yunliang Zang, Dingchang Zheng*, Ling Xia

Tuesday, September 24, 2013, 13:15

P53: Heart Rate Variability: Software and Implementation

Room: Central Hall

- 109-234 **A Software Toolkit for Nonlinear Heart Rate Variability Analysis**
Constantino A García*, Abraham Otero, Jesús Presedo, Xosé Vila, Paulo Félix
- 110-239 **Implementation of Heart Rate Variability Signal Processing into FPGA: System on-Chip Design**
Shahab Rezaei*, Hossein Ajourloo, Sadaf Moharreri
- 111-259 **VARVI: A Software Tool for Heart Rate Variability Analysis in Response to Visual stimuli**
Leandro Rodríguez-Liñares, Pedro Cuesta, Raúl Alonso, Arturo J Méndez, María J Lado, Xosé A Vila*
- 112-420 **Trend Strips: a New Tool to Analyze RR Time Series**
Antônio Carlos Silva Filho*, Regiane Máximo Souza, Fátima Maria Helena Simões Pereira da Silva, Júlio Cesar Crescêncio, Lourenço Gallo Júnior

Tuesday, September 24, 2013, 13:15

P54: Heart Rate Variability: Methodology

Room: Central Hall

- 113-64 **Variability of Left Ventricular Ejection and Diastolic Times Obtained from Impedance Cardiography: A Comparison with Heart Rate Variability**
Salvador Carrasco-Sosa, Alejandra Guillén-Mandujano*
- 114-333 **A Modified Hilbert-Huang Algorithm to Assess Spectral Indices in Intense Exercise**
Rebeca Goya-Esteban*, Óscar Barquero-Pérez, Elena Sarabia-Cachadiña, José Naranjo-Orellana, José-Luis Rojo-Álvarez
- 115-392 **Seismocardiograms Return Valid Heart Rate Variability Measures**
Alexandre Laurin*, Andrew Blaber, Kouhyar Tavakolian
- 116-406 **Fast Detrending of Unevenly Sampled Series with Application to HRV**
Valeria Villani*, Antonio Fasano

Tuesday, September 24, 2013, 13:15

P55: Heart Rate Variability: Analysis and Information Measures

Room: Central Hall

- 117-401 **Higuchi's Fractal Complexity of RR and QT Interval Series during Transient Myocardial Ischemia**
Rudys Magrans, Pedro Gomis*, Pere Caminal, Andreas Voss
- 118-174 **On the Early Detection of Perinatal Hypoxia with Information-theory based Methods**
Ricardo Santiago-Mozos*, Beatriz García-Vizuetete, José María Lillo-Castellano, José Luis Rojo-Álvarez, Carlos Martín-Caballero
- 119-213 **Sample Entropy Parametric Estimation for Heart Rate Variability Analysis**
M Aktaruzzaman*, R Sassi
- 120-295 **Enhancing Scaling Exponents in Heart Rate by means of Fractional Integration**
A Leite*, AP Rocha, ME Silva
- 121-222 **Indices of Symbolic Dynamics' Distributions in Cardiac Patients**
Giovanni D'Addio*, Maria Romano, Roberto Maestri, Paolo Bifulco, Mario Cesarelli
- 122-129 **In-vivo and Ex-vivo HRV discrimination by Complex Correlation Measure**
Oto Janoušek*, Sara Francisco, Petr Veselý, Veronika Olejníčková, Marina Ronzhina, Ivo Provazník, Marie Nováková, Peter Scheer, Jana Kolářová
- 123-217 **Fractal Behaviour of Heart Rate Variability reflects Abnormal Respiration Patterns in OSAS Patients**
Giovanni D'Addio*, Agostino Accardo, Mario Cesarelli, Alberto De Felice

Tuesday, September 24, 2013, 13:15

124-31 **Non-linear dynamic analysis of RR signals in patients with and without Excessive Daytime Sleepiness**

Umberto Melia, Marc Guaita, Montserrat Vallverdu*, Francesc Claria, Pere Caminal, Cristina Embid, Isabel Vilaseca, Manel Salamero, Joan Santamaria

125-326 **Development of Fetal Heart Rate Dynamics Before and After 30 Weeks of Gestation**

Ahsan Khandoker*, Chandan Karmakar, Yoshitaka Kimura, Marimuthu Palaniswami

Tuesday, September 24, 2013, 13:15

P56: Novel Techniques

Room: Central Hall

- 126-1 **High Resolution 16-channel ECG Test Simulator for Online Digital-to-Analogue Conversion of Data from PC**
Tatyana Neycheva, Todor Stoyanov, Roger Abächerli, Ivaylo Christov*
- 127-18 **A Comparison of Heartbeat Detectors for the Seismocardiogram**
Miguel Angel Garcia-Gonzalez*, Ariadna Argelagos-Palau, Mireya Fernandez-Chimeno, Juan Ramos-Castro
- 128-20 **Electrical Impedance Tomography vs. Whole Thoracic Impedance for Monitoring Heart Failure Patients**
Marina Arad*, Shimon Abboud
- 129-95 **Improved Estimation of V-Index Based on Analytic Forms of Dominant T-Wave**
Luca Mainardi*, Davide Di Donato, Denise Falcone, Roberto Sassi
- 130-113 **The Effect of Breathing on Stroke Volume Estimation in Patients with Implanted Cardiac Device Using Parametric Electrical Impedance Tomography**
Muhammad Mhajna*, Shimon Abboud
- 131-219 **Night and Day Changes in Heart rate and Blood Pressure Fractal Dimensions from 24-hour Ambulatory Blood Pressure Monitoring Devices**
Andrea Faini*, Gianfranco Parati, Marco Di Rienzo, Paolo Castiglioni
- 132-267 **Heart Auscultation Learning using Multi-labeler Evaluation Feedback**
Santiago Murillo Rendón, Diego Hernán Peluffo Ordoñez, Liliana Patricia Ramírez Zuluaga, Mario Iván Ruano Restrepo, Germán Castellanos Domínguez, Alvaro Angel Orozco* Gutiérrez

Tuesday, September 24, 2013, 13:15

- 133-336 **On the Sparsest Representation of Electrocardiograms**
Roopak Tamboli, Manas Savkoor, Soumya Jana*
- 134-350 **The Effect of Automated Preprocessing of RR Interval Tachogram on Discrimination Capability of Heart Rate Variability Parameters**
Faezeh Marzbanrad, Herbert Jelinek, Ethan Hambly, Craig McLachlan, Slade Matthews, Marimuthu Palaniswami, Ahsan Khandoker*
- 135-434 **Characterizing Complexity of Atrial Arrhythmias through Effective Dynamics from Electric Potential Measures**
Oriol Pont*, Binbin Xu
- 136-34 **A Pilot Study of Photoplethysmographic Peripheral Pulse Transit Times in Paediatric Heart Transplant Recipients and Healthy Children**
Costanzo Di Maria, Emma Sharkey, Annette Klinge, Dingchang Zheng*, Alan Murray, John O'Sullivan, John Allen

Tuesday, September 24, 2013, 13:15

P57: Health Informatics

Room: Central Hall

- 137-207 **An Easy System to Follow the Evolution of Cardiac Patients**
Rene Gonzalez-Fernandez*, Margarita Mulet-Cartaya, Daniel Jimenez-Gonzalez, Juan Dayron Varona
- 138-209 **The Design and Testing of a Heart Monitor for Home Care**
Yanesis Lorenzo-Costa, Rene Gonzalez-Fernandez*, Ronny Guardarrama-Mieres
- 139-257 **Neural Network Approach to Incomplete Data Applied to Assessing Cardiac Health**
Joanna Grabska-Chrzastowska*
- 140-58 **Clair-DB: A Standardized Departmental Research Database**
Enno van der Velde*, Thekla Jansen, Victoria Delgado, Douwe Atsma
- 141-317 **Biometric Personal Identification System using ECG Signal**
Emna Rabhi*, Zied Lachiri

Tuesday, September 24, 2013, 13:15

P58: ECG Measurement

Room: Central Hall

- 142-418 **Measurement of Noise in ECG Signals to Improve Automatic Delineation**
Loriano Galeotti*, Lars Johannesen, Jose Vicente, David G Strauss
- 143-238 **Detection of P wave in Electrocardiogram**
Rene Gonzalez-Fernandez*, Martha Rivero-Varona, Gisela Montes de Oca-Colina
- 144-145 **Detection of Electrode Interchange in Precordial and Orthogonal ECG Leads**
Irena Jekova*, Vessela Krasteva, Roger Abächerli
- 145-359 **Noncontact Sensing of Electrocardiographic Potential and Body Proximity by In-bed Conductive Fabrics**
Kei Ito*, Yutaka Fukuoka, Gert Cauwenberghs, Akinori Ueno
- 146-115 **A Suppression of Impulsive Noise in ECG Signal using Adaptive Filters**
Shankar Gupta, Ramchandra Manthalkar*, Suhas Gajre
- 147-80 **An Algorithm for the Detection of ST Segment Elevation Myocardial Infarction in Body Surface Potential Maps**
Dewar Darren Finlay*, Daniel Guldenring, Raymond Robert Bond, Michael John Daly

Tuesday, September 24, 2013, 13:15

P59: Miscellaneous ECG

Room: Central Hall

- 148-176 **The Effect of Precordial Leads Displacement on P-wave Morphology in Body Surface Potential Mapping**
Michał Kania*, Hervé Rix, Małgorzata Fereniec, Dariusz Janusek, Roman Maniewski
- 149-151 **Analysis of Spatial Variability for the Development of Reduced-Lead Body Surface Maps**
Frederique J Vanheusden*, Xin Li, Gavin S Chu, Tiago Paggi de Almeida, G André Ng, Fernando S Schindwein
- 150-396 **An artificial model of the Electrocardiogram during paroxysmal Atrial Fibrillation**
Julien Oster*, Gari D Clifford
- 151-185 **Effects of Heart Orientation on Isolated Heart Electrograms**
Marina Ronzhina*, Veronika Olejníčková, Oto Janoušek, Jana Kolářová, Marie Nováková, Ivo Provazník
- 152-16 **Load Dependent Changes of Cardiac Depolarization and Repolarization during Exercise ECG Test**
Ivaylo Christov*, Giovanni Bortolan, Iana Simova
- 153-77 **Prediction of Sudden Death in Patients with HCM Using Late Potential Analysis**
Nader Jafarnia Dabanloo*, Azadeh Parham, Keyvan Maghooli, Gholamreza Attarodi
- 154-253 **The Isolated Rabbit Hearts – Database of Electrograms and Monophasic Action Potentials**
Jana Kolarova, Marie Novakova, Marina Ronzhina*, Oto Janousek, Petr Vesely, Veronika Olejnickova, Ivo Provaznik

Tuesday, September 24, 2013, 13:15

P5A: Cardiac Imaging

Room: Central Hall

- 155-339 **Classification of Delayed Enhancement Scar Islands by Means of their Local Subendocardial Transmurality**
Susana Merino-Caviedes*, Lucilio Cordero-Grande, Teresa Sevilla, M Teresa Pérez, Marcos Martín-Fernández, Carlos Alberola-López
- 156-319 **A Software Tool for the Computation of Arterial Pulse Wave Velocities from Flow-sensitive 4D MRI Data**
Johann Drexl*, Hanieh Mirzaee, Andreas Harloff, Markus Hüllebrand, Anja Hennemuth, Horst Hahn
- 157-307 **Registration and Fusion of Contrast-Enhanced MRI Myocardial Substrate Maps and X-ray Angiograms**
Juan E Ortuño*, Esther Pérez-David, Ángel Arenal, Javier Bermejo, Andrés Santos, María J Ledesma-Carbayo
- 158-342 **Global Tractography in Cardiac Diffusion-Tensor MRI**
Matthew Ozon*, Marc Robini, Pierre Croisille, Carole Frindel, Yue-Min Zhu
- 159-311 **Computational Mesh as a Descriptor of Left Ventricular Shape for Clinical Diagnosis**
Pablo Lamata*, Merzaka Lazdam, Anna Ashcroft, Adam Lewandowski, Paul Leeson, Nic Smith
- 160-161 **Regional Comparison of Left Ventricle Systolic Wall Stress reveals Non-uniformity in Healthy Subjects**
Soo-Kng Teo, Si-Yong Yeo, May-Ling Tan, Chi-Wan Lim, Liang Zhong, Ru-San Tan, Yi Su*
- 161-183 **3D Bilateral Filtering of Cardiac DT-MRI Data**
Tomasz Pieciak*

Tuesday, September 24, 2013, 15:15

S61: Myocardial Ischemia

Room: Sal3n de Actos

Chair(s): Roger Abächerli and Olle Pahlm

162-156 **Tuning a Real-Time Detector of Transient Cardiac Ischemic Episodes on the Long-Term ST Database according to the Annotation Protocol B.**

Lacramioara Dranca*, Alfredo Goñi, Arantza Illarramendi

163-168 **Automated Detection of the Culprit Artery from the ECG in Acute Myocardial Infarction**

Elaine Clark*, Yama Fakhri, Abdul Waduud, Maria Sejersten, Peter Clemmensen, Peter Macfarlane

164-29 **Depolarization Morphologic Features of the ECG for Detection of Stress Induced Ischemia**

Mariano Llamedo*, Mariano Albertal, Pablo Laguna, Juan Pablo Martínez

165-231 **High resolution ECG Changes in Survivors of Out-of-Hospital Cardiac Arrest during and after Mild Therapeutic Hypothermia**

Martin Rauber*, Dušan Štajer, Marko Noč, Todd T Schlegel, Vito Starc

166-232 **T-Wave Alternans Identification in Routine Exercise ECG Tracings: Comparison of Methods**

Silvia Bini*, Cees A Sweene, Sumche Man, Laura Burattini

167-201 **T-wave Alternans Predicts ICD Discharge in MADIT II Patients with Elevated Resting Heart Rate**

Violeta Monasterio*, Juan Pablo Martínez, Scott McNitt, Pablo Laguna, Arthur J Moss, Mark C Haigney, Wojciech Zareba, Jean-Philippe Couderc

Tuesday, September 24, 2013, 15:15

S62: Clinical Electrophysiology

Room: Aula 0.01

Chair(s): José Luis Rojo Álvarez and Omar Escalona

168-211 Non-Invasive Epicardial Imaging of Human Ventricular Fibrillation

John R Fitz-Clarke*, John L Sapp, B Milan Horáček

169-250 Dynamic Changes in Intracardiac Impedance as a Prognostic Marker During Internal Cardioversion of Atrial Fibrillation

Philip Richard Walsh, Omar Jacinto Escalona*, Vivek Kodoth, Noel Camilo Castro, David McEneaney, Ernest Lau, Ganesh Manoharan

170-47 Wavelet-Based Electrogram Onset Identification for Ventricular Electroanatomical Mapping

Alejandro Alcaine*, David Soto-Iglesias, David Andreu, Juan Fernández-Armenta, Antonio Berruezo, Pablo Laguna, Oscar Camara, Juan Pablo Martínez

171-54 Nonlinear Characteristics of Ventricular Fibrillation depending on Myocardial Infarction Locations

María González-González, Óscar Barquero-Pérez*, Cristina Soguero-Ruiz, José Luis Rojo-Álvarez, Juan José Sánchez-Muñoz, Arcadi García-Alberola

172-263 Analyzing Electrical Patterns in an Experimental Wwine Model of Dyssynchrony and CRT

David Soto-Iglesias*, Nicolas Duchateau, Constantine Butakoff, David Andreu, Juan Fernández-Armenta, Antonio Berruezo, Marta Sitges, Oscar Camara

173-270 Electrophysiological Predictors of Malignant Arrhythmias in Patients with Wolff-Parkinson-White Syndrome

Amarild Cuko*, Massimo Saviano, Luigi Giannelli, Cristiano Ciaccio, Andrea Petretta, Mario Baldi, Alessia Pappone, Gabriele Vicedomini, Carlo Pappone

Tuesday, September 24, 2013, 15:15

S63: Cardiac MRI

Room: Aula 1.03

Chair(s): Cristiana Corsi and Trygve Eftestøl

- 174-341 **Automated MRI-Based Biventricular Segmentation Using 3D Narrow-Band Statistical Level-Sets**
Giacomo Tarroni*, Davide Marsili, Federico Veronesi, Cristiana Corsi, Amit Patel, Victor Mor-Avi, Claudio Lamberti
- 175-264 **Automatic Segmentation of the Epicardium in Late Gadolinium Enhanced Cardiac MR Images**
Kjersti Engan*, Valery Naranjo, Trygve Eftestøl, Stein Ørn, Leik Woie
- 176-162 **Assessment of the Fibrotic Myocardial Tissue Mechanics by Image Processing**
Lucilio Cordero-Grande*, Teresa Sevilla, Ana Revilla, Marcos Martín-Fernández, Carlos Alberola-López
- 177-187 **Automatic Detection of Myocardial Perfusion Defects using Object-based Myocardium Segmentation**
Teodora Chitiboi*, Anja Hennemuth, Lennart Tautz, Paul Stolzmann, Olivio Donati, Lars Linsen, Horst Hahn
- 178-411 **Relationship between Cardiac Imaging Data and Simultaneous Physiological Measurements**
Wenfeng Duan*, Dingchang Zheng, Christopher Eggett, Philip Langley, Alan Murray
- 179-391 **Measuring the Degree of Fibrosity in Myocardial Scars from LGE-CMR Images**
Frode Måløy*, Leik Woie, Trygve Eftestøl, Kjersti Engan, Stein Ørn

Tuesday, September 24, 2013, 15:15

S64: Novel Techniques

Room: Sala de Juntas

Chair(s): Eduardo Gil and Piotr Augustyniak

- 180-287 **Simultaneous Registration of ECG and Cardiac Motion by a Single Esophageal Probe**
Thomas Niederhauser, Sergio Sánchez Martínez*, Andreas Haeberlin, Thanks Marisa, Josef Goette, Marcel Jacomet, Rolf Vogel
- 181-136 **Electrocardiogram Derived Respiration from QRS Slopes: Evaluation over Stress Testing Recordings**
Jesús Lázaro Plaza*, Alejandro Alcaine Otín, Daniel Romero Pérez, Eduardo Gil Herrando, Pablo Laguna Lasaoa, Leif Sörnmo, Raquel Bailón Luesma
- 182-297 **Bayesian Voting of Multiple Annotators for Improved QT Interval Estimation**
Tingting Zhu*, Alistair EW Johnson, Joachim Behar, Gari D Clifford
- 183-192 **The Feasibility of Impedance Cardiography to Assess Hemodynamic Changes and Fluid Loss Related to Pleural Drainage**
Mark Ulbrich*, Jens Muehlsteff, Matthias Zink, Steffen Leonhardt
- 184-394 **High-Power Current Source with Real-Time Arbitrary Wave Form Control for in Vivo and in Vitro Studies of Defibrillation**
Ilija Uzelac*, Mark Holcomb, Ron Reiserer, John Wikswo
- 185-348 **Using Piezoelectric Sensor for Continuous-contact-free Monitoring of Heart & Respiration Rates in Real-life Hospital Settings**
Tal Klap*, Zvika Shinar

Tuesday, September 24, 2013, 17:00

S71: Ischemia Modelling

Room: Aula 0.01

Chair(s): Peter Macfarlane and Henggui Zhang

- 186-50 **Computing Ischemic Regions in the Heart: On the Use of Internal Electrodes**
Ola Marius Lysaker*, Bjørn Fredrik Nielsen, Samuel Wall
- 187-59 **Observability of Ischemia and the Need for Patient Specific Models**
Glenn Terje Lines*, Ola Marius Lysaker, Bjørn Fredrik Nielsen
- 188-126 **Effect of RyR2 Refractoriness and Hypercalcemia on Calcium Overload and Spontaneous Release**
Enric Alvarez-Lacalle*, Angelina Peñaranda, Inma R Cantalapiedra, Leif Hove-Madsen, Blas Echebarria
- 189-310 **Avoiding the Inverse Crime in the Inverse Problem of Electrocardiography: Estimating the Shape and Location of Cardiac Ischemia**
Carlos Eduardo Chávez*, Felipe Alonso-Atienza, Diego Álvarez
- 190-384 **Ionic Mechanisms underlying Arrhythmogenic Biomarkers in Ischemia: A Population-based Study**
Ana Mincholé*, Sara Dutta, John Walmsley, Blanca Rodriguez
- 191-398 **Recent Human Ventricular Cell Action Potential Models Under Varied Ischaemic Conditions**
Sara Dutta*, Ana Mincholé, T Alexander Quinn, Blanca Rodriguez

Tuesday, September 24, 2013, 17:00

S72: Modelling Electrophysiology

Room: Sala de Juntas

Chair(s): Yoram Rudy and Ralf Köhler

- 192-435 **The Effect of Gap Junction Uncoupling on Spatial Dispersion of Action Potential Duration at Sites of Abrupt Tissue Expansion**
Marjorie Letitia Hubbard*, Craig S Henriquez
- 193-282 **A Steklov-Poincaré Variational Formulation of the Inverse Problem in Cardiac Electrophysiology**
Nejib Zemzemi*
- 194-203 **Identification of Ablation Sites in Atrial Flutter by Causal Method**
Miguel Rodrigo*, Alejandro Liberos, Andreu M Climent, Maria S Guillem
- 195-361 **Computational Probabilistic Quantification of Pro-arrhythmic Risk from Scar and Left-to-right Heterogeneity in the Human Ventricles**
Mikael Wallman*, Alfonso Bueno-Orovio, Blanca Rodriguez
- 196-340 **Volumetric Imaging of Cardiac Current Sources using Lp-Norm Regularization**
Azar Rahimi*, Jingjia Xu, Linwei Wang
- 197-316 **A Methodology to Characterize the Causal Interactions Between Depolarization and Repolarization Temporal Changes in Unipolar Electrograms: Application to Human Epicardial Mapping**
Michele Orini*, Luca Citi, Ben Hanson, Peter Taggart, Pier Lambiase

Tuesday, September 24, 2013, 17:00

S73: Atrial Fibrillation Detection and Prediction

Room: Salón de Actos

Chair(s): José Millet and Valentina Corino

- 198-380 **Application of the Preoperative ECG to Predict Cox Maze Surgery Mid-term Outcome**
Antonio Hernández Alonso*, Raúl Alcaraz Martínez, Fernando Hornero Sos, José Joaquín Rieta Ibáñez
- 199-308 **Combination of Clinical and Electrocardiographic Indices to Predict Cox-Maze Surgery Outcome at Discharge**
Antonio Hernández Alonso*, Raúl Alcaraz Martínez, Fernando Hornero Sos, José Joaquín Rieta Ibáñez
- 200-390 **Open source Java-based ECG analysis software and Android app for atrial fibrillation screening.**
Julien Oster*, Joachim Behar, Roberta Colloca, Qiao Li, Gari D Clifford
- 201-62 **Dynamic Risk Assessment of the Onset of Paroxysmal Atrial Fibrillation**
Claudia Vega*, Irene Garcia, Juan Jiménez
- 202-104 **A Noise-Adaptive Method for Detection of Brief Episode Paroxysmal Atrial Fibrillation**
Andrius Petrėnas*, Leif Sörnmo, Vaidotas Marozas, Arūnas Lukoševičius
- 203-51 **Real Time Detection of Atrial Fibrillation using a Miniature, Low-power ECG Monitor**
Greg Hayes*, Paul D Teal

Tuesday, September 24, 2013, 17:00

S74: Multivariate Cardiovascular Signal Modelling and Analysis

Room: Aula 1.03

Chair(s): Philip de Chazal and Olivier Meste

- 204-318 **Comparing Model-free and Model-based Transfer Entropy Estimators in Cardiovascular Variability**
Alessandro Montalto*, Daniele Marinazzo, Dimitris Kugiumtzis, Giandomenico Nollo, Luca Faes
- 205-65 **Correlations between Spectral Measures of Baroreflex Sensitivity Variability and HRV during Supine Position, Paced Breathing, Standing and Exercise**
Salvador Carrasco-Sosa, Alejandra Guillén-Mandujano*
- 206-73 **Association of Ankle Brachial Pressure Index with Heart Rate Variability**
Herbert F Jelinek*, Hayder Al-Aubaidy, Kinda Khalaf, Ahsan H Khandoker
- 207-119 **Granger Causality Analysis of Baroreflex in Obese Children and Adolescents**
Michal Javorka*, Ingrid Tonhajzerova, Barbora Czippelova, Zuzana Turianikova, Lenka Chladekova, Kamil Javorka
- 208-105 **Comparison of Baroreflex Sensitivity Gain during mild Lower Body Negative Pressure in Presence and Absence of Long Duration Bed Rest**
Guadalupe Dorantes-Mendez*, Manuela Ferrario, Giuseppe Baselli, Philippe Arbeille, Kevin J Shoemaker, Danielle K Greaves, Richard L. Hughson, Federico Aletti
- 209-386 **Echocardiovariability - Low and High Frequency Beat-to-beat Variability in Echocardiographic Signals**
Amanda Albano, Sandra Gustavsson, Per Lindqvist, Urban Wiklund, Christer Grönlund*

Wednesday, September 25, 2013, 09:15

S81: ECG Measurement

Room: Salón de Actos

Chair(s): Shen Luo and Arie Maan

210-124 Use of Dominant T-wave to Reduce T-Wave Offset Location Uncertainty

Corrado Giuliani*, Angela Agostinelli, Laura Burattini

211-365 ECGlab: User Friendly ECG/VCG Analysis Tool for Research Environments

Jose Vicente*, Lars Johannesen, Lorian Galeotti, David G Strauss

212-303 An Interactive Tool Developed for the Evaluation of ECG Formats

Elizabeth Martin*, Dewar Finlay, Chris Nugent, Raymond Bond, Cathal Breen

213-89 Ultra-high-frequency ECG Measurement

Pavel Jurák*, Josef Halánek, Pavel Leinveber, Petr Klimeš, Josef Šumbera, Karel Zeman, Miroslav Novák

214-37 Coherence-Based Measure of Instantaneous ECG Noise

Piotr Augustyniak*

215-241 Improved Respiration Rate Estimation using a Kalman filter and Wavelet Cross-coherence

Alistair EW Johnson*, Andrew A Kramer, Sharath Choletti, Joel H Saltz, Timothy G Buchman, Gari D Clifford

Wednesday, September 25, 2013, 09:15

S82: Cardiac Mechanics

Room: Sala de Juntas

Chair(s): Dingchang Zheng

- 216-276 **Characterization of Patients with Different Ventricular Ejection Fractions using Blood Pressure Signal Analysis**
Andres Arcentales, Andreas Voss, Pere Caminal, Antonio Bayés-Genís, Maria Teresa Domingo, Beatriz F Giraldo*
- 217-375 **Empirical Mode Decomposition for Respiratory and Heart Rate Estimation from the Photoplethysmogram**
Ainara Garde*, Walter Karlen, Parastoo Dehkordi, J Mark Ansermino, Guy A Dumont
- 218-393 **Study on the Linear Relation Between Chest Compression Depth and the Fluctuation Caused in the Thoracic Impedance Acquired by Defibrillation Pads**
Erik Alonso*, Digna González-Otero, Elisabete Aramendi, Sofía Ruiz de Gauna, Jesús Ruiz, Unai Ayala, James Russell
- 219-169 **A Simple Impedance-Based Method for Ventilation Detection During Cardiopulmonary Resuscitation**
Digna González-Otero*, Erik Alonso, Jesús Ruiz, Elisabete Aramendi, Sofía Ruiz de Gauna, Jo Kramer-Johansen, Trygve Eftestøl
- 220-334 **The Influence of Cardiac Trabeculae on Ventricular Mechanics**
Marta Serrani*, Maria Laura Costantino, Roberto Fumero
- 221-227 **Effects of Physical Exercise on the Photoplethysmogram Waveforms Recorded on Fingertip and Forehead**
Andrius Rapalis*, Vaidotas Marozas, Arūnas Lukoševičius

Wednesday, September 25, 2013, 09:15

S83: Cardiac Computed Tomography

Room: Aula 1.03

Chair(s): Alan Murray and Victor Mor-Avi

- 222-108 **Automatic Right Ventricle Segmentation in CT Images Using a Novel Multi-Scale Edge Detector Approach**
Sofia Antunes*, Caterina Colantoni, Anna Palmisano, Antonio Esposito, Sergio Cerutti, Giovanna Rizzo
- 223-3 **3D Analysis of Myocardial Perfusion from Vasodilator Stress Computed Tomography: Can Accuracy Be Improved by Iterative Reconstruction?**
Victor Mor-Avi*, Nadja Kachenoura, Nicole Bhave, Benjamin Freed, Michael Vannier, Karin Dill, Roberto Lang, Amit Patel
- 224-272 **Extracting Myofibre Orientation from Micro-CT Images: An Optimisation Study**
Haibo Ni*, Simon J Castro, Robert S Stephenson, Jonathan C Jarvis, Tristan Lowe, George Hart, Mark R. Boyett, Henggui Zhang
- 225-82 **Mitral valve regurgitation: assessment with dual source computed tomography**
Liping Yao, Kun Sun*, Sun Cheng, Linwei Yu, Ming Liu, Xin Yang
- 226-48 **Multi-Parametric Model of the Heart from CT Images to Guide Ventricular Tachycardia Ablation**
Sofia Antunes*, Daniele Tresoldi, Anna Palmisano, Caterina Colantoni, Antonio Esposito, Sebastiano Colombo, Giuseppe Maccabelli, Paolo della Bella, Sergio Cerutti, Giovanna Rizzo

Wednesday, September 25, 2013, 09:15

S84: Ventricular Cell-Tissue Modelling

Room: Aula 0.01

Chair(s): Stefano Severi

- 227-328 **Combined Action Potential- and Dynamic-Clamp for Accurate Computational Modeling of the Kinetics of Cardiac IKr Current**
Chiara Bartolucci*, Claudia Altomare, Marco Bennati, Simone Furini, Antonio Zaza, Stefano Severi
- 228-337 **Extracellular Calcium and L-Type Calcium Current Inactivation Mechanisms: a Computational Study**
Elisa Passini*, Stefano Severi
- 229-152 **IKr Impact on Repolarization and its Variability Assessed by Dynamic-Clamp**
Claudia Altomare, Luca Sala, Chiara Bartolucci, Gaspare Mostacciuolo, Stefano Severi, Antonio Zaza*
- 230-262 **Deactivation of Per-Arnt-Sim Domain Mutation Increases the Proarrhythmic Risk of Dofetilide**
Rodolfo Gonzalez*, Edgar Cardenas, Alain Manzo, Fernando Martinez, Julio Gomis, Javier Saiz
- 231-301 **Validation of a Computational Model of Cardiac Defibrillation**
Jean Bragard*, Jorge Elorza, Elizabeth M Cherry, Flavio H Fenton
- 232-360 **Population of Human Ventricular Cell Models Calibrated with in vivo Measurements Unravels Ionic Mechanisms of Cardiac Alternans**
Xin Zhou*, Alfonso Bueno-Orovio, Michele Orini, Ben Hanson, Martin Hayward, Peter Taggart, Pier Lambiase, Kevin Burrage, Blanca Rodriguez

Wednesday, September 25, 2013, 11:15

S91: Clinical Aspects of Electrocardiography

Room: Sal3n de Actos

Chair(s): Paul Kligfield and Guy Carrault

- 233-147 **Detection of Sleep Apnea in Infants using ECG and Oximetry Signals**
Gregory Cohen*, Philip de Chazal
- 234-368 **Detection of Epileptic Seizures by means of Morphological Changes in the ECG**
Carolina Varon*, Katrien Jansen, Lieven Lagae, Sabine Van Huffel
- 235-403 **Evaluation of the Relation Between Changes in R-wave Amplitude and LV Mass and Dimensions in a Model of “Reversed Hypertrophy”**
Enrico G Caiani*, Angelo Auricchio, Mark Potse, Rolf Krause, Alessandro Pellegrini, Roberto M Lang, Pierre Vaïda
- 236-85 **Cardiac Repolarization Analysis: Immediate Response**
Josef Halamek*, Pavel Jurak, Eleonora Tobaldini, Nicola Montano, Pavel Leinveber
- 237-149 **Atrial Fibrillation Classification Method for Patients with Different Pharmacological or Surgical Therapies**
Nuria Ortigosa*, Antonio Galbis, Carmen Fern3ndez, Guillermo Ayala, 3scar Cano, Ana Andr3s
- 238-109 **Towards Standardization of Non-invasive Atrial Fibrillation Substrate Complexity Quantification: Effect of Choice of ECG-leads and Complexity Measure on Prediction of Pharmacological Cardioversion**
Stef Zeemering*, Theo Lankveld, Harry Crijns, Ulrich Schotten

Wednesday, September 25, 2013, 11:15

S92: Vascular Mechanics

Room: Sala de Juntas

Chair(s): José F Rodriguez and Elisabete Aramendi

- 239-32 **Effect of Pre-measurement Relaxation Time on Manual Blood Pressure Measurement**
Dingchang Zheng*, Fan Pan, Alan Murray
- 240-408 **Pulse Arrival Time and Pulse Width as Potential Measure for Estimating Beat-to-beat Systolic and Diastolic Blood Pressure**
Adriana Arza*, Raquel Bailon, Jordi Aguiló, Jesús Lázaro, Pablo Laguna, Eduardo Gil
- 241-137 **Exploring the Stationary Wavelet Transform Detail Coefficients for the Detection and Identification of the S1 and S2 Heart Sounds**
Nuno Marques, Ana Paula Rocha, Rute Almeida*, Miguel Coimbra
- 242-70 **Effect of Stethoscope Position on Auscultatory Blood Pressure Measurement**
Fan Pan*, Dingchang Zheng, Alan Murray
- 243-245 **Influence of Intraluminal Thrombus Topology on AAA Passive Mechanics**
Fabian Riveros, Giampaolo Martufi, T Christian Gasser, Jose F Rodriguez*
- 244-131 **A Complete Riemann Solver for Arterial flow with Application to the Systemic Arterial Tree**
Javier Murillo*, Pilar García-Navarro

Wednesday, September 25, 2013, 11:15

S93: 3D Atrial Modelling

Room: Aula 0.01

Chair(s): Javier Saiz and Felipe Atienza

- 245-23 **Approximate Entropy can Localize Rotors, but no Ec-topic Foci during Chronic Atrial Fibrillation - a Simulation Study**
Andrés Orozco-Duque, Juan P Ugarte*, Catalina Tobón, Javier Saiz, John Bustamante
- 246-60 **3-Dimensionality in Determining the Stability of Atrial Fibrillation**
Ali Gharaviri*, Sander Verheule, Nico HL Kuijpers, Ulrich Schotten
- 247-164 **Cell Repolarization Variability Modulates Atrial Fibrillation Dynamics in 3D Virtual Human Atria**
Carlos Sanchez*, Alfonso Bueno-Orovio, Esther Pueyo, Blanca Rodriguez
- 248-362 **Body Surface Potential Propagation Maps During Macroreentrant Atrial Arrhythmias. A Simulation Study**
Alejandro Liberos*, Jorge Pedrón-Torrecilla, Miguel Rodrigo, José Millet, Andreu M Climent, María S Guillem
- 249-371 **Computational Simulation and Analysis of 3D Body Surface Potential Patterns Generated by Common Atrial Arrhythmias**
Ana Ferrer*, Rafael Sebastian, Jose F Rodriguez, Catalina Tobón, María Guillem, Eduardo J Godoy, Javier Saiz
- 250-373 **Influence of Three-Dimensional Fibrotic Patterns on Simulated Intracardiac Electrogram Morphology**
Matthias W Keller*, Armin Luik, Mohammad Soltan Abady, Gunnar Seemann, Claus Schmitt, Olaf Dössel

Wednesday, September 25, 2013, 11:15

S94: Sensor Technology and Heart Rate Analysis

Room: Aula 1.03

Chair(s): Beatriz Giraldo and Urban Wiklund

- 251-389 **Sensitivity of a Wearable Bioimpedance Monitor to Changes of Thoracic Fluid Content in Heart Failure and Hypertension Patients**
Silviu Dovancescu*, Azam Torabi, Thato Mabote, Jennifer Caffarel, Emile Kelkboom, Ronald Aarts, Erik Korsten, John Cleland
- 252-397 **Detection of Ischemia Using Electromechanical Signals for a Remote Diagnostic Device**
Farzad Khosrow-Khavar*, Carlo Menon
- 253-6 **Modeling of Motion Artifacts in Contactless Heart Rate Measurements**
Tobias Wartzek*, Christoph Brüser, Thomas Schlebusch, Christian Brendle, Susana Santos, Anna Kerekes, Kurt Gerlach-Hahn, Sören Weyer, Katrin Lunze, Christoph Hoog-Antink, Steffen Leonhardt
- 254-197 **Photoplethysmography-based Ambulatory Heartbeat Monitoring Embedded into a Dedicated Bracelet**
Simon Arberet*, Mathieu Lemay, Philippe Renevey, Josep Solà, Olivier Grossebacher, Daniela Andries, Claudio Sartori, Mattia Bertschia
- 255-12 **Is Cross-sample Entropy a Valid Measure of Synchronization between the Sequences of RR Interval and Pulse Transit Time?**
Chengyu Liu*, Dingchang Zheng, Peng Li, Changchun Liu
- 256-284 **Physiological Feature Analysis in Heart Rate Turbulence using LASSO Model**
Óscar Barquero-Pérez*, Rebeca Goya-Esteban, Carlos Figuera, Inmaculada Mora-Jiménez, Arcadi García-Alberola, José Luis Rojo-Álvarez

Wednesday, September 25, 2013, 13:15

PA1: ECG Signal Processing

Room: Central Hall

- 257-204 **A Real Time ECG Preprocessing System based on ADS1298**
Daniel Campillo Montes de Oca*, Ronny Guardarrama, Rene Gonzalez Fernandez, Jorge Rodriguez Rubio, Daniel Jimenez Gonzalez
- 258-255 **ECGlib: Library for Processing Electrocardiograms**
Lars Johannesen*, Jose Vicente, Lorian Galeotti, David Strauss
- 259-260 **Sufficient Dimension Reduction for Heartbeat Classification**
Long Ma*, Minyi Chen, Lerong Li, Momiao Xiong
- 260-148 **A Switchable Feature Extraction System for ECG Heartbeat Classification**
Philip de Chazal*
- 261-437 **Cepstrum Feature Selection for the classification of Sleep Apnea-Hypopnea Syndrome based on Heart Rate Variability**
Antonio Gabriel Ravelo-García*, Juan Luis Navarro-Mesa, Eduardo Hernández-Pérez, Sofía Martín-González, Pedro Quintana-Morales, Iván Guerra-Moreno, Gabriel Juliá-Serdá
- 262-19 **Enhanced Turning Point Algorithm for the Visualization and Printing of Long Term ECG Curves**
Sándor Hargittai*
- 263-419 **Proposed New Requirements for Testing and Reporting Performance Results of Arrhythmia Detection Algorithms**
John Wang*
- 264-133 **Automatic Classification of Arrhythmic Heartbeats Using Linear Prediction Model**
Chun-Cheng Lin, Weichih Hu*, Chun-Min Yang

Wednesday, September 25, 2013, 13:15

PA2: Health Informatics

Room: Central Hall

- 265-409 **Web-based Online Consulting System for Quasi Real-time Consultations of Cardiac Images**
Csaba Jenei, Tamás Ivánfai, Bálint Kószegi, Zsolt Kószegi*
- 266-224 **Towards Semantic Interoperability for Cardiovascular Risk Stratification into the Electronic Health Records Using Archetypes and SNOMED-CT**
Cristina Soguero-Ruiz, Teresa Quintanilla-Fernández, Luis Lechuga-Suárez, Óscar Barquero-Pérez, José García-Muñoz, Inmaculada Mora-Jiménez, José Luis Rojo-Álvarez*, Silvia Del Castillo-Arrojo, Pablo Serrano-Balazote, Arcadi García-Alberola
- 267-198 **Information System for Surveillance of Hospital Infections in Cardiac Surgery**
Alessandro Taddei*, Giuseppe Rossi, Marina Marchi, Elaine Laws, Stefano Dalmiani, Maurizio Mangione, Stefano Bevilacqua
- 268-304 **An HTML5-based ECG Viewer**
Jesús Daniel Trigo*, Miguel Martínez-Espronedada, Aitor Eguzkiza, Luis Serrano
- 269-7 **Internet Based ST Map Software: A Web Service, a Decision Support System and an Educational Tool**
Raymond Robert Bond*, Dewar Darren Finlay, Daniel Guldenring
- 270-36 **Portable Platform Independent Patient Monitoring**
Rogier Barendse*, Teus van Dam, Stefan Nelwan
- 271-33 **Telemedicine Network for Diagnosis and Care of Congenital Heart Malformations**
Alessandro Taddei*, Pierluigi Festa, Nadia Assanta, Tiziano Carducci, Emiliano Rocca, Bruno Murzi

Wednesday, September 25, 2013, 13:15

PA3: Heart Rate Variability in Disease

Room: Central Hall

- 272-139 **Heart Rate Asymmetry in Aortic Valve Stenosis Patients**
Monika Petelczyc*, Olga Lipińska, Jan, Jacek Żebrowski, Ewa Orłowska-Baranowska, Rafał Baranowski
- 273-412 **Analysis of Heart Rate Variability in Elderly Patients with Chronic Heart Failure and Periodic Breathing**
Beatriz F Giraldo*, Joan P Téllez, Sergio Herrera, Salvador Benito
- 274-195 **Age Related Changes in Variability of Short-Term Heart Rate and Diastolic Period**
Peng Li, Chengyu Liu*, Xin Sun, Yongai Ren, Chang Yan, Zhonghan Yu, Changchun Liu
- 275-53 **Validation of the Use of Heart Rate Variability Measurements during Meal Intake in Humans**
Sebastian Päßler, Alexander Noack*, Rüdiger Poll, Wolf-Joachim Fischer
- 276-99 **Combining HRV Features for Automatic Arousal Detection**
Jerome Foussier*, Pedro Fonseca, Xi Long, Berno Misgeld, Steffen Leonhardt
- 277-215 **OSAS Severity is Associated to Decreased Heart rate Turbulence Slope**
Giovanni D'Addio*, Mario Cesarelli, Maria Romano, Alberto De Felice
- 278-97 **Obstructive Sleep Apnea in a Rat Model: Effects of Anesthesia on Autonomic Evaluation from Heart Rate Variability Measures**
Raimon Jané*, Jesús Lazaro, Puy Ruiz, Eduardo Gil, Daniel Navajas, Ramon Farré, Pablo Laguna

Wednesday, September 25, 2013, 13:15

- 279-357 **Pulse Rate Variability in Children with Sleep Disordered Breathing in Different Sleep Stages**
Parastoo Dehkordi*, Ainara Garde, Walter Karlen, J Mark Ansermino, Guy A Dumont
- 280-413 **Heart rate variability analysis of pre and post awakening of 10 years children**
Taher Biala*, Syamil Muhammad, Michael Wailoo, Fernando Schindwein
- 281-424 **Detection of Cardiac Autonomic Neuropathy using Linear Parametric Modeling of QT dynamics**
Mohammad Hasan Imam*, Chandan Karmakar, Ahsan Khandoker, Herbert Jelinek, Marimuthu Palaniswami
- 282-233 **A New Methodology for Nonlinear Heart Function Analysis: Studying Just the Beat Morphology**
Constantino A García*, David G Márquez, Abraham Otero, Jesús Presedo, Paulo Félix
- 283-9 **Gender Comparison of Heart Rate Variability in Epileptic Seizures**
Soroor Behbahani*, Nader Jafarnia Dabanloo, Ali Motie Nasrabadi
- 284-228 **Heart Rate Variability Associated with Different Modes of Respiration during Zen Meditation**
Masaki Hoshiyama*, Asagi Hoshiyama
- 285-61 **Ageing of ECG Characteristics at Five Years Distance**
Neus Carmona*, Juan Carlos Rúa-Seoane, Jorge Elorza, Edurne Sáenz de Pipaón, Jean Bragard
- 286-243 **Discrimination of Heart Arrhythmia using Novel Features in Heart Rate's Phase Space**
Sadaf Moharreri*, Shahab Rezaei, Hossein Ajorloo

Wednesday, September 25, 2013, 13:15

PA4: Atrial Fibrillation

Room: Central Hall

- 287-221 **Study on the Generalized Hurst Exponents Optimal Use to Estimate Noninvasively Atrial Fibrillation Organization**
M Julián*, R Alcaraz, JJ Rieta
- 288-244 **Point Process Modeling of R-R Interval Dynamics during Atrial Fibrillation**
Marianna Meo*, Vicente Zarzoso, Olivier Meste, Decebal G Latcu, Nadir Saoudi, Riccardo Barbieri
- 289-265 **A Support Vector Machine Approach for Reliable Detection of Atrial Fibrillation Events**
Roberta Colloca*, Alistair EW Johnson, Luca Mainardi, Gari D Clifford
- 290-189 **Measures of Right Atrial Organization as a Means to Select Candidates for Sinus Rhythm Restoration by Catheter Ablation**
Andrea Buttu*, Andrei Forclaz, Patrizio Pascale, Philippe Maury, Anne Rollin, Jean-Marc Vesin, Etienne Pruvot
- 291-268 **Different Definitions of Complex Fractionated Atrial Electrograms do not Concur with Clinical Perspective**
Tiago Paggi de Almeida*, João Salinet, Gavin S. Chu, G André Ng, Fernando S. Schlindwein
- 292-163 **Assessment of Cycle Lengths during Human Atrial Fibrillation using Phase Information from Electrocardiographic Imaging Signals**
Adam Quotb*, Guillaume Attuel, Carole Pomier, Yuki Komatsu, Pierre Jäis, Meleze Hocini, Michel Haissaguerre, Rémi Dubois

Wednesday, September 25, 2013, 13:15

293-367 **Atrial Fibrillation Quantification by Implantable Leadless Device Equipped with Automatic Remote Monitoring**

Amarild Cuko*, Daniele Giacomelli, Massimo Saviano, Diego Grassini, Alessia Pappone, Andrea Petretta, Raffaele Vitale, Luigi Giannelli, Cristiano Ciaccio, Mario Baldi, Gabriele Vicedomini, Carlo Pappone

Wednesday, September 25, 2013, 13:15

PA5: Atrial Modelling

Room: Central Hall

- 294-370 **The Ionic Expression Gradients Affect the Paroxysmal Atrial Fibrillation Dynamic: A Simulation Study**
Catalina Tobón*, Karen Cardona, Sandeep V Pandit, José Jalife, Omer Berenfeld, Javier Saiz
- 295-423 **Frequency Dependency of Pacing Determinants of an IK1-mediated Rotor Drift in the Posterior Left Atrial Wall toward the Pulmonary Veins**
Conrado J Calvo*, Makarand Deo, Sharon Zlochiver, José Millet, Omer Berenfeld
- 296-237 **Modeling Calcium Dynamics in Human Atria**
Inmaculada R Cantalapiedra*, Carlos Lugo, Angelina Peñaranda, Leif Hove, Blas Echebarria
- 297-324 **Diagnosis of Atrial Ectopic Origin from Body Surface ECG – Insights from 3D Virtual Human Atria and Torso**
Erick Andres Perez Alday*, Michael Alan Colman, Daniele Giacomelli, Philip Langley, Henggui Zhang
- 298-261 **Paroxysmal Atrial Fibrillation Caused by Interaction of Pacemaker Waves and Reduced Excitability: Insights from the Bueno-Orovio Model Adapted to Atria**
Claudia Lenk*, Frank M Weber, Martin Bauer, Mario Einax, Gunnar Seemann, Philipp Maass

Wednesday, September 25, 2013, 13:15

PA6: Ventricular Arrhythmia

Room: Central Hall

- 299-273 **Effects of Physical Exercise and Glibenclamide in Local Activation Waves During Ventricular Fibrillation**
Juan Caravaca*, Antonio J Serrano-López, Emilio Soria-Olivas, Manuel Bataller, Alfredo Rosado-Muñoz, Luís Such-Belenguer, Juan F Guerrero
- 300-274 **Temporal Evolution of Spatial Regularity in Ventricular Fibrillation Modified by Physical Exercise**
Juan Caravaca*, Antonio J Serrano-López, Emilio Soria-Olivas, Manuel Bataller, Alfredo Rosado-Muñoz, Luís Such-Belenguer, Juan F Guerrero
- 301-206 **Performance of Heart Rhythm Analysis during Chest Compressions in Out-of-Hospital Cardiac Arrest**
Vessela Krasteva, Irena Jekova*, Todor Stoyanov, Sarah Ménétré, Jean-Philippe Didon
- 302-132 **Towards the Selection of Patients Requiring ICD Implantation by Automatic Classification from Holter Monitoring Indices**
Charles-Henri Cappelaere*, Rémi Dubois, Pierre Roussel, Oliver Baumann, Amel Amblard, Gérard Dreyfus

Wednesday, September 25, 2013, 13:15

PA7: Cardiac Mechanics

Room: Central Hall

- 303-292 **The Effect of the Sensor Position of the Pressure Wire Distal to a Coronary Stenosis on the Calculated Fractional Flow Reserve**
Balázs Tar, Sándor Bakk, Zoltán Béres, János Sánta, Péter Polgár, Shengxian Tu, Zsolt Kőszegi*
- 304-312 **Diagrammatic Reasoning with Interactive P-V Curves**
Marc Cavazza*, Fred Charles
- 305-254 **Analysis of Seismocardiogram Capability for Prediction of Mild to Moderate Hemorrhage**
Kouhyar Tavakolian*, Guy Dumont, Andrew Blaber
- 306-353 **Haemodynamic Parameters for Assessment of Orthostatic Intolerance in Older People**
Fernando García*, Lisa Cogan, Richard Reilly, José Millet, Raquel Cervigón

Wednesday, September 25, 2013, 13:15

PA8: Electrophysiology

Room: Central Hall

- 307-433 **Hurst Exponent to Analysis Atrial Fibrillation Recurrence after Ablation Procedures**
Raquel Cervigón*, Javier Moreno, Francisco Castells, Julián Pérez-Villacastín, José Millet
- 308-229 **Experimental Study of Arrhythmia due to Mild Therapeutic Hypothermia after Resuscitation of Cardiac Arrest**
Binbin Xu*, Oriol Pont, Gabriel Laurent, Sabir Jacquir, Stéphane Binczak, Hussein Yahia
- 309-55 **Spectral and Nonlinear Analysis in Surgical Ventricular Fibrillation**
Francisco Javier Pulido-Hidalgo, Óscar Barquero-Pérez*, Cristina Soguero-Ruiz, José Luis Rojo-Álvarez, Juan José Sánchez-Muñoz, Arcadi García-Alberola
- 310-122 **Classification of Inverse Solutions to Two Dipoles**
Jana Svehlikova*, Michal Teplan, Milan Tysler
- 311-116 **Clustering of Re-entry Close to Scar Boundaries in Ventricular Tissue during Simulated Ventricular Fibrillation**
Sathyavani Malyala*, Richard Clayton
- 312-285 **A Machine Learning Technique Regularization of the Inverse Problem in Cardiac Electrophysiology**
Nejib zemzemi*, Remi Dubois, Yves Coudiere, Olivier Bernus, Michel Haissaguerre
- 313-4 **Novel Potent Small Molecule Modulators of Cardiac KCa2 and KCa3.1 Channels: Potential Utility for Treating Cardiac Ischemia and Atrial Fibrillation**
Aida Olivan-Viguera*, Marta Sofia Valero, Ralf Kohler

Wednesday, September 25, 2013, 13:15

PA9: Cardiac Imaging

Room: Central Hall

- 314-120 **Automatic Detection of Mitral Annulus in Echocardiography based on Prior Knowledge and Local Context**
Wei Song, Wei Xu, Xin Yang*, Liping Yao, Kun Sun
- 315-2 **Role of 3D Echocardiography Derived Color-Coded Parametric Models of the Mitral Valve in Differential Diagnosis of Prolapse and Billowing**
Karima Addetia, Lynn Weinert, Roberto Lang, Victor Mor-Avi*
- 316-49 **Vendor-Independent Software for Rapid Comprehensive Assessment of Changes in Left Ventricular Function During Serial Echocardiographic Studies**
Gillian Murtagh*, Victor Mor-Avi, Wendy Tsang, Nicole Bhawe, Brent DeManby, Eric Kruse, Megan Yamat, Roberto Lang, Jeanne DeCara
- 317-376 **Multivariate Classification of Cardiac Autonomic Function and Echocardiographic Abnormalities**
Gabriel Granåsen*, Urban Wiklund
- 318-345 **Development of Fetal Cardiac Intervals Throughout 16 to 41 Weeks of Gestation**
Faezeh Marzbanrad, Yoshitaka Kimura, Kiyoe Funamoto, Rika Sugibayashi, Miyuki Endo, Takuya Ito, Marimuthu Palaniswami, Ahsan Khandoker*
- 319-84 **Non-Photorealistic Volume Visualization with Color Distance Gradient and Two-Level Volume Rendering**
Yong Xia*, Libing Zeng, Kuanquan Wang

Wednesday, September 25, 2013, 15:15

SB1: ECG Signal Processing

Room: Aula 0.01

Chair(s): Luca Faes and Joel Xue

- 320-17 **QRS Delineation Algorithms Comparison and Model Fine Tuning for Automatic Clinical Classification**
Antonio Casanez-Ventura, Francisco-Javier Gimeno-Blanes*, Jose-Luis Rojo-Alvarez, Jose-Maria Lopez-Ayala, Juan-Ramon Gimeno-Blanes, Arcadi Garcia-Alberola
- 321-106 **ECG Baseline Wander Removal and Impact on Beat Morphology: A Comparative Analysis**
Antonio Fasano*, Valeria Villani
- 322-407 **Baseline Wander Removal in ECG and AHA Recommendations**
Antonio Fasano*, Valeria Villani
- 323-298 **Transposition of Any Lead Placement to the Standard 12 Lead ECG Configuration on a Personalized Thorax Geometry**
Peter M van Dam*, Arie C Maan, Niek HJJ van der Putten, Nico Bruining, Arnold W A Dijk

Wednesday, September 25, 2013, 15:15

SB2: Physiological Atrial Modelling

Room: Aula 1.02

Chair(s): Maria S. Guillem and Gunnar Seemann

- 324-5 **Hyperpolarization-activated ‘Pacemaker Current’ — a Funny Current in Models of SA Nodal Pacemaker Cells**
Ronald Wilders*, Arie O Verkerk
- 325-208 **Accuracy of Non-invasive Frequency Estimation during Atrial Fibrillation**
Jorge Pedrón-Torrecilla*, Alejandro Liberos, Jose Millet, Andreu M Climent, Maria S Guillem
- 326-144 **Atrial Myocyte Model Parameter Optimization via Dynamic Electrophysiology Protocols and Automated Search Algorithms**
Willemijn Groenendaal, Lala Tanmoy Das, Trine Krogh-Madsen, David Christini*
- 327-177 **Influence Of Transmural Slow-Conduction Zones On Long-Time Behaviour Of Atrial Arrhythmia. A Numerical Study With a Human Bilayer Atrial Model**
Simon Labarthe*, Edward Vigmond, Yves Coudière, Jacques Henry, Pierre Jaïs, Hubert Cochet

Wednesday, September 25, 2013, 15:15

SB3: Atrial Fibrillation Physiology

Room: Aula 1.03

Chair(s): Leif Sörnmo and Rob MacLeod

- 328-63 **Recording and Identification of Cardiac Neuron Activity in the Right Atrium Ganglionated Plexus**
Siamak Salavatian*, Alain Vinet, Eric Beaumont, J Andrew Armour, Jeffrey L Ardell, Vincent Jacquemet
- 329-39 **Modification of Atrioventricular Node Conduction Increases RR Variability but not RR Irregularity nor Atrial Fibrillation Rate in Atrial Fibrillation Patients**
Valentina DA Corino*, Fredrik Holmqvist, Luca T Mainardi, Pyotr G Platonov
- 330-220 **Generalized Hurst Exponents as a Tool to Estimate Atrial Fibrillation Organization from the Surface ECG**
M Julián*, R Alcaraz, JJ Rieta
- 331-103 **Spectral Analysis of Blood Pressure Variability in Atrial Fibrillation: the Effect of Tilting**
Valentina DA Corino*, Federico Lombardi, Luca T Mainardi

Wednesday, September 25, 2013, 15:15

SB4: Intravascular Imaging

Room: Sala de Juntas

Chair(s): Nico Bruining

- 332-22 **Computer-assisted Quantitative Analysis of New
Interventional Treatment Methods**
Giulia Paoletti*, Francesco Prati, Sebastiaan de Winter, Ronald
Hamers, Nico Bruining
- 333-404 **Automatic Segmentation of Intravascular Ultrasound
Images based on Temporal Texture Analysis**
Adithya Gangidi*, CH Chen, Ahmet Umit Coskun, Prakash
Manandhar, Prakruthi Siddaramu
- 334-344 **Computer-Assisted Quantitative Evaluation of Coronary
Stent Platforms by Different Intracoronary Imaging
Methods**
Elżbieta Pociask*, Klaudia Proniewska, Nico Bruining
- 335-140 **Automatic Stent Segmentation in IOCT images Using
Combined Feature Extraction techniques and
Mathematical Morphology**
Matheus Cardoso Moraes*, Diego Armando Cardona Cárdenas,
Sérgio Shiguemi Furuie

Wednesday, September 25, 2013, 15:15

SB5: Prediction of Hypotension and Blood Pressure Variability

Room: Salón de Actos

Chair(s): Frida Sandberg and Raquel Bailón

- 336-160 **Cross-Entropy of Systolic Blood Pressure - Pulse Interval: Automatic Threshold and its Reliability**
Tamara Čeranić, Tatjana Lončar-Turukalo*, Branislav Milovanović, Nina Japundžić-Žigon, Dragana Bajić
- 337-300 **Prediction of Intradialytic Hypotension Based on Oxygen Saturation Variations**
Claudia Perazzini*, Piergiorgio Bolasco, Luca Corazza, Michele Tramonti, Elena Mancini, Antonio Santoro, Stefano Severi
- 338-155 **Prediction of Intradialytic Hypotension using PPG and ECG**
Frida Sandberg*, Raquel Bailón, David Hernando, Pablo Laguna, Juan Pablo Martínez, Kristian Solem, Leif Sörnmo
- 339-302 **Heart Rate Variability Analysis for the Prediction of Hypotension during Spinal Anesthesia in Programmed Cesarean and its Relation with Fetal Cord Acid-base Equilibrium**
José M Remartínez*, Raquel Bailón, Eva M Rovira, Juan Bolea, Pablo Laguna, Augusto Navarro

Wednesday, September 25, 2013, 16:30

MC: Plenary

Room: Sal3n de Actos

Chair(s): Pablo Laguna and George Moody

- 340-199 **Non-invasive Location of Re-entrant Propagation Patterns during Atrial Fibrillation**
Miguel Rodrigo*, Andreu M Climent, Alejandro Liberos, Jorge Pedr3n-Torrecilla, Jos3 Millet, Francisco Fern3ndez-Avil3s, Felipe Atienza, Omer Berenfeld, Maria S Guillem
- 341-66 **Computational Modelling of LQT1 in Human Induced Pluripotent Stem Cell Derived Cardiomyocytes**
Michelangelo Paci*, Jari Hyttinen, Stefano Severi
- 342-158 **Drug Effect Evaluation during Permanent Atrial Fibrillation using an AV-node Model**
Frida Sandberg*, Valentina Corino, Sara Reinvik Ulimoen, Steve Enger, Arnljot Tveit, Luca Mainardi, Pyotr Platonov, Leif S3rnmo
- 343-225 **Online Apnea-Bradycardia Detection using Recursive Order Estimation for Auto-regressive Models**
Di GE*, Alain Beuch3, Guy Carrault, Patrick Pladys, Alfredo Hernandez

Abstracts

Fluid-structure Interaction Analysis of Representative Left Coronary Artery Models with Different Angulations

Jingliang Dong*, Zhonghua Sun, Kiao Inthavong, Jiyuan Tu

RMIT University
Melbourne, Australia

The aim of this study is to elucidate the correlation between coronary artery angulation and local mechanical forces at the vicinity of bifurcation using a coupled fluid-structure interaction (FSI) modelling approach. Four representative left coronary arteries with different angles ranging from 75° to 120° were used to demonstrate the relation between circumferential stress and angulation. In order to increase simulation fidelity, the arterial wall was modelled as an isotropic hyperelastic material, and physiologically reasonable waveforms were imposed at the boundaries. The results show that circumferential stress is positively correlated with left coronary artery angulation. In addition, the hemodynamic differences between the FSI modelling and rigid wall modelling was also addressed and analysed through comparing those two modelling techniques. The instantaneous wall shear stress (WSS) distributions were substantially affected by the arterial wall compliance.

Improved Electrocardiographic Detection of Hyperacute Ischemia by Difference Vector Analysis

C Cato ter Haar*, Arie C Maan, Martin J Schalij, Cees A Swenne

Leiden University Medical Center
Leiden, Netherlands

The ECG is important in diagnosis and triage in the hyperacute phase of the acute coronary syndrome (ACS), especially during the "golden hours", during which myocardial salvage possibilities are largest. An important triaging decision to be taken is whether or not a patient requires primary PCI, for which the guidelines mention an ST elevation (STE) pattern in the ECG as major criterion. This criterion has, however, a relatively low sensitivity and specificity.

We investigated the diagnostic possibilities of ischemia detection by means of changes in the ST vector, ΔST , and changes in the VG (QRST-integral) vector, ΔVG . We studied vectorcardiograms (VCGs) synthesized of the ECGs of 84 patients who underwent elective PTCA. Mean \pm SD balloon occlusion times were 260 ± 76 s. The ECG ischemia diagnosis, STE or non-STE (NSTE), and the differences ΔST and ΔVG with the baseline ECG were measured after 3 min. of occlusion.

Linear regression of ΔVG on ΔST yielded $\Delta VG = 324 \cdot \Delta ST$ ($r = 0.85$; $P < 0.0001$, ΔST in mV). With ΔST thresholds of values 0.025, 0.050, 0.075 and 0.100 mV and corresponding ΔVG thresholds of 8.1, 16.2, 24.3 or 32.4 mV \cdot ms, respectively, we determined the sensitivity for ischemia detection, that varied from 55% for the STE criterion to 87 or even 99% for the one but most and the most sensitive ΔST and ΔVG criteria, respectively.

Differential diagnosis by ΔST and ΔVG (requiring an earlier made non-ischemic baseline ECG) could dramatically improve ECG guided detection of patients who urgently require catheter intervention.

Semi-automated Detection and Quantification of Aortic Atheromas from Three-Dimensional Transesophageal Echocardiography

Concetta Piazzese*, Wendy Tsang, Miguel Sotaquira, Roberto M Lang, Enrico G Caiani

Politecnico di Milano
Milano, Italy

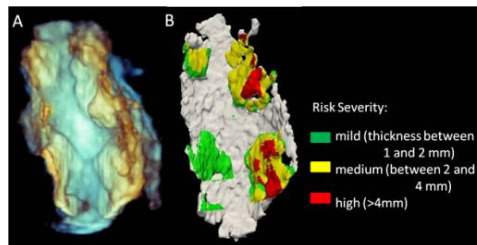
Aim: Atherosclerosis is a chronic disease characterized by the presence of atheromas (AT) in medium and large arteries. Transesophageal echocardiography (TEE) is the best imaging modality for diagnosing aortic AT. Our aim was: 1) to develop a semi-automated method to detect and quantify AT from 3D TEE images of descending aorta; 2) to assess algorithm accuracy against expert cardiologist “gold standard” analysis (GS).

Method: Five points describing the aortic lumen (AL) were manually initialized on 7 equally-spaced 2D cut-planes in the 3D TEE volume and used to obtain an elliptical contour, which was extended in-between cut-planes by interpolation. By automated thresholding and marching cubes algorithm a 3D mesh of the original data was obtained. The AT were defined as the regions lying inside the AL, composed by >300 nodes of the 3D mesh. Based on its maximum thickness, a risk severity (mild, medium, high) was associated to each AT. Algorithm accuracy was tested in 58 consecutive patients by comparing the number, location and severity of the GS manual analysis (see figure). Also,

in 15 AT, the GS manual volumes were compared with the automatically computed AT volumes by linear correlation and Bland-Altman analyses.

Results: Computerized analysis required on average 5 min, versus 5 to 30 min of the GS, depending on AT complexity. GS detected 163 AT, of which 145 were found also automatically (accuracy, 89%). In 116/145 AT, no difference in severity (80%) was found. High correlation ($r^2 = 0.98$) with minimal underestimation (9%) were reported for AT volumes.

Conclusion: We developed a semi-automated method for the detection and quantification of descending aortic AT from 3D TEE images. This analysis is rapid, feasible and accurate in determining AT number, severity, and volume. This methodology could allow standardization of 3D AT quantification, with great potential benefits in clinical practice.



Prediction of Sudden Cardiac Death in Chronic Heart Failure Patients by Analysis of Restitution Dispersion

Julia Ramírez, Ana Mincholé, Juan Bolea, Pablo Laguna, Esther Pueyo

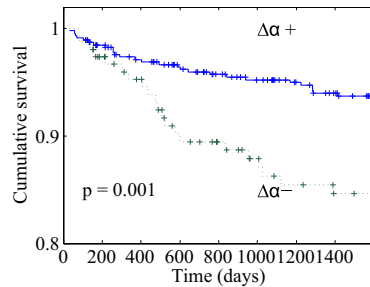
University of Zaragoza
Zaragoza, Spain

Background: The dynamic restitution of the action potential duration (APDR) measures the relationship between the action potential duration and the RR interval at steady-state pacing. Due to heterogeneities in the ventricles, APDR presents spatial variations generally termed APDR dispersion. Enhancement of APDR dispersion has been associated with higher propensity to suffer from ventricular arrhythmias and sudden cardiac death (SCD). Recently, a marker, $\Delta\alpha$, was proposed to non-invasively quantify APDR dispersion from the electrocardiogram (ECG) by computing the ratio between differences in the T-peak-to-T-end (T_{pe}) and RR intervals at different steady-state conditions.

Methods: Holter ECG recordings of 609 subjects (48 victims of SCD, 64 of other cardiac causes, 25 of non-cardiac death causes and 472 survivors) from the “MUSIC” database were analyzed. ECGs were delineated using a single-lead procedure over the first principal component calculated to emphasize the T-wave. RR and T_{pe} series were computed and T_{pe} /RR dynamics was estimated using a nonlinear system with memory, from which the risk marker $\Delta\alpha$ was derived.

Results: $\Delta\alpha$ discriminated between the group formed by SCD victims and the group composed of the other subjects, with mean \pm SEM values of: $\Delta\alpha = 0.049 \pm 0.012$ for the former and $\Delta\alpha = 0.029 \pm 0.003$ for the latter ($p = 0.048$). In a survival analysis where a threshold on the third quartile of $\Delta\alpha$ values was set, statistically significantly different event probabilities were obtained in both stratas of the population ($p = 0.001$).

Conclusions: The marker $\Delta\alpha$ stratifies patients according to their risk of suffering from ventricular arrhythmias that could lead to SCD, with larger repolarization dispersion indicating lower survival probability.



Event-free curves for SCD

LightWAVE: Waveform and Annotation Viewing and Editing in a Web Browser

George Moody*

Massachusetts Institute of Technology
Cambridge, United States

S21

Within the PhysioNet project, software for viewing ECGs and other physiologic waveforms and associated annotations (event markers) is in high demand by researchers and students for finding and examining data relevant to their studies. Interactive annotation editing is essential for creating and curating new data collections. Since the inception of PhysioNet, we have relied for these capabilities on WAVE (Waveform and Annotation Viewer and Editor), an X11/XView application that we created on SunOS in 1989 and later ported to Solaris, GNU/Linux, Mac OS X, and MS-Windows. WAVE has become increasingly expensive to maintain as evolving X11 technology introduces incompatibilities with the XView library that provides WAVE's GUI. A replacement built on modern standards has been clearly needed. We have recently designed a lightweight successor, LightWAVE (<http://physionet.org/lightwave/>), that provides WAVE's features and more while running in any modern web browser without requiring installation in the user's computer, tablet, or smart phone. As for all software from PhysioNet, this application is open-source software that can be freely used, studied, and adapted by its users. LightWAVE's back end is a CGI application written in C for speed and efficiency. It retrieves data from its data repository and delivers them in response to requests generated by the front end. It has been tested successfully using Apache (on Fedora 64-bit Linux and Ubuntu 32-bit Linux); it does not have explicit system dependencies and should be usable with Apache on other platforms. The API is designed to ease development of alternative front ends with the aim of encouraging experimentation. LightWAVE's front end is a web application written using HTML5, Javascript, and SVG, with fast high-resolution graphics. Annotations can also be created and edited using mouse and touchscreen interfaces. Although it was created for PhysioNet, LightWAVE can be used independently of PhysioNet.

eLab: A web-based Platform to Perform HRV Analysis and Store Cardiac Signals

Óscar Barquero-Pérez¹, Teresa Quintanilla², José García-Muñoz, Cristina Soguero-Ruiz¹, Mark Wilby³, José Luis Rojo-Álvarez¹, Arcadi García-Alberola⁴, Manuel de la Rosa², Miguel Cabañas², Iván González², Roberto Bravo²

¹ University Rey Juan Carlos, Madrid Spain, ² Persei Consulting, Spain, ³ Universidad Politécnica de Madrid, Spain, ⁴ Hospital Virgen de la Arrixaca de Murcia, Spain

This study aimed to develop a user-friendly, modular and scalable web-based system to calculate risk stratification markers of Sudden Cardiac Death (SCD) and it can be used in daily clinical practice.

Development of eLab platform began in the project Vpredict+, funded by the Ministry of Industry, Tourism and Commerce.

eLab allows to upload and save cardiac signals into a custom database, perform a complete heart rate variability (HRV) analysis of each anonymous RR-interval time series from holter records. These results are stored and can be presented to the user using plots and tabular information or downloaded in commonly formats (txt, csv, etc). Users only need a web browser to use this tool.



eLab principal access web page.

The main components of eLab are: (1) Signal analysis toolbox HRV analysis. (2) Database of ECG and RR-interval time series. It stores a large amount of data. In order to improve indexed access to the information and reduce search time significantly, values are divided into several time interval segments. Measurements are stored within each correspond segment, following an AVL tree structure. (3) User-friendly Web Interface. The components of eLab are communicated by mean of connections client-server through a ICE interface. Zero ICE middleware technology has been chosen, due to its independence from any programming language or platform and its great efficiency in terms of bandwidth load, allowing high data transfer rate.

The design of eLab as isolated modules interconnected using ICE interface allows to replace or add new modules in an efficient way, without affecting the interoperability of the system. It has a data model flexible and extensible.

We are integrating eLab with an EHR system that uses Selene and expanding to analyse HRT.

Seamless Integration of Watermarks in DICOM Images

Óscar J Rubio*, Álvaro Alesanco, José García

University of Zaragoza
Zaragoza, Spain

S21

This study aimed at introducing watermarks in the DICOM protocol, to implement an additional security layer. In this context, the watermarks were of use to bind tightly the test image with some fields of interest (e.g. patient name and diagnosis), ensuring that these data vanish if the image loses its clinical value. Other interesting uses were to improve the authentication of the image, even when it is seriously distorted, and the integrity control, tuned to allow only mild modifications of the image. To be fully consistent with this medical standard, the watermarking needed to meet a series of formalities: distortion-free embedding algorithm, security in harmony with the policies of DICOM and endurance of the watermarks to medical modifications, such as gamma correction, contrast change or compression. A new distortion-free watermarking algorithm was specifically designed for medical images. It works on the region-of-interest of the image, encoding the watermark bits as positions of the sign bit of the highest energy coefficients in the wavelet domain, generating a compact access key that is protected with Cryptographic Message Syntax, supported by the standard. The most sensitive DICOM fields are embedded into the image as watermarks, and the corresponding access keys replace the original field values. This security design prevents eavesdropping, collusion and forgery attacks. Different configuration of the watermarks were proposed to implement in-image diagnosis, image authentication and integrity control. Echocardiograms of 20 patients from Lozano Blesa hospital were used for the evaluation. The watermarks resisted all tested medical modifications, obtaining bit-error-rate < 3%, which was reduced to zero by means of BCH codes. The watermark embedding-retrieval delays were < 0.2s (each), half if the watermarking is integrated with JPEG2000 image compression. Although a n bit watermark generated a $7n$ access key, the overhead was very low compared to the image size (< 6% in highly compressed images).

An Interactive Digital Platform for Arterial Wave Intensity Analysis

John L Tassone*, Ashraf W Khir

Brunel University
Uxbridge, United Kingdom

Background: Wave intensity analysis (WIA) is a technique that is used for the evaluation of the working condition of the heart and the arterial system. Simultaneous measurements of blood pressure (P) and velocity (U) are required for calculating wave intensity (WI), which can also be determined non-invasively using U and diameter (D) of the vessel at the measurement site. The technique allows for the separation of P, U, D and WI into their forward and backward directions.

Aim: This paper describes the development of an interactive digital platform that can be used to analyse arterial waves, determine WI, providing a range of cardiac and arterial indices.

Methods and results: The platform is developed in Matlab, and operates interactively by allowing the user to select the data and the type of analysis based on the availability of the acquired signals. The user chooses to visualise the analysis of the raw signals or part of, and decide which set of results would be saved either in excel or .txt files, together with all the automatically generated graphs and tables. The wave speed is calculated using the PU-Loop or InDU-Loop techniques, automatically taking into consideration the lag between the velocity and pressure, or diameter using linear regression techniques. Also, the platform shows the separation of the forward and backward waves, whose meaningful indices are tabulated interactively with variations of wave speed. The platform is designed for batch analysis of large data-sets, and has been used for investigating signals taken in vivo of dogs which have undergone different hemodynamic manipulations. The results are in good agreement with those processed manually.

Conclusion: the proposed platform is easy to use, saves computational time and effort for the assessment of a cardiac performance and arterial stiffness.

A Cardiovascular Patient Follow-up System using Twitter and HL7

Jesús Daniel Trigo*, Aitor Eguzkiza, Miguel Martínez-Espronedada, Luis Serrano

Public University of Navarre
Pamplona, Spain

S21

Aims: This project aimed at designing and developing a system for following-up cardiovascular patients integrating social networks and healthcare communications standards. **Methods:**

The system was designed using Twitter as social network and Health Level 7 (HL7) version 2.6 as health care standard. An android application was developed to gather a number of cardiovascular signs (weight, blood pressure, pulse rate and temperature). Thereafter, the plain measurements were encapsulated into HL7 v2.6 messages and tweeted to the hospital twitter account. Finally, a desktop Java application simulating the front-end of the health care provider received the incoming tweets and parsed the HL7 messages, so that the new measurement could be adequately committed to the patient's Electronic Health Record.

Results: Two applications – an android-based tool for gathering and tweeting vital cardiovascular signs and a Java-based desktop tool for receiving and parsing the information – were created within the framework of this project. The two applications developed provided a feasible prototype for following-up cardiovascular patients.

Discussion: A number of considerations concerning this novel approach are discussed in this paper. The modification of the health care flow empowers the patient and enhances the patient-physician communication. On the other hand, both patients and physicians may be reluctant to use the system as a daily basis due to security and privacy concerns. In any case, the use of a health care standard assures an extra layer of interoperability.

Conclusion: The integration of healthcare standards into social networks provides user-friendly applications that help bridge the gap in the patient-physician communication in a standard-compliant fashion. However, some research questions are still open and further projects are needed to guarantee the secure use of social networks in healthcare environments.

Computational Modeling of Human Fetal Normal Sinus Rhythm and Arrhythmia

Alan Benson, Adam Bleakley, Arun Holden*, Nikki Pelech, Eleftheria Pervolaraki, Catherine Whitfield, Sam Hodgson

University of Leeds
Leeds, United Kingdom

Introduction: The foetal electrocardiogram can be recorded from the maternal abdominal surface from ~ 12 weeks gestational age (WGA), and RR, PR, QR and QT intervals, and T and P wave dispersions extracted. These non-invasive measures provide quantitative approximations to sino-atrial node pacemaking rate (via RR), propagation times and velocities (via PR, QT), and ventricular action potential duration and its restitution (QT-RR) during foetal normal sinus rhythm. Arrhythmias are observed in <5% of recordings.

Methods: The parameters of biophysically detailed models of adult human cardiac cell electrophysiology, derived from voltage clamp, immunohistochemical and mRNA expression data were modified, informed by data from the literature on animal foetal tissue and cardiomyocytes derived from human stem cell lines, to reproduce human foetal RR and QT intervals. One dimensional partial differential equation models of SAN, atrial, AVN and ventricular tissue, with lengths from MRI and intercellular coupling informed by PR and QR intervals, were constructed for hearts from 15-40 WGA. Numerical solutions, with zero-flux boundary conditions, were by the explicit Euler method, with integration time and space steps of 0.005 ms and 0.1 mm.

Results: The 1D model at 15, 30 WGA gave NSR intervals RR :400, 450; QR: 200, 280 ms. Spatially uniform progressive reduction of the calcium maximal conductances slowed the SAN, extended the PR interval, and led to AV conduction blocks. Self-terminating ventricular re-entry was obtained within a 1-D ring ventricular tissue model.

Conclusion: The preliminary 1-D family of models reproduces the observed timings of fECG intervals from 15-40 WGA, the characteristics of development of foetal AV block, and self terminating ventricular tachycardia.

HCN and SCN5A Channel Mutations: Implications for Impaired Atrioventricular Nodal Conduction in a Heterogeneous Computer Model of Whole Mouse Heart

S22

Simon Joseph Castro*, Michael Alan Colman, Henggui Zhang

University of Manchester
Manchester, United Kingdom

AIMS: The atrioventricular (AV) node is a specialised region of the cardiac conduction system, allowing electrical excitation to propagate from the atria to the ventricles. AV block occurs when the AV node prevents electrical stimuli reaching the ventricles, ultimately leading to a decrease in cardiac output. HCN and SCN5A genetic mutations have previously been identified in patients with AV block, but the mechanisms underlying impaired AV node conduction remain incompletely understood. The aim of this study was to assess the functional impacts of HCN knockout and SCN5A gene mutations (T220I, P1298L, delF1617 and E161K) on AV block.

METHODS: Recently published single cell models for mouse sinoatrial node (SAN) and ventricular cells were modified based on extant experimental data to create new models for murine AV node and Purkinje fibre cells. These newly developed cell models, along with an existing model for SAN, atrial and ventricular tissue were incorporated into 1D and 2D whole heart models. Using these computational platforms we investigated the effects of HCN and SCN5A ion channel mutations on the initiation and conduction of electrical excitation waves in the heart.

RESULTS: Both HCN knockout and SCN5A mutations had a significant effect on cardiac pacing as illustrated by a remarkable reduction in cardiac pacing rate. They also caused a slowing of conduction velocity in the conduction system of the heart, particularly in the AV node region, resulting in enhanced susceptibility to AV block.

CONCLUSION: We have developed a 1D and 2D whole heart model of mouse electrophysiology which can be further extended to a 3D anatomical model in the future. Our computational simulations show that HCN knockout and SCN5A mutations provide the conditions required for AV block and result in impaired conduction. The computational models presented will allow further investigation of AV block including potential drug therapy.

Modeling the Influence of High Fibroblast Level on Arrhythmia Development and Obstructed Depolarization Spread

Sándor Miklós Szilágyi*, László Szilágyi, Béat Hirsbrunner

University of Fribourg
Fribourg, Switzerland

Aims: In the focus of this study exists the fibroblast cells that under physiological terms are providing structural support for the heart, but under patho-physiological conditions such as myocyte aging or death, various injuries and inflammation, can accumulate in the cardiac tissue, obstructing the pacemaker activity and excitation spread function of the heart that may develop arrhythmia.

Methods: We investigated the influence of high fibroblast level under several patho-physiological conditions. The simulation was performed on a 3D heart model, adopting a 0.25 mm spatial and 2 μ s temporal maximal resolution, using Nygren atrial and Luo-Rudy II ventricular cell models. In our simulation 25% volume of the normal cardiac tissue is occupied by fibroblast, and in presence of regional inflamed or injured tissue, fibroblast cells accumulates up to 40%-80% volume. Aging increases the volume of fibroblasts up to 30%-50% in cardiac tissue and up to 40%-60% among sino-atrial cells. We employed the effect of cardio-myocyte death (up to 5%-15% of cardiac cells), and laminar sheet isolation (depolarization velocity in trans-sheet direction is 2-9 times slower than in in-sheet orientation). In our consideration the high level of fibroblast cells conducted to a 25-200 times more frequent spontaneous ectopic-firing (SEF) than develops in normal circumstances.

Results: In presence of 30%/35%/40%/45%/50% fibroblast in cardiac myocyte the spread velocity of depolarization was obstructed by 3%/7%/11%/15%/19%, while regional inflammation and injures reduced locally the propagation speed of excitation by at least 20%. Due to aging the normal cardiac pacemaker activity was reduced by 20%-50% that yield a 10-100 times increased chance to evolve irregular cardiac activity. The prevalent SEF makes the development of arrhythmia 50-500 times more frequent.

Conclusion: A high fibroblast cell concentration not only detains significantly the spread velocity of excitation, but it can completely swoon the depolarization wave evolving cardiac arrhythmia.

Heterogeneous Electrical Remodeling of the Failing Heart Modulates the Arrhythmogenic Substrate

Juan Fco Gomez*, Karen Cardona, Lucia Romero, Javier Saiz, Beatriz Trenor

Universitat Politècnica de València
Valencia, Spain

S22

Introduction: Failing hearts undergo electrical and structural remodeling, setting the stage for malignant arrhythmias. Increased dispersion of repolarization has also been related to arrhythmogenesis in human heart failure (HF), but it remains unknown whether heterogeneous electrical remodeling is responsible for an increased dispersion of repolarization in the setting of HF. Several experimental studies focused on the controversial changes of transmural dispersion of repolarization in the failing heart. In this simulation work, we try to elucidate the mechanisms of modulation of transmural gradients in the failing human heart and their implication for arrhythmogenesis.

Methods: The human ventricular action potential (AP) models formulated by O'Hara et al. (ORd) and Grandi et al. (GPB) were modified to simulate the electrical cellular behavior observed in human HF. Several biomarkers were calculated from ventricular cellular simulations under conditions of heterogeneous remodeling of the sodium-calcium exchanger (INCX) and SERCA (ISERCA) in endocardial, midmyocardial, and epicardial cells.

Results: Computer simulations showed that heterogeneous electrical remodeling of ISERCA and INCX in failing ventricular cells could reduce APD transmural gradient in 13% in the HF model of endocardial and epicardial cells using GPB model. This gradient was reduced in 8% when ORd model was used, which considers epicardial, endocardial, and M cells. A heterogeneous remodeling also led to an increase of transmural calcium decay gradient of 2500% in the absence of M cells (GPB model) versus an increase of 929% when M cells were present (ORd model). Systolic sodium transmural gradient level was reduced in 43% in the HF model heterogeneously remodeled using GPB model versus 6% using ORd model.

Conclusions: The results of this study uncover the importance of the controversial presence of M cells in the human transmural wall and how heterogeneous remodeling can modulate the repolarization gradient in failing hearts.

Kalman Filter Based Estimation of Ionic Concentrations and Gating Variables in a Cardiac Myocyte Model

Laura Munoz*, Niels Otani

Cornell University
Ithaca, United States

Background: The purpose of this study is to give researchers improved access to important electrophysiological quantities, such as ion-channel gating variables, that are difficult or impossible to measure during in vitro experiments, yet are thought to be critical to the formation of dangerous arrhythmias. To help fulfill this goal, we used a Kalman filtering approach to reconstruct gating and concentration variables from simulated time-series observations of cellular membrane potential. This research is relevant to human health, since it could be used to provide more information about the response of a single cell to the influence of pharmacological agents or other anti-arrhythmic therapies, over a larger range of cellular variables than are typically monitored during an in vitro study.

Methods: A Luo-Rudy dynamic (LRd) cell model was stimulated at a one-second cycle length. The model was linearized after its fixed point was identified with a Newton-Krylov solver. To determine whether measurements of any individual variable were sufficient to estimate the remaining variables, we analyzed a model property called observability. Next, the linearized model was augmented with process and measurement noise, and a Kalman filter was designed. Matlab was used to perform all computations.

Results: The observability results showed that membrane potential measurements were sufficient for estimating the other variables in the LRd model. In simulation tests, the Kalman filter reduced the norm of the estimation error covariance; with process and measurement noise variances of 1.0 and 0.10, the covariance norm over ten cycles was 32% smaller compared to the case without measurement feedback.

Conclusion: The concentration and gating variables in the LRd model can be reconstructed from membrane potential data. Kalman filtering methods constitute a promising approach for allowing researchers to gain a more complete understanding of the dynamical behavior of cardiac ion-channel quantities.

Uncertainty Visualization in Forward and Inverse Cardiac Models

Brett M Burton, Burak Erem, Kristin Potter, Paul Rosen, Chris R Johnson, Dana H Brooks, Rob S Macleod

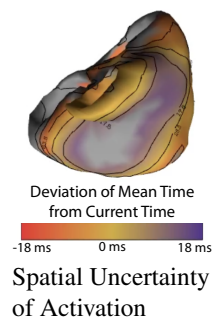
University of Utah, Scientific Computing and Imaging Institute
Salt Lake City, Utah, USA

S22

Introduction: The complex nature of cardiac structure and the inherent need to regularize inverse solutions lead to poorly quantified or visualized uncertainty in cardiac forward and inverse simulations. To better understand such variations, we have developed new three-dimensional techniques to visually analyze ECG simulation uncertainty. To highlight the utility of these techniques, we address uncertainty associated with modeling myocardial potentials, during the ST segment, as a function of variability in tissue conductivities of the ischemic heart, as well as spatial uncertainty of reconstructed activation times on the epicardium resulting from variation in the Tikhonov inverse method's regularization parameter.

Methods: We characterized uncertainty in the results as the variations caused by perturbing the parameters around some assumed ground truth. Anisotropic conductivity ranges for bidomain forward simulations were determined and applied to what are known as second-order polynomial chaos methods. In the second case, Tikhonov regularization parameters were uniformly distributed between 0.09 to 0.11 and used to compute activation-based inverse solutions. Visualization of these uncertainty results included mean and standard deviation 3D volume rendering and isosurfacing, 2D clipping, transfer function coloring, and video activation animations.

Results: Our visualization techniques provide novel insight into simulation uncertainty. Regions of high uncertainty were easily identified after combining several visualization techniques - highlighting key regions of interest. Forward models of ischemia produced large variations along longitudinal fiber pathways and in regions where fiber orientation was more variable. In the activation-based inverse problem, we observed that certain spatial regions had greater standard deviations in the estimated timing of electrical excitation than others, suggesting higher uncertainty in those regions. Animation of mean and standard deviation values over the time course of activation further illustrated this uncertainty.



Exploring QT Variability Dependence from Heart Rate in Coma and Brain Death on Pediatric Patients

Rute Almeida, Marta João Silva, Ana Paula Rocha

S23

CMUP, University of Porto
Porto, Portugal

Introduction

Patients with acute brain injury (ABI) present dysfunctions of the Autonomic Nervous System producing alterations on the cardiac parameters, particularly in brain death (BD). Therefore the study of cardiovascular variabilities can provide a complementary tool for time course predicting and prognostic. Moreover, early reliable predictors of BD would contribute for the efficiency of organ transplantation programs.

Methods

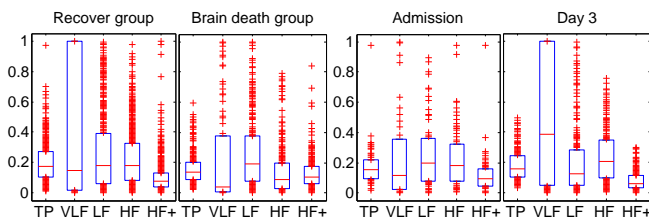
QT variability (QTV) versus heart rate variability (HRV) interactions were explored using a low order AR-ARARX model previously validated which allows quantifying the QTV Fraction (F %) driven by HRV. High resolution 12-lead ECG Holter recordings were taken from 6 pediatric patients admitted to the intensive care unit with ABI. For 3 patients BD has been confirmed later by the usual protocol (BD), while other 3 have recovered (R). RR and QT beat-to-beat series were computed from automatic delineation and detrended. Segments with 250 valid consecutive measures in both series, for which valid models were obtained, were used. Power of HRV, QTV total and fractions were calculated considering the frequency bands: < 0.04 (VLF), $0.04 - 0.15$ (LF), $0.15 - 0.4$ (HF), $> 0.4\text{Hz}$ (HF+) and all frequencies (TP).

Results

The median of F% was found to be for each frequency band, respectively, 0.1505, 0.1778, 0.1802, 0.0774, 0.1776 for R patients and 0.0387, 0.1939, 0.0881, 0.1032, 0.1358 for BD group. F% in BD group was found to be significantly lower for TP, VLF and HF bands and significantly higher for HF+ ($p < 0.00001$). Moreover for one of the R cases, in which data is available with 3 days apart, median F% has significantly ($p < 0.005$) increased for VLF and decreased for HF+, what can reflect an improvement in the patient state.

Conclusion

Uncoupling of QT/RR have clinical potential in differentiating the progression of the disease within children with ABI, providing a better individual adjustment in treatment type and timing, and as early prognostic predictor of BD.



Comparing the Relationship Between QT/RR Slope and Basal QTc in LQT1 Patients and Healthy Subjects

Josef Halamek*, Jean-Philippe Couderc, Pavel Jurak

Institute of Scientific Instruments, AS, Brno
Brno, Czech Republic

S23

Introduction: Conventional QT analysis has shown that the QT/RR slope (QTRR) is steeper in LQTS patients leading to an increased propensity for life-threatening arrhythmias. Yet, little attention has been given to the relationship between QTRR and the basal QTc interval. We hypothesize that relationship between QTRR and basal QTc is consistent with the arrhythmogenic role of both QT prolongation and the lack of QT adaptation to adrenergic stimulation in the LQT1 syndrome.

Method: Holter ECGs from the THEW database, healthy (n=154, age 36±14 years, 73 women) and LQT1 subjects (n=97, age 23±16 years, 57 women) were analyzed. QTc and QTRR were given by linear and dynamic model using three optimized parameters and so both QTc and QTRR slope were corrected for hysteresis. The relationship was analyzed using correlation and linear regression with QTc as independent variable, i.e. $QTRR = a_0 + a_1 \times QTc$.

Results: QTRR values shows strong relationship to basal QTc interval in healthy (R=0.58; P<0.00001) and in LQT1 patients (R=0.56; P<0.00001). The linear regression between QTRR and QTc were $a_0 = -0.42$; $a_1 = 0.0016$ in healthy and $a_0 = -0.24$; $a_1 = 0.0010$ in LQT1 subjects. Therefore, LQT1 subjects have flatter QT/RR slope than controls but higher intercept. This is consistent with the high risk for syncope primarily during high adrenergic states such as exercise and strong emotion in LQT1.

Conclusion: The steeper QT/RR slope relative to basal QTc preserves proper shortening of QT intervals during increased heart rate in healthy while in LQT1 patients the QT intervals does not adapt to increased heart rate (lack of shortening). We believe the proposed analysis of the QTRR relationship to basal QTc could be complementary to QTc interval in the risk stratification of LQTS patients.

Lack of Autonomic Influence on QT Interval Variability In Patients With Heart Failure

S23

Sachin Nayyar, Muhammad Hasan, Thomas Sullivan, Judith Hunt, Prashanthan Sanders, Kurt Roberts-Thomson, Mathias Baumert*

Background: Beat-to-beat QT interval variability (QTV) is a marker of repolarization lability and increased QTV was shown to be predictive of malignant ventricular arrhythmia. Autonomic nervous system dysfunction has been implicated in the genesis of QTV, but it is not clear whether it drives elevated QTV that has been reported in heart failure.

Methods. The study was performed in 29 subjects: 10 heart failure patients with spontaneous ventricular tachycardia [HFVT(+)], 10 heart failure patients without spontaneous VT [HFVT(-)], 9 subjects with structurally normal heart (HNorm). Beat-to-beat QT interval was measured by automated analysis on 8-minutes records of surface ECG at baseline and during interventions [atrial pacing at 80bpm and 100bpm, esmolol (0.3 mg/kg/min), isoprenaline (3 µg/min) and atropine (0.04 mg/kg single dose) infusion]. Variability in QT intervals was expressed as the standard deviation of all QT intervals (SDQT) at baseline and in the last 3-minutes during interventions. An index of QTV normalized to heart rate variability (QTV/HRV) was calculated as ratio of SDQT to SDRR.

Results. Baseline QTV/HRV veered to be higher in HFVT(+) group compared to HFVT(-) and HNorm groups ($p=0.09$). QTV turned significantly higher in HFVT(+) and HFVT(-) groups compared to HNorm patients during fixed rate atrial pacing ($p=0.008$). Compared to baseline, isoprenaline increased QTV in HNorm group ($p=0.02$), but not in HF patients. QTV remained elevated in HFVT(+) group relative to HNorm group despite acute beta-adrenoceptor blockade with esmolol ($p=0.02$).

Conclusion. Patients with HF and spontaneous VT have larger fluctuations in beat-to-beat QT intervals. This repolarization instability appears to persist despite uncoupling the effect of heart rate. Importantly, acute beta-adrenoceptor blockade fails to reduce QTV in these patients at risk of VT.

QT Interval Analysis in Electrograms of Isolated Guinea Pig Hearts Treated with Haloperidol

Petr Vesely*, Josef Halamek, Tibor Stracina, Lenka Krejčírova, Marie Novakova

S23

Aims: Antipsychotic drug haloperidol exhibits serious cardiac side effects including QT interval prolongation. Repeated haloperidol treatment influence on QT interval of isolated guinea pig hearts was studied.

Methods: The experiments were performed on 10 guinea pigs (male only), divided into haloperidol-treated (8 animals) and control (2 animals) groups. The experimental protocol consisted of four 30 minutes lasting phases: stabilization, haloperidol 1, wash-out, haloperidol 2. ECG in three orthogonal leads was continually recorded (sampling rate 2000 Hz, resolution 16 bits) during the whole experiment. The Q waves, R waves and the end of T waves were automatically detected, manually corrected and served to RR and QT intervals computing. The QTc interval was computed according to three models: Bazett's, Fridericia's, and dynamic model (TRF) with three parameters. Mean value and standard deviation were consequently assigned from the interval of 2000 beats in the middle of all four experimental phases.

Results: Significant ($P < 0.01$) prolongation of QTc (in all models) occurs during haloperidol applications in haloperidol-treated hearts. The relative increases of QTc were 0.042 ± 0.0198 , 0.053 ± 0.0298 , and 0.0046 ± 0.002 for QTcB, QTcF, and QTc TRF, respectively. The prolongation in control group was insignificant. Relative accuracy of QTc given as STD/mean over all phases and experiments was 0.020 ± 0.022 , 0.023 ± 0.025 , and 0.005 ± 0.004 for QTcB, QTcF, and QTc TRF, respectively.

Conclusion: The QTc prolongation occurs during haloperidol application in comparison with the previous phases of stabilization or washout. This was confirmed by all models. If the exact value of QTc is important, the sample specific model must be used and the hysteresis must be eliminated as it is in case of TRF model. Determination of the haloperidol effect in control experiments was not possible, but it seems that haloperidol prolongs QT interval dynamically, with long time constant.

Comparative Analysis of Short-Term Variability of RR and QT Intervals for the Assessment of Autonomic Nerve Activity

Yi Zhu*, Xiaolin Yang, Zhigang Wang, Yi Peng

Institute of Basic Medical Sciences, Chinese Academy of Medical Sciences & School of Basic Medicine, Peking Union Medical College Beijing, China

Aims: The purpose of this study is to investigate the behavior of autonomic nervous system (ANS), reflected by short-term variability (STV), in the patients with high risk for cardiac arrhythmias and sudden cardiac death (SCD). Comparison was performed with normal people.

Methods: The data were provided by the Telemetric and Holter ECG Warehouse (THEW). 43 Holter recordings were selected from database ESRD (E-HOL-12-0051-016), containing the recordings of hemodialysis patients with high risk for cardiac arrhythmias and SCD (ESRD-HRAS), and 83 Holter recordings as age-matched normal controls from database Normal (E-HOL-03-0202-003). STV of RR intervals (STVRR) and QT intervals (STVQT) were calculated using 30 consecutive beats. Two resting episodes lasting 1 h were selected in each Holter record, one in the period of 7:00~20:00 (day), the other in 0:00~6:00 (night). For each 1 h interval series, a sliding window with width of 30 beats was implemented and STVs of each sliding window within the episode were averaged as the feature indexes (MSTVRR and MSTVQT) of this episode. Mann-Whitney U test was used to compare the indexes in Normal and ESRD.

Results: MSTVRR in ESRD-HRAS was much lower than that in normal people though the level of heart rate was comparable in these two groups. MSTVRR significantly increased at night and MSTVQT significantly decreased at the same time in normal people. While for ESRD-HRAS, MSTVRR significantly increased at night but MSTVQT almost remained the same level as that by day. The decreased heart rate variability (HRV) and more dispersion of ventricular repolarization in ESRD-HRAS suggest the sympathetic superactivity in these patients, having the tendency to result in malignant arrhythmia.

Conclusions: Comparative analysis of HRV and QT variability using Holter data might be a potential approach to get information of ANS modulation.

The Linear Dependence of Ventricular Repolarization Variability on Heart Rate Variability in Head-Down Bed Rest Studies

Juan Bolea, Enrico G. Caiani, Pablo Laguna, Rute Almeida

Universidad de Zaragoza, CIBER-BBN
Zaragoza, Spain

S23

Background: It is known that the cardiac function is affected by head down bed rest (HDBR) microgravity simulation. Nevertheless its consequences for the health both during the HDBR at recovery are still a matter of research. In particular, the effects over ventricular repolarization (VR) are not well known, while VR dysfunctions could lead to cardiac arrhythmias and eventually to sudden cardiac death.

Objectives: To evaluate the changes in interactions of VR variability with heart rate variability (HRV), used as pro-arrhythmic marker, elicited by 5-days HDBR.

Methods: Three VR beat-to-beat indexes were extracted from ECG signals acquired before (PRE), during (HDBR) and after HDBR (POST): QT , QT_p and T_{pe} (peak to end of T wave). ARARX modeling was used to estimate the VR variability fraction driven by HRV at different time periods.

Result: In all VR indices, the VR variability content linearly driven by HRV was significantly increased during HDBR versus PRE by multiple comparisons statistical analysis. Furthermore, in a pairwise comparison between PRE and POST, a significant increase in T_{pe} variability driven by HRV was also found.

Conclusions: HDBR increases the linear dependency of VR variability to HRV. The results evidence a reduced recovery capacity for the T_{pe} repolarization variability to restore its linear dependency values to HR in the first moments at the end of BR that might be related with changes in the pro-arrhythmic substrate.

Fetal Heart Rate Pattern in Prenatal Diagnosis

Dirk Hoyer*, Uwe Schneider

S24

Jena University Hospital
Jena, Germany

Aims: Fetal heart rate patterns provide valuable information about the fetal normal maturation as well as maturation disturbances due to potential risk factors such as intrauterine growth restriction (IUGR) and administration of glucocorticoids (GC). Heart rate variability (HRV) analysis that is successful in prenatal diagnosis requires the selection of appropriate HRV indices. Those indices were organized according to the physiological rhythms of autonomic modulations as well as according to universal principles of developmental biology. The present work aims at the introduction and evaluation of HRV based scores of normal fetal maturation and its disturbances.

Methods: All magnetocardiographic recordings of our study data base were performed with a sampling rate of 1024 Hz in a magnetically shielded room at the Biomagnetic Center of the Jena University Hospital. We investigated 30 min recordings of normal, IUGR and GC singleton fetuses in a nonstress situation. Stable 10 min intervals of active and quiet state were selected according to standard criteria. In the selected group of normal fetuses (21.4-40.3 weeks of gestation), we estimated the age dependency separately in quiet (n=113, 63 females) and active (n=286, 145 females) state by cross-validated multivariate linear regression models in a cross-sectional study. HRV indices were designed according to physiological and developmental principles.

Results: The scores of the normal developmental explained 66/63% (coefficient of determination R^2 of training and validation set) of the variance by age in quiet state, while 51/50% in active state. IUGR and GC fetuses showed remarkable differences compared to the normal group models.

Conclusions: With respect to autonomic regulation, functional fetal age can be assessed based on universal developmental indices obtained from short HRV patterns of pre-classified activity states. The proposed scores may have implications for early identification of fetal developmental disturbances.

Subspace Detection of the Impulse Response Function from Intrapartum Uterine Pressure and Fetal Heart Rate Variability

Philip Warrick*, Emily Hamilton

Perigen, Inc.
Montreal, Canada

S24

Objectives: Using clinically measured intrapartum cardiotocography (CTG) data, the objective of this study was to detect the impulse response function (IRF) of the system composed of uterine pressure as the input and one of three frequency band powers of fetal heart rate variability (fHRV) as the output.

Methods: We used CTG with at least three hours of tracing just prior to delivery. 89 of the cases were normal (N) while 142 had developed metabolic acidemia (M). We first estimated the fHRV using an autoregressive model of the CTG FHR signal to estimate the power spectral density (PSD) [Warrick2012]. The PSD was integrated over low frequency (LF, 30-150mHz) and movement frequency (MF, 150-500mHz) and high frequency (HF, 500-1000mHz) bands to obtain three instantaneous components of fHRV. We performed system identification over 20min epochs using the CTG uterine pressure (UP) as an input and one of the fHRV components as an output. Subspace methods are well-suited to these noisy signals because of their inherent singular-value decomposition and because they permit inclusion of non-contiguous data. We used the PO-MOESP subspace method [Verhaegen2007] to estimate two-dimensional state-space system models. Because of UP periodicity, there was no unique system model; we searched for a best model by shifting the output signal with respect to the input to find an IRF beginning with a first coefficient near 0. This shift represented the response delay relative to the input.

Results: Figure 1 shows that the IRF delay had statistically significant differences between N and M cases in each of the three bands. The HF band had the most(3) epochs with significant differences. In all bands the differences in the final 120min (HF band) and 90min (LF,MF bands) preceding delivery.

Conclusions: IRF estimates from UP and fHRV are useful discriminants of fetal state, potentially for automated clinical decision-making.

Increased Instability of Heartbeat Dynamics in Parkinson's Disease

Riccardo Barbieri*, Gaetano Valenza, Luca Citi, Maria Guerrisi, Stefano Orsolini, Carlo Tessa, Stefano Diciotti, Nicola Toschi

Massachusetts general Hospital
Boston, United States

Introduction: Parkinson's disease (PD) has been reported to involve postganglionic sympathetic failure and, in 25% of patients, autonomic failure. Recently, measures of heart rate variability (HRV) have been employed to explore autonomic alterations in PD. In this work we investigate autonomic dynamics in PD using a novel methodology able to provide instantaneous estimates of the Lyapunov spectrum within a point process framework.

Methods: Physiological signals were recorded from 10 healthy controls (5 males, 5 females, age 53.1 +/- 15.4 years) and 9 cognitively preserved PD patients (6 males, 3 females, age 64.9 +/- 7.2 years). Subjects were placed horizontally in a supine position and remained at rest during the whole recording (600 s). We computed mean values (over the whole recording period) of conventional HRV features as well as of the full Lyapunov spectrum and tested for significant effects of group (PD vs. controls) using both nonparametric statistics and a general linear model taking into account age and gender as nuisance covariates. Additionally, the discriminatory power of all features was tested by training a Support Vector Machine (SVM) classifier (linear kernel and complexity parameter=0.001, Recursive Feature Elimination (RFE), 10 fold cross-validation).

Results: In both statistical comparisons, The first (LE1) and second (LE2) Lyapunov exponents were significantly ($p=0.01$) higher in PD patients vs. controls (LE1: 0.108 +/- 0.105 vs. -0.012 +/- 0.055; LE2: -0.115 +/- 0.042 vs. 0.167 +/- 0.038). Additionally, RFE retained exclusively LE1 and LE2 and SVM resulted in classification with 75% sensitivity and 80% specificity (area under ROC curve 0.8). No other HRV measure differed significantly between groups.

Conclusions: Our results suggest that autonomic control in PD entails a preponderance of nonlinear, less stable heartbeat dynamics with respect to controls. This could point to possible autonomic dysfunction which cannot be detected by conventional HRV measures.

Assessment of Fetal Development using Multiscale Multifractal Analysis of Heart Rate Variability

Jan Gierałtowski*, Dirk Hoyer, Uwe Schneider, Jan Żebrowski

Warsaw University of Technology
Warszawa, Poland

S24

Two lowest bands (very low frequencies and ultra-low frequencies) of human heart rate variability (HRV) account for 95% of the total signal power. Nonetheless their physiological background is still uncertain. The problem is in the lack of methods capable of analyzing these bands, other than the basic power spectral analysis, which is usually insufficient. Lately fractal scaling methods, such as DFA have been used to analyze fetal heart rate [1]. In our study we assessed 158 magnetocardiographic HRV time series. 30 minute signals were recorded from fetuses of 21-38 weeks of age. A novel method was employed for analyzing the data: Multiscale Multifractal Analysis (MMA) [2]. As a method result, we obtain the Hurst surface. Resulting surface describes in a very compact form, fluctuation scaling properties (i.e. nonlinear correlation properties) depending on fluctuation's magnitude and frequency range. Note that the MMA method is designed specifically to analyze the VLF band of heart rate variability. Using the MMA method we developed a model which is able to predict gestational age based only on heart rate variability recordings [3]. The possibility to predict the APGAR score of a child, a few weeks before it is born, also based only on its heart rate variability recordings, will be discussed at the conference. We hope that our work will bring a significant input to noninvasive, efficient and accurate prenatal diagnosis methods. [1] D. Hoyer, S. Nowack, S. F. Tetschke, S. Ludwig, L. Moraru, A. Rudolph, U. Wallwitz, F. Jaenicke, J. Haueisen, E. Schlußner, U. Schneider, *Comput. Biol. Med.* 42, 335-341 (2012) [2] J. Gierałtowski, J. J. Żebrowski and R. Baranowski, *Phys. Rev. E* 85, 021915 (2012) [3] J. Gierałtowski, D. Hoyer, F. Tetschke, S. Nowack, U. Schneider, J. Żebrowski, *Auton. Neurosci.* (2013)

<http://dx.doi.org/10.1016/j.autneu.2013.01.009>

Time-series Network Analysis for Detecting Cardiac Autonomic Neuropathy using RR Interval Data

Chandan Karmakar*, Ahsan Khandoker, Herbert Jelinek, Marimuthu Palaniswami

Cardiovascular autonomic neuropathy (CAN) is highly prevalent and a serious complication in patients with diabetes mellitus. The change in heart rate variability (HRV) is regarded as one of the early signs of CAN. In this study, we investigate the effect of degree and data length on complex network (mapped from RR interval time-series) properties (transition asymmetry and network efficiency) to differentiate negative CAN (NCAN) subjects from definite CAN (DCAN). Forty-one patients with Type 2 diabetes mellitus were included in the study: 15 patients had definite CAN (DCAN), whilst the remaining 26 were negative for CAN (NCAN), being without clinical signs and symptoms of CAN. Symbolic Aggregate approximation (SAX) was used as the discretization procedure of HRV time-series signal and the transition graph (τ) was generated from the discretized signal. Finally, transition asymmetry ($A(G)$) and network efficiency EF were calculated. The optimal degree (m_{opt}) and data length n_{opt} selected for differentiating DCAN from NCAN subjects are 270 and 200 respectively. Mean $A(G)$ of NCAN group was higher than DCAN group, which represents higher variations in dynamics of HRV signal in NCAN than DCAN. Similarly, EF was also higher in NCAN group, which means that the network topology of NCAN group is strongly connected compared to DCAN group. Moreover, both $A(G)$ and EF were found equally strong in classifying NCAN and DCAN group with an accuracy 85.37%. In conclusion, complex network theory based HRV parameters can be used as a potential tool for analysing CAN in diabetes.

Quantification of Cardiorespiratory Coupling in Acute Schizophrenia Applying High Resolution Joint Symbolic Dynamics

Steffen Schulz, Karl-Juergen Baer, Andreas Voss*

University of Applied Sciences Jena
Jena, Germany

S31

Schizophrenia is one of the most severe psychiatric disorders where patients have a relative risk to suffer from cardiovascular disease. Different studies demonstrated a cardiac autonomic dysfunction reflecting altered heart rate variability (HRV) in those patients. However, less information are available regarding to respiration and its variability and especially the corresponding cardiorespiratory regulation (coupling) in patients suffering from acute schizophrenia. The aim of this study was to quantify short-term nonlinear cardiorespiratory couplings in acute schizophrenia applying a new high resolution joint symbolic dynamics (HRJSD) analysis approach based on a redundancy reduction strategy. The latter is characterised by 8 coupling pattern families (resulting in 64 different coupling patterns) which represent different patterns of interactions of the branches of the autonomic regulation. HRJSD is able to provide detailed information about short-term nonlinear cardiorespiratory physiological regulatory mechanisms (patterns) of autonomic nerve system. To avoid the influence of very low variabilities we defined a threshold for the symbol transformation based on the individual physiological variability of the heart rate and respiratory frequency time series. In this study, 23 unmedicated patients with acute schizophrenia (SZO; 12 male; 30.4±10.3 years) and 23 age and gender matched healthy controls (CON, 13 male; 30.3±9.5 years) were investigated. HRJSD revealed 24 significant ($p < 0.01$) cardiorespiratory coupling patterns quantifying changes of cardiorespiratory regulation in SZO. Seven significant ($p < 0.01$) respiratory and three significant ($p < 0.01$) heart rate pattern families showed also univariate changes in SZO in comparison to CON. The altered cardiorespiratory coupling in SZO was mainly characterized by a larger amount of increased short-term alternating and fluctuating patterns. Further on, the respiratory regulation is more complex in SZO and dominates the cardiorespiratory coupling. These results indicate to an impairment of short-term cardiorespiratory regulation probably due to an altered or suppressed interplay of the brainstem and higher regulatory centres in the patients.

Analysis of Cardio-respiratory Dynamics during Mental Stress using (Partial) Time-Frequency Spectra

Devy Widjaja*, Michele Orini, Elke Vlemincx, Sabine Van Huffel

KU Leuven
Leuven, Belgium

S31

Aim: Mental stress is a growing problem in today's society. Although it is recognized that stress has an important effect on both the variability of the heart rate (HRV) and on respiration, the precise stress mechanisms are still unknown. In this study, we aim to investigate how the cardio-respiratory coupling is affected by stress.

Methods: A quadratic time-frequency distribution is used to conduct bivariate time-frequency analysis of HRV and respiration. The time course of spectral indices (LF and HF power), the coherence and phase delay between both signals, were analyzed. In addition, HRV was partialized in two spectra: one which contains components locally coupled to respiration, representing respiratory sinus arrhythmia, and one which contains components which are not synchronous with respiration. Data of 40 subjects, undergoing a baseline recording, two mental stress tasks (MT1 and MT2) and an attention task (AT), are analyzed.

Results: The results indicate that the phase delay was not influenced by stress nor attention and that the coherence between HRV and respiration slightly increased during AT. On the other hand, a significant decrease ($p < 0.05$, Wilcoxon signed rank test) in coherence was observed during MT1 and MT2 around respiratory frequency. The time courses of LF and HF power show reductions during AT and MT1 compared to baseline. During MT2, only LF power was significantly ($p < 0.01$) lower. The partialization of HRV reveals that, in the HF band, respiratory-related changes due to stress were faster (10-15 s), and larger, than changes unrelated to respiration.

Conclusion: The time-frequency analysis of cardio-respiratory interactions shows interesting dynamic courses of several features as a result of stress and attention. Moreover, partial spectra reveal differing time scales of stress responses related and unrelated to respiration.

Cardiorespiratory Coherence Analysis of Abnormal Heart Rate Responses during Deep Breathing

Urban Wiklund, Amir Kadkhodae, Kennet Andersson

Department of Radiation Sciences, Biomedical Engineering, Umeå University, Sweden

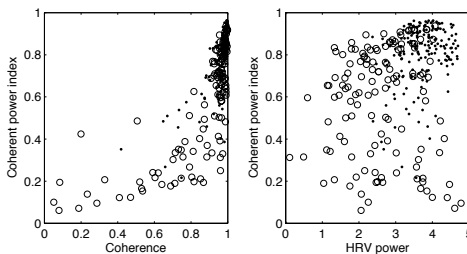
S31

Background: Deep breathing normally causes a marked response in the heart rate variability (HRV), but in patients with transthyretin amyloidosis (ATTR) we occasionally observe abnormal heart rate responses due to arrhythmia, e.g., atrioventricular blocks, or other irregular heart rate responses despite regular breathing patterns. We evaluated the use of cardiorespiratory coherence analysis for detection of these abnormal patterns.

Methods: One-minute sequences from paced deep breathing (6/min) were retrospectively obtained from 131 recordings in adult ATTR patients and 176 healthy subjects. The total power of HRV was estimated, including the corresponding age-dependency in controls. The magnitude-squared coherence was determined at the breathing frequency using bivariate autoregressive (AR) modelling and Welch's averaged, modified periodogram method. Finally, we calculated the coherent power index (CPI) as the fraction of HRV that was coherent with respiration.

Results: HRV scores were within normal limits in 55 patients (42%). AR-based coherence increased from 0.67/0.87 (means for patients/controls) for AR(2) to 0.86/0.96 for AR(8). The Welch-based coherence decreased markedly with increasing number of segments used for averaging. Both methods showed significantly lower coherence and CPI in patients than in controls. For AR(8) mean CPI was 0.57 vs 0.79 ($p < 0.001$, Mann-Whitney test). Among the subjects with normal HRV scores, CPI was lower than 0.50 in 35% of patients and in 6% of controls (for Welch the corresponding proportions for patients/controls were 50%/13%).

Conclusion: Cardiorespiratory coherence analysis can be used to identify subjects with "falsely" increased HRV scores during deep breathing. If the coherent power index is very low, most of the power in the HRV spectrum appears at other frequencies than the breathing frequency. The recorded signals must then be carefully inspected, e.g., to detect cardiac arrhythmia or other factors that could explain the lack of the expected heart rate response.



Left panel: CPI and coherence (for AR). Right panel: CPI and log-transformed total power of HRV. Data from all subjects: o patients, • controls.

Information decomposition of short-term cardiovascular and cardiorespiratory variability

Luca Faes*, Alessandro Montalto, Giandomenico Nollo, Daniele Marinazzo

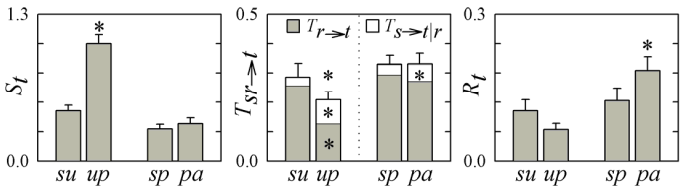
University of Trento, Trento, Italy

S31

Aims: We present an entropy decomposition strategy aimed at quantifying how the rate of information generated by heart period variability (t) is dynamically stored in t and is transferred to t from systolic pressure (s) and respiration (r) variability according to synergistic or redundant cooperation. The strategy is applied to head-up tilt (HUT) and paced breathing (PB) protocols to describe the related physiological regulatory mechanisms.

Methods: We decompose the predictive information about t , i.e. the information carried by t that is explained by the past of t, s, r , into a sum of contributions reflecting the information stored in t (S_t) and the information transferred to t from s and r ($T_{sr \rightarrow t}$). The information transfer was further decomposed as total (direct+indirect) transfer from r plus direct transfer from s : $T_{sr \rightarrow t} = T_{r \rightarrow t} + T_{s \rightarrow t|r}$. Moreover, a redundancy measure describing the informational character of the information transfer was defined as $R_t = T_{s \rightarrow t} - T_{s \rightarrow t|r}$. All measures were computed as conditional entropy differences; entropies were estimated by linear regression exploiting the Gaussian assumption. The method was applied on short (300 beats) r, s , and t series from 15 healthy subjects in the supine (su) and upright (up) positions during HUT, and further 15 subjects with spontaneous (sp) and paced (pa) breathing during PB.

Results and Conclusions: From su to up , we found significant increases (paired t-test, $p < 0.05$) of S_t and $T_{s \rightarrow t|r}$, and significant decreases of $T_{sr \rightarrow t}$ and $T_{r \rightarrow t}$ that were related respectively to baroreflex activation and dampening of respiratory sinus arrhythmia consequent to HUT. From sp to pa , we found significant increases of $T_{s \rightarrow t}$, $T_{s \rightarrow t|r}$ and R_t , that were related to an enhanced respiratory driving on arterial pressure induced by PB. These results indicate that physiological transitions are associated with a re-modulation of the storage and transfer of information in heart period variability which reflects specific cardiovascular and cardiorespiratory control mechanisms.



Heart period variability information storage, transfer, and transfer redundancy during HUT and PB. (* $p < 0.05$ up vs. su , or pa vs. sp)

Influence of Respiration in the Very Low Frequency Modulation of QRS slopes and Heart Rate Variability in Cardiomyopathy Patients

David Hernando, Alejandro Alcaine, Esther Pueyo, Pablo Laguna, Andrs Arcentales, Beatriz F. Giraldo, Andreas Voss, Antonio Bayés-Gens, Raquel Bailón

Aragón Institute for Engineering Research (I3A), IIS, University of Zaragoza, Zaragoza, Spain
CIBER de Bioingeniería, Biomateriales y Nanomedicina (CIBER-BBN), Zaragoza, Spain

S31

Aims: This work investigates the very low frequency (VLF) modulation of QRS slopes and heart rate variability (HRV). Our hypothesis is that the main source of that modulation is respiration, either directly or indirectly through linearly-related autonomic nervous system (ANS) effects. Other non-linearly-related autonomic effects are secondary.

Methods: Electrocardiogram (ECG) and respiratory flow signal were acquired from 19 patients with dilated cardiomyopathy and 29 patients with ischemic cardiomyopathy. HRV as well as the upward QRS slope (I_{US}) and downward QRS slope (I_{DS}) were extracted from the ECG. The relation between HRV and I_{US}/I_{DS} in the VLF band was measured using ordinary coherence in 5-minute segments. To remove the respiration influence, partial coherence was used. A statistical threshold has been determined, below which coherence values do not represent linear relation.

Results: Approximately 5% of the analyzed segments (12 for I_{US} and 15 for I_{DS}) presented the VLF modulation in QRS slopes, HRV and respiration. Those segments showed a linear relation between QRS slopes and HRV, with ordinary coherence values of 0.78 ± 0.06 (above the threshold in all cases), and all of them presented a decrease in partial coherence. For I_{US} , 9 segments had a partial coherence value below the threshold, and 7 segments for I_{DS} . The rest of the segments also presented a notable decrease in partial coherence (around 10%), but still above the threshold.

Conclusion: The decrease in partial coherence with respect to ordinary coherence suggests that the origin of the VLF modulation of QRS slopes and HRV can be explained by respiration or is linearly related to it. However, the removal of respiration influence does not always lead to a partial coherence value below the threshold, which means that other ANS effects non-linearly-related to respiration may also affect this modulation.

Estimating Respiratory Frequency from Heart Rate Variability During Treadmill Exercise Testing

L.M. Sepúlveda-Cano*, E. Sierra*, G. Castellanos-Domínguez*, R. Bailón-Luesma**, P. Laguna**

S31

*Universidad Nacional de Colombia, Sede Manizales, Colombia

**Instituto de Investigación en Ingeniería de Aragón (I3A), IIS Aragón, Universidad de Zaragoza, Zaragoza, Spain

**Centro de Investigación Biomédica en Red - Biomedicina, Biomateriales y Nanomedicina (CIBER-BBN), Spain

This paper aims to discuss a methodology for assessing respiratory frequency, from heart rate variability (HRV) signals during treadmill exercise testing based on the HR modulation synchronous with respiration, called respiratory sinus arrhythmia. During exercise, HRV signals are highly non-stationary and may be influenced by false detections or misdetections of QRS complexes due to muscular noise and motion artifacts present in the ECG signal. Respiratory frequency during exercise is in itself a highly dynamic quantity and changes with effort and work load. Moreover, in HRV signals during treadmill exercise testing it has been observed the appearance of a component at the running stride frequency which complicates respiratory frequency estimation. In this work respiratory rate is estimated from HRV during treadmill exercise testing using a methodology which combines empirical mode decomposition (and its ensemble version) with the time-frequency representation of the main modes. A tracking algorithm is used to track respiratory rate in time and modes. The method is evaluated in 22 physically active volunteers from whom ECG, RR series and respiratory variables were simultaneously recorded during maximal treadmill exercise testing. The proposed methodology estimates respiratory rate with an error of media $5.95 \pm 3.86\%$. As an additional outcome, since each mode or represents different dynamics present in the HRV signal other kind of information about the signal behavior can be also estimate such the influence of the stride frequency.

Probabilistic Classification Approaches for Cardiac Arrest Rhythm Interpretation during Resuscitation

Ali Bahrami Rad, Trygve Eftestøl, Jan T Kvaløy, Unai Ayala, Jo Kramer-Johansen, Kjersti Engan

University of Stavanger
Stavanger, Norway

S32

Aims: Our ultimate objective is to develop methodology for resuscitation data analysis that involves monitoring of the patients response, the quality of therapy, and the interplay between therapy and response. To this end, methods to reliably detect the rhythm types during a resuscitation episode are needed. The objective of this study was thus to develop machine learning algorithms to recognize the rhythms appearing during a resuscitation episode.

Materials: The database of ECG from cardiac arrest rhythm segments consisted of 269 ventricular fibrillation (VF), 25 ventricular tachycardia (VT), 262 asystole (AS), 411 pulseless electrical activity (PEA), and 155 pulse generating rhythms (PGR). The first two rhythms (VF/VT) are shockable, and the others are non-shockable.

Methods: 16 different features were extracted in the wavelet domain as follows: two different statistical descriptors (variance and the first quartile) of the approximation and detail coefficients of Daubechies 4 (D4) wavelets in 4-level decomposition (10 features), the parameters of the fourth-order autoregressive model (5 features) and autocorrelation (1 feature) of the approximation coefficients in level 4. The data were classified by two different methods; firstly, by using naive-Bayes classifier, which makes a conditional independence assumption on the features, and secondly by logistic regression classifier with L-BFGS quasi-Newton methods and Gaussian prior on the parameters.

Results: The detection accuracy for the five different rhythms for 3s segments was 70% and 67% for naive-Bayes and logistic regression classifiers respectively. The sensitivity/specificity for shockable/non-shockable rhythms were 94/90 and 75/94(%) for naive-Bayes and logistic regression classifiers.

Conclusion: This study is our initial work to address automatic cardiac arrest rhythm analysis. The results are promising, and the performance can be improved by adding sub-algorithms like QRS detection and extracting more informative features.

A New Rhythm Analysis Algorithm for Chest Compression Intervals: Effect on Cardiopulmonary Resuscitation Delivery

Unai Ayala, Unai Irusta, Jesús Ruiz, Digna González-Otero, Erik Alonso, Jo Kramer-Johansen, Trygve Eftestøl

University of the Basque Country (UPV/EHU)
Bilbao, Spain

S32

Aim: Rhythm analysis during cardiopulmonary resuscitation (CPR), i.e. a shock advice algorithm (SAA) combined with a CPR artifact suppression method, has been evaluated in terms of sensitivity and specificity. Recently, a new methodology was developed to evaluate to which degree these methods reduce unnecessary CPR prolongations (shockable rhythms) and interruptions (nonshockable rhythms), compared to the 2-minutes of uninterrupted CPR established by the guidelines. This study evaluates the real effect on CPR delivery of using a new SAA specially designed to analyse the rhythm during CPR.

Materials: We used 214 shockable and 634 nonshockable records from 247 patients with median duration 120 seconds (65–180) and 162 seconds (90–180), respectively.

Methods: The SAA classified the rhythm each consecutive 9-second segment as shockable, nonshockable or unreliable (large CPR artifacts). For this study, the SAA was modified to also classify borderline cases as unreliable. In our implementation scenario, rhythm assessment would start 1-minute after the beginning of CPR. On-going CPR would be delivered until the first shock diagnosis or until a consecutive minute of unreliable diagnoses. The probability of stopping CPR as a function of time was estimated using Kaplan-Meier curves.

Results: The SAA classified as unreliable 10.8% of the segments, 4.4% had large CPR artifacts and 6.4% were borderline cases. For the rest of segments, the sensitivity, specificity and the positive predictive value (confidence in shock diagnosis) were 93.2%, 97.4% and 88.0%, respectively. For the shockable records, the probability of advising the shock before 2-minutes was 95.0% (95% confidence interval, 92.0-97.9). For the nonshockable records, the probability of prolonging CPR beyond 2 and 3-minutes were 92.5% (90.5-94.6) and 90% (87.6-92.8), respectively.

Conclusions: Our method would improve the recommended 2-minute CPR cycles by avoiding unnecessary CPR prolongations in 95.0% of shockable cases, and decreasing unnecessary CPR interruptions in 92.5% of nonshockable cases.

Increase of QRS Duration as a Short-Term Predictor of Ventricular Arrhythmias During Coronary Artery Occlusion.

Alba Martín-Yebra*, Marina Demidova, Pyotr Platonov, Pablo Laguna, Juan Pablo Martínez

Centro de Investigación Biomédica en Red- Bioingeniería, Biomateriales y Nanomedicina (CIBER-BBN), Zaragoza, Spain
Zaragoza, Spain

S32

Aims: Increased QRS duration (QRSd) has been observed during acute myocardial ischemia and infarction, indicating conduction deterioration in the myocardial tissue. It has been reported that intramyocardial conduction velocity slowing induced by ischemia is associated with the occurrence of malignant ventricular arrhythmias, however, clinically useful QRSd cut-offs that would predict ventricular fibrillation (VF) onset have not been identified. In this work, we study the association between QRSd prolongation and VF in a porcine model of myocardial infarction.

Materials and Methods: In 32 pigs, infarction was induced by 40-minute-long balloon inflation in LAD coronary artery under continuous 12-lead ECG monitoring. After applying a wavelet-based delineator to the ECG precordial leads (V1-V6), beat-to-beat multilead QRSd was measured using post-processing rules. Using a short-term sliding window, local increments of QRSd (DQRSd) were continuously computed along the 40-minute occlusion. Association between (DQRSd) and subsequent VF onset was studied using ROC curve analysis. Pigs were classified as QRSd(+) if at any moment $QRSd \geq 120$ ms and at the same time the local increment DQRSd exceeded a threshold and as QRSd(-) if not.

Results: VF occurred in 10 of 32 pigs (onset ranging from 12 to 30 min). Using a 3-min sliding window, we found that QRSd(+) recordings showed a higher presence of VF episodes. Choosing a threshold for DQRSd of 28 ms, obtained from the ROC curve analysis, 8 out of 10 recordings with VF were classified as QRSd(+), while only 3 out of 22 recordings without VF were QRSd(+) (Se=80%, Sp=86.4%, NPV=90.48%, PPV=72.73%). In pigs with VF the threshold for QRSd increase was first exceeded, on average, 4.36 ± 3.89 minutes (median=3.16 minutes) before the VF episode.

Conclusion: This study suggests that a transient increase in QRSd may be a sensitive and specific index for monitoring the immediate risk of malignant ventricular arrhythmias during acute myocardial ischemia.

Dependency of T-Wave Alternans Predictive Power for the Occurrence of Ventricular Arrhythmias on Heart Rate

Laura Burattini*, Sumche Man, Cees A Sweene

Polytechnic University of Marche
Ancona, Italy

S32

T-wave alternans (TWA), consisting of every other beat alternation of the T wave amplitude, is a promising index of cardiac electrical instability and sudden cardiac death. It is well known that TWA amplitude (TWAA) tends to increase with increasing heart rate. However, the effect of heart rate on the TWA predictive power for the occurrence of ventricular arrhythmias remains unclear. Thus, the aim of the present study was to evaluate if fast heart rates, besides inducing higher amplitude TWA, also enhances TWA ability to discriminate patients at greater risk of major cardiac events. To this aim we analyzed heart-rate increasing routine exercise ECG tracings from 266 implanted cardioverter-defibrillator (ICD) patients who were classified, at the end of the 4-year follow-up, as either ICD_Cases (76 patients), if they had developed ventricular tachycardia or ventricular fibrillation, or ICD_Controls (190 patients), if they had not. For each patient, TWA was measured at 80 bpm and 120 bpm using our heart-rate adaptive match filter method. Eventually, TWA ability to discriminate the ICD_Cases from the ICD_Controls was evaluated using the area under the receiver operating curve (AUC). Our results show that at 80 bpm TWAA was significantly higher among the ICD_Cases than the ICD_Controls (median values: 23 μ V vs. 16 μ V; $P=0.0018$), and the AUC was 0.6718. As expected, when heart rate increased to 120 bpm, TWAA also significantly ($P<0.005$) increased (median values: 36 μ V for both the ICD_Cases and ICD_Controls). However, TWAA statistical differences could no longer be observed between the two ICD groups and the AUC decreased to 0.4872. In conclusion, in our ICD populations, TWA predictive power for the occurrence of ventricular arrhythmias was higher at low heart rates when TWAA was smaller, than at fast heart rates when TWAA was higher.

Risk Stratification for Arrhythmic Sudden Cardiac Death in Heart Failure Patients using Machine Learning Techniques

George Manis, Stavros Nikolopoulos, Petros Arsenos, Konstantinos Gatzoulis, Polychronis Dilaveris, Christodoulos Stefanadis

Dept. of Computer Science, University of Ioannina
Ioannina, Greece

S32

Arrhythmic Sudden Cardiac Death (SCD) is still a major clinical challenge even though much research has been done in the field. Machine learning techniques give a powerful tool for stratifying arrhythmic risk.

We analyzed 40 Holter recordings from heart failure patients, 20 of which were characterized as high arrhythmia risk after 16 months followup. The two groups (high and low risk) were not statistically different in basic clinical characteristics (Age: 62.8 vs 70.4 years, $p=0.107$. Male gender: 17 vs 16, $p=0.686$. LVEF: 27% vs 32%, $p=0.160$. 24h mean heart rate: 77 vs 71 bpm, $p=0.088$).

Summary table

Classifier:	SVM with RBF		
	low risk	high risk	p-value
Recordings:	20	20	
Age (years):	70.4±13.3	62.8±15.6	0.107
Male gender:	16/20	17/20	0.686
LVEF(%):	32.0±10.9	27.1±10.4	0.160
Heart Rate (bpm):	71.5±8.7	77.4±11.5	0.088
Features:	27		
Observations:	3697		
Accuracy:	82.20%		
Sensitivity:	85.76%		
Specificity:	78.72%		

We performed windowed analysis and computed 27 heart rate variability (HRV) indices for non overlapping windows of size 1024 beat intervals. The metrics computed were: approximate entropy, β spectral exponent, Hurst exponent (three variations), detrended fluctuation analysis (α_1 and α_2), decorrelation time, Hjorth mobility and complexity, indices from 3D and 2D Poincaré plot, indices from spectral analysis, statistical moments, statistical and geometrical indices from the guidelines of taskforce on HRV. We fed these indices as input to a Support Vector Machine (SVM) and trained it with a radial basis function (RBF). We obtained a classification accuracy of 82.20%, sensitivity of 85,76% and specificity of 78.72%.

Deceleration Capacity Alterations before Non Sustained Ventricular Tachycardia in Post Myocardial Infarction Patients

Petros Arsenos, George Manis, Stavros Nikolopoulos, Konstantinos Gatzoulis, Polychronis Dilaveris, Christodoulos Stefanadis

S32

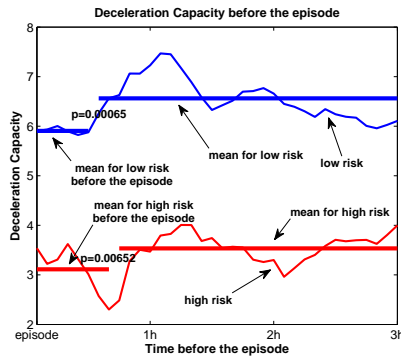
First Dept. of Cardiology, National Kapodistrian University of Athens Athens, Greece

Non Sustained Ventricular Tachycardia (NSVT) episodes are considered as electrical activity associated with increased risk of Sudden Cardiac Death (SCD). Deceleration Capacity (DC) of heart rate quantifies the inter-beat deceleration duration reflecting the parasympathetic nervous system (PNS) activity on sinus node. Experimental and clinical data indicate that PNS has a protective role for the heart against malignant arrhythmias. Impaired PNS activity reflected through decreased DC values may be of prognostic value.

We study the differences between the behavior of DC before NSVT episodes and the rest of the signal in patients suffered myocardial infarction. We study two groups of subjects that presented NSVT episodes, those (9 patients) characterized as high risk for SCD after 16 months of followup and those (11 patients) considered as low risk (Age: 72 vs 62, $p=0.035$. LVEF(%): 40.5 vs 40.9, $p=0.894$. Heart rate (bpm) 73 vs 70, $p=0.444$).

For each NSVT episode, we compare the 30 min period before the episode and the 150 min period before the first period. In the 150 min period no NSVT episodes were observed. We break these periods into overlapping windows of 20 minutes, starting from the window just before the episode and continuing by shifting the window every 5 min.

Mean values for these periods showed that DC is reduced before NSVT episodes in both high ($p=0.00652$) and low risk ($p=0.00065$) patients. DC extracted from 24 hours signal was also statistically significant for these two groups ($p=0.014$).



DC is reduced before an NSVT episode.

Noninvasive Fetal ECG: the PhysioNet/Computing in Cardiology Challenge 2013

Ikaro Silva*, Joachim Behar, Gari D Clifford, George B Moody

Massachusetts Institute of Technology
Cambridge, United States

S33

Since the late 19th century, decelerations of fetal heart rate (FHR) have been known to be associated with fetal distress. The 14th annual PhysioNet/Computing in Cardiology Challenge aims to accelerate development of accurate algorithms for locating QRS complexes and estimating the QT interval in noninvasive fetal electrocardiograms (FECGs), acquired using electrodes placed on the mother's abdomen. Unlike direct FECGs obtained using a fetal scalp electrode, noninvasive FECGs (NIFECGs) can be observed throughout the second half of pregnancy with negligible risk, but it is often difficult to detect fetal QRS complexes in NIFECGs, since maternal QRSs are usually of greater amplitude. Beyond FHR, features such as FHR variability and fetal QT interval may be useful independent indicators of fetal status. There are no accepted techniques for assessing such features from NIFECGs, however. Multiple challenge events are designed to test basic FHR estimation accuracy, as well as accuracy in measurement of inter-beat (RR) and QT intervals needed as a basis for derivation of other ECG features. Data for the challenge consist of a collection of one-minute, four-channel NIFECGs. The data were obtained from multiple sources using a variety of instrumentation with differing frequency response, resolution, and configuration.

In Phase 1 of the challenge, we provided reference annotations for 75 training records (set A), an additional 100 records (set B) for which reference annotations had been withheld, and source code for a sample entry for study.

We scored annotations for set B submitted by 50 participant-teams; 40 teams outperformed the sample entry with respect to FHR estimation, and 42 did so with respect to fetal RR interval measurement. Phase 2 of the challenge takes place over summer 2013, culminating in final evaluations of participants' entries using a hidden data set (set C).

Cancellation of the Maternal and Extraction of the Fetal ECG in Noninvasive Recordings

Ivaylo Christov*, Iana Simova, Roger Abächerli

S33

Background: Heart defects are among the most common birth defects and are the leading cause of birth defect-related deaths. Noninvasive fetal electrocardiographic (ECG) monitors have been designed but their outputs are often unreliable and difficult to interpret, resulting in increased rates of Caesarean deliveries of healthy infants. In an attempt to solve the problem a Physio-net/Computing in Cardiology announced the 2013 Challenge: Noninvasive fetal ECG.

Method: Filtering of mains interference and electromyographic (EMG) noise is inapplicable, because the fetal ECG (fECG) has very low amplitude and its frequency range is totally overlapping with the range of the noise. We created a method to indicate the presence of noise in certain segments in order to ignore them during the analysis of the fECG. The suggested method for cancellation of the maternal ECG consists of: maternal QRS detection, heart rate dependant P-QRS-T interval selection, location of the fiducial points inside this interval for best matching by cross correlation, superimposition of the intervals, calculation of the mean signal of the P-QRS-T interval, and sequential subtraction of the mean signal from the whole fECG recording. A combined lead of all the 4 channels is synthesized and fetal QRS detection is performed on it.

Results: All 100 recordings of set B were processed, the times of occurrence of the fetal QRSs were recorded and sent to the organizers of the Challenge as Entry 1. The calculated average scores are: 5051.57 for Events 1 and 4: Fetal heart rate measurement; 72.49 for Events 2 and 5: Fetal RR interval measurement. Ranking of these scores was not provided by the Organizers at the time when this Abstract was created.

Extracting R-wave Position from an FECG Record using Recognition of its Multi-channel Shapes

Filip Plešinger*, Josef Haláček, Pavel Jurák

Institute of Scientific Instruments, Academy of Sciences of the Czech Republic, Brno, Czech Republic
Brno, Czech Republic

S33

Aims: The goal of this study is to develop a method for extracting the positions of a child's R-waves from a four-channel non-invasive FECG record (according to CinC 2013 Challenge).

Methods: The method is based on eliminating the influence of the mother's heartbeats, defining the presumed multi-channel shapes of the child's R-wave and its recognition in the record. 1. Mother R-wave (MR) areas are detected within the record using thresholds of the derivative signal (processed on filtered channels, band pass 1–45 Hz). 2. The impact of the mother's heartbeats is eliminated from all channel derivations by subtracting the average shape (5 iterations) of the MR and surrounding areas from each MR shape. 3. The most probable positions of the child's R-wave (CR) are selected from areas outside the MR influence (where significant central symmetry in corrected derivations and significant axial symmetry in the original signal can be found). 4. Waveforms of all channels are detected in these positions and multi-channel CR shapes and their reliabilities are stated. 5. The whole record is tested for the presence of these multi-channel shapes and the positions of reliable CRs are stated. 6. Adjacent CRs are searched recursively. 7. Result annotations are refined with a post-processing algorithm and saved to text file. The method was programmed using the C# language. The tested FECG data series were "set A" and "set B" from CinC Challenge 2013.

Results: The success rate of this method depends heavily on the number of usable channels. However, reliable results can be generated from technically poor records. The computing time for this method is approximately 3.3 s for a one-minute record (at 1,000 Hz) processed by one core at 3GHz. The mechanism of this method allows the usage of any number of channels. Event 4 score: 395.06 Event 5 score: 10.45

Advanced Maternal ECG Removal and Noise Reduction for Application of Fetal QRS Detection

Jukka A Lipponen*, Mika P Tarvainen

University of Eastern Finland
Kuopio, Finland

S33

The fetal heart rate (fHR) have been commonly used as indirect indicators of fetal condition. Noninvasive fHR monitoring uses electrodes placed on the mother's abdomen. However it is challenging to detect fetal QRS (fQRS) complexes from the signals measured in this way. In this paper we introduce an augmented multi-lead principal component regression (PCR) approach for maternal ECG removal and multichannel correlation based fHR detector. In the multi-lead PCR approach, P-,T-waves and QRS-complexes of all four leads are segmented based on maternal R-peaks and collected into augmented observation matrices. Hence, the QRS-complex matrix, for example, contains complexes from all four leads. Maternal ECG waveforms are then modeled using six most significant eigenvectors of augmented correlation matrices and removed from all four leads. After the maternal ECG is removed to improve the signal-to-noise ratio linear combinations of the four leads are computed. The noise levels of all channels are then estimated and equalized using an envelope detector. The fQRS complexes are then detected using a multi-lead template matching technique. First, fQRS templates for all channels are constructed by detecting strongest peaks from regions with minimum noise level (acquired from the envelope). The cross-correlations between the fQRS templates and the ECG channels are then computed and a resultant correlation time series showing fQRS occurrence times is formed. The fQRS times are then detected using normal QRS detection algorithm. In the PCR model, prior information of the shape of ECG waveforms is maximized by using augmented observation matrices which contains waves from all leads. The shapes of the maternal ECG waves are thus well modeled and maternal ECG can be removed successfully. The envelope detector gives good approximation of the noise level and signal periods with less noise can be weighted more. Challenge score for event 4 was 72.16 and event 5 2.13.

A Novel Algorithm for Fetal QRS Detection in Abdominal ECG Recordings

Andrea Fanelli*, Giovanni Magenes, Maria Gabriella Signorini

The 14th annual Physionet/CinC challenge for 2013 proposes the problem of developing and testing automated algorithms for fetal QRS detection in non-invasive FECG signals. For this purpose, a new algorithm for fetal QRS detection in abdominal recordings is presented. The algorithm is based on a first phase of signal preprocessing, organized in 3 steps: (i) signal resampling, (ii) pass-band filtering and (iii) baseline wander removal. Subsequently the algorithm detects maternal QRS on the abdominal lead characterized by the highest variability, which is quantified through a simple regularity parameter. Subsequently, maternal QRS are detected through a template matching approach. Maternal QRS are then subtracted from each abdominal lead, in order to obtain FECG signals. This is accomplished by constructing a maternal QRS template as adaptive average of ten subsequent maternal QRS. The template is subtracted from the current maternal QRS after the multiplication of the template by a constant, which minimizes the least mean square difference between the template and the current QRS. This allows extracting one FECG signal per lead. Fetal QRS detection is then accomplished on each extracted FECG signal, through the same template matching approach employed for maternal QRS detection. Finally, a novel quality parameter allows identifying the most reliable fetal QRS detection among the different leads. The algorithm was tested on open test set B (composed of one hundred 60-seconds abdominal ECG recordings) for events 4 and 5 of the 2013 PhysioNet Challenge. The algorithm scored 860.62 for event 4, which is approximately 75% better than the average score of the sample submission (3258.56) (the lower the score the better). The algorithm scored 25.00 for event 5 (75% better than the average score of the sample submission, 102.75). The results suggest the novel developed algorithm presents a valid approach to detect fetal QRS in abdominal ECG data.

S33

Fetal QRS Detection and RR Interval Measurement in Noninvasively Registered Abdominal ECGs

C Maier, H Dickhaus

Heidelberg University
Heidelberg, Germany

S33

Background: This contribution relates to the CinC Challenge 2013 on noninvasive fetal ECG analysis. The aim is to detect fetal QRS complexes and derive fetal RR intervals in ECGs registered from the expectant mother's abdomen.

Methods: Our approach follows the 'classic' sequence signal preprocessing, maternal QRS detection and maternal PQRST cancellation. A final three-step-process identifies fetal QRS complexes in the residual signal.

Preprocessing for each channel includes high-pass-filtering (median, 151ms) and power-line notch-filtering. After maternal QRS detection, an average PQRST template is RR-adjusted and subtracted from the ECG at each QRS position. Moreover, the first three principal components of the PQRST residuals are eliminated to suppress remaining physiological PQRST variability. A final median high-pass-filter (width 51ms) provides a signal dominated by the fetal QRS's.

To locate fetal QRS candidates, a 'matched' filtering process is performed in each channel. The impulse response consists of 10 triangular pulses of 50ms width. Their interspacing varies iteratively over the range of expected fetal interevent-intervals (280ms-660ms in steps of 1ms). For each 1s-segment of the signal, the filter output providing the maximum energy is selected and fetal QRS candidates are assumed at the positions of the output maxima. Moreover, the filter output energy is used to estimate the SNR.

Finally, the QRS positions are refined on a detection signal (DS) derived by weighted combination of the four available channels according to the estimated SNR. A triangular window (width 50ms) is placed at each candidate position and multiplied with the DS. The final QRS position is assumed at the center of gravity of the windowed DS.

Results: On data set B, our entry received average scores of 64.97 for event 4 and 5.77 for event 5.

Conclusion: For acceptable SNRs, noninvasive fetal QRS detection seems possible using conventional signal processing techniques. A key in our approach is the 'matched' filter which robustly identifies the average local fetal heart rate and QRS candidate positions under non-arrhythmic conditions.

Noninvasive Fetal QRS Detection Using Linear Combination of Abdomen ECG Signals

Or Perlman*, Amos Katz, Yaniv Zigel

Ben Gurion University of the Negev, Israel

S33

Background: The fetal ECG may serve as a tool for fetal distress detection. However, the abdominal ECG (AECG) of a pregnant woman contains mainly the maternal ECG and a relatively small amplitude fetal ECG signal, contaminated by various noises. As part of the 2013 PhysioNet/CinC Challenge, this study aimed to develop an algorithm for noninvasive fetal QRS (fQRS) detection. The proposed algorithm is mainly based on fetal ECG source signal enhancement using a modified linear combiner.

Methods: *Filtering and fQRS candidates detection:* After noise reduction, the maternal QRS (mQRS) complexes are detected. Then, 10-49.5 Hz band pass filtering is performed (the signal in Figure 1.a) and peaks between each two subsequent mQRS complexes (from all 4 AECG leads) are considered as fQRS candidates. *Modified linear combiner:* For each candidate, a Gaussian-like synthetic fQRS signal is created (Figure 1.b). This signal is considered as an observation signal for the modified linear combiner. The 4 filtered AECG signals then undergo maternal ECG cancellation and serve as reference signals in this linear combiner; hence by finding the appropriate weight coefficients, their linear combination (that is actually the enhanced fQRS source signal f_e) is forced to minimize the error between f_e and the observation signal. The peaks in f_e that are higher than a predefined threshold are located and determined as fQRS complexes (Figure 1.c). *Post-processing:* The fetal heart-rate is calculated and used for fQRS outliers rejection.

Results: The method was developed using the entire 75 1-minute-long AECG training set, and its evaluation on the test set led to scores of 541.41 for event 4 (fetal heart rate measurement) and 26.73 for event 5 (fetal RR interval measurement).

Conclusions: The proposed method has the potential to constitute an effective tool for fetal heart rate and RR interval extraction and measurement.

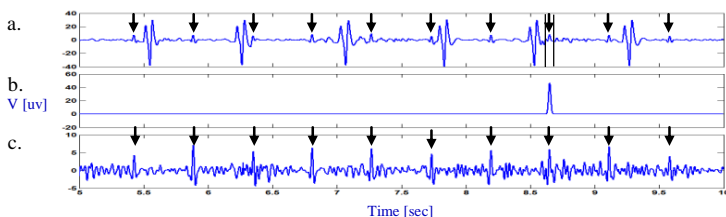


Fig 1. a. Filtered AECG (lead #1), the two vertical lines mark an fQRS candidate. The arrows indicate the true fQRS complexes. b. The synthetic signal. c. The enhanced fQRS signal (f_e), the arrows indicate the detected fQRS complexes.

Fetal ECG Extraction From Abdominal Recordings using Array Signal Processing

Masoumeh Haghpahani*, David A Borkholder

Rochester Institute of Technology
United States

S33

Motivation: Despite huge interest in noninvasive monitoring and processing of fetal ECG (fECG) signals, reliable measurement of fECG signals has remained to be a challenging task; this is largely due to the contamination of such recordings with mother ECG (mECG), mother and fetus myographic signals and other movement artifacts. The aim of this year's PhysioNet/CinC Challenge was to develop accurate algorithms for locating QRS complexes in noninvasive fECG signals obtained by a set of four electrodes placed on the mother's abdomen.

Methods: Our method consisted of two steps: separation of the desired fECG signals from the noisy electrode recordings and performing peak detection on fECG signals. In the fECG extraction step, data preprocessing was performed at first to fill in missing values and remove non-cardiac interferences. A series of semi-blind decomposition, denoising (through the use of extended Kalman filtering) and back-projection were then applied iteratively to the electrode recordings until the mECG signals were removed from the measurements. The resulting fECG signals from the four electrode measurements were next divided into chunks of 2-second intervals. At each time interval, signals that passed a series of time and frequency qualification tests were fused using weighted averaging to generate a single fECG signal with a higher signal to noise ratio than each individual recording. Fetal QRS complexes were then detected for the fused signal using a matched filter algorithm.

Results: We achieved a score of 99.34 in event 4 for the fetal heart rate measurement, and a score of 6.39 in event 5 for the RR interval measurement. The average performances for these two events were reported to be 3258.56 and 102.75, respectively.

Advanced Signal Processing Techniques for Fetal ECG Analysis

Jakub Kuzilek*, Lenka Lhotska

FEE, CTU in Prague
Prague, Czech Republic

S33

In response to the PhysioNet/CinC Challenge 2013: Noninvasive Fetal ECG we developed the algorithm for fetal QRS (fQRS) positions estimation based on set of classical filters, which enhances the fetal ECG, combined with robust QRS detection technique based on Christov's beat detection algorithm. These steps enable us to reduce maternal ECG (mECG) recording efficiently. In order to extract fetal QRS complexes we used BSS/JADE algorithm, which is based on joint diagonalization of cross-cumulant matrices. The fQRS complexes is then identified using set of features computed for each candidate fQRS detected in second step of beat detection applied on preprocessed recording. Misdetection of fQRS is solved by back search procedure with lowered thresholds for QRS detection algorithm. This set of features contains basic statistical measures such as mean, standard deviation, etc. but also contains several features such as information entropy. We used CART algorithm for discriminating of falsely detected candidates from set of detected fQRS. The preliminary results of our method are 616.84 for Events 1 and 4 and 35.19 for Events 2 and 5. The originally proposed method has scores 3258.56, 102.75 respectively.

Fetal QRS Complex Detection using Semi-blind Source Separation Framework

Fatemeh Razavipour*, Reza sameni, Marzieh Fatemi

Iran (Islamic Republic of)

S33

Fetal heart rate (FHR) variability is one of the valuable features of fetal electrocardiography that could be useful to obtain reliable information about the fetal heart activity. In noninvasive systems, the major obstacle for the accurate detection of the fetal QRS (fQRS) complex is the presence of abdominal noise and the maternal ECG (mECG). In this study, we propose a method to remove the mECG and other abdominal interferences to improve the detection of fQRS complexes.

Methods: In order to improve the signal to noise ratio and to reduce susceptibility to noise, the noninvasive recordings are processed at different stages. First, the multichannel signals are band-pass filtered to remove out of band noise. Next, a semi-blind source separation (SBSS) technique was applied to find the mECG sources. These sources are next ranked automatically to determine the maternal channel reference and their mECG R-peaks. Using the peaks, the maternal artifacts are reduced from the signals using the quasi-periodicity of cardiac activities. The fetal ECG is estimated by applying a secondary SBSS stage to the residue of the previous stage. Another channel selection technique, based on a measure of variance, is applied to the channels to rank the channels according to their resemblance with the fetal ECG. The channel most resembling the fQRS is finally used in the peak detection algorithm for finding the fQRS complexes.

Results: The procedure was applied to the CinC challenge 2013 dataset B, which consists of 100 noninvasive signals containing the mECG, fECG, and some abdominal noises. The FHR (Entry 4) and RR interval (Entry 5) time series was calculated respectively with obtained average scores 1879.78 and 63.05.

Conclusion: This study and other relative research present the good ability of the here by employed SBSS framework for the step-wise cancellation of the mECG, noises, and fQRS detection.

Fetal QRS Complex Detection Based on Three-Way Tensor Decomposition

Mohammad Niknazar, Bertrand Rivet, and Christian Jutten

GIPSA-lab (UMR CNRS 5216) - University of Grenoble
Grenoble, France

S33

This study is focused on detection of fetal QRS complexes in multichannel ECG signals recorded from mother's abdomen, containing both fetal and maternal ECGs. Assuming different values for maternal and fetal heart rates, the proposed method relies on a deterministic tensor decomposition method, which aims at deterministic blind separation of sources having different symbol rates. In the ECG context, due to the quasi-periodic nature of ECG signal, maternal ECG R-peaks are firstly detected from the mixture to identify maternal beats as maternal ECG symbols. Then the maternal ECG beats are stacked into a three-dimensional array. Decomposition of this tensor yields three loading matrices that are now used to reconstruct the maternal ECG. The residue of subtraction of the maternal ECG estimate from the original mixture is then used to detect fetal QRS complexes. The obtained average scores of event 4 and 5 on the set B of Physionet Challenge 2013 data are 1514.59 and 57.01, respectively.

Fetal Electrocardiogram R-peak Detection using Robust Tensor Decomposition and Extended Kalman Filtering

Mahsa Akhbari, Mohammad Niknazar, Christian Jutten, Mohammad B. Shamsollahi, and Bertrand Rivet

S33

GIPSA-lab, University of Grenoble, Grenoble, France
BiSIPL, Sharif University of Technology, Tehran, Iran

In this paper, we propose an efficient method for R-peak detection in non-invasive fetal electrocardiogram (ECG) signals which are acquired from multiple electrodes on mother's abdomen. The proposed method is performed in two steps: first, we employ a robust tensor decomposition-based method for fetal ECG extraction from mixtures of fetal and maternal ECG; then a method based on Extended Kalman Filter (EKF) is used for fetal R-peak detection. In order to obtain a rough estimate of fetal ECG, a weighted tensor decomposition method is utilized to capture weak traces of fetal ECG mixed with maternal ECG and noise. In this method, it is assumed that maternal and fetal heart rate values are different. After fetal ECG extraction, a previously introduced non-linear dynamic model for generation of synthetic ECG signals is adopted and modified such that each ECG wave (P, QRS and T) has a separate state in the EKF formulation. Each parameter of the Gaussian functions used for modeling each ECG wave is considered as a simple auto-regressive (AR) model and estimated via the EKF. The results show that the proposed method is efficiently able to estimate the location of peak, onset and offset of all fetal ECG waves. Average score of our proposed method for the PhysioNet 2013 Challenge on set B from entry 1 are 1326.21 and 45.06 for event 4 and 5 respectively which are better than average score for sample submission `physionet2013.m` (available at PhysioNet) on set B which were 3258.56 and 102.75 for event 4 and 5 respectively.

Maternal signal estimation by Kalman Filtering and Template Adaptation for fetal heart rate extraction

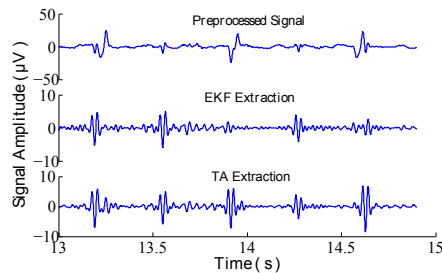
Fernando Andreotti, Maik Riedl, Tilo Himmelsbach, Daniel Wedekind, Sebastian Zaunseder, Niels Wessel, Hagen Malberg

Dresden University of Technology
Dresden, Germany

S33

The fetal electrocardiogram derived from abdominal leads provides a mean to monitor the fetal heart rate (fHR) noninvasively. Limitations arise from the low signal-to-noise ratio of the fetal component in the abdominal leads. To obtain the fHR, processing methods are pursued which usually consist of three stages: preprocessing, extraction of the fetal signal and fetal QRS detection. Concerning the extraction of the fetal signal, i.e. maternal ECG cancellation, template subtraction techniques are widely used. Previous own works revealed that the extraction can be altered depending on the template's creation.

This contribution exploits the varying behaviors by combining the outputs of two approaches, namely Extended Kalman Filter (EKF) and Template Adaptation (TA), to obtain estimates for the maternal interference. The extraction procedure consists of four stages: preprocessing (band-pass and power line filtering), multichannel maternal QRS detection, extraction of fetal signal (subtraction of maternal estimate) and multichannel fetal QRS fusion.



Exemplary extraction process

For set-A each technique was solely applied (as in the figure) and its average sensitivity (SE) and positive predictive value (PPV) determined (according to ANSI/AAMI EC57 - 50 ms acceptance interval). The EKF-based approach resulted in 86.3% SE and 88.0% PPV. Meanwhile, the TA approach resulted in 87.2% and 89.1%. The combination of both methods yielded 89.7% and 90.0%. In terms of challenge scores, for set-A the combined algorithm obtained an average score of 211.09 (event 4) and 13.63 (event 5). Even better results were obtained for set-B: 122.98 (event 4) and 9.48 (event 5). Compared to the reference scores - 3258.56 (event 4) and 102.75 (event 5) - an improvement of 96.2% and 90.8% was achieved.

The Physionet / Computing in Cardiology Challenge 2013: Detection of fetal heart-rate and fetal RR interval from Fetal Electrocardiogram signals

Srinivasan Vairavan*, Syed Haider, Eric Carlson, Minnan Xu, Saeed Babaeizadeh

S33

Philips Research
Briarcliff Manor, United States

Fetal Electrocardiography (fECG) is one of the established non-invasive methods of recording fetal cardiac activity using electrodes placed over the maternal abdomen. However, the analysis of fECG is still in its infancy because of the difficulties in separating the fetal cardiac signal from interference. In order to detect fetal heart-rate (fHR) from fECG with improved accuracy, we use a modified version of Extended Kalman filter (EKF) based fetal cardiac signal extraction (Sameni et al, 2005). To this end, we use two different techniques to detect the fHR. The first technique is based on a template matching using adaptive threshold (TMAT) and the second technique is real-time QRS detector (RTQ). Both these techniques are evaluated on training set A containing 75 fECG records provided by Physionet as a part of the 2013 challenge. These records have the exact location of the fetal R wave identified using the fetal scalp electrode and it serves as the gold standard. The scoring metric for HR detection (Event 4) is the mean square error between the HR generated by the proposed techniques and the reference HR provided by the gold standard and the scoring metric for RR interval detection (Event 5) is based on the ANSI EC38:1998 standard. TMAT outperformed RTQ and its average scores for set A are 1450 and 44 for Events 4 and 5 respectively. TMAT was further validated on a new dataset, set B containing 100 fECG records and the average scores are 1319 and 38 for Events 4 and 5 respectively. As a reference, Physionet provided a technique (Martens et al, 2007) which achieved average scores of 3258 and 102 for both events in the validation dataset. Based on the validation results, TMAT is better than the reference technique and could be a robust approach in detecting fHR from fECG.

A Sequential Multiscale Bayesian Tracker for Maternal ECG Removal in Non-invasive Fetal ECG Recordings

Guojun Li, Xiaoping Zeng, Xiaona Zhou

Chongqing University, Chongqing Communication Institute
Chongqing, China

S33

Motivation: The location of QRS complexes in the fetal ECG (FECG) recorded on the maternal abdominal wall (non-invasive FECG) is generally faced with a serious interference, namely the maternal ECG (MECG). The MECG usually possesses a high amplitude many times exceeding the level of FECG and the spectra of both ECG signals overlap. Thus, existing methods often attenuate the FECG in suppressing the MECG. This study aimed to cancel the MECG while preserving the FECG, in order to enable the location of fetal QRS complexes.

Methodology: The accurate MECG suppression for the non-invasive FECG signal is usually confronted with a contradiction. For one thing, the temporal variations of MECG waveform requires a strong tracker to account for beat-to-beat variability. For another, an improved tracking performance of MECG entails an increased risk that the FECG signal could be tracked out. Thus, existing Bayesian trackers constitute a tradeoff between improvement of MECG subtraction and attenuation of FECG. In this study, the differences in scale characteristics between the maternal and fetal QRS complexes, as new a priori information, were incorporated into the traditional Bayesian filtering framework, where only temporal features of MECG were considered. Thus, a novel time-scale domain filtering algorithm, named sequential multi-scale extended Kalman smoother (SMEKS) was proposed to accurately separate the MECG from the FECG, even in the case of coincidence of fetal and maternal QRS complexes.

Results: With this method, our initial scores for the PhysioNet 2013 Challenge on set B were 666.52 for fetal heart rate measurement and 38.55 for fetal RR interval measurement. Experiments on both synthetic data and realistic data show that our method outperforms the other Bayesian trackers in the MECG suppression.

Conclusion: The proposed SMEKS tracker incorporating the temporal and scale information of MECG signal is fit to discriminate the MECG from the FECG.

2013 PhysioNet Challenge: A Markov Chain Monte Carlo Approach to Locating Features in Noninvasive Fetal ECG Signals

Tom Pollard*, Jack Carlyle, Jamie Jasinski, Alice Foster, Matthew Hills, Kirthika Narasimhan, Emma Gale, David Williams

S33

University College London
Dorking, United Kingdom

Aims: Identifying fetal features within an ECG obtained from a mother's abdomen has been difficult to accurately achieve. If a reliable technique could be developed, problems such as fetal hypoxia might be identified earlier. We aim to develop an algorithm which can reliably identify the fetal contributions to the combined maternal-fetal ECG.

Methods: Our approach is to model and subtract the maternal ECG signal from the combined signal using a Markov Chain Monte Carlo (MCMC) method. The MCMC method is applied with considerable success to a similar problem in astrophysics, where exoplanets are identified through features in the light-curve of the parent star.

Results: A provisional algorithm was submitted to the 2013 PhysioNet Challenge, which received an Event 4 score of 3637.92 and an Event 5 score of 219.84 on Test Set B. For reference, the sample algorithm received an Event 4 score of 3258.56 and an Event 5 score of 102.75 for the same dataset. Lower scores in the challenge indicate more accurate identification of the target features.

Conclusion: We are optimising the MCMC algorithm through better constraints on the initial parameter space for modelling the maternal signal. We hope to develop a robust method of noninvasive fetal ECG characterisation based on this approach.

Fetal Electrocardiogram QRS Detection Using Ensemble Empirical Mode Decomposition and Normalized Correlation Coefficient

Paschalis Bizopoulos*, Evaggelos Karvounis, Dimitrios Tsalikakis, Dimitrios Koutsouris, Dimitrios Fotiadis

Biomedical Engineering Laboratory, School of Electrical and Computer Engineering, National Technical University of Athens Athens, GreeceGreece

S33

The fetal heart rate (fHR) can be derived from the abdominal electrocardiogram (abdECG) acquired from skin electrodes placed on the abdomen of the pregnant woman. In that framework, a novel three-stage method for the detection of fHR from multivariate abdECG recordings is presented. In the first stage, the maternal QRS complexes are detected and eliminated from the abdECG recordings. The process is based on the Ensemble Empirical Mode Decomposition (EEMD) that is employed for removing the baseline wander and the Electromyogram (EMG) related noise by rejecting the Intrinsic Mode Functions (IMFs) which primarily contain frequencies related to baseline wander and EMG. In the second stage, the change of the RR Interval (RRI) shape is used as a feature for evaluating possible QRS series and the physiological threshold which is connected to RRI does not exceed 150 millisecond. A measure of similarity of the signal around QRSs, using the Template Matching and Normalized Correlation Coefficient (NCC), is also used to evaluate individual QRSs related to the average template of the selected series. The feature space is constructed using the RRI and the individual NCC (iNCC) of QRSs. The Euclidean distance between each feature and the point of reference (RRR=0, iNCC=1) is used for select the channel, and for feature insertion and rejection. The maternal PQRST complexes (P-wave, QRS complex, T-wave) are eliminated from the abdECG recordings using the RR Intervals and correlation techniques. The extraction of the fHR is accomplished in the third stage, using the first two stages. The method was evaluated on real multichannel abdominal ECG signals from the Physionet database, by CINC reviewers, with results that indicate promising performance; the average score of the test set B for event 4 was 320.45 and for event 5 was 13.85.

A Robust Framework for Noninvasive Extraction of Fetal Electrocardiogram Signal

Marzieh Fatemi

Biomedical Engineering, Shiraz University, Shiraz, Iran
(Email: marziehfatemi@gmail.com)

S33

Aims: Noninvasive extraction of fetal electrocardiogram (fECG) from multichannel maternal abdomen recordings is an emerging technology used for fetal cardiac diagnosis. A well-known technique for extraction of fECG is *Independent Component Analysis* (ICA). However, basic limitations in conventional ICA are statistical independence of the sources and equal number of sources and sensors. Moreover, its performance degrades for distributed sources and in presence of full-rank Gaussian noise.

Method: In this work, we have presented a robust framework that can deal with fECG extraction problems even in the case that ICA assumptions are not satisfied. This method consists of the set of algorithms for signal subspace extraction, iterative multichannel subspace decomposition based denoising and Bayesian filtering. The suitable combination of these effective methods, introduced in recent literatures, gathers advantages of multichannel and single channel model based adaptive filtering. The proposed framework has also exploited the benefits of both temporal and statistical properties of the ECG signals. Moreover, ranking property of these algorithms, in comparison to permutation ambiguity of the ICA methods, helps reliable automatic detection of fECG signal in long last recordings.

Result: The algorithm is tested over 100 different maternal abdomen ECG signals to find QRS complex and RR interval of the fECG signal. The data set consists of four channels one minute signals, taken from the physioNet challenge, with high level noise and full rank maternal ECG interference and somehow correlated channels. The proposed framework leads to 541.40 score on fetal QRS detection and 22.25 score for RR interval detection that is very good in comparison to the reference scores of 3258.56 and 102.75 respectively.

Conclusion: The results have shown that the proposed frame can work effectively in the presence of the full rank maternal interference in both low and high *Signal to Interference and Noise Ratio* (SINR) scenarios.

Noninvasive Fetal QRS Detection using Echo State Network

Mantas Lukoševičius*, Vaidotas Marozas

Kaunas University of Technology
Kaunas, Lithuania

S33

Aim: The aim of this work is to develop an accurate algorithm for locating QRS complexes of fetus in noninvasive fetal ECG signals recorded on mother's abdomen.

Method: The proposed method combines established cardiology-specific techniques based more on domain knowledge with powerful supervised general-purpose machine learning approaches that are more data-driven. After filtering and normalization, maternal QRS complexes are detected and averaged maternal ECG is removed. The key task of detecting fetal QRS complexes is performed by an Echo State recurrent neural Network (ESN) trained by supervised machine learning. The training of the model is made possible by the availability of correctly annotated training data. Finally, fetal QRS annotations are obtained by a statistics-based dynamic programming approach interpreting the outputs of the ESN. The approach is capable of detecting fetal QRS complexes in high quality signals directly, without the need of recognizing and removing maternal ECG first, but this step significantly improves performance in most cases. Since the data is rarely perfect, it also helps to take special provisions to ensure that the model is only trained on correct annotations.

Results: The algorithm participates in "Noninvasive Fetal ECG: the PhysioNet/Computing in Cardiology Challenge 2013" announced in www.physionet.org. It was developed and trained using a dataset A (25+50 records) provided by the organizers. The method has been independently evaluated by the organizers on another dataset B (100 records) for which the correct annotations were not given. The preliminary average error scores obtained are: 109.56 for the fetal heart rate measurement (event 1/4) and 9.04 for fetal RR interval measurement (event 2/5). The scores of the provided baseline algorithm are 3258.56 and 102.75, respectively.

Conclusion: The proposed ESN-based algorithm shows a very promising performance in noninvasive fetal QRS detection compared to the baseline.

Peripheral Blood Volume Changes in Response to Ventricular Premature Beats During Dialysis

Eglé Grigonyté*, Eduardo Gil, Pablo Laguna, Leif Sörnmo

Lund University, Lund, Sweden

S34

Introduction. Patients treated with dialysis often suffer from cardiovascular disorders and uremic neuropathy. This leads to homeostatic imbalance, which may result in intradialytic hypotension. Ventricular premature beats (VPBs) can be viewed as an internal disturbance which increases the imbalance through instantaneous blood pressure drop and prolonged tissue deoxygenation due to a cardiac compensatory pause.

Aims. Our study aims at employing VPB-induced peripheral blood volume changes from photoplethysmographic (PPG) recordings in order to characterize physiological recovery to an “original” circulatory state.

Materials. PPG data acquired during dialysis from 10 patients, with a total of 22 treatments, were analyzed. 5 patients, with 12 treatments, qualified for further analysis once the following two criteria were fulfilled: the absence of other VPBs around the analysed VPB, and the amount of VPBs satisfying the previous criterion (>10 per treatment).

Methods. A new approach to PPG signal analysis was studied. After preprocessing of the PPG, the pulse upslope amplitude was evaluated on a peak-to-peak basis in the pulsatile PPG intervals preceding and following a VPB. Cumulative, normalized post-VPB amplitudes were used to track variation in ratio of averaged amplitude values corresponding to normal pulses that surround VPB.

Results. During treatments with hypotensive symptoms, the initial drop in peripheral blood volume after a VPB was found to be 18-24% followed by a slow recovery period lasting for more than 20 pulses. On the contrary, a smaller drop in peripheral blood volume (5–16%) and faster recovery to initial conditions (~ 10 pulses) were observed in asymptomatic dialysis treatments.

Conclusion. We propose a new indicator to differentiate between normal dialysis treatments and those at risk of hypotension, based on relative peripheral blood volume changes caused by a VPB.

Modeling of the Oxygen Saturation Pattern for Detecting Anomalies During Clinical Interventions

Diego Martín*, Pablo Casaseca, Marcos Martín, Carlos Alberola

Laboratory of Image Processing. Universidad de Valladolid
Valladolid, Spain

S34

Aims: This study is aimed at detecting in real time the anomalies that the oxygen saturation (SaO_2) pattern suffers during a clinical intervention. This approach circumvents most of the drawbacks associated to the use of SaO_2 ; specifically, (a) the interpretation of readings is far simpler since a measure of deviation from the reference pattern is given; (b) the well-known biases inherent to this technique are avoided as a consequence of using the data so affected in the reference patterns; (c) the index on which the classifier is based does not require long signal records, so it is amenable for real time analysis.

Methods: A two-stages methodology is proposed. During the first stage, the reference patterns – based on a simplified Markov Models (sMM) of the signal acquired from the patient before the beginning of the intervention– and the testing patterns –the sMMs of the windows to be tested– are extracted. In the second stage, the similarity between both patterns is assessed through the Williams' Index (WI), which uses the Kullback-Leibler divergence metric as the agreement measurement. The classification task mainly consists of comparing the WI with the threshold 1.0: the pattern of the testing window is normal for $WI \geq 1.0$, and abnormal otherwise.

Results: Four experiments that emulate situations in which the respiratory function is altered have been undertaken: (1) shortening the breath, (2) interrupting the breath, (3) hyperventilation and (4) CO_2 increase in blood. For the experiments (1) and (2), the anomalous patterns have been detected one minute after the beginning of the impairment, whereas for the experiments (3) and (4) the anomalies were detected immediately. These results were as expected, since the effects of the procedures carried out for the first two experiments are not immediate. The last two experiments have also shown the appropriate behavior of the proposal during the recovery intervals, since the WI increases along time to reach values greater than 1.0 when the respiratory function is actually recovered.

Conclusion: The proposal here presented is sensitive to some situations in which the respiratory function is impaired, even when the way the impairment is reflected in the SaO_2 signals is not evident by direct visual inspection.

Determining Heart Activity Present in the Pressure Sensors of a Dialysis Machine

Mattias Holmer*, Eglé Grigonyté, Frida Sandberg, Kristian Solem, Bo Olde, Leif Sörnmo

Lund University
Lund, Sweden

S34

Introduction: Patients with renal failure usually have problems with the cardiovascular system. Determination of heart status during dialysis can improve patient monitoring. Heart pressure pulses propagate in the body and enter the extracorporeal blood circuit of the dialysis machine, where the pressure sensors capture them. A peristaltic blood pump, located in the same circuit, introduces strong periodic pressure pulses that interfere with much weaker cardiac component. Additionally, the pump rate may overlap with the heart rate. These signal characteristics make the extraction of the heart signal challenging. In the present study, we explore the possibility to extract and analyze the cardiac component by using artificial signals.

Methods: The artificial signal was built from three components: Pump, heart and noise. The pump component was based on pressure recordings from the dialysis machine without any heart signal present. The shape of the heart pulsations was based on clinical data. A modified integral pulse frequency modulation (IPFM) model was used to account for variability in heart rate. The pump component was estimated based on information contained in the artificial signal. Using a least squares criterion, the resulting pump component was scaled to match the observed signal so that estimates of the heartbeat occurrence times can be produced.

Results: The estimates of the occurrence times were compared with the occurrence times from the simulated heart component. The results showed that the timing of each heart pulse can be determined with an accuracy of about 2 ms when the heart-to-pump amplitude ratio is 50%, 4 ms at 20%, and 25 ms at 5 %.

Conclusions: The extracorporeal sensors of a dialysis machine can be used for monitoring the status of the patient's heart. Timing information can be determined accurately when the heart-to-pump amplitude ratio is large enough.

Empirical Mode Decomposition Based Real-Time Blood Pressure Delineation and Quality Assessment

Vladimir Ostojic, Tatjana Loncar-Turukalo, Dragana Bajic

Faculty of Technical Sciences, University of Novi Sad
Novi Sad, Serbia

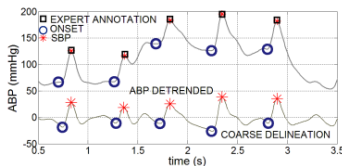
S34

INTRODUCTION: Noise and artifacts compromise the fidelity of arterial blood pressure (ABP) waveform, resulting in unreliable parameter estimation and high false alarm rate, both in intensive care and home-health monitoring solutions. This study proposes empirical mode decomposition (EMD) based algorithm that integrates real-time ABP delineation and quality assessment. The data-driven decomposition ensures patient-specific adjustments. Adaptive EMD detrending procedure, combined with short-term memory parameter tracking, solves the problem of abrupt waveform morphology changes.

METHODS: Ensemble Empirical Mode Decomposition (EEMD) was used to decompose ABP signal into intrinsic mode functions (IMFs) based on characteristic local time scales. EEMD decomposition was done on fixed number of IMFs with 10 iterations in sifting process, minimizing computational time and memory usage. Adaptive, data-dependent threshold strategy for ABP delineation was applied on sum of first four IMFs resulting in coarse ABP parameterization with minimal computational effort. The fine parameter adjustment was done in corresponding time-windows of original signal. The final correction procedure implied adaptive amplitude and time position tests. In real-time application the signal was processed in windows of 4 seconds, using sliding window approach with 0.8s overlap. The overlap served as guard band providing for EEMD edge effects. The signal quality was constantly monitored by inspection of the first two IMFs for high frequency and impulse artifact detection, whereas saturation and reduced pulse pressure artifacts were identified straightforwardly.

RESULTS: Algorithm was validated on an annotated public database of human ABP signals sampled at 125Hz consisting of 13079 beats. The algorithm achieved sensitivity of 99.79% and positive predictivity of 99.75% in systolic BP estimation without exclusion of segments with compromised

quality. In real-time scenario processing of 4s ABP window in Matlab took in average 0.66s. The frequency band separation of IMFs proved as relevant feature for selective artifacts detection on the most affected IMF.



An example of ABP delineation during a change in ABP mean level

Detection of Glaucoma based on the Analysis of Cardiovascular Signals

Andreas Voss*, Katharina Witt, Eva Koch, Matthias Fuest, Niklas Plange

University of Applied Sciences Jena
Jena, Germany

S34

Previous studies have shown that vascular risk factors are relevant in the pathogenesis of glaucomatous optic neuropathy. Especially vascular dysfunctions seem to play an important role in the development of glaucoma. Therefore, the aim of this study was to characterize the cardiovascular regulation by analyzing heart rate (HRV), blood pressure variability (BPV) and the coupling between these signals in patients with glaucoma (GC) and healthy controls (CON). From 19 GC and 10 age-matched CON, the 30min ECG and continuous blood pressure were recorded. The time series of heart rate, systolic and diastolic blood pressure were extracted and analyzed applying univariate linear methods of HRV / BPV (Task Force time and frequency domain) and nonlinear uni- and bivariate methods (symbolic dynamics (SD) and joint symbolic dynamics (JSD)). The index $plvar2_Dia$ of SD (measure of lower variability) revealed high significant differences between GC (0.23 ± 0.16) and CON (0.67 ± 0.24) leading to a sensitivity of 90% and specificity of 80%. The combination of this parameter $plvar2_Dia$ with SP101 (sum of the measures of couplings between systolic blood pressure and HRV; GC: 0.14 ± 0.03 , CON: 0.08 ± 0.04) led to an increased specificity of 90% while the sensitivity was maintained at 90%. Linear HRV and BPV indices could not discriminate between GC and CON. Especially uni- and bivariate nonlinear parameters from the symbolic dynamics were able to characterize the diastolic blood pressure and the coupling between heart rate and systolic blood pressure and separated the GC and CON. These changes in short term blood pressure regulation patterns and the coupling with heart rate are a sign of a vascular dysfunction. Therefore, this method might contribute to an improved and preterm diagnosis of glaucoma.

Waving at the Heart: Implementation of a Kinect based Real-time Interactive Control System for Viewing Cineangiogram Loops During Cardiac Catheterization Procedures

Bart Suelze, Robin Agten, Philippe B Bertrand, Thijs Vandenryt, Peter Dedrij, Ronald Thoelen, Pieter Vandervoort, Lars Grieten*

Hasselt University
Genk, Belgium

S34

Introduction: Combining human gestures and voice commands may provide an interesting solution for human interaction with high tech clinical equipment. As proof of concept we focused on the setting of the cardiac catheterization laboratory where during an invasive cardiac procedure there are many interactions required to scroll between fluoroscopic cine-recordings and between frames within one recording in order to visualize and locate coronary artery lesions. As the cardiologist is draped with sterile clothing, he has to rely on an assisting nurse to review the recorded cineloops.

Aim: The aim of this study was to build an interface allowing the cardiologist to view and review during the procedure all recorded fluoroscopic cineloops without the need for an assisting person.

Methods: The new Kinect for Windows was used to create a multilayer application with a front-end that captures gestures and audio commands. A second layer developed in .NET and c# language was used to analyze the body gestures and voice commands. The back-end layer was developed to allow easy interfacing with the software and triggering actions.

Results: Programmed gesture-software interactions were 'play', 'stop', 'next/previous image' and 'next/previous frame' when images were frozen. All commands were based on single arm movements to limit interference with invasive procedures. In addition, actions could also be triggered using voice commands when immobilized. In all situations there was a good skeletal capture, gesture recognition and the application resulted in an improved procedural efficiency with more freedom for the cardiologist and a lower burden on the assisting nurse.

Conclusion: The application of our system offers a straightforward, out of the box application for establishing a natural user interface between interventional cardiologists and cineloop viewing software during invasive cardiac procedures. This application improved procedural efficiency, is flexible for implementation in other interventional or surgical settings, independent of current infrastructure.

Quantitative Characterization of Mitral Annulus and Leaflets from Transesophageal 3D Echocardiography

Miguel Sotaquira*, Laura Fusini, Mauro Pepi, Roberto M Lang, Enrico G Caiani

Politecnico di Milano
Milan, Italy

S41

Aims: To propose and validate versus manual tracing a novel algorithm for the segmentation and quantification of the mitral annulus (MA) and anterior (A) and posterior (P) mitral leaflets (ML) from transesophageal real-time 3D echocardiography (3D TEE).

Methods: After manual initialization of 8 MA points, and of 4 to 6 points on the coaptation line, the MA and the anterior (A) and posterior (P) ML are automatically obtained. Several global morphological parameters as well as novel regional parameters (ML thickness, tenting and curvedness) are computed. The algorithm accuracy was tested on a group of 33 patients: 9 controls, with normal MA dimensions, 12 patients with dilative cardiomyopathy and 12 patients after mitral valve repair with insertion of annuloplasty ring on the posterior MA region. For each 3DE TEE volume, both MA and ML were manually traced by an expert, and point to point distances between manual and automatic segmentations were used as the error metric; in addition, the accuracy of ML regional thickness and tenting measures was also assessed.

Results: The semi-automated analysis including the quantification of MA, A and P ML parameters, required 3 min (including initialization). Compared to manual tracings, a high level of accuracy was found both for MA and ML automatic delineation: for MA, the median error was of 1.2 pixels, while for ML it was around 1.0 pixel. Conversely, regional thickness and tenting computation exhibited median errors of 0.1 and 0.2 pixels, respectively. For the lowest available volume resolution (1.0 mm), errors in segmentation were below 1.2 mm, whereas the quantification of ML parameters offered higher accuracy (of the order of 0.2 mm).

Conclusions: Besides computing both global and regional novel morphological parameters, our algorithm outperforms previous MA and ML segmentation approaches, offering high accuracy and reduced computation time, making it suitable for clinical settings.

Dynamic Registration of Multiple-view-US and MRI for the Characterization of Hypertrophic Cardiomyopathy

Julián Betancur^{1,2}, Antoine Simon^{1,2}, Frederic Schnell^{1,2,3}, François Tavard^{1,2}, Erwan Donal^{1,2,4}, Alfredo I. Hernandez^{1,2}, Mireille Garreau^{1,2}

¹ INSERM, UMR 1099, Rennes, France

² Université de Rennes 1, LTSI, Rennes, France

³ Université de Rennes 1, Lab. Physiologie Médicale, Rennes, France

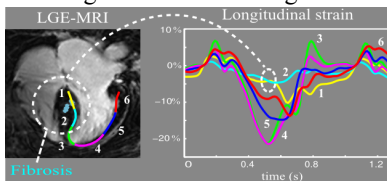
⁴ CHU Rennes, Service de Cardiologie, Rennes, France

S41

Aims: The relationship between strain and fibrosis for patients with hypertrophic cardiomyopathy (HCM) remains unclear. This work aims to fuse (i) myocardial fibrosis assessed from late-gadolinium-enhanced (LGE) sequence in cardiac-magnetic-resonance images (CMRI) and, (ii) myocardial strain from multiple-view 2D speckle tracking echocardiography (STE).

Methods: The proposed registration framework performs the spatio-temporal alignment between (i) left-ventricle (LV) contours from STE apical two- and four-chamber views (2CH, 4CH) and (ii) LV endocardial surfaces segmented from cine-MR short-axis-view (MR-SAX) images. The computation of a spatio-temporal metric applies the dynamical-time-warping (DTW) to the -translation and rotation invariant- Fourier descriptors of LV contours. DTW handles the non-linear relationship between the cardiac phases of input sequences. Fourier descriptors allow to compare corresponding 2D contours by weighting their global and fine shape details. Finally, an optimization finds the position of the US-views in the MR coordinate system.

Results: Rest-US and CMRI of four non-ischemic patients with HCM were acquired. Temporal alignment evaluation compares, for both modalities, the end-systolic (ES) instant given by the registration to a manually obtained reference. An average misalignment of 4.4% (US) and of 10.5% (MR-SAX) were obtained. Also, a cardiologist assessed the number of LV segments that are correctly aligned at the peak of R-wave and at ES instants. An average of 105 out of 120 segments were exploitable. Finally, LGE-MR image was superimposed to the corresponding mid-diastolic STE contours to assess the feasibility of performing the combined tissue and strain analysis. The cardiologist detected a change of strain in the regions with fibrosis.



Fusion of LGE-MRI with STE-4CH and corresponding regional strain.

Conclusions: Dynamic registration using Fourier decomposition and DTW shows to be suitable to integrate tissue and strain information from multiple-view 2D-US and 3D-MR. Preliminary results suggest that the magnitude of the longitudinal strain peak decreases in presence of fibrosis.

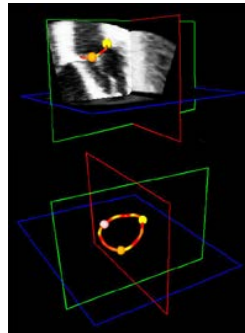
3D Evaluation of Tricuspid Annulus Morphology in Patients with Pulmonary Hypertension

Federico Veronesi, Karima Addetia, Claudio Lamberti, Roberto M Lang, Victor Mor-Avi

DEI, Alma Mater Studiorum – Università di Bologna, Italy

S41

Background. Tricuspid valve (TV) dilatation is associated with tricuspid regurgitation and right ventricular failure. Pulmonary hypertension (PH) secondary to mitral valve disease is a common cause of TV dilatation. Decision regarding when to surgically repair the TV, while operating on the mitral valve, is a topic of debate, and is frequently based solely on 2D measurement of TV diameters. To facilitate decision-making, we sought to develop software for 3D analysis of TV morphology from real-time 3D echocardiographic images.



Methods. Novel custom software was used to trace and measure TV annulus (TVA) in 10 patients with PH and 10 control subjects (CTRL). To trace the TVA, 10 rotated planes (18° apart) were displayed and two TVA points were selected in each plane. Points were interpolated using smooth splines (figure). Manually identified commissures were used to divide the TVA into three parts pertaining to different leaflets. The following parameters were automatically computed in 3D : area, perimeter, height, eccentricity, inter-commissural distance (ICD), diameters and segmental annulus curvature.

Results. Compared to CTRL, in patients with PH , the TVA was: (1)

	PH	CTRL
Area (cm ²)	12.4 ± 2.2	8.0 ± 1.6*
Eccentricity	0.57 ± 0.10	0.67 ± 0.10*
Annulus Height (mm)	6.4 ± 1.3	5.0 ± 1.3*
Anterior ICD (cm)	5.1 ± 0.9	4.0 ± 0.6*
Posterior ICD (cm)	4.1 ± 0.6	3.2 ± 0.5*
Septal ICD (cm)	3.9 ± 0.6	3.3 ± 0.7
Anterior Curvature (mm ⁻¹)	0.051 ± 0.007	0.065 ± 0.011*
Posterior Curvature (mm ⁻¹)	0.048 ± 0.009	0.064 ± 0.017*
Septal Curvature (mm ⁻¹)	0.060 ± 0.011	0.067 ± 0.011

* significant difference (p-value < 0.05, unpaired t-test)

bigger and less planar; (2) less elliptical, i.e. more round (table). Interestingly, changes in annular shape were not uniform, as the anterior and posterior segments showed altered ICD and curvature, while the septal segment remained

unchanged, probably because the septal leaflet is fixed between the fibrous trigones, while the other two are free to expand.

Conclusions. Our new software revealed that PH affects both size and shape of the TVA, suggesting that 3D analysis may be useful for pre-surgical evaluation of TV pathology.

Evaluation of Computed Tomography to Ultrasound 2D Image Registration for Atrial Fibrillation Treatment

Zulma L Sandoval, Jean-Louis Dillenseger

INSERM, URM1099, Rennes, France
 Université de Rennes 1, LTSI, Rennes, France

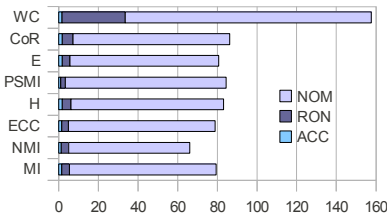
S41

Aims: This work aims to evaluate intensity-based similarity measures used in rigid or elastic registration techniques to align preoperative computed tomography (CT) and transesophageal ultrasound (US) images of the left atrium and the pulmonary veins, in order to guide the high intensity focused ultrasound (HIFU) ablation therapy in patients with atrial fibrillation.

Methods: The evaluation of the registration techniques has four steps: (i) design of anatomical 2D models including the left atrium and the pulmonary veins from the cryosections of the Visible Human Project (male and female), (ii) application of a known rigid/nonrigid transformation in order to produce a gold standard, (iii) creation of a pair of synthetic US images (based on the acoustical impedance and spatial distribution of speckle for each type of tissue) and CT slices (using the Hounsfield value corresponding to the type of tissue), (iv) estimation of the transformation by rigid/elastic registration of the simulated images and comparison with the gold standard.

The performance of eight measures was evaluated for rigid registration: mutual information (MI), normalized mutual information (NMI), entropy correlation coefficient (ECC), joint entropy (H), point similarity measure based on MI (PSMI), energy of histogram (E), correlation ratio (CoR) and Woods criterion (WC). The evaluation follows the protocol defined by Skerl et al allowing to estimate the accuracy (ACC), distinctiveness of the optimum (DO), number of minima (NOM), capture range (CR) and risk of non-convergence (RON). For the elastic registration we use the Dice index between the original anatomical model and the deformed model corrected by the estimated deformation field.

Results:



Performance of the rigid registration

Performance of the elastic registration

Metric	Dice
MI	84.27%
NMI	82.75%

Conclusion: NMI performed the best for the rigid registration of US and CT images. For elastic registration, MI had the best behavior.

Early Detection of Cardiotoxicity in Chemotherapy-Treated Patients from Real-time 3D Echocardiography

Cinzia Lorenzini, Cristiana Corsi*, Michele Aquilina, Alberto Farolfi, Andrea Rocca, Luca Frassinetti, Emanuela Scarpi, Dino Amadori, Claudio Lamberti

DEI, University of Bologna
Cesena. Italy

S41

Cardiotoxicity is a well-known adverse effect of various chemotherapeutic agents that can be monitored by 3D echocardiography. Following the recommendation, a temporal decrease of left ventricular ejection fraction (LVEF) might indicate dangerous effects of the drug on the myocardium and triggers consideration of therapy modification or interruption. However, myocardial deformation could identify preclinical myocardial dysfunction earlier than conventional LVEF allowing the administration of treatments to avoid cardiac side-effects. The aim of this study was to investigate whether changes in tissue deformation are able to identify LV dysfunction earlier than LVEF in patients treated with anthracyclines and trastuzumab. **Methods:** Sixty-five patients who were newly diagnosed with breast cancer, were enrolled to be evaluated before cancer therapy, during the therapy at 16 weeks (16w) and at follow up after 32 weeks (32w). Echocardiographic examination included 3D and 3D speckle tracking imaging for LVEF, circumferential, radial and longitudinal strain assessment. **Results:** Following the recommendation, 24 patients (36.9%) showed cardiotoxicity (LVEF mean reduction of 22% at 16w ($p < 0.0001$)); 11 (16.9%) patients interrupted the therapy due to a severe cardiac dysfunction and at 32w only 4 patients recovered. In this group at 16w, strain analysis showed a significant reduction for all strain values (table) that were all predictive of cardiotoxicity independently from LVEF. Applying a logistic backward stepwise regression model, the radial strain resulted an independent prognostic index of cardiotoxicity (OR=0.90, 95% CI: 0.85-0.96, $p=0.0006$). **Conclusion:** The evolving use of myocardial deformation indexes might provide additional echocardiographic tools to assess cardio-toxic effects beyond LVEF.

Strain (%)	Before therapy		16 w		32 w	
	Group 1	Group 2	Group 1	Group 2	Group 1	Group 2
Longitudinal	-20.2 (4.0)*	-19.3 (3.6)	-14.0 (3.2)	-18.3 (4.1)	-17.8 (2.8)	-18.9 (3.5)
Circumferential	-18.0 (3.3)*	-16.4 (3.4)	-13.3 (3.3)	-16.4 (4.9)	-15.9 (3.1)	-16.2 (3.1)
Radial	56.2 (11.6)*	51.3 (11.6)	36.7 (9.4)	48.9 (12.2)	47.3 (8.6)	49.9 (10.6)

Values expressed as mean (SD); Group 1: Patients with cardiotoxicity (n=24); Group 2: Patients without cardiotoxicity (n=41); * $p < 0.0001$ group 1 before therapy vs 16w.

Comparison of 2D and 3D Echocardiographic Measurement of Mitral-Aortic Angle

Federico Veronesi, Enrico G Caiani, Cristiana Corsi, Claudio Lamberti

Department of Electrical, Electronic and Information Engineering, Alma Mater Studiorum – Università di Bologna, Italy

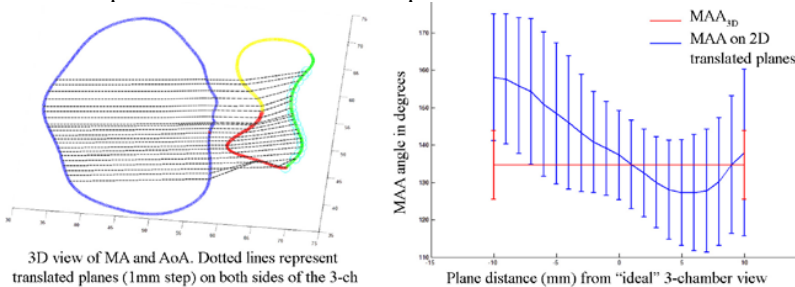
S41

Background: The angle between the mitral and aortic valves (MAA) facilitates blood flow ejection in physiological condition. The narrowing of MAA increases the risk of systolic anterior movement and thus is an important parameter in preoperative evaluation. Usually, MAA is measured in the 2D echo image (2DE) representing the 3-chambers view (3-ch); however, changes in 3-ch view selection may lead to significant changes in the measured 2D angle, due to the 3D shape of the two annuli. Real-time 3D echo (3DE) represents an alternative way to compute MAA. Accordingly, Our aim was to measure the impact of minimal variation in 3-ch selection on MAA computation, compared to MAA measured with 3DE (MAA_{3D}).

Methods: On 3DE data of 18 randomly chosen subjects, aortic and mitral annuli (AoA, MA) were traced using custom software. MAA_{3D} was measured as the angle between the best fitting planes of the two traced annuli. To simulate 2D MAA measurements, the 3D data was sliced: 1) at the position corresponding to 3-ch; 2) using 20; 3) using 40 rotated planes (1 degree step) around MA saddle point. The intersection of the traced annuli with these planes was used to automatically measure MAA in 2D.

Results: MAA_{3D} was $134.7^{\circ} \pm 9.2^{\circ}$ and MAA on 2DE 3-ch was $137.3^{\circ} \pm 12.0^{\circ}$. MAA measured on translated planes (± 10 mm) ranged from $137.9^{\circ} \pm 22.3^{\circ}$ to $158.1^{\circ} \pm 16.9^{\circ}$, while on rotated planes ($\pm 20^{\circ}$) ranged from $147.7^{\circ} \pm 14.4^{\circ}$ to $135.6^{\circ} \pm 12.9^{\circ}$. MAA measured in 2D was significantly different (paired t-test, $p < 0.05$) from MAA_{3D} already starting from translation greater than 1mm and rotation greater than 1° .

Conclusions: Even a slight misalignment (>1 mm and $>1^{\circ}$) of 2D cut-plane from the ideal 3-ch leads to MAA measures that differ from MAA_{3D}. 3DE should be preferred to 2DE for the computation of MAA.



An Evidence Based Android OSA Screening Application

Joachim Behar*, Aoife Roebuck, Mohammed Shahid, Jonathan Daly, Niclas Palmius, Andre Hallack Miranda Pureza, Gari D. Clifford

S42

Obstructive Sleep Apnoea (OSA) is a disorder characterized by pauses in breathing during sleep which lead to deoxygenation and consequent arousals. Long term consequences include sleep-related issues and cardiovascular diseases. OSA is often diagnosed with an overnight sleep study or polysomnogram. Monitoring can be costly and wait time for diagnosis can be high. In this paper we describe a novel OSA screening framework and prototype phone application. This is the first proof of concept of a fully automated smartphone medical diagnostic system which uses more than simple logic branching/decision support. A database of 856 patients that underwent at-home polysomnography was collected. Features were derived from audio, actigraphy and demographics; then used as the inputs of a support vector machine (SVM) classifier. The SVM was trained on 735 patients (278 treatment and 457 non-treatment) and tested on 121 patients (60-61 split). Classification on the test set resulted in accuracy of 74.4% with sensitivity of 55.5% and specificity of 93.4% validating the scientific approach. The signal processing and machine learning algorithms were ported to Java to be integrated into the phone application. The app records audio and actigraphy; implements the clinically validated STOP-BANG questionnaire; derives features from the signals; classifies the patient as needing treatment or not. Computational time for deriving the features and classifying a patient on the phone was on average 10.82 seconds (plus/minus 0.87 seconds). This paper provides a framework for an evidence-based phone application. The resulting software could provide a new, easy-to-use, low-cost and widely available modality for OSA screening (for users of smartphones). The research application is released as an open source software under the GNU licence. Future work will encompass assessing the performance of the algorithms on signals recorded by the phone.

Long-term Effect of Telecare on Patients with Heart Failure and High Blood Pressure

Masatsugu Tsuji*, Yuji Akematsu

University of Hyogo
Kobe, Japan

S42

Objective: This paper aims to examine the long-term effect of telecare on patients with chronic diseases including heart failure, high blood pressure, stroke and diabetes in Nishi-aizu Town, Fukushima Prefecture, Japan from the data of 2002-2010, by comparing medical expenditures and treatment days between users (treatment) and non-users (control) of the system based on the receipt data issued by National Health Insurance. Our previous papers used five years data from 2002 and 2006, while this paper expands to four more years and examines the same residents as used in the previous analysis. The number of samples in this study is 90 of users and 118 of non-users.

Method: Subjects' medical expenditures and treatment days were used dependent variables in estimation. Individual characteristics of the two groups, including age, sex, income, and health conditions, were obtained from the questionnaire survey and the above receipts were used for explanatory variables. For estimation, system GMM (Generalized Method Moments) is used to prove the causality between telecare use and outcomes.

Results: The coefficients of telecare use are negatively significant for both outcomes ($p < 0.05$). In particular, telecare use reduces medical expenditures of chronic diseases by JPY 64,944 per user per year. Similarly, treatment days of chronic diseases is reduced by 4.2 days. In contrast to the previous estimation, only hypertension is positively significant for the outcomes.

Conclusion: Our previous papers showed telecare reduced medical expenditure of chronic diseases and treatment days from 2002-2006 data by PY 15,302 and 1.6 days, respectively. Whereas this paper thus demonstrates that telecare has a possibility to yield the much larger long-term effect. There is no research to examine the long-term economic effect of telemedicine thus far, and accordingly this paper presents a new dimension of research in this field.

Remote Monitoring of Respiratory Rate in Critical Environments

Kian Davoudi, Moein Shayegannia, Bozena Kaminska*

Masters Student
Burnaby, Canada

S42

Respiration rate (RR) derived from photoplethysmography (PPG) can be estimated accurately regardless of age, anesthesia, ventilated or spontaneous breathing [1]. The user owned, wireless system with location tracking is used for monitoring physiological variations to determine critical conditions [2,3]. The high reliability method is needed to estimate critical conditions. PPG is used in our research.

Aim: We propose an algorithm based on Respiratory Induced Intensity Variation (RIIV) contained in AC and DC components of PPG signal to determine RR and HRV (Heart Rate Variability) to detect critical conditions and compatible with Wireless Network [2,3].

Method: Two pulse oximetry sensors, on finger and forehead were used on 10 subjects. Our references were Co₂ sensor and respiration rate transducer (RRT) belt. Three measurement sets were obtained from each subject: breathing at normal pace, controlling respiration rate by following a visual sinusoidal signal at 0.2Hz and at 0.3Hz. An algorithm that consists of Hilbert Transform followed by a Butterworth low pass filter processed data. This algorithm detects upper envelope of the PPG signal that corresponds to the respiration synchronous variations.

Results: Using Bland-Altman analysis of mean difference, upper and lower limit for Co₂= 0,0,0 at normal pace; 0, 0.92, -0.92 at 0.2Hz; 0.1, 0.71, -0.51 at 0.3Hz were obtained. For PPG of forehead values of -0.2, 2.09, -2.6 at normal pace; -0.5, 1.8, -2.8 at 0.2Hz, and -0.3, 0.64, -1.24 at 0.3Hz followed by values for PPG of finger -0.1, 1.84, -2.04 at normal pace (fig 1); -0.7, 1.37, 2.77 at 0.2Hz and -0.2, 1.6, -2.001 at 0.3Hz were obtained.

Conclusion: By self-calibration of the algorithm on each subject, all data points from PPG and Co₂ were close to the mean value and between the upper and lower limit of standard deviation. This confirms that PPG could be used to detect critical conditions.

Technical Verification of Applying Wearable Physiological Sensors in Ubiquitous Health Monitoring

Eliasz Kańtoch*

AGH University of Science and Technology
Kraków, Poland

With recent advances in electronics, wireless communication and computer science it is possible to develop miniaturized pervasive health monitoring devices that are capable of monitoring physiological signals during daily life activities. The aim of the research is to design, implement and verify health monitoring system to monitor and analyze human physiological signals. System incorporates central processing unit with Bluetooth module, dedicated ECG sensor, temperature sensor and movement sensors placed on the human body or integrated with clothes and network gateway to forward acquired data to remote medical server. The main advantage of the system is the ability to acquire, process and wirelessly transmit physiological data during daily activities. Moreover, system includes dedicated transmission protocol and remote web-based graphical user interface for real time data analysis. Experimental results for a group of human who performed various activities (ex. working, running etc.) show maximum 5% absolute error compared to certified medical devices. The results are promising and indicate that developed wireless wearable monitoring system faces challenges of multi-sensor human health monitoring during performing daily activities and open new opportunities in threatening and evaluating the treatment of number of patients who suffer from chronic diseases including cardiac disorders, asthma or diabetes.

S42

Proposal of Real-Time Echocardiogram Transmission based on Visualization modes with WiMAX access

Eva Cavero, Álvaro Alesanco, Ljiljana Trajkovic, Constantinos Pattichis, José García

University of Zaragoza
Zaragoza, Spain

S42

Aims: This study developed a methodology to improve the echocardiogram transmissions over WiMAX networks using a compression method based on visualization modes.

Methods: In a previous work we proposed a Set Partitioning in Hierarchical Trees (SPIHT)-based echocardiogram compression method that employed various codification approaches for each visualization mode. This method distinguished two visualization modes: the 2-D and the sweep modes. In the previous work, the minimal transmission rates to guarantee adequate clinical quality for these two modes were 200 Kbps and 40 Kbps, respectively. These requirements, especially the latter, were very low compared to previously reported results.

In this paper, it is proposed to apply the compression method based on visualization modes described previously but now considering the transmission in order to improve the overall process. However, the errors produced by the channel may affect the clinical quality, particularly for the 2-D modes since they required a higher transmission rate. Hence, a reliable method for the 2-D modes where retransmissions were combined with forward error correction techniques was proposed. The transmission results were analyzed using OPNET Modeler. The transmitter station had WiMAX access while the received station had ADSL access. Both networks were connected through the Internet.

Results: Nine echocardiograms videos were sent over the WiMAX network using the recommended transmission rates given in the previous study. The results showed that in order to visualize the video with a guaranteed diagnosis quality, the compression method based on visualization modes compared to the compression without distinguishing the visualization modes (compressing all the modes as the 2-D modes) introduced delay that was 100 ms smaller and achieved a reduction in the total transmission rate in the range of 17 Kbps to 113 Kbps depending on the echocardiogram distribution.

Conclusions: The echocardiogram transmission using the compression method based on visualization modes achieves lower bandwidth requirements for the available dataset. As a result, better transmission performance than compressing the echocardiogram without distinguishing the visualization modes.

Context-aware Cardiac Monitoring System for Early Detection of Heart Diseases

Abdur Rahim Mohammad Forkan*, Ibrahim Khalil, Zahir Tari

National ICT Australia (NICTA) and RMIT University, Melbourne, VIC, Australia
Melbourne, Australia

Cardiovascular disease (CVD) is the most common disease in Australia especially for elderly people which caused 50,000 mortalities in 2008. Aged people living alone in home die from CVD more than other members of the population. Death rate can be minimized if the causes of any potential CVD are automatically detected before the patient is in high risk situation. The aim of this research is to propose a scalable context-aware framework for early detection of several CVDs by continuous patient monitoring using smart sensors and utilizing the strength of cloud computing. The system consists of a target user, body worn sensors (ECG, pulse oximeter, BP sensor, accelerometers), environmental sensors (pressure, temperature, smoke), monitoring and communication devices (RFIDs, cameras, speakers, microphone, monitor), smart phone, and cloud-based repository and server. The developed system generates high level context of the patient by fusing information from low level physiological signals, ambient conditions, patterns of daily activities, personal profile, social interactions and medical history. By continuous sampling of heart, physical conditions and activities our system is able to detect possible symptoms of heart disease and can alert user by delivering context-aware service using flexible output modalities. As a proof of concept, we have developed a simulated prototype to detect which is a Premature Atrial Contraction (PAC), a common cardiac arrhythmia. By appropriate feature selection and learning algorithm, our system can classify ECG signals as PAC. By tracking the stored context history and personal profile in cloud database, the system detects smoking habit and alcohol consumption of the user. It can also detect caffeine intake, nicotine, stress and anxiety level using physiological and activity history and capable of sending warning notification to the user. Thus, this model can lead to a new mechanism for heart disease detection.

S42

A multi-step Approach for Non-invasive Fetal ECG Analysis

Maurizio Varanini, Gennaro Tartarisco*, Lucia Billeci, Alberto Macerata, Giovanni Poggia, Rita Balocchi

CNR
Pisa, Italy

S43

Non invasive monitoring of fetal cardiac activity is of great clinical interest to assess fetal health. To date, however, difficulties in detecting foetal beats from abdominal mother recordings prevented the possibility of obtaining reliable results. Difficulties mainly arise from the low signal-to-noise ratio, small amplitude of the fetal compared to the maternal ECG, baseline drifts, power line, artefacts of movement, maternal breath and muscle contraction. In this study a multi-step approach for the analysis of non-invasive fetal ECG is proposed. The analysis is focused on fetal beat detection based on a learning set of 75 annotated records and a test set of 100 records: each 60s record consists of 4 channels of mother abdominal ECG. The pre-processing steps concern the baseline removal with a forward/backward IIR, power line cancelling using a notch filter and signal interpolation to 4KHz. Successive steps are performed for: 1) source separation, 2) mother ECG identification, 3) mother ECG cancelling, 4) fetal ECG selection and analysis. Signal sources are identified using Independent Component Analysis (ICA) whereas mother QRS detection is based on adaptive threshold on filtered derivative signal. The mother ECG contribution is then cancelled from all 4 ECG signals using a QRST approximation obtained by weighted Singular Value Decomposition. After cancelling, ICA is repeated to separate sources in the residual signal. Among the sources, the best fetal signal is selected based on a priori information on ECG pseudo-periodicity. Lastly, fetal QRS is detected by an algorithm searching the maxima on filtered derivative signal. Results obtained on the learning set are: sensitivity=96.3% and positive predictive accuracy=96.3%. The average score on test set obtained from our second entry is (event 1/4)=97.69, (event 2/5)=5.28.

Noninvasive Fetal ECG Estimation based on Linear Transformations

Llamedo M*, Martín-Yebra A, Laguna P, Martínez JP

Electronic Department, National Technological University, Buenos Aires, Argentina

The most accurate method for measuring fetal heart rate is direct fetal electrocardiographic (FECG) monitoring using a fetal scalp electrode. Noninvasive FECG monitoring makes use of electrodes placed on the mother's abdomen, and sophisticated algorithms to separate fetal and mother activity. This year Physionet's challenge consists in locating fetal QRS complexes and estimating QT interval in FECG recordings. The approach presented in this work is based on previously validated algorithms, such as a wavelet based ECG delineator, the Woody QRS complexes alignment algorithm, and other techniques as independent (ICA), periodic (π CA) and principal components analysis (PCA). The algorithm consists in a common ECG preprocessing stage, followed by a mother ECG (MECG) removal, obtaining a raw FECG. The FECG is rotated by two kind of linear transformations, ICA and PCA, in order to get a more clear representation of the fetal activity isolated. Following that, QRS complexes are detected in these 3 representations, each with 4 FECG leads. An statistical model, trained in set A, is applied to the detections obtained from the 12 resulting leads, in order to rank the leads with higher degree of FECG content. With the detections of those leads, an average QRS complex is calculated with the Woody algorithm, which is used later as a matched filter for the refinement of the fetal QRS detections (fQRS). The final decision is performed with an estimation of the SNR gain produced by coherent averaging with the fQRS. Finally, the QT interval is measured in an average heartbeat. Results in set B were 5284.12 for event 4 (sample entry score was 3258.56), and 60.5 for event 5 (sample entry score was 102.75). This algorithm presented promising results specially for event 5. Future improvements will include π CA in order to obtain a clearer representation of the FECG.

S43

A Wavelet-Based Method for Assessing Fetal Cardiac Rhythms from Abdominal ECGs

Rute Almeida, Hernâni Gonçalves, Ana Paula Rocha, João Bernardes

CMUP, Universidade do Porto
Porto, Portugal

S43

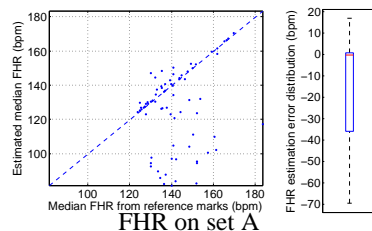
Introduction Fetal heart rate (FHR) monitoring is widespread all over the world. However, despite recent advances in FHR analysis methods, there are still inherent technical limitations. One of the main challenges in this field is to extract accurate and useful information from the external fetal ECG, which may provide a better non-invasive characterization of the fetal cardiovascular system during the third trimester of pregnancy.

Methods Data provided from PhysioNet 2013 Challenge was considered. Segments with signal loss were first detected and eliminated from the analysis and a notch filter at 0Hz is applied. Maternal ECG waves were located using a wavelet based system previously developed and validated. Then similar processing with adapted wavelet scales and thresholds was applied to detect fetal QRS, excluding signal singularities that were associated to maternal heartbeats. Along with the 4 lead provided, fetal QRS detection uses derived principal components based leads. Single lead based annotations were combined in a single annotator relative to fetal QRS locations from which RR and HRV fetal measures could be taken.

Results The rate of true positives, false positives and false negatives, normalized by number of fetal beats, found in the (training) set A was, respectively: 68%, 55% and 33%. Median FHR estimation error was -0.376bpm. Correlation between reference and estimated median FHR was 0.78 for estimated FHR > 120bpm. The average scores on set B from entry 1 were: 2236.59 for event 4 and 47.57 for event 5.

Conclusions The proposed approach seems promising for assessing fetal cardiac rhythms from abdominal ECGs.

Further evaluation is required through the analysis of the fetal ECG morphology and through the use of linear and nonlinear FHR indices. The performance of the detector strongly depends on the quality of the data, and thus pre-processing methods for discarding very low quality signals should be considered.



PhysioNet/CinC Challenge 2013: A Novel Noninvasive Technique to Recognize the Fetal QRS Complexes from Noninvasive Fetal Electrocardiogram Signals

Ali Ghaffari, Seyyed Abbas Atyabi*, Mohammad Javad Mollakazemi, Maryam Niknami, Ali Soleimani

CardioVascular Research Group (CVRG), Department of Mechanical Engineering at K.N Toosi University of Technology, Tehran, Iran
Tehran, Iran (Islamic Republic of)

S43

The aim of this study is the intelligent recognition of the fetal heart rate and its R-R intervals. At first, after eliminating the non-value data, the missing data was then regenerated based on the statistical distribution of the data. In order to remove the power line noises a band stop finite impulse response filter was implemented. Then Using the discrete wavelet transform, the low frequency noises were removed by eliminating the reconstructed signals in approximations of level 10 and both details of levels 9 and 10. The final preprocessing stage was using wavelet denoising technique based on the estimation of noise of wavelet coefficients. The denoised signal was then decomposed again using discrete wavelet transform with Daubechies 6 wavelet function in level 10. The results showed that both maternal and fetal QRS complexes were discriminated in the reconstructed signals from the details of the first decomposition level D1. At the next stage, a variable threshold criterion was designed to detect the maternal R-waves. By eliminating the special limit ranges of the maternal R waves from D1 signal the remaining data described merely the fetal QRS complexes. Next a window with a specific length was slid on D1 signals and the envelope curves were extracted. The locations of each local maximum on the envelope curve represent the fetus's R waves. In order to improve both the performance of the proposed method and the robustness of the algorithm versus noise, an amendment technique with respect to the fetal and maternal R-R intervals was implemented. This algorithm was applied on 75 noninvasive Fetal ECG signals in the train data set A. The algorithm was also applied on the test data set B. consequently as the preliminary challenge scores, the average scores 177.58 and 12.98 was achieved for the events 4 and 5, respectively.

Non Invasive FECG Extraction From a Set of Abdominal Sensors

Joachim Behar*, Julien Oster, Gari D Clifford

Oxford
Oxford, United Kingdom

S43

Aims: The PhysioNet/Computing in Cardiology Challenge 2013 aims at developing an efficient algorithm able to locate foetal QRS (FQRS) complexes and estimate FQT intervals using non invasive foetal electrocardiograms (FECG) recorded on the mother's womb.

Methods: A total of 75 one minute segments of various quality and FECG signal to noise ratio were available for the training set along with the FQRS annotations. Another 100 one minute segments without reference annotations were used for validation. ECGs were first preprocessed by cascading a low pass and a high pass filter in order to remove higher frequency and baseline wander. A Notch filters to remove power interferences at 50Hz or 60Hz was applied only in the case where a spike was detected on the power spectrum at these respective frequencies. The signals were then normalised before applying various source separation techniques to cancel the maternal ECG. These techniques included: template subtraction, principal component analysis (PCA) and a combination of these methods. FQRS detection was then performed on all residuals and on the PCA transformation of the residual signals using a Pan and Tompkins QRS detector. The regularity of the time series obtained on each individual residual channel were evaluated and the most regular one was selected as containing the FECG.

Results: Best preliminary scores using our method for event 4 and 5 were 227.96 and 20.79 respectively which are much better than the 3258.56 and 102.75 scores obtained using the sample submission available on the challenge web page.

Conclusion: At this stage the method shows good performance on the training set-a and validation set-b.

Multi Stage Principal Component Analysis Based Method for Detection of Fetal Heart Beats in Abdominal ECG

Robertas Petrolis, Algimantas Krisciukaitis*

Kaunas, Lithuania

Electrical activity of fetal heart is present in registered abdominal signals, however in real clinical recordings energy of this signal is so small that classical multivariate analysis based methods (e.g. Independent Component Analysis) fail to extract it for further analysis. Principal Component Analysis based method was used for truncated representation and subtraction of cardiocycles of maternal ECG. The energy of fetal ECG component then remains sufficient when compared to other components of the remaining signal to be concentrated in the first component obtained during the second stage Principal Component Analysis. This stage was performed not for extracted cardiocycles, but for the whole leads of the signal. The procedure extracts maximal amplitude of the sought signal regardless to the orientation of the fetus in multilead recording cases. Two stage detection of fetal heart beats is performed in band-pass filtered first principal component. Maximization of correlation with sliding QRS model gives the final time point of fetal heart beat in the region preliminary detected by means of simple amplitude thresholding. Third stage Principal Component Analysis was used to reconstruct the cardiocycles of fetal ECG for further analysis. The algorithm was tested with PhysioNet Challenge 2013 signals. Preliminary results of the detection of fetal heartbeats by our method for the PhysioNet Challenge 2013 on set B were: Average Score (event 1/4): 1391.70; Average Score (event 2/5): 45.49.

S43

An Algorithm for the Analysis of Foetal ECG from 4-channel Non-invasive Abdominal Recordings

Costanzo Di Maria, Wenfeng Duan, Marjan Bojarnejad, Fan Pan, Susan King, Dingchang Zheng, Alan Murray, Philip Langley*

Newcastle upon Tyne Hospitals
Newcastle upon Tyne, United Kingdom

S43

The foetal ECG (fECG) is one of the most important tools for monitoring the health of the foetus throughout pregnancy. Various valuable parameters could be extracted from the fECG, including foetal heart rate (fHR) and its variability, foetal RR (fRR), and foetal QT (fQT) time interval. However, its clinical use has been limited by the difficulty of analysing non-invasive fECG recordings. The aim of this study was to develop a robust algorithm for the analysis of 4-channel abdominal fECG recordings and test its performance in the Computing in Cardiology Challenge 2013. Signals were pre-processed by a combination of frequency filtering and wavelet denoising. Adaptive cancellation of the maternal ECG (mECG) was performed using maternal QRS time markers obtained from the principal component containing the largest mECG. Following further wavelet denoising of the residuals, the fQRS time markers were computed with a local peak detection algorithm from the first principal component. From the average foetal beat, the fQT interval was derived automatically from detected Q-wave to T-wave end (determined by mathematical model of the terminal portion of the T-wave). The derived fHR (event 4) and fRR (event 5) traces were compared to the reference values obtained from a scalp electrode signal. The algorithm scored 223.23 for Challenge event 4 and 19.34 for Challenge event 5, versus 3258.56 and 102.75 respectively obtained by the sample algorithm provided by the Challenge organisers. As the lower the score the better the performance, this algorithm performed 15 (event 4) and 5 (event 5) times better than the sample algorithm. Targeted wavelet denoising and principal component analysis made possible the computation of fECG parameters from recordings heavily affected by large amplitude noise. The proposed algorithm outperformed the sample submission and, therefore, represents a more robust approach for the analysis of the foetal ECG from abdominal recordings.

Systematic Methods for Fetal Electrocardiographic Analysis: Determining the Fetal Heart Rate, RR Interval and QT Interval

Chengyu Liu*, Peng Li

In the present study, we aimed to propose systematic methods for accurately locating the fetal QRS complexes and estimating the QT interval in noninvasive FECG signals. The methods included 5 steps. Step 1: we firstly validated that if there were any invalid value in the original FECG signals and used the spline interpolation when the invalid value occurred. Then we used the wavelet transformation to acquire the trend and the FECG signals removed the trend were analyzed in the following process. Step 2: we used the entropy method and peak detection method based on parabolic fitting weights to assess the signal quality of FECG signals. At least two channels were selected for the following analysis. Step 3: we used the principal components analysis (PCA) method to locate the maternal QRS complexes. Then we determined the accurate location of maternal QRS complexes in each channel and used the coherent averaging method to reconstructing the maternal ECG signals. The reconstructed signals were adjusted around the maternal QRS complexes to achieve the optical matching. Step 4: we obtained the fetal ECG signals by subtracting the reconstructed maternal ECG signals from the FECG signals. Then the fetal ECG signals were pre-processed using wavelet transformation. Step 4: the fetal QRS complexes were detected from each channel of the de-trended fetal ECG signals. The fetal ECG template from the channel with the highest signal quality was constructed using coherent averaging and the fetal QT interval was determined from the start of QRS complexes to the end of T wave. Our entry results on set B were: average score for event 1/4 is 309.43 and average score for event 2/5 is 9.04, which is a significant improvement compared with the sample submission (event 1/4 is 3258.56 and event 2/5 is 102.75)

S43

Comparison of Three Methods for Fetal QRS detection

Aruna D Deogire*, Satish T Hamde

MET's Institute of Engineering,
Nashik, India

S43

Aim: Aim of this work is to detect fetal QRS accurately and reliably in the presence of noise. Further work will be extended to measure QT interval. This work is result of a participation in Physionet/CinC challenge 2013 on Noninvasive Fetal Analysis. Results of phase 1 entry to detect fetal QRS are submitted along with score obtained.

Methods: Presently three approaches are implemented to detect fetal QRS using four abdominal signals. First one is a single lead approach, where each channel is processed independently for preprocessing, detection and cancellation of mother QRS, post processing. One of the outputs generated from four is considered for fetal QRS detection. Second and third are multilead approaches where preprocessing is done on all four channels independently and Principal Component Analysis (PCA) is used to reduce the outputs. Like in second approach the maternal peak detection and cancellation is done and the signal is given for PCA. The first component of PCA is the signal for fetal QRS detection. While in third approach after preprocessing itself signals are given to PCA and first component of PCA is used for mother R peak cancellation and fetal QRS detection.

Results: For all three approaches algorithms were tested on 100 set B records. Score for method three is not known currently but other two are as in table 1.

Table 1 Results of Fetal QRS Detection Scores

	Score of Proposed Methods			Sample Score (Provided by organizers)
	1	2	3	
Average Score (event 4)	863.28	932.28	Waiting	3258.56
Average Score (event 5)	38.37	45.22		102.75

Conclusion: Thus the proposed methods show potential to detect the fetal QRS. Although multilead approach is better option than single lead as it gives single output.

A Robust Algorithm for Fetal QRS Detection using the Non-invasive Maternal Abdomen ECG

Martin Kropf*, Günter Schreier, Robert Modre-Osprian, Dieter Hayn

Ludwig Boltzmann Society
Graz, Austria

Fetal electrocardiography (FECG) analysis has the potential to be a reliable technology to prevent fetal hypoxia and to detect heart defects, which are the most common birth defect and leading cause for deaths during birth. However, state-of-the-art noninvasive FECG analysis techniques show only little reliability and, therefore, FECG is currently used in a rather small band of applications, only. We present an algorithm for automated fetal QRS detection, developed with the PhysioNet FECG database. This database provides noninvasive ECG signals recorded from the mother's abdomen, and expert annotations for fetal QRS locations. The database consists of three sets: Set-a (75 records, signals and annotations provided), set-b (100 records; only signals but no annotations published), and set-c (neither signals nor annotations publicly available). Our algorithm consisted of four separate steps: 1. Maternal QRS complexes were detected using our QRS detector, featuring adaptive thresholds and automated, ECG-quality-based channel selection. 2. Averaged maternal QRS complexes were calculated and – for each QRS complex – the averaged beat was subtracted. 3. On the remaining signal (with predominantly fetal components), QRS complex detection was applied again. 4. Finally, fetal QRS event sequences were optimized using statistical methods. PhysioNet's set-a was used for training our fetal QRS detector, leading to a sensitivity of 90 % and specificity of 84 %. Thereafter, by taking part in the Computing in Cardiology Challenge, the algorithm was evaluated using set-b. The algorithms results were sent to the challenge organizers, who determined the accuracy of our fetal HR and fetal RR sequences against the reference annotations that were available to them only. Compared to PhysioNet's sample code, our preliminary results look quite promising. Scores were 380.61 for fetal HR (optimum = 0.00; PhysioNet sample code scored 3258.56) and 18.07 for fetal RR interval measurement (optimum = 0.00; PhysioNet sample code scored 102.75).

S43

Noninvasive Fetal ECG Detection from Maternal Abdominal Recording: the Physionet/CINC Challenge 2013

Vito Starc*

University of Ljubljana, Faculty of Medicine
Ljubljana, Slovenia

S43

The PhysioNet Challenge 2013 focused to develop accurate algorithms for locating QRS complexes and estimating the QT interval in noninvasive fetal ECG (FECG) signals obtained from noninvasive abdominal recordings in pregnant women. Maternal abdominal signals were obtained from multiple sources using a variety of instrumentation with differing frequency response, but all in the form of four ECG leads with the sampling rate of 1 kHz. We upgraded our custom automated software was used in the previous Challenges using the following algorithm. First, signals were preprocessed using median filtering to remove spikes, a two pole low pass Chebyshev filter (0.003 Hz) to remove baseline wandering and a high pass Chebyshev filter (0.06 Hz) to remove noise of higher frequencies. R wave peaks were identified with an automated peak detection algorithm proposed by Pan and Tompkins. Then, templates of the P, QRS and T wave of the maternal ECG were obtained by averaging beats that belonging to the same cluster. For the construction of templates we used our time shifting method considering an appropriate delay of the waves due to the QT and PQ variability. The maternal ECG was removed by subtracting the appropriate templates. The processed abdominal ECG signals were again filtered (0.06 Hz Chebyshev high pass filter) and then decomposed using PCA. Finally, the first principal signal was used to identify fetal R wave peaks using the peak detection algorithm. From the provisional fetal RR interval series, a median RR interval was determined and used to identify missing or false detected peaks. The program was written in the Pascal implemented in the Delphi 5.0. For the PhysioNet 2013 Challenge on set B from obtained an average score 977.41 for event 4, and score 33.33 for event 5.

Fetal QRS Detection using Maternal Template Matching and Modified Pan Tompkins Algorithms

Akshay Dhawan

Cornell University, Ithaca, NY, USA

Aims: This study developed a template matching approach to annotate the fetal QRS complexes in a database of fetal electrocardiograms (FECG) for the CinC 2013 Challenge. FECG monitoring offers physicians the ability to detect and treat arrhythmia and other heart conditions as early as possible. However, the non-invasive recording of FECGs presents a signal processing challenge since the fetal signal is masked by the maternal electrocardiogram (MECG) as well as breathing, fetal movement, and muscle activity.

Methods: The training set contained 25 sets of 4 abdominal surface recordings, each recorded for 1 minute. A running average template of the MECG was calculated for each set and used to cancel out the maternal signal. A modified version of the famous Pan Tompkins algorithm with low and high pass Butterworth filters was then used on the FECG, resulting in a signal with relatively large spikes around the locations of the QRS complexes. Each of the abdominal signals was processed separately. The final locations were annotated by correlating peaks from all 4 signals as well as enforcing periodicity in an interval between 80 – 200 beats per minute.

Results/Conclusions: The preliminary average scores of this algorithm on events 4 and 5 in the CinC challenge were 1444.60 and 26.17 respectively. The algorithm exhibits higher performance on the RR intervals than the fetal heart rate, which suggests that the current iteration exhibits high specificity but poor sensitivity to QRS detections. Phase 2 iterations of this algorithm use independent component analysis to perform blind source separation of the fetal QRS complex following MECG cancellation. The resulting signal is less noisy and leads to improved outcomes from the modified Pan Tompkins approach.

S43

Identification of Fetal QRS Complexes in Low Density Non-Invasive Biopotential Recordings

Alessia Dessì*, Danilo Pani, Luigi Raffo

University of Cagliari
Cagliari, Italy

S43

The PhysioNet/CinC Challenge 2013 aims at addressing the extraction of the fetal electrocardiogram (FECG) from non-invasive biopotential recordings in order to access specific features such as the heart rate and the location of the fetal R peaks. On a 4-channel recordings dataset, the solution of the problem through methods such as Independent Component Analysis is not possible. In this paper, a technique based on the maternal interference cancellation has been developed. After the ADC errors correction by spline fitting, FIR filtering has been performed both to correct the baseline drift without phase distortion and to suppress the frequency components above 46 Hz. This also limits the mains interference. Templates of parts of the filtered signals possibly representing QRS complexes are automatically extracted from the signal and incremental synchronized averaging performed in order to smooth over the noise components. The reference points for the templates extraction are identified by a QRS enhancement technique based on a feature signal created exploiting a wavelet denoising stage. For every channel, the maternal template (identified as the most frequent) is cross-correlated to the signal extracting the occurrences of the maternal QRS, and then subtracted after Tuckey windowing. The channel with the highest number of fetal templates is identified as the best candidate for FECG detection. Fetal R peaks are obtained after a correction stage aimed at removing redundancies due to residual maternal peaks or isolated noise peaks considering a maximum fetal frequency of 300 bpm. The algorithm has been trained using the dataset A and tested on the dataset B, obtaining an average score of 622.83 for event 4 and of 29.07 for event 5.

Fetal ECG Detection in Abdominal Recordings: a Method for QRS Location

Rui Rodrigues*

Faculdade de Ciencias e Tecnologia, Universidade Nova de Lisboa
Caparica, Portugal

The Physionet/Cinc Challenge 2013 consists of locating the Fetal QRS(FQRS) and estimating the QT interval in a one-minute non invasive Fetal ECG recording. The only goal of our method is to detect the FQRS complex. Each recording contains four abdominal channels. The same procedure was applied to each channel and, after having a set of FQRS detections for each, one of them was chosen. In order to achieve baseline and high frequency noise removal, our approach starts with filtering. The next step is mother QRS(MQRS) locating: we used our own algorithm. To be able to detect the FQRS, a segment of the filtered ECG was set to zero, in the neighborhood of each MQRS detection. We developed an algorithm to detect the FQRS in this last signal, using also the MQRS detections. To choose the best among the four sets of FQRS detections, a linear function was used to score each set. The arguments to that function are 20 statistics obtained from the FQRS detections and from the MQRS detections. A sort of perceptron algorithm was applied to learn the weights of the linear function, using the Challenge training set A. The Challenge test set B contains 100 recordings. Challenge events 4 and 5 consist on detecting the FQRS on this set of records. Scoring on event 4 is based on the mean square error between the algorithm FQRS location and the reference location. Our average score was 197.93. Scoring on event 5 is based on RR interval estimation: our average score was 17.06.

S43

A Neural Network Model for Noninvasive Fetal ECG

Xiaopeng Zhao

Department of Mechanical, Aerospace, and Biomedical Engineering
University of Tennessee, Knoxville, TN

S43

Monitoring fetal heart rate is an important means to reduce fetal hypoxia. Fetal heart rate can be accurately measured using a fetal scalp electrode, which is known as direct fetal electrocardiograph. However, the direct fetal ECG is available only during labor and cannot be used in clinical practice. This work is a response to Physionet Challenge 2013, which aims to estimate fetal heart rate using noninvasive electrodes placed at the mother's abdomen.

Physionet provides three databases for detection of FECG signals. We develop an artificial neural network model to identify patterns of fetal QRS. An ECG record is passed through template filters to generate features to characterize different waves. The features are then utilized to train the network model. Figure 1 shows the results of the model when tested on the record a01. The model can capture most of the fetal QRS waves but will miss those fetal QRS waves that are too close to a maternal QRS. The model also reports false positive results at the beginning of the record, probably due to boundary effects. Our scores for the Challenge on set B are 283.61 for event 4 and 15.72 for event 5.



Figure 1. Wave detection on the record a01: detected maternal QRS (+), annotated fetal QRS (*), detected fetal QRS (o).

Multichannel Foetal Heartbeat Detection by Combining Source Cancellation with Expectation-weighted Estimation of Fiducial Points

Luigi Yuri Di Marco*, Alberto Marzo, Alejandro Frangi

University of Sheffield
Sheffield, United Kingdom

BACKGROUND: Non invasive monitoring of foetal heart rate (FHR) is important in detecting foetal distress and morbidity. The accuracy of current non-invasive FHR monitors is not satisfactory.

AIM: To improve accuracy of foetal heart beat detection from abdominal recordings of maternal ECG.

METHODS: A dataset of 75 recordings of 4-channel abdominal ECG provided by Physionet was used for training (SetA). Signals were notch-filtered (50 Hz) and high-pass filtered (8 Hz). Maternal QRSs were detected and subtracted (window of +/- 80 ms about the R peak). For each channel, the residual ECG signal was further processed (1st derivative squared and low-pass filtered by 49-tap moving-average). On the resulting signals, an expectation-weighted estimate of the “next” fiducial point (foetal QRS) was built using a Gaussian distribution $G(\mu, \sigma)$ with μ indicating the most probable time distance of the “next” fiducial point. A grid search was used to determine (μ, σ) minimising the standard deviation of the resulting estimated time series (fQRS) for each recording. The source code of the algorithm, together with the output (fQRS) were submitted to enter Physionet Challenge Events 1,2,4,5. In Events 1 (unpublished test set of 100 recordings, SetC) and 4 (published set of 100 recordings, SetB), a test FHR time series was built by Physionet’s Scoring System (PSS) from fQRS annotations and matched to the reference. Scores were based on test vs. reference mismatches (lower scores indicate better performance). In Events 2 (SetC) and 5 (SetB), the RR time series replaced FHR.

RESULTS: Our algorithm scored 135.18 (7.11) in Event 4 (Event 5). The reference algorithm provided by Physionet scored 3258.56 (102.75) in Event 4 (Event 5). PSS was not available for Events 1 and 2 by the abstract submission deadline.

CONCLUSIONS: The proposed method substantially improved the foetal heart beat detection accuracy with respect to the reference algorithm.

S43

Fetal Heart Rate Discovery (FHRD) Algorithm for Detection of Fetal Heart Rate from Noisy, Noninvasive Fetal ECG Recordings

Piotr Podziemski*, Jan Gierałtowski

Warsaw University Of Technology
Warsaw, Poland

S43

Fetal heart rate variability is known to be of a great meaning in assessing fetal health status [1]. The simplest way of measuring fetal heart rate is of course to record a signal with noninvasive fetal ECG (FECG). Unfortunately, amplitude of fetal ECG is often small and usually we need mother's ECG (of high amplitude) to be removed. Moreover, the electrodes placement on the mother's abdomen is known but it is not clear what is the placement of electrodes in relation to the child. Last but not least, signal is almost always very noisy (e.g. because of mother's muscles contractions). A novel and efficient algorithm for detection of fetal ECG is needed. We analyzed 75 FECG recordings from PhysioNet Challenge 2013 database. Each recording has 4 channels, sampling rate of 1 kHz and duration of 60 s. Detected RR interval peaks were compared with reference fetal scalp electrode measurements. Our algorithm focuses on detecting the most prominent part of a fetal QRS complex i.e. RS slope. First we remove long-range trends, find the channels with the best quality fetal ECG. Then, we localize decelerations with the required characteristics (adequate amplitude and slope). Note, that algorithm is adaptive and finds by itself optimal RS slope characteristics for every recording. After this final steps of a "fine-tuning" are done, i.e. removal of incorrect detections and in the case of missing ones re-check with lower requirements. These steps allowed us to obtain very accurate and reliable results of fetal R peak detection, even in the case of very noisy data. The preliminary test score of the PhysioNet Challenge were 143.83 for event 4 and 8.92 for event 5.

Validation of the V-index through Finite Element 2D Simulations

Roberto Sassi*, Luca T Mainardi, Pablo Laguna, Jose F Rodriguez

Università degli Studi di Milano
Crema, Italy

Aims: Spatial heterogeneity of ventricular repolarization (SHR) is a property of the human heart and it is responsible for the T-wave on the ECG. However, an increased SHR might favor the development of ventricular arrhythmias. Hence, being able to assess SHR from ECGs would be of clear clinical and scientific value. The V-index is a metric recently introduced with this purpose.

Methods: First, we validated the V-index by means of 2D computer simulations. A vertical slab with 101 x 751 nodes was inserted in a circular volume conductor. At each node, the electrophysiological behavior of the cell was described using a modified version of the tenTusscher and Panfilov (TP06) model that accounts for repolarization variability. The mono-domain model was used to simulate the tissue. Finally, synthetic electrocardiographic recordings (ECG) were simulated at 12 different positions at the external surface. Second, we present a theoretical proof that V-index holds in situations where the beat-to-beat variability of the repolarization times (BBVRT) (i) have different variance at each node, and (ii) are correlated across them.

Results: We considered two different positions of the slab in the volume conductor, and for each, 5 minutes of ECG were simulated (fixed pacing time of 800 ms). The standard deviation of the BBVRT varied slightly across the slab (0.3-0.6 ms), with a mean value of 0.42 ms, and was strongly correlated across nearby nodes. The values of the V-index numerically estimated from the ECG were in good agreement with the repolarization heterogeneity at the node level (15.5 ms and 15.4 ms vs 16.6 ms).

Conclusion: We showed numerically and theoretically that even when the BBVRT is strongly correlated across nearby nodes, the V-index provides an approximate measure of the standard deviation of repolarization times. Further extensive tests are expected with a bi-ventricular model of the human heart.

S44

Repolarization Variability Mechanisms and its Relation with Cardiac Arrhythmogenesis

Jose F Rodriguez*, Roberto Sassi, Esther Pueyo, Luca Mainardi

Universidad de Zaragoza
Zaragoza, Spain

S44

Background: Temporal and spatial variability of ventricular repolarization has been related to increased ventricular arrhythmic risk. Even though causes and modulators of variability in repolarization have been studied, most attention has been focused on the slow component of the delayed rectifier potassium current (IKs). In this study we investigate the influence of several mechanisms that have been proposed as influential on Action Potential (AP) repolarization variability: inactivation IKs gating, inactivation L-type Calcium current (ICaL) gating, and Sarcoplasmic Reticulum Calcium Release gating.

Methods: Different levels of white noise were introduced by means of a stochastic differential equation for the inactivation gating variables of the three considered currents. Two stimulation protocols were applied to the ten Tusscher human ventricular model (TP06) and a number of arrhythmic risk biomarkers and their variations were evaluated: steady state AP and $[Ca^{2+}]$ transient properties, and AP duration (APD) dynamic restitution curve. In addition, a multi-scale study in 1D, 2D and 3D was conducted in order to determine the influence of the electrotonic interaction on biomarkers variability.

Results: IKs and SR calcium release were the main contributors to biomarkers variability at the cellular level (1.0% and 2.0% for IKs and SR calcium release, and $<0.1\%$ for ICaL). Differently to IKs and ICaL, large fluctuations on the SR calcium release led in some cases to non-physiological APs and caused the APD to follow a non-normal distribution. At the tissue level, the effect of electrotonic coupling masked the effects of current variability for all biomarkers. In particular, a very notable reduction on variability was obtained for 2D and 3D tissue models (80% reduction with respect to 1D models, and more than 20 folds with respect to single cells). Hence, much larger fluctuations at the cellular level are required in order to reproduce the fluctuation levels observed at tissue level.

Evaluating the Differences of Simulated Long-QT Syndromes in Body Surface ECGs

Gunnar Seemann*, Maider Alvarez de Eulate, Niko Konrad, Julian Maier, Mathias Wilhelms, David Keller, Olaf Dössel, Eberhard Scholz

Karlsruhe Institute of Technology
Karlsruhe, Germany

Congenital Long-QT Syndrome (LQTS) is a genetic disorder affecting the repolarization of the heart in around 1 out of 2500 people increasing their risk for sudden cardiac death. Genes that encode for various cardiac ion channels are mutated, which tends to prolong the ventricular action potential duration (APD) thus increasing the risk for ventricular arrhythmias. The most prevalent subtypes of LQTS are LQT1-3. In this work, we aim to evaluate the differences in the T-waves of simulated LQT1-3 in order to identify markers in the body surface ECG that might help to classify patients solely based on ECG measurements. Voltage clamp recordings of mutated channels co-expressed with wild-type channels were performed to gather mutant ion channel characteristics for LQT1 and LQT2. For LQT1, mutation S277L was used to characterize IKs and mutation S818L in IKr for LQT2. The data was used to parametrize the respective ion channel equations of the ten Tusscher and Panfilov model of human ventricular electrophysiology. LQT3 was integrated using an existing mutant INa model. The monodomain model was used in a transmural and apico-basal heterogeneous model of the ventricle (tuned to reconstruct realistic T-waves) to calculate ventricular excitation propagation. The forward calculation on a torso model was performed to calculate body surface ECGs. Compared to the physiological case with a QT-time of 375 ms, this interval was prolonged in all LQTS (LQT1 405ms; LQT2 423ms; LQT3 394ms). The T-wave amplitude was changed (Einthoven lead II: LQT1 108%; LQT2 91%; LQT3 103%). Also, the width of the T-wave was enlarged (full width at half maximum: LQT1 111%; LQT2 125%; 109%). These and further extractable data from the simulated ECGs might help to identify genotype-specific differences in the ECGs of patients in order to classify patients fast and cheap compared to the current method using genetic testing.

S44

Simulation of KCNJ2-linked Short QT Syndrome in Human Ventricular Tissue

Cunjin Luo, Yongfeng Yuan, Kuanquan Wang*, Henggui Zhang, Yongfeng Yuan

Harbin Institute of Technology
Harbin, China

S44

The aim of this study was to investigate the mechanisms by which the Kir2.1 D172N mutation induces short QT syndrome (SQT3). We developed a SQT3 syndrome model based on both I_{K1} equations on SQT3 from one paper published in *Cardiovascular Research* (2012) and the ten Tusscher et al. model for human ventricular action potentials. Based on the published paper above, we did further research to explore the functional effects of Kir2.1 D172N mutation-induced electrical properties of cardiac cells on ventricular electrical wave conduction. This modified model takes two factors into consideration, one factor is three situations which include wild type (WT), heterozygous (WT-D172N) and homozygous (D172N), the other factor is three kinds of cells which include EPI, MIDDLE, ENDO cells because of the heterogeneity of ventricular wall. In the cellular simulation, we computed action potential duration (APD), amplitude and magnitude of I_{K1} current, channel activation coefficient, the restitution curves of APD (APDR), and effective refractory period (ERPR). In the 2D model simulation, the functional effects of the SQT3 on the characteristics of ECG were simulated. It was shown that under SQT3 condition, the action potential duration was abbreviated, amplitude and magnitude of I_{K1} current was increased, channel activation coefficient was enlarged, the APDR and ERPR were both decreased, QT interval in pseudo ECG was abbreviated clearly. Further more, the results under the D172N condition were more serious than under the WT-D172N condition. Increased I_{K1} under SQT3 condition accelerates the repolarization, enhances the excitability of the tissue, and probably induces ventricular fibrillation and sudden cardiac death.

Electrocardiographic T-wave Flattening and Action Potential Triangulation before TdP Onset

Tanveer A Bhuiyan*, Claus Graff, Morten B Thomsen, Johannes J Struijk

Aalborg øst, Denmark

Inhibition of the cardiac IKr current results in prolonged phase-3 duration of the monophasic action potential (MAP) which is manifested in the ECG as a broadened and flattened T-wave. In separate studies, both phase-3 duration (triangulation) and flattening of the T-wave have been linked to Torsades de Pointes (TdP) arrhythmia, but the association between their simultaneous change and TdP is still to be reported. We therefore developed a measure of T-wave flatness which captures MAP triangulation and investigated the development of the ECG-MAP relationship from baseline to immediately before the occurrence of TdP. The IKr inhibitor sertiindole was administered at supratherapeutic dose in five dogs with complete AV-block. Simultaneous recordings of 10 lead ECGs and left and right ventricular MAPs were obtained. All five dogs developed TdP. T-wave flatness was calculated as the ratio of the T-wave area (A1) to the area of an adaptive rectangle (A2) connecting the ascending and descending segments of the T-wave between the QRS complex and T(end), see figure. Therefore, the T-wave Ratio (TR) = $A1/A2$, a number between 0 and 1. A flat T-wave occupies a larger area of the surrounding rectangle compared to a peaked T-wave. Triangulation was calculated using the standard definition of MAP duration between the 30-90% repolarization points. TR reached a maximum immediately prior to TdP onset and increased from a baseline value of 0.44 ± 0.01 to 0.53 ± 0.036 just before TdP. Concurrently, the phase-3 durations changed from their baseline value of 100 ± 12.1 ms to 151.2 ± 26.5 ms before TdP onset. About 10-15 minutes after TdP termination, both TR and MAP duration returned to their baseline values (0.43 ± 0.01 and 101 ± 14 ms, respectively) T-wave flatness in the ECG is directly associated with triangulation of the monophasic action potential and both measurements can be used to indicate TdP onset in the dog.

S44

Computational Analysis of Head-Down Bed-Rest Effects on Cardiac Action Potential Duration

Elisa Passini*, Alessandro Pellegrini, Enrico G Caiani, Stefano Severi

University of Bologna
Cesena, Italy

S44

Introduction and Aim: Microgravity can possibly affect cardiac electrophysiology: several episodes of arrhythmias during spaceflight have been reported, as well as QTc interval prolongation. To better understand this phenomenon, our aim was to assess the effects of 21 days strict head-down (-6°) bed-rest (HDBR) on blood electrolyte concentrations and evaluate their impact on cardiac action potential (AP), using a computational model of human ventricular myocyte.

Methods: 10 healthy men (age 25-42 years) were enrolled at DLR (Köln, Germany) as part of the European Space Agency HDBR studies. Blood samples were collected before (PRE), during (BR) and after HDBR (POST). Holter 24h-ECG was recorded weekly, and repolarization duration (RT interval) derived during the night period from the vectorcardiogram by selective beat averaging technique. A human AP ventricular model has been improved to reproduce the inverse relationship between extracellular calcium and AP duration (APD): L-type calcium current formulation was modified, by strengthening calcium-dependent inactivation; minor changes were included to preserve whole cell physiology. Extracellular concentrations was considered in equilibrium with blood.

Results and Conclusion: Interestingly, BR induced RT interval shortening, that recovered at POST reaching values even higher than PRE (-20 ± 4.0 ms BRvsPRE, $+30 \pm 3.6$ ms POSTvsBR, $p < 0.001$). As for electrolyte concentrations, significant changes occurred in calcium (0.023 ± 0.018 mM BRvsPRE, -0.052 ± 0.077 mM POSTvsBR, $p < 0.05$), while only minor differences were found in sodium and potassium. Simulation of the AP ventricular model with average concentrations at PRE, BR and POST revealed a consistent but small biphasic time course of APD (-5.6 ms BRvsPRE, $+3.4$ ms POSTvsBR). When considering individual patients with larger electrolyte variations, APD changes became even more relevant (-18 ms BRvsPRE, $+12$ ms POSTvsBR). These results suggest that BR-induced alterations of repolarization can be partially linked to electrolyte unbalances, even if other factors should be taken into account for a more comprehensive analysis.

Computer Simulation of the Rabbit Purkinje Fibre Action Potential in Heart Failure

Jue Li*, Sunil Jit Logantha, Joseph Yanni-Gerges, Xue Cai, Halina Dobrzynski, George Hart, Mark Boyett

University of Manchester
Manchester, United Kingdom

The His-Purkinje network conducts the action potential from the atrioventricular node to the ventricles and causes them to contract. However, this network is also an important source of ventricular arrhythmias. ~25% of heart failure (HF) patients have left bundle branch block. Computer simulation is a useful tool to understand the physiology and pathophysiology of cardiac tissues, and we are using computer simulation to investigate the influence of HF on the His-Purkinje network. We have used a rabbit model of congestive HF induced by volume and pressure overload. In the left ventricular Purkinje fibres the expression level of the key cardiac ion channels was measured at the mRNA level using qPCR. Major changes were observed: for example, in HF, Kv4.2 (responsible for Ito) was downregulated by 96%, hERG (responsible for IK,r) was downregulated by 64% and Kir2.1 and Kir2.2 (responsible for IK,1) were downregulated by 79% and 97%, respectively. To simulate the effect of these changes, we began with a model of the healthy rabbit Purkinje fibre action potential. In the absence of ionic current measurements from failing rabbit Purkinje fibres, we have assumed that changes in ionic currents in HF mirror changes in ion channel expression—ionic conductances were adjusted, based on changes in expression of the relevant ion channels. In the simulations, if all the observed changes were incorporated, the Purkinje fibre is predicted to become inexcitable. Such an outcome would result in left bundle branch block, as is commonly observed in HF patients. The simulations predict that the HF-dependent changes in Ito, IK,r and IK,1 have the most influence on the Purkinje fibre action potential. The predicted changes in the Purkinje fibre action potential are now being compared to actual changes measured using sharp microelectrodes. Reference (1) Aslanidi OV et al. *Biophys J* 2009;97:20-39

P51

Simulation of Arrhythmia using Adaptive Spatio-temporal Resolution

Sándor Miklós Szilágyi*, László Szilágyi, Béat Hirsbrunner

1 University of Fribourg, Fribourg, Switzerland
Fribourg, Switzerland

P51

Aims: This study is aimed to present the simulation of several types of cardiac arrhythmias using adaptively selected spatio-temporal resolution. This task involves the accuracy analysis of the experiment in function of applied resolution. The promoted method may throw light upon the limits and necessary granulation of modeling during several cardiac rhythm malfunctions such as tachycardia, bradycardia, atrial and ventricular fibrillation (AF/VF).

Methods: We developed a spatio-temporal adaptive whole-heart simulation algorithm that handles automatically and regionally the proper resolution. The limits of upper and lower resolutions (0.2-5 mm; 1-500 μ s) are a-priori established, while the granularity at a given moment depends from the type, place and state of each modeled compartment. The simulation was performed using Nygren atrial and Luo-Rudy II ventricular cell models. We employed the effect of muscle fiber direction (ratio between longitudinal-transversal conductivity varies from 2-15), laminar sheet effect (in-sheet transversal conduction is 2-6 times faster than trans-sheet conduction), average and minimal depolarization period (considered 70-280 ms), and cell inhomogeneity (using conduction speed differences for base-apex gradient (5%-25%), transmural epicardial-endocardial gradient (5%-45%), left-right ventricular gradient (5%-20%)).

Results: The estimation errors were maximal during fast depolarization phase of the activation potential. Under normal circumstances, tachycardia and bradycardia, a 2/5/10 times lower spatial resolution induced a 3%/7%/12% estimation error of the depolarizing front line's shape, while a 5/10/20 times lower temporal resolution altered the spreading wave's aspect by 6%/11%/17%. In presence of AF/VF, under similar simulation conditions, the estimation error has raised up to 6%/11%/16% for lower spatial resolution, while the lower temporal resolution has elevated the differences to 9%/16%/27% level.

Conclusion: The simulation of cardiac arrhythmia demands high spatio-temporal resolution during fast depolarization phase. In presence of AF/VF an even higher resolution is claimed due irregular spread of depolarization.

Coherent Structures and Nonlinear Control of Cardiac Tissue

Roman Grigoriev*, Christopher Marcotte

Georgia Institute of Technology
Atlanta, United States

While ionic models of cardiac cells get progressively more detailed, including many tens of variables, and more detailed information about the shape and heterogeneity of the tissue and fiber rotation is incorporated in tissue models, numerical simulations becomes progressively more time-consuming. This makes them unsuitable for real-time applications such as advanced pacemakers and defibrillators that could exploit the dynamics to gently steer the tissue away from arrhythmic behaviors towards the normal rhythm using very weak electrical feedback, thereby preventing tissue damage and extending the life time of those devices. While the detailed models of cardiac tissue are very high-dimensional (at a minimum, the number of variables equals the number of cells times the number of gating variables plus intra- and extracellular potential), the real dynamics are not, due to a large degree of temporal and spatial coherence resulting from dissipation, even for very complicated rhythms such as fibrillation. Hence, a much lower-dimensional (and hence computationally more tractable) description of the tissue dynamics is possible. We show that detailed PDE/ODE models of cardiac tissue could in fact be reduced to an ensemble of low-dimensional systems of linear ODEs enabling real-time prediction and control. This reduction is based on periodic orbit theory which describes tissue dynamics corresponding to spatiotemporally complex rhythms such as fibrillation as a walk through neighborhoods of a hierarchy of coherent structures which represent exact unstable solutions (equilibria, time-periodic states, traveling waves) of the detailed tissue model. We also describe a computational approach based on Arnoldi iteration and matrix-free Newton-Krylov method for extracting these unstable solutions and using them and their dynamical connections (heteroclinic orbits) to guide the dynamics through phase space, e.g., from fibrillation to normal rhythm.

P51

Inverse Reconstruction of Epicardial Potentials Improves by Vectorcardiography and Realistic Potentials

Matthijs JM Cluitmans, Pietro Bonizzi, Joël MH Karel, Paul GA Volders, Ralf LM Peeters, Ronald L Westra

Maastricht University, Maastricht, the Netherlands

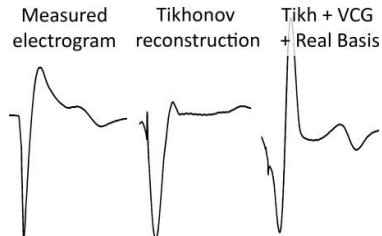
P51

The inverse problem of electrocardiography is to reconstruct electrical activity at the level of the epicardium from body-surface electrograms and a patient-specific torso-heart geometry. Previously, we have shown that the use of realistic epicardial training electrograms can improve reconstruction quality *in silico*. Here, we apply this method in a patient and compare the resulting computed electrograms with selected intracardiac measurements. Additionally, we utilize a new method that yields further improvements by incorporating characteristics of vectorcardiographic patient-specific information.

In a patient, 256 body-surface electrograms were recorded simultaneously. A CT scan was performed to obtain the position of electrodes and the heart contour. Based on the digitized torso-heart geometry and measured body-surface potentials, Tikhonov regularization was applied to compute the associated epicardial electrograms. As a novel step, these electrograms were then improved by optimizing their vectorcardiographic characteristics to match those from body-surface potentials by means of subspace alignment. Next, improved epicardial electrograms were projected on a realistic basis, constructed from computer-generated (FitzHugh-Nagumo) electrograms.

Two intracardiac leads provided measurements: at the left ventricular epicardium, and the right ventricular endocardium. The measured electrograms were compared to the reconstructed electrograms at those locations, for a paced beat and a native beat. Tikhonov reconstruction alone yielded reconstructed electrograms with a Spearman correlation coefficient (CC) of the QRS-complexes of 0.03. Vectorcardiographic improvement yielded electrograms with $CC=0.64$, and subsequent projection onto the realistic basis resulted in electrograms with $CC=0.77$, which was a significant improvement. More importantly, as the figure illustrates for a paced beat on the left ventricle, significant deflections showed up in the reconstructed electrograms after applying vectorcardiographic improvement and projection on the realistic basis (“Tikh+VCG+RealBasis”).

These results indicate that computer-generated electrograms are useful for improving reconstruction of epicardial electrograms, and that the combined use of patient-specific vectorcardiographic characteristics yields further improvements.



Automatic Parametrization Strategy for Cardiac Electrophysiology Simulations

Caroline Mendonca Costa, Elena Hoetzel, Bernardo Martins Rocha,
Anton Prassl, Gernot Plank

Medical University of Graz
Graz, Austria

Aims: This study aims to develop a novel, fully automatic strategy for the parametrization of tissue properties in the cardiac bidomain equations. Instead of relying upon direct measurements of material properties which cannot be conducted with sufficient accuracy, an numerical scheme is proposed which iteratively refines material properties for a given spatial resolution, h , until a sufficiently accurate match between model and experiment is achieved. Conduction velocity and anisotropy ratios are the parameters we aim to fit.

Methods: A monodomain model using harmonic mean conductivities as tensor eigenvalues is spatially discretized with varying space steps, h , to evaluate the impact of numerical errors due to the choice of h on the conduction velocity of planar wave fronts along the principal axes of conduction. Based on the proportionality relationship between conduction velocity and harmonic mean conductivity, $C_{\zeta}^v \propto \sqrt{\frac{\sigma_{m\zeta}}{\beta}}$, an iterative refinement scheme is derived to determine conductivity values which yield the prescribed conduction velocity. In a final step, harmonic mean conductivities are split into intracellular and extracellular components, a process that is governed by prescribed anisotropy ratios, $\alpha_{\zeta} = \frac{\sigma_{i\zeta}}{\sigma_{e\zeta}}$.

Results: When keeping harmonic mean conductivities, determined on a fine grid of $h = 1\mu m$, during simulation runs on coarser grids, deviations in conduction velocity increased with h . When equations were re-parametrized on grids of coarser h using the automatic parametrization strategy, wave fronts propagated with the exact prescribed velocity. Re-parametrized values varied slightly, between -6% up to 24%, within a range that is well below experimental uncertainty. Moreover, using the derived expressions with prescribed anisotropy ratio to obtain intracellular and extracellular conductivity values of the bidomain model yielded matching propagation patterns in full bidomain simulations.

Conclusion: Using an iterative approach to compute bidomain material parameters we demonstrate that activation sequence of cardiac electrophysiology simulations can be matched very well with experimental data, independently of h .

P51

Cardiac Spiral Waves Drifting Due to Spatial Tissue Temperature Gradients

Guy Malki*, Sharon Zlochiver

Tel Aviv University
Tel Aviv, Israel

Aims: This study aimed to simulate a rotor drifting due to temperature heterogeneity. Our hypothesis is that temperature gradients will cause to excitability heterogeneity, which will affect the spiral waves' dynamics. This may help to detect, map and characterize cardiac spiral waves, and improve their traditional treatment.

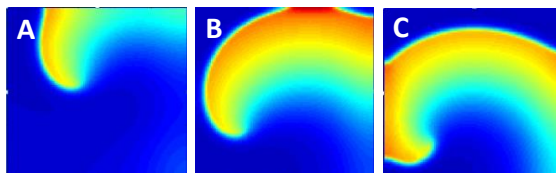
Methods: Cardiac electrical conduction was simulated in 2D square tissue models and stable rotors were initiated. Human atrial kinetics were employed (Courtemanche-Kneller model), and the effect of temperature on the rate constants of gating variables was incorporated using the temperature adjustment function:

$$k(T) = Q_{10}^{\frac{T-T_0}{10}}$$

where T_0 is the reference temperature (normally set to 37°C), T is the temperature, and Q_{10} is the ratio by which the rate constants increase following a temperature change of 10°C . Q_{10} factors for each gating variable were taken from the literature. Two types of temperature heterogeneity were modeled: 1) linear spatial temperature gradient, and 2) a regional (4mm-wide square) temperature perturbation.

Results: The linear temperature gradient simulations showed spiral wave drifting according to the gradient direction (figure). The specific gradient parameters (minimum temperature T_1 , maximal temperature T_2 , and $\Delta T = T_2 - T_1$) had a major impact on the resulting drift dynamics, and could result in unstable rotors or to insignificant drifting. The regional temperature perturbation simulations generally yielded faster rotor drifting and rotor anchoring around the temperature heterogeneity location.

Conclusion: Local temperature perturbation can be employed to control rotor drifting and trajectory due to its effect on tissue excitability heterogeneity. While this type of heterogeneity is not physiological, it is possible to artificially introduce it by localized heating, in order to improve arrhythmia research and its treatment.



Spiral wave location after 4 rotations post formation for : A) uniform temperature of 37°C , B) temperature gradient along the y-axis of $\Delta T=1^\circ\text{C}$, and C) regional square temperature perturbation of $\Delta T=1^\circ\text{C}$. The spiral wave drifts and anchors around the perturbation.

Realistic 3D Bidomain Model of Whole Heart Electrical Activity and ECG Generation

Siniša Sovilj¹, Ratko Magjarević¹, Nigel H. Lovell², Socrates Dokos²

¹University of Zagreb, Zagreb, Croatia

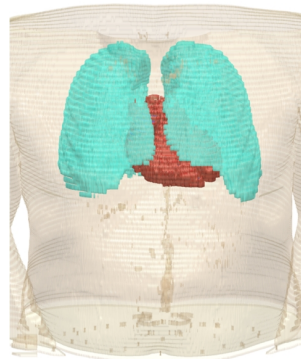
²University of New South Wales, Sydney, Australia

Aims: This study aimed to develop a realistic 3D bidomain model of whole-heart electrical activity. The heart was embedded in the torso and incorporated spontaneous activation in the sinoatrial node, accompanied by conduction through the specialized conduction pathways. It also included heterogeneous action potential (AP) morphologies in various regions of realistic heart.

Methods: The realistic 3D model geometry was assembled from segmented CT images of the Visual Human Project male dataset and the mesh was imported into Comsol Multiphysics finite element solver. Due to computational simplicity we used modified FitzHugh–Nagumo (FHN) equations to simulate the myocyte APs for different heart areas. The realistic mesh geometry incorporated the whole-heart as a volume source, with heart cavities, lungs and torso as passive volume conductors. We placed four surface electrodes at the limbs of the torso: V_R (right arm), V_L (left arm), V_F (left leg) and V_{GND} (right leg or ground) to simulate the Einthoven leads of a standard 12-lead system. The simulations were performed on an Intel Core i7-970 processor workstation with 24 GB of memory, 2x6 cores and processing power of about 100 Gflops.

Results: The model was able to simulate and generate realistic electrocardiogram (ECG) morphologies under normal and pathological heart states. The time dependent solver took about 12 hours to solve 1 simulated second of ECG with 1 ms resolution.

Conclusion: A realistic 3D cardiac model was developed using broadly available commercial finite element software that could run on relatively standard computer hardware. Apart from its educational value, the model can be used as a simulator for induction of various arrhythmias such as atrial/ventricular fibrillation, for simulating effects of changes in tissue conductivity, AP duration or AP shape on ECG morphology. As a continuous bidomain model it also allows simulation of fibrillation and defibrillation waveforms.



Geometry of the realistic 3D bidomain model of the whole-heart embedded in a torso.

P52

Effects of species-dependent differences in action potential shape in setting β -adrenergic-stimulation induced current.

Luca Sala, Chiara Bartolucci, Claudia Altomare, Marcella Rocchetti, Gaspare Mostacciolo, Stefano Severi, Antonio Zaza

University of Milano - Bicocca
Milano, Italy

P52

Background: The cardiac action potential (AP) shape is a species-dependent feature related to differences in ionic currents underlying repolarization. In guinea pigs (GP), large mammals and humans, the AP is prolonged by a pronounced plateau phase. In canine and human, but not GP, myocytes, a spike-and-dome profile characterizes repolarization of specific regions within the heart and to a different extent according to heart rate. It is still unclear whether the response to β -adrenergic stimulation is dictated by peculiarities of ion channels properties, or may simply results from differences in AP contour.

Aim: The aim of this project is to test whether the presence of the spike-and-dome in the AP contour is, by itself, able to modify the response of membrane current to β -adrenergic stimulation in a rate-dependent fashion.

Methods: In this study we performed AP-clamp experiments on GP myocytes with dog epicardial and endocardial AP waveforms to assess the contribution of the spike-and-dome in isoprenaline (ISO) sensitive current (I_{ISO}) at cycle lengths (CL) of 2000 ms and 500 ms. We also performed dynamic clamp experiments on GP myocytes with a computational simulated canine transient outward current (I_{to}) to evaluate the ISO response on the AP duration (APD) in presence of an artificial spike-and-dome.

Results: We found that: 1) at CL2000, I_{ISO} is more inward with dog endocardial rather than dog epicardial waveform; this difference was not evidenced at CL500. 2) The injection of a simulated canine I_{to} is not sufficient by itself to affect the direction of APD changes during β -adrenergic stimulation.

Conclusions: The differences between dog and GP in setting β -adrenergic stimulation response are a species-dependent feature not related to the presence of I_{to} and might be explained as a more complex mechanism involving AP shape and a diverse contribution of Ca^{2+} and K^+ channels during the AP.

A Comparison of Two Models of Human Ventricular Tissue: Simulated Ischaemia and Re-entry

Mitra Abbasi*, Richard Clayton

University of Sheffield
Sheffield, United Kingdom

Introduction: Several models of the human ventricular action potential have been developed. The aim of this study was to compare the dynamical behaviour and impact of simulated ischaemia in two cell models: the O'Hara-Rudy dynamic (ORd) model, and the Ten Tusscher-Panfilov 2006 (TP06) model.

Methods: The epicardial variant of each cellular model was embedded in a 2D monodomain tissue model, and solved with an explicit finite differences approach with a fixed space step of 0.02 mm and time step of 0.005 ms. Action potential duration (APD) and conduction velocity (CV) restitution were measured using an S1S2 protocol with S1=1000ms. An ATP activated potassium current was added to each model. To obtain stable re-entry in the ORd model, the Na⁺ current formulation was replaced by the Na⁺ current formulation from the TP06 model. Ischaemia was simulated by elevating extracellular potassium concentration from 5.4 mM to 6.0 and 8.0 mM, and by reducing intracellular ATP concentration from 6.8 mM to 6.0, 5.0, and 4.0 mM. For each combination, APD and CV restitution was determined, as well as the period of spiral wave rotation.

Results: The response of both models to simulated ischaemia was qualitatively similar. Elevated extracellular potassium acted to reduce CV, but had little effect on APD. Reduced ATP acted to decrease APD, but had only a small effect on CV. These modifications had only small effects on the shape of the action potential down stroke. Elevated extracellular potassium increased re-entry period from 221.9 ms (TP06) and 310 ms (ORd) to around 450 ms. Reduced intracellular ATP decreased the period of re-entry to between 195 and 290 ms.

Conclusion: Despite different formulations for both transmembrane currents and calcium handling in these models, the dynamical behaviour and their response to simulated ischaemia in these models was similar.

P52

Modelling the Integrated Regulation Role of β -adrenergic Signaling and CaMKII in Human Myocyte Electrophysiological Properties

Ling Dai, Yunliang Zang, Dingchang Zheng*, Ling Xia

Zhejiang University
Hangzhou, China

P52

Both β -adrenergic receptor (β -AR) signaling pathway and Ca^{2+} /Calmodulin-dependent protein kinase II (CaMKII) play important roles in regulating cardiac excitation-contraction coupling (ECC). Because the laboratory experiment can not quantify these regulatory roles easily, computer modelling has been used as an alternative way. However, the majority of published computer models were based on the ventricular myocyte of different animals, and there was few for human ventricular myocyte. The aim of this study was to use computer models to preliminarily investigate the combined role of β -AR and CaMKII in human cardiac myocyte properties, including the rate dependence of action potential duration (APD), Ca^{2+} and $[\text{Na}^+]$ transient amplitude. With the hypothesis that β -AR is mainly mediated by targets of protein kinase A (PKA) phosphorylation, the influence of PKA was incorporated into a modified ORd's model. The formulations of L-type Ca^{2+} current (ICaL), slow-activating delayed rectifier K^+ current (IKs) and phospholamban (PLB) were then modified. The simulation results were finally compared with and without the administration of isoproterenol (ISO). Our simulation showed that, in comparison with the control, ISO shortened APD₉₀ by 15ms (265 ms vs 250 ms) at the cycle length of 1000 ms. At the same cycle length, the amplitude of Ca^{2+} transient was increased by approximate 60%. This increase was not observed for $[\text{Na}^+]$. Our findings agree well with some published experimental observations. In conclusion, a human ventricular myocyte model has been developed to investigate the role of β -AR and CaMKII in human myocyte electrophysiological properties. This model can be used as a platform to further investigate their separate or integrated role in cardiac arrhythmias.

A Software Toolkit for Nonlinear Heart Rate Variability Analysis

Constantino* A. García, Abraham Otero, Jesús Presedo, Xosé Vila, Paulo Félix

Centro Singular de Investigación en Tecnoloxías da Información (CI-TIUS), University of Santiago de Compostela, Santiago de Compostela, Spain

Introduction: The use of nonlinear time series techniques in the analysis of Heart Rate Variability (HRV) is growing. However, support for these techniques in HRV toolkits is weak. Often, they only permit the calculation of the more basic nonlinear statistics, and completely lack functionality to perform nonlinearity tests –which should be performed before applying nonlinear analysis techniques–, support for nonlinear noise reduction, or for dealing with the problems that arise when searching for nearest neighbors in a phase space calculated from a discretized temporal series –such as the RR intervals. Thus, researchers who use these techniques have to either implement the algorithms themselves –which is prone to errors and makes it harder to reproduce their results– or use general nonlinear analysis packages not geared towards RR analysis. Both solutions are suboptimal.

Aims: This paper presents an extension to the RHRV open source package to endow it with nonlinear RR analysis support. RHRV is an open source package for the R environment for statistical computing which already has support for a wide variety of time and frequency HRV analysis methods.

Results: We have implemented a phase space reconstruction algorithm that uses the delays method and that deals with the problem of discretization in the RR series. The package provides automatic estimation of both the embedding dimension and the time lag needed for the phase space reconstruction. Functionality to perform nonlinearity tests and nonlinear noise reduction is also provided. A wide variety of nonlinear statistics can be calculated, including largest Lyapunov exponent, correlation dimension, SD1/SD2 of Poincaré plots, detrended fluctuation analysis, approximate entropy and recurrence quantification analysis.

Conclusions: An open source package such as RHRV can provide invaluable support when performing nonlinear HRV studies and it makes the results more reproducible.

P53

Implementation of Heart Rate Variability Signal Processing into FPGA: System on-Chip Design

Shahab Rezaei*, Hossein Ajourloo, Sadaf Moharreri

Khomeini Shahr Branch, Islamic Azad University
Isfahan, Iran

P53

The analysis of HRV signal provides more valuable information for the physiological interpretation of heart rate fluctuations. The importance of this signal needs more investigation of methods as aids to clinical evaluation. Many works have been done to extract different kinds of information from HRV signal in various ways. Time, Frequency and nonlinear analysis of this signal are the majors processing that have been done on HRV signal and the resulted features are useful tools for diagnosis different problems in heart function. In this paper, we try to develop and implement the HRV signal processing into a Field Programmable Gate Array (FPGA) for extracting this signals feature. The hardware implementing algorithm was developed in Verilog Hardware Description Language (HDL). In designed hardware, after defining the number of samples in the input, it extracts and analyses the time domain features of HRV signal and also the parameters that can be extracted from the Poincare plot of this signal. The number of 15 recorded HRV signal from the Physionet database (Normal Sinus Rhythm (NSR), Congestive Heart Failure (CHF) and Atrial Fibrillation (AF) used as test input to test the modules implemented on FPGA. The performance of the system was tested using MATLAB and validated based on the mentioned input signals. Simulations show that the proposed system is able to achieve appropriate HRV analyses in the hardware. This system can be develop and use for more feature extraction by different kinds of analysis on HRV signal. The proposed system is suitable for portable monitoring devices and arrhythmia detection and as a biomedical signal processor on a system-on-chip (SOC) design.

VARVI: A Software Tool for Heart Rate Variability Analysis in Response to Visual stimuli

Leandro Rodríguez-Liñares, Pedro Cuesta, Raúl Alonso, Arturo J Méndez, María J Lado, Xosé A Vila*

University of Vigo
Ourense, Spain

Aim: this paper describes VARVI: a free software tool developed in our research group to perform heart rate variability (HRV) analysis in response to different visual stimuli. The tool was developed after realizing that this type of studies are becoming popular in fields such as psychiatry, psychology and marketing, and taking into account the lack of specific tools for this purpose. **Tool description:** VARVI has been developed in python programming language and tested on Linux, but keeping portability as a key feature. It requires the subject to wear a Polar WearLink Bluetooth chest strap. Then, the researcher selects a set of video files and the tool plays them in a predefined or random order, while the subject's heart rate is recorded. As a result, two text files are obtained that can be read by other HRV tools developed in our group (RHRV and gHRV). HRV indices in both time and frequency domains and also nonlinear parameters corresponding to each video are obtained, and can be statistically analyzed. **Current and future use:** it has already been used for analyzing the HRV response of 90 subjects while viewing spots of the last Galician election campaign. Results from this study will be presented in the IBERCOM-2013 conference. In the near future, VARVI will be used in at least two research projects to analyze the impact of a traffic accidents prevention campaign in Spain, and also in a research work with depressed patients in collaboration with the Hospital of Ourense. **Download:** VARVI is freely available in <http://varvi.milegroup.net>

P53

Trend Strips: a New Tool to Analyze RR Time Series

Antônio Carlos Silva Filho*, Regiane Máximo Souza, Fátima Maria Helena Simões Pereira da Silva, Júlio Cesar Crescêncio, Lourenço Gallo Júnior

Uni-FACEF - Centro Universitário de Franca
Ribeirão Preto, Brazil

P53

There are many different tools and parameter that can be used to analyze RR time series, as the Correlation Dimension, the Lyapunov Exponents, the Higher Reconstruction Step and so on. Here we address the problem of discriminating between two populations: one with some cardiac disease and another with healthy people, in a non-invasive way, through RR time series. The mathematical tool used to analyze the series is called Trend Strips (TS) and was proposed recently in the scientific literature. TS are a sequence of "0" and "1", where "1" means that the value in some position is greater than the value in a previous position in the series, while "0" means the opposite. We can use TS of any size, where the size is the amount of "0" and "1" considered. If we choose TS of size 4 we will have 16 different sequences at our disposal, from "1111" to "0000". What we do, then, is to compute the relative frequency of occurrence of each of them in a particular time series and to compare the frequencies in both groups. We collected RR time series from two groups of men at rest: one group with a cardiac chagasic disease (24 individuals) and a second one of healthy people (21 individuals). We analyzed TS of sizes from 2 to 5 and found significant TS that discriminate the two groups at all sizes. The statistical test used was a t-test and some of the TS useful, with a $p < 0.01$ were: (a) for $n=2$, TS "00" ($p=0.0009$); (b) $n=3$, TS "101" ($p=0.0055$) and TS "000" ($p=0.0061$); (c) for $n=4$, TS "1011" ($p=0.0059$), TS "1000" ($p=0.0071$) and TS "0001" ($p=0.0073$), etc. The set of significant TS can be useful, then, for diagnostic purposes. SUPPORT OF FAEPA-HC-FMRP-USP AND FAPESP AND CNPq.

Variability of Left Ventricular Ejection and Diastolic Times Obtained from Impedance Cardiography: A Comparison with Heart Rate Variability

Salvador Carrasco-Sosa, Alejandra Guillén-Mandujano*

División de Ciencias Biológicas y de la Salud, Universidad Autónoma Metropolitana-I, DF, México
Mexico City, Mexico

Despite ejection time (ET) has been widely used for evaluating left ventricular function, its variability remains unclear. Our aim was to compare the time-frequency spectral measures of HRV with those of the variability of: impedance heart periods (IHPV), ejection time (ETV) and diastolic time (DTV), computed from impedance cardiography (ICG) traces in four maneuvers that elicit different vagal activity. ECG and ICG were recorded from 17 healthy volunteers during 5-min supposedly steady-state conditions: supine position (SP), controlled breathing (CB), standing (S) and dynamic exercise (E). Diastolic time (DT), ET and impedance heart period (IHP) were computed from the ICG derivative. Time-frequency spectra of RR intervals (RR), IHP, RR-IHP difference, ET, and DT series were estimated via the smoothed pseudo-Wigner-Ville distribution to compute their corresponding high-frequency (HFRR, HFIHP, HFRR-IHP, HFET, HFDT) and low-frequency powers (LFRR, LFIHP, LFRR-IHP, LFET, LFDT). Time-frequency coherences of LFRR and HFRR with the respective components of the other series were obtained. For statistical analysis, 50-s epochs of the indexes dynamics were used. Slopes of relations, correlations and coherences of LFRR and HFRR with LFIHP, HFIHP, LFDT and HFDT ranged from 0.89 to 0.99 in SP, CB and S, decreasing in E ($p < 0.01$), and were greater ($p < 0.001$) than those corresponding to LFET and HFET in all maneuvers. S condition reduced ($p < 0.02$) both HFRR-IHP and LFRR-IHP. Powers of HFRR-IHP were much greater ($p < 0.005$) than LFRR-IHP in all maneuvers. In SP, CB and S, ETV accounted for $4 \pm 3\%$ of IHPV, percentage that increased substantially in E ($p < 0.001$). Although HRV determines most of IHPV, the latter contains additional respiratory modulation that limits their interchangeability, especially in E. DTV, accounting for $96 \pm 9\%$ of IHPV, indicates that DT is the portion of the cardiac cycle where autonomic modulation occurs, contrasting with the minimal ETV required for the appropriate timing of systolic processes.

P54

A Modified Hilbert-Huang Algorithm to Assess Spectral Indices in Intense Exercise

Rebeca Goya-Esteban*, Óscar Barquero-Pérez, Elena Sarabia-Cachadiña, José Naranjo-Orellana, José-Luis Rojo-Álvarez

Rey Juan Carlos University
Fuenlabrada, Spain

P54

Introduction: Spectral indices are widely used to assess Heart Rate Variability (HRV) during exercise. HRV signal spectrum comprises two main spectral bands, High Frequency (HF) and Low Frequency (LF), the first related to parasympathetic activity and the second related to both parasympathetic and sympathetic activity. During exercise, it is generally assumed that heart rate increases due to both a parasympathetic withdraw and an augmented sympathetic activity. However, the literature presents conflicting results when HF and LF bands powers are assessed during exercise. HF and LF powers are mostly obtained through Fast Fourier Transform (FFT) based algorithms, however there is a major problem due to the non-stationary and non-linear properties of the signal.

Methods: In the present study we used a modified version of the Hilbert-Huang (HH) algorithm. After performing Empirical Mode Decomposition, the two last Intrinsic Mode Functions (IMF) were eliminated to detrend the signal. Next, two band pass filters with pass bands matching the LF and HF bands were used to filter the remaining IMFs. The instantaneous amplitudes and frequencies were obtained through the Hilbert Transform. Finally, the instantaneous LF and HF powers were obtained to assess the HRV evolution in an All Out Exercise Test (AOET) on eight male amateur triathletes.

Results: Both techniques revealed depressed LF and HF powers during exercise, but FFT-based approach gave systematically nearly zero LF power values while HH-based approach showed higher variability. Furthermore, with the FFT-based approach the LF/HF ratio was always lower than one during intense exercise, while the mean of the instantaneous LF/HF ratio was lower than one only in one case.

Conclusion: In contrast to the FFT-based approach the HH-based approach allows a detailed tracking during AOET and it may allow a more accurate insight about the sympathetic and parasympathetic balance during exercise.

Seismocardiograms Return Valid Heart Rate Variability Measures

Alexandre Laurin*, Andrew Blaber, Kouhyar Tavakolian

Simon Fraser University
Vancouver, Canada

Low heart rate variability (HRV) is a risk factor for angina pectoris, myocardial infarction, as well as death following coronary heart disease and congestive heart failure. It is also correlated with depression and insomnia. HRV indices have traditionally been acquired using electrocardiogram RR intervals. We propose to use low frequency vibration signals recorded from the sternum using accelerometers (seismocardiogram) instead. The validity of such measurements would present an interesting discovery due the recent ubiquity of very affordable accelerometers of satisfactory sensitivity in mobile phones.

Eighteen healthy subjects were taken to -20, -30, -40, and -50 mmHg of lower body negative pressure (LBNP) preceded and followed by supine rest. Each step lasted 5 minutes. We compared heart period (ms) as obtained from aortic-opening to aortic-opening (AO-AO), mitral-closure to mitral-closure (MC-MC), isovolumic moment to isovolumic moment (IM-IM) to that obtained from RR intervals. The largest absolute mean difference was computed to be smaller than 0.00015% and the largest amplitude of 95% confidence interval was computed to be smaller than 0.07%.

We computed all 14 time-domain statistical and frequency-domain measures specified by the Task Force of the European Society of Cardiology and the North American Society for Pacing and Electrophysiology. All amplitudes of 95% confidence intervals were smaller than 2%.

We further compared, at initial rest and -50 mmHg LBNP, all 12 measures that did not require recordings over 5 mins. All measures that exhibited statistical difference using one technique exhibited statistical difference using all techniques.

We conclude that AO-AO, MC-MC, and IM-IM are valid measurements of heart period and lend themselves validly to time-domain and frequency-domain analysis. It is our recommendation that AO-AO intervals be used as they represent well defined events and are obtainable without the use of ECG markers.

P54

Fast Detrending of Unevenly Sampled Series with Application to HRV

Valeria Villani*, Antonio Fasano

Università Campus Bio-Medico di Roma
Rome, Italy

P54

Aims: In this paper we propose a novel approach to detrending RR series, which is both effective and fast. Detrending RR series is a common processing step prior to HRV analysis. In the classical approaches RR series, which are inherently unevenly sampled, are interpolated and uniformly resampled, thus introducing errors in subsequent HRV analysis. **Proposed Approach:** To cope with this problem, we introduce a suitable measure of “variability” that contains information about the (possibly uneven) sampling grid. Trend is estimated by solving a constrained convex optimization problem that exploits the measure of “variability” to track the slowly varying components of the RR series. The solution is in closed form and the resulting algorithm is fast, since its computational complexity is linear in the size of the vector to process.

Results: Performances were investigated both on real and synthetic RR series and compared to state-of-art algorithms, namely smoothness priors (SP) and Gaussian process priors (SGP). Measuring performance in terms of detrending error, the proposed approach returned a mean error of 255 s^2 with variance $2.12 \times 10^{-4} \text{ s}^4$; SP returned a mean error of 258 s^2 with variance $1.61 \times 10^{-3} \text{ s}^4$; SGP returned a mean error of 255 s^2 with variance 9.56 s^4 . Regarding execution time, the proposed approach required 0.82 s to detrend an RR series of 10^7 double precision floating point samples, whereas SPG required 690 s, and SP could not complete the task due to out of memory error.

Conclusion: The proposed approach can handle RR series without resorting to interpolation and resampling. It outperforms competing algorithms in terms of performance and it is remarkably fast, due to its linear complexity. This makes it suitable for long-term HRV analysis. To the best of the authors' knowledge, it is the fastest algorithm for detrending RR series.

Higuchi's Fractal Complexity of RR and QT Interval Series during Transient Myocardial Ischemia

Rudys Magrans¹, Pedro Gomis¹, Pere Caminal¹, Andreas Voss²

¹Dept ESAll, Universitat Politècnica de Catalunya, Barcelona, Spain

²Dept MEB, University of Applied Sciences, Jena, Germany

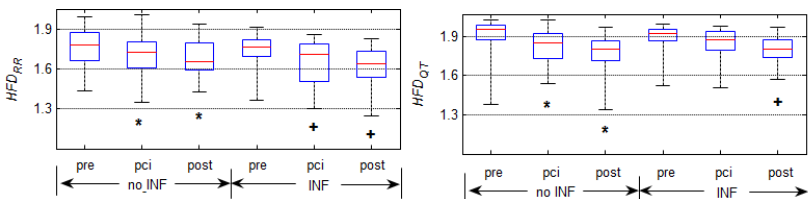
P55

Introduction: Myocardial ischemia may lead to significant changes in autonomic control of heart rate (HR) affecting its variability and alter beat-to-beat ventricular repolarization periods. We hypothesized that transient myocardial ischemia affects the complex dynamics of the HR and QT. The aim of this study was to assess the RR and QT interval time series complexity using Higuchi's fractal dimension (HFD) during prolonged balloon occlusion of one of the major coronary arteries.

Methods: Eighty-five patients who underwent elective percutaneous coronary intervention procedures were selected. Patients were classified into 2 groups according to the presence of prior healed myocardial infarction (INF) (n = 29) or not (No_INF) (n = 56). RR, QT and QTc (Bazget's formula) time series were obtained from continuous ECG with mean occlusion period of 4.66 ± 1.08 minutes. Three 3-minute stages were chosen: (1) preinflation (baseline), (2) from the start of occlusion (pci), and (3) immediately post deflation (post_pci). HFD was calculated on each 3-minute stage time series to quantify the changing complexity and self-similarity of R-R, QT and QTc time series (HFD_RR, HFD_QT and HFD_QTc, respectively). Cohen's d statistics were included to measure the effect size of the procedure.

Results: HFD decreased throughout the PCI procedure in the three time-series. From baseline to pci: HFD_RR, 1.76 ± 0.13 vs. 1.69 ± 0.15 ($p < 0.001$, Cohen's d = -0.64); HFD_QT, 1.90 ± 0.11 vs. 1.82 ± 0.13 ($p < 0.001$, d = -0.67); HFD_QTc, 1.88 ± 0.09 vs. 1.83 ± 0.11 ($p < 0.01$, d = -0.46). The HFD reduction was greater from baseline to post_pci ($p < 0.001$, d = -0.99 (RR), d = -1.02 (QT)). The figure shows the HFD reduction in each group.

Conclusions: The time series studied, related to autonomic control of HR and to the variability of ventricular repolarization, exhibit a reduced complexity provoked by transient myocardial ischemia.



HFD for RR and QT time series throughout the PCI. (*) $p < 0.001$ and (+) $p < 0.01$ vs. pre_pci.

On the Early Detection of Perinatal Hypoxia with Information-theory based Methods

Ricardo Santiago-Mozos*, Beatriz García-Vizueté, José María Lillo-Castellano, José Luis Rojo-Álvarez, Carlos Martín-Caballero

Dep of Signal Theory and Communications. Universidad Rey Juan Carlos

P55

Background: Perinatal hypoxia is a severe condition that might harm fetus organs permanently. When the fetus brain is partially deprived from oxygen, the normal control of the fetal heart rate (FHR) is affected. We hypothesized that advanced processing of the FHR, readily available at the hospital bed, can reveal whether the fetus is under perinatal hypoxia, which allows for quick action minimizing fetus organ damage.

Methods. We analyzed FHR morphology with normalized compression distance (NCD), a powerful measure coming from Information Theory, which compares two arbitrary sequences and outputs the dissimilarity between them. This measure exploits linear and non-linear relations in the data and allows the comparison of sequences of different sizes. In addition, NCD is parameter free and simple to apply. It was applied to raw FHR sequences and to a set of statistics computed from them (e.g. moments on 5 minutes signal windows). We classified the cases from the NCD dissimilarity matrix by using a simple nearest neighbour classifier and leave-one-out crossvalidation.

Results. FHR records were acquired with Philips cardiocograph for a total of 26 recordings, 13 controls and 13 cases. A case was declared whether: 1) the PH of the umbilical artery ≤ 7.05 ; or 2) the APGAR score 5 minutes after delivery was ≤ 7 and a reanimation type III or greater was required. Our best result was obtained with the sequences of the central moment of order 3 calculated over sliding windows of 5 minutes on the interval from 4 to 3 hours to delivery. Accuracy was 0.88 with sensitivity 0.92 and specificity 0.85, which is remarkable taking into account that visual expert interpretation of the FHR recording gives many false positives.

Conclusion: The NCD is a useful criterion for perinatal hypoxia prediction, with simple methods and good accuracy 3 hours before delivery.

Sample Entropy Parametric Estimation for Heart Rate Variability Analysis

M Aktaruzzaman*, R Sassi

Università degli Studi di Milano
Crema, Italy

Aims: Sample Entropy (SampEn) is a powerful approach for characterizing heart rate variability (HRV) regularity. On the other hand, autoregressive (AR) models have been employed for maximum-entropy spectral estimation for more than 40 years. The aim of this study is to explore the feasibility of a parametric approach for SampEn estimation through AR models.

Methods: Differential entropy measures were successfully employed to detect the reduction of complexity before paroxysmal atrial fibrillation (AF). Therefore, we re-analyze the Physionet paroxysmal AF database, where RR series are provided before and after an AF episode, for 25 patients. In particular, we selected short RR series, close to AF episodes, to fit an AR model. Then, theoretical values of SampEn, based on each AR model, were analytically derived (SEth) and also estimated numerically (SEsyn), on 200 synthetic series. Finally, starting from the original series, surrogate data were constructed to verify the impact of non-Gaussianity on the estimates.

Results: The value of SampEn (SErr), computed on the 50 RR series with $r=0.2 \times SD$, $m=1$ and $N=120$, were within the standard range of SEsyn in 30 cases (39 for SEth). The figure increases to 82% of cases if shorter series are selected ($N=75$), and if RR series are replaced by surrogates with Gaussian amplitude distribution. The editing method employed largely affects the results: ectopic beats are more likely before an AF episode. Interestingly, without removing ectopic beats, every estimates of SampEn considered was significantly different between pre- and post-AF series (SErr: $p=0.020$; SEsyn: $p=0.0024$; SEth: $p=0.023$).

Conclusion: Parametric SampEn estimation through AR model is influenced by lack of stationarity (common on longer series) and non-Gaussianity (i.e. ectopic beats). These limits are shared with AR power spectral estimation. However, when an AR model is appropriate and the theoretical estimates differ, this approach might enlighten additional information brought by SampEn.

P55

Enhancing Scaling Exponents in Heart Rate by means of Fractional Integration

A Leite, AP Rocha, ME Silva

CMUP, CM-UTAD, Universidade de Trás-os-Montes e Alto Douro
Vila Real, Portugal

The characterization of Heart Rate Variability (HRV) series has become important for clinical diagnosis. These series are non-stationary and exhibit long and short-range correlations. In recent years, the non-parametric methodology Detrended Fluctuation Analysis (DFA) has become widely used for the detection of these correlations. The standard procedure is to apply DFA to the RR series, estimating the desired scaling exponents.

P55

In this work we pursue an alternative approach which consists in applying DFA to the fractionally differenced RR series, $\Delta^d RR$, where $0 < d < 1$ is the long-range correlation parameter. Then, the usual scaling exponents α_1 and α_2 are calculated according to the time scales $4 \leq n \leq 11$ and $12 \leq n \leq 32$. Both methodologies are applied to 24h HRV series from the Noltisalis data base: 10 Healthy subjects, 10 patients suffering from Congestive Heart Failure (CHF) and 10 heart Transplanted patients.

The results (mean \pm standard deviation) for DFA scaling exponents calculated over RR series during 6 hours of the day period are, for each group: Healthy ($\alpha_1 = 1.53 \pm 0.26$, $\alpha_2 = 0.95 \pm 0.12$); CHF ($\alpha_1 = 1.19 \pm 0.32$, $\alpha_2 = 1.21 \pm 0.21$); Transplanted ($\alpha_1 = 0.66 \pm 0.29$, $\alpha_2 = 0.85 \pm 0.38$). The corresponding results for DFA scaling exponents calculated over $\Delta^d RR$ series are: Healthy ($\alpha_1 = 1.25 \pm 0.30$, $\alpha_2 = 0.65 \pm 0.17$); CHF ($\alpha_1 = 0.71 \pm 0.26$, $\alpha_2 = 0.69 \pm 0.28$); Transplanted ($\alpha_1 = 0.29 \pm 0.13$, $\alpha_2 = 0.26 \pm 0.27$). Similar results were obtained in 6 hours of the night period. The results indicate that the scaling exponents have circadian variation and decreased scaling exponent α_1 for sick subjects. Furthermore the scaling exponents α_1 and α_2 are combined for discriminating purposes. The scaling exponents obtained from $\Delta^d RR$ increase the discriminatory power among the 3 groups: from 76% to 83% during the day period and 60% to 80% during the night period.

We conclude that changes in HRV are better quantified by DFA scaling exponents calculated over fractionally differenced RR series than by the standard procedure.

Indices of Symbolic Dynamics' Distributions in Cardiac Patients

Giovanni D'Addio*, Maria Romano, Roberto Maestri, Paolo Bifulco, Mario Cesarelli

S. Maugeri Foundation
Telese Terme, Italy

Symbolic analysis (SA) of HRV is an emerging technique providing parameters independent of those derived from time and frequency-domains. Although SA has been proposed encoding different words of L-length of K-symbols, the resulting rapidly growing patterns, contrasting the need of synthetic evaluation's indices, have until now limited its clinical use. Aim of this study is to propose a patterns' redundancy reduction procedure, defining new SA indices to test on a clinical data-set of normal and cardiac patients. We studied forty 24h-ECG Holter of normal (N), post-MI (MI), heart failure (HF) and transplanted (TR) subjects. RR consecutive differences has been encoded into 5 symbols by a primary (10 ms) and secondary (50 ms) threshold and the resulting 3, 5 and 7 length words have been derived. Independently from length, all words have been classified by a dominance's criterion depending on the symbols' prevalence, in pattern words (PW) with a predominant vagal content (V), decelerating content (D) accelerating content (A) sympathetic content (S) and without variability content (0). Given the Gaussian shape of PW distributions, it has been derived the Kurtosis, measuring the distribution's peakedness, and the Chi-square, measuring deviation of the PW distribution from those observed in normals. Results showed an optimum word-length of 3, exhibiting the maximum F-value of the ANOVA test for PW between groups. For this distributions, both Kurtosis (2.2 ± 0.6 ; 2.2 ± 0.9 ; 3.1 ± 0.9 ; 4.0 ± 0.4) and Chi-square (7 ± 5 ; 8 ± 5 ; 26 ± 17 ; 106 ± 42 , respectively for N, MI, HF and TR) showed very significant $p < 0,0001$ value at the ANOVA test between groups, mainly discriminating HF and TR subject by Tukey's post-test. SA is an helpful technique in interpreting the encoded HRV information. The PW distributions clearly tend to lose their tails to the worsening of the autonomic impairment as immediately described by Kurtosis or chi-square index, especially for risk stratification of HF patients.

P55

In-vivo and Ex-vivo HRV discrimination by Complex Correlation Measure

Oto Janoušek*, Sara Francisco, Petr Veselý, Veronika Olejníčková, Marina Ronzhina, Ivo Provazník, Marie Nováková, Peter Scheer, Jana Kolářová

Brno University of Technology
Brno, Czech Republic

P55

Aims: Poincaré plot is a valuable technique for heart rate variability (HRV) assessment due to its ability to visualise nonlinear aspect of time series. In contrast to standard Poincaré plot descriptors SD1 and SD2, a recently published descriptor Complex Correlation Measure (CCM) can quantify the temporal aspect of the Poincaré plot. In this study, the potential of CCM as a more sensitive indicator than SD1 and SD2 in discriminating of the in-vivo and isolated heart beat-to-beat series was investigated.

Methods: Five New Zealand white rabbits and five isolated New Zealand rabbit hearts in Langendorff setup were studied. The R-peaks from five-minutes long ECG records have been manually detected and SD1, SD2, and CCM were computed in custom made software in Matlab.

Results: All three examined Poincaré plot descriptors (SD1, SD2, CCM) measured from isolated hearts were smaller than those measured from the in-vivo hearts. Only CCM exhibited statistically significant ($\alpha = 0.046$) difference between in-vivo and isolated hearts, however. Poincaré plot descriptor SD1 decreased from 5.6 ± 2.3 ms in in-vivo to 4.5 ± 6.7 ms in isolated hearts, SD2 decreased from 19.5 ± 6.6 ms in in-vivo to 11.6 ± 8.4 in isolated hearts, and CCM decreased from 0.106 ± 0.016 in in-vivo to 0.050 ± 0.051 in isolated heart, respectively.

Conclusion: CCM, a novel descriptor for Poincaré plot that measures the beat-to-beat dynamic of heart rate variability, has been found to be more significant parameter than widely utilised SD1 and SD2 in discriminating of in-vivo and isolated beat-to-beat series. Overall variability and temporal dynamics of beat-to-beat series decreased in isolated hearts.

Fractal Behaviour of Heart Rate Variability reflects Abnormal Respiration Patterns in OSAS Patients

Giovanni D'Addio*, Agostino Accardo, Mario Cesarelli, Alberto De Felice

S. Maugeri Foundation
Telese Terme, Italy

Although heart rate variability (HRV) decreasing has been usually described in obstructive sleep apnea syndrome (OSAS), some studies have recently questioned the validity of spectral HRV analysis in presence of respiratory and arrhythmic disorders. Fractal analysis (F) of HRV is an emerging nonlinear technique overcoming these limitations and allowing short term HRV assessment during hypo/apnea phases. This is one of the first studies on F-features in sleep apnea and its aim is to find out whether and to which extend F-HRV reflects abnormal respiration patterns in OSAS. We studied 30 polysomnographic recordings (PR) of severe OSAS ($AH\geq 30$) pts. (age 55 ± 9) and 10 PR of normal subjects (age 46 ± 4). Hypo/apnea phases and related beat-to-beat time series have been detected and classified by automated algorithms and manually verified by expert technicians. F-analysis has been performed by Huiguchi fractal dimension algorithm (FD), separately for normal breath (NB), hypopneas (HY), obstructive (OS) and mixed (MX) apneas epochs. Results showed that while FD does not significantly (Mann Whitney test $P>0.05$) differ between Normals (1.61 ± 0.09) and NB epochs in OSAS pts., it significantly (Friedman test $p<0.005$) tends to a less fractal structure from NB (1.60 ± 0.15) to HY (1.52 ± 0.13), OS (1.50 ± 0.12) and MX apneas (1.48 ± 0.11) epochs, with a significant Dunn's multiple comparisons post test only between NB vs. OS and MX apneas. Data demonstrate that F-HRV reflects abnormal respiration patterns in severe OSAS patients with a novel finding suggesting that the observed HRV decreasing in OSAS is not related to NB periods as mainly to the loss of variability just during abnormal respiration patterns.

P55

Non-linear dynamic analysis of RR signals in patients with and without Excessive Daytime Sleepiness

Umberto Melia, Marc Guaita, Montserrat Vallverdu*, Francesc Claria, Pere Caminal, Cristina Embid, Isabel Vilaseca, Manel Salamero, Joan Santamaria

Universitat Politècnica de Catalunya
Barcelona, Spain

P55

Non-linear measures of heart rate variability can be used to quantify modulation of sympathetic and parasympathetic branches of the autonomic nervous system (ANS). Thus, RR signals were obtained from the ECG recorded during two tests: MWT, which measures the ability to maintain wakefulness for a defined time; MSLT, which measures the ability or tendency to fall asleep. Patients with sleep disorder breathing underwent 5 trials of MWT and MSLT, interspersed throughout the day. Two end-points were considered: Study A, excessive daytime sleepiness (EDS) versus without daytime sleepiness (WDS), both groups of 20 patients; Study B, pre-CPAP versus post-CPAP (continuous positive airway pressure therapy) in EDS. After removing artifacts and ectopic beats with adaptive filtering, RR signals were resampled at 4 Hz. For each MWT and MSLT, 180-second windows of RR signals during awaking state were considered in the following frequency bands: VLF, <0.04 Hz; LF, 0.04-0.15 Hz; HF, 0.15-0.4 Hz; TB, total-frequency band. ANS activity was described by measures obtained from time-frequency representation (TFR). Correntropy (CORR) and auto-mutual-information function (AMIF) were used to describe the RR regularity. Results Study A: TFR, CORR and AMIF analysis showed that EDS presented higher parasympathetic activity and RR regularity than WDS (p -value<0.05) during MSLT. Discrimination accuracies of 77.5%, 82.5% and 85% were achieved by measures from TFR in HF band, from CORR in TB and from AMIF in HF and VLF bands, respectively. Study B: During MWT, parasympathetic activity and RR regularity in EDS were affected by CPAP therapy. All measures obtained from EDS in post-CPAP differed from pre-CPAP (p -value<0.05) and tended to be similar to WDS. Conclusions Non-linear dynamic analysis applied to RR signals improves the sensitivity of this analysis and detects statistically significant changes in MSLT events, in VLF, HF and TB bands, when comparing patients from EDS and WDS groups.

Development of Fetal Heart Rate Dynamics Before and After 30 Weeks of Gestation

Ahsan Khandoker*, Chandan Karmakar, Yoshitaka Kimura,
Marimuthu Palaniswami

Khalifa University

In this study, we have investigated how the dynamics of fetal beat-to-beat heart rate variability (fHRV) changes during development prior to and after 35 weeks of gestation. Noninvasive fetal electrocardiogram (ECG) signals [extracted from abdominal ECG by previously published method, Sato et al, IEEE Trans Biomed Engg, 2007, 54(1):49-58] from 45 pregnant women (27 cases before and 18 cases after 35 weeks) at the gestational age from 16 to 41 weeks with normal single pregnancies were analysed. A nonlinear parameter called complex correlation measure (CCM) which measures the variability in the temporal structure of Poincaré plot was used to understand the dynamics of fHRV. Dependency of CCM on gestational age was evaluated with correlation analysis and was found to be significantly ($p=0.003$) inversely correlated ($r=-0.74$) with gestational ages prior to 35 weeks only. However, CCM was weakly ($p>0.05$) correlated after 35 weeks. Results also showed that CCM decreases with enhancement of parasympathetic activity as measured by RMSSD of fHRV. We conclude that fetal heart rate dynamics as captured by CCM is strongly developed before 35 weeks of gestation. It may be linked to the maturation of the autonomic nervous system before 35 weeks and could help identify the pathological autonomic nervous system development.

P55

High Resolution 16-channel ECG Test Simulator for Online Digital-to-Analogue Conversion of Data from PC

Tatyana Neycheva, Todor Stoyanov, Roger Abächerli, Ivaylo Christov*

Institute of Biophysics and Biomedical Engineering, Bulgarian Academy of Sciences
Sofia, Bulgaria

P56

Recent design of electrocardiographic (ECG) simulators should be consistent with the international standard IEC 60601-2-47 issued 2012, which recommends the measurements, detections and interpretative statements of the ECG to be tested by digitized ECGs signals taken from five standard databases. In accordance to this recommendation we designed a high-resolution ECG tester simulator for direct digital-to-analogue conversion of data from PC. The signals selected from a database are sent from the PC to the Simulator via USB. The 16 independent channels of the simulator permit representation of the 10-channels of the 12-Standard leads plus any kind of additional leads configuration: bipolar leads, extra chest leads, etc. The prototype has high sampling frequency of 2 KHz, and high amplitude resolution of 286 nV weight of the least significant bit. The mass production of the used audio DAC keeps a relatively low cost of the device. The power-line interference is minimized by a galvanic isolation of the communication between the PC and the simulator. The need of build-in circuit for a Wilson Central Terminal is avoided by the use of 12-Standard-leads to 8-primary-leads transfer formulas. The power supply of the Simulator is by a rechargeable battery (6V, 1.3Ah). In-house PC software in Visual C is developed to select and control the operation mode of the simulator. Using this software the operator can: visual-ise the appropriate database, select specific ECG from the database, select a part of the record or the whole record to be continuously repeated. The transmitted signals are real-time visualized on the PC monitor. Simulator's functionality tests for: 12- to 8-leads transfer formulas, pacemaker pulses representation, channel-to-channel crosstalk and keeping of a constant DC level are successfully performed.

A Comparison of Heartbeat Detectors for the Seismocardiogram

Miguel Angel Garcia-Gonzalez*, Ariadna Argelagos-Palau, Mireya Fernandez-Chimeno, Juan Ramos-Castro

Universitat Politecnica de Catalunya
Barcelona, Spain

Aims: The study aimed to study the accuracy in RR time series derived from the seismocardiogram when employing different heartbeat detectors in subjects measured in a quiet environment.

Methods: The ECG and seismocardiogram of 15 healthy volunteers was recorded at a sampling frequency of 5 kHz using a Biopac acquisition system. The seismocardiogram was acquired using a triaxial accelerometer (LIS344ALH, ST Microelectronics). For each volunteer, three recordings were done in supine position: the first and last have durations of 5 min while the second lasts around 50 min and was recorded while the volunteer was listening to music. Three detectors of the heartbeat from the seismocardiogram were employed: The first detector (D1) locates local maxima above a threshold in a properly filtered signal, the second (D2) uses pattern matching techniques to refine the heartbeat location of D1 while the third (D3) relies on the Continuous Wavelet Transform. The reference heartbeat locations were obtained from the ECG using the Pan-Tompkins detector with a pattern matching refinement. Differences between the reference RR and the detected RR time series greater than 20 ms were rejected. The standard deviation of the difference of RR time series (SDdRR) was used as an agreement indicator.

Results: SDdRR was higher when using D1 ($3.12 \text{ ms} \pm 0.87 \text{ ms}$) than when using D2 ($2.84 \text{ ms} \pm 0.91 \text{ ms}$) or when using D3 ($2.52 \text{ ms} \pm 1.11 \text{ ms}$). SDdRR is reasonably low when compared with the standard deviation of the RR time series but depends on the subject under measurement and the employed detector.

Conclusion: The seismocardiogram, when measured in a quiet environment, can be used instead of the ECG to obtain reliable RR time series when using proper heartbeat detectors.

P56

Electrical Impedance Tomography vs. Whole Thoracic Impedance for Monitoring Heart Failure Patients

Marina Arad*, Shimon Abboud

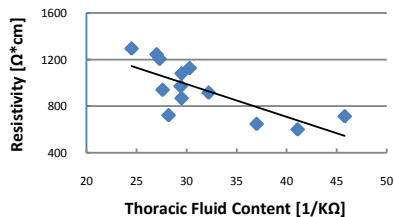
Sheba Medical Center, Tel Hashomer, Israel

P56

Acute decompensate heart failure is accompanied with pulmonary congestion resulting from elevated left ventricular filling pressures. Since pulmonary edema causes changes in lung conductivity, an approach such as bio-impedance is appropriate for monitoring the level of fluids accumulated in the lungs. The purpose of this study is to compare two approaches, the whole-thoracic impedance and the Electrical Impedance Tomography, for monitoring pulmonary congestion level.

The study was conducted on a group of 14 subjects (all males, aged 59 ± 12 years). All subjects signed an informed consent. To ensure minimal inter-subject variance, all EIT measurements were taken in similar postures on a seated subject during tidal respiration, with 8 electrode belt attached to the patients' thorax on the plane of the fifth intercostal space in the midclavicular line using conventional ECG Ag/AgCl disposable electrodes. Eight specially designed elongation mechanisms on the electrode belt were used for adapting the electrode belt length to the thoracic perimeter of the subject, ensuring a fixed angular distance between the electrodes. In addition the whole thoracic impedance for each subject was measured.

Figure 1 shows the relationship between the EIT ($\Omega \cdot \text{cm}$) and the whole thoracic impedance ($1/K\Omega$). A good correlation ratio of $R=0.75$ ($p\text{-value} < 0.01$) was found between the two data sets.



The results suggest that the EIT method with 8 electrodes belt has the potential to be used for monitoring lung fluid content in patients with congestive heart failure.

Improved Estimation of V-Index Based on Analytic Forms of Dominant T-Wave

Luca Mainardi*, Davide Di Donato, Denise Falcone, Roberto Sassi

Politecnico di Milano
Milano, Italy

The spatial heterogeneity of ventricular repolarization (RH) is a key quantity for the development of cardiac arrhythmias. To assess spatial RH (SRH), we introduced the V-index, a metric based on a biophysical model: each T-wave is described, on a given lead, as the projection of the Dominant T-Wave (DTW) and its derivatives, weighted by scalars (lead factors). To compute the V-index, the lead factors are estimated from the ECG. Theoretically, the larger the number of derivatives, the better the adherence to the model. However, in our original method (OM), only the first derivative was taken into account. In fact, the DTW numerical computation induces noise in the derivatives, which are progressively corrupted as order increases. In this work, we introduced a parametric method (PM), based on analytic definitions of the DTW, to allow analytical computation of its derivatives. We adopted three analytic forms based of combination of: sigmoidal (S), Gaussian (G) or exponentials (E) functions. To assess the improvement in the estimation procedure, simulated ECGs were generated using a forward ECG model (ECGSIM re-implemented in MATLAB). SRH was varied from 5 to 40 ms (5 ms-steps). To simulate real recordings, noise available from the MIT-BIH Noise Stress Test Database was added with different peak-to-peak amplitudes (30, 60, 120 and 180 μV). The use of parametric DTW allowed the inclusion of a larger number of derivatives in the model (3 vs 1, PM vs OM) and reduced the difference between actual and estimated T-waves. This reduction was more pronounced for methods S and G. However, the E method resulted in a lower estimation bias of V-index with respect to the actual SRH. Finally all the three considered parametric forms proved resistant to noise addition, being G method the most robust.

P56

The Effect of Breathing on Stroke Volume Estimation in Patients with Implanted Cardiac Device Using Parametric Electrical Impedance Tomography

Muhammad Mhajna*, Shimon Abboud

Tel Aviv University
Umm Al Fahem, Israel

P56

Introduction: During the cardiac cycle, changes in the thoracic conductivity distribution might be a result of changes in the fluid content of the vascular bed or changes in the lungs' volumes due to breathing. Correlating these conductivity changes with the volume changes of the heart can help providing a non-invasive Stroke Volume (SV) quantification method.

Methods: Electrical Impedance Tomography is a non-invasive non-ionizing imaging and monitoring technique in which tissues can be differentiated based on their electrical properties. The method uses measured surface potentials in order to reconstruct information of the spatial conductivity distribution within the thorax. In the current study, parametric EIT (pEIT) scheme was applied in a high-resolution 4D model of the human thorax with implanted cardiac device to determine the left ventricular volume (LVV) at different cardiac cycle phases. The effect of breathing is examined by allowing both heart and respiratory motions.

Results: The results emphasize the fact that the estimation of the LVV using pEIT is affected by breathing. About 10% change in the lungs' volume (during tidal breathing) causes 8% change in the estimated SV. In order to neutralize this effect a new algorithm was developed. By assuming that the respiratory rate is lower than the heart rate, the contribution of both motions to the change of potential distributions can be separated. The separated potential distributions are used to estimate the LVV while neutralizing the effect of breathing. The preliminary results show a decrease in the SV estimation error; 3% compared to 12% without using the correction algorithm.

Conclusion: The results suggest that the LVV can be estimated using pEIT method while neutralizing the effect of respiratory motion and that the method has the potential to be used for monitoring patients with implanted cardiac pacemaker.

Night and Day Changes in Heart rate and Blood Pressure Fractal Dimensions from 24-hour Ambulatory Blood Pressure Monitoring Devices

Andrea Faini*, Gianfranco Parati, Marco Di Rienzo, Paolo Castiglioni

Istituto Auxologico Italiano, IRCCS, Milan, Italy
Milan, Italy

Ambulatory blood pressure monitoring (ABPM) describes 24-hour changes of blood pressure (BP) and heart rate (HR) by periodically inflating an arm cuff. ABPM provides clinically important information quantifying daytime and night-time mean values of BP and HR without interfering with daily activities and sleep. However, due to the low number of measures (usually 2-4 per hour), few indices of variability have been considered so far, typically the standard deviation (SD) or the variation coefficient ($VC=SD/mean$) over daytime or night-time periods. Recently we showed[1] that it is possible to quantify a more specific feature of ABPM dynamics: the fractal dimension (FD). Aim of this study is to describe changes between day and night in FD of BP and HR over a large population of subjects, and to evaluate whether FD provides complementary information to SD or CV. We analysed time series of HR and of systolic (S) and diastolic (D)BP from ABPM recordings performed with an oscillometric device (Spacelabs 90207, USA) in 67 untreated hypertensives (36M/31F). ABPM readings are taken every 15' during the day (06:00-22:00), every 30' during the night (22:00-06:00). We compared SD, VC and FD (Higuchi's algorithm) calculated for daytime and night-time with paired t-test/Wilcoxon-Mann-Whitney-test (significance level 0.05). From day to night, SD decreased significantly ($p<0.001$; SBP: 13 ± 4 mmHg and 10 ± 4 mmHg; DBP: 10 ± 3 mmHg and 8 ± 3 mmHg; HR: 9 ± 3 bpm and 5 ± 3 bpm; respectively). VC decreased significantly for HR only ($11\pm 4\%$ and $8\pm 5\%$, $p<0.001$) remaining the same for SBP ($8\pm 2\%$ and $8\pm 3\%$) and DBP ($11\pm 3\%$ and $11\pm 4\%$). FD showed a different behaviour, increasing significantly for DBP only (from 1.83 ± 0.12 to 1.92 ± 0.26 , $p<0.001$) while it changed only slightly for SBP (from 1.83 ± 0.11 to 1.86 ± 0.21) and HR (from 1.78 ± 0.13 to 1.80 ± 0.26). Therefore FD provides information on night/day changes of ABPM dynamics not included in SD or VC. [1]Computing in Cardiology 2011;38:593–596.

P56

Heart Auscultation Learning using Multi-labeler Evaluation Feedback

Santiago Murillo Rendón, Diego Hernán Peluffo Ordoñez, Liliana Patricia Ramírez Zuluaga, Mario Iván Ruano Restrepo, Germán Castellanos Domínguez, Alvaro Angel Orozco* Gutiérrez

UNAL
Manizales, Colombia

P56

Aims: this work discusses an automated tool to improve learning and discrimination of heart sounds for medical students. It is common that the ear training in semiology sceneries is a complex process involving hard work and even after a huge effort it is possible that the student is not able to make an appropriate discrimination. A methodology capable to contribute in the auscultation learning is proposed by introducing an evaluation feedback based on measuring the statistical distance of each one of the answers provided by the student.

Methods: The students hear a set of recorded heart sounds to provide the corresponding label set. To evaluate the quality of the introduced labels by each student towards the previous label set provided by an expert team (i.e., the teacher panel), the use of a modiflicated SVM formulation is considered, that allows to measure the student performance in terms of the statistical SVM distance. The method can be applied also to a group of students, allowing for ranking their relative learning performance in accordance to the expert team.

Results: For training purposes, 400 signals obtained from the four traditional auscultation focuses and labeled by three physicians is considered. For testing, the methodology is applied in a team of five medical students, four of which are formally in the semiology course. Another involved student with no auscultation skills comes outside from different program. As a result, the methodology ranks the student labeler panel under evaluation, showing the high concordance with the teacher evaluation.

Conclusion: The use of statistical multilabeler strategies can be also introduced in the learning environment making more objective the evaluation quality. This work is a powerful tool to the heart sound teaching and it can be implemented in e-learning environments and to spread its capabilities to students around the world.

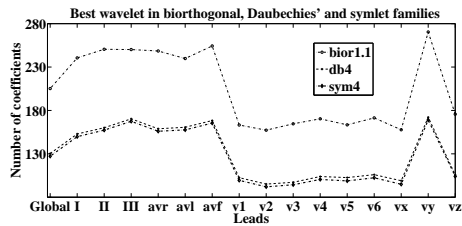
On the Sparsest Representation of Electrocardiograms

Roopak R. Tamboli, Manas A. Savkoor, Soumya Jana

Indian Institute of Technology Hyderabad
Yeddumailaram, Andhra Pradesh, India

Telecardiology has been growing in importance owing to shortage of qualified local caregivers in various regions. It often involves acquisition and transmission of electrocardiogram (ECG) signals to a remote facility, where diagnosis is performed towards possible intervention. Perhaps the most in need of telecardiology are the remote under-privileged segment. Unfortunately, they often have limited access even to nominal infrastructure such as bandwidth and power. Thus it becomes imperative to design healthcare systems taking infrastructural constraints into account. In this backdrop, one can reduce storage and transmission requirements by compressing ECG signals. In dire circumstances, where inadequate power makes intensive compression algorithms infeasible, one may adopt the low-power alternative of compressive sampling, albeit sacrificing on compression efficiency.

Whether one uses compression or compressive sampling, the efficacy depends on signal sparsity. In compression, the sparsest representation provides the least dimension in which the signal space could be embedded. Alternatively, such representation allows perfect reconstruction from the least number of compressive samples. In this context, we consider a large set of wavelet bases, drawn from various families including symlets and Daubechies' wavelets, and compare the sparsity of a broad collection of ECG signals in those bases. In particular, twelve standard and three Frank leads are considered for this study. We order the transform coefficients in decreasing order of magnitude, and count the number of coefficients accounting for 99% of the signal energy (sparser representation requires less number). In the process, two interesting phenomena are observed. First, symlets tend to outperform Daubechies' wavelets, with the fourth order symlet ('sym4') proving the most efficient overall. Second, among the aforementioned leads, 'v1' through 'v6' and 'vx' (Frank X) appear to admit sparser representation. The latter observation could also guide efficient subset selection while reconstructing the full set of leads from a subset (key to portable design).



P56

The Effect of Automated Preprocessing of RR Interval Tachogram on Discrimination Capability of Heart Rate Variability Parameters

Faezeh Marzbanrad, Herbert Jelinek, Ethan Hambly, Craig McLachlan, Slade Matthews, Marimuthu Palaniswami, Ahsan Khandoker*

Khalifa University
Abu Dhabi, United Arab Emirates

P56

Ectopic beats and noise within the ECG can change the estimated value of Heart rate variability (HRV) features and reduce classification accuracy. Although preprocessing of the RR tachogram can improve the accuracy of HRV analysis and discriminatory power, it is often not performed. In this paper, a practical example shows how different automated preprocessing methods can improve discrimination using HRV features. HRV features are estimated without preprocessing and applying three different automated preprocessing methods. Two automated preprocessing approaches differ in that they remove RR intervals based on a deviation of more than 10% (A) and 20% (B) between two beats and substituting the deviated interval with the mean of the two preceding RR intervals. The third method (C) is to take five consecutive intervals and replace the middle RR interval by the mean of the two preceding and two following RR intervals, if they differ by more than 20%. Both linear and nonlinear HRV features are compared across the four groups comprising diabetic and control patients attending a diabetes screening clinic that had their Angiotensin-Converting Enzyme (ACE) gene polymorphism determined. Group comparisons were undertaken using the nonparametric Kruskal-Wallis test with a $p < 0.05$ set as significant. Entropy showed no significant difference in HRV if preprocessing is not used, but demonstrated a significant difference between groups by using preprocessing. However the methods do not have the same effect for all HRV features; for entropy method C and for SDRR method B provide a better discriminatory power. However part of our finding is dependent on how the HRV feature is calculated, whether it is sensitive to beat by beat variations or global change over several beats. Therefore it is recommended to use appropriate preprocessing before obtaining each HRV feature to optimize classification

Characterizing Complexity of Atrial Arrhythmias through Effective Dynamics from Electric Potential Measures

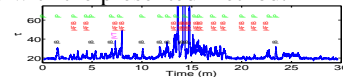
Oriol Pont, Binbin Xu

INRIA Bordeaux Sud-Ouest, F-33405 Talence, France
L'Institut de rythmologie et modélisation cardiaque LIRYC, Université de Bordeaux, F-33000 Bordeaux, France

The cardiac electrical activity follows a complex dynamics whose accurate description is crucial to characterize arrhythmias and classify their complexity. Rhythm reflects the connection topology of pacemaker cells at their source. Hence, characterizing the attractors as nonlinear, effective dynamics can capture the key parameters without imposing any particular model on the empirical signals. A dynamic phase-space reconstruction from appropriate embedding can be made robust and numerically stable with the presented method.

Methods: Time series evolution is mapped to an object embedded in a phase space in abstract coordinates. m independent observations construct an mD phase space, as per the embedding theorem. The dimension m is the least one that embeds the dynamics (which is twice plus one the Minkowski dimension of its attractor set) and the time lag τ is the shortest for which the m coordinates do not mutually interfere. With appropriate filtering, the method is robust and adapted to empirical signals. The result is a compact dynamical description that characterizes complexity degree and information distribution.

Results and Conclusion: Nonlinear analysis provides appropriate tools to characterize cardiac dynamics. Singularity analysis and phase-space reconstruction are physically meaningful complexity measures with minimal assumptions on the underlying models. We validate our approach on ECG, endocavitary catheter measures and electrocardiographic maps. Key parameters vary infrequently and exhibit sharp transitions, which show where information concentrates and correspond to actual dynamical regime changes. In space domain, extreme values highlight arrhythmogenic areas whose ablation stopped the fibrillation. We observe a correspondence of time lag fluctuations of phase-space reconstructions with atrial fibrillation episodes in the same way as with the dynamical changes coming from singularity exponents. This opens the way for improved model-independent complexity descriptors to be used in non-invasive, automatic diagnosis support and ablation guide for electrical insulation therapy, in cases of arrhythmias such as atrial flutter and fibrillation.



Time lags (in samples, at 360Hz) of phase-space reconstruction for MIT-BIH Arrhythmia Database case #217: a fragmented electrogram with many intermittent episodes of atrial flutter and fibrillation, which appear well segmented by the lags.

P56

A Pilot Study of Photoplethysmographic Peripheral Pulse Transit Times in Paediatric Heart Transplant Recipients and Healthy Children

Costanzo Di Maria, Emma Sharkey, Annette Klinge, Dingchang Zheng*, Alan Murray, John O'Sullivan, John Allen

Newcastle upon Tyne Hospitals
Newcastle upon Tyne, United Kingdom

P56

Introduction: Previous studies using expensive SphygmoCor pulse measurement technology (requiring a highly trained operator) have demonstrated increased blood pressure and arterial stiffness (AS) in paediatric heart transplant recipients (HTR) [1]. Photoplethysmography (PPG) is an alternative pulse technology which is low-cost and easy-to-perform. It can measure the pulse from different peripheral body sites and provide valuable cardiovascular information [2].

Aim. To use PPG to assess pulse transit times at three different body sites in HTR, in comparison to healthy controls. **Methods.** PPG waveforms and an ECG timing reference were recorded from 12 HTR (5 males; age range 8-17 years) and 30 healthy children (15 males; age range 8-16 years) from the right and left ear lobes, index fingers, and great toes. Signals were digitised and stored to computer for off-line analysis. The median values for pulse transit time to PPG-pulse foot (PTTf) were calculated over a period of 60 heart beats, with right and left sides averaged at each segmental site.

Results. There were no significant differences between age, sex, and height. Toe PTTf was significantly lower in HTR (median 290ms) compared to controls (324ms, Mann-Whitney $p < 0.05$). No significant differences were found for ear and finger PTTf. Furthermore, toe PTTf significantly correlated with subject height both in HTR (Spearman $\rho = 0.776$, $p < 0.01$, slope = 88ms/m) and controls ($\rho = 0.755$, $p < 0.001$, slope = 132ms/m).

Conclusion. A smaller PTTf at the toe is consistent with increased AS in paediatric heart transplant recipients and the results from correlation analysis further corroborate this finding. This pilot study has also shown the value of photoplethysmographic assessment in this group.

References. [1] Klinge A., Allen J., Murray A., O'Sullivan J., Increased pulse wave velocity and blood pressure in children who have undergone cardiac transplant. *J Heart Lung Transplant* 2009;28:21-25 [2] Allen J., Photoplethysmography and its application in clinical physiological measurement. *Physiol Meas* 2007;28:R1-R39

An Easy System to Follow the Evolution of Cardiac Patients

Rene Gonzalez-Fernandez*, Margarita Mulet-Cartaya, Daniel Jimenez-Gonzalez, Juan Dayron Varona

Central Institute of Digital Research
Havana, Cuba

Aims: This paper is focused on the main characteristic of a new system oriented to follow the evolution of cardiac patients. The main features of this system will be discussed.

Methods: The proposed system is composed by three parts: a small battery-powered device designed to acquire an ECG channel; a mobile application based on Android operating system and a web application. The ECG device was designed to acquire and transmit via Bluetooth the ECG continuously. The mobile application is able to receive and store the ECG data in the phone memory, QRS complexes are detected and heart rate is computed. All these information is transmitted to the web application using the GPRS network. The web application stores each ECG data in a SQL database and it is available for the users connected to this service. Cardiologists can review all the ECG from any patient and they can analyze the heart rate and premature beat trends. These features are useful for medical treatment adjustments and to follow-up the cardiac arrhythmias. The ECG device is easy to use, patient only have to attach the electrodes to his skin and press the ON/OFF button.

Results: Two ECG device's prototypes have been tested according to the IEC 60601-2-47 standard; all the IEC tests were passed successfully. The mobile application has been finished and one hundred of three-minute ECG strips have been received from the ECG devices without communication errors. QRS complex detection algorithm was tested in previous research projects with good results. 98,05% of the QRS complexes were detected and false positives were not present. The web application is being developed, but the communication with the mobile application has been tested.

Conclusions: The proposed system seems easy to use for patients and cardiologist, it could be useful to follow the cardiac arrhythmias evolution.

P57

The Design and Testing of a Heart Monitor for Home Care

Yaniesis Lorenzo-Costa, Rene Gonzalez-Fernandez*, Ronny Guardarrama-Mieres

University of Informatic Sciences
Havana, Cuba

Aims: The aim of this paper is to discuss the design of a new battery-powered cardiac monitor for Homecare. It should be a powerful tool to follow the evolution of patients prone to suffer cardiac arrhythmias.

Methods: The device is able to acquire two ECG channels; these signals can be processed, stored and transmitted through a Bluetooth's communication channel. The monitor is based on the MSP430F5438 microcontroller from Texas Instruments and includes a graphic liquid crystal display, a simple keypad, a two-channel ECG amplifier, and two NiMH batteries. The electrocardiographic signal is displayed in real time with the heart rate; QRS complexes are automatically detected to compute heart rate. The QRS complex detection is based on an auxiliary energy function computed sample by sample for each ECG channel. There is an innovative element in the ECG acquisition; one ECG channel can be acquired by holding with hands the device because its cabinet has two embedded electrodes for that purpose. On the other hand, the two ECG channels can be acquired by connecting the appropriated patient cable to the monitor.

Results: The method developed for QRS complex detection has been tested with twelve ECG strips from MIT-BIH annotated ECG database; 98,05% of the QRS complexes were detected and false positives were not present. The Bluetooth's communication process was tested with simulated ECG; this signal was transmitted continuously for ten hours. Communication was not aborted and there was no change in the received ECG from the original signal.

Conclusions: The proposed device seems to be a useful tool to follow the cardiac arrhythmias evolution. Also, this device could be integrated to a Telemedicine system easily.

P57

Neural Network Approach to Incomplete Data Applied to Assessing Cardiac Health

Joanna Grabska-Chrzastowska

AGH University of Science and Technology
Krakow, Poland

The classification problem with missing data is an important issue especially in the case of medical data. There is no standard procedure for collecting data for the particular disease. For this reason, for example, in assessing the degree of degradation of the heart muscle, some centers established group of parameters in order to create a knowledge base. Unfortunately, the records of the database are often incomplete. This article aims to develop a general method for optimal selection of input data to neural networks in case of missing data.

The project is based on data from the Cleveland Clinic Foundation Clinic, located in Cleveland. Data were collected from accessible web base UCI Machine Learning Repository. In the database, there are 13 variables: age, sex, type of chest pain, resting blood pressure, serum cholesterol, blood sugar levels, results of the resting ECG, maximum heart rate, angina, decrease the

value of the ECG ST, slope of the ST segment on the ECG, number of large blood vessels, scintigraphy results. The patient is assigned to one of the two groups: healthy - sick (0 or 1). Using a neural network (MLP) for all 13 parameters 93% of correct classification was achieved. Unfortunately, even a best-chosen neural network is not suitable for classification of incomplete data. With the

Results of the Classification

Id	The database name	Quality
0	Cleveland (297 full data)	81,5 %
1	Hungarian (294 incomplete data)	68 %
2	V.A. (200 incomplete data)	71 %
3	Switzerland (123 incomplete data)	78,9 %

help of genetic algorithm used to select the input group, we find the most important parameter: maximum heart rate, which determines the classification of a fairly good result (71.5%). Most of the databases have this parameter. Other easily available parameters were added in order to improve the quality of classification. New set included the first 10 data from 13. The results obtained for incomplete data sets are shown in the table. The results demonstrate the possibilities of neural networks to classify vectors of incomplete content.

Clair-DB: A Standardized Departmental Research Database

Enno van der Velde*, Thekla Jansen, Victoria Delgado, Douwe Atsma

Leiden University Medical Center
Leiden, Netherlands

P57

Background: The efficacy of implementation of a common standardized central database to be used by an investigational group for several lines of research remains unknown. The objective of the CLAIR-DB (Cross Linked Advanced Integrated Research Database) project is to create one single, controlled research database for our department (Cardiology) from which all clinical research will be carried out. Existing research databases (in Excel, Access, etcetera) are migrated into the new research database.

Methods. The ProMISe system from the Leiden University Medical Center (LUMC) department of Medical Statistics and Bioinformatics is used as the underlying database system (www.msbi.nl/promise). The approach: definition of a small set of database tables; definition of common variables; all variables unambiguously defined (based on international standards and guidelines). All data in CLAIR-DB are automatically transferred from our Cardiology Information System (EPD-Vision), which means that all data are directly available from the source; no retyping of data; data are always up-to-date. To perform statistical analysis, an export from CLAIR-DB (ProMISe) can be made in SPSS format. The export file can be limited to exactly those variables as defined in the original research project setup, or can contain additional data to allow correlation with novel parameters. Data can only be analyzed from patients that have been included in the specific study.

Results. Data harmonization from 15 existing databases has resulted in one single well defined data set (CLAIR-DB). The data transfer tool in EPD-Vision is further refined.

Conclusion. The CLAIR-DB research database may help to facilitate and improve retrospective analysis of standardized clinically acquired data common to several research lines developed within a single department.

Biometric personal identification system using ECG signal

Emna Rabhi¹, Zied Lachiri^{1,2}

¹National School of Engineers, Tunis, Tunisia

²National Institute of Applied Science and Technology, Tunis, Tunisia

The Electrocardiogram has unique cardiac features to each individual, which motivated us to use it as a biometric, hence, its robust nature against falsification makes it rather reliable for security systems, as it offers ultimate security in all situations. This paper presents a new approach applying this ECG particularity. A robust ECG Biometrics based on the features extraction with fiducial detection in the time domain is proposed. After preprocessing, ten morphological descriptors are extracted from each heartbeat and which were divided into homogenous groups (amplitude, surface, interval and slope). Later, sixty Hermite Polynomials Expansion (HPE) coefficients are extracted from the ECG signal. Finally, classification is based on the Hidden Markov Model (HMM) with the (HTK) recognition toolkit using a Bakis model with one Gaussian. A particular strategy is adopted for personal identification: the groups of morphological parameters were used separately in the classification then were made associations between these groups them in one input vector. On the other hand, the Hermite Polynomials Expansion coefficients were classified apart. In order to improve performance, a combination between 10 morphological parameters and 60 HPE coefficients was performed in a one system. Our algorithm is tested on 18 healthy signals of the MIT_BIH database. Each recording lasts about 30 minutes, 20 min of the data were used for training and the last 10 min were used for testing. The analysis of different groups separately showed that the best recognition performance is 96.7% for the Hermite Polynomials Expansion coefficients and the results of experiments showed that the proposed hybrid approach has led to an overall maximum of 99%.

P57

Measurement of Noise in ECG Signals to Improve Automatic Delineation

Loriano Galeotti*, Lars Johannesen, Jose Vicente, David G Strauss

US Food and Drug Administration
Silver Spring, United States

P58

Introduction: Quality evaluation of digital ECG recordings is of importance when analyzing data archives or for automatic patient monitoring. In these settings, using noisy signals may lead to incorrectly measured ECGs or triggering false alarms in patient monitoring; thus empirically defined thresholds are usually employed to exclude noisy recordings. We developed a method to measure and correct the amount of noise in an ECG dividing it in three different categories (baseline wander, power-line and residual). To decide whether a signal is valid for its intended use (e.g. to measure T-offset), we characterized the amount of errors introduced on the ECG measurements as a function of the measured input noise.

Methods: We first synthesized twenty-eight 10-second ECGs and annotated fiducial points (e.g. QRS onset/offset and T-wave offset). Next, to characterize the noise measurement system, we added 216 different amounts of artificial noise to the ECGs. For each lead we evaluated the correlation (Pearson) between the effective and measured noise present in the signal (root mean square [RMS] across the 10-second ECG). We then characterized the error in the detection of biomarkers of interest (e.g. the QRS duration and T-wave offset) as a function of measured noise. Finally, we computed the maximum amount of noise allowed in order to keep the error (95%CI) on the measured biomarker within a certain threshold, e.g. 10ms for T offset detection.

Results: We found a linear correlation ($R^2 > 0.98$ p-value < 0.0001) between the effective and measured amount of noise present in the signal. We found that to have a T-offset error within 10 ms, the maximum allowed RMS noise is 1.0, 0.1 and 0.3 mV for baseline wander, power-line and residual respectively.

Conclusion: This method provides a generalized way to evaluate noise levels of ECGs and to determine if it is of sufficient quality for the intended use

Detection of P wave in Electrocardiogram

Rene Gonzalez-Fernandez*, Martha Rivero-Varona, Gisela Montes de Oca-Colina

Central Institute of Digital Research
Havana, Cuba

Aims: This study aimed to develop an algorithm to detect P wave on the ECG. This kind of algorithms is complex because of the characteristics of that wave.

Methods: One hundred ECG from CSE-study, specified in the IEC 60601-2-51 standard, were studied. All the QRS complexes and T-wave offsets were detected to look for P waves in TQ segments only. A QRS detector, developed by the authors previously, was used. The QRS onset identification process was based on a derivative function and a set of adaptive thresholds. The proposed detector was applied to lead II to identify the P zones where this wave was measured lead by lead. The proposed method can be broken down in several stages; the first step was to square each TQ segment sample in lead II to emphasize the differences. A Difference Collector (DC) was computed in forward and reverse way; this function was defined as a collector of differences between samples in 100 ms-duration moving window across each TQ segment. The forward way was from the T wave to the QRS complex and the reverse was from QRS complex to the previous T wave. The next step was to identify DCF significant peaks in forward and reverse ways. A P wave was located always between a forward and a reverse significant peaks, an amplitude threshold was applied to lead II in order to determine the presence of P wave.

Results: The proposed algorithm was tested with the ECG data stated in the IEC 60601-2-51 standard. The sensitivity for P wave detection reached 99.24%. False positives were not produced.

Conclusions: The proposed algorithm had a good performance with the CSE data collection used, but it should be assessed under the influence of such elements as skin impedance and the internal noise of an ECG machine.

Detection of Electrode Interchange in Precordial and Orthogonal ECG Leads

I Jekova^{1*}, V Krasteva¹, R Abächerli²

¹Institute of Biophysics and Biomedical Engineering, Sofia, Bulgaria

²Schiller AG, Baar, Switzerland

Misplacement of electrodes in multi-channel ECGs is reported in 0.4-4% of all clinical recordings – a severe cause of erroneous diagnosis due to simulated false or concealed true ECG abnormalities. This study aims to present methods for automated detection of interchanged ECG leads that may prevent from incorrect diagnosis and treatment, and reduces costs.

The first method detects precordial electrodes interchange by analysis of leads V1–V6. Matrix R (6x6) with correlation coefficients between P-QRS-T waveforms in each pair of leads is constructed. Analyzing rows and columns of Matrix R, any deviation from the trend for gradual increase of the correlation coefficients towards the cell where a lead is compared to itself is suspected as incorrect lead. The method also estimates the time-alignment of R and S-peaks with monotonically increasing time-shift V1-V6. The final decision for chest leads interchange summarizes all suspicious elements from waveform and time-alignment of leads.

The second method detects Frank bipolar leads (X,Y,Z) interchange by analysis of 15-lead ECG. Four criteria are implemented: (1) difference between angles of QRS loops in the frontal plane ([I,avF],[X,Y]); (2) correlation coefficients of I,II,V1-V6 (measured vs. Dower transform); (3) correlation coefficients of (I,X), (I,Y), (V2,-Z); (4) Time-alignment of (Y,Z).

Both methods are implemented in Matlab. They are trained on 77 healthy controls in PTB database and tested on 1220 files from CSE database, containing various arrhythmias. Lead interchange is simulated:

- Precordial leads: 23 different swaps between V1-V6, including the most difficult cases of sweep between 2 adjacent leads, and various reversals of 3 and more leads;
- Orthogonal leads: able to simulate only 47 reversals of electrode couples A/I, F/H, M/E by swapping X,Y,Z and changing their polarity.

The accuracy is reported as specificity (Sp) for detection of the correct electrode placement and sensitivity (Se) for interchanged leads (see table).

	Training set (77 files)			Test set (1220 files)		
	Sp (%)	Se-mean (%) 23 reversals	Se-range (%) 23 reversals	Sp (%)	Se-mean (%) 47 reversals	Se-range (%) 47 reversals
Precordial leads	93.5	95.7	77.9 – 100	91.8	95.0	84.6 – 99.3
Orthogonal leads	98.7	98.5	77.9 – 100	93.3	98.5	83.2 – 100

P58

Noncontact Sensing of Electrocardiographic Potential and Body Proximity by In-bed Conductive Fabrics

Kei Ito¹, Yutaka Fukuoka², Gert Cauwenberghs³, Akinori Ueno¹

¹Tokyo Denki University, Tokyo, Japan

²Kogakuin University, Tokyo, Japan

³University of California San Diego, CA, USA

Aging populations call for pervasive monitoring of activity of elderly patients and their electrocardiographic potential (ECG) in the hospital or at home. In this study, we propose a noncontact approach for continuous sensing of presence, position and ECG of a human body on a bed.

Six pieces of belt-like conductive fabrics were used as sensing electrodes, placed on a mattress and covered with a commercial cotton bed sheet. Three of the pieces were connected to a newly developed ECG amplifier featuring ultra-high input impedance. The other three pieces were connected to two sets of capacitance meters. Each meter measures coupling capacitance between electrodes, clothes and a part of the body. Capacitances for upper and lower bodies were separately measured. A male volunteer subject was instructed to sit down on a bed, lie on the bed in a supine position, and change to a lateral position at fixed time intervals. In addition to our developed devices under test, a commercial ECG amplifier and a webcam were used to record a reference ECG and a video sequence of the subject.

As shown in Fig. 1, the combination of two voltages, inversely proportional to the upper and lower body coupling capacitances, varied in accordance with the change in the subject's position. In addition ECG was detected in the periods when the subject was in supine or lateral position. In Fig. 2 distinct QRS complexes and T-waves were confirmed, though some distortion can be observed. These results demonstrate the potential of the proposed approach for noncontact sensing of ECG and lying body capacitance toward awareness-free pervasive and continuous monitoring.

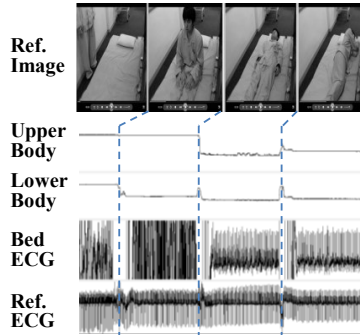


Fig.1. Simultaneously recorded signals of lying body capacitance and ECG

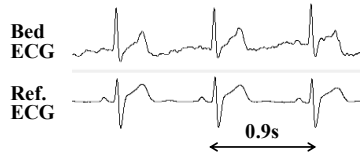


Fig.2. Enlarged waveforms of simultaneously measured ECGs

A suppression of impulsive noise in ECG signal using adaptive filters

Shankar S Gupta*, Ramchandra R Manthalkar, Suhas S Gajre

S.G.G.S.Institute of Engineering and Technology, Nanded.
Maharashtra,India.

The electrical activity of muscles is usually modeled using Gaussian probability distribution function. Such assumption is not always true, because real-life muscle noise has impulsive character as well. Adaptive threshold technique is one important step in the detection of QRS Complexes. However, presence of impulsive noise may trigger false positives. The proposed system uses adaptive filters to suppress impulsive noise in ECG signal and avoid the false positives.

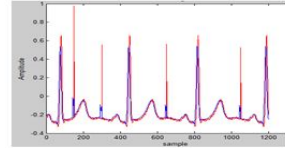


Fig. Filtered ECG (blue) superimposed on ECG (red) corrupted with impulsive noise.

In fixed threshold algorithm, it was observed that defining high values for threshold leads to missed complex and defining low values causes incorrect detection of the peaks present in the signal. In adaptive threshold algorithm, detection is done by using a pair of threshold. If in each stage of threshold the number of detected peak by up and down limits are not equal, then error component is defined and fixed value is deduced from respective limits and threshold operation repeated.

The adaptive algorithm used to suppress impulsive noise is based on a system identification application with impulsive noise contribution. In this algorithm, $x(n)$ is the stimulus signal, which is applied to the unknown system and the adaptive filter. The output of the unknown system, $d(n)$ or desired signal, is corrupted by impulsive noise and contaminated with Gaussian noise, not correlated to the adaptive system input $x(n)$. Weights are updated using delta learning rule. The algorithm has been evaluated with the MIT-BIH Arrhythmia Database, MIT-BIH Compression database and University of Glassgow noisy and normal database.

It was observed that despite the noise, the algorithm identifies the system and adjusts coefficients accordingly. The desired signal and output signal were same except for the noise. Measuring the performance in terms of signal-to-noise-interference ratio (SNIR) in dB, the proposed approach was able to achieve {84,10,100,72} {mean,sd,max,min} on highly corrupted ECG records with initial SNIR as low as {39,3,42,32} {mean,sd,max,min}.

Acknowledgement:- The work was supported by funds from All India Council for Technical Education (AICTE), New Delhi under Research Promotion Scheme Grant Number 8023/RID/RPS-86/2011-12.

An Algorithm for the Detection of ST Segment Elevation Myocardial Infarction in Body Surface Potential Maps

Dewar Darren Finlay*, Daniel Guldenring, Raymond Robert Bond, Michael John Daly

University of Ulster
Belfast, United Kingdom

Criteria for the detection of ST segment elevation myocardial infarction (STEMI) in the 12-lead Electrocardiogram (ECG) are widely published. Such criteria allow highly specific detection of STEMI however sensitivity is low. Body surface potential maps have the potential to improve diagnostic performance by sampling information from areas of the torso not interrogated by the 12 lead ECG. In this study we investigate a BSPM STEMI detection algorithm that is based upon an extension of recently published 12-lead ECG STEMI criteria. The algorithm detects STEMI when J-Point potentials exceed predefined thresholds in two contiguous leads. Thresholds were set at 0.05 mV for posterior leads, 0.05 mV for right ventricular leads and 0.1 mV for remaining anterior leads with the exception of leads in close proximity to V2 and V3. Thresholds for leads in close proximity to V2 and V3 were set at 0.15 mV for females and 0.2 mV for males ≥ 40 years of age and 0.25 mV in males < 40 years of age. Our algorithm was applied to 45 subjects who had 120 lead BSPMs recorded during percutaneous transluminal coronary angioplasty (PTCA).

A total of 90 BSPMs (j-point iso-potential maps) were studied representing the 45 subjects at baseline and the same 45 subjects during peak balloon inflation (15 left anterior descending, 15 left circumflex and 15 right coronary artery). When our algorithm was applied to BSPM leads STEMI, corresponding with peak balloon inflation, was detected with a sensitivity of 84.4% and specificity of 75.6%. Standard STEMI criteria, applied to 12-lead ECGs extracted from the same data, resulted in a sensitivity of 46.7% and a specificity of 95.6%.

P58

The effect of precordial leads displacement on P-wave morphology in body surface potential mapping

Kania M¹, Rix H², Fereniec M¹, Janusek D¹, Maniewski R¹

¹Nalecz Institute of Biocybernetics and Biomedical Engineering Warsaw, Poland

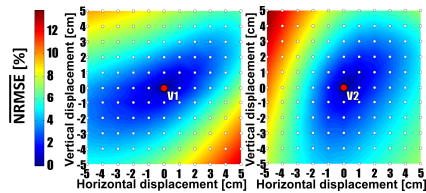
²Lab. I3S, University of Nice Sophia Antipolis, France

Inaccurate ECG electrode placement on the chest can lead to misinterpretation or even to significant diagnostic errors. The aim of this study was to investigate the variability of P wave morphology recorded in a close distance to precordial ECG leads.

The study consisted of 60 patients with diagnosed cardiac disease. The shapes of ECG signals interpolated at the 120 points located at a distance up to 7 cm from the precordial lead location were compared to shape of signals recorded from precordial leads. For this interpolation the 67-channel high-resolution ECG data were used. Mean differences in P-wave shape were quantified using the distribution function method (*DF*), correlation coefficient (*R*) and normalized root mean square error (*NRMSE*). The relative variability (*RV*) index was computed to quantify inter-individual variability of measured body surface potentials.

Up to 5 cm there were not visible changes in values of *R* in all studied electrode positions. The P-wave morphology changes were prominent in values of *DF* and *NRMSE* beyond 2 cm distance to precordial leads *V*₁ and *V*₂. The dispersion of the signal morphology was growing with the increase of the distance from the reference point. No significant ECG morphology changes up to 5 cm from location of leads *V*₃, *V*₄, *V*₅ and *V*₆ were observed. *V*₁ electrode is more sensitive to vertical than to horizontal displacements in contrary to *V*₂ electrode. The *RV* ranged from 0.47 to 0.79.

The issue of P-wave morphology change due to electrode displacement is complex. The distortions in ECG increase with the distance from precordial lead, especially above 2 cm and are specific for chosen electrode and direction of displacement. Large ECG inter-individual variability suggests important influence of human anatomy on measured ECG signals.



Normalized RMS error quantifying the mean differences in P wave shape referred to signals in *V*₁ and *V*₂ positions (red dot).

Analysis of Spatial Variability for the Development of Reduced-Lead Body Surface Maps

Frederique J. Vanheusden, Xin Li, Gavin S. Chu, Tiago Paggi de Almeida, G. André Ng, Fernando S. Schindwein

University of Leicester
Leicester, UK

Introduction: Detailed cardiac analysis requires a minimum number of ECG channels. Solutions have been proposed based on reduced-lead Body Surface Potential Maps (BSPMs), but these have not as yet entered clinical practice, partly due to a lack of standardization. This situation could be improved by determining the minimal spatial sampling frequency needed to reproduce a complete BSPM. A classical method for finding the required sampling frequency for any signal is to determine the Nyquist frequency using Fourier analysis, but this cannot be applied to spatial sampling in BSPM, as it is a non-uniformly sampled signal. The aim of this study is to identify the minimum spatial sampling frequency for BSPM using spatial Lomb-Scargle spectral analysis (LSSA).

Methodology: A 128-electrode BSPM system was used to acquire body surface potentials from 10 healthy male volunteers. Distances between electrodes were measured. Signals were measured for one minute at 2048 Hz and band-pass filtered (0.16 Hz and 50 Hz cut-offs). LSSA was performed on 3 s windows, followed by an analysis on 400 ms windows containing one QRS complex to determine the Nyquist spatial frequency and, consequently, the minimum distance between electrodes needed for a complete representation of the BSPM.

Results: The 3 s window spectra indicated a need for a high electrode density (1 every 4.5 cm) due to small amplitude, high frequency variations occurring during diastole. However, QRS intervals corresponded to a lower dominant spatial frequency, such that if one is mainly interested in studying the QRS phase, then one electrode every 10.4 cm, uniformly spread over the entire torso, would be sufficient.

Conclusion: This study on healthy volunteers identified a minimum inter-electrode distance for QRS analysis using BSPM which may help to standardize future BSPM deployment.

Further evaluation on cardiac arrhythmia patients is under way.

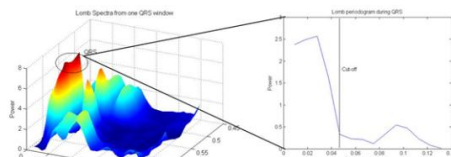


Figure: Overview of Lomb spatial spectral behavior. A significant frequency could be found at 0.048/mm.

An artificial model of the Electrocardiogram during paroxysmal Atrial Fibrillation

Julien Oster*, Gari D Clifford

University of Oxford
Oxford, United Kingdom

Introduction: We present an extension of an artificial ECG model for the simulation of multi-lead ECG during paroxysmal Atrial Fibrillation (AF).

Method: This new method was based on previously published models, the first one consisting in the generation of the cardiac dipole by a sum of Gaussian kernels and the second model consisting in a saw-tooth like shaped function simulating the atrial activity during AF. The proposed model allowed also for the generation of ectopic beats. The generation of paroxysmal AF was made possible by the use of a multiple layer-based Hidden Markov Model (HMM). The first layer allowed for the switching between different rhythms (AF or normal sinus rhythm). The second layer enabled the simulation of short and long RR intervals, as AF is usually accompanied with the succession of short and long RR intervals. The values of the transition matrix were defined as described in the literature for a realistic AF rhythmicity. The final HMM layer allowed for the simulation of ectopic beats independently of the rhythm. The cardiac dipole was generated with a sum of Gaussian kernels. During AF, the Gaussians for the P wave were replaced by the saw-tooth like atrial activity function. Each parameter of the different models was allowed to evolve randomly to simulate the inherent non-stationarity of a physiological signal. Finally, some physiological noises extracted from the noise-stress database were added to enhance the realism of the simulation.

Results: The model was used to assess the SNR of the atrial activity by a method based on a Echo State network and gave an average 2.2dB SNR.

Discussion: The simulation of ECG signal with paroxysmal AF allows a quantitative assessment of any new atrial activity extraction technique, and is useful for preliminary validation before application on real ECG data.

P59

Effects of Heart Orientation on Isolated Heart Electrograms

Marina Ronzhina*, Veronika Olejníčková, Oto Janoušek, Jana Kolářová, Marie Nováková, Ivo Provazník

Brno University of Technology
Brno, Czech Republic

INTRODUCTION: During certain experiments, the position of isolated heart has to be changed. It may result in incorrect analysis and interpretation of recorded electrograms (EGs). Study of effects of heart orientation on EG recording can help to avoid such troubles.

METHODS: The orthogonal EGs were recorded in isolated hearts of ten New Zealand rabbits by touch-less method with sampling frequency of 2 kHz. The hearts were rotated around longitudinal axis in 10° steps. In some preparations ($n=5$), rotation was made before and after ischemia. After suppression of low-frequency baseline wander, four points (fiducial point of QRS, beginning of Q, J point, and the end of T) were detected. QRS-T segments were selected for further analysis. Each heart position was represented with the first principal component calculated from 30 segments. Pearson's correlation coefficient was used to study the segment correlation within certain group (position) and between all groups for both whole segment and for Q-J and JT individually. The areas under QJ and JT were also computed and used to estimate electrical axis of the heart (parameters α QRS and α JT).

RESULTS: In correlation maps, there are two large regions (approx. $-40^\circ..+100^\circ$ and $+150^\circ..+240^\circ$) without substantial changes (correlation > 0.9) in EG morphology. There are significant differences between highly correlated regions in EG from transverse and frontal lead and no significant changes in EG recorded in longitudinal lead. Regions of high correlation in EG after ischemia are wider (by 5-15%) than in EG from control phase. These regions for JT are shifted by $25-40^\circ$ in comparison with those for QJ. The course of α JT during experiment is more consistent than of α QRS, where α QRS changes rapidly at approx. $120^\circ-140^\circ$ and $320^\circ-340^\circ$. Presented results can be suitable in studies aimed at analysis of animal EG and design of experimental protocol.

P59

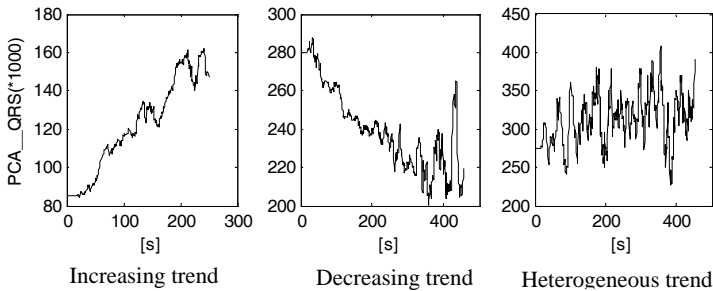
Load Dependent Changes of Cardiac Depolarization and Repolarization during Exercise ECG Test

Ivaylo Christov, Giovanni Bortolan, Iana Simova

Institute of Biophysics and Biomedical Engineering,
Bulgarian Academy of Sciences, Sofia, Bulgaria

Background: Preliminary studies have suggested that QRS and T-wave amplitude changes due to exercise-induced alterations in ventricular functionality can improve the diagnostic value of the exercise test. We hypothesize that the trends of these changes have a relevant relationship with cardiac risk factors, which will let to better risk stratification.

Method: The stress ECG test and the clinical data of 106 individuals were examined. The complexity index (the ratio between the second and the first eigenvalues of Principal Component Analysis) was considered for all QRS and T waves. Examples of homogeneous (increasing and decreasing) and heterogeneous trends of PCA_QRS are shown in the figures.



Results and discussions: The increasing and decreasing trends of PCA_QRS and PCA_T were classified as homogeneous and the rest as heterogeneous, and their relationship with clinical data was studied.

Depolarization: A predominance of the heterogeneous trends was observed in most of the groups with cardiac risk factors. This trend was statistically significant in the dyslipidemia group ($p < 0.05$).

Repolarization: Opposite to the depolarization, a prevalence of the homogeneous trends was obtained in the groups with cardiac risk factors, with statistically significant differences in the groups of coronary artery disease and percutaneous coronary intervention ($p < 0.05$).

Conclusions: The study of the load dependent behavior of PCA index during stress test in relation to clinical data has revealed the predominance of homogeneous and heterogeneous trends respectively in T and QRS wave, which can help to a better characterization of the exercise test in relation to cardiac risk factors.

Prediction of Sudden Death in Patients with HCM Using Late Potential Analysis

Nader Jafarnia Dabanloo*, Azadeh Parham, Keyvan Maghooli,
Gholamreza Attarodi

Department of Biomedical Engineering, Science and Research
Branch, Islamic Azad University, Tehran, Iran
Tehran, Iran (Islamic Republic of)

Prediction of sudden death in patients with heart diseases is very important to manage their treatments. Many researchers have been working in this area. In patients with Hypertrophic Cardiomyopathy (HCM) the risk of sudden death is very high. The question is this if late potential signals can be used as good markers of this risk in such patients. In this paper we used late potential signals in patients with HCM and after extracting features from this signal we applied Principal Component Analysis (PCA) to reduce the number of features and then we used a proper Neural Network (NN) as predictor for prediction of sudden death. Our results showed accuracy was more than 70%.

P59

The Isolated Rabbit Hearts – Database of Electrograms and Monophasic Action Potentials

Jana Kolarova, Marie Novakova, Marina Ronzhina*, Oto Janousek, Petr Vesely, Veronika Olejnickova, Ivo Provaznik

Brno University of Technology
Brno, Czech Republic

P59

INTRODUCTION: During last decade, the myocardial ischemia was studied in our laboratory in isolated hearts. The three orthogonal electrograms (EGs) and monophasic action potentials (MAPs) recorded by optical method from the surface of the left ventricle were continuously recorded according to specific experimental protocol. The original data are stored, labelled, provided with comments and may be useful for other researcher.

METHODS: Three orthogonal EGs were recorded in isolated New Zealand rabbit hearts by leads positioned orthogonally around the preparation by touch-less method. MAPs were recorded from the heart surface by optical method (fluorescence measurement). Fluorescence method is based on use of voltage-sensitive dye (VSD); in our experiments, di-4-ANEPPS was employed. Signals were amplified and digitized with sampling rate of 2 kHz and 16-bit AD converter. EGs and MAPs were recorded during the whole experiment focused on ischemia, which contains eight periods (control, loading of the VSD, three ischemia, and three reperfusion periods).

RESULTS: Twenty-four isolated rabbit hearts are included in this signal database. Since all 24 hearts were loaded with VSD, the data enable to study the effects of VSD on heart electrophysiology. In 9 cases, the incomplete numbers of ischemia-reperfusion periods were acquired. Thus, only 15 experiments were fully successful and signals from all eight periods were recorded, analysed and commented. These complete experiments are therefore suitable for ischemia preconditioning studies using EGs and MAPs signals. Also, various arrhythmias occurring in this experimental set-up may be studied from the signals included in this database.

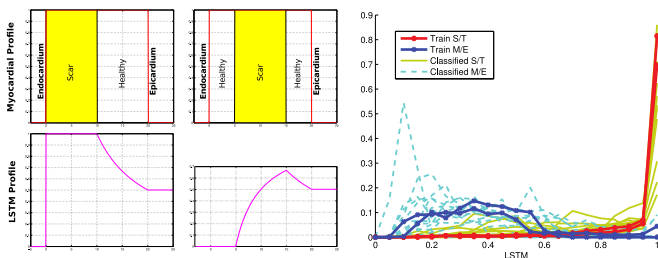
Classification of Delayed Enhancement Scar Islands by Means of their Local Subendocardial Transmurality

Susana Merino-Caviedes, Lucilio Cordero-Grande, Teresa Sevilla, Teresa Pérez, Marcos Martín-Fernández, Carlos Alberola-López

Laboratorio de Procesado de Imagen, Universidad de Valladolid
Valladolid, Spain

Introduction: Delayed Enhancement Magnetic Resonance (DE-MR) has clinical relevance in the diagnosis and prognosis of, among others, ischaemic cardiopathy and hypertrophic cardiomyopathy (ICM and HCM respectively), which have different etiologies. DE-MR hyperenhancement in ICM appears as a subendocardial scar, while in HCM, when present, it generally appears as mid-wall islands near the right-left ventricle junction. **Purpose:** To classify between subendocardial or transmural (S/T) scar islands and mid-wall or subepicardial (M/E) ones by means of their local subendocardial transmurality (LSTM), presently unpublished, defined at any myocardial point as the ratio of the thickness occupied by scar between that point and the endocardium. **Methods:** 20 short-axis DE-MR, with available myocardial and scar segmentations were employed and their LSTM computed. A connectivity analysis was conducted to identify isolated scar islands, where their LSTM was inspected. After excluding false positives, a total of 30 islands were available for training (5) and testing (25). The normalized histogram of every test island LSTM was computed and correlated with those of the train islands (3 for S/T and 2 for M/E), and the class of the train island with the highest correlation value was chosen for the test island. **Results:** A paired Mann-Whitney U-test that was performed between S/T and M/E train islands indicating that their medians are different with $p < 1e-65$. The classifier had a success rate of 96%, with only one S/T island misclassified as M/E. **Conclusion:** Inspecting a local magnitude such as LSTM within isolated scar islands in DE-MR allows to determine its type, which is important in the diagnosis of different types of cardiomyopathies.

P5A



LSTM for two myocardial scar 1D profiles and classified LSTM normalized histograms of the island set.

A Software Tool for the Computation of Arterial Pulse Wave Velocities from Flow-sensitive 4D MRI Data

Johann Drexl*, Hanieh Mirzaee, Andreas Harloff, Markus Hüllebrand, Anja Hennemuth, Horst Hahn

Fraunhofer MEVIS
Bremen, Germany

P5A

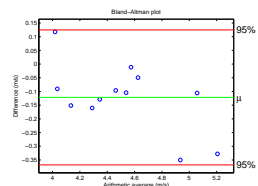
Aims: Measurement of aortic pulse wave velocity (PWV) is of high clinical importance, as PWV is an important predictor of atherosclerosis progression. As demonstrated in previous studies, PWV can be measured non-invasively based on flow-sensitive 4D MRI. However, this interactive approach is very time-consuming (~ 3 h per case). Thus, we propose a more efficient PWV computation through automatizing major steps of the processing pipeline.

Method: The presented approach is integrated into a workflow oriented software assistant, supporting data import, offset error correction, phase-unwrapping, vessel segmentation and PWV computation. A centerline calculation forms the basis for automatically placing the cross-sectional analysis planes. The flow curves used to derive the pulse wave arrival information are calculated for measurement regions defined through the intersections with the vessel mask.

Materials: To ensure correctness, we systematically validated our implementation on a realistic digital phantom. Furthermore, we evaluated our method on in-vivo data from 12 volunteers from a recent study conducted by Markl et al; consequently a comparison between the outcomes was possible. Data acquisition had been performed on a Siemens TRIO scanner (3 Tesla). Scan parameters were spatiotemporal resolution= $1.7 \times 2.0 \times 2.2 \text{ mm}^3 \times 42.8 \text{ ms}$, TE/TR= $2.6-3.5 \text{ ms} / 5.1-6.1 \text{ ms}$, flip angle= $7-15^\circ$, VENC= 1.50 m/s .

Results: After the data was processed with the above mentioned workflow, two observers independently measured the PWVs. Mean and standard deviation for the two observers were: $4.46 \text{ m/s} \pm 0.35 \text{ m/s}$ and $4.58 \text{ m/s} \pm 0.43 \text{ m/s}$. To further analyze the degree of agreement between the two observers, the Bland-Altman method was used. We found a small bias of $0.12 \text{ m/s} \pm 0.13 \text{ m/s}$, and a maximum discordance of 0.35 m/s between the observers (still within the 95% confidence interval). Mean time per case for preprocessing and segmentation was 30min, and 4min for PWV measurement.

Conclusion: Comparing our PWV results to those of Markl et al (PWV $4.39 \text{ m/s} \pm 0.32 \text{ m/s}$), we find that our method gives similar accuracy and reproducibility, but at a significantly reduced processing time.



Registration and Fusion of Contrast-Enhanced MRI Myocardial Substrate Maps and X-ray Angiograms

Juan E Ortuño*, Esther Pérez-David, Ángel Arenal, Javier Bermejo, Andrés Santos, María J Ledesma-Carbayo

Universidad Politécnica de Madrid and CIBER-BBN, Spain

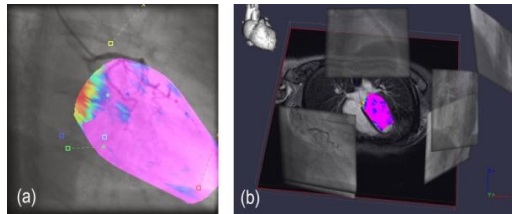
Background and Aim: Contrast-enhanced MRI (ceMRI) has been proved to be reliable for the identification of viable and scar tissue. The aim of this work is to provide the necessary methods to register and fuse the endo-epicardial signal intensity maps (SI_m) extracted from ceMRI data with X-ray coronary angiograms using an intrinsic registration-based algorithm to help pre-planning and guidance of catheterization procedures.

Methods: Fusion of angiograms with ceMRI derived maps was treated as a 2D-3D pose estimation, where each image point is projected to a Plücker line, and the screw representation for rigid motions is minimized using a gradient

descent method. The procedure is optionally combined with an iterative closest point algorithm (ICP) that aligns the ventricular contour from a ventriculogram with the SI_m surface. The resultant transformation is applied to the SI_m that is then projected on each angiogram. ceMRI images were performed with a 1.5T Philips Intera scanner. Endo-epicardial contours were manually defined using QMass software (MEDIS) and reconstructed as a 3D-mesh on which sub-epicardial or sub-endocardial scar SI_m was projected. Left ventricular angiographies in typical orientations were performed using a Siemens Axiom-Artis system.

Experiments and Results: The proposed methods were tested in clinical datasets from 6 patients with prior myocardial infarction. 5 points (apex, coronary junctions, bony structures and catheter) were identified in each ceMRI and their correspondence in one angiogram. Additionally in two cases the combination with the ICP algorithm was tested. Fusion results were validated by experts in cardiac imaging and intervention.

Conclusions: Internal marker-based 2D-3D registration has proved to be robust and to perform correctly. Additionally an ICP contour to surface strategy has been combined to provide a more flexible data-input. The proposed methods provide a flexible solution for typical clinical settings with promising clinical relevance.



(a) Endocardial SI_m fused with angiogram; (b) display of the ceMRI, the SI_m and the angiograms in the application tool.

P5A

Global Tractography in Cardiac Diffusion-Tensor MRI

Matthew Ozon, Marc Robini, Pierre Croisille, Carole Frindel, Yue-Min Zhu

CREATIS, INSA-Lyon, France

Aims: Our objective is to extract global myocardial fiber architecture from diffusion-tensor MRI data under the degraded conditions of in-vivo imaging (i.e., small number of gradient directions and noisy diffusion-weighted images). The underlying aim is to assess the spatio-temporal fiber architecture of the myocardium to improve the understanding of the heart dynamics and of cardiac diseases.

Methods: The fiber architecture is modeled by a binary-weighted graph whose vertices represent voxel locations and whose edges connect neighboring voxels. The vertex and edge sets characterize the possible fiber paths, and the discrete fibers are sequences of adjacent edges with non-zero weights—the actual fibers are splines controlled by the vertices of the discrete fibers. The optimal fiber set is defined as the global minimum of an energy function that we specifically designed for cardiac tractography: the fidelity to the data is balanced by a prior term that enforces locally coherent fiber architectures. The minimization of the proposed energy function is a difficult optimization task that is performed by simulated annealing. We assess the robustness of our algorithm to noise by considering synthetic data sets with increasing (Rician) noise level. We also test our algorithm on real cardiac data sets with 12 and 6 gradient directions. Our results are compared to that obtained with another graph-based algorithm and with streamlining. The accuracy of the extracted fiber sets is measured via the deviation to the tensor fields (synthetic and real data cases) and via the distance to the “true” fibers (synthetic case only).

Results: Our experiments on synthetic data show that the proposed algorithm outperforms the two others when the signal-to-noise ratio is low, which suggests that our approach is the most suitable for in-vivo cardiac tractography. This conclusion is corroborated by our experiments on real data when using only 6 directions.

P5A

Computational Mesh as a Descriptor of Left Ventricular Shape for Clinical Diagnosis

Pablo Lamata*, Merzaka Lazdam, Anna Ashcroft, Adam Lewandowski, Paul Leeson, Nic Smith

King's College of London
London, UK

Shape and size of the left ventricle are cardiac biomarkers used in clinical routine practice typically assessed through medical imaging and analysis tools that capture key partial metrics like volume, length, diameter or wall thickness. The aim of this work is to illustrate the potential of an alternative shape analysis methodology based on a comprehensive description of the anatomy using a computational atlas. 40 cardiovascular magnetic resonance scans of young women defined the cohort data set. A stack of 7 to 8 slices from end diastolic frames of dynamic MRI studies, were analysed by manual segmentation and automatic personalization of high order computational meshes. The most significant modes of variation of shape of this population were identified by principal component analysis. Statistical significant differences in shape were found in women with higher cardiovascular risk profiles ($P < 0.05$, Hotelling T2 test). The analysis revealed differences in the position of the apex in the left to right direction, which had not been captured by standard clinical parameters. These results show computational statistical atlases may offer potential to improve stratification of cardiac diseases.

P5A

Regional Comparison of Left Ventricle Systolic Wall Stress reveals Non-Uniformity in Healthy Subjects

Soo-Kng Teo¹, Si-Yong Yeo¹, May-Ling Tan¹, Chi-Wan Lim¹, Liang Zhong², Ru-San Tan^{2,3}, Yi Su^{1,*}

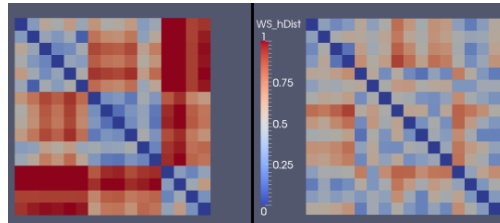
¹Institute of High Performance Computing, A*STAR, Singapore

²National Heart Centre, Singapore

³Duke-NUS Graduate Medical School, Singapore

P5A

Aims: This study assessed the feasibility of using the regional uniformity of the left ventricle (LV) wall stress (WS) to diagnosis patients with myocardial infarction (MI). Previously, we had shown that the mean systolic WS was significantly increased at each LV segments in ischemic dilated cardiomyopathy patients. However, this mean value comparison might obscure subtle local variations in the systolic WS across the different segments within the same patient. Here, we present a novel similarity map that indicates the degree of uniformity in systolic WS across the different segments within the same patient.



LV systolic WS similarity map between a normal subject (left panel) and a MI patient (right panel).

Methods: The 3D LV geometries at end-diastolic (ED) and end-systolic (ES) phases were reconstructed from border-delineated MRI images. For each data sample, an automatic algorithm was used to generate a 1-to-1 corresponding mesh pair of the LV for the ED and ES phases based on a geometrical-mechanical minimization approach. The systolic WS at each vertex point and a WS histogram distribution for each of the 16 LV segment were computed. A similarity index was then computed for each pair of histogram distributions to generate a 16-by-16 similarity map. Segments with similar (dissimilar) distribution of WS were reflected by a similarity index (denoted by $hDist$) with values close to 0 (1).

Results: Based on an initial study involving 4 MI patients and 4 normal subjects, we observed that the mean $hDist$ for segments in the following groups: (i) basal against mid, (ii) basal against apical and (iii) mid against apical were significantly higher in normal subjects compared to patients (p-value = 0.0073, 0.00026 and 0.0079 < 0.05 using a 1-tailed student t-test, respectively), reflecting greater non-uniformity.

Conclusions: Our results suggest that the regional uniformity of the LV systolic WS in the form of a similarity map can be used as a discriminant between MI patients and normal subjects.

3D Bilateral Filtering of Cardiac DT-MRI Data

Tomasz Pieciak

AGH University of Science and Technology
Krakow, Poland

Introduction: Diffusion tensor magnetic resonance imaging (DT-MRI) is a modern imaging modality, which, as the only one, can assess fiber structure arrangement on a microscopic level in a non-invasive way. However, inherent cardiac cycle and respiratory system considerably affect the data quality, e.g., change the directions of the principal eigenvectors of the diffusion tensors (DTs). In consequence, it leads to ambiguities in quantitative analysis of DTs (e.g., fractional anisotropy measure – FA) and fiber tracts obtained with tractography algorithms.

Purpose: We performed Monte Carlo noise simulation at $S_0 = 250$ amplitude with negligible small diffusion gradient and b-value fixed at 1000 s/mm^2 . The quantitative analysis of primary eigenvector of the DT shows their significant changes even up to 45° .

Method: The proposed technique integrates information both coming from 3D spatial localization of the DTs and also their similarities. However, an Euclidean metric on DTs leads to a specific “swelling effect”, thus, we take advantage of P-average that distinctly reduces undesirable tensors averaging distortions. The DTs similarity measures, in turn, are based on the principal eigenvectors angle between tensors (angle similarity – AS) and Jensen-Bregman LogDet (JBLD) divergence for covariance matrices.

Results: We generated Rician noise and conducted experiments both on synthetic and real cardiac DT-MRI datasets. Our investigation shows, that AS as well as AS+JBLD measures highly reduce root mean-squared error (RMSE) of FA parameter and primary eigenvector angle difference (AD) mean (results in the bottom table). Also, we notice, that for low signal-to-noise ratio and high cut-off AS value, the filtering process result in the most accurate results.

Conclusion: The 3D bilateral filtering approach allows one to enhance cardiac DT-MRI data, therefore, the principal eigenvectors field could be reflected in a more reliable way. Moreover, the proposed algorithm decreases uncertainties for incorrect fiber tracts reconstruction procedure and keeps positive-semi defined property of the DTs.

Noise Variance	FA RMSE			AD mean [°]		
	Noisy	AS	AS+JBLD	Noisy	AS	AS+JBLD
$\sigma^2 = 5$	0.075	0.016	0.014	8.550	1.901	1.757
$\sigma^2 = 20$	0.316	0.163	0.245	33.787	18.862	18.978

P5A

Tuning a Real-Time Detector of Transient Cardiac Ischemic Episodes on the Long-Term ST Database according to the Annotation Protocol B.

Lacramioara Dranca*, Alfredo Goñi, Arantza Illarramendi

Centro Universitario de la Defensa de Zaragoza
Zaragoza, Spain

This study revisits a real-time ischemia detector trained over the Long-Term ST (LTST) database according to the transient ST episode annotations (ischemic and heart-rate-related episodes considered together) for protocol A. However, the results for annotation protocol B are more used in the literature when comparing performance.

Aims: We have studied to adapt the initial detector in order to comply with the ischemia annotation protocol B requirements on the LTST database and make easier a fair comparison with related works. Secondly have we studied to improve the initial algorithm.

Methods: The detection algorithm consists of a detection step of ST events and a discrimination step of ischemic from non-ischemic events. In the detection step: 1) a new measurement method proposed in the literature for the ST level has been adopted; 2) detection thresholds have been adjusted to comply with the ischemia annotations for protocol B and additional checks have been done on the continuity and maintenance of the ST deviation trend over time. In the discrimination step, we evaluated different features, recently proposed in the literature, for ischemia discrimination from non-ischemic events. The individual predictive ability of each feature and the degree of redundancy between them have been considered. Several new features have been found suitable and used for the REAL-TIME ischemia discrimination. A bagged decision tree model has been trained according to the annotations for protocol B. The model uses a voting scheme that allows the posterior adjustment of the final decision according to their confidence level.

Results: The intermediate results in terms of sensitivity/positive predictivity after the detection step were 81.61%/55% and improved to 80.95%/73.92% after the discrimination step. These improve our previous results and are comparable to other results reported for this database with the advantage that this algorithm could analyze the ECG signal in real-time.

S61

Automated Detection of the Culprit Artery from the ECG in Acute Myocardial Infarction

Elaine Clark, Yama Fakhri, M Abdul Waduud, Maria Sejersten, Peter Clemmensen, Peter W Macfarlane

University of Glasgow
Glasgow, UK

Introduction: The AHA/ACC guidelines recommend that, for patients with acute myocardial infarction(MI), the likely culprit artery is reported on ECG interpretations. The aim of this study was to develop, implement and evaluate criteria for automated detection of the culprit artery.

Methods: ECG and PCI data was retrospectively gathered in Zealand, Denmark, from patients who had presented with symptoms suggesting an acute coronary syndrome. Those eligible for the study had a prehospital ECG recorded between January 1st,2003 and June 1st 2012 and a PCI on the same day as the ECG recording, and were subsequently identified as having single vessel disease. 307 patients were selected (218 male, 89 female, age 61.8 ± 12.3 years). ECG criteria for locating the culprit artery were based on the presence of STEMI, the wall or walls in which acute MI was present and individual lead ST elevation levels. These criteria were implemented in the Glasgow program which was run on the dataset to determine the suspected culprit artery as LAD, RCA, LCX, unknown or none. The automated results were evaluated by calculating sensitivities and specificities for each type of occlusion against the gold standard location determined from the coronary arteriogram.

Results: There were 136 LAD, 119 RCA, 23 LCX and 29 other locations of the culprit artery. 231 (75%) of the 307 cases were reported as STEMI by the program. The sensitivities and specificities for reports of LAD, RCA and LCX are given below.

Culprit Artery	Sensitivity	Specificity
LAD	69%	94%
RCA	64%	94%
LCX	57%	96%

Conclusion: Detection of the culprit artery from an ECG can be automated. The approach was accurate for this data set which was used as a training set but a new database requires to be established for use as a test set.

Depolarization Morphologic Features of the ECG for Detection of Stress Induced Ischemia

Llamedo M*, Albertal M, Laguna P, Martínez JP

Electronic Department, Universidad Tecnológica Nacional, Buenos Aires, Argentina

Introduction: Exercise electrocardiography is widely used for diagnosing coronary artery disease. The objective of this study is to develop an algorithm for detecting stress-induced ischemia in the ECG. For this purpose, we evaluated several morphologic features measured in a multilead signal representations using the wavelet transform (WT) and principal components analysis (PCA). Some of these features were previously used for arrhythmia classification [Llamedo M, *IEEE TBME* 2010].

Materials and Methods: The diagnostic performance of this technique has been studied in a public database available at the THEW project (UIDB: 15). It includes 996 patients (age: 56 ± 10 years, 670 men) referred for exercise myocardial perfusion imaging (MPI), which served as the gold standard of ischemia. The performance was compared with results reported in the same database with other techniques such as high frequency QRS components (HFQRS), or the ST segment change [Sharir T, *Am. J. Card.* 2012]. A class-balanced linear classifier was used to classify patients as ischemic or not.

Results: The best performing features were found in the first two principal components, as the first zero-crossing in the autocorrelation function of the WT, which can be interpreted as a robust surrogate of the QRS complex width. The best model found as in [Llamedo M, *IEEE TBME* 2010], resulted of 2 features, and achieved a sensitivity (Se) of 67% and specificity (Sp) of 77% assessed with a $k=10$ cross-validation scheme.

Discussion: This performance is comparable to HFQRS (Se 69%, Sp 86%), and better than using the ST segment (Se 39%, Sp 82%), with the additional advantage that it can be used with the standard ECG recording bandwidth, while HFQRS requires special recording equipment to preserve the HF band (>150 Hz). Although other features to improve the performance of the current model are under study, the model presented represents an useful tool.

High resolution ECG Changes in Survivors of Out-of-Hospital Cardiac Arrest during and after Mild Therapeutic Hypothermia

Martin Rauber, Dušan Štajer, Marko Noč, Todd T. Schlegel, Vito Starc
University of Ljubljana, Faculty of Medicine, Ljubljana, Slovenia

Induced mild therapeutic hypothermia (MTH) improves neurologic outcome and probably also myocardial damage in comatose survivors of heart arrest. We were interested in conventional and advanced ECG parameters during and after recovering from hypothermia.

The study population consisted of 62 comatose survivors of out-of-hospital primary cardiac arrest, caused by coronary artery thrombosis, who were admitted to the Ljubljana University Medical Centre (2011 - 2013) and treated with MTH for 24 hours. In all subjects, resting 5-minute 12-lead high resolution ECG during and one day after MTH were recorded and evaluated via custom software programs. Eighty-five conventional and advanced ECG parameters, including beat-to-beat QT and RR variability, waveform complexity, and signal-averaged ECG parameters were assessed. Parameters during hypothermia and in normothermia were compared using a paired T-test.

After recovering from hypothermia the mean RR interval, QTc interval, PR interval, and ventricular gradient (VG) decreased (all $p < 0.0001$). RRV parameters, the total power of the autoregressive function (AR TP), its HF component (AR HFP), and RMSSD also decreased significantly (all $p < 0.0001$). QTV parameters slightly deteriorated: QTVI and the unexplained part of QTVI (uQTVI) increased, and the repolarization parameter QTcor decreased (all $p < 0.005$).

Reduction of several ECG intervals and variability parameters and slight deterioration in repolarization has been observed after recovery from hypothermia. This might be related beneficial effect of hypothermia on the heart.

ECG Parameters	Hypothermia	Recovery	P value
RR interval (ms)	1019 ± 332	660 ± 161	<0.0001
QTc interval (II ms)	471 ± 129	453 ± 41	<0.0001
PR interval (ms)	175 ± 54	143 ± 38	<0.0001
VG (mV*ms)	33.1 ± 18.1	19.6 ± 1.4	<0.0001
AR TP (Ln ms ² /Hz)	6.4 ± 2.5	4.7 ± 2.6	<0.0001
AR HFP (Ln s ² /Hz)	5.5 ± 2.8	3.6 ± 3.1	<0.0001
RMSSD (ms)	79 ± 93	44 ± 73	<0.0001
QTVI (II, units)	-0.68 ± 0.99	-0.13 ± 0.93	0.002
uQTVI (II, units)	-0.47 ± 1.2	0.23 ± 1.0	0.001
QTcor (II, units)	0.53 ± 0.18	0.44 ± 0.14	0.005

S61

T-Wave Alternans Identification in Routine Exercise ECG Tracings: Comparison of Methods

Silvia Bini*, Cees A Sweene, Sumche Man, Laura Burattini

Polytechnic University of Marche, Ancona, Italy
Ancona, Italy

S61

T-wave alternans (TWA) is widely accepted as an index of electrical cardiac vulnerability and is often measured on clinical exercise ECG recordings specifically made for TWA testing in order to minimize the noise level. Since TWA amplitude (TWAA) increases with heart rate (HR), measurements are usually performed at high HR when TWAA is maximum and HR variability is minimum. Indeed, both conditions are fundamental for a reliable TWA identification by any automatic method. Still, TWA utility in clinical evaluation would be magnified by the possibility of measuring TWA on a broad variety of recordings, including routine standard exercise ECGs usually affected by a high noise level. Thus, aim of this study was to evaluate the performances of 3 automatic TWA identification methods, namely the spectral method (SM), the modified-moving-average method (MMAM) and the HR-adaptive-match-filter method (AMFM) on routine exercise (biking) ECGs of 46 implanted-cardiac-defibrillator patients (ICDP). TWA was identified in 1-min windows characterized by stable HR and the absence of artifacts and ectopic beats in correspondence of the minimum (MinHR=83±12 bpm) and maximum (MaxHR=123±19 bpm) HR. Results show that the SM was able to identify TWA in only 12 ICDP during MinHR and 23 ICDP during MaxHR (median TWAA: 4 μV and 29 μV, respectively; P<10⁻³) due to the presence of some levels of noise and HR variability. Instead, the MMAM and AMFM always identified TWA in all ICDP; however, the former method provided much higher median TWAA estimates (MinHR: 1507 μV, MaxHR: 1602 μV; P=0.5258) than the latter one (MinHR: 22 μV, MaxHR: 38 μV; P<10⁻⁴), suggesting that the MMAM is likely measuring noise. Eventually, the SM and AMFM detected the expected significant TWAA increment at MaxHR. In conclusion, among the analyzed methods, the AMFM appears as the most reliable for TWA identification in routine exercise ECG recordings.

T-wave Alternans Predicts ICD Discharge in MADIT II Patients with Elevated Resting Heart Rate

V Monasterio^{1,2}, JP Martínez^{2,1}, S McNitt³, P Laguna^{2,1}, AJ Moss³, M Haigney⁴, W Zareba³, JP Couderc³

¹CIBER de Bioingeniería, Biomateriales y Nanomedicina, Zaragoza, Spain

²University of Zaragoza, Zaragoza, Spain

³University of Rochester Medical Center, Rochester, NY, USA

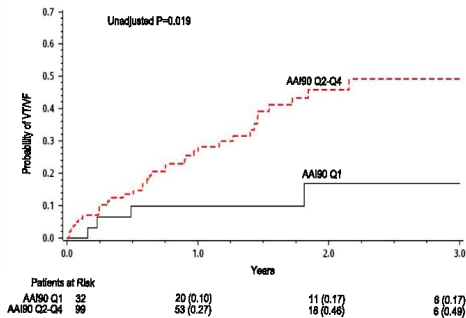
⁴F. Edward Hébert School of Medicine, Bethesda, MD, USA

Introduction: The identification of MADIT II patients who might benefit the most from ICD therapy remains a clinical challenge. We proposed to measure T-wave alternans (TWA) using the multilead Laplacian likelihood ratio method (mLLR) in MADIT II patients, and to evaluate its ability to predict ventricular tachycardia (VT) or ventricular fibrillation (VF) events requiring an ICD shock and to predict sudden cardiac death (SCD). mLLR is a robust alternative to existing single-lead TWA techniques which improves the accuracy of TWA detection in noisy ECG signals.

Methods: We studied MADIT II patients with baseline heart rate ≥ 80 beats/min, free of atrial fibrillation who had 10-min resting Holter ECG recorded prior to implantation. We measured the index of average alternans (IAA) and the heart rate restricted value of IAA (80 beats/min \leq HR < 90 beats/min) called IAA₉₀. Cox's proportional hazard models were adjusted for relevant clinical variables, and appropriate ICD therapy (VT/VF events) and SCD were considered as independent and combined endpoints.

Results: We identified 175 MADIT II patients in whom IAA and IAA₉₀ could be computed. Out of the 131 patients in the ICD arm, 40 (30%) experienced ICD therapy for VT/VF. Amongst the overall study population, 15 (8.6%) subjects had SCD. IAA and IAA₉₀ indices did not predict SCD, but Cox's models revealed that appropriate ICD therapy was predicted by IAA₉₀ (hazard ratio: 1.05 per μV ; 95%CI: 1.01-1.09, $p=0.008$) after adjustment for QRS duration, NYHA class, diabetes, creatinine and blood urea nitrogen levels. The Kaplan-Meier graph revealed that patients with an elevated IAA have 40% more risk for VT/VF at 2 years after ICD implantation.

Conclusion: The average TWA measured between 80 and 90 beats/min in resting ECGs is associated with future ICD therapy in MADIT II patients.



Non-Invasive Epicardial Imaging of Human Ventricular Fibrillation

John R Fitz-Clarke*, John L Sapp, B Milan Horáček

Dalhousie University
Halifax, Canada

S62

Introduction: ECG signals from ventricular fibrillation (VF) contain information about the electrical status of the myocardium. Novel signal analysis might improve techniques for tailoring decisions during cardiac resuscitation. We hypothesized that spatial distribution of potentials on the torso surface would correlate with underlying fibrillation dynamics. ECG data of human VF was obtained through high-resolution body surface mapping. Inverse solution was used to construct images of epicardial activity.

Methods: A 120-lead ECG mapping system was used to record torso potentials from seven anesthetized patients during controlled VF induction following implantable cardioverter-defibrillator placement. Body surface potential map (BSPM) sequences ($n = 12$) were acquired for 8-second intervals prior to device shock delivery. Epicardial potential maps of VF were calculated mathematically by inverse solution using Tikhonov regularization and L-curve method, assuming a homogenous bounded torso. Spatial features of epicardial and torso activity were each characterized by principal component analysis using the Karhunen-Loève transform. To aid interpretation, VF was simulated in a large-scale numerical anisotropic heart model with dynamics varied over ranges of ionic current parameters. Potential fields were simulated within the torso volume conductor to assess spatiotemporal information attenuation.

Results: Torso maps exhibited high spatial organization, with 92 percent of BSPM variance captured by the largest three eigenvectors. Spatial features of VF diminished with distance from the heart within the volume conductor, however multiple dipolar components were recoverable on the torso surface. Derived epicardial images exhibited dynamical regions resembling propagating action potentials of varying spatial scales. Statistical characteristics of epicardial activity and spatial eigenvectors were reproducible with computer simulation.

Conclusion: Epicardial images of VF were derived non-invasively from body surface potentials. Although torso volume attenuated signal features, spatial information from VF was measurable at the body surface. Computer simulation revealed how the torso volume conductor imposes fundamental limitations on spatial information extraction.

Dynamic Changes in Intracardiac Impedance as a Prognostic Marker During Internal Cardioversion of Atrial Fibrillation

Philip Richard Walsh, Omar Jacinto Escalona*, Vivek Kodoth, Noel Camilo Castro, David McEneaney, Ernest Lau, Ganesh Manoharan

University of Ulster
Newtownabbey, United Kingdom

Introduction: Voltage, current and impedance are major determinants of success during internal cardioversion of atrial fibrillation (AF). However, there is limited data on the dynamic change in intracardiac impedance (ICI) as a predictor of success.

Methods: Thirty patients with persistent AF were randomised to treatment with a biphasic very low-low-tilt rectilinear (B-VLTR) chronosymmetric (6ms/6ms) amplitude asymmetric (negative phase at 50% amplitude) waveform or a monophasic very low-low-tilt rectilinear (M-VLTR) waveform (12ms) using a step up protocol (50V to 300V; 6-step). Cardioversion success was defined as the restoration of sinus rhythm for a minimum of 30 seconds. Data gathered was grouped into four categories: patients cardioverted using the B-VLTR step-up protocol (Group I), patients treated with the B-VLTR step-up protocol but who failed to cardiovert (Group II), patients cardioverted using a M-VLTR step-up protocol (Group III) and patients treated with the M-VLTR step-up protocol who failed to cardiovert (Group IV). Intracardiac impedance was calculated across each group and a standard student t-test (two tailed paired distribution) used to investigate the significance of dynamic changes in ICI between successive electrical shocks.

Results: For both B-VLTR and M-VLTR treatment protocols, all patients who cardioverted exhibited a significant reduction in ICI between the first and third shock ($[\Delta Z=5.66\pm 2.71\Omega(\text{mean}\pm\text{SD})$, $p<0.01$] and $[\Delta Z=4.72\pm 1.62\Omega(\text{mean}\pm\text{SD})$, $p<0.003$] for B-VLTR and M-VLTR, respectively). However, no significant reduction in ICI between these initial shocks was noted in patients who failed to cardiovert ($[\Delta Z=3.85\pm 5.63\Omega(\text{mean}\pm\text{SD})$, $p>0.05$] and $[\Delta Z=8.12\pm 6.57\Omega(\text{mean}\pm\text{SD})$, $p>0.05$] for B-VLTR and M-VLTR, respectively). The data suggests that reaction of the cardiac substrate to a minimum quantum of energy may ultimately be of more importance than waveform type in determining the outcome to treatment.

Conclusion: Significant decrease in ICI during the first three shocks was identified as a positive predictor of success in a step-up protocol using both B-VLTR and M-VLTR waveforms.

S62

Wavelet-Based Electrogram Onset Identification for Ventricular Electroanatomical Mapping

Alejandro Alcaine, David Soto-Iglesias, David Andreu, Juan Fernández-Armenta, Antonio Berruezo, Pablo Laguna, Oscar Camara, Juan Pablo Martínez

Communication Technologies Group, Universidad de Zaragoza
Zaragoza, Spain

S62

Aims: Catheter ablation guided by an electroanatomical mapping system is frequently used to treat different arrhythmias. Identification of the earliest activation area is a common task specially in focal tachycardias. However, those systems do not automatically locate the activation onset and a technician usually does it manually during the intervention, which is may be highly observer-dependent and very time-consuming. In this work, we propose a method combining surface ECG information with electrogram (EGM) signals to automatically delineate the onset and offset of EGM activations.

Materials and methods: A total of 14 electroanatomical maps from 10 patients suffering from ventricular extrasystole beats admitted for ablation procedure at Hospital Clínic (Barcelona, Spain) were used. The map acquisition was made at 1 kHz sampling frequency using the CARTO[®] system. In each mapping point 2.5 seconds of 12-lead standard ECG and bipolar EGM signals were recorded.

QRS complex was detected and delineated in each lead, and then, multi-lead delineation was achieved by applying rules. The estimated QRS complex width define the search window of the EGM activation. Then, the EGM signal envelope was estimated and the detection and delineation were performed on its Wavelet Transform (WT). The main wave of EGM activation was located at the zero-crossings between a pair of local maxima-minima through the WT scales, and the onset and offset of the EGM activation were located in the first sample crossing a threshold in the second scale of the WT.

Results: The assessment of the proposed method was made by comparing the EGM onset points manually measured by an expert technician during the intervention with the automatic ones. The difference in the local activation time (LAT) between our algorithm and the manual measurements were 4.0 ± 13.7 ms evaluated in 2163 mapping points.

Conclusions: The proposed method allows automatic LATs estimation with an accuracy comparable with the manual measurements achieved during the procedure.

Nonlinear Characteristics of Ventricular Fibrillation depending on Myocardial Infarction Locations

María González-González, Óscar Barquero-Pérez*, Cristina Soguero-Ruiz, José Luis Rojo-Álvarez, Juan José Sánchez-Muñoz, Arcadi García-Alberola

University Rey Juan Carlos
Fuenlabrada, Spain

Background The location of the myocardial infarction (MI) might induce a change in the characteristics of cardioelectric signals recorded during ventricular fibrillation (VF). In the literature, spectral analysis has been used to characterize VF, however, spectral parameters do not account for nonlinear information on these signals.

Objective. Our aim was to analyze the effect of the location of the infarcted area on VF signals by using nonlinear parameters, hence complementing their spectral characterization..

Materials and Methods. We included patients with chronic MI (28 anterior, 29 inferior) from Hospital Universitario Virgen de la Arrixaca (Murcia) and Hospital Universitario Gregorio Marañón (Madrid) in Spain. VF was induced during cardioverter defibrillator implant. Spectral parameters (dominant frequency -FD-, organization index -OI-, and regularity index -RI-) were obtained on every VF episode, and compared to nonlinear measurements, namely entropy indices (sample entropy -SampEn-) and higher order moments (kurtosis -K- and skewness -S-). A nonparametric resampling statistical hypothesis test was used to evaluate the effect of the location of the MI on VF parameters.

Results. Nonlinear parameters, SampEn, K, and S were all significantly different regarding the location. SampEn was higher on inferior (0.57 ± 0.17) compared to anterior (0.47 ± 0.20 , $p < 0.05$) MI patients, whereas K and S were significantly lower on inferior MI patients (K; inferior: 2.71 ± 0.89 , anterior: 3.32 ± 1.05 , $p < 0.05$) and (S; inferior: 0.34 ± 0.41 , anterior: 0.62 ± 0.61 , $p < 0.05$). None of the spectral parameters showed significant differences, FD (4.83 ± 0.52 vs 4.85 ± 0.52 Hz), RI (0.82 ± 0.10 vs 0.79 ± 0.12), OI (0.82 ± 0.10 vs 0.83 ± 0.10).

Conclusions. Nonlinear and higher order moments parameters (SampEn, K and S) showed significant differences during VF depending on the MI localization. Indeed, VF signals were more complex (irregular) on patients with inferior MI location.

S62

Analyzing electrical patterns in an experimental swine model of dyssynchrony and CRT.

David Soto-Iglesias, Nicolas Duchateau, Constantine Butakoff, David Andreu, Juan Fernández-Armenta, Antonio Berruezo, Marta Sitges, Oscar Camara

PhySense, DTIC, Universitat Pompeu Fabra
Barcelona, Spain

Aims: Cardiac resynchronization therapy (CRT) is an innovational therapy for the treatment of specific types of cardiac dyssynchrony. However its cost and the still elevated rate of non-responders maintain it as a very challenging issue. Electroanatomical maps (EAM) are currently used to visualize electrical activation patterns jointly with the patient anatomy. Nonetheless they are intrinsically specific to each subject and suffer from the lack of a common space of coordinates in which intra- and inter-subject comparisons can be performed. We propose a method for mapping this EAM surface-based information to a common geometry (homeomorphic mapping to a disk) to solve this issue.

Material and methods: A total of 10 pigs were studied, under baseline, LBBB and CRT conditions. Contact mapping data was collected with an electroanatomical mapping device. EAMs were subsequently generated by reconstructing the local activation time (LAT) information obtained.

The proposed methodology provides a simple method for mapping a ventricle surface to a disk. This disk will be used as a common reference geometry for all the ventricles in the dataset. The high variability observed in different activation times, requires a normalization between 0 and 100

Results: Median-interquartile range for left ventricle activation time show statistically significant differences between the different experimental stages, except for total activation time between LBBB and CRT.

Conclusions: Delay in early activation can be seen for the LBBB stage as compared to baseline. Besides, the low inter-subject variability of the LBBB global activation indicates the high reproducibility of the observations induced by the ablation performed. In addition, almost complete recovery of the global activation pattern after CRT is observed.

Electrophysiological Predictors of Malignant Arrhythmias in Patients with Wolff-Parkinson-White Syndrome

Amarild Cuko*, Massimo Saviano, Luigi Giannelli, Cristiano Ciaccio, Andrea Petretta, Mario Baldi, Alessia Pappone, Gabriele Vicedomini, Carlo Pappone

Maria Cecilia Hospital, GVM Care&Research, Cotignola (RA), Italy

BACKGROUND: Limited amount of long-term data are available for malignant arrhythmias (MAs) in patients with Wolff-Parkinson-White syndrome (WPW). There are no clinical studies using electrophysiological testing (EPT) to evaluate predictors of sudden cardiac death (SCD) in symptomatic WPW.

METHODS AND RESULTS: Among 8575 symptomatic WPW patients with atrioventricular reentrant tachycardia (AVRT) referred for EPT, 369 (23±12.5 years-old) declined catheter ablation and were followed up. The primary end point of the study was to evaluate over a 5-year follow-up the predictors and characteristics of patients who develop MAs. After a mean follow-up of 54.1±10 months, MAs developed in 29 patients (13.9±5.6 years-old; 26 male), resulting in syncope (25 patients), hemodynamic collapse (3 patients), or SCD due to ventricular fibrillation (1 patient). Considering the rest of the patients (n=340), 168 (34.2±9.0 years-old) remained asymptomatic up to 5 years, and 172 (13.6±5.1 years-old) had benign recurrence, including sustained AVRT (132 patients) or non pre-excited atrial fibrillation (40 patients). The group with MAs had shorter accessory-pathway effective refractory period (APERP) (P<0.001), higher incidence of multiple accessory pathways (P<0.001), and higher incidence of AVRT triggering sustained pre-excited atrial fibrillation (P<0.001). Multivariable analysis demonstrated that short APERP and AVRT triggering sustained pre-excited atrial fibrillation were independent predictors of MAs.

CONCLUSIONS: Even if symptomatic patients with WPW generally have a good outcome, evidence of multiple accessory pathways, short APERP and AVRT triggering sustained pre-excited atrial fibrillation during EPT are independent predictors of MAs on the long term follow-up confirming the results of the studies made for asymptomatic patients. So EPT is useful to identify patients at higher risk of MAs in whom catheter ablation should be strongly encouraged and performed contextually with EPT.

S62

Automated MRI-Based Biventricular Segmentation Using 3D Narrow-Band Statistical Level-Sets

G Tarroni¹, D Marsili¹, F Veronesi¹, C Corsi¹, AR Patel², V Mor-Avi² and C Lamberti¹

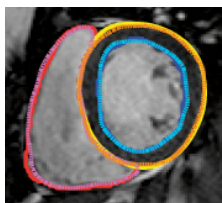
¹ University of Bologna, Italy; ² University of Chicago, IL, USA

Background. The quantification of left and right ventricular (LV, RV) volumes and masses from cardiac magnetic resonance (CMR) images is important for the management of a variety of cardiac diseases. Despite considerable research aimed at the development of tools for automated endo- and epicardial contour identification, the problem remains only partially solved, particularly for the right ventricle, because of its unique shape and prominent trabeculations. We sought to develop and test a near-automated technique for the segmentation of LV endo- and epicardial as well as RV endocardial contours.

Methods. The technique is based on 3D narrow-band statistical level-set algorithms (which are applied to a stack of CMR short-axis images), followed by several refinement steps, involving anisotropic filtering, 2D edge-based level-set evolution, and convex hull closing. Boundary initialization requires manual placement of two seed points, one inside each ventricle, in one slice. The technique was initially tested on steady-state free precession (SSFP) images acquired during 10-15 sec breath-holds in 4 patients, a total of 84 images. For performance evaluation, an experienced interpreter manually traced ventricular contours, which were used as reference. Quantitative error metrics between automatically identified and manually traced contours included: Hausdorff distance (HD), mean absolute distance (MAD), and dice coefficient (DC).

Results. In all slices, the automatically detected and manually traced contours were similar visually (figure, solid versus dashed lines). Computed error metrics showed excellent inter-technique agreement (table). Time required for the segmentation of the ventricular contours using the proposed technique in a stack of 10 slices was around 3 min on a Quad-Core Intel Xeon® PC, while the manual segmentation of the same stack required around 15 min.

Conclusion. Fast and accurate identification of LV and RV contours using 3D narrow-band statistical level-sets aimed at the quantification of ventricular volumes and LV mass on CMR images is feasible.



	HD (px)	MAD (px)	DC (a.u.)
LV Endo Contour	3.8±1.8	1.4±0.7	0.9±0.1
RV Endo Contour	6.6±5.1	1.6±1.2	0.8±0.2
LV Epi Contour	3.6±1.6	1.4±0.6	0.9±0.0

S63

Automatic Segmentation of the Epicardium in Late Gadolinium Enhanced Cardiac MR Images

Kjersti Engan, Valery Naranjo, Trygve Eftestol, Stein Orn, Leik Woie

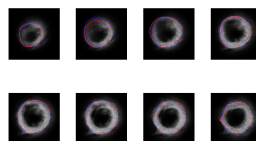
University of Stavanger, Stavanger, Norway

Aims: This study aimed to automatically produce a probability model for the myocardial muscle in Late Gadolinium Enhanced Cardiac Magnetic Resonance (LGE-CMR) images, short axis slices, and to automatically segment the epicardium using the probability model.

Materials: The Department of Cardiology at Stavanger University Hospital provided LGE-CMR images of 33 patients, all with previous myocardial infarction. The myocardium in all short axis slices are segmented by expert cardiologists for comparison.

Methods: As a first step the heart center is detected in all the short axis slices using a method based on morphological image processing and the Circular Hough Transform (CHT). The 3D information in the consecutive slices is utilized to improve detection accuracy. An a priori probability model of a typical heart is made using prior information about typical sizes of the heart muscle in the different short axis slices. The a priori model is combined with the detected heart centers in each slice. In an iterative process, using a pre-processed version of the images and information from neighboring slices, the probability model is updated in a couple of iteration. After terminating the iterations, a postprocessing by image smoothing gives the final probability model. The epicardium is segmented from the probability model using the detected image center in each slice and evaluate the differential radial values.

Results and Conclusion: The resulting probability model is a good 3D input image for doing final automatic segmentation of the epicardium. We have compared the manually marked epicardium and the automatically segmented epicardium on the 33 patients. The mean Dice index is 0.83 and variance 0.003. The mean Jaccard index is 0.71 with variance 0.006. We are currently working on an automatic segmentation of the endocardium based on the probability model, as well. Large myocardial scars make the problem harder, especially in detecting the endocardium.



Probability model with doctors segmentations of epicardium in red, and automatic in blue.

Assessment of the Fibrotic Myocardial Tissue Mechanics by Image Processing

Lucilio Cordero-Grande, Teresa Sevilla, Ana Revilla, Marcos Martín-Fernández, Carlos Alberola-López

Universidad de Valladolid
Valladolid, Spain

Introduction. We propose an image processing method to study the mechanical properties of fibrotic and normal tissue of the myocardium in magnetic resonance (MR). The procedure fuses cine MR (C-MR) and late enhanced MR (LE-MR) images and estimates the myocardial motion in C-MR images. It has been applied to the analysis of MR studies of hypertrophic cardiomyopathy (HCM) patients.

Methods. The differences in the contractility patterns between hyperenhanced and normal zones in a set of 12 patients affected by HCM are investigated. For the joint processing of C-MR and LE-MR images the following steps are considered: 3D information reconstruction, breath-derived misalignment correction, constrained Delaunay tetrahedralization of the myocardial volume, Markov random field (MRF) based motion estimation, scar segmentation, and mechanical feature extraction. A novel fast and robust tracking procedure is proposed in which the deformation is modeled by a MRF and quasi-incompressible, spatio-temporally smooth and homeomorphic transformations are promoted.

Results. The tracking method has been validated by comparing its results with respect to manual myocardial segmentations at end systole in 7 patients affected by different cardiomyopathies. It has proven to be able to recover the surface deformation (with a mean 3D myocardial Dice coefficient of 0.823) and to estimate reasonable values for myocardial mechanics parameters. Regarding its application to the mechanical analysis of fibrosis in HCM patients, the absolute value of both the mean radial and circumferential components of the Green ejection strain tensor has been encountered significantly lower when hyperenhancement is present (respectively with $p = 10^{-3}$ and $p = 1.5 \cdot 10^{-3}$).

Conclusion. A method has been proposed to fuse C-MR and LE-MR and to estimate the motion in the former which enables the precise characterization of the mechanical properties of hyperenhanced myocardial tissue. Statistically different contractile properties have been found in normal and fibrous areas of 12 HCM patients.

S63

Automatic Detection of Myocardial Perfusion Defects Using Object-based Myocardium Segmentation

Teodora Chitiboi, Anja Hennemuth, Lennart Tautz, Paul Stolzmann, Olivio F. Donati, Lars Linsen, Horst K. Hahn

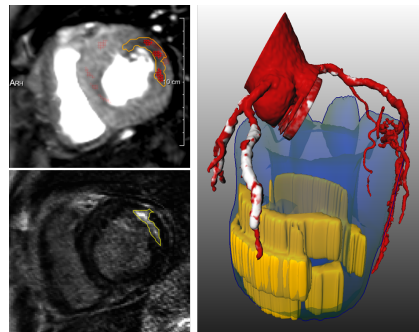
Fraunhofer MEVIS,
Bremen, Germany

Goal: Magnetic resonance perfusion imaging provides non-invasive means to assess the relevance of coronary artery stenosis in the diagnosis of coronary heart disease (CHD). We propose the first fully automatic analysis approach for perfusion MRI that supports voxel-based segmentation of suspicious myocardium regions, besides the conventional AHA model quantification.

Methods: Our pipeline consists of three steps: motion correction, myocardium segmentation, and local perfusion analysis. The registration method uses local image features in a multi-scale fashion, enabling the correction of both stronger breathing displacements and local contractions. After correction, the myocardium is segmented in a temporal maximum intensity projection, using an object-based image analysis approach. While pixel-based approaches fail due to missing contrast, we use image regions (super-pixels) described by a set of properties (shape, orientation, intensity statistics, and relative position) to model the image context. Regions belonging to the myocardium or blood pool are successively merged based on the compactness and circularity of the left ventricle and the homogeneity and ring-like shape of the heart muscle. Finally, perfusion analysis uses a Gaussian mixture model to determine suitable thresholds for quantitative perfusion parameters such as myocardial blood flow. The thresholds are used to detect initial markers for a subsequent watershed segmentation step for delineating the suspicious regions.

Results: The algorithm was applied to six patient datasets with known multivessel CHD. Results showed good agreement with findings from delayed enhancement examinations and conventional coronary angiography. 75.5% of the marked necrotic regions were successfully detected, while the missed regions were fairly small ($<30\text{mm}^2$). The myocardium segmentation showed an average distance to ground truth of 1.35mm.

Conclusion: The automatic segmentation of underperfused regions has great potential for assessing the extent and transmural of perfusion defects as well as classifying the tissue state in combination with delayed enhancement imaging, which would improve therapy planning for CHD.



Top: temporal MIP perfusion defect segmentation (with initial markers hashed). Bottom: corresponding necrotic region in delayed enhancement (bright). Right: 3D visualization of diseased vessel branches, perfusion defect (yellow), and myocardium (blue).

S63

Relationship between Cardiac Imaging Data and Simultaneous Physiological Measurements

Wenfeng Duan*, Dingchang Zheng, Christopher Eggett, Philip Langley, Alan Murray

S63

This study aimed to quantitatively link cardiac imaging and simultaneous physiological measurements. Thirty healthy subjects were studied (age: 41 ± 13 years, mean \pm SD). Mitral and aortic valve movement and valve blood flow were examined by M-mode and Doppler echocardiography simultaneously with cardiac electrical activity, thoracic impedance and peripheral pulse. Following time features were obtained from synchronized images and physiological waveforms: P-QRS-T waves from ECG; valves motions (open, maximum and close) and blood flow (start, peak and end) from images; impedance waveform (start, minimum and end) and pulse waveform (foot, notch, peaks). Times were measured with reference to ECG R peak to reconstruct the timing sequence of cardiovascular events during atrial contraction, ventricular contraction and ventricular relaxation phases, and mean \pm SDs calculated across all subjects. The relationships between valve movement/blood flow and physiological measurements were investigated. Expected sequence of cardiac mechanical events and electrical activities has been demonstrated. The timing of mitral and aortic flow was quantified as starting within 20 ms of the valves opening, and ending within 31 ms of the valves closing, except at the end of ventricular relaxation when mitral flow stopped 18 ms after valve closure. Mitral peak flow always occurred after the valve was fully open. Thoracic impedance started to fall soon after aortic flow onset (12 ± 26 ms), while the minimum impedance occurred 101 ms (± 28 ms) before the flow stopped, with impedance taking account of both left ventricular volume and aortic blood volume changes. Similarly, left ventricular ejection produced a significantly ($p < 0.001$) longer effect on peripheral pulse (from foot to the notch, 347 ± 26 ms). In conclusion, with simultaneously recorded cardiac images and physiological signals, we have analyzed the cardiovascular timing sequence through the cardiac cycle and linked echocardiograms to thoracic impedance and peripheral pulse.

Measuring the Degree of Fibrosity in Myocardial Scars from LGE-CMR Images

Frode Måløy*, Leik Woie, Trygve Eftestøl, Kjersti Engan, Stein Ørn

Department of Electrical and Computer Engineering, University of Stavanger

Introduction: Analysis of LGE-CMR images has previously shown that myocardial infarction (MI) patients with ventricular tachycardia (VT) have more fibrotic scars than MI patients without VT. We seek to define and measure the degree of scar fibrosity, and to see if the measures help in separating a group of VT patients from a group of patients without VT.

Method: LGE-CMR images of 20 MI patients with VT and 34 MI patients without VT were taken, and the myocardia and scars demarcated by cardiologists. For each patient the myocardium was normalised by dividing its signal intensity values by its highest occurring value. Various fibrosity measures were defined by integrating the product $w(x) * p(x)$ on the interval $[0, 1]$, where $w(x)$ is a monotonically increasing linear or exponential weighting function and $p(x)$ the relative frequency signal intensity distribution of the scar. We also calculated the skewness of each $p(x)$ to use as a fibrosity measure, since the tail of $p(x)$ might indicate how fibrotic the scar is. The fibrosity measures were used as input to a neural network classifier together with the left ventricular ejection fraction (LVEF) and the relative scar size. The classification problem being separating the two patient groups and done in a leave-one-out fashion.

Results: The best results were achieved using skewness as fibrosity measure: At a sensitivity of 90%, combining skewness with LVEF and relative scar size gave a specificity of 91% (with 95% confidence interval (CI) 76-98%), whereas LVEF combined with relative scar size yielded 85% (CI: 69-94%) and LVEF alone 82% (CI: 60-87%).

Conclusion: Capturing the degree of fibrosity of myocardial scars using the skewness of the scar's signal intensity distribution can be of assistance in evaluating the risk of MI patients getting VT.

Simultaneous Registration of ECG and Cardiac Motion by a Single Esophageal Probe

Thomas Niederhauser, Sergio Sánchez Martínez*, Andreas Haeberlin, Thanks Marisa, Josef Goette, Marcel Jacomet, Rolf Vogel

ARTORG Cardiovascular Engineering, University of Bern, Bern, Switzerland

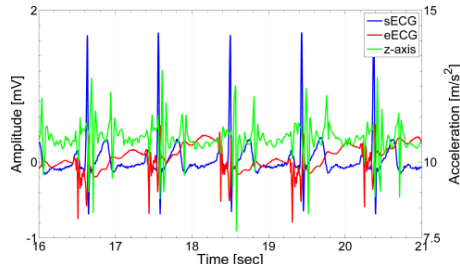
An increasing number of patients suffer from heart rhythm disorders (arrhythmias), e.g. atrial fibrillation, as a result of the aging population. Long-term surface ECG (sECG) recordings are routinely used to screen for and diagnose paroxysmal arrhythmias. Recent literature has shown that long-term esophageal ECG (eECG) provides more detailed atrial signals than sECG and is helpful in the diagnosis of supraventricular arrhythmias. However, sECG and eECG only measure the heart's electrical excitation and provide no information about the cardiac motion, i.e. heart's contractility.

S64

We investigated a novel esophageal catheter that is able to record the eECG and mechanical motions simultaneously. The system was realized by integrating an ultra-small, 3-axis accelerometer (BMA250, Bosch Sensortec) into an 9F esophageal tube. The acceleration signals are sampled with 60 Hz and 10 bits per axis. Four electrodes mounted on the tube's surface are connected to a biopotential amplifier and capture 2 bipolar eECG signals. A dedicated software (LabVIEW) reads out and synchronizes all signals.

A pilot study including three healthy volunteers has shown that the accelerometer provide detailed information about cardiac motion that is highest in the z-axis; the dominant signal waves with amplitudes $<5 \text{ m/s}^2$ and $<2 \text{ m/s}^2$ are correlated with the contraction and relaxation of the ventricles and atria, respectively, in the eECG. The mechanical actions of the small atria are registered because the esophageal catheter is located closely to the left atrium. Slow accelerations occurring in the frontal plane represent major motion ($<1.5 \text{ m/s}^2$) that are related to the baseline wander in eECG signals caused by respiration and esophageal peristalsis.

The investigated accelerometer is a low-power chip and, thus, dedicated for a long-term eECG and cardiac motion recorder. Such a device may allow for long-term outpatient myocardial contractility surveillance, which would be a highly innovative tool for future heart failure monitoring.



Example segment of sECG, eECG and acceleration signal

Electrocardiogram Derived Respiration from QRS Slopes: Evaluation over Stress Testing Recordings

Jesús Lázaro, Alejandro Alcaine, Daniel Romero, Eduardo Gil, Pablo Laguna, Leif Sörnmo, Raquel Bailón
Aragón Institute for Engineering Research (I3A), IIS, University of Zaragoza, Zaragoza, Spain
CIBER de Bioingeniería, Biomateriales y Nanomedicina (CIBER-BBN), Zaragoza, Spain

A method for respiratory rate estimation from electrocardiogram (ECG) signals, based on variations in QRS complexes slopes, is presented. Besides the 12 standard leads, and the 3 vectorcardiogram (VCG) leads, 2 additional non-standard leads derived from VCG loops were analyzed. These leads are denoted loop derived lead (LDL) and N loops derived lead (NLDL), and they are designed to maximize QRS complexes variations and, therefore, enhance respiratory influence on the corresponding lead.

A total of 34 slope series were studied, 2 for each analyzed lead: slopes between the peak of Q and R waves, and between the peak of R and S waves. Each one of these QRS slope series lead to an ECG derived respiration (EDR) signal. Respiratory rate was estimated by using a time-frequency based algorithm which can combine information from several EDR signals.

Evaluation was performed over a database containing ECG and respiration signals simultaneously recorded from 30 subjects spontaneously breathing during a stress test. Stress test recordings are challenging due to their non-stationarity (respiratory rate and depth variations, exercise-induced ECG changes) and noise contamination (muscular activity, motion artifacts). Respiratory rate was estimated from 4 different combinations of QRS slopes series: those obtained from 12 standard leads, from 3 VCG leads, from LDL, and from NLDL. For comparison purposes, respiration rate was also estimated from other known methods based on the variations of the heart electrical axis rotation angles (Φ).

Respiratory rate estimation error (mean \pm SD)

	Relative (%)	Absolute (mHz)
12ECG	3.39 \pm 13.55	2.37 \pm 43.95
VCG	0.11 \pm 11.06	-8.73 \pm 44.99
LDL	-0.01 \pm 13.58	-10.67 \pm 49.06
NLNL	-1.74 \pm 10.86	-9.52 \pm 42.70
Φ	4.51 \pm 18.53	10.80 \pm 52.16

those obtained from rotation angles (4.51 \pm 18.53%; 10.80 \pm 52.16 mHz), and suggest that proposed methods based on QRS slopes are highly suitable for respiratory rate estimation from ECG signals.

The best results in respiratory rate estimation error terms were obtained by the combination of the 3 VCG leads QRS slope series (0.11 \pm 11.06%; -8.73 \pm 44.99 mHz). These results outperform

S64

Bayesian Voting of Multiple Annotators for Improved QT Interval Estimation

Tingting Zhu, Alistair Johnson, Joachim Behar and Gari D. Clifford

University of Oxford
Oxford, UK

Introduction: Human bias and significant intra- and inter- observer variance exist in most manual labelling tasks. Automated algorithms can eliminate these biases, offer time efficiency, and reduce costs associated with acquiring expert annotation.

Aim: This article focuses on devising a method for electrocardiogram (ECG) QT interval evaluation through combining measures from human or automated algorithms.

Methods: The 2006 Physionet/Computing in Cardiology (PCinC) challenge QT database provides 549 ECG records with annotations from 20 independent humans and 69 automated algorithms. A Bayesian approach, that combine measures from multiple humans or algorithms as well as contextual information (such as heart rate and signal quality) was developed for inferring the true QT length. The developed method is compared to the commonly used mean and median voting approaches by computing the root-mean-square (RMS) error between the computed QT lengths and the reference annotations provided by the PCinC challenge.

Results and Conclusion: The Bayesian algorithm (BA) with features can reduce the human RMS error of QT estimates to 6.02ms and 13.93ms for automated algorithms, out-performing the results in the Challenge of 6.67ms and 16.34ms respectively. The BA with features consistently outperformed the mean voting strategy in all entries. It outperformed the median voting algorithms for less than nine human annotators and for any number of automated algorithms. For only three annotators, the BA provides an 11.02% improvement over the next best voting strategy for manual annotations, and a 13.31% improvement for combining automated algorithms. For large numbers of annotators, the BA estimates became approximately equal to the best-performing annotator, even though the identity of the best annotator is unknown. Combining human annotators using the BA could potentially provide an optimal 'gold standard' for QT estimation even when the ground truth is not available.

S64

The Feasibility of Impedance Cardiography to Assess Hemodynamic Changes and Fluid Loss Related to Pleural Drainage

Mark Ulbrich, Jens Mühlsteff, Matthias Zink, Steffen Leonhardt

RWTH Aachen University, University Hospital Aachen
Aachen, Germany

Aims: This work aimed to verify if impedance cardiography (ICG) as a non-invasive measurement method for hemodynamic parameters is feasible for the detection of hemodynamic changes and fluid loss due to pleural drainage in heart failure (HF) patients with pleural effusion. Therefore, stroke volume (SV) and thoracic fluid content (TFC) before and after pleural drainage should be compared.

Methods: Six patients with HF and pleural effusion as indication were treated in the University Hospital Aachen. By the insertion of an intercostal drain, between 1 and 2 liters of fluid were removed from the pleural space in sitting position. ICG measurements were made before and after the drainage using standard electrode positions at neck and abdomen. Therefore, a sinusoidal current of 1.5 mA at a frequency of 85 kHz was injected into the body. SV was calculated according to Kubicek, Sramek and Bernstein. TFC was calculated using the static base impedance (Z_0). A paired-sample t-test was made at 5 % significance level.

Results: The morphology of the measured impedance curves allowed the extraction of all standard characteristic points in order to calculate SV. The calculated SV difference varies between 45 ml and 17 ml, whereas Z_0 changes between 0.9Ω and 2Ω . The t-tests showed significant changes of SV ($p \leq 0.015$) and TFC ($p \leq 0.03$).

Conclusion: Since all measured and calculated values show significant changes before and after pleural drainage, ICG reflects the influence of the removed fluid of the thorax on the body. Prospectively, ICG might be a valuable technology to predict decompensation in heart failure patients by detecting pleural effusion.

S64

Computer driven device for arbitrary biphasic wave-form current shocks applied in real time for in vivo and in vitro studies of defibrillation

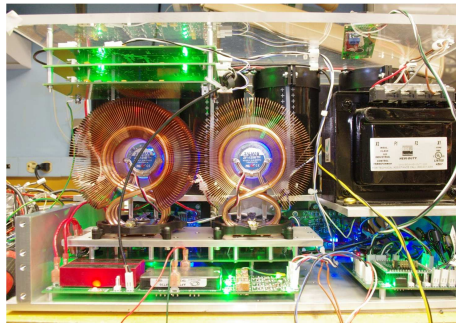
Ilija Uzelac, Mark Holcomb, Ron Reiserer, John P. Wikswo

Georgia Institute of Technology
Atlanta, GA, USA

Aims: Study of new methods for defibrillation require the use of a simple to use, yet robust device that can deliver multiple shocks of arbitrary wave-forms of various energies.

Methods: We present a custom-made computer controlled arbitrary wave-form voltage to current converter (V2CC) with an output that is isolated from the Earth ground, capable of delivering up to 1 A continuously and up to 5 A into a 40 Ω load for >500 ms in a pulsed regime. For currents lower than 5 A, the load resistance can be higher, so that the product current times resistance is guaranteed to be up to 200 V. The bandwidth is in excess of 1 kHz, and the timing accuracy is better than 10 μ s. A set of safety measures is implemented that keeps the output disconnected through reed relays and H-bridge MOSFETs. Shock duration is limited by the voltage across the main capacitor bank. With the 120V AC main, the internal voltage across the main capacitor bank will reach above the 305 V necessary for the 500 ms long, 5 A current shocks. If longer shocks are needed, the 120V AC main power supply can be increased to 140V AC using an autotransformer. In this case, the voltage across the main capacitor bank will reach above 340 V, allowing 50% longer shock durations.

Conclusions: The V2CC is a device designed to be used in vivo and in vitro cardiac experiments and is suitable for a wide variety of settings that require arbitrary waveforms with high current source. We demonstrate its use with activations on rabbit hearts for several wave-forms with amplitudes varying from 50mA to 5A and frequencies from a DC up to 1 kHz, as well as defibrillation examples.



V2CC without the front panel and chassis

Using Piezoelectric Sensor for Continuous-Contact-Free Monitoring of Heart & Respiration Rates in Real-Life Hospital Settings

Tal Klap, Zvika Shinar

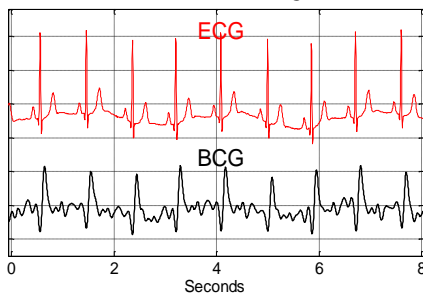
Earlysense ltd.

Introduction: The ballistocardiogram (BCG) was used in the past to explore mechanical properties of the heart before the age of ultrasound and Doppler. It was never widely used as the ECG is, and was more a subject of research than of clinical practice.

While it is common practice to measure respiration with piezoelectric sensors, it is much less common to measure the mechanical properties of the heart with a piezoelectric sensor, let alone to apply the measurements in real life hospital settings, continuously and contact-free, with real patients.

Aim: Validate a practical piezoelectric sensor for continuous measurement of heart rate (HR) and respiration rate (RR) in real clinical setting.

Methods: A single sensor placed under the mattress was used to collect data continuously from 16 patients in a sleep lab & 44 patients in an Intensive Care Unit (ICU) unit. The collected signals were filtered to separate the waveforms of respiration and BCGs (see figure), and to extract the instantaneous HR and RR. The extracted rates were tested in a variety of clinical events and were compared with gold standard reference.



Example of the simultaneous ECG (upper curve) vs. BCG (lower curve)

Results: Comparison to gold standard reference devices achieved accuracy in sleep-lab setting of 95% for HR and 94% for RR with detection at 94% and 96% of the evaluated time period for HR and RR, respectively.

During the study period, several episodes of tachycardia, bradycardia, tachypnea and bradypnea were recorded, during these episodes the BCG and respiration waveforms measured were compatible with measurements of reference devices.

Consistent and accurate measurements of HR and RR were demonstrated also during a variety of clinical events such as arrhythmias, sleep apneas and death.

Conclusions: The contact-free piezoelectric sensor allows continuous monitoring of RR and HR, during normal rates as well as during tachycardia, bradycardia, tachypnea and bradypnea cases recorded at ICU ward.

Computing Ischemic Regions in the Heart: On the Use of Internal Electrodes

Ola Marius Lysaker*, Bjørn Fredrik Nielsen, Samuel Wall

Simula Research Laboratory
Porsgrunn, Norway

Aims: In order to locate ischemic regions in the heart, using electrical measurements and inverse solutions, we explore the possibility for supplementing BSPM data sets with additional internal electrodes in the esophagus. We investigate whether such internal electrodes closer to the heart's surface could significantly improve the ability to pinpoint ischemic regions.

Method: A framework based on exercise ECG testing and a mathematical model for identifying ischemic regions from ECG measurements is implemented to test the effect of internal electrodes. This method identifies areas with abnormal perfusion by minimizing the difference between recorded and simulated ECGs. To investigate the effect of the extra electrodes in the esophagus, we computed the location of the ischemic zones with and without the internal electrodes for both synthetic data and using clinically obtained BSPMs.

Results: Computations based on pure synthetic data illuminate that, if an ischemic region is close to an electrode in the esophagus, then the use of internal electrodes might improve the result significantly. However, the simulations also indicate that ischemic areas further away from the internal electrodes are not better recovered with the use of such additional ECGs. The procedure was also tested on clinical BSPMs recorded at Oslo University Hospital. This study indicates that the use internal electrodes, along with standard BSPMs, might improve the accuracy of the inverse ECG technology. To validate our findings, the computed ischemic regions were visualized in terms of images and compared with images taken with perfusion scintigraphy.

S71

Observability of Ischemia and the Need for Patient Specific Models

Glenn Terje Lines*, Ola Marius Lysaker, Bjørn Fredrik Nielsen

Simula Research Laboratory
Porsgrunn, Norway

Introduction: Non ST-elevation ischemia (NSTEMI) can by definition not be detected by ST shifts using the standard 12 lead ECG. The non-observability of NSTEMI can be due to placement of the ischemia, or due to canceling effects. In this work we present a quantitative approach to analyzing the observability.

Methods: Using patient specific geometries, which included lungs and cardiac fiber directions, we used forward simulations to compute the response of ischemia at various locations in the heart. For each patient, 4 cases in total, the left ventricular was divided into 60 segments. A step-wise constant function was used to represent the pathological membrane potential distribution associated with an ischemic segment. The corresponding ST-shift at the body surface was computed for each configuration. A subset of 64 positions at the body surface was chosen for the analysis.

Results: As expected, the chest leads provided most information. Furthermore, there were clear similarities between patients with respect to ischemic location and response in the body surface potential. However, the simulations also revealed significant differences in response, with correlation coefficients in the range 0.6-0.8. In particular, the surface potential crucially depended on heart orientation and body size. It was not possible to make general, precise statements about amplitude in specific electrodes and the corresponding ischemic location. Furthermore, for some patients there were silent areas, i.e. ischemic locations that showed a weak response in the surface potential in all leads.

Conclusion: Our analysis suggests that accurate and reliable results from inverse computations might only be obtained with the use of patient specific geometrical models.

S71

Effect of RyR2 Refractoriness and Hypercalcemia on Calcium Overload and Spontaneous Release

Enric Alvarez-Lacalle*, Angelina Peñaranda, Inma R Cantalapiedra, Leif Hove-Madsen, Blas Echebarria

Universitat Politècnica de Catalunya
Barcelona, Spain

Some cases of cardiac arrhythmias have been associated with dysfunctions in calcium dynamics at the cardiomyocyte level. Instabilities in the calcium transient may give rise to the appearance of calcium alternans, or to the generation and propagation of intracellular calcium waves. The latter provide a proarrhythmogenic substrate through the generation of either delayed (DAD) or early afterdepolarizations (EAD), that may give rise to ectopic beats and lead to reentry and conduction blocks. Similarly, a large synchronous spontaneous release of calcium during afterdepolarization may also generate ectopic beats due to the increased activity of the sodium-calcium exchanger. In both situations, calcium overload is critical to the generation of these arrhythmias. In this work we use a computer model of a ventricular rabbit myocyte to study several factors that affect sarcoplasmic reticulum (SR) calcium load, such as hypercalcemia, SR calcium buffering, or ryanodine receptor (RyR2) dynamics. General conditions for the appearance of calcium spontaneous release in situations with calcium overload are obtained as a function of the different dynamical regimes of the RyR2. Furthermore, we study the appearance of alternans under these conditions. Recent studies have shown that calcium alternans may be due to either a steep calcium load release relation, resulting in oscillations in SR Ca content, or to a slow recovery from refractoriness of the RyR2. We find that a change in calsequestrin buffering dynamics or extracellular calcium concentration greatly affects the appearance of the former type of alternans, but not of the latter.

S71

Avoiding the Inverse Crime in the Inverse Problem of Electrocardiography: Estimating the Shape and Location of Cardiac Ischemia

Carlos Eduardo Chávez*, Felipe Alonso-Atienza, Diego Álvarez

Universidad Carlos III de Madrid
Leganes, Spain

The Inverse Problem of electrocardiography (IPE) can be summarized as the characterization of the electrical behavior of the heart using measurements obtained by electrodes that are not directly in contact with the cardiac surfaces. Given a data ensemble provided by electrodes, the solution of the IPE requires the design of a mathematical procedure that matches a theoretical model of estimated measurements with that ensemble of data. Common tests of inversion procedures were often made with synthetic data using the same model for computing both predicted and estimated measurements, yielding into overoptimistic results; this is called the Inverse Crime. In practice, the test of an inversion process avoiding the Inverse Crime could be done using a model for the numerically produced simulated data and a different one to invert the data. This work shows the behavior of a procedure designed to characterize regions in the heart with a lack of blood supply (ischemia) avoiding the Inverse Crime. Realistic and experimentally supported models constitute the forward procedure (the Luo-Rudy model for the electrical activity and the volume conductor theory for simulating the electrode measurements) while a simple phenomenological model (the two-current model proposed by Mitchell and Schaeffer) is used during the inversion process.

S71

Ionic Mechanisms underlying Arrhythmogenic Biomarkers in Ischemia: A Population-based Study

Ana Mincholé*, Sara Dutta, John Walmsley, Blanca Rodriguez

Oxford, United Kingdom

Electrophysiological heterogeneities in ischemia provide a pro-arrhythmic substrate that can lead to ventricular arrhythmias. However, the underlying mechanisms in the human ventricles are unclear. We investigated the ionic basis of variability in arrhythmogenic biomarkers in normal and acutely ischemic human ventricular cardiomyocytes using a population-based simulation study. We constructed a population of human ventricular AP models based on the ten-Tusscher model by first sampling the following parameters of interest to $\pm 50\%$ of the original values: the conductances of the sodium (g_{Na}), calcium (g_{CaL}) and potassium currents (g_{Kr} , g_{Ks} , g_{K1} , g_{to}), Na^+/Ca^{2+} exchanger (g_{NaCa}) and Na^+/K^+ pump (g_{NaK}). We paced 200 beats at different cycle lengths (CLs) from 1500 to 400ms. The normal population was calibrated by ensuring the restitution curve is monotonic and that APDs were within experimental ranges: 225 to 400ms for CL=1000ms and up to 350ms for CL=500ms. Ischemic conditions were applied to the control population by increasing the extracellular concentration of potassium to 8mM and activating the K_{ATP} channel by 10%. A decrease in the maximum restitution slope under ischemia was observed and, APD alternans appeared in the normal population at CLs below 550ms while in the ischemic population they appeared at CLs below 1200ms. Regression shows that under ischemic conditions, g_{Na} and g_{NaCa} become important while g_{NaK} and g_{CaL} reduce their influence on the maximum restitution slope. Acidosis, an early ischemia response, inhibits dynamically the sodium current, affecting in turn the restitution slope. The relative importance of the conductances in determining changes in the amplitude of APD alternans are similar in both populations, g_{CaL} being the most important, followed by g_{NaK} and g_{NaCa} . We conclude that ischemic conditions promote AP alternans at longer CLs than observed in control conditions and less steep restitution slopes. The population-based approach reveals the key parameters underlying these processes.

S71

Recent Human Ventricular Cell Action Potential Models Under Varied Ischaemic Conditions

Sara Dutta, Ana Mincholé, T Alexander Quinn, Blanca Rodriguez

University of Oxford
Oxford, UK

Aims: Cardiac ischaemia greatly increases vulnerability to lethal cardiac arrhythmias. Human data is scarce and computational techniques provide an ideal tool to bridge this gap. The applicability of recent human ventricular cell action potential models to the study of ischaemia, however, has not been investigated. Our aim was to investigate the use of the most recent human models under ischaemic conditions, to assess their utility for future studies of arrhythmogenesis.

Methods: Simulations were run at the single cell and tissue level, under normal conditions and varied degrees of ischaemia. Four human models were assessed: ten Tusscher et al. 2006 (TP06), Grandi et al. 2010 (GPB), Carro et al. 2011 (CRLP), and O'hara et al. 2011 (ORD). The ATP-sensitive inward-rectifying potassium current ($I_{K(ATP)}$) was added to each model. Extracellular potassium concentration ($[K^+]_o$) and peak $I_{K(ATP)}$ (two parameters thought to be important for arrhythmogenesis in ischaemia) were varied and action potential duration (APD) and post-repolarisation refractoriness (PRR), pro-arrhythmic biomarkers, were calculated to quantify model response.

Results: Results were compared to published experimental data in human. In single cell and tissue, all models showed the expected APD shortening under ischaemic conditions due to $I_{K(ATP)}$ activation and elevation of resting membrane potential due to hyperkalaemia (increase in $[K^+]_o$). Most models also reproduced the expected increase in PRR. The ORD model, however, did not display the increased PRR in single cell and, with the GPB model, excitation did not propagate in tissue for $[K^+]_o=9\text{mM}$.

Conclusion: Within the scope of this study, which investigated the APD and PRR of 4 recent human models under varied ischaemic conditions, results show that the TP06 and CRLP models are the most suitable for performing human-specific simulations of arrhythmogenesis during myocardial ischaemia.

S71

The Effect of Gap Junction Uncoupling on Spatial Dispersion of Action Potential Duration at Sites of Abrupt Tissue Expansion

Marjorie Letitia Hubbard*, Craig S Henriquez

Duke University
Durham, United States

S72

Spatial dispersion of action potential duration has been linked to arrhythmogenesis in the diseased heart; however, the complex dynamic between action potential properties during repolarization and microstructural heterogeneity in critical regimes with geometric source-load mismatch is largely unexplored. The objective of this study was to use microstructural computer models of adult monolayers to study the effect of abrupt tissue expansion on the dispersion of action potential duration (APD) in well-coupled and poorly coupled tissue. Two-dimensional computer models of ventricular monolayers ($dx=10\ \mu\text{m}$) that incorporated discrete, uniformly distributed gap junctions (gj) were randomly generated to represent the cardiac microstructure. Narrow strands of tissue with varying width ($60\ \mu\text{m}$ or $200\ \mu\text{m}$) were connected to a larger cell area that was $0.20\ \text{cm} \times 0.20\ \text{cm}$. Gap junction conductance throughout the strand and the larger cell area was uniformly set to a value between $0.50\ \mu\text{S}$ and $0.003\ \mu\text{S}$. The LRD cell model was used to model ion channel kinetics. In well-coupled strands ($gj=0.50\ \mu\text{S}$) with a width of $180\ \mu\text{m}$ or a width of $60\ \mu\text{m}$, APD declined from $183\ \text{ms}$ within the strand to $179\ \text{ms}$ as the wavefront propagated away from the site of abrupt expansion. In poorly coupled strands ($gj=0.003\ \mu\text{S}$) with a width of $180\ \mu\text{m}$, APD increased from $178\ \text{ms}$ within the strand to maximum of $182\ \text{ms}$, a difference of $4\ \text{ms}$, at the site of abrupt expansion. In poorly coupled strands with a width of $60\ \mu\text{m}$, APD increased from $174\ \text{ms}$ within the strand to maximum of $186\ \text{ms}$, a difference of $12\ \text{ms}$. Decreased intercellular coupling alters the APD profile at sites of abrupt tissue expansion, which may increase the likelihood of successful propagation of rapidly paced beats in regions of diseased tissue with source-load mismatch.

A Steklov-Poincaré Variational Formulation of the Inverse Problem in Cardiac Electrophysiology

Nejib Zemzemi*

INRIA Bordeaux Sud-Ouest
Talence, France

Aims: The classical mathematical formulation of the inverse problem in cardiac electrophysiology is based on a transfer matrix that maps the electrical potential on the heart to the body surface potential (BSP). Lots of works have been concentrating on the regularization term without thinking of reformulating the problem itself. We propose in this study to solve the inverse problem based on the Steklov-Poincaré formulation.

Methods The method splits the problem in two auxiliary problems: A Dirichlet operator and a Neumann operator. We then define a function cost as the L2 norm in space of the two auxiliary problem solutions difference. The derivative of the function cost with respect to the extra-cellular potential on the heart surface is exactly the difference of the fluxes between the Dirichlet and Neumann operators solutions on the heart surface. We use the finite element method to solve both of the auxiliary problems and compute the derivative of the function cost. We use a gradient-descent method to minimize the function cost. We use an ECG simulator to construct a heart potential and the corresponding body surface potential (BSP). As geometry, we use concentric spheres to define the volume of the heart and the torso. We add noise to the BSP and reconstruct the heart surface potential.

Results We added 10% of noise to the BSP and compute the heart surface potential. Although we obtain quantitatively an error of 15% due to the fact that the noise does not satisfy the compatibility condition, we remark that the wave front is correctly captured (see Figure 1).

S72

Identification of ablation sites in atrial flutter by causal method

Miguel Rodrigo, Alejandro Libereros, Andreu Climent, Maria S Guillem

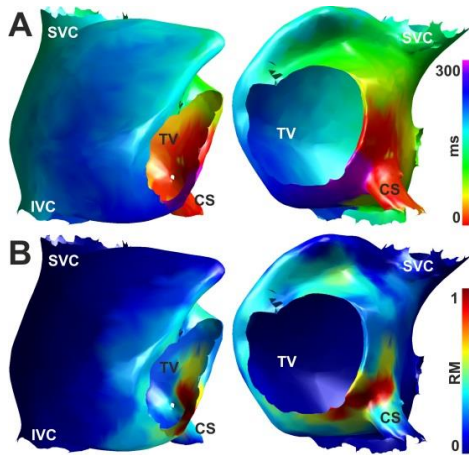
Universitat Politècnica de València, València, Spain

Hospital General Universitario Gregorio Marañón, Madrid, Spain

Atrial flutter is a cardiac arrhythmia for which ablation therapy provides satisfactory outcomes in most patients. However, in patients with atypical atrial flutter isochronal maps are complex and thus the identification of the target sites for ablation is complicated and success rates are lower than in typical atrial flutter. In this study we propose the use of the causal method to analyse the intracardiac atrial signal in order to automatically obtain the optimal target site for ablation.

A 3D atrial model was used to simulate the electrical activity of three different flutter propagation patterns: typical flutter, reverse typical flutter and superior vena cava flutter. The causal method summarizes the electrical activity recorded by the electrograms in a single map, called recurrence map (RM). In recurrence maps three main regions can be identified: (1) atrial tissue that does not belong to the re-entrant circuit, (2) atrial tissue belonging to the re-entrant circuit and (3) the thinnest path in the re-entrant circuit, with RM values of 0.04 ± 0.05 , 0.41 ± 0.15 and 0.94 ± 0.06 , respectively. The region with highest RM values corresponds to the optimal site for the ablation therapy.

The results obtained with atrial models during atrial flutter suggest that the proposed method allows the identification of target sites for ablation in patients with atrial flutter. This method may be useful in clinical practice to interpret isochronal maps from patients with atypical atrial flutter circuits and identify the best target regions for ablation.



Right atrial maps in typical counterclockwise atrial flutter: (A) Isochronal map; (B) Recurrence map. SVC: superior vena cava, IVC: inferior vena cava, TV: tricuspid valve, CS: coronary sinus.

Computational Probabilistic Quantification of Pro-arrhythmic Risk from Scar and Left-to-right Heterogeneity in the Human Ventricles

Mikael Wallman*, Alfonso Bueno-Orovio, Blanca Rodriguez

University of Oxford
Oxford, United Kingdom

BACKGROUND: Both scar and left-to-right ventricular (LV/RV) differences in repolarization properties have been implicated as risk factors for lethal arrhythmias. As a possible mechanism for the initiation of re-entry, a recent study has indicated that LV/RV heterogeneities in APD adaptation to a change in heart rate can promote unidirectional block of conduction at the LV/RV junction. In the presence of scar tissue and ectopic activation, this increases the risk of re-entry. However, the exact location and timing of the ectopic activation play a crucial role in arrhythmogenesis, and certain combinations may lead to re-entry even under a normal LV/RV dispersion in repolarization. This suggests that the phenomenon needs to be investigated in a probabilistic manner using modelling and simulation, but high computational costs of whole-ventricular simulations has prevented wide spread application of this methodology.

METHODS: In this study we present a computationally efficient, phenomenological model, allowing faster-than-realtime simulations of electrical re-entry. Using this method, we investigate the pro-arrhythmic properties of over 16000 of combinations of position and timing of an ectopic activation in a CT-derived human geometry. The study compares normal and pathological LV/RV heterogeneities in APD adaptation, derived from human in vivo measurements. This allows us to probabilistically quantify how increasing interventricular dispersion of repolarization increases arrhythmic risk.

RESULTS: Results indicate that a larger LV/RV dispersion in repolarization allows ectopic beats to initiate re-entry during a significantly larger time window and from a greater number of locations compared to the case of smaller LV/RV dispersion. Specifically, for the investigated scenarios, we observe that the larger LV/RV leads to a doubling of the length of the vulnerable time window and a 300% increase in the maximal probability of re-entry.

S72

Volumetric Imaging of Cardiac Current Sources using Lp-Norm Regularization

Azar Rahimi, Jingjia Xu, Linwei Wang

Rochester Institute of Technology
Rochester, NY, USA

Introduction: Volumetric cardiac current source imaging aim to mathematically reconstruct 3-dimensional current source activities from noninvasive body-surface measurements. However, this inverse problem is severely ill-posed and lacks a unique solution. Progress towards 3D cardiac source reconstruction is further hindered by the complex structure of cardiac current sources, which decides that common L1 and L2-norm constraints are no longer proper because the underlying assumption is either too focal or too smooth to reflect the structure of the source activity.

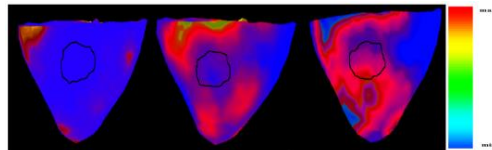
Method: We propose a novel yet simple regularization with Lp-norm ($1 < p < 2$) constraint to bridge the gap between an overly-smoothed L2 and overly-focal L1 solutions in 3D cardiac source reconstruction. Lp-norm penalty term promotes different forms of structural sparsity as often observed in the heart. The nonlinear Lp-norm regularization is solved after being cast to second-order cone programming problem.

Results: In a set of phantom experiments ($n = 44$), we investigate the optimal p value in imaging cardiac current sources with increasing extents (from 1% to 45% of the heart) in the presence of 20 dB noise. Our results show the optimal solutions are obtained at $p = 1.5 - 1.7$ for sources with different sizes. Paired student's t-test shows that the accuracy of the proposed method in preserving the source structure is significantly higher than that of L1 ($p < 0.0001$) and L2 ($p < 0.001$).

Through computer-simulated as well as real-data experiments, we further demonstrate the feasibility of the proposed method in imaging the complex structure of current source activity along the infarct border.

Conclusions:

This feasibility study shows the ability of Lp-norm to preserve the spatial structure of cardiac current source distribution. Our future work focuses on casting the problem into a Bayesian framework and treating p as a hyperparameter to be estimated simultaneously from the data.



(A) L1-norm (B) L1.5-norm (C) L2-norm
Estimation of current source activity along the infarct border using Lp vs. L1 and L2-norm regularizations for a post-infarction human subject (Black contour shows the infarct center).

A Methodology to Characterize the Causal Interactions Between Depolarization and Repolarization Temporal Changes in Unipolar Electrograms: Application to Human Epicardial Mapping

Michele Orini*, Luca Citi, Ben Hanson, Peter Taggart, Pier Lambiase

University College London
London, United Kingdom

INTRODUCTION: The temporal variability of the repolarization is associated with arrhythmogenesis. The mechanisms which determine this variability are undetermined. The aims of this study are: - Present a methodology to assess whether repolarization variability is determined by depolarization variability, - Assess whether these causal relationships can be inferred from unipolar electrograms.

METHODS: Depolarization and repolarization time series (DT and RT) are modelled as bivariate autoregressive processes, including lag-0 interactions. A hypothesis test based on surrogate data is proposed to determine the direction of the causal interactions. A simulation study was conducted: - Bivariate processes, DT and RT, characterized by either absence of interactions (DT:RT), or unidirectional interaction in either direction (DT→RT or DT←RT), or bidirectional interactions (DT↔RT), were generated. - DT and RT were utilized as inputs of a 257-node heart analytical model to generate action potentials. - Electrograms were derived as the difference between local action potentials and a position-independent remote component. - DT and RT were estimated from inflection-points in the electrograms. - Causal relationships in estimated DT and RT were characterized.

RESULTS: The analysis was performed for different levels of noise, sampling frequency and variance of DT and RT. For typical conditions, i.e. $F_s=1000\text{Hz}$, $\text{SNR}=30\text{dB}$ and variance of DT and RT of 4ms^2 and 16ms^2 , respectively, the interactions DT:RT, DT→RT, DT←RT and DT↔RT were revealed with an accuracy of 97%, 91%, 89% and 96%, respectively. 217 epicardial electrograms recorded in one patient undergoing cardiac surgery (CABG) were analysed. Interactions DT→RT, DT←RT and DT↔RT were found in 28%, 5% and 13% of the electrograms, respectively.

CONCLUSION: The proposed methodology to characterize activation-repolarization dynamic relationships from electrograms is robust and accurate in typical conditions. Preliminary results have identified where regions of causality occur across one example patient's epicardium, and suggest that depolarization variability may contribute to repolarization variability.

572

Application of the Preoperative ECG to Predict Cox Maze Surgery Mid-term Outcome

Antonio Hernández Alonso*, Raúl Alcaraz Martínez, Fernando Hornero Sos, José Joaquín Rieta Ibáñez

Biomedical Synergy
Valencia, Spain

S73

Although several therapy strategies have been developed to restore normal sinus rhythm (NSR) in patients with atrial fibrillation (AF), the Cox-Maze surgery still maintains the highest long-term cure rate. Regardless of the rhythm presented, all the patients are currently treated at the discharge with anticoagulant and antiarrhythmic drugs. During the follow-up, patients relapsing to AF are electrically cardioverted, whereas pharmacologic treatment is withdrawn in those who present a stable NSR at six months post-surgery. Hence, a preoperative prediction of patient's rhythm during the first six months could avoid the application of an aggressive pharmacologic treatment in patients under low risk of developing mid-term AF. Although some clinical parameters have provided to be successful predictors of the long-term Cox-Maze outcome, three indices computed from the preoperative ECG recording have shown higher effectiveness to identify immediate result of the procedure. These indices are the fibrillatory waves amplitude (fWP), the dominant atrial frequency (DAF) and the sample entropy (SampEn). Hence, given that the ability of these metrics to predict the patient's rhythm after a six months follow-up has not been assessed yet, the present work focuses on this analysis. For that purpose, a preoperative 20 second-length ECG recording from 24 patients with permanent AF was assessed. Six months after Cox-Maze surgery, 7 patients were in AF and the remaining 17 were in NSR. Prediction results reported sensitivity, specificity and accuracy values of 71.43%, 52.94% and 58.33% for fWP, 85.71%, 52.94% and 62.5% for DAF and 85.71%, 58.82% and 66.66% for SampEn, respectively, providing no statistically significant differences between patient in NSR or AF. Therefore, in contrast to the significant prediction yielded by the same parameters at discharge, these parameters did not reveal ability to successfully predict the patient's rhythm at six months after the surgery. The atrial substrate alteration due to pharmacological and electrical cardioversion during the patient's follow-up could be the main reason for this result. Nonetheless, further analyses are required to clarify this question.

Combination of Clinical and Electrocardiographic Indices to Predict Cox-Maze Surgery Outcome at Discharge

Antonio Hernández Alonso*, Raúl Alcaraz Martínez, Fernando Hornero Sos, José Joaquín Rieta Ibáñez

Biomedical Synergy
Valencia, Spain

The most effective procedure to terminate atrial fibrillation (AF) is the Cox-Maze surgery. After the intervention and before the discharge, patients still in AF are electrically cardioverted to restore normal sinus rhythm (NSR). Moreover, independently of the post-surgery rhythm, all the patients are habitually treated with oral anticoagulants and antiarrhythmic drugs at the moment of discharge. Hence, a preoperative prediction of the patient's rhythm at discharge would help to plan in advance drug therapy and cardioversion decisions. Previous studies used only clinical parameters to predict long term Cox-Maze outcome whereas electrocardiographic parameters have been used to predict immediate AF termination after Cox-Maze surgery. Therefore, in this work the combined ability of clinical and electrocardiographic parameters to predict patient's rhythm at discharge is evaluated. The analyzed database consisted of 29 patients with permanent AF lasting more than 3 months undergoing Cox-Maze surgery. At the moment of discharge, 16 patients were in AF and the remaining 13 in NSR. From each patient, a preoperative 20 second-length ECG segment was extracted and an adaptive QRST cancellation method was applied to lead V1 to obtain its atrial activity (AA). Next, the dominant atrial frequency (DAF), Sample Entropy (SampEn) of its main atrial wave and fibrillatory waves average power (fWP) were obtained as potential predictors. Additionally, clinical information of the patients, as age, left atrial size and preoperative time in AF, was also considered under analysis. Finally, a decision tree was applied to investigate non-monotonic relationships among parameters and, thus, group classification. Results showed that the best single predictor was fWP, yielding sensitivity, specificity and accuracy values of 87.50%, 84.62% and 86.21%, respectively. Another interesting outcome was that parameters computed from the AA signal revealed higher discriminant ability than the clinical ones. Nonetheless, the combination of clinical and ECG indices through a decision tree reported sensitivity, specificity and accuracy values of 87.5%, 100% and 93.1%, respectively. As a consequence, clinical and ECG parameters contain complementary information that could lead to a robust prediction of patient's rhythm at discharge.

S73

Open source Java-based ECG analysis software and Android app for atrial fibrillation screening.

Julien Oster*, Joachim Behar, Roberta Colloca, Qiao Li, Gari D Clifford

University of Oxford
Oxford, United Kingdom

S73

The development of mHealth applications could facilitate the decrease of the healthcare costs in both high income and low to middle income regions. However, it is essential that mHealth software is validated on public databases. Moreover, public scrutiny of the algorithms is likely to lead to faster and lower cost innovation. In this paper, we therefore present a novel Android application offering advanced Electrocardiogram (ECG) processing techniques, including signal quality analysis and Atrial Fibrillation screening. The application connects the phone to a wireless Shimmer ECG device for ECG signal recording. The application then processes the acquired signal in three stages. First a peak detector, based on peak energy-amplitude detection, is applied. The detector has been adapted to deal with high noise environments and frequent signal loss or saturation. A Signal Quality Index (SQI) is then computed which is based on the comparison of two different peak detectors, one being more sensitive to noise and artifacts. Finally, an Atrial Fibrillation (AF) detection algorithm, based on the regularity of the extracted RR interval time series, is performed. The peak detection achieved 99.8% sensitivity and 98.7% positive predictive value on the MIT-BIH arrhythmia database. The SQI had 96.9% accuracy on an extension of the CinC 2011 competition database. This AF detector achieved 92.7% sensitivity and 94% positive predictive value on the MIT-BIH AF database, on short 12 beat-length segments with as few as 10% of the beats being related to AF. This application opens the way for advanced ECG analysis in the mHealth context and more specifically for the screening of AF in developing countries. The software will be released under the BSD Open Source License to increase the engagement of the user community in the use of the software platform.

Dynamic Risk Assessment of the Onset of Paroxysmal Atrial Fibrillation

Vega C Author, García I Too, Also Jiménez J

Universidad Simón Bolívar
Sartenejas, Venezuela

Atrial fibrillation is the most common cardiac arrhythmia. The development of predictors of the acute onset of paroxysmal atrial fibrillation (PAF) is clinically important in patients who might benefit from prophylactic therapy.

In this work we propose a computational approach to evaluate the temporal evolution of risk of the onset of PAF. Our study uses a database of 75 hours of ambulatory ECG records from a set of healthy volunteers. We build a representative catalog of patterns of the behavior of heart rate in this group by storing all the possible patterns contained in the 75 records. For each record, the patterns are defined as standardized sequences of 5 consecutive RR intervals.

In a second stage, using 25 records of one hour ending with self-terminating episodes of PAF, we implement a numerical procedure to compare the patterns belonging to this second group with the catalog. This allows us to determine if any of these patterns is very similar to some pattern of the catalog, then we perform a hypothesis test by considering moving windows of 500 consecutive RR, each time closer to the PAF event. Our null hypothesis is that the patterns contained in each window are statistically indistinguishable from any subgroup of patterns in the catalog.

Our results show that the potency, P , with which the hypothesis is rejected, increases as we approach the event of arrhythmia. They also show that P exceeds, at least five minutes before the episode, the maximum value of the rejected potency obtained when the methodology is applied to a third group of healthy volunteers.

Hence, P could be useful in designing early warning systems of atrial fibrillation.

A Noise-Adaptive Method for Detection of Brief Episode Paroxysmal Atrial Fibrillation

Andrius Petrėnas*, Leif Sörnmo, Vaidotas Marozas, Arūnas Lukoševičius

Biomedical Engineering Institute, Kaunas University of Technology
Kaunas, Lithuania

Background: Recently it was shown that brief episodes of paroxysmal atrial fibrillation (PAF), lasting only 5–30 seconds, appeared in 10 % of patients who had cryptogenic ischemic stroke. The hypothesis was raised that it might be possible to prevent subsequent strokes if all patients were monitored for PAF during their first month after stroke.

Aim: The aim of this work is to develop a method for detection of brief episode PAF that could recognize episodes with a duration of just a few seconds.

Methods: The proposed method utilizes four different features: RR interval irregularity, absence of P waves, presence of f-waves and noise level. Features characterizing atrial activity are included for the reducing the number of false alarms. The echo state neural network, which is well-suited for nonlinear adaptive filtering, is used for ventricular activity cancellation. The obtained features are applied to the Mamdani-type fuzzy inference method for decision-making. The performance was evaluated on one hundred 90 s long surrogate ECG signals with brief PAF episodes (< 30 s). The robustness to noise in ECGs where noise level in each set is incremented in steps of 0.02 mV from 0 to 0.2 mV was examined as well. The method was compared to the coefficient of sample entropy (COSEn) method. Both methods were evaluated using the area under the receiver operating characteristic (AUC).

Results: When compared to the COSEn, our method is significantly better for low noise levels (< 0.03 mV) with an AUC of 0.9 and 0.97, respectively. Both methods showed similar performance for high levels (> 0.1 mV) with an AUC of 0.9, reflecting that atrial activity is no longer used in the detection process.

Conclusion: The results suggest that our method achieves significantly better performance at low to moderate noise levels when compared to the COSEn.

Real Time Detection of Atrial Fibrillation using a Miniature, Low-power ECG Monitor

Greg Hayes*, Paul D Teal

Victoria University of Welling
Wellington, New Zealand

Aims: This study was carried out to determine the feasibility of designing a miniature ECG monitor capable of real time, automatic detection of atrial fibrillation by using fast algorithms running on a low-cost, low-power device.

Methods: The target device was designed using the ADS1198 ECG front-end and the MSP430F5528 microcontroller. Algorithms for QRS detection, estimation of RR interval statistics and P-wave presence were developed on a PC and then ported to the assembly language of the target device. Nine hundred and eighteen samples of ECG heartbeats were extracted from the PhysioNet online ECG databases, manually classified and processed into ten features which were subsequently presented to a Support Vector Machine (SVM) classifier for training and testing using a leave-one-out, round robin testing scheme. The feature set comprised six frequency sub-band energy levels, the current RR interval, the RR mean and RR standard deviation of the previous 16 samples, and P-wave presence using correlation.

Results: In simulations, SVM classification achieved 89.14% sensitivity and 92.13% specificity, with 40% of data points retained as support vectors. Power consumption was measured at 30mW's with 96 hours of continuous operation using an 850mAH Li-Pol battery. Time to carry out the signal sub-band filtering and P-wave correlation was measured at 2.1mS at 8mS intervals, and heartbeat classification by the SVM at 10.2mS for every beat detected.

Conclusion: This research demonstrates that the design of a low-powered, low-cost, miniature ECG monitor having the ability to automatically detect atrial fibrillation in real time is feasible.

S73

Comparing model-free and model-based transfer entropy estimators in cardiovascular variability

Alessandro Montalto*, Daniele Marinazzo, Dimitris Kugiumtzis, Giandomenico Nollo, Luca Faes

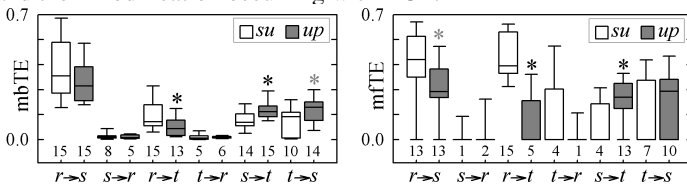
University of Gent, Gent, Belgium

Aim: We present a comparison between model-free (MF) and model-based (MB) approaches to estimate the multivariate transfer entropy (TE) between heart period (t), systolic pressure (s) and respiration (r) variability in a head-up tilt (HUT) protocol.

Methods: Given three variables x, y, z , $TE_{x \rightarrow y|z}$ is an information-theoretic measure of direct causality quantifying the information transfer from x to y conditioned to z . $TE_{x \rightarrow y|z}$ was computed from the error covariances of restricted (including the past of y and z only) and unrestricted (including also x) linear regressions of y for the MB approach, and combining time series binning with a non-uniform embedding scheme optimized in explaining y from the past of x, y, z for the MF approach. Statistical significance of each estimated TE was assessed by an F-test for MB, while for MF it was implicitly tested in non-uniform embedding resulting in strictly positive values of $TE_{x \rightarrow y|z}$. The approaches were applied on short (300 beats) r, s , and t series from 15 healthy subjects in the supine (su) and upright (up) positions during HUT.

Results: Both approaches detected unidirectional information transfer from r to s and t (high $TE_{r \rightarrow s|t}$, $TE_{r \rightarrow t|s}$ vs. low $TE_{s \rightarrow r|t}$, $TE_{t \rightarrow r|s}$), reflecting respiratory driving on pressure and respiratory sinus arrhythmia; the transfer was comparable in the two conditions, except for a reduction of $TE_{r \rightarrow t|s}$ from su to up denoted by the MF approach. The interaction between s and t was bidirectional; from su to up , $TE_{s \rightarrow t|r}$ increased significantly, reflecting HUT-induced baroreflex activation, and $TE_{t \rightarrow s|r}$ increased only using the MB approach. MF yielded significant separation between su and up in more subjects.

Conclusion: While both TE estimators were able to describe cardiovascular, cardiopulmonary and vasculo-pulmonary interactions, the significance test associated with the MF approach better elicited directional information transfers and their modification occurring with HUT.



TE values and no. of subjects with significant TE using MB and MF (* $p < 0.05$ su vs. up)

S74

Correlations between Spectral Measures of Baroreflex Sensitivity Variability and HRV during Supine Position, Paced Breathing, Standing and Exercise

Salvador Carrasco-Sosa, Alejandra Guillén-Mandujano*

División de Ciencias Biológicas y de la Salud, Universidad Autónoma Metropolitana-I, DF, México
Mexico City, Mexico

Baroreflex sensitivity (BRS) presents highly dynamic features that are poorly understood. To provide insight on this issue, we assessed the relations between spectral and temporal measures of baroreflex sensitivity variability (BRSV) and heart rate variability (HRV) during four maneuvers that induce distinctive vagal activity. ECG and arterial pressure were recorded from 30 healthy volunteers during 5-min supposedly steady-state maneuvers: supine position (SP), standing (S), controlled breathing (CB) and dynamic exercise (E). Auto- and cross-spectra of RR intervals (RR) and systolic arterial pressure (SAP) series were estimated with the smoothed pseudo-Wigner-Ville distribution to compute high-frequency power of RR (HFRR), low-to-high-frequency ratio (LFRR/HFRR), low-frequency power of SAP (LFSAP), BRS level by time-frequency alpha index in the low-frequency band, and, as criteria for BRS estimation, time-frequency coherence and phase between LFSAP and LFRR. Standard deviation and time-frequency spectra of instantaneous BRSV were also computed. Indexes dynamics were segmented and mean values of the 50-s epochs were used to obtain linear correlations between temporal and spectral estimators of BRS level, BRSV and HRV. BRSV spectra showed a single component in the very low-frequency band (VLFBRS), whose correlations with HFRR and mean RR (RRm) were 0.84 ± 0.09 and 0.78 ± 0.13 respectively. Correlations of standard deviation of BRSV with HFRR and with RRm were 0.91 ± 0.08 and 0.85 ± 0.10 respectively. Instantaneous frequency of VLFBRS fluctuated around 0.021 ± 0.001 Hz and was similar in the four maneuvers ($p>0.05$). Correlations of BRS level with HFRR and RRm were 0.93 ± 0.05 and 0.91 ± 0.07 respectively. RRm-BRS level correlation was greater ($p<0.01$) than the correlation between RRm and LFRR/HFRR (-0.51 ± 0.38). BRSV has a single spectral component, VLFBRS. Both BRS level and VLFBRS power are strongly correlated with vagal activity. BRS level is a better index of sympatho-vagal balance than the usual LFRR/HFRR ratio.

S74

Association of Ankle Brachial Pressure Index with Heart Rate Variability

Herbert F Jelinek*, Hayder Al-Aubaidy, Kinda Khalaf, Ahsan H Khandoker

Kalifa University
Abu Dhabi, United Arab Emirates

Background: Atherosclerosis, and hardening of the peripheral arteries are associated with PVD and an increased risk of cardiovascular disease (CVD). The ankle brachial pressure index (ABPI) is considered a practical, cost effective, and noninvasive tool to investigate PVD. Previous studies have shown that ABPI values below 0.8 are associated with atherosclerosis, while values above 1.2 with hardening of the vascular wall. This study aims to investigate whether a minor decrease or increase in ABPI is reflected in a change in the magnitude of heart rate variability (HRV), where HRV is used as the quantitative marker for cardiovascular disease risk.

Methods: One hundred and twenty five records of individuals attending a diabetes screening clinic were analyzed. Thirty seven percent had an ABPI below 1.0 and above 0.8, and 88% above 1.2. ECGs of 10 minute duration were also recorded to determine the heart rate variability, which is an indicator of CVD risk. HRV was determined using time and frequency domain measures in addition to other nonlinear measures including detrended fluctuation analysis and approximate entropy.

Results: No statistically significant differences were detected between the low and high ABPI groups for any HRV variables. But HRV values were lower in the group with decreased ABPI compared to the group with increased ABPI. Participants with low ABPI also had significantly longer reported hypertension with higher systolic blood pressure indicating a possible sympathetic preponderance.

Conclusion: Our study investigated whether HRV differs in individuals with moderate decrease or increase in ABPI. Sympathovagal balance may be affected when ABPI decreases from the normal range and associated with increased blood pressure.

S74

Granger Causality Analysis of Baroreflex in Obese Children and Adolescents

Michal Javorka*, Ingrid Tonhajzerova, Barbora Czippelova, Zuzana Turianikova, Lenka Chladekova, Kamil Javorka

Comenius University, Jessenius Faculty of Medicine
Martin, Slovakia

Background: Obesity is an important risk factor of arterial hypertension. The impairment of baroreflex – a principal blood pressure (BP) control mechanism – could contribute to the development of hypertension in obese patients. Previous studies have found a decreased baroreflex sensitivity (BRS) measured by transfer function analysis of spontaneous BP and heart rate (HR) oscillations in obese subjects. However, this method ignores the causality and directionality of HR and BP oscillations interactions. In classical BRS analysis, an assumption of unidirectional influence from BP to HR is applied. However, interaction of BP and HR is bidirectional - HR also influences BP by changes in diastolic heart filling. The novel method for separate analysis of feedback (baroreflex) and feedforward (mechanical) interactions between HR and BP was recently developed based on Granger causality concept.

Aim: The aim of the study was to analyse BRS in obese normotensive children and adolescents using causal baroreflex analysis method.

Methods: Continuous noninvasive recordings of BP (volume-clamp method) and R-R intervals (ECG) were obtained from 40 obese subjects (age: 14.7 ± 0.3 yrs, BMI: 32.7 ± 0.6 kg m⁻²) and gender and age matched non-obese control subjects (age: 14.7 ± 0.3 yrs, BMI: 20.4 ± 0.3 kg m⁻²). Causal close loop model was used to measure classical (noncausal) BRS and causal feedback interaction from BP to HR (causal BRS).

Results: The noncausal BRS did not show any significant difference between groups. On the other hand, causal BRS was significantly lower ($p = 0.030$) in obese group.

Conclusion: The causal BRS analysis is more sensitive in early detection of baroreflex impairment in obese children and adolescents compared to classical BRS method. The results points towards baroreflex as one of the mechanisms involved in future hypertension development in obese patients. The study was supported by project of CEPV no 26220120036, grants VEGA 1/0059/13 and 0223/12.

S74

Comparison of Baroreflex Sensitivity Gain during mild Lower Body Negative Pressure in Presence and Absence of Long Duration Bed Rest

Guadalupe Dorantes-Mendez*, Manuela Ferrario, Giuseppe Baselli, Philippe Arbeille, Kevin J Shoemaker, Danielle K Greaves, Richard L. Hughson, Federico Aletti

Politecnico di Milano
Milano, Italy

S74

Lower body negative pressure (LBNP) and head down bed rest (HDBR) are protocols used to simulate hypovolemia and cardiovascular deconditioning, causing an alteration of autonomic control of circulation. The objective of this study was to investigate the combined effects of LBNP and bed rest on cardiac baroreflex sensitivity (BRS). RR and systolic blood pressure (SBP) recordings from seven participants in the WISE (Women's International Space Simulation for Exploration) study were analyzed during a mild LBNP protocol consisting of three different levels of LBNP (-10 mmHg, -20 mmHg, -30 mmHg) with a duration of at least 2 min per cycle, before (pre-HDBR) and on day 50 of a HDBR study. Spectra of RR and SBP were computed and BRS was assessed in the low frequency (LF) and high frequency (HF) bands through a bivariate model that takes into account the causal relationships between heart rate (HR) and arterial blood pressure. HR significantly increased from BL in HDBR for \geq LBNP -20 mmHg. A significant increase in LF% of RR was found on day 50 of HDBR, with increasing levels of LBNP. LF power of SBP was significantly lower in pre-HDBR than on day 50 of HDBR. BRS gain decreased significantly in the LF band with increasing levels of LBNP in both conditions. BRS gain was significantly lower on day 50 of HDBR with respect to pre-HDBR at -20 mmHg. Regarding the feedforward pathway, no changes were reported, as expected, since the mechanical coupling between HR and arterial blood pressure should not be altered by bed rest. These data suggest that BRS in the LF range is reduced in bed rest, and these changes may be due primarily to a reduction in plasma volume associated with bed rest, which impacts the physiological responses of autonomic control of circulation.

Echocardiovariability - Low and High Frequency Beat-to-beat Variability in Echocardiographic Signals

Amanda Albano, Sandra Gustavsson, Per Lindqvist, Urban Wiklund, Christer Grönlund*

Radiation sciences, Umeå university, Umeå, Sweden
Umeå, Sweden

Introduction: The cardiovascular system comprises several oscillating components, e.g. respiration (~0.3Hz, HF), Meyer waves (~0.1Hz, LF). Since echocardiographic variables are known to be load and respiration dependent, the guidelines say that images should be taken end-expired. However, this does not account for low frequency variations. This work aims at assessing this low and high frequency beat-beat variability in healthy and diseased subjects.

Methods: Five young and two older healthy subjects (20-35y and 50-60y), and two patients with amyloid cardiac disease (50-70y), participated in this pilot study. A two-minute B/CDI-mode echocardiographic exam was performed with acquisition of ECG, respiration and blood pressure (BP) signals. Simultaneous blood flow velocity and myocardial motion echo-variables, and systolic BP were extracted per heart-beat off-line. Variability of the unfiltered, LF (bandpassed BP), and the HF signals was calculated using the coefficient of variation (CV). Coupling strength to Meyer waves and respiration signals was quantified by the coherence power index (CPI). Analysed signals included: early and late peak diastolic flow velocity (E, A), peak myocardial velocity (E'), E/E', and E/A.

Results: The echovariables had wider band spectra than BP, respiration and RR signals. Variability of unfiltered signals was 10-30% and was lower in patients and old compared to healthy subjects. The variability in the LF and HF bands were similar (~10%) except for the A and E/A (higher in HF band). The coupling strength (CPI) between echo-variables and respiration was overall stronger (20-80%) than coupling to Meyer waves 10-50%, and was lower in patients than in healthy subjects.

Discussion: The magnitude of high and low-frequency variations was similar and may influence clinical evaluation. Echocardiovariability is a novel approach which seems promising for the development of novel diagnostic indices.

S74

Use of Dominant T-wave to Reduce T-Wave Offset Location Uncertainty

Corrado Giuliani*, Angela Agostinelli, Laura Burattini

Polytechnic University of Marche, Ancona, Italy
Ancona, Italy

Abnormalities in the cardiac repolarization, and thus in the electrocardiographic (ECG) T wave, are known to be associated to cardiac electrical instability and sudden cardiac death. Despite the QT-interval prolongation being the standard indicator of cardiac safety in clinical trials, it suffers of a major limitation identifiable in the T-wave offset (Toff) uncertainty due to a significant variability (tens of ms) of the Toff location provided by different automatic methods. Thus, the aim of the present study was to evaluate if the dominant T wave (DTW), defined as a weighted mean of the T-waves over the ECG leads, can be used to reduce Toff uncertainty. Our clinical data consisted of a sinus 15-lead (I to III; aVI, aVr, aVf, V1 to V6, X, Y, Z) ECG beat randomly extracted from ECG recordings (www.physionet.org) of 36 control healthy subjects (CHS) and 62 acute myocardial infarction patients (AMIP). Toff was independently identified in the DTW and in each single lead by means of Zhang's (M1) and Daskalov's (M2) methods. Distributions of the temporal distances between Toff locations by the two techniques computed in the DTW were found to be characterized or by a significantly ($P < 0.05$) lower median value than those measured over the 15 leads (CHS: 5 ms in DTW and 5-18 ms in 15 leads; AMIP: 10 ms in DTW and 10-20 ms in 15 leads), or by a comparable median value but a significantly lower variability around the median in both populations (median variability values: CHS: 5 ms in DTW and 3-10 ms in 15 leads; AMIP: 5 ms in DTW and 5-13 ms in 15 leads). In conclusion, in our CHS and AMIP, the use of the DTW allowed a significant reduction of Toff uncertainty quantifiable in a reduction of the Toff-location differences provided by M1 and M2.

S81

ECGlab: User Friendly ECG/VCG Analysis Tool for Research Environments

Jose Vicente^{*1}, Lars Johannesen^{2,3}, Lorian Galeotti¹, David G Strauss^{1,3}

¹Division of Physics, Office of Science and Engineering Laboratories, Center for Devices and Radiological Health, US Food and Drug Administration

²Division of Pharmacometrics, Office of Clinical Pharmacology, Office of Translational Sciences, Center for Drug Evaluation and Research, US Food and Drug Administration

³Department of Clinical Physiology, Karolinska Institutet, Stockholm, Sweden

Introduction: We present ECGlab, a cross-platform, user friendly, graphical user interface (GUI) for assessing results from automated analysis of ECG tools in research environments. ECGlab allows visual inspection and adjudication of ECGs. It complements our recently developed framework to automatically analyze ECGs from the US Food and Drug Administration (FDA) ECG Warehouse. The Warehouse contains over 6 million digital ECGs from more than 200 Thorough-QT studies, which are required to assess pro-arrhythmic potential of almost all new drugs since 2005.

Methods / Results: ECGlab was written in C++ using open-source libraries and its GUI was developed using Nokias QT application framework. Supported ECG formats include Physionet, ISHNE and FDA XML HL7. ECG processing and automated analysis is done with ECGlib, our recently developed ECG analysis framework. ECGs can be loaded individually or grouped using ECGlib's index format, which includes subject, treatment and time-point information. Additional information, such as demographics or signal quality metrics, can be loaded from metafiles and used to navigate through the loaded ECGs, and guide ECG reviewing. ECG assessment can be done on screen using the ECG display, which includes different views (single-lead, overlay, 4x3 view and vectorcardiogram) and allows the user to graphically adjudicate the annotations in semi-automatic or manual fashion (Figure 1). Vectorcardiograms can be derived from 12-leads ECGs using four different methods and visually assessed in 3D or projection view. It is possible to use heart rate stability and signal quality criteria to automatically extract 10s ECG segments from continuous Holter.

Discussion: ECGlab has been tested successfully in Linux and Microsoft Windows. Currently it is being used to assess automatic measurements obtained from Thorough-QT studies and other studies. We are currently working on making ECGlab open-source in order to facilitate ECG research.

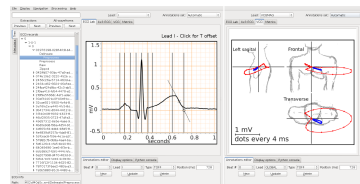


Figure 1: ECGlab GUI

S81

An Interactive Tool Developed for the Evaluation of ECG Formats

Elizabeth Martin*, Dewar Finlay, Chris Nugent, Raymond Bond, Cathal Breen

University of Ulster
Newtownabbey, United Kingdom

Electrocardiograms (ECGs) are typically printed on graph paper and clinicians look for changes in the various waveforms when they make a diagnosis. In some cases however, these changes are not always obvious on the standard printed 12-lead ECG. For this reason researchers have developed different methods for presenting ECG information. This paper reports on the development of an interactive system that supports display of ECG information in a number of formats. The system was designed to run as a web based platform as this offers the best method of data capture for a large group simultaneously. The system consists of a backend database written in MySQL where all images/ECG files and user information are stored. The main user interface was developed using a combination of PHP and HTML to allow user interactivity. Further languages used include jQuery and JavaScript. The main interface consists of functionality that includes an initial login screen, followed by a diagnosis input screen. The system is currently configured to display ECGs in either 12 lead ECG, Body Surface Potential Maps (BSPMs) and ST Map format. The system is currently hosted on a live University of Ulster server and has been tested for compatibility with a number of web browsers. e.g. Mozilla, Chrome and Safari. This compatibility test has highlighted compatibility issues with Internet Explorer and system functionality that uses jQuery development technology. Refinements are currently being implemented to ensure interoperability with all commonly used desktop browsers. The system has been designed to provide basic ECG viewing functionality and it is planned that it will see use in the evaluation of ECG interpretation skills in students undergoing training in ECG interpretation. Future work would like to see this system compatible with mobile computing platforms, allowing access even when the users are not near a desktop computer.

S81

Ultra-high-frequency ECG Measurement

Pavel Jurák*, Josef Haláček, Pavel Leinveber, Petr Klimeš, Josef Šumbera, Karel Zeman, Miroslav Novák

1Institute of Scientific Instruments, AS, Brno
Brno, Czech Republic

Introduction: Cardiac ischemia and various kinds of cardiomyopathies frequently result in structural damage to the heart muscle which can lead to heart rhythm disturbances or even risk of sudden cardiac death. Pathological changes often manifest themselves in the electrical conductivity of the heart and cannot be clearly identified from standard ECG records. A lot of work has been devoted to high-frequency analysis of the QRS complex from ECG recordings (HF-QRS). The HF-QRS frequency range currently used is limited to 250Hz, as ECG measured at higher frequencies are influenced by noise and artifacts. Here, we introduce ultra-high-frequency high-dynamic-range 12-lead QRS (UHF-QRS 250–1000Hz) measurement, using a Faraday cage electromagnetic shielding environment and battery-powered ECG monitor with a sampling of 25 kHz and 24-bit resolution.

Methods: We measured 12 subjects – 6 healthy volunteers and 6 ischemic patients. We analyzed 15-minute resting supine recordings. 25kHz data was filtered and down-sampled to 5kHz with a pass band of 2kHz. Wide-band 0-1 kHz time-frequency-analysis (TFA) was applied on each QRS complex region. Artifact-free TFA matrixes from 500 beats were averaged with the R-wave maximum from lead II as a trigger.

Results: In healthy young volunteers, the TFA consisting of a single 30-60 ms narrow line positioned in the middle of the QRS complex going over frequencies up to 1 kHz in each lead. In ischemic patients, there is a significant expansion and splitting of frequency components and differentiation in measured leads. The width of UHF-QRS activation is up to 140 ms, much more than the detectable QRS complex width.

Conclusions: Compared with the commonly used power envelope of 150–250Hz HF-QRS calculations, the TFA UHF-QRS can identify the time-frequency-spatial distribution of wide frequency range QRS components. The UHF-QRS technique presented here can accurately identify the inhomogeneity of the electric impulse propagation in the heart muscle.

S81

Coherence-Based Measure of Instantaneous ECG Noise

Piotr Augustyniak

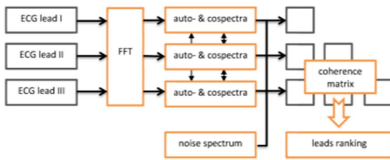
AGH University of Science and Technology
Krakow, Poland

This paper presents a coherence-based method for estimation of spatial or temporal variability of leads quality in a multichannel ECG record. The method is dedicated to stress test or Holter analyzers and aimed at providing an objective criterion for local assessment of data reliability (e.g ST-segment elevation or depression) in presence of variable noise.

The coherence is a frequency-domain measure of similarity between signals and helps to assess the contribution of additive random noise when its spectral distribution is uneven and different to the ECG spectrum.

The procedure starts with heartbeat segmentation followed by Fast Fourier Transform to the frequency domain. Consequently, autospectra and cospectra for each pair of signals are determined and the resulted coherence function is normalized and weighted by the noise spectrum (NS). Finally, the triangular matrix summarizes the coherence power and the ECG sections (beats or channels) are sorted accordingly to the value of Noise Estimate.

The proposed method was tested with the CSE Multilead Database and the artificially added muscular noise of level ranging from -30 dB to 0 dB RMS. In a channel selection test, the noise was increasingly added to different ECG channels of a multilead record and the proper channel ranking was assessed. In a noise tracking test the added noise was modulated with time and the proper value of noise level was checked at each heartbeat report.



Scheme of lead quality ranking

S81

Accuracy of Noise Estimate

noise level	regular	NS-weighted
-20 dB	-19.1 dB	-20.8 dB
-10 dB	-8.81 dB	-10.2 dB
-5 dB	-4.33 dB	-5.15 dB

With average accuracy of noise estimate of 11.23% for regular and of 3.0% for NS-weighted coherence the method is accurate enough for beat-to-beat noise tracking and reliable selection of best channel in a multichannel ECG record.

Although the a priori knowledge on the noise spectrum is not mandatory, it significantly improves the performance. Shortening the length of time epoch decreases the accuracy of noise estimation, and thus the interval corresponding to one heartbeat seems to be reasonable in aspect of assessment of ECG data reliability.

Improved Respiration Rate Estimation using a Kalman filter and Wavelet Cross-coherence

Alistair EW Johnson*, Andrew A Kramer, Sharath Choletti, Joel H Saltz, Timothy G Buchman, Gari D Clifford

University of Oxford
Headington, Oxford, United Kingdom

Introduction: Respiration rate is a common measurement in the intensive care unit (ICU) which is well correlated with patient severity. However, automated estimation of the respiration rate, especially when the patient is not intubated, is prone to large errors. Here we present a method of merging respiration estimates from the electrocardiogram (ECG) merged based on a novel signal quality index.

Methods: Data from 133 patients admitted to a mixed ICU were recorded for 2.93 \pm 0.55 hours during a spontaneous breathing trial. Respiration waveforms were derived from each of the 4 available ECG leads by extracting waveforms known to be modulated by breathing from the R-R intervals, the R peak amplitude, the R-S amplitude, and the QRS area amplitude all resampled at 4 Hz. Respiration rate was derived from these waveforms using a previously described autoregressive model. For each individual lead, the four respiration estimates were fused using a Kalman filter whose state covariance matrix depended on a novel signal quality index (SQI). The normalized Wavelet Transform Coherence (WTC) between a given two respiration waveforms in an adaptive band was used as the SQI. This resulted in four fused respiration estimates: one for ECG each lead. The respiration rates were compared to a reference rate extracted from simultaneous capnography measured on each patient.

Results: Overall, the root mean square error of our new approach was 5.4-6.1 breaths per minute depending on the ECG lead. These errors were statistically significantly better than all component respiration estimates.

Conclusions: Respiration rate can be robustly estimated from ECG leads during a spontaneous breathing trial. The use of a novel SQI within a Kalman filter allows for proper assessment of the accuracy of each component respiration estimate, even though the estimates are derived from the same underlying ECG lead.

S81

Characterization of Patients with Different Ventricular Ejection Fractions using Blood Pressure Signal Analysis

Andres Arcentales, Andreas Voss, Pere Caminal, Antonio Bayés-Genís, Marí Teresa Domingo, Beatriz F. Giraldo

Institut de Bioenginyeria de Catalunya, Universitat Politècnica de Catalunya. Barcelona, Spain

Aims: The aim of this study is to obtain parameters from the blood pressure signal that allow to characterize the behavior of patients with different values of ventricular ejection fraction.

Methods: 48 cardiomyopathy patients characterized by NYHA ≥ 2 were studied: 19 patients with dilated cardiomyopathy (DCM) and 29 patients with ischemic cardiomyopathy (ICM). The non-invasive continuously Blood Pressure (BP) signal was obtained. The ventricular ejection fraction (EF) percentage was used to classify patients in low ($LR : EF > 35\%$, 17 patients) and high ($HR : EF \leq 35\%$, 31 patients) risk groups. From BP signal, maximal systolic slope (BP_{sl}), difference between systolic and diastolic BP (BPA), and systolic time intervals (STI) were extracted, and calculated systolic blood variability (SBV). Mean and statistical dispersion parameters were calculated for each time series. Power spectral density of these series were estimated, using the Minimum Variance Distortion-less Response (MVDVR) method, and were characterized on different spectral bands: VLF (0-0.04 Hz), LF (0.04-0.15 Hz), and HF (0.15-0.8 Hz).

Results: In time domain analysis, when comparing LR versus HR, the best parameters with statistical significant differences were standard deviation (SD) of $1/STI$ ($p = 0.003$), kurtosis (K) of BP_{sl} ($p = 0.002$), and K of BPA ($p < 0.0001$). Considering DCM patients group (LR vs. HR), the best parameters were interquartile range of BP_{sl} ($p = 0.004$) and SD of BPA ($p < 0.0001$). The same parameters showed the best significances considering ICM patients group. In frequency domain analysis, all frequency bands showed statistical significance differences when comparing LR and HR groups. Similar results were obtained when analysing only DCM or ICM patients group.

Conclusion: Several parameters extracted from BP signals (in time and frequency domain analysis) presented statistical significance differences when comparing patients with $EF \leq 35\%$ and patients with $EF > 35\%$.

Empirical Mode Decomposition for Respiratory and Heart Rate Estimation from the Photoplethysmogram

A. Garde, W. Karlen, P. Dehkordi, J. M. Ansermino, and G. A. Dumont

Electrical and Computer Engineering in Medicine Group, University of British Columbia and BC Children's Hospital, Vancouver, BC Canada

Aim: We introduce a method based on empirical mode decomposition (EMD) to estimate both respiratory rate (RR) and heart rate (HR) from the photoplethysmographic (PPG) signal obtained from pulse oximetry.

Methods: The spectral analysis of the EMD applied to the PPG signal was used to extract two signals, the respiratory and cardiac modulation respectively. Another spectral analysis was applied to these signals to calculate their frequency peaks. To improve spectral resolution a parametric power spectral analysis based on autoregressive modeling was performed. The frequency peak found in the respiratory and cardiac signals reflects RR and HR, respectively. The PPG signals were analyzed using a 1-min sliding window with 50% overlap. The RR and HR estimation accuracy was assessed using the unnormalized root mean square (RMS) error. Median errors (quartiles) were calculated to account for the non-normal RMS distribution.

Dataset: The dataset contains 8-min PPG and capnometric signals from 29 pediatric and 13 adults cases (42 subjects in total) containing reliable recordings of either spontaneous or controlled breathing. A research assistant manually labeled the signals. The reference RR (from capnogram) and HR (from PPG) were manually extracted.

Results: The median RMS error (quartiles) obtained for RR was 2.4(0.4, 6.8) breaths/min and for HR was 1.4(0.9, 2.0) beats/min, see Figure 1.

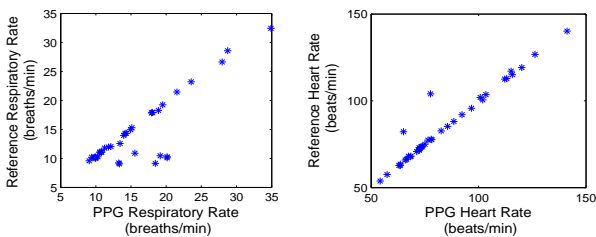


Figure 1. Reference and estimated RR and HR for each subject.

Conclusion: The spectral analysis of the respiratory and cardiac signals extracted through EMD, introduces a new method to estimate RR and HR simultaneously from the PPG signal. This method provides a useful tool to monitor RR and HR noninvasively.

Study on the Linear Relation Between Chest Compression Depth and the Fluctuation Caused in the Thoracic Impedance Acquired by Defibrillation Pads

Erik Alonso*, Digna González-Otero, Elisabete Aramendi, Sofía Ruiz de Gauna, Jesús Ruiz, Unai Ayala, James Russell

University of the Basque Country UPV/EHU
Bilbao, Spain

Poor quality chest compressions during cardiopulmonary resuscitation (CPR) may compromise the resuscitation probability during cardiac arrest. Accelerometers have been attached to automated external defibrillators (AEDs) to provide real-time feedback to rescuers on the depth of the compressions during CPR. Alternatively, the thoracic impedance (TI) signal, available in current AEDs, has been proposed as an indicator of the compression depth (CD) in animal models of cardiac arrest. This study analyzed the linear relationship between the maximum CD as measured by an accelerometer and the fluctuation caused in the TI in out-of-hospital cardiac arrest. 19 episodes were extracted from monitor/defibrillator files collected from out-of-hospital cardiac arrests between 2006 and 2010 by an EMS agency using the Philips HeartStart MRx monitor/defibrillator. Each episode contained the TI signal recorded through defibrillation pads, and the CD signal. Duration of the records was 1763 ± 581 s, with 2162 ± 831 compressions per episode, and a mean depth of 42.77 ± 1.36 mm. The mean of the CD maxima, D_{max} , was computed for every 5s of the CD signal. Each compression interval was marked automatically in the TI, and the mean peak-to-peak fluctuation, Z_{pp} , computed. Three analyses were performed: - Distributions of D_{max} and Z_{pp} in all episodes. - Linear relation between D_{max} and Z_{pp} : correlation coefficient for every episode (R_e) and for the complete dataset (R_c). - Time evolution of the correlation coefficient (R_i) for three consecutive intervals along the episode. Z_{pp} was $1.20 \pm 0.57\Omega$, $1.46 \pm 0.7\Omega$, $1.76 \pm 0.87\Omega$ for $D_{max} < 38$, $38 < D_{max} < 51$ (correct compressions range), and $D_{max} > 51$ ($p < 0.01$). High overlap between the three distributions was observed. R_e varied between 0.02-0.82 (mean=0.41), and $R_c = 0.26$. Time evolution of R_i did not show any tendency. R_i varied between 0.01-0.92 (mean=0.51). Unlike previous results with animals, linearity between D_{max} and Z_{pp} showed high variability between episodes in humans. The correlation coefficient for the complete dataset was low.

S82

A Simple Impedance-Based Method for Ventilation Detection During Cardiopulmonary Resuscitation

Digna González-Otero, Erik Alonso, Jesús Ruiz, Elisabete Aramendi, Sofía Ruiz de Gauna, Unai Ayala, Jo Kramer-Johansen, Trygve Eftestøl

University of the Basque Country UPV/EHU
Bilbao, Spain

Aim: During cardiac arrest, quality of cardiopulmonary resuscitation (CPR) is key to the survival of the patient. Current resuscitation guidelines recommend a 30:2 compression-ventilation ratio before intubation and a ventilation rate of around 10 ventilations/min afterwards, when compressions and ventilations are provided simultaneously. Compressions and ventilations induce identifiable fluctuations on the impedance signal acquired through the defibrillation pads. In this context, we developed a simple impedance-based method to automatically detect ventilations during CPR.

Materials: We used 18 out-of-hospital cardiac arrest episodes recorded with a Heartstart 4000SP defibrillator. All the episodes included intervals before and after intubation, and their mean duration was 45 ± 18 min. Five reviewers independently annotated each ventilation using the impedance signal. A majority criterion was adopted for the reference annotations. The episodes were randomly split into a training and a test set.

Methods: The detection algorithm first searched for the relative maxima of the preprocessed impedance signal and determined the fluctuation cycle. Then, it characterized every cycle by features for amplitude, duration and slope. Finally, to classify the cycles as ventilation or non-ventilation it followed a decision system based on thresholds. Using the training set, we adjusted a fixed threshold for the duration and two dynamic thresholds for amplitude and slope.

Results: Sensitivity (Se) and positive predictive value (PPV) for the test set (2831 ventilations) were 97% (95% confidence interval, 96-97) and 94% (94-95), respectively. Results per episode varied between 95-100% (Se) and 88-100% (PPV). Before intubation (343 ventilations), Se and PPV were 92% (89-95) and 79% (75-83), and 97% (96-98) and 97% (96-98) after intubation.

Conclusions: Our system accurately detected ventilations during CPR, even when compressions and ventilations were provided simultaneously. Our results were comparable to those reported in recent publications. However, further research is needed to validate our results with a larger database and with a more reliable gold-standard.

S82

The Influence of Cardiac Trabeculae on Ventricular Mechanics

Marta Serrani*, Maria Laura Costantino, Roberto Fumero

Politecnico di Milano
Milano, Italy

Cardiac trabeculae are cylindrical structures arranged in a complex shape which cover the endocardial surfaces of ventricles. They consist of axially arranged cardiac fibres and they represent a significant percentage of ventricular mass (between 10% and 20%). Aim of the project is to study the influence of the trabecular mass on heart performances. A finite-element model of the left ventricle was developed to simulate the entire cardiac cycle (ABAQUS®, SIMULIA Corp.). To compare different models (with or without trabecular structures) the ventricle was simplified as a truncated ellipsoid and the trabeculae, if present, as cylindrical strands oriented in the ventricular axis direction laying onto the endocardium. The total muscular mass and the intra-ventricular volume were kept constant in all the models. To reproduce the mechanical behaviour of the cardiac tissue, the Holzapfel constitutive relation was chosen and the material parameters were estimated by literature experimental data. Cardiac fibres were oriented helically in the ventricular wall and along the axial direction in the trabeculae, according to the literature. The muscular contraction was simulated by a stiffening of the material during the systole; namely the material stiffening was modulated by imposing the contraction curve of a muscular cardiac cell. To avoid rigid motion of the structure, kinematic boundary conditions were applied at the ventricular base. Physiologic atrial pressure was set during the ventricular filling phase, while an adequate RCR model was connected downstream to the ventricle to simulate the systemic circulation. The results show an influence of the trabecular mass on ventricular behaviour. The pressure-volume relationships show an increment of the tele-diastolic volume of about 7% for the trabeculated model with respect to the “smooth” one. This difference in the ventricular filling has a significant effect also on the systolic phase: the ventricular systolic pressure increases, as well as the ejection fraction.

S82

Effects of Physical Exercise on the Photoplethysmogram Waveforms Recorded on Fingertip and Forehead

Andrius Rapalis*, Vaidotas Marozas, Arūnas Lukoševičius

Biomedical Engineering Institute
Kaunas, Lithuania

Aims: The aim of this exploratory study is to compare PPG waveforms and parameters recorded on fingertip and forehead at rest and at different physical exercise intensities. This information might be useful for objective assessment of exercise intensity.

Methods: Synchronous fingertip and forehead PPG data was acquired for eleven healthy volunteers by using physiological signal recording system. The experiment was accomplished in 5 stages: 1) 10 min. rest; 2) 5 min. physical activity, 1 min. break; 3) 5 min. physical activity, 1 min. break; 4) 5 min. physical activity; 5) 10 min. rest. PPG cardiac cycles were selected from each activity stage then these cycles were filtered and normalized in amplitude from 0 (valley) to 1 (peak). Several parameters were estimated from extracted PPG cycles: systolic front angle (SFA), pulse interval (PI), diastolic and systolic amplitude ratio (RAS), large artery stiffness index (SI), pulse width (PW), pulse area (PA) and pulse area ratio (IPA). Statistical methods (Student t-tests and box plots) were used to study variability of parameters and confirm the consistent differences among physical activity stages.

Results: Dicrotic notch recorded on forehead is not as clearly expressed as dicrotic notch on fingertip and with increasing intensity of physical activity this point becomes almost invisible. The main differences between forehead and fingertip PPG signals are found in PW and PA parameters. The mean PW's in 4-th stage on forehead and fingertip PPG's decreased by 48.2 % and 43.6 % respectively. The same tendency is visible in case of PA parameter: decreases by 45.8 % and 39.9 % were observed for forehead and fingertip in 4-th stage.

Conclusion: The experiment results indicate that PPG signal recorded on forehead is more appropriate location for assessment of intensity of physical activity because larger differences were observed among activity stages.

S82

Automatic Right Ventricle Segmentation in CT Images Using a Novel Multi-Scale Edge Detector Approach

Sofia Antunes, Caterina Colantoni, Anna Palmisano, Antonio Esposito, Sergio Cerutti, Giovanna Rizzo

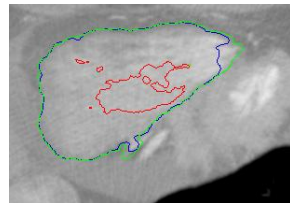
Politecnico di Milano, Milan, Italy

CNR, Segrate, Italy

Scientific Institute H. S. Raffaele, Milan, Italy

In this study we present a novel approach for the 3D automatic segmentation of the right ventricle (RV) in computed tomographic (CT) images.

We use a geodesic active contour with a new optimized stopping function based on a multi-scale approach. The stopping function contains oriented filters and acts along a scale space, being able to properly drive the curve evolution in three steps (see Figure). This is the first published approach presenting scale reduction of bar filters on a curve evolution segmentation, obtaining promising results from a low level based segmentation perspective.



The three steps of the multi-scale edge detector

This multi-scale approach can be used as a post-processing technique for refining the segmentation results. The proposed method was evaluated over 18 volumes acquired for clinical diagnosis and follow-up of patients with suspected cardiac problems (9 normal subjects and 9 subjects with ischemic heart disease) in ED phase. The original volumes, as well as the automatic segmentations, were re-oriented in short axis and 30 slices were extracted for each volume containing the RV. For all of the 540 slices, RV was manually outlined by a team of expert radiologists; the contours are used as ground truth for the automatic segmentation performance validation. Our results (see Table) show that the automatic segmentation method is in good agreement with manual segmentation, with approximately 79% of the surface voxels presenting distance errors less than 1mm and the mean surface distance (MSD) error below 1 mm. We are confident that, based on the presented results, our method offers a reliable performance in RV segmentation.

Results of the Segmentation

Metric	Healthy	Pathologic
DICE	0.89 ± 0.08	0.87 ± 0.06
MSD	0.64 ± 0.30	0.95 ± 0.43
% < 1mm	82.10 ± 7.42	75.18 ± 7.86

The original volumes, as well as the automatic segmentations, were re-oriented in short axis and 30 slices were extracted for each volume containing the RV. For all of the 540 slices, RV was manually outlined by a team of

expert radiologists; the contours are used as ground truth for the automatic segmentation performance validation. Our results (see Table) show that the automatic segmentation method is in good agreement with manual segmentation, with approximately 79% of the surface voxels presenting distance errors less than 1mm and the mean surface distance (MSD) error below 1 mm. We are confident that, based on the presented results, our method offers a reliable performance in RV segmentation.

3D Analysis of Myocardial Perfusion from Vasodilator Stress Computed Tomography: Can Accuracy Be Improved by Iterative Reconstruction?

Victor Mor-Avi, Nadjia Kachenoura, Nicole M. Bhave, Benjamin H. Freed, Michael Vannier, Karin Dill, Roberto M. Lang, Amit R. Patel

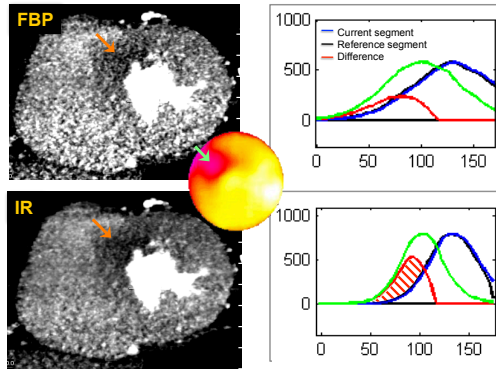
University of Chicago, Chicago, Illinois, U.S.A.
Inserm U678, Paris, France

Background. Computed tomography (CT) is an emerging tool to detect stress-induced myocardial perfusion abnormalities. We hypothesized that iterative reconstruction (IR) could improve the accuracy of the detection of significant coronary artery disease using quantitative 3D analysis of myocardial perfusion during vasodilator stress.

Methods. We studied 39 patients referred for CT coronary angiography (CTCA) who agreed to undergo additional imaging with regadenoson (Astellas). Images were acquired using 256-channel scanner (Philips) and reconstructed using 2 different algorithms: filtered back-projection (FBP) and IR (iDose7, Philips). Custom software was used to analyze both FBP and IR images. An index of severity and extent of perfusion abnormality was calculated for each 3D myocardial segment and compared to perfusion defects predicted by coronary stenosis >50% on CTCA.

Results. 5 patients with image artifacts were excluded. Ten patients with normal coronaries were used to obtain reference values, which were used to correct for x-ray attenuation differences among normal myocardial segments. Compared to the conventional FBP images, IR images had considerably lower noise levels, resulting in tighter histograms of x-ray attenuation (figure). In the remaining 24 patients, IR improved the detection of perfusion abnormalities (table).

Conclusions. Quantitative 3D analysis of MDCT images allows objective detection of stress-induced perfusion abnormalities, the accuracy of which is improved by IR.



P83

		Sensitivity	Specificity	PPV	NPV	Accuracy
By segment	FBP	0.54	0.75	0.21	0.93	0.73
	IR	0.66	0.79	0.28	0.95	0.78
By territory	FBP	0.75	0.72	0.25	0.96	0.72
	IR	0.88	0.78	0.33	0.98	0.79

Extracting Myofibre Orientation from Micro-CT Images: An Optimisation Study

Haibo Ni*, Simon J Castro, Robert S Stephenson, Jonathan C Jarvis, Tristan Lowe, George Hart, Mark R. Boyett, Henggui Zhang

The University of Manchester
Machester, United Kingdom

Introduction: Anisotropic myofibre architecture has a significant impact on electric wave propagation in the heart and is important in developing structurally detailed 3-D anatomical models of cardiac electrophysiology. We have recently developed a method for extracting fibre orientation from micro-CT images. The aim of this study was to quantitatively assess the robustness and accuracy of this extraction method, optimising it for micro-CT image processing.

Methods: The fibre structure extraction algorithm was based on the Eigen-analysis of the structure tensor derived from image gradients using derivative filters. A “synthetic cardiac tissue wedge” consisting of artificial fibers with predefined inclination angles was constructed for accuracy assessment and parameter optimization. Using this as a test volume, the performance of several derivative filters (including derivative of Gaussian and a derivative filter developed by Farid et al.) was evaluated under various conditions including noisy background. Multi-scale approach and coherency measurement were implemented to determine the feature scales. Finally, the proposed approach with optimized parameters was applied to extract myofibre orientations in micro-CT scanning images of the rabbit heart.

Results: Tests on the “synthetic wedge” shows that the use of appropriate smoothing filter scales plays an important role in assuring accurate fibre reconstruction, which can be achieved using multi-scale approaches. Farid and Gaussian derivative filters were found to be more precise than finite difference methods, resulting in errors $< 1^\circ$ for idealised fibres. However, the Farid filter demonstrated some limitations when fibres are closely packed. The extracted myofibre structure from cardiac micro-CT scans in the atrial and ventricular regions are consistent with data reported in literature.

Conclusion: The implemented algorithm robustly and accurately extracted fibre orientations from micro-CT cardiac images. This together with micro-CT provides a rapid and powerful tool for noninvasively characterizing the structural properties of cardiac tissues and its remodeling by various cardiac diseases.

Mitral valve regurgitation: assessment with dual source computed tomography

Liping Yao, Kun Sun*, Sun Cheng, Linwei Yu, Ming Liu, Xin Yang

Heart Center, Xinhua Hospital Affiliated to Shanghai Jiaotong University School of Medicine
Shanghai, China

Aim: To evaluate diagnostic accuracy of dual source computed tomography(DSCT) for evaluation of mitral valve regurgitation(MR) with transthoracic echocardiography (TTE).

Material and Methods: We evaluated a total of 60 patients who underwent both DSCT and TTE. According to Doppler echocardiography, we divided the patients into two groups: 40 with MR and 20 without MR. We assessed the presence and severity of MR on the basis of systolic regurgitant orifice size on DSCT images and compared the results with two-dimensional Doppler echocardiography. We graded the morphology of the mitral apparatus of the 40 patients with MR using Real-time three-dimensional echocardiography (RT-3DE) and DSCT. Features such as calcification, valve thickening, valve prolapse, flail leaflet movement and local limitation of stretching on DSCT images were used to diagnose each patient and the results were compared with RT-3DE findings.

Results: Diagnosis of MR by DSCT was in good agreement with traditional two-dimensional Doppler echocardiography ($Kappa = 0.883$, $P < 0.01$); for the severity of MR, the correlation coefficient between the two methods was 0.94. DSCT was able to diagnose five different types of pathologic morphology with no statistically significant difference to RT-3DE.

Conclusions: DSCT can provide quick, multi-angle, multiphase observations of the mitral valve. Also DSCT can accurately assess the severity of regurgitation and pathologic morphology in MR disease.

P83

Multi-Parametric Model of the Heart from CT Images to Guide Ventricular Tachycardia Ablation

Sofia Antunes*, Daniele Tresoldi, Anna Palmisano, Caterina Colantoni, Antonio Esposito, Sebastiano Colombo, Giuseppe Maccabelli, Paolo della Bella, Sergio Cerutti, Giovanna Rizzo

Politecnico di Milano
Segrate, Italy

In ventricular tachycardia (VT) radio-frequency (RF) ablation, the exact location and extent of myocardial scar is important to decide whether the procedure will be epicardial or endocardial, and may be potentially useful to increase ablation success reducing intervention time. Today, contrast enhanced magnetic resonance imaging (CE-MRI) is considered the standard of reference for the assessment of myocardial scar. However, computed tomography (CT) could be an interesting alternative, since at least 2/3 of patients with recurrent VT are carriers of implantable cardioverter defibrillator (ICD) that contraindicates the MR evaluation for safety concerns and for the strong artifacts linked to the ICD electrocatheters. Beside the assessment of scars, segmentation of epicardial fat is also useful because, if not recognized, thick layer of fat are responsible of false scar voltages during epicardial procedures. However, fat is often neglected in RF ablation because it needs a very time consuming manual segmentation. The purpose of this work was to construct a 3D multi-parametric model of the heart by segmenting automatically cardiac cavities, left myocardium, scar and epicardial fat from CT images, using a level set algorithm based on a new multi-scale stopping function. This method was applied to 4 patients with recurrent VT undergoing angi-ographic and delayed CT before electro-anatomic mapping and RF ablation. The segmented structures were integrated into the clinical software system for electrophysiological procedures. The adequacy of our model was verified by expert radiologists and an arrhythmologist by visual inspection; scar position from CT images was judged in good agreement with that obtained from Bi-polar map sampled during VT ablation. These preliminary results suggest that our method could be used as an effective tool to assist the surgeon during the ablation procedure.

P83

Combined Action Potential- and Dynamic-Clamp for Accurate Computational Modeling of the Kinetics of Cardiac IKr Current

Chiara Bartolucci*, Claudia Altomare, Marco Bennati, Simone Furini, Antonio Zaza, Stefano Severi

University of Bologna
Cesena, Italy

Aims: To optimize an IKr model by fitting it to IKr recorded under AP-clamp and validate the optimized model by testing its suitability to replace native IKr under dynamic clamp conditions.

Methods: AP clamp technique was used to impose to the cell its AP waveform and obtain the dynamical behaviour of drug (E4031) – sensitive current (IE4031, representative of IKr) to compare it with the LRd formulation. IKr model parameters were then optimized by minimization of a cost function. For the validation we used the dynamic clamp technique; the protocol consisted in recording the AP in control, adding the blocker E4031, then injecting into the cell a “synthetic” current computed by the formulation of LRd or the optimized one.

Results: AP clamp recordings pointed out that the IE4031 current is very different from the IKr LRd model. The main changes in the optimized model with respect to the original one are a more pronounced inactivation at negative potential and a positive shift of the voltage dependence of activation time constant. After the IKr block the APD90 prolonged of 9% respect the control but the LRd current injection shorted to much the APD90 (-13% respect the control), instead of the optimized model which restored the APD90 with a difference of 2%. Similar percentages were maintained for APD50 and APD30.

Conclusions: The IKr model was successfully optimized by fitting it to IKr recorded under AP-clamp and validated by performing the dynamic clamp technique. The LRd model during the plateau phase led to over reduction of AP duration while the optimized model restore the AP control. The optimized model could be used to explore the effects of changes in single kinetic parameters on the AP and to study pathologies linked with IKr alterations.

S84

Extracellular Calcium and L-Type Calcium Current Inactivation Mechanisms: a Computational Study

Elisa Passini*, Stefano Severi

University of Bologna
Cesena, Italy

Introduction and Aim: It is well known that extracellular calcium concentration $[Ca]_o$ affects cardiac action potential (AP): the inverse relationship between AP duration (APD) and $[Ca]_o$ has been experimentally observed in vivo and in vitro. Both shortening and prolongation of AP are associated with an increased risk of arrhythmias. Calcium variations may occur in many clinical contexts (e.g. pathological hypo/hypercalcemia, hemodialysis therapy, bed-rest experiments) and computational modeling could be a useful tool to explore this phenomenon: however, most of the commonly used ventricular cell models are not able to reproduce $[Ca]_o$ effect properly. The aim of this study has been to modify one of the most recent human ventricular AP model, in order to improve its response to $[Ca]_o$ variations.

Methods: O'Hara-Rudy AP model (ORd) has been used as basis. Since L-type calcium current is the one mainly responsible for APD- $[Ca]_o$ dependence, its original Hodgking-Huxley formulation has been replaced by a novel Markov chain. Calcium-dependent inactivation (CDI) has been strengthened, with respect to the Voltage-dependent one (VDI). Simulations were run with the original and modified models, $[Ca]_o$ ranging from 1 to 3mM and APD were compared to experimental data available in literature. Other minor changes were included to preserve the physiology of the whole cell. The modified model has been validated against the same experimental data used in the original ORd paper.

Results and Conclusion: In control conditions ($[Ca]_o=1.8mM$), the modified and original ORd model APs and ionic currents were very similar. However, when changing $[Ca]_o$ from 1mM to 3mM APDs varied in an opposite way: -7.9% vs +24.2%, modified and original ORd respectively. Therefore, the modified model constitute a useful framework to explore effects of electrolyte changes in silico. Moreover, these results suggest that CDI mechanism is usually underestimated in ventricular human AP models.

S84

I_{Kr} impact on repolarization and its variability assessed by Dynamic-Clamp.

Claudia Altomare, Luca Sala, Chiara Bartolucci, Gaspare Mostacciolo, Stefano Severi, Antonio Zaza

University of Milano - Bicocca
Milano, Italy

Background: action potential duration (APD) and its short-term variability (BVR) are linked by mathematical proportionality. Nevertheless, loss of the rapid delayed rectifier K^+ current (I_{Kr}) leads to outstanding BVR increment, thus suggesting mechanisms beyond simple dependency on APD. It is unclear whether this may be explained by known I_{Kr} gating properties and which among them prevails in setting I_{Kr} profile and APD.

Aims: to investigate whether 1) BVR changes caused by I_{Kr} blockade (by E4031) are fully expected from APD prolongation; 2) specific gating parameters may have different weight in reproducing native I_{Kr} profile and APD.

Methods: A deterministic numerical I_{Kr} model (mI_{Kr}) was constructed to fit E4031-sensitive current in guinea-pig ventricular myocytes. At cycle lengths (CL) of 1 and 0.3 s, native myocyte I_{Kr} was blocked by E4031 and replaced by mI_{Kr} under Dynamic-Clamp (DC) conditions. The BVR/APD relationship of data pooled from all interventions (control, E4031, E4031+DC at both CLs) was linearly fitted and the sum of raw residuals ($\sum rR$) obtained for each intervention. Recovery of E4031 effect on APD by mI_{Kr} was tested with different values for maximal conductance (g_{max}), mid-potentials of activation ($V_{0.5A}$) and inactivation ($V_{0.5I}$), activation/deactivation time-constant (τ).

Results: E4031 increased APD and BVR ($p < 0.01$). mI_{Kr} injection restored control APD and BVR (NS vs control). $\sum rR$, positive and large in the E4031 group ($p < 0.01$), was negative and small in the control and E4031+DC groups (NS). Preliminary observations suggest that $V_{0.5I}$ was most influential in setting I_{Kr} profile and APD, followed by $V_{0.5A}$, τ and g_{max} .

Conclusions: 1) $\sum rR$ analysis suggests that E4031-induced increment in BVR exceeds the one expected from APD prolongation only; 2) Restoration of the control BVR/APD relation by mI_{Kr} indicates that known I_{Kr} properties are adequate to account for I_{Kr} impact on BVR; 3) I_{Kr} inactivation gating may prevail in APD modulation.

Deactivation of Per-Arnt-Sim Domain Mutation Increases the Proarrhythmic Risk of Dofetilide

Rodolfo Gonzalez*, Edgar Cardenas, Alain Manzo, Fernando Martinez, Julio Gomis, Javier Saiz

Instituto Tecnológico de Morelia
Tarimbaro, Mexico

The human ether-a'-go-go-related gene (hERG) encodes the major subunit of the rapidly activating delayed-rectifier potassium current (IKr), which plays an essential role in the final repolarization of the ventricular action potential. Two types of potentially lethal cardiac arrhythmias are associated with hERG: inherited mutations in the hERG gene underlie type 2 long QT syndrome (LQT2), and drug inhibition of hERG channels underlies acquired long QT syndrome. hERG exhibits characteristic slow closing (deactivation) kinetics that are regulated by an N-terminal Per- Arnt-Sim (PAS) domain, which help to specialize the channels for their role in the heart. Loss of hERG function, and thus, loss of IKr, can occur through a number of mechanisms, including defects in channel opening and closing (gating), ion permeation, or protein trafficking. The aim of this work was to study the influence of PAS hERG R56Q mutation on the effects of dofetilide. Markovian models of R56Q/WT mutation and dofetilide have been introduced in mammalian (modified Faber-Rudy) ventricular cellular model. The R56Q/WT mutation acts to increase the rate of deactivation. Using this mutated ventricular cellular model we have studied the effects of dofetilide concentrations (IKr blocker). The results showed that increased rates of deactivation produce a rightward shift in the voltage dependence of activation and rectification. Deactivation occurs earlier, resulting in less repolarizing current late in the action potential where IKr usually plays a major role in repolarization and determining APD. Moreover, the action of dofetilide increases the APD in the R56Q/WT epicardial and endocardial cells, enhancing the difference in APD between both cell types. In addition, dofetilide amplifies the amplitude of the EADs that the R56Q/WT mutation provokes in midmyocardial cells. In conclusion, the heterozygous R56Q hERG mutation increases the proarrhythmic risk of dofetilide prolonging the APD and enhancing the dispersion of repolarization.

S84

Validation of a Computational Model of Cardiac Defibrillation

Jean Bragard*, Jorge Elorza, Elizabeth M. Cherry, Flavio H. Fenton

University of Navarra
Pamplona, Spain

Aims: Currently, electrical defibrillation is the only reliable method for terminating ventricular fibrillation clinically. Improvements to this therapy depend on a better understanding of how defibrillation works to reset the electrical state of the heart. The aim of the present study is to validate a model for studying cardiac defibrillation that can be run using existing computational capabilities.

Methods: For our study, we developed a 3D bidomain model of the electrical activity of the ventricles. The geometry was taken from a rabbit heart and fiber orientation information was included in the model. A 5-variable model (generalization of the Fenton-Karma model) was used for the description of cell electrophysiology. We initiated a sustained ventricular state in the model and saved 10 separate uncorrelated full states of the system. These 10 states were then used as independent initial conditions for testing the efficacy of a 12-ms monophasic external defibrillation shock applied to the ventricles. The shock intensity (applied electric field) was increased up to a maximum of 18 V/cm. We fit the simulation results with a dose-response curve and obtained a value of $E=6.35 \pm 0.35$ (V/cm) for a 50 percent probability of successful defibrillation, in close agreement with the value of the critical defibrillation threshold known from experiments which is of about $E=6$ V/cm. Therefore, our model reproduces the defibrillation threshold accurately without the need for introducing any adjustable parameters.

Conclusions: We have validated a simple, yet computationally efficient, realistic 3D bidomain model that reproduces the experimentally observed defibrillation curve response and threshold. This validation paves the way for more ambitious computational studies aimed at improving our understanding of defibrillation mechanisms and designing and testing new and more efficient external defibrillation protocols by using tailor-made waveforms in next-generation defibrillation devices.

S84

Population of Human Ventricular Cell Models Calibrated with in vivo Measurements Unravels Ionic Mechanisms of Cardiac Alternans

Xin Zhou*, Alfonso Bueno-Orovio, Michele Orini, Ben Hanson, Martin Hayward, Peter Taggart, Pier Lambiase, Kevin Burrage, Blanca Rodriguez

University of Oxford
Oxford, UK

Cardiac alternans is a repetitive beat-to-beat fluctuation between subsequent action potentials, and is regarded as an important risk factor for ventricular arrhythmia and fibrillation. It can be seen in many pathological conditions under significant metabolic stress and chronotropic stimulations. The goal of this study is to investigate the mechanisms underlying alternans generation in human using combined computational and in vivo electrophysiological studies. We constructed and calibrated a population of human cell models to consider variability in the ionic properties of different myocytes. 11 key parameters reported experimentally to be related to alternans generation were varied across the population and Latin hypercube sampling was used to generate the initial population of 10000 models. Activation-recovery interval (ARI) ranges from patients were used to calibrate the population of models by constraining APD90 (action potential duration to 90% repolarization): any parameter sets that generated a model with unphysiological APD90 were excluded from the population (top panel). The occurrences of voltage and calcium alternans were defined as a difference of greater than 5ms between APD80 (APD to 80% repolarization) or CaTD80 (CaT duration to 80% of repolarization) in the penultimate and final pacing beats. Parameters that generated alternating or normal action potentials were divided into two groups. In the Alternans group, GNa (fast sodium conductance) and Jup (Ca²⁺ uptake flux via SERCA pump) were statistically smaller than in the Normal group (bottom panel). Further analysis suggested that GNa and Jup may determine the generation of alternans through different mechanisms, respectively modulating the generation of voltage and calcium alternans in human ventricular tissue.

S84

Detection of Sleep Apnea in Infants using ECG and Oximetry Signals

Gregory Cohen*, Philip de Chazal

University of Western Sydney
Australia

Algorithms for detection of sleep apnea hypopnea syndrome in adults using combined night-time electrocardiogram (ECG) and pulse oximetry recordings have been successfully designed. In this study we investigate detection of sleep apnea hypopnea syndrome in infants using the same signals. The study draws upon the polysomnogram recordings found inside the National Collaborative Home Infant Monitoring Evaluation (CHIME) database. The CHIME database contains both overnight polysomnogram recordings and expert-scored sleep analysis for infants. Viable ECG data, pulse oximetry data and scored arousal information was extracted for 408 subjects from this dataset and time-aligned to 30s epochs. Due to the large movement of the infants during sleep, a key first step in processing the signals was the detection and removal of movement artefact on the ECG and the SpO₂ signals. ECG features based on RR intervals were extracted after QRS detection. SpO₂ features based on identification of oxygen desaturation events were also extracted. The features were then used alongside the scored apnea information to train a classifier based on linear discriminants. Performance of the classifier was evaluated using a leave-one-out cross-validation scheme and an accuracy of 68% was achieved, with a specificity of 68.6% and a sensitivity of 55.9%.

S91

Detection of Epileptic Seizures by means of Morphological Changes in the ECG

Carolina Varon*, Katrien Jansen, Lieven Lagae, Sabine Van Huffel

KU Leuven
Heverlee, Belgium

Aims: This study aims to develop a method for the detection of epileptic seizures from ECG recordings. Traditionally these seizures are detected using the electroencephalogram (EEG). However, it has been shown that epileptic seizures also change the morphology of the ECG. The ECG has an inherent advantage over EEG in the sense that it is easier to measure in a long-term setting, and changes can be observed before the EEG onset.

Methods: ECG segments were selected from single-lead recordings of 35 patients admitted to the epilepsy clinic. In total 80 segments of 5 minutes were selected, starting 3 minutes before the onset of 40 partial and 40 generalized seizures. First, the R peaks were identified and the RR interval time series were computed. Then, a moving window of 5 heartbeats was shifted with an overlap of 4 heartbeats throughout the whole segment. Each matrix of 5 QRS complexes was analyzed using principal component analysis. Last, the normalized 4th and 5th eigenvalues were selected as features, as they get higher when the variability of the QRS becomes more complex. Additionally, they are less influenced by the respiratory modulation of the ECG. The mean RR per window was also selected as feature.

Results: The best positive predictive value (PPV) obtained was 79.17% for partial seizures, which were identified within a 7.4 ± 14.3 seconds range. For generalized seizures, the performance was lower (PPV=57.38%). For both types of seizures, about 75% of the changes in the ECG were lagging the onset in the EEG, while the rest was leading or simultaneous.

Conclusions: The proposed methodology can be used to improve monitoring systems for detection of epileptic seizures. It can complement other approaches such as those based on accelerometers and EMG. Furthermore, it has an added value in the fact that it can be used online.

S91

Evaluation of the Relation Between Changes in R-wave Amplitude and LV Mass and Dimensions in a Model of “Reversed Hypertrophy”

Enrico G Caiani*, Angelo Auricchio, Mark Potse, Rolf Krause, Alessandro Pellegrini, Roberto M Lang, Pierre Vaïda

Politecnico di Milano
Milan, Italy

Background. Electrocardiographic (ECG) diagnosis of left ventricular (LV) hypertrophy is based on the so-called voltage criteria, i.e. the increased amplitude of the QRS complex, considered to be specific for diagnosis of LV hypertrophy. However, these criteria suffer from low sensitivity, and correlation between QRS amplitude and LV mass is poor, so that the dominant cardiac factors influencing the QRS voltage have not been fully elucidated.

Aims. Our aim was to evaluate the correlation between changes in R-wave amplitude (R-AMP) and LV mass and volumes in a model of “reversed hypertrophy”, such as that induced by 5-days head-down (-6°) bed rest (HDBR).

Methods. ECG Holter-24h and 2D and 3D echocardiographic imaging obtained before (PRE) and the last day (HDT5) of HDBR in 11 healthy volunteers (age 21-41 years) were considered. The experiments took place at MEDES (Toulouse, France) as part of the European Space Agency HDBR studies. At each epoch, the R-peak amplitude (R-AMP) was derived from the vectorcardiogram by selective beat averaging applied to the night period, and LV mass (area-length method) and end-diastolic (EDV) and end-systolic (ESV) volumes semi-automatically obtained (QLab, Philips).

Results. Compared to PRE, R-AMP was found decreased by 8.9% at HDT5 ($p < .001$), while LV mass, EDV and ESV were reduced by 15%, 10% and 16% ($p < .01$), respectively. Linear regression between percent changes in R-AMP and percent changes in EDV ($y = -.53x + .1$, $r^2 = .34$) was found significant ($p < .05$), while regression with LV mass ($y = -.39x + .11$, $r^2 = .17$, $p = .1$) was poor. No relation was found with ESV.

Conclusions. A decrease in R-wave amplitude could be partially explained by a concomitant decrease in LV EDV, while the relationship with decrease in LV mass was weaker. Further studies using electrophysiologic model could better elucidate the phenomenon.

S91

Cardiac Repolarization Analysis: Immediate Response

Josef Halamek*, Pavel Jurak, Eleonora Tobaldini, Nicola Montano,
Pavel Leinveber

Institute of Scientific Instruments, AS, Brno
Brno, Czech Republic

QT adaptation to RR changes has two phases: immediate response (restitution, dependence on preceding interval) and the slow adaptation (memory, dependence on previous intervals). The analysis of restitution is mostly neglected, even if this parameter significantly differ between controls and LQT, may be modified by drugs and is important in analysis of short term QT variability. The reason for this is due to the low reproducibility of the measure. We tested the reproducibility with two different algorithms QT detection: D1 - detection on a beat to beat basis, and classic D2 detection, on a 10-beats average basis. Graded head-up tilt from 15° to 90° with steps 15° was analyzed. Analyzed QT parameters provided by linear, dynamic model with 3 optimized parameters, were: QTc, QT/RR slope (GL), and QT gain for fast variability RR (GF), i.e. QT restitution. Analysis on simulated data and theoretical analysis were also performed. QT parameters (mean±STD over 6 angles of tilt, for one subject) using D1 detection were 0.171±0.006; 0.024±0.002; 362.8±2.2 respectively for GL, GF and QTc, while using D2 were: 0.171±0.006; 0.005±0.004; 361.7±2.3. Relative reproducibility (STD/mean per subject, mean over three subjects) was for D1: 0.063; 0.100; 0.007 and for D2: 0.063; 0.587; 0.007 for GL, GF and QTc respectively. The difference in mean levels of GF when comparing D1 and D2 was explained by theoretical analysis; with D2 no proper level of GF may be achieved. The detection D1 must be used when QT restitution is assessed and reproducibility of GL and GF are comparable. The reproducibility of GL and QTc is the same with D1 or D2. Significant raises of heart rate and the length of the RR interval series are other prerequisite of QT analysis. The QT parameters with 15° of tilt (minimal RR interval decrease) showed maximal differences from mean levels.

S91

Atrial fibrillation classification method for patients with different pharmacological or surgical therapies

Nuria Ortigosa *, Antonio Galbis, Carmen Fernández, Guillermo Ayala, Óscar Cano, Ana Andrés

I.U. Matemática Pura y Aplicada, Universidad Politécnica de Valencia, Spain

Aims: This method aimed to assess electrophysiologists to choose the most suitable therapy for patients suffering from atrial fibrillation (AF), depending on whether a paroxysmal or persistent episode is presented. Since the surface ECG masks the differentiation between subtypes of AF, an early detection of paroxysmal episodes allows a clinically preventive treatment to stop recurrence and the natural progression towards persistent AF.

Methods: 76 consecutive unselected ECG AF signals of a tertiary center (15 paroxysmal and 61 persistent) conformed the study population (including first AF episodes, and recurrent AF with pharmacological or electrical cardioversion treatments). Variations of the modulus of the General Fourier-family time-frequency transform were used as inputs of a Linear Discriminant Analysis classifier. Training was performed with 6 paroxysmal and 9 persistent signals. Accuracy (total correct classifications), sensitivity and specificity (paroxysmal and persistent subjects correctly classified, respectively) were used as performance measures.

Results: Of the 61 testing patients (9 paroxysmal and 52 persistent), 43 were correctly classified (7 paroxysmal and 36 persistent). Obtained performances were: accuracy 70%, specificity 69%, and sensitivity 78%.

Conclusion: AF episodes are mostly correctly classified, having into account that, from a clinical point of view, it is more important to detect almost every paroxysmal episode than viceversa, in order to stop the progression of these patients towards persistent AF.

S91

Towards Standardization of Non-invasive Atrial Fibrillation Substrate Complexity Quantification: Effect of Choice of ECG-leads and Complexity Measure on Prediction of Pharmacological Cardioversion

Stef Zeemering*, Theo Lankveld, Harry Crijns, Ulrich Schotten

Maastricht University
Maastricht, Netherlands

Introduction: Current studies on non-invasive outcome predictors in patients with atrial fibrillation (AF) vary widely in choice of ECG lead and features used to estimate AF complexity. Consequently, the predictive power of different techniques cannot be compared based on current literature. We performed a retrospective analysis of ECGs of patients undergoing cardioversion (CV) using flecainide to compare the ability of several non-invasive AF substrate complexity parameters to predict CV success and to study the effect of the number and location of ECG leads on outcome prediction.

Methods Patients were selected from our institutional database of patients that underwent CV with intravenous flecainide between 2008-2010 (n=125, success rate 68%, CV within 1 hour). AF substrate complexity parameters were computed on all 12 leads of the ECG recorded before the flecainide administration, consisting of dominant atrial frequency (DF), spectral organization index (OI), spectral entropy (SE), fibrillation wave amplitude (FWA), and sample entropy (SampEn). For each parameter, logistic regression models were estimated to predict CV outcome, containing single lead or multiple lead information.

Results Single lead prediction was best using SampEn, but performance was poor (Lead II | 54% sensitivity | 75% specificity | AUC 69%). Exploiting multi-lead information enhanced performance of all parameters, with SampEn performing best (I, II, AVR, V6 | 80% | 78% | AUC 78%), followed by DF (I, II, III, V1, V6 | 67% | 80% | AUC 77%). Combining parameters and leads further improved prediction (AUC 83%).

Conclusion Successful CV with flecainide may be predicted from the surface ECG during AF. Prediction is notably improved by combining information derived from multiple ECG-leads as opposed to a single lead. Best performing ECG-derived AF substrate complexity parameters are sample entropy and dominant atrial frequency. Useful information is predominantly located in the limb leads and precordial lead V6.

Effect of Pre-measurement Relaxation Time on Manual Blood Pressure Measurement

Dingchang Zheng*, Fan Pan, Alan Murray

Newcastle University
Newcastle upon Tyne, United Kingdom

In clinical practice, blood pressures (BPs) are often measured without time to relax before the measurement is taken, allowing little time for BP to stabilise. However, there is little evidence on the effect of any pre-measurement relaxation time on manual BP measurement. This study aimed to provide these data. Twenty subjects (aged from 24 to 61 years) were studied. Manual systolic and diastolic BPs (SBP and DBP) were obtained by a trained observer while the subjects were seated on a chair. There were two sessions for each subject with two pre-measurement relaxation times (none and 10 min). Within the first session, the subjects were asked to sit relaxed at the reception for at least 10 min before entering the measurement room. Three sequential BP measurements were then taken at 0, 10, and 20 min. For the second session, the subjects were asked to walk around for 800 m at their normal walking speed before a similar series of BP measurements were taken. The measured BPs were then compared between the three sequential measurements and between the two pre-measurement relaxation times. ANOVA analysis showed no significant sequential changes in BPs ($P=0.7$). For SBP, the paired changes (mean \pm SD) at 10 and 20 min from 0 min were -1.1 ± 5.6 and 0.6 ± 6.8 mmHg (with 10 min relaxation), and -0.7 ± 7.1 and -0.9 ± 6.5 mmHg (without relaxation). Their corresponding changes for DBP were 1.3 ± 5.2 and 1.9 ± 7.8 mmHg (with 10 min relaxation), and 0.8 ± 3.3 and 1.7 ± 4.3 mmHg (without relaxation). There was also no effect of pre-measurement relaxation time on SBP. However, the effect of the two relaxation times (none and 10 min) on DBP was significant ($P<0.001$). On average, the DBP measured with no relaxation was 1.7 mmHg higher than with 10 min relaxation. In conclusion, this study quantified the effect of relaxation period on manual BP measurement.

S92

Pulse arrival time and pulse width as potential measure for estimating beat-to-beat systolic and diastolic blood pressure.

Adriana Arza¹, Raquel Bailon², Jordi Aguiló¹, Jesús Lázaro², Eduardo Gil², Pablo Laguna²

¹Dto de Microelectrónica y Sistemas Electrónicos, Universidad Autónoma de Barcelona, España

²Instituto de Investigación en Ingeniería de Aragón, Universidad de Zaragoza, España

Two cardiovascular parameters of emerging interest suitable for estimation of non-invasive, beat-to-beat and without cuff blood pressure parameters are pulse width (PW) and pulse transit time (PTT). In this study the performance of both parameters in estimating beat-to-beat systolic blood pressure (SBP) and diastolic blood pressure (DBP) is analyzed. The overall data set used in the study includes synchronous electrocardiogram signal, pulse photoplethysmography signal and continuous blood pressure signal of 17 healthy subjects during tilt table test, which provokes significant changes in SBP and DBP due to postural changes.

Blood pressure was estimated using different linear models, mean error (mmHg) and correlation were calculated between estimated and measured blood pressure for each model:

Model	PAD				PAS			
	Error	Std	Corr	<i>p</i>	Error	Std	Corr	<i>p</i>
$BP = c_0 + c_1 TTP$	1,0	6,1	0,270	0,045	0,7	9,9	0,212	0,0001
$BP = c_0 + c_1 PW$	2,8	5,2	0,348	0,026	0,1	9,4	0,364	0,0197
$BP = c_0 + c_1 TTP + c_2 PW$	4,6	3,4	0,609	0,0001	7,3	6,5	0,714	0,00010

Real and estimated SBP and DBP series were filtered in the very low frequency (VLF, 0.003-0.04Hz), low frequency (LF, 0.04-0.15Hz), and high frequency (HF, 0.15-0.4Hz) bands, and estimation error was computed in each of the bands:

Model		PAD			PAD		
		Error	Std	Corr	Error	Std	Corr
$BP = c_0 + c_1 TTP$	VLF	0,9	5,2	0,457	0,6	8,8	0,444
	LF	0,0	2,5	0,367	-0,1	3,6	0,622
	HF	0,0	1,4	0,003	0,0	1,8	0,675
$BP = c_0 + c_1 PW$	VLF	2,8	4,3	0,536	-0,1	8,1	0,572
	LF	0,0	2,4	0,369	0,0	4,3	0,476
	HF	0,0	1,3	0,356	0,0	2,2	0,471
$BP = c_0 + c_1 TTP + c_2 PW$	VLF	4,1	2,5	0,794	5,8	5,2	0,755
	LF	-0,1	1,7	0,683	0,0	2,3	0,852
	HF	0,0	0,8	0,730	-0,1	2,0	0,935

The result suggests that these two parameters can be used to estimate blood pressure, TTP is better than PW to detect rapid changes, while PW shows better result in slow changes, but together they are a potentially measure for estimating beat-to-beat systolic and diastolic blood pressure.

Exploring the stationary wavelet transform detail coefficients for the detection and identification of the S1 and S2 heart sounds

N.Marques, A.P.Rocha, R.Almeida, M.Coimbra

CRACS, University of Porto
Porto, Portugal

Heart sound auscultation is a cheap, non-invasive procedure that can detect a number of cardiac pathologies. For this reason, automatic detection of heartbeats is a crucial step for heart pathology detection and classification. The heart sound can be decomposed into 4 different events, the first heart sound(S1), the systole, the second heart sound(S2) and diastole. S1 represents the closure of the mitral and tricuspid valves, while S2 represents the closure of the pulmonary and aortic valves. An algorithm that attempts to detect heart sounds faces several problems: high noise levels, inter-personal variations with age and pathology, etc. We propose a new method that uses the Stationary Wavelet Transform to segment the signal and hierarchical clustering to distinguish the S1 and S2 heart sounds from noise. The used wavelet is the Daubechies of order 18. This particular wavelet function was chosen due to its similarity with S1 and S2. The inflection points in the detail coefficients at scale 10 mark the beginning and end of S1 and S2. After segmenting the signal, we compute the energy of each segment. We use hierarchical clustering as an unsupervised procedure to cluster the energy of the segments into 2 classes, the information cluster, composed by the S1's and S2's, and the noise cluster. In order to distinguish the S1's from the S2's, we also use clustering. This approach was tested in the Dataset B of the Classifying Heart Sounds PASCAL Challenge <http://www.peterjbentley.com/heartchallenge/>. The following table shows the results of blind scoring, using the information provided by the data owners.

Results of the Challenge and our approach

Team	Total Error
UCL	75569
Stanford	76444
ISEP	72242
Our approach	62116

Correct labeling of the event is not available at the moment. The results of the detection and identification of heart sounds with our proposed method outperformed the winning approach of the Classifying Heart Sounds Challenge.

S92

Effect of Stethoscope Position on Auscultatory Blood Pressure Measurement

Fan Pan*, Dingchang Zheng, Alan Murray

Sichuan University
Chengdu, China

When measuring blood pressure (BP) using the auscultation method, a stethoscope is commonly used. Various international societies of hypertension recommend that the stethoscope should be placed gently over the brachial artery at the point of maximal pulsation. In clinical practice, it is sometimes placed under the cuff, but more usually outside the cuff on the antecubital fossa. However, there is little scientific evidence to quantify the BP difference between the BP measurements taken with the stethoscope under the cuff or outside the cuff. The aim of this study was to provide these data. Nine healthy subjects were studied. The cuff pressure was linearly deflated at a recommended rate. Two electronic stethoscopes (one under the cuff, the other outside the cuff) were used to record the Korotkoff sounds. The signals of cuff pressure and two Korotkoff sounds were simultaneously and digitally recorded to a computer for off-line analysis. A repeat measurement was performed for each subject. Next, the recorded Korotkoff sound data were converted into wav files, and replayed with an interactive Matlab program. Two operators were asked to determine the BPs independently from the sounds recorded from the two positions. Their BP difference was finally compared. ANOVA analysis showed that there was no significant BP difference (for both SBP and DBP) between the repeat measurements and between the two operators (all $P > 0.05$). There was also no significant SBP difference between results with the stethoscopes placed at the two positions (mean \pm SD, under the cuff: 105 ± 8.9 vs outside the cuff: 104 ± 8.7 mmHg). However, a significant difference for DBP was observed (under the cuff: 66 ± 8.9 vs outside the cuff: 69 ± 8.6 mmHg), with a mean \pm SD difference of -3.0 ± 1.4 mmHg ($P < 0.001$). In conclusion, this study quantified the effect of stethoscope position on BP measurement.

S92

Influence of Intraluminal Thrombus Topology on AAA Passive Mechanics

Fabian Riveros, Giampaolo Martufi, T Christian Gasser, Jose F Rodriguez*

Universidad de Zaragoza
Zaragoza, Spain

Background: An intraluminal thrombus (ILT) is found in most AAAs of clinically relevant size. Some authors have suggested that ILT growth and volume may be related to AAA risk of rupture. Even though some studies seem to indicate a protective role of the ILT against AAA rupture, there is still great controversy on this regard. In addition, patient-specific AAA models are generated from gated medical images in which the artery is under pressure. Therefore, identification of the AAA zero pressure geometry would allow for a more realistic estimate of the aneurysmal wall mechanics and a better understanding of the role of the ILT. This study looks into the influence of the ILT on the stress field on patient specific AAA accounting for the zero pressure geometry.

Methods: Ten patient specific AAA of similar maximum diameter (4.8-5.2cm) and ILT volumen, but with different ILT topology are considered. A novel iterative algorithm is used to determine the zero pressure configuration of the model, and the anisotropic hyperelastic behavior of the arterial wall is considered for the nonlinear stress-strain analysis.

Results: Our results suggest that the geometrical configuration of the ILT relative to the arterial wall may be an influential factor not only on the ensuing peak wall stress, but also on its location within the lesion. The effects of the ILT topology are enhanced when the zero pressure configuration of the lesion is accounted for. It is important to point out that when the zero pressure configuration is not accounted for, the peak wall stress is underestimated by a 20% (47 kPa).

Conclusions: This study suggests that, it is not only the symmetry, or the curvature, but also the topology of the ILT that greatly influence the zero-pressure geometry and therefore the stress field at the systolic pressure on AAA.

S92

A complete Riemann solver for arterial flow with application to the systemic arterial tree

Javier Murillo and Pilar García-Navarro

Universidad de Zaragoza
Zaragoza, Spain

Complete Riemann solvers are able to describe the evolution in time of the variables involved in a specific system of equations, attending to the actual number of waves that may appear. Here, a complete approximate solver based on the upwind discretization of the source terms and a genuinely Roe solver for the one-dimensional blood flow equations in arteries is presented. The systemic circulation is modeled as a 1D network of elastic tapering vessels, where equations for arterial blood flow are presented using mass and momentum arguments and a closure relation between vessel cross-sectional area and internal pressure. The complete solver involves source terms and ensures convergence to the exact solution even in presence of variable material properties. The resulting numerical solver allows the simulation of pulsatile waves without creating non-physical oscillations. The numerical scheme is applied to an specific person model and validated with non-invasive measurements of flow and pressure on the same person. The specific arterial tree includes 94 arterial segments, extending the arterial tree via the carotids and the vertebrales to include a detailed cerebral arterial tree. Numerical simulation is performed by providing the inlet blood discharge at the ascending aorta. Peripheral resistances for terminal vessels are defined using the three-element Windkessel model. This model considers the compliant-capacitive effects due to microvessels and arterioles.

S92

Approximate Entropy can Localize Rotors, but no Ectopic Foci during Chronic Atrial Fibrillation. A Simulation Study

Andrés Orozco-Duque¹, Juan P. Ugarte¹, Catalina Tobón², Carlos A. Morillo³, Javier Saiz⁴, John Bustamante¹

¹Centro de Bioingeniería, Universidad Pontificia Bolivariana, Medellín, Colombia

²GI²B, Instituto Tecnológico Metropolitano, Medellín, Colombia

³McMaster University, Hamilton, Canada

⁴I3BH, Universitat Politècnica de València, Valencia, Spain

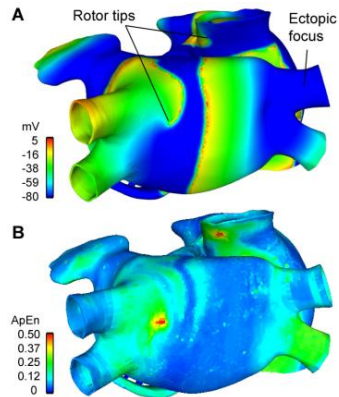
Introduction: Atrial fibrillation (AF) is the most prevalent cardiac arrhythmia. AF is often sustained by rotors and ectopic foci, which are stable over time and thus suitable targets for ablation. Focal impulse and rotor modulation-guided ablation substantially improved long-term freedom from AF over conventional ablation alone. Analyses of dominant frequency and regularity indexes have proven to be effective to localize ectopic foci but no rotors on chronic AF. Some studies suggest that fractionated electrograms are generated by the rotor tips. Approximate entropy (ApEn) is a non-linear statistic that can be used as a measurement that quantifies the complexity of a signal. We hypothesized that the ApEn could locate rotors.

Methods: Electrical remodeling was introduced in the Courtemanche atrial cellular model to simulate chronic AF in a 3D model of human atria. AF episode of 10 seconds was generated by a continuous ectopic focus applied in the right superior pulmonary vein at high frequency. Pseudo-unipolar electrograms were simulated in the atrial surface and ApEn was calculated for every 500 ms of simulation.

Results: During AF activity, two stable rotors were observed, one located in the posterior wall of the left atrium near the left pulmonary vein and the remaining in the superior vena cava.

The ApEn map showed two areas with high ApEn values, which matched with the rotor tips. Low values of ApEn were observed in the rest of the atria.

Conclusion: Targeting ApEn areas may potentially be effective in identifying the rotor tips for ablation in chronic AF.



A) Chronic AF propagation. Rotor tips and ectopic focus location are showed. B) ApEn map showing high values in the rotor tips.

3-Dimensionality in Determining the Stability of Atrial Fibrillation

Ali Gharaviri*, Sander Verheule, Nico HL Kuijpers, Ulrich Schotten

Maastricht University
Maastricht, Netherlands

Background: Disruption of side to side electrical connection between muscle bundles has been described as a phenomenon that promotes atrial fibrillation (AF). Putatively, such electrical uncoupling also occurs between the endocardial bundle network and the epicardial layer. Paradoxically, clinical and experimental studies revealed an increased incidence of “breakthroughs” (BT) during later stages of AF.

Method: In a computer model consisting of 2 layers with realistic atrial membrane behavior and endo-epicardial conduction was simulated. Progressive disruption of endo-epicardial electrical connections was simulated by limiting connectivity to 48, 24, 12 or 6 connections representing the transition to moderate and severe remodeling. 100% endo-epicardial connectivity served as control (healthy atrium). The effect of endo-epicardial connectivity on conduction velocity (CV), AF cycle length (AFCL), excitable area (EA), and breakthrough rate (BTR) was studied.

Results: Eliminating endo-epicardial connections did not change CV, AFCL, and EA but endo-epicardial dissociation (EED) increased. BTR increased by eliminating connections to 48 and 24 but declined at lower numbers of connections. The stability of AF episodes increased with progressive loss of connections and correlated significantly ($r = 0.82$, $p < 0.05$) with EED but not with AFCL, CV, and EA.

Conclusion: During the development of a substrate for AF, EED increases. Since EED was the only parameter correlating well with AF stability, we conclude that the three-dimensional conduction pattern during AF, i.e. transmural conduction and EED, were the most important determinants of AF persistence.

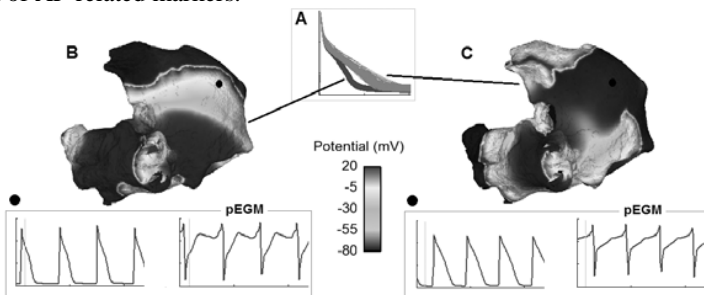
S93

Cell Repolarization Variability Modulates Atrial Fibrillation Dynamics in 3D Virtual Human Atria

C Sánchez*, A Bueno-Orovio, B Rodríguez, E Pueyo

University of Zaragoza, Zaragoza, Spain

Variability in cardiac electrophysiology between patients is an intrinsic feature of nature. It underlies the biological proneness to suffer and/or sustain arrhythmia episodes, such as atrial fibrillation (AF). In this study, we compare arrhythmogenic properties between pairs of simulated 3D human atria in AF with notable differences in their cellular repolarization dynamics. To account for intercellular variability, a population of models within physiological range was generated by simultaneously modifying ionic current conductances within a $\pm 30\%$ range obtaining 2275 combinations, and calibrated to fit experimental observations in chronic-AF patients. Out of the obtained population, subpopulations were extracted according to their action potential duration (APD) measured at 20%, 60% and 90% repolarization, separating those models over the third quartile from those below the first quartile (Figure, panel A). Models of the subpopulations were randomly assigned to each node in the heterogeneous 3D-mesh. Following periodic sinoatrial stimulation until reaching the steady-state, fibrillatory activity was initiated by applying ectopic stimulation near the right pulmonary veins. Analysis of calculated pseudo-electrograms showed the dominant frequency was lower in the short APD₉₀ (Figure, panel B) than in the long APD₉₀ subpopulation (Figure, panel C): 5.4 vs. 5.9 Hz. Calcium transient decay time was shorter in the short subpopulation (66 vs. 75 ms) while the amplitude was similar (0.24 vs. 0.22 μM). Regularity was higher in the long APD₉₀ subpopulation, and organization was also slightly higher (0.88 vs. 0.96). For APD₆₀ and APD₂₀, short and long subpopulations had slight differences in dominant frequency, regularity and organization, but unequally affected wave-break likelihood and electric propagation through calcium transient amplitude modulation: 0.18 vs. 0.24 μM (short/long APD₆₀); 0.20 vs. 0.24 μM (short/long APD₂₀). In conclusion, inter-patient variability in cell repolarization underlies differences in modulation of AF-related markers.



S93

Body Surface Potential Propagation Maps During Macroreentrant Atrial Arrhythmias. A Simulation Study

Alejandro Liberos*, Jorge Pedrón-Torrecilla, Miguel Rodrigo, José Millet, Andreu M Climent, María S Guillem

Universitat Politècnica de València
Valencia, Spain

Atrial flutter (AFL) is a supraventricular arrhythmia perpetuated by a macroreentrant circuit around an obstacle. Typical AFL is caused by a rotation around the tricuspid annulus and atypical AFL by a rotation around any other structure. The identification of the circuit in atypical AFL is complicated by using the techniques of the clinical practice. Location of the circuit responsible of the reentrance prior to the ablation procedure may help in planning the intervention and thus reducing intervention times and improving success rates. In this work, we present mathematical simulations describing several macroreentrant behaviors and its reflection on the torso. Atrial activity was calculated by using an anatomically realistic atrial structure. Potentials on the surface of the torso were computed with the forward problem. The calculated BSPMs were summarized by phase maps and the detection and tracking of phase singularities. Specifically, it discusses in detail a clockwise typical flutter and two atypical flutters depending on IVC and SVC respectively, a calculated BSPM during sinus rhythm is also included. The propagation during typical AFL shows an ascending propagation through the front of the torso continued by a descending propagation through the back according to previous studies. Two stable PSs were detected in the underarms with diagonal lengths (0.16Y, 0.12Y) for the left one and (0.3Y, 0.22Y) for the right one, being Y the height of the torso. The phase maps representing clockwise macro-reentrant arrhythmias around IVC and SVC presented a counterclockwise propagation through the anterior part of the torso. A PS remained at the front of the torso with lengths (0.12Y, 0.11Y) for IVC and (0.25Y, 0.16Y) for SVC. The results of this study reinforce the reliability of BSPM as a tool for distinguishing among different cardiac behaviours, this technique may help new ablation procedures to be planned in the near future.

S93

Computational Simulation and Analysis of 3D Body Surface Potential Patterns Generated by Common Atrial Arrhythmias

Ana Ferrer*, Rafael Sebastian, Jose F Rodriguez, Catalina Tobón, María Guillem, Eduardo J Godoy, Javier Saiz

Universidad Politécnica de Valencia, Valencia, Spain
Valencia, Spain

Motivation: Atrial fibrillation (AF) is the most common cardiac arrhythmia and the variety of mechanisms of AF onset and progression are not well understood. This has motivated the development of multi-scale computer models for investigating mechanism that underlie atrial rhythm disturbances.

Aims: This study presents a set of numerical indicators calculated from in-silico body surface potential maps (BSPM) able to discriminate and characterize a normal sinus rhythm (SR) and different types of arrhythmic atrial propagations. Attention was paid to the correlation between atrial sites with high frequency arrhythmic activity and the corresponding torso surface activity to help in the non-invasive diagnosis of electrical cardiac problems.

Methods: A 3D human torso model that includes an anatomically realistic atrium was used to obtain biophysical simulations of electrical atrial depolarisation and BSPMs. Three indicators - dominant frequency (DF), sample entropy (SE) and phase-space diagram (PD) - were studied on the torso surface (12371 points) to characterize SR, flutter (AFL), tachycardia (AT) and AF. Furthermore, DF and SE were graphically represented by 3D maps on the torso surface to describe characteristic patterns and facilitate visual diagnosis and correlation inside-outside.

Results: DF was in agreement with published experimental measurements: SR [0.78~8.59]Hz, AFL [5.47]Hz, AT [5.08~10.2]Hz, AF [5.08~7.81]Hz. DF maps revealed homogeneous patterns in SR and AFL meanwhile AT and AF showed well-defined regions with different frequency. SE was, as expected, low in regular arrhythmias (0.15 in SR and AFL) and high in AF (0.58~0.67). Corresponding surface maps revealed high complexity degree of AF. PD registered at chest leads showed a spread trajectory all over the space in AF versus definite loops around the central attractor in SR, AFL and AT.

Conclusion: The numerical indicators and gradients in surface maps revealed important differences in spatial and temporal distributions and allowed classifying each type of arrhythmia.

S93

Influence of Three-Dimensional Fibrotic Patterns on Simulated Intracardiac Electrogram Morphology

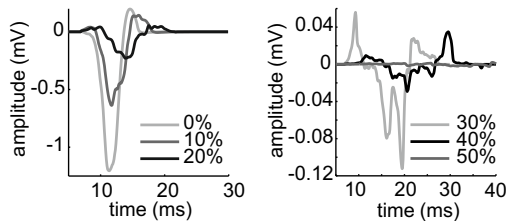
Matthias W Keller, Armin Luik, Mohammad Soltan Abady,
Gunnar Seemann, Claus Schmitt, Olaf Dössel

Institute of Biomedical Engineering, Karlsruhe Institute of Technology
Karlsruhe, Germany

Aims: Complex fractionated atrial electrograms (CFAE) are linked to areas of slow conduction and therefore ablated to cure atrial fibrillation. We investigated the influence different three-dimensional fibrotic patterns on simulated intracardiac electrograms (EGM) and compared the results to clinical data.

Methods: Catheter signals were simulated for two types of fibrosis (diffuse (DF), patchy (PF)) on a regular spaced grid (resolution $50 \mu\text{m}$). Each setup included a plane sheet of myocardium and highly conducting catheter electrodes. Fibrosis was modeled by uniformly distributed cube like elements for DF, compared to disks with Poisson distributed length and width for PF. We simulated fibrotic volume fractions (FVF) of 0-50%. Cardiac excitation was calculated by solving the monodomain equation followed by a forward calculation of extracellular potentials. Simulated results were compared to characteristic features extracted from a database of 605 annotated clinical CFAEs.

Results: Conduction velocity (CV) decreased linearly for both types of fibrosis with increased FVF (1.1 m/s for 0%, 0.4 m/s for 40%). EGM amplitude decreased and EGM width increased



Simulated EGM for different FVF of PF

with increasing degree of fibrosis. However fractionated EGMs only occurred for the patchy case for a FVF above (30%). Amplitude reduction from non-fractionated to fractionated simulated EGMs was 88 % comparing to 84 % for clinical signals. Number of zero crossings ranged from 4 to 10 for simulated EGM and 6 to 10 for medium fractionation in the clinical case.

Discussion: Simulated EGM for PF show fractionation, which was not the case for DF. However DF bears the same arrhythmogenic potential due to low CV. Characteristic parameters extracted from simulated EGMs matched those received from a database of clinical CFAE-signals.

Sensitivity of a Wearable Bioimpedance Monitor to Changes of Thoracic Fluid Content in Heart Failure and Hypertension Patients

Silviu Dovancescu¹, Azam Torabi², Thato Mabote², Jennifer Caffarel¹, Emile Kelkboom¹, Ronald Aarts^{1,3}, Erik Korsten^{3,4}, John Cleland²

¹Philips Research, Eindhoven, The Netherlands

²Department of Cardiology, Castle Hill Hospital, Kingston-upon-Hull, UK

³Technical University Eindhoven, The Netherlands

⁴Dept. of Anesthesiology, Catharina Ziekenhuis, Eindhoven, The Netherlands

Aims: This study aims to assess the ability of a wearable bioimpedance monitor to detect variations of thoracic fluid content induced in stable chronic heart failure (HF) and controlled hypertension patients by means of withholding medication and a range of physiological maneuvers.

Methods: Transthoracic spectroscopic bioimpedance measurements using a quadripolar textile electrode arrangement integrated into a vest were acquired under clinical laboratory conditions in outpatients in the context of the EU-funded project HeartCycle (FP7–216695). A measurement session included a range of physiological maneuvers aimed at inducing changes in hemodynamic parameters e.g. posture changes, administration of vasodilators, moderate exercise. HF patients attended two measurement sessions: while following normal medication regime (Condition A) and after omitting medication e.g. diuretics for 48 hours prior to the session (Condition B). Hypertension patients participated in one session while following normal medication regime (Condition C).

The extracellular resistance R_0 of the Cole-Cole model extracted from each spectroscopic impedance measurement was used as the marker for thoracic fluid content. Effects of maneuvers and conditions on extracellular resistance were analyzed with repeated measurements ANOVA. Post-hoc test identified the exact sources of variance.

Results: Data from 8 HF and 9 hypertension patients showed that (1) Physiological maneuvers had significant effect on R_0 : Posture changes from supine and semi-recumbent to sitting resulted in a decrease of 5.87% and 3.49%, respectively. Administration of vasodilators and moderate exercise resulted in an increase of 2.28% and 3.75%, respectively. (2) The effect of medication omission by HF patients before the second visit was an R_0 decrease of 9.41% accounting for the expected fluid buildup. (3) The effect of physiological maneuvers was similar among conditions.

Conclusions: Impedance measurements taken in a consistent position could be used to study therapy effectiveness in HF and hypertension patients.

Further analysis will follow upon study completion (20 HF and 10 hypertension patients)

S94

Detection of Ischemia Using Electromechanical Signals for a Remote Diagnostic Device

Farzad Khosrow-Khavar*, Carlo Menon

Simon Fraser University

Objective - The main objective of this project is to design a portable remote diagnostic device (RDT) for detection of ischemia to be used in rural area where equipment such as echocardiography is not accessible. **Method** - Electrocardiogram (ECG) and seismocardiogram (SCG) signals were used as an input to the RDT for ischemia detection. The ECG signal captures the electrical and the SCG signal captures the mechanical activity of the heart. The SCG signal is extracted by mounting an accelerometer on the chest of the patient. A low pass 30Hz filter is used to extract seismocardiogram from the accelerometer.

It is known that specific peaks of the SCG signal correspond to specific mechanical activity of the heart. In particular, mitral valve closure (MC) and atrial valve closure (AC) can be extracted. The ECG can be used as a reference signal in order to find these peaks. The interval of MC to AC corresponds to the diastolic period and the interval of AC to MC corresponds to the systolic period. The variability of the ratio of the systolic (SYS-HRV) and diastolic (DIA-HRV) period to the heart rate (autoregressive model of order 16), standard deviation of SYS-HRV and DIA-HRV and the square root of mean of the sum of the SYS-HRV and DIA-HRV features were extracted from the SCG signals. Various classifications models such as linear discriminant analysis, random forest, support vector machine and neural networks were used to classify between normal and ischemic patients.

The data were manually annotated for training purposes. **Result**- The following table shows the specificity and sensitivity of algorithms: Table 1 - Sensitivity and Specificity of Various Classification Models

Classification Method	Specificity (%)	Sensitivity (%)
Random Forest	93.3	96.6
Support Vector Machine	86.6	90.0
Neural Network	86.6	93.3
Linear Discriminant Analysis	76.6	80.0

S94

Modeling of Motion Artifacts in Contactless Heart Rate Measurements

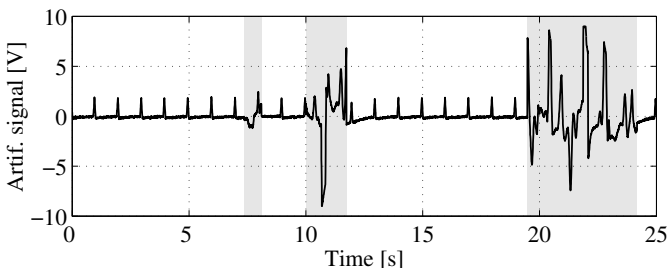
T Wartzek, C Brüser, T Schlebusch, C Brendle, S Santos, A Kerekes, K Gerlach-Hahn, S Weyer, K Lunze, C Hoog Antink, S Leonhardt

Chair for Medical Information Technology, RWTH Aachen University
Aachen, Germany

While contactless vital sign monitoring technologies provide the great opportunity of fast and simple measurements, all these technologies have the unavoidable drawback that they suffer from strong motion artifacts. These motion artifacts may severely disrupt the signal of interest, which could lead to false peak detections and hence, result in false conclusions or diagnoses. Extensive and robust signal processing is needed for a reliable detection of these artifacts.

In this work, a mathematical model of the motion artifacts is derived based on capacitive ECG measurements, as an example for contactless heart rate estimation. It arises that the amplitude distribution of the artifacts follows a t-distribution instead of a normal distribution. The spectrum of the artifacts follows a $1/f^{1.4}$ function in a double logarithmic scale, while the distribution of the lengths of the artifacts follows an exponential distribution.

With the results presented in this paper, it is, for the first time, possible to generate an arbitrary large database of heavily distorted capacitive ECG signals with a selectable percentage of artifacts. This allows to test and verify algorithms for the robust detection of motion artifacts. Since the location of artifacts is a priori known, it can be used as a gold standard for the assessment of the artifact classification algorithms. Analyses have shown, that the presented method is also valid for other types of contactless heart rate measurements (e. g. optical) with only slight changes in the parameters of the distributions.



Artificially generated signal containing undistorted intervals and synthetic artifacts (shaded in grey).

Photoplethysmography-Based Ambulatory Heartbeat Monitoring Embedded into a Dedicated Bracelet

Simon Arberet^a, Mathieu Lemay^a, Philippe Renevey^a, Josep Solà^a, Olivier Grossenbacher^a, Daniela Andries^b, Claudio Sartori^b, Mattia Bertschi^a

^a Swiss Center for Electronics and Microtechnology (CSEM)
Neuchâtel, Switzerland

^b University Hospital Center of Lausanne (CHUV)
Lausanne, Switzerland

Since the introduction of portable devices in 1957 by Dr Holter, ambulatory electrocardiogram (ECG) monitors have been intensely used. Even with important device improvements such as weight, volume and autonomy, these systems are still associated to clinical/ambulatory cumbersome procedures and, therefore have a limited generalized use. The question of this research is the following: what is the performance of a photoplethysmography (PPG)-based device located at the wrist in terms of heart rate variability (HRV) monitoring?

PPG and ECG signals were recorded simultaneously on patients in clinical conditions. Heartbeat (RR) intervals were estimated from both devices. For PPG signals, an approach based on the detection of local minima of the time-derivative was used to estimate RR time series. For ECG signals, a state-of-the-art approach based on adaptive threshold was used (gold standard). The resulting time series of RR were compared in terms of error (mean \pm standard deviation) and distribution using Wilcoxon signed-rank test (hypothesis test for distributions with different median values, rejected with $p > 0.05$). The normalized differences observed on state-of-the-art time-domain and frequency-domain HRV features were also computed (standard deviation of RR intervals (SDRR), powers of very low frequency (VLF), low frequency (LF), high frequency (HF)).

Preliminary results based on 563 minutes of recordings showed an overall agreement 0.17 ± 18.2 ms and a correlation coefficient of 0.987 between PPG and ECG-based RRs ($N=28420$). The hypothesis that both RR distributions have different median values was rejected (p -value=0.59). Regarding HRV analysis, the difference between the PPG-based and ECG-based temporal and frequency features was the following: -0.02 ± 0.02 for SDRR, -0.05 ± 0.21 for VLF, -0.07 ± 0.19 for LF, and -0.03 ± 0.05 for HF.

In view of these preliminary but promising results, it appears that the proposed wrist sensor opens the door towards a new generation of comfortable and easy-to-use cardiac HRV tool especially well adapted for long-term monitoring.

Is Cross-sample Entropy a Valid Measure of Synchronization between the Sequences of RR Interval and Pulse Transit Time?

Chengyu Liu*, Dingchang Zheng, Peng Li, Changchun Liu

Newcastle University
Newcastle upon Tyne, United Kingdom

Synchronization provides an insight into the underlying interaction mechanisms among multivariable physiological signals where their coupling is not known a priori. Cross-sample entropy has been used to quantify their synchronization. However, traditional cross-sample entropy has a poor statistical stability because a rigid decision rule is applied to define the similarity between two vectors. To overcome this limitation, in this study, a fuzzy membership degree function was implemented to redefine the decision rule. Both the traditional and modified cross-sample entropy measurements were then applied to the sequences of RR interval and pulse transit time for both normal subjects and heart failure patients. 10 normal subjects (58 ± 7 years) and 10 heart failure patients (60 ± 6 years) were studied and they were matched by age. Electrocardiograms (ECG) and radial pulses were simultaneously recorded to obtain the sequences of RR interval and pulse transit time (from the R wave peak of the ECG to the foot of the corresponding pulse). Both the traditional and modified cross-sample entropy measurements were applied to the two sequences for each subject. The mean \pm SD of the values from the cross-sample entropy measurements were then calculated and compared between the two groups. The values from the traditional cross-sample entropy measurement showed that there was no significant difference between the two groups (normal 1.96 ± 0.24 vs. heart failure 1.93 ± 0.27 , $P > 0.05$). However, with the modified cross-sample entropy, they were significantly different (normal 2.05 ± 0.23 vs. heart failure 1.94 ± 0.25 , $P < 0.01$). In conclusion, the synchronization between the sequences of RR interval and pulse transit time has been measured by cross-sample entropy, and our modified approach provides a potential solution to understand the different cardiovascular coupling between normal subjects and heart failure patients.

S94

Physiological Feature Analysis in Heart Rate Turbulence using LASSO Model

Óscar Barquero-Pérez*, Rebeca Goya-Esteban, Carlos Figuera, Inmaculada Mora-Jiménez, Arcadi García-Alberola, José Luis Rojo-Álvarez

University Rey Juan Carlos
Fuenlabrada, Spain

Background. Heart Rate Turbulence (HRT) is a relevant cardiac risk stratification criterion. It is usually assessed by turbulence slope (TS) and turbulence onset TO parameters. HRT is known to be affected by several physiological factors, mainly heart rate (HR) and coupling interval (CI). Baroreflex source of the HRT is the physiological hypothesis accepted. However, several studies showed different results about the relationship between CI and HRT.

Objective. Our aim was to propose a LASSO model using CI and sinus cardiac length (SCL), their powers and an interaction term as explanatory variables to account for the physiological dynamic of the TS parameter. **Methods.** We used a database of 61 recording holters from acute myocardial infarction (AMI) patients (Hospital Universitario Virgen de la Arrixaca de Murcia, Spain). The database was split into two groups; low-risk patients ($TS > 2.5$ & $TO < 0$), and high-risk patients ($TS < 2.5$ & $TO > 0$). We performed a feature analysis by means of LASSO paths, in which the regularization parameter is changed from high values, where all weights of the explanatory variables are zero, to small values where all the weights are different from zero. The first variable with a coefficient different from zero were SCL on low-risk patients and the two following were related to CI. Whereas the first variable activated on high-risk was CI and the two following were relate to SCL.

Conclusions. Results from LASSO paths suggest that the influence of physiological variables on HRT is broken on AMI high-risk and completely different from low-risk. Also, the features selected by LASSO model on AMI low-risk are in agreement with baroreflex hypothesis as source of the HRT, in which SCL is the most important variable, and CI has a negative correlation with TS, so that premature VPC implies higher TS values.

A Real Time ECG Preprocessing System Based on ADS1298

Daniel Campillo, Ronny Guardarrama, René González, Jorge Rodríguez, Daniel Jiménez

Central Institute of Digital Research, Havana, Cuba

Aims: Discuss the main characteristics of a real time ECG preprocessing multichannel system whose basic premises are: an improvement on parametric characteristics of ECG signal over previous solutions and compliance with the international standard IEC60601-2-25 {ed2.0} 2011.

Methods: The solution is based on the integrated circuit multichannel high-resolution (24- bits) ADS1298 and the microcontroller MSP430F5529 (16-bit), both from Texas Instruments. This solution is used in electrocardiographs which process 12 bit samples so it was necessary to reduce signal to 12bit/samples. To limit the signal frequency band set by the standard, from 0.05Hz to 150 Hz, digital filters were implemented with integer coefficients that run in real time on the MSP430F5529. Once ECG is acquired a 1st order high pass IIR filter, Butterworth type, with a cutoff frequency of 0.04Hz is applied. Resulting signal is reduced to 12bit/samples using a reduction factor. After a 28th order low pass FIR, Equiripple type, with a cutoff frequency of 150Hz is applied. The ECG acquisition frequency is 500Hz. The solution establishes synchronization with the processing layer by means of a protocol for transmitting ECG signal, the electrode status and the presence of pacemaker.

Results: Three system's prototypes have been made and evaluated according to the standard IEC60601-2-25{ed2.0}2011 successfully. The recovery time has decreased to 1.33 seconds and the Common mode rejection (dB) has been increased to 94.32 in lead I and 93.71 in lead II compared to previous solutions 91.12 in lead I and 90.86 in lead II. The noise level has decreased from 11uV to 9uV.

Conclusions: Developed acquisition system provides improvements in parametric characteristics of the signal with respect to previous solutions. Also it is more compact and reliable so it can be used in different equipment's for real time ECG preprocessing.

PA1

ECGlib: Library for Processing Electrocardiograms

Lars Johannesen*, Jose Vicente, Lorian Galeotti, David Strauss

US Food and Drug Administration
Silver Spring, United States

Since 2005, all new non-cardiovascular drugs have had to undergo a Thorough-QT study, a dedicated clinical study to assess the potential to induce fatal arrhythmias. The US Food and Drug Administration (FDA) has required the digital ECGs recorded during the Thorough-QT study to be uploaded to the FDA ECG Warehouse, which currently houses ECGs from more than 200 Thorough-QT studies. Recently, there have been several research efforts within the FDA to analyze the ECGs collected in these studies for various purposes. In order to analyze these ECGs, it was necessary to develop a framework for this. We developed a framework for loading various ECG formats (currently Physionet, ISHNE and FDA XML HL7) into a common structure that is used in all our methods. Afterwards, we implemented previously developed methodologies for detecting and delineating QRS complexes, performing template-based QRS complex classification and implementing a wavelet-based approach for delineating QRS-T waveforms. The code was written in C++ using open-source libraries. Currently, there is a complete interface for Matlab/Octave and we are working on making an interface for Python and R. We used publicly available databases to evaluate the performance of the implementation of the detector, classifier and waveform delineator. Our implementation performed on par with previously published implementations. The results show that the implemented methods in the library are capable of detecting, delineating and classifying QRS-T waveforms. The developed framework is currently being used for analysis of data from Thorough-QT studies and additional studies. We are currently developing a graphical user interface for evaluation and adjudication of measurements. We believe that frameworks such as the one described in this abstract can be used to facilitate ECG research and we are working to make our framework open-source.

PA1

Sufficient Dimension Reduction for Heartbeat Classification

Long Ma*, Minyi Chen, Lerong Li, Momiao Xiong

University of Texas School of Public Health
Houston, United States

QRS complex is an essential part of ECG signal. Develop accurate QRS complex classification systems is important in clinic management of cardiac disorders. Dimension reduction and feature selection are a key to the successful classification of heartbeat. Sufficient dimension reduction (SDR) and coordinate hypothesis which project the original high dimensional data to very low dimensional space while preserving all information on response phenotypes are important concepts and efficient tools for dimension reduction and feature selection. To explore the morphology of QRS complex, we used the functional principal component analysis to compress the QRS complex signals into a few principal components which can remove the noise hidden in the QRS complex. Using the compressed functional principal component scores we formulated the heartbeat classification problem into sparse SDR problem which is in turn formulated as sparse optimal scoring problem, but with penalty which can remove row vectors from the basis matrix. To speed up computation, we apply the alternating direction method for multipliers to solving the sparse optimal scoring problem. The proposed method was applied to the MIT/BIH database with a total of 2,930 QRS records to classify normal and abnormal heartbeat. We can reach as high as 94.10%, 91.63% and 96.34% average classification accuracy, sensitivity and specificity, respectively, in the test datasets.

PA1

A Switching Feature Extraction System for ECG Heartbeat Classification

Philip de Chazal

MARCS Institute
University of Western Sydney, Australia

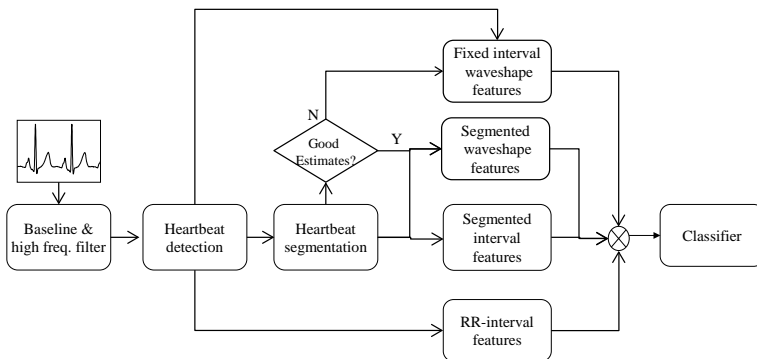
In this study we looked at two methods for extracting ECG waveform features useful for ECG heartbeat classification. The first method (segmented features) sampled the ECG waveform between the QRS and T wave boundary points, calculated QRS and T wave durations, and used RR-interval features. The second method (fixed interval features) used a fixed window to capture the ECG waveform shape and RR-interval features.

Data was obtained from the 44 nonpacemaker recordings of the MIT-BIH arrhythmia database. We investigated the problem of discriminating ventricular ectopic beats (VEB) from non-VEBs and supraventricular ectopic beats (SVEB) from non-SVEBs.

For heartbeats where the QRS and T wave boundaries could be found reliably, the segmented features resulted in higher classification performance than the fixed interval features. When the waveform boundaries could not be found reliably, the fixed interval features performed best. A hybrid approach that used segmented features when waveform boundaries could be reliably found, and fixed interval features otherwise was the most robust solution.

The hybrid approach resulted in a sensitivity of 76%, a positive predictivity of 38%, and a false positive rate of 5% for the SVEB class. For the VEB class, the sensitivity was 78%, the positive predictivity was 82%, and the false positive rate was 1%. These results are an improvement on previously reported results for automated heartbeat classification systems.

PA1



A switching feature extraction system

Cepstrum Feature Selection for the classification of Sleep Apnea-Hypopnea Syndrome based on Heart Rate Variability

Antonio Gabriel Ravelo-García*, Juan Luis Navarro-Mesa, Eduardo Hernández-Pérez, Sofía Martín-González, Pedro Quintana-Morales, Iván Guerra-Moreno, Gabriel Juliá-Serdá

Departamento de Señales y Comunicaciones
Las Palmas de Gran Canaria, Spain

The underlying regulatory mechanisms during apnea are still poorly understood. This fact makes necessary to explore appropriate feature estimation techniques in order to extract as much information as possible. A sequential forward feature selection technique is applied in order to know for one thing, what parameters can extract better information about the influence of breath sleep disorder on the heart rhythm, and on the other hand, trying to detect apneas based on the Heart Rate Variability (HRV) obtained from the electrocardiogram (EKG). 70 EKG recordings have been divided into a learning set and a test set of equal size. Each set consists of 35 recordings, containing a single ECG signal. Each recording includes a set of reference annotations, one for each minute, which indicates the presence or absence of apnoea during that minute. These reference annotations were made by human experts on the basis of a complete polysomnographie. There are two main important properties that make the cepstrum useful. Firstly, contributions to the cepstrum due to periodic structures will occur at integer multiples of the fundamental period. In fact, if the signal under analysis is quasi-periodic the contributions due to periodic structures will occur around the fundamental period. And secondly, contributions due to parameters usually modeled by the filter-type elements will concentrate in the low time lag (quefreny) region. Our results show that these two properties make easy to extract relevant information. An automatic statistical classification method based on Linear Discriminant Analysis (LDA) is applied to the classification of sleep apnea epochs. LDA presents a sensitivity of 80.14% and specificity of 70.11% (auc=0.8395).

PA1

Enhanced Turning Point Algorithm for the Visualization and Printing of Long Term ECG Curves

Sándor Hargittai*

Meditech
Budapest, Hungary

Aims: In the modern ECG signal processing systems the typical sampling rate is 100 to 2000 Hz. However, in many situations we have to reduce the amount of samples preserving the significant morphology features such as peaks, valleys and turning points. For example visualising and printing of the full disclosure ambulatory ECG curves. In these cases diagnostic quality of ECG signal is not necessary but retaining of important turning points is crucial. For solving this problem a very efficient enhanced turning point algorithm was developed.

Method: The original turning point algorithm has been proposed by Mueller. His essential idea was to eliminate one point from every pair of samples preserving the points where the sign of slope of signal is changed. This method gave a compression factor of 2:1. The presented enhanced algorithm provides arbitrary integer reduction in real-time preserving of the peaks, valleys and turning points. The method has been evaluated using CSE, MIT and CTS databases.

Results: The original method allows of compression rate more than 2:1 in several steps, but the factor can be only power of 2. Our method permits of reduction with arbitrary integer factor in one step. We achieved 20 Hz sampling rate for CTS test curves without losing any waves. Disadvantages of the method are not equally spaced sampling and widening of waves. But it does not cause any problems for visualizing and printing long term ECG curves.

Conclusion: A new enhanced turning point algorithm has been presented. It has demonstrated itself a very efficient real-time method suitable to use in visualizing and printing of long term ECG. The fraction reduction factor also can be achieved with previous dilating.

PA1

Proposed New Requirements for Testing and Reporting Performance Results of Arrhythmia Detection Algorithms

John Wang*

Philips Healthcare
Andover, United States

Background: In 1987, AAMI published a recommended practice document for reporting arrhythmia algorithm performance. While the original document seeks to define performance measures that are relevant to the clinical practice, over the years it has become clear that some of the performance measures do not adequately reflect clinicians' experience in using these algorithms for real-time monitoring application. Additional reporting requirements that are more clinically relevant are thus needed. New reporting requirements: 1) Due to the large number of QRS complexes that need to be analyzed (~100,000 complexes/patient/day at heart rate of 70), even an algorithm with high specificity will generate a large number of false-positives. Currently used performance measure, false-positive-rate, only indirectly reflect this fact. A new proposed recommendation is to report the actual number of false-positives/patient/day at heart rates of 70 and 140. 2) Due to the low PVC prevalence in most monitored patients, even an algorithm with high sensitivity and specificity will have a very low positive-predictive-value (PPV). The high PPVs reported using the AHA and MIT-BIH databases (with PVC prevalence of ~9%, and ~8%, respectively) are not clinically relevant. A proposed recommendation is to report PPV for PVC prevalence at rates of 10/hr and 1/hr. 3) Contrary to performance reporting in other applications, the arrhythmia performance measures as specified in the recommended practice do not include performance bounds. A new proposed recommendation is to use the bootstrap method with sample replacement to generate the mean values and 95% confident intervals for all the reported performance measures.

Conclusions: Several statistical measures used for reporting arrhythmia performance do not adequately reflect the actual clinical experience in patient monitoring. Additional performance measures are proposed to further improve the clinical relevance of the reported performance results. These new measurements should be considered for inclusion as part of the standard performance reporting.

PA1

Automatic Classification of Arrhythmic Heartbeats Using Linear Prediction Model

Chun-Cheng Lin, Weichih Hu*, Chun-Min Yang

National Chin-Yi University of Technology
Taichung, Taiwan

Automatic classification of heartbeats is an essential technique for identifying arrhythmic beats from large amounts of data in the long-term ambulatory ECG recordings. It can also provide quantification information for the diagnosis of the risk of arrhythmias or sudden cardiac death such as the presence of ventricular premature beats and nonsustained ventricular tachycardia, and for the further inspection, e.g. long-term heart rate variability and heart rate turbulence. However, the limitation of the automatic heartbeat classification was the variation in the morphologies of ECG waveforms, not only among different patients or patient groups but also within the same patient. This study developed an automatic heartbeat classification system based on the morphological features extracted using linear prediction model with a 10th-order finite-impulse-response and the normalized RR interval features using the averaged heart rate to reduce the effects of the inconsistent heart rates among patients. Three heartbeat types including normal beats, supraventricular ectopic beats and ventricular ectopic beats obtained from MIT-BIH arrhythmia database were tested the performance of the proposed method. The data was divided into training and testing datasets, each containing about 50,000 heartbeats. The training dataset was first used to train the optimized linear discriminant classifier, and then the testing dataset was applied to test the classification performance. The study results demonstrated that the sensitivity and positive predictive value of the proposed method were 91.4 and 99.1% for normal beats, 87.1% and 31.9% for supraventricular ectopic beats, and 83.2% and 77.3% for ventricular ectopic beats respectively. If the RR interval features without normalization were used, the sensitivity and positive predictive value for supraventricular ectopic beats decreased to 77.0% and 31.6%, respectively. The results also show an improvement in comparison with a previous Wavelet-based method.

PA1

Web-based Online Consulting System for Quasi Real-time Consultations of Cardiac Images

Csaba Jenei, Tamás Ivánfai, Bálint Kőszegi, Zsolt Kőszegi*

Institute of Cardiology, Medical and Health Science Centre, University of Debrecen
Debrecen

The authors have constructed a web base consulting program (Online Consulting System: OCS) for cardiac images especially for coronary angiograms. The DICOM movies from the PACS server of the catheterization laboratory are uploaded by secured 128 bit Virtual Private Network (VPN) connection without compression by a “send to DICOM node” command to a mini PACS hosting the OCS. After then the php modul checked the AETITLE + IP source, the communication is taking place on the TCP/IP 104 port. The uploads of the images of one patients takes 1-15 minutes depending on the bandwidth and the size of the DICOM files. After the upload, the movies can be downloaded by a real-time-like speed from any Internet connected place. The secured connection is performed by SSL protocol (https) which identifies the “receiver”. The viewer is based html5, therefore it runs in any browser program without the need for further application; however it is also possible to download the original DICOM files for further evaluations. Tablets and mobiles with the usual platforms can also be used for the consultations, the latter has the advantage in urgent cases, because sending an SMS or E-mail containing the link of the uploaded urgent coronary angiography enables the consultant invasive cardiologist to see immediately the movies on his/her smartphone or tablet or PC. The OCS can integrate the consultations of cardiac imaging modalities (echocardiography, CT, MR, IVUS, OCT) in DICOM forms. Using the OCS also for ECG trace transmission, the system is also useful for prehospital consultations during the treatment of acute coronary syndrome.

PA2

Towards Semantic Interoperability for Cardiovascular Risk Stratification into the Electronic Health Records Using Archetypes and SNOMED-CT

Cristina Soguero-Ruiz, Teresa Quintanilla-Fernández, Luis Lechuga-Suárez, Óscar Barquero-Pérez, José García-Muñoz, Inmaculada Mora-Jiménez, José Luis Rojo-Álvarez*, Silvia Del Castillo-Arrojo, Pablo Serrano-Balazote, Arcadi García-Alberola

University Rey Juan Carlos
Fuenlabrada, Spain

Background. Clinical data exchange between different organizations could be of great value in the field of Cardiovascular Risk Stratification (CVRS) research. Semantic interoperability is an essential key in order to integrate and exchange medical records and to automate the clinician workflow. **Objective.** We present a proposal to smooth out a way towards the exchange of CVRS data, prototyped and focused on Heart Rate Turbulence (HRT), and connecting the Electronic Health Record (EHR) in the Hospital Information System (HIS) of two different hospitals.

Materials and Methods. The same way of representing and storing data, based on CEN/ISO13606 standard for semantic interoperability, is considered for EHR communications. It is proposed to access data from cardiac patients in Fuenlabrada and Arrixaca Hospitals. Starting from a previously developed prototype of HRT ontology, based on the conceptual model of SNOMED-CT in the EHR, an HRT archetype is created, yielding an agreed, formal, and interoperable specification for representing a given clinical entity within EHR. This archetype compiles clinical and ECG signal processing information of 24h Holter recording, in order to have a standard data structure to infer the CVRS in terms of HRT values and of clinical data.

Results. The built archetype achieves: (1) a standardized HRT data structure involving domain specialists; (2) the interoperability in HRT data exchange between the two hospitals; (3) structured HRT recordings for a simple follow up by medical societies and with statistical, research and educational purposes.

Conclusion. Interoperability between heterogeneous systems in Holter recordings for HRT analysis can be obtained by designing a HRT data structure where specialist from different fields work together.

PA2

Information System for Surveillance of Hospital Infections in Cardiac Surgery

Alessandro Taddei*, Giuseppe Rossi, Marina Marchi, Elaine Laws, Stefano Dalmiani, Maurizio Mangione, Stefano Bevilacqua

CNR - G.Monasterio Foundation
Massa, Italy

BACKGROUND: Hospital infections affect significantly morbidity and mortality of both adult and pediatric patients. Particularly in cardiac surgery infection rate ranges from 3 to 10 percent while associated mortality more than 20% has been reported. While the surveillance of infections is challenging Aim of our project was to set up an information system for prospective monitoring of infections since hospital admission. A database for representation of patient care pathway and for characterization of infections is challenging for assessing quality of care and for developing models for risk prediction.

METHODS: According to “Matrix” model (previously reported at CinC) a clinical repository was set up by integration with Hospital Information System (HIS, Oracle RDBMS), applied in all health care activities at our hospital, from diagnostic, intervention and operation reports to medical records. The dataset consists of 159 parameters, concerning patient’s medical history, clinical conditions, cardiac surgery operations, perioperative prophylaxis as well as patient’s follow-up both one month and one year after discharge. Each new patient was enrolled into the repository on the recommendation of physicians discovering or suspecting infection development. Embedded SQL queries allowed to retrieve any information from HIS. Web secure access to on-line patient records and statistics were provided.

RESULTS: Since 2011, 2081 patients undergoing cardiac surgery were enrolled for infection surveillance. Patients were followed-up after hospital discharge (29 died after one month and 22 after one year). Statistical analysis (CUSUM) allowed early detection of infection number over time.

CONCLUSIONS: The developed repository, integrated with HIS, was useful for evaluating care pathways in patients, assessing correlation between infections and mortality and driving improvement of patient care delivery.

PA2

An HTML5-based ECG Viewer

Jesús Daniel Trigo*, Miguel Martínez-Espronedca, Aitor Eguzkiza,
Luis Serrano

Public University of Navarre
Pamplona, Spain

Background: Hospitals and health care systems usually need to install appropriate, ad-hoc software in every computer that requires access to an electrocardiogram (ECG). To work around that problem, some solutions provide the ECGs as images, hindering thereby more advanced features such as, for example, measures over the waveform.

Aims: This project aimed to design, implement and assess the feasibility of an independent ECG viewer requiring no specific software. Besides, further features such as e.g. the capability of making annotations, measurements or zoom, were also design pre-requisites of the system.

Methods: The designed solution was based on web standards. More specifically, HTML5 was used, which combines the fifth revision of the HyperText Markup Language (HTML), the third level of Cascading Style Sheets (CSS), and a number of JavaScript Application Program Interfaces (APIs). Besides, a specific charts library using the HTML5 canvas tag, namely RGraph, was used. A number of tests for different browsers – including desktop, tablet, and mobile browsers – were performed within the framework of the project.

Results: An independent, web-based ECG viewer in compliance with the latest web standards was designed, developed and successfully tested in different browsers.

Conclusions: By using this software, only a web browser (an HTML5-compliant one) is needed. No further, specific software is required. Moreover, the use of the chosen technologies facilitates the creation of complex applications displaying high-performance graphics that previously could only be developed for desktop platforms. Finally, as a web-based platform, ECGs can be visualized anywhere with an internet connection and in different types of devices.

Internet Based ST Map Software: A Web Service, a Decision Support System and an Educational Tool

Raymond Robert Bond*, Dewar Darren Finlay, Daniel Guldenring

University of Ulster
Newtownabbey, United Kingdom

ST segment values from a 12-lead electrocardiogram (ECG) are used to assess patients with suspected myocardial ischemia. The ST segment is assessed through interpretation of ECG complexes either presented on a computerised display or on paper printouts. Given ST segment changes can be missed in busy clinical environments, researchers have proposed alternative methods for visualising ST segment data. One such method is the ST Map and given this has recently been integrated into the clinical environment, we investigated the feasibility of a Web based system that could be used to further the acceptance and understanding of this approach. Methods: An ST Map system was developed using ActionScript 3.0 (a programming language for Adobe Flash). The software uses ST values to display two ST Maps to represent the horizontal and frontal planes respectively. Each ST Map consists of 1mm concentric circles. The user can choose to visualise ST values as vectors or as polygons, which are both generated using simple trigonometric functions. Discussion: The software is available online (<http://tinyurl.com/a7dsvp9>) and can be accessed on any device that supports the Adobe Flash Player. This tool can potentially be used as a decision support system where a user can input ST segment values and use the resulting visualisation to assist in making a diagnosis. This software can also be used as an educational tool for learning the relationship between the ST vector and the ischemic regions. Thirdly, the tool can be used as a Web service by other ECG machines/applications, i.e. an ST Map can be automatically generated by transmitting ST0 values through a REST (HTTP/GET) Web service. ST Maps can then be saved as image files (.PNG). Conclusion: The authors developed ST Map software that can potentially be used as a Web service, a decision support system and as an educational tool.

PA2

Portable Platform Independent Patient Monitoring

Rogier Barendse*, Teus van Dam, Stefan Nelwan

Erasmus MC
Rotterdam, Netherlands

Background and objective: Medical applications are becoming increasingly available on portable devices such as smart phones, tablets and small notebooks in healthcare organizations. However, application development for diagnostic and monitoring purposes on these devices is still limited, because of regulatory requirements and significant development time and complexity for the multiple mobile operating system platforms in use. HTML5 has become a stable and mature platform that is implemented in all major browsers on almost every platform. With the introduction of web sockets and the canvas element, HTML5 could provide the necessary tools to display the patient monitor data in the same fashion as a patient monitor. Our objective was to create a cross-platform patient monitor solution, with the main focus on tablets and test the feasibility of this platform for patient monitoring.

Methods: We developed an HTML5-based portable patient monitoring application to be a cross-platform based solution for a broad range of tablet operating systems (iOS, Android, Windows 8). The application shows the vital signs, curves and trend parameters as a monitor would display. The system could be capable of annunciating and suppressing alarms as well. The backend, running on a web server (IIS7) captures the patient monitor data from the network and sends it to through a web service using the SignalR library. The web service extracts the information and sends it to the clients with SignalR. The client draws the signal and parameter data onto the HTML5 canvas object.

Results: We evaluated the usability of the portable patient monitoring application on the iPad 3, Samsung Tab 2 10.1 and the Windows 8 platform. We tested the main browser on each platform and also the latest version of additional (mobile) browsers as Chrome, Firefox and Opera. All browsers were capable to display the monitor curves and trend parameters.

Conclusion: Platform independent patient monitoring is possible by using standard tablet operating systems and the HTML5 standard without requiring app-development.

PA2

Telemedicine Network for Diagnosis and Care of Congenital Heart Malformations

Alessandro Taddei*, Pierluigi Festa, Nadia Assanta, Tiziano Carducci, Emiliano Rocca, Bruno Murzi

CNR / G.Monasterio Tuscany Foundation
Massa, Italy

Diagnosis and care of congenital heart malformations is usually referred to specialized centers. Given the wide-bandwidth networks, interconnecting today main health institutions, it is conceivable to set up low-cost telemedicine services, from reference hub centers to secondary health centers, providing collaborative diagnosis, care and follow-up of congenital heart malformations (in the fetus, in the newborn or child up to GUCH patient). A new telemedicine network is currently developed in Tuscany, using the regional WAN interconnecting the FTGM Heart Hospital in Massa with the neonatology and prenatal centers. The aim is to provide regular services for collaborative diagnosis and care planning of congenital heart malformations. Using videoconferencing instrumentation, equipped for video signal acquisition from echocardiograph, real-time tele-echocardiography is implemented, as experienced by FTGM in the cooperation with Balkan countries (reported at CinC 2011). Real-time tele-echocardiography during videoconferencing allows the specialist from the hub center to interact with the echo-operator, next to patient at the remote center, guiding correct examination to assure comprehensive diagnostic evaluation. Telemedicine services for elective cases will be regularly scheduled weekly, involving cardiac specialist teams, assisted by nurses and computer technicians, while 24h emergency service will be assured for urgent cases. Quality of care is improved by inter-institutional collaboration and continuity of care across the region is achieved with benefits for patients. Clinicians at secondary center, through collaborative examination and on-line case discussion, will learn faster improving their skillness. Mobility of patients (pregnant women or neonates/infants) will be limited to cases of complexity or urgency. Overall costs for health-care will be reduced saving examinations, hospitalizations and unnecessary transfers.

PA2

Heart Rate Asymmetry in Aortic Valve Stenosis Patients

Monika Petelczyc*, Olga Lipińska, Jan, Jacek Żebrowski, Ewa Orłowska-Baranowska, Rafał Baranowski

Warsaw University of Technology
Warsaw, Poland

Background: Heart rate asymmetry is a measure of the imbalance of the autonomic nervous system activity. The simplest quantification of the heart rate asymmetry is given by a non-equal number of lengthenings and shortenings of RR-intervals in the time series. The most popular measures are related to the geometry the Poincaré plots (more points above the diagonal line than below). But a different approach is based on the Phase Rectified Signal Averaging Method, which initially was used to determine characteristic frequencies from noisy data. Two parameters - deceleration (DC) and acceleration (AC) capacity can be computed from four main anchor points in the PRSA curve. The first parameter seems to be a good prognostic for several cardiac regulation dysfunctions.

Methods: We compute the DC and AC parameters for heart rate variability data measured in 105 patients with aortic valve stenosis (AS) just before surgical replacement of the aortic valve (age 60-71 y). In the study, we use 6-hour nighttime data. We suggest a new definition for the DC (DCn) and AC (ACn) parameters and assessment of their uncertainty. In addition, a novel measure of heart rate asymmetry is introduced based on these two new factors.

Results: The DC and AC parameters as defined by Bauer et al. are not effective factors for risk assessment for the uniform group of patients studied here. On the other hand, the DCn and ACn shows that a better assessment of the ability to lengthen and shorten RR intervals can be obtained. With the new definitions, we obtained essentially increased new values for DC (decreased for AC) in comparison to those obtained from the old definitions (new minimum value: DCn=9.63ms versus DC=2.53ms). Note that $DC < 2.5ms$ indicates increased mortality risk. For high risk AS patients is always $DC > 2.53ms$.

PA3

Analysis of Heart Rate Variability in Elderly Patients with Chronic Heart Failure and Periodic Breathing

Beatriz F. Giraldo, Joan P. Téllez, Sergio Herrera, Salvador Benito.

Universitat Politècnica de Catalunya, Institut de Bioenginyeria de Catalunya and CIBER de Bioingeniería, Biomateriales y Nanomedicina. Barcelona, Spain

Aims: The aim of this study is to analyze the heart rate variability (HRV) in elderly patients with and without chronic heart failure (CHF), and with periodic (PB) and non-periodic (nPB) breathing pattern.

Methods: Electrocardiogram (ECG) and respiratory flow signal were recorded in 36 elderly patients admitted in the short stay unit of the hospital (21 males, 15 females, aged 82 ± 5 years): 18 patients CHF and 18 without CHF. According to the clinical criteria, the patients were classified into the follow groups: 19 patients with nPB pattern, 7 with PB pattern, 4 with Cheyne-Stokes respiration (CSR), and 6 patient non-classified (problems with respiratory signal). From HRV, in time domain, SDANN, SDNN, RMSSD, and SDSD were calculated. Power spectral density of HRV were estimated using modified covariance method, and were characterized on different spectral bands: total power (Tot_P: 0-0.4 Hz), VLF (0-0.04 Hz), LF (0.04-0.15 Hz), and HF (0.15-0.4 Hz).

Results: The most discriminants parameters when comparing patients with and without CHF, were in frequency domain: Tot_P ($p = 0.02$), power of LF ($p = 0.022$), frequency peak (f_p) of HF ($p = 0.021$) and power ratio LF /HF ($p = 0.037$). Comparing nPB vs. CSR patients groups, the best parameters were RMSSD ($p = 0.028$), SDSD ($p = 0.028$), and f_p of HF ($p = 0.016$). When comparing nPB vs. PB patients group no differences were obtained.

Conclusion: Several parameters of HRV frequency domain presented statistical significance differences when comparing patients with and without CHF. The best differences were obtained, when comparing nPB and CSR patients, with time and frequency domain parameters. On the other hand, between nPB and PB patients there were no differences. These results appear to suitable for enhanced diagnosis of decompensated CHF patients, and the possibility to developed periodic breathing, and further, CSR pattern.

PA3

Age Related Changes in Variability of Short-Term Heart Rate and Diastolic Period

Peng Li, Chengyu Liu*, Xin Sun, Yongai Ren, Chang Yan, Zhonghan Yu, Changchun Liu

Shandong University

Previous studies have proved that the heart rate variability (HRV) is preferentially expressed in cardiac diastolic period variability (DPV). Does that mean that DPV analysis should act as an alternative approach for characterizing the autonomic regulation? And do they behave in accordance with each other in all subjects with various ages? Our aim was thus to assess the age related changes in: 1) HRV and DPV through frequency domain analysis, and 2) the interactions between HRV and DPV in a nonlinear coupling analysis framework. Totally 60 healthy subjects were enrolled. Results showed that both LF and HF powers of DPV decreased with the increasing of age (both $p < 0.001$), which behaved generally in the same way with HRV. However, their coupling, especially in terms of short-range correlations ($p < 0.01$), decreased significantly with aging, which suggests that the interactions between HRV and DPV might provide additional valuable information for characterizing the autonomic regulation in aged individuals.

Validation of the Use of Heart Rate Variability Measurements during Meal Intake in Humans

Sebastian Päßler, Alexander Noack, Rüdiger Poll, Wolf-Joachim Fischer

Fraunhofer Institute for Photonic Microsystems (IPMS)
Dresden, Germany

Aims: Food intake is an essential function for a living organism. Analyzing food intake provides an estimation for a healthy or unhealthy lifestyle of a person. Misbalanced eating behavior often is a result from psychological disturbances like mental stress. To plan a proper therapy, the reasons for this misbalance have to be investigated. As the activity of the autonomous nerve system (ANS) affects food intake, this activity should be monitored in combination with food intake to get a deeper insight on eating disorders. This could help to understand the complex interactions between different eating stimuli and food intake. However, the ANS itself is affected by food intake as well. In this study, we aimed to assess the influence of food intake on the heart rate variability (HRV) computed on ECG recordings.

Methods: ECG recordings of 27 participants were taken before, during and after a short meal session. 11 different HRV parameters were calculated as a measurement of ANS activity in these three phases. For the calculation, a trained cardiologist manually selected segments of 2.5 minutes duration without disturbances. Using Wilcoxon-test and Mann-Whitney-U-test we analyzed the HRV parameters for inter-individual similarities.

Results: Based on the HRV parameters SDNN, RMSSD, pNN50 and total power clusters could be formed. In the biggest cluster, the values of these parameters tended to decrease during food intake and increased afterwards ($p < 0.005$). In a second cluster, these HRV values increased from the resting period to the eating period and from the eating period to the second resting period ($p < 0.05$).

Conclusions: The formation of clusters on HRV trends showed that food intake influences the ANS activity in a defined way. The identification of ANS alterations caused by stress should be noticeable. HRV parameters can therefore be used in simultaneous measurements of the eating behavior and the ANS activity.

PA3

Combining HRV Features for Automatic Arousal Detection

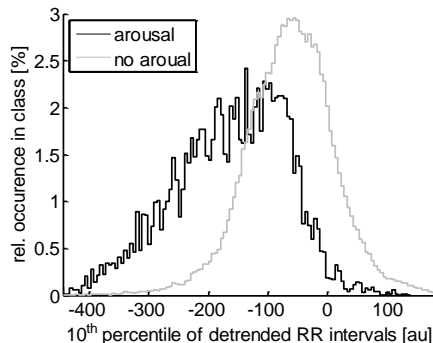
Jerome Foussier*, Pedro Fonseca, Xi Long, Berno Misgeld, Steffen Leonhardt
RWTH Aachen University, Aachen, Germany

Aims: Arousals are vital for sleep as they ensure its reversibility. However, increased occurrence of arousals might indicate sleep disturbances or disorders. Physiologically, arousals usually lead to a sudden increase in heart rate, in blood pressure and in pulse arterial tone (PAT). It has been shown that arousals can be detected automatically with less obtrusive sensing modalities, such as respiratory, actigraphy or cardiac. Therefore, we develop and adapt known features solely based on ECG which allow the automatic, accurate detection of arousals during sleep.

Methods: For this work, arousal events and sleep stages in polysomnographic data of 15 subjects with healthy sleep were annotated by sleep technicians according to the AASM guidelines. Based on the observation that arousals affect the heart rate variability (HRV), 72 HRV features were extracted from the ECG signal in the time and frequency domain with a time step interval of one second. The discriminating power of each feature in identifying the presence or absence of arousals was evaluated using the multivariate analysis of variances (MANOVA). A feature selection (FS) algorithm based on Mahalanobis distance (MD) ranking was used to reduce the feature space.

Results: Changes in the cardiac signals are visible in the time- and in the frequency-domain. For the first ranked feature of the FS (10th percentile of detrended RR intervals) a χ^2 -test value of 16633 (df=1, p<0.001) with MD=1.16 has been found (significance level $\alpha=5\%$). Combining the best 20 features chosen by FS, leads to an improved χ^2 -test value of 33117 (df=20, p<0.001) and MD=3.75.

Conclusion: It is shown that the combination of multiple known HRV features on a one second basis improves arousal detection capability compared to a single feature. Being able to detect arousals automatically and non-obtrusively has the potential to introduce new screening and diagnosis techniques for sleep related disorders.



PA3

OSAS Severity is Associated to Decreased Heart rate Turbulence Slope

Giovanni D'Addio*, Mario Cesarelli, Maria Romano, Alberto De Felice

S. Maugeri Foundation
Telese Terme, Italy

Obstructive sleep apnea syndrome (OSAS) has been associated to impaired baroreflex sensitivity (BRS) which has recently been shown to be non-invasively assessed by heart rate turbulence (HRT) analysis. Although HRT seems to be better suited than traditional heart rate variability indexes for autonomic assessment in presence of respiratory and arrhythmic disorders, very few papers addressed its evaluation in OSAS. Aim of the study is to find out whether and to which extent HRT is associated to OSAS severity. HRT consists of sinus cycle length fluctuations following spontaneous isolated VPC composed by an early rate acceleration phase, namely turbulence onset (TO), and by a late deceleration phase, namely turbulence slope (TS). We studied HRT in polysomnographic recordings of 82 mild ($5 < \text{AHI} < 15$), 74 moderate ($16 < \text{AHI} < 30$) and 65 severe ($\text{AHI} > 30$) OSAS pts. (age 62 ± 14 , 71% males). Results showed that, while TO values did not significantly differ between mild ($-0,78 \pm 1,50$), moderate ($-0,89 \pm 1,78$) and severe ($-0,70 \pm 1,28$) pts., TS significantly decreases (Kruskal-Wallis P value < 0.05) from mild ($3,27 \pm 2,7$) to moderate ($2,6 \pm 2,6$) and severe ($1,98 \pm 2,5$) pts., with a significant Dunn's multiple comparisons post test only between mild vs. severe OSAS pts. Data indicate that the main BRS alterations do not appear in the early HRT phase triggered by transient vagal inhibition, with $\text{TO} < 0$ normal values in mild to severe pts., but during the slow one, due to the sympathetic hyperactivity affecting the heart rate recovery, with $\text{TS} < 2.5$ abnormal values associated to increasing OSAS severity. These findings support the conclusion that HRT assessment could have a prognostic value related to the development of cardiovascular disease in OSAS.

PA3

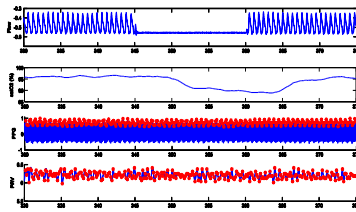
Obstructive Sleep Apnea in a Rat Model: Effects of Anesthesia on Autonomic Evaluation from Heart Rate Variability Measures

Raimon Jané, Jesús Lázaro, Puy Ruiz, Eduardo Gil, Daniel Navajas, Ramon Farré, Pablo Laguna

Institute for Bioengineering of Catalonia (IBEC)
Barcelona, Spain

Aims: Rat model of Obstructive Sleep Apnea (OSA) is a realistic approach for understanding and studying physiological mechanisms involved in sleep apnea. Rats are usually anesthetized and therefore autonomic nervous system (ANS) could be blocked. This study aimed to assess the effect of anesthesia on ANS activity during OSA episodes and therefore to assess the validity of the model to extrapolate results to unanesthetized OSA.

Methods: Six male Sprague-Dawley rats (390 - 465 g) were anesthetized intraperitoneally with urethane (1g/kg). The experiments were conducted applying airway obstructions, simulating OSA episodes. Recurrent 15s-apnea episodes for 15 minutes intervals, with a subsequent resting period of 15 minutes were used. Apnea index of 20, 40 and 60 apnea/hour were applied. Five signals were simultaneously acquired: respiratory pressure and flow, SaO₂, ECG and photoplethysmography (PPG). In total, 210 apnea episodes were studied.



Respiratory Flow, SaO₂, PPG and PRV signals during a 15s-apnea episode.

Power spectrum of Pulse Rate Variability (PRV) was analyzed in the appropriated bands for a rat model: 0.04-1 Hz for Low Frequency (LF) and 1-3 Hz for High Frequency (HF). Normalized LF and HF bands were calculated for each episode in consecutive 15s intervals (before, during and after the apnea).

Results: All episodes showed changes in respiratory flow and SaO₂ signal (desaturation <90%). Conversely, decreases in the amplitude fluctuations of PPG (DAP) were not observed during apnea episodes. Normalized LF presented extremely low values during breathing (median=7,66%), suggesting inhibition of sympathetic system probably due to anesthetic effect. Although subtle increases of LF were observed during apnea (median=8,00%), no significant differences were found in both LF and HF.

Conclusion: This rat model is suitable to study the consequences of OSA in respiratory pattern, but anesthetic effects can limit assessment of ANS response. Consequently, HRV and PPG analysis during apnea could be an indirect tool to assess the effect and deep of anesthesia.

Pulse Rate Variability in Children with Sleep Disordered Breathing in Different Sleep Stages

Parastoo Dehkordi, Ainara Garde, Walter Karlen, J. Mark Ansermino and Guy A. Dumont

Electrical and Computer Engineering, Faculty of Applied Science
University of British Columbia, BC, Canada

Aim- The main objective of the study is to observe the heart rate response of the autonomic nervous system in children during sleep and sleep disordered breathing (SDB) by analysing the variability of heart rate derived from the photoplethysmogram (PPG) signal (Pulse Rate Variability (PRV)). PPG is recorded by an oximeter sensor connected to a mobile phone (phone oximetry).

Method- Pulse to pulse intervals of the PPG signal were converted to a tachogram. Mean and standard deviation of all PP intervals (SDNN) and the square root of the mean squared differences of successive PP intervals (RMSSD) were estimated in time domain. For spectral analysis, an autoregressive model was applied to the evenly sampled tachogram and low (LF) and high (HF) frequency components and LF to HF ratio (LF/HF) were estimated. For both time and frequency domain, analysis was performed using a 1-min sliding window with 50% overlap. All annotated periods of NREM and REM sleep were analysed separately for the subjects with and without SDB.

Database- The database contains the sleep studies of 72 children referred to the BC Children's Hospital for PSG in addition to the PPG signals recorded simultaneously for each subject with the phone oximetry.

Result- The results show the increase in the LF/HF ratio in the SDB group in both REM and NREM sleep compared with the normal group. For both normal and SDB groups, REM sleep shows increased LF/HF ratio in comparison with NREM sleep. Increased LF/HF ratio may indicate increased sympathetic and/or decreased parasympathetic activities.

Conclusion- This study shows the feasibility of using the phone oximetry PPG signal for observing the contribution of sympathetic and parasympathetic activities in controlling heart rate in children during sleep and SDB.

Table 1. Parameters of PRV in sleep and SDB

	NREM			REM		
	SDB	Normal	P-value	SDB	Normal	P-value
RMSSD	0.11	0.07	< 0.01	0.09	0.07	< 0.05
Normalized LF	0.31	0.29	ns	0.42	0.37	ns
Normalized HF	0.53	0.57	ns	0.43	0.46	ns
LF/HF Ratio	0.96	0.67	< 0.01	1.5	1.1	ns

PA3

Heart rate variability analysis of pre and post awakening of 10 years children

Taher Biala*, Syamil Muhammad, Michael Wailoo, Fernando Schlindwein

University of Leicester
leicester, United Kingdom

It is well known in clinical practice and research that sudden cardiac death (SCD) has high occurrence around the wake up time. There is much interest in finding indicators which could help stratify a person's risk for SCD at a young age. This work analyses the heart rate variability (HRV) during one hour pre- and post-wakening from intra-uterine growth restricted (IUGR) children against healthy children. The RR signal of a unique set of data was tested. IUGR children represents 44 of the cohort and 31 are normal. The analysis consists of detecting the start of the day and night by specifying an RR threshold. When the threshold value is reached the algorithm marks the start of the day and night. The RR signal was subjected to cubic spline interpolation and fast Fourier transform was computed for every 5 min segment along the 1 hour before and after wakening. Welch method was used to calculate low frequency, high frequency, and low over high frequency components of the signal. The results of all frequency domain indices were calculated for the 75 children and a t-test was used to compare between the two groups of children and between boys and girls. Table 1 shows that the p value is significantly different between HRV indexes of IUGR and normal before wakening up (wake up after segment 12), and between males and females, possibly suggesting an increased risk of SCD.

PA3

Detection of Cardiac Autonomic Neuropathy using Linear Parametric Modeling of QT dynamics

Mohammad Hasan Imam*, Chandan Karmakar, Ahsan Khandoker, Herbert Jelinek, Marimuthu Palaniswami

University of Melbourne
Melbourne, Australia

Model-based signal processing is a promising advancement in the description of the regulation of physiological systems (e.g., cardiovascular system) controlled by external and internal factors such as respiration, stress and autonomic nervous system. QT-RR modelling is used in various fields such as the evaluation of drug safety, determining QT adaptation patterns with rapid HR changes and effect of alteration of autonomic nervous system on heart rate. One of the serious clinical complications of diabetes is cardiac autonomic neuropathy (CAN) which gradually causes damage to the autonomic nerve fibers that innervate the heart and blood vessels, resulting in abnormalities in heart rate control and vascular dynamics. The main objective of this study is to investigate whether QT-RR modelling could be used for the detection of cardiac autonomic neuropathy. In this study, first 250 beats of 20 minutes ECG signal collected from total 32 subjects (20 with no CAN (CAN-) and 12 with definite CAN (CAN+)) were used to model QT dynamics using ARXRRAR and ARXRR XEDRAR model. The results showed that, compared to ARXRRAR model, inclusion of respiration increases the model fit for both QT_{peak} and QT_{tend} dynamics. Moreover, the tri-variate (ARXRR XEDRAR) model significantly differentiates the model fit values between CAN- and CAN+ groups. This indicates that the effect of respiration on QT dynamics is different in CAN- and CAN+ group. Since, the model fit values of CAN- group is higher than CAN+ group, it can be concluded that respiration better estimates the QT dynamics of subjects in CAN- group than CAN+ group.

PA3

A New Methodology for Nonlinear Heart Function Analysis: Studying Just the Beat Morphology

Constantino* A. García, David G. Márquez, Abraham Otero, Jesús Presedo, Paulo Félix

Centro Singular de Investigación en Tecnoloxías da Información (CI-TIUS), University of Santiago de Compostela, Santiago de Compostela, Spain

Aims: Nonlinear analysis techniques have been used to study the RR series –which only contains RR interval information–, and the ECG –which contains both RR interval and beat morphology information. It is still an open issue whether the RR series is chaotic or stochastic. Nonlinear properties of ECG are less controversial, but ECG nonlinear analysis is very resource intensive due to its large data volume. Both RR and ECG nonlinear analysis usually achieve phase space (PS) reconstruction by the delays method. We tried to achieve PS reconstruction through a different method: using only beat morphology information –thus avoiding possible PS contamination from stochastic components of the RR intervals.

Methodology: PS vectors were built using parameters derived from each beat's morphology. Two different approaches were tested: beat segmentation –PS vector components are features such as PQ segment, QRS width and height...– and Hermite representation of the beat –PS vector components are Hermite polynomial coefficients. To find the proper embedding dimension – i.e. the vector's length– the number of vector components was increased until the slope of the scaling regions saturated in the correlation sum. This occurred for embedding dimension of 12 or more in the Hermite PS –i.e., proper PS reconstruction was achieved. No saturation in the correlation sum was found in the beat segmentation PS. This is consistent with these PS vectors being too noisy for proper attractor reconstruction due to inaccuracies in beat segmentation.

Results: Several nonlinear statistics were calculated from the Hermite PS for the 30 recordings of the Normal Sinus Rhythm and the Congestive Heart Failure databases. Many of these statistics presented statistically significant values for both databases. Just by establishing a threshold on the length of the maximum vertical line of the recurrence plot, sensitivity 100% and specificity 87% were achieved when classifying the recordings.

Gender Comparison of Heart Rate Variability in Epileptic Seizures

Soroor Behbahani*, Nader Jafarnia Dabanloo, Ali Motie Nasrabadi

Islamic Azad University
Tehran, Iran (Islamic Republic of)

The analysis of the heart rate variability (HRV) has been used to assess autonomic control of heart rate especially in diabetes, chronic heart failure and epilepsy. The purpose of this study was to investigate sex-dependent changes of heart rate variability (HRV) in epileptic patients. Our results indicate that HR variables of seizures in females were significantly less than males which represent the lower sympathetic influence on the heart during ictal phase in females compared to males.

PA3

Heart Rate Variability Associated with Different Modes of Respiration during Zen Meditation

Masaki Hoshiyama*, Asagi Hoshiyama

Meisei University
Kamakura-shi, Japan

Zen is a traditional meditation method which utilizes unification of body, respiration and mind. Zen is spreading widely into western world today, realizing deeper meditation with minimum body movement and distraction. While heart rate variability (HRV) during controlled breathing by the subject has been studied in the past, there remains a lack of consensus whether heart rate during Zen practice elicit consistent HRV differences for different modes of respiration. To better understand the effect of respiration modes on hemodynamic events elicited by deep Zen meditation during Zazen, we studied heart rate in 2 intermediate Zen meditators. The study took place over 9 sets of Zen meditations in a quiet, Zen practice hall. Each set of Zazen lasted at least for 25 minutes. The first sets were used for habituation, and the data obtained from the following eight sets were used for analysis, where 2 modes of respiration, i.e., fast inhalation followed by slow exhalation (FISE) and slow inhalation followed by fast exhalation (SIFE), were allocated alternately. Power spectrum analysis showed distinctive change in frequency components. Very low frequency (VLF) components decreased for FISE ($p=0.05$). Most notably, detrended fluctuations analysis (DFA) of HRV were around 1/2 for FISE and 0.74 for SIFE. During Zen practice, we seat ourselves in a lotus posture, practice Tanden respiration, i.e., lower abdominal breathing, and keep mind free from specific state of consciousness. We attribute the decrease of VLF components and DFA exponent in FISE to the spontaneous and passive regulation of respiratory muscles during slow exhalation, as contrasted with the active use of respiratory muscles during slow inhalation in SIFE, hence to the effective regulation of mind during meditation toward the edge of sleep, but not quite over it. This result suggests the possibility of HRV as a handy and quantitative evaluator for Zen meditation.

PA3

Ageing of ECG Characteristics at Five Years Distance

Neus Carmona*, Juan Carlos Rúa-Seoane, Jorge Elorza, Edurne Sáenz de Pipaón, Jean Bragard

Universidad de Navarra
Pamplona, Spain

Aims: The aim of this work was to design an application which analyzes ECG signals in order to find indicators related to potential heart pathologies in young population. Our objective was to compare the ECG signals from a sample of population (17 men, 31 women) between 18 and 22 years old at a certain time and five years later to find significant differences between the recorded signals.

Methods: 52 people's ECG signals with recorded sampling rate 10 kHz were obtained and examined in two temporal series of 5 minute duration: firstly in 2002, secondly in 2007. For each patient and each year two different data were registered, the first one at rest and the second one after a mild effort. Therefore, a total of 208 electrocardiographic signals were examined by computational techniques in order to extract the RR and QT intervals. Then, we compared the data using first return maps and measured the covariance ellipses. Data with too much noise were excluded from the analysis leaving a sample of 48 people. Relations between each of the four data series were studied. The statistical analysis was done using the Kruskal-Wallis and Mann-Whitney tests for non parametric statistics. It also included the gender and the categorical aspect "practicing sport".

Results and conclusions: 1. Young population showed a significant reduction of the area of the ellipse after an ageing of 5 years. 2. This decrease was more significant for the interval RR than for the QT intervals. 3. The area reduction was more important in the effort state signals than in the registers at rest. 4. Women were more affected by this area reduction than men. 5. "Not practicing sport" also showed a more significant area reduction.

PA3

Discrimination of Heart Arrhythmia using Novel Features in Heart Rate's Phase Space

Sadaf Moharreri*, Shahab Rezaei, Hossein Ajorloo

Khomeini Shahr Branch, Islamic Azad University
Isfahan, Iran

In today's world, death rate due to heart diseases is a major threat to human beings, so early diagnosis of cardiac arrhythmia is very important. Various Signal processing methods have been applied to improve the accuracy for the detection of ECG arrhythmia. In this paper, we try to recognize and distinguish different groups of arrhythmia using novel features which have been obtained from the heart rate's phase space in recent years. We used Triangular Phase Space Mapping (TPSM) which is obtaining by using RR interval time series signal consist of all the ordered pairs: $(\overline{RR}_i, \text{abs}(\overline{RR} - \overline{RR}_i))$, $i=1, \dots, N$ where \overline{RR} is the mean of RR intervals. In the other mapping, Parabolic Phase Space Mapping (PPSM) which consists of ordered pairs: $(RR(i), (\text{mean}(RR) - RR(i+1))^2)$ is used estimating a two degree polynomial equation in the form of $y = Ax^2 + Bx + C$. For recognition, we used three groups of 15 subjects using the Physionet database (Arrhythmia, Congestive Heart Failure (CHF), and Atrial Fibrillation (AF)) with Normal Sinus Rhythm (NSR). Kruskal-Wallis test which is a nonparametric version of ANOVA analysis distribution was used to define the level of significance of each feature for different groups of subjects in cardiac arrhythmia diagnosis. The results show that these features in both mapping have significant effect on arrhythmia detection. For instance, the obtained features discriminate arrhythmia from NSR by $p < 10^{-5}$; CHF from NSR by $p < 10^{-4}$; AF from NSR by $p < 10^{-5}$; CHF from arrhythmia by $p < 10^{-2}$; CHF from AF by $p < 10^{-4}$; and arrhythmia from AF by $p < 10^{-3}$. The results show that PPSM is more useful in detection of cardiac arrhythmia from normal, while TPSM is more effective to recognize different arrhythmia from together.

PA3

Study on the Generalized Hurst Exponents Optimal Use to Estimate Noninvasively Atrial Fibrillation Organization

M Julián¹, R Alcaraz², JJ Rieta¹

¹Biomedical Synergy, Electronic Engineering Department, Universidad Politécnica de Valencia, Spain

²Innovation in Bioengineering Research Group. University of Castilla-La Mancha, Cuenca, Spain

The Generalized Hurst Exponent $H(q)$ relates to the existence of long-term self-dependencies in the autocorrelation function of a time series. In this work, the optimal use of $H(q = 2)$ in the study of Atrial Fibrillation (AF) organization from noninvasive ECG recordings has been analyzed. 60 signals from the Physionet AF Termination Database, classified as non-terminating (N) and terminating (T) were studied. After preprocessing the signals, the atrial activity was extracted via adaptive QRST cancelation.

First, the optimal data length was determined by computing $H(2)$ over all non-overlapping segments of the signals ranging from 30 to 1 second and then the average value over the whole recording was obtained. Next, the application of a previous band-pass filtering step was assessed to reduce noise and ventricular residua in the signal. Two different filters were proposed: a 3 to 9 Hz band-pass filter and the extraction of the main atrial wave (MAW) using a band-pass filter centered on the dominant atrial frequency. Finally, the optimal recording length to compute $H(2)$ was determined analyzing a gap of the last seconds of the signals and using, as computational parameters, the optimal segment length together with the optimal filtering stage.

Results indicated that the optimal segment length to compute $H(2)$ is 15 seconds, providing an accuracy of 71,66%. In addition, the use of band-pass filtering improved the performance. Thus, classification accuracy increased up to 91,67% with the 3-9Hz filter and reached 95% with the MAW filter, which notably outperforms most of the previous studies on the same database. Finally, the total recording length had lower influence, but the highest performance was obtained by considering the last 15 seconds of each recording, thus proving its applicability to short ECG recordings. Therefore, $H(2)$ is able to discriminate organization-dependent AF signals and it can be proposed as a promising alternative to non-invasive organization estimation in AF.

PA4

Point Process Modeling of R-R Interval Dynamics during Atrial Fibrillation

Marianna Meo*, Vicente Zarzoso, Olivier Meste, Decebal G Latcu, Nadir Saoudi, Riccardo Barbieri

Nice Sophia Antipolis University
Sophia Antipolis Cedex, France

Atrial fibrillation (AF) is the most common arrhythmia, and one of the main causes of ictus and strokes. Effective treatments for AF are still unknown, as its effects on the heart substrate have not been clearly quantified yet. One of the main lines of investigation aims at characterizing ventricular response by looking at its effects on heartbeat interval dynamics. Most of the standard approaches have focused on RR interval (RRI) histogram parameters albeit with several shortcomings, such as bin width dependence or lack of attention to the time-varying dynamical structure. In this study, we model heartbeat interval series as a history-dependent inverse Gaussian (HDIG) point process where the history for each RRI prediction is a linear regression of the previous RRIs. As opposed to classical nonparametric methods, the heart rate (HR) variability features derived from the proposed parametric model provide a physiologically more consistent characterization during AF, and can clearly discriminate AF from sinus rhythm (SR) subjects. Analysis of 36 patients affected by persistent AF and 18 controls shows that RRI distributions are more right-skewed and affected by higher variability during AF (skewness of 0.63 ± 0.29 in AF and of 0.17 ± 0.16 in SR, $p=7.6 \times 10^{-8}$; HR standard deviation of 18.73 ± 10.64 bpm in AF and 4.66 ± 4.75 bpm in SR, $p=2.3 \times 10^{-6}$). Our results demonstrate that we can extract valuable information associated with AF from RRI series by using a point process framework.

PA4

A Support Vector Machine Approach for Reliable Detection of Atrial Fibrillation Events

Roberta Colloca*, Alistair EW Johnson, Luca Mainardi, Gari D Clifford
Lamezia Terme, Italy

There is a continued need to provide clinicians with accurate and reliable methods to detect asymptomatic atrial fibrillation (AF). Several ECG-based algorithms have been described in the literature, but no open comparison of features on out of-sample data is available. In this work, ten RR features were selected; CosEn, SampEn, AFEvidence, OriginCount, PACEvidence, IrregularityEvidence, median heart rate, minimum RR interval, mean RR interval and MAD. We assessed the classification performance of the features both univariately and when combined using a Support Vector Machine (SVM) using a radial basis function. The MIT-BIH Atrial Fibrillation database was used as the training set, and the MIT-BIH Normal Sinus Rhythm database and the MIT-BIH Arrhythmia database were used for out-of-sample test performance assessment. During the training phase, the optimal window length (i.e. the number of beats required for accurate detection) was determined using cross validation. A grid search was employed to optimize SVM's hyper-parameters. On the held out fold of cross-validation the SVM showed a Sensitivity (Se) of 99.07% and a Positive Predictive Value of 98.27%. These results exceeded all other results published in the literature, which are confined to in-sample results. During independent testing on the MIT-BIH Normal Sinus Rhythm database the SVM gave a better Specificity (Sp=99.77%) than the three best single features: AFEvidence (Sp=99.39%), MAD (Sp=98.37%) and CosEn (Sp=94.58%). The SVM also provided a Sp=100% on series 100 of the MIT-BIH Arrhythmia database and a Sensitivity of 100% on series 200 of the same dataset, higher than CosEn (Se=99.19%), AFEvidence (Se=99.12%) and MAD (Se=97.62%). A good Specificity (Sp=80.86%) and Accuracy (Acc=84.53%) was also obtained. In conclusion, fusion of AF-related features using machine learning provided a best-in-class model to detect AF and could be considered for AF screening applications.

PA4

Measures of Right Atrial Organization as a Means to Select Candidates for Sinus Rhythm Restoration by Catheter Ablation

Andrea Buttu*, Andrei Forclaz, Patrizio Pascale, Philippe Maury, Anne Rollin, Jean-Marc Vesin, Etienne Pruvot

Swiss Federal Institute of Technology
Lausanne, Switzerland

Purpose: Stepwise catheter ablation (step-CA) can terminate long standing persistent AF (LS-pAF) within the left atrium (LA) or may require additional right atrial (RA) ablation, but predictive parameters of procedural success are lacking. We hypothesized that the variability of interbeat intervals (IBI) of RA and LA EGMs as a measure of AF organization before step-CA is lower in LA terminated (LT) patients (pts) compared to RA terminated (RT) and non terminated (NT) pts. Methods: 24 consecutive pts (60 ± 7 y, LS-pAF duration 19 ± 12 m) underwent step-CA consisting in pulmonary vein isolation and LA ablation, followed by RA ablation if NT. Multipolar catheters were placed into the RA (RAA) and LA (LAA) appendages. Time series of RAA and LAA IBI were resampled at 20 Hz and their variability was characterized using the power spectrum mean frequency (μF) and variance (σF), and compared to RAA and LAA AF cycle length (AFCL). Results: LS-pAF was terminated in 79% (19/24) of the pts: 17 LT, 2 RT and 5 NT. RT/NT pts were pooled and their results compared to LT pts. The figure shows before ablation that LT pts display longer bi-atrial AFCL, similar LAA but lower RAA μF and σF compared to RT/NT pts. Conclusion: pts whose LS-pAF is terminated within the LA display a lower variability of RA IBI suggestive of a higher bi-atrial organization compared to RT/NT pts. Parameters of RA organization in LS-pAF may help to select best candidates for restoration of sinus rhythm by step-CA.

PA4

Different Definitions of Complex Fractionated Atrial Electrograms do not Concur with Clinical Perspective

Tiago P. de Almeida, João Salinet Loures Jr., Gavin S. Chu, G. André Ng, Fernando S. Schlindwein

University of Leicester,
Leicester, UK

Introduction: Complex fractionated atrial electrograms (CFAEs) are potential targets for ablation for persistent AF, but there is no consensus on its definition including among different commercial systems. This study aimed to quantify the impact of different CFAE definitions on automated CFAE detection, when compared to visual assessment.

Methodology: Pre-/post-ablation bipolar electrograms (50 s duration; bandpass 30-250 Hz; notch 50 Hz) recorded from a decapolar catheter placed into the coronary sinus from six longstanding-persistent AF patients were analysed in different time windows (2.5 s, 5 s and 8 s). Caution was taken to exclude electrograms with ventricular far-field. Automatic CFAE detection algorithm based on selected (peak-to-peak \geq 0.05 mV; slope duration \geq 10 ms) negative deflections (-dV/dt) was developed. CFAE_{mean} was defined as the mean time interval between local deflections in a time window. Three different CFAE definitions, as described in the literature, were evaluated. Electrograms were considered fractionated if CFAE_{mean} fell within the following limits: (1) CFAE_{mean} \leq 120 ms; (2) 30 ms \leq CFAE_{mean} \leq 120 ms; (3) 50 ms \leq CFAE_{mean} \leq 120 ms. CFAE_{mean} for each definition were compared on pre-/post-ablation electrograms groups. Electrograms segments were labelled as fractionated or non-fractionated according to the CFAE_{mean} thresholds for each definition, followed by a blinded visual inspection of a clinician. An ‘error (%)’ was quantified based on the disagreement between clinician inspection and the labels from definitions.

Results: Electrogram window size did not affect CFAE_{mean}. However, different CFAE definitions influenced CFAE_{mean} significantly on both pre-/post-ablation groups ($p<0.0001$ and $p<0.02$) (Figure A). Definition 3 using 5s windows presented the smallest error when confronted with visual inspection (34%). The error between visual inspection and remaining two definitions was bigger than 50% and 38% for definition 1 and 2, respectively, considering all pre-/post ablation electrograms (Figure B).

Conclusion: Although non-subjective automated algorithms are appreciated in clinical practice, different CFAEs definitions might influence clinical ablation strategies.

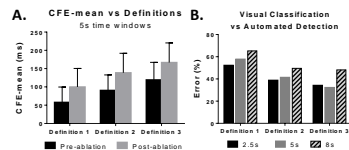


Figure A. CFAE_{mean} pre-/post-ablation 5s time window. B. Error (%) between definitions and visual inspection

PA4

Assessment of Cycle Lengths during Human Atrial Fibrillation using Phase Information from Electrocardiographic Imaging Signals

Adam Quotb*, Guillaume Attuel, Carole Pomier, Yuki Komatsu, Pierre Jäis, Meleze Hocini, Michel Haissaguerre, Rémi Dubois

Lyric
Pessac, France

Background: Cycle Length (CL) measurement is considered an efficient way to monitor Atrial Fibrillation (AF). Routinely, CL mapping using contact catheters in the atria provides indications on the localization of regions involved in AF. Particularly, this technique assists practitioners to identify the driving chamber (right or left), fast regions, and AF complexity. In this study, we propose a non-invasive mapping of CL (niCL) using phase information extracted from electrocardiographic imaging signals (ECGI). niCL mapping provides a real-time bedside ablation planning, prior to the catheter exploration. The aim of this study is to validate the method by finding a direct correlation between endocardial measurements of the CL (enCL) and niCL mapping.

Methods: The unipolar potential on the surface of the atria are estimated from the 252 body surface recordings by solving the inverse solution with standard algorithm. A phase mapping is computed with post-processing, which is justified by the search of pseudo periodic events during AF. The performance of the algorithm is evaluated in N=73 patients (mean age: 59, minimum age: 21, maximum age: 79) who underwent AF ablation (mean AF duration: 8.6 month). niCL were mapped bedside within an hour prior to procedure. enCL were measured in left and right appendages as routinely done during AF mapping. Other regions identified as involved in AF mechanisms have also been tested (Total region number: 16).

Results: niCL and enCL are well correlated in both appendages (RAA: $r=0.88$, $p<0.0001$; LAA: $r=0.91$, $p<0.0001$). These results are confirmed in the other regions ($r=0.89$, $p<0.0001$). This study together with recent case-reports supports the reliability of this technique in providing guidance information prior to ablation procedure of AF.

PA4

Atrial Fibrillation Quantification by Implantable Leadless Device Equipped with Automatic Remote Monitoring

Amarild Cuko*, Daniele Giacomelli, Massimo Saviano, Diego Grassini, Alessia Pappone, Andrea Petretta, Raffaele Vitale, Luigi Giannelli, Cristiano Ciaccio, Mario Baldi, Gabriele Vicedomini, Carlo Pappone

Maria Cecilia Hospital, GVM Care & Research, Cotignola (RA), Italy

Introduction: Characterization and quantification of atrial fibrillation (AF) is essential for optimal management of this arrhythmia. Continuous monitoring with implantable loop recorders (ILRs) and specific AF detection algorithms was demonstrated to have higher performances respect short-term monitoring systems. This pilot study is the first experience of AF quantification with implantable leadless BioMonitor® (Biotronik) device that use a three-vector signal detection to ensure higher precision.

Methods: Twenty patients suffering from paroxysmal AF were successfully implanted with BioMonitor® and equipped with the Home Monitoring® System (CardioMessenger II-S) which provides daily remote data transfer without patient interaction. The device automatically transmits daily the AF burden, 40 seconds of subcutaneous electrocardiogram (sub-ECG) triggered by the onset of the arrhythmic event and 40 seconds of periodic sub-ECG. Each AF sub-ECG was analysed and classified by a physician as: “true positive”, “false positive” or “non diagnostic”. The positive predictive value (PPV) for AF detection was reported.

Results: We analyzed an overall of 310 sub-ECGs, 132 triggered by the onset of AF and 178 periodic one. In the group of AF events 130 sub-ECGs were classified as “true positive” with a PPV value of 98%. Only 2 AF events were classified as “false positive” and this was due to myopotentials interference or noise. The duration reported for these two incorrect AF events was short, only 2 minutes, so it does not affect significantly the AF quantification. All the 178 periodic sub-ECGs were considered “diagnostic” by the physician (100%). The average of the AF burden over the period of the study was 21,9%.

Conclusions: Considering the PPV value, the rate of AF quantification with BioMonitor® devices may be very higher compared with standard ILRs. Daily sub-ECGs allows to physicians to have a real diagnostic tool for evaluating arrhythmias. Further studies are needed to better evaluate this important data.

PA4

The Ionic Expression Gradients Affect the Paroxysmal Atrial Fibrillation Dynamic: A Simulation Study

Catalina Tobón^{1,2}, Karen Cardona², Sandeep V. Pandit³, José Jalife³, Omer Berenfeld³, Javier Saiz²,

¹GI²B, Instituto Tecnológico Metropolitano, Medellín, Colombia

²13BH, Universitat Politècnica de València, Valencia, Spain

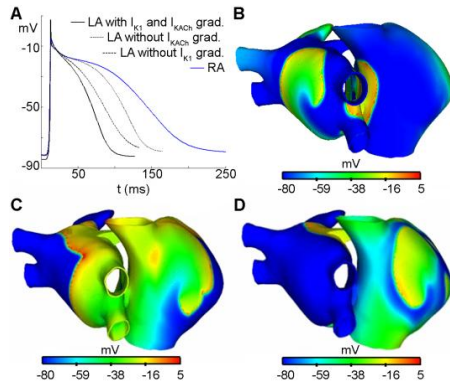
³Center for Arrhythmia Research, University of Michigan, Ann Arbor

Introduction: Ionic expression gradients could determine the dynamics of excitation during paroxysmal atrial fibrillation (pAF). Recently, it has been demonstrated that the acetylcholine (ACh)-activated potassium current ($I_{K_{ACh}}$) and the inward rectifier K^+ current (I_{K1}) densities are ≈ 2 -fold larger in left atrium (LA) versus right atrium (RA) during pAF, which could result in a greater increase in LA than RA rotor frequency. In this work, we study how the ionic expression gradients affect the pAF dynamic.

Methods: Experimental LA-RA I_{K1} and $I_{K_{ACh}}$ gradients were incorporated in the Courtemanche-Kneller atrial kinetics to simulate pAF in a 3D model of the human atria in the presence of $0.005 \mu M$ of ACh. As controls, models without the I_{K1} gradient and without $I_{K_{ACh}}$ gradient were used. pAF episodes of 10 seconds were generated by a burst of 6 ectopic beats in the right superior pulmonary vein.

Results: In pAF model with I_{K1} and $I_{K_{ACh}}$ gradients, the action potential duration (APD) gradient observed between two points at the free LA and RA walls was of 53% (Panel A). However, without I_{K1} gradient and without $I_{K_{ACh}}$ gradient; the APD gradient was decreased to 39% and 28%, respectively. In pAF model, reentrant activity in the LA in a form of single and then figure-of-eight reentry that maintained the AF, without reentrant activity in RA (Panel B). When one of the two ionic expression gradients was not present, the pAF was maintained by multiple reentrant waves that collided and fragmented in the RA (Panels C, D).

Conclusion: LA-RA gradients in both $I_{K_{ACh}}$ and I_{K1} expression are important in establishing APD gradients and LA reentrant activity maintaining pAF.



A) LA and RA action potentials in the pAF models. Propagation dynamics in B) pAF with I_{K1} and $I_{K_{ACh}}$ gradients, C) pAF without I_{K1} gradient and D) pAF without $I_{K_{ACh}}$ gradient.

Frequency Dependency of Pacing Determinants of an IK1-mediated Rotor Drift in the Posterior Left Atrial Wall toward the Pulmonary Veins

Conrado J Calvo*, Makarand Deo, Sharon Zlochiver, José Millet, Omer Berenfeld

Universitat Politècnica de Valencia
Valencia, Spain

Introduction: Maintenance of paroxysmal atrial fibrillation (AF) by fast rotors near or at the pulmonary veins (PVs) is not fully understood. We believe that heterogeneous distribution of transmembrane currents in the PVs and LA junction (PV-LAJ) in the localization of rotors in the PVs. We seek for pacing protocols and measurements that could be used to predict drift direction.

Methods: Experimentally observed heterogeneities in the PV-LAJ were incorporated into 2D and pseudo-3D models using validated human atrial kinetics to simulate various conditions and investigate rotor drifting mechanisms and its correlation to electrophysiological pacing predictors.

Results: Simulations with various gradient conditions and various current-voltage relationships, substantiated IK1 major role in the rotor drift through its impact on the global excitability and refractoriness gradients in the vicinity of the rotor core. PV rotors were slightly slower and of reduced wavelength measured as radial distance from the core along the wavefront. Among various action potential properties tested, only MDP gradient was found to be a pacing-rate independent predictor of rotor drift direction during pacing studies.

Conclusions: Our simulations suggest that regardless of a particular ionic dispersion of the PV-LAJ, measuring with high-resolution refractoriness, excitability and diastolic potentials during pacing could provide a mechanistic guidance for the unstable components of rotors that are believed to underlie AF. Interestingly our results attract attention into the interpretation of frequency dependent electrophysiological measurements from pacing studies (commonly performed at 2Hz) and its correlation to the AF activation sequence.

PA5

Modeling Calcium Dynamics in Human Atria

Inmaculada R Cantalapiedra*, Carlos Lugo, Angelina Peñaranda, Leif Hove, Blas Echebarria

Universitat Politècnica de Catalunya. BarcelonaTech
Barcelona, Spain

Mathematical models of cardiac electrophysiology are an important tool to investigate the underlying mechanisms responsible of arrhythmias. In particular, an important question is the origin of atrial fibrillation (AF). Often, AF initiation is preceded by action potential duration (APD) alternans, i.e., beat to beat oscillations in the APD, that arise at slower rates in patients with persistent AF than in those without AF or with paroxymal AF. Most of these arrhythmias appear as a consequence of malfunctions in calcium dynamics that produce oscillations in intracellular calcium, inducing subsequent APD alternans through electromechanical coupling. The aim of this work is to present a human atrial mathematical model that gives insight into the presence of calcium alternans. For that the model by Nygren et al was modified in order to reproduce calcium alternans at high and moderate pacing rhythms, as has been observed in experiments. The modified model includes three different compartments i) a dyadic (junctional) space with the presence of LCC and RyR channels, ii) a subsarcolemmal space where the other transmembrane currents act, and iii) the bulk cytosolic compartment where the calcium concentration transient is caused by diffusion from the subsarcolemma and luminal calcium efflux from the SR through the RyR channels. For the RyR dynamics we consider a markovian four state model. The SR Ca release includes inactivation/adaptation and SR Ca load dependence of activation and inactivation. The model reproduces the nonlinear dependence of gain and fractional SR Ca release upon SR Ca load. At fast pacing rates it presents alternans, due to slow recovery from inactivation of the RyR. Finally, we compare the results from this new model with other human atrial models well established in the literature.

PA5

Diagnosis of Atrial Ectopic Origin from Body Surface ECG – Insights from 3D Virtual Human Atria and Torso

Erick Andres Perez Alday*, Michael Alan Colman, Daniele Giacomelli, Philip Langley, Henggui Zhang

University of Manchester
Manchester, United Kingdom

Aims: Atrial tachycardia (AT), resulting from ectopic atrial activity, may predispose to atrial fibrillation (AF). Such abnormal excitation may be reflected as an alteration in the P-wave morphology (PWM) of the body surface potential (BSP). Identifying the best electrocardiogram (ECG) lead configuration to obtain information on the presence and origin of ectopic atrial activity can help to diagnose the early onset of AF in a cost effective manner. In this study we use a biophysically detailed computational model of the human atria and torso to investigate the correlation between PWM in different ECG configurations and origins of atrial ectopic activity.

Methods: We developed a 3D human atrial model to simulate electrical activity during normal sinus rhythm and ectopic activity. The atria model is placed into a newly developed torso model, taken from the visible human dataset with consideration for the lungs and liver. A boundary element method is used to compute the electrical activity from the surface of the atria to the surface of the torso. Elements of the torso mesh corresponding to the locations of the electrode placement are selected to simulate different ECG systems. PWM associated with ectopic and rotor wave activity from a variety of regions throughout the atria are analyzed.

Results: During sinus rhythm, the simulated P-waves of different ECG leads and BSP dipole direction show strong agreement with experimental data. Marked changes in PWM are observed in the BSP associated with ectopic atrial activity and the presence of rotor waves, with some areas of the torso being more sensitive to specific activity than others.

Conclusion: Our simulation data suggested that atrial ectopic activity can be reflected on changes of PWM. This study established a correlation between PWM and ectopic activity or rotor waves presence, which requires detailed analysis of PWM registered from specific anterior-posterior leads.

PA5

Paroxysmal Atrial Fibrillation Caused by Interaction of Pacemaker Waves and Reduced Excitability: Insights from the Bueno-Orovio Model Adapted to Atria

Claudia Lenk*, Frank M Weber, Martin Bauer, Mario Einax, Gunnar Seemann, Philipp Maass

Technische Universität Ilmenau, Ilmenau, Germany
Ilmenau, Germany

Paroxysmal atrial fibrillation (AF) is characterized by an alternation of fibrillation episodes with normal sinus rhythm. Despite much research in the past, its origin is not well understood. A recently proposed mechanism for the initiation of AF and its intermittent occurrence is the interaction of waves from two different pacemakers located in separate regions. The primary pacemaker represents the sinus node in the right atrium while the secondary one represents a self-excitatory source in the left atrium such as an ectopic focus or reentrant wave. The pacemakers waves can only get in contact through a small bridge. Studies of this mechanism based on the FitzHugh-Nagumo (FHN) model revealed three different types of irregular patterns. Which type occurs depends on the frequency of the pacemakers. In the Bueno-Orovio model adapted to atrial electrophysiology (aBO) only one type is found, because in this more realistic model a reduction of excitability due to high pacing frequencies is not present. By a reduction of excitability in the aBO model, as e.g. by increasing the relaxation time of the fast inward current, all three types of irregularities are recovered. In addition, a further type IV is found that is initiated by a partial conduction block of the waves passing the bridge. The strength of irregularity, classified by an order parameter for phase coherence, is significantly increased compared to the other irregularities. Because transitions from regular to fibrillation-like patterns can be induced by a change of the pacemaker frequencies, our studies provide a possible explanation for paroxysmal AF.

PA5

Effects of Physical Exercise and Glibenclamide in Local Activation Waves During Ventricular Fibrillation

Juan Caravaca*, Antonio J Serrano-López, Emilio Soria-Olivas, Manuel Bataller, Alfredo Rosado-Muñoz, Luís Such-Belenguer, Juan F Guerrero

University of Valencia
Burjasot, Spain

Aims: This study aimed to characterize cardiac mapping recordings during Ventricular Fibrillation (VF) according to the fragmentation level and occurrence ratio of its Local Activation Waves (LAW), in order to analyze the effects of physical exercise in the electrical activity of VF, compared to the effects of Glibenclamide.

Methods: Isolated rabbit hearts were perfused by a Langendorff system, and cardiac recordings were acquired with a 240-electrodes array. Three groups of rabbits were used. G1: control (sedentary rabbits), G2: trained (rabbits submitted to a running program) and G3: drugged (sedentary rabbits treated with Glibenclamide). VF was induced during each experiment, and two recordings were acquired: maintained perfusion and ischemic damage. LAW were detected using the maximal derivative, and were classified according to its fragmentation. Single activations have a unique deflection in a 40 ms period, and fractionated LAW have two or more deflections. The complexity level was measured with the Fractionated LAW Ratio (FLR), i.e. fractionated/total ratio. Finally, the activation rate was quantified using the LAW Occurrence Ratio (LOR), i.e. mean interval between consecutive LAW. These parameters were computed each 5 seconds, and compared using two sample permutation tests.

Results: The temporal evolution of FLR have shown that, with maintained perfusion or ischemic damage, the trained group has the lowest values ($p=0.05$), and no differences were found between drugged and control groups. Regarding LOR, the results depend on the perfusion conditions. When perfusion is maintained, drugged group has the lowest values ($p<0.05$). On the contrary, when there is ischemic damage, drugged group has the highest LOR values ($p<0.05$). No significant differences were found between LOR of control and trained groups.

Conclusion: Physical exercise and Glibenclamide modify different LAW properties. Physical exercise reduces its fragmentation, decreasing the complexity of LAW. By contrast, Glibenclamide modifies the activation interval, related to quickness of fibrillation.

PA6

Temporal Evolution of Spatial Regularity in Ventricular Fibrillation Modified by Physical Exercise

Juan Caravaca*, Antonio J Serrano-López, Emilio Soria-Olivas, Manuel Bataller, Alfredo Rosado-Muñoz, Luís Such-Belenguer, Juan F Guerrero

University of Valencia
Burjassot, Spain

Aims: This study tackles the analysis of cardiac mapping recordings during Ventricular Fibrillation (VF), with the aim of analyze its modifications produced by physical exercise, compared to the ones produced by Glibenclamide.

Methods: Isolated rabbit hearts were perfused by a Langendorff system, and cardiac recordings were acquired with a 240-electrodes array. Three groups of rabbits were used. G1: control (sedentary rabbits), G2: trained (rabbits submitted to a running program) and G3: drugged (sedentary rabbits treated with Glibenclamide). VF was induced during each experiment, and two recordings were acquired: maintained perfusion and ischemic damage. The recordings were analyzed in consecutive 4-second segments, and Regularity Index (RI) was obtained for every segment and electrode. RI quantifies the morphological regularity among local activation waves found in a electrode. A map with the RI value in each electrode was computed for each segment. To analyze the spatial distribution of RI, a threshold value was experimentally determined, and applied to each map in order to obtain the Regions Of Interest (ROI). Two parameters were calculated: ROI spatial number (ROI_{sn}, a measure of spatial fragmentation), and ROI spatial area (ROI_{sa}, the percentage of area map occupied by ROI). The time course of ROI_{sa} and ROI_{sn} in the three groups was compared using two sample permutation tests.

Results: Control group has shown higher values of ROI_{sn} than trained and drugged groups ($p < 0.05$), in both conditions (maintained perfusion or with ischemic damage). Regarding ROI_{sa}, control group has the lowest values ($p < 0.05$) in maintained perfusion, while these differences where less marked with the presence of ischemic damage. On the contrary, no differences were found between drugged and trained groups in terms any of the analyzed parameters.

Conclusion: The performed ROI analysis has shown that physical exercise and Glibenclamide decrease the fragmentation of VF cardiac response, increasing its spatial uniformity.

Performance of Heart Rhythm Analysis during Chest Compressions in Out-of-Hospital Cardiac Arrest

V Krasteva¹, I Jekova^{1*}, T Stoyanov¹, S Ménétré², JP Didon²

¹Institute of Biophysics and Biomedical Engineering, Sofia, Bulgaria

²Schiller Médical SAS, Wissembourg, France

Interrupting chest compressions (CC) for rhythm analysis by automated external defibrillators (AEDs) can adversely affect hemodynamics during cardiopulmonary resuscitation and can decrease resuscitation success rates in cardiac arrest patients. CC-artifacts in ECG considerably affect the accuracy of conventional AED rhythm analysis algorithms. This study aims to validate a method dedicated to ECG analysis in AEDs during CC that advises the rescuer to stop CC for rhythms which should be terminated by a defibrillation shock and to continue CC in all other cases.

The ECG database is collected with Fred Easy AEDs (Schiller Médical SAS, France) used by the fire brigade of Paris in out-of-hospital cardiac arrest interventions in 2011. A subset of 2528 ECG strips is identified, including episodes during CC which are followed by noise-free AED analysis periods. Reviewers have annotated CC-episode boundaries and rhythm during AED analysis, including: 74 normal sinus rhythms (NSR), 1671 asystoles (ASYS), 632 other non-shockable rhythms (N), 151 ventricular fibrillations (VF). Assuming consistence of the ECG rhythm till 20s before the AED analysis period, these annotations are also considered for the preceding CC episode.

We validate a method, which is previously introduced for heart rhythm analysis during CC, based on assessment of time and frequency components of band-pass filtered CC-artifacts and reconstructed ECG. The first analysis uses 10-second window to take a decision: 'Continue-CC' (for non-shockable rhythms) or 'Stop-CC' (for shockable rhythms). Next analyses are applied on windows slid by 2s.

The performance of the first analysis is improved by combining the decisions of three consecutive analyses: the correct advice 'Continue-CC' is increased by 1.4% for NSR, 4.8% for N, 4.8% for ASYS; the correct warning 'Stop-CC' is increased by 2.6% for VF (see table). Improving specificity of such algorithms is of tremendous importance, allowing patient treatment (CC delivery) instead of delivering unnecessary shocks.

	VF Sensitivity	NSR Specificity	N Specificity	ASYS Specificity
1 st Analysis	86.8% (131/151)	97.3% (72/74)	84.7% (535/632)	76.4% (1277/1671)
Combined 1 st -3 rd analyses	89.4% (135/151)	98.7% (73/74)	89.6% (566/632)	81.2% (1357/1671)

PA6

Towards the selection of patients requiring ICD implantation by automatic classification from Holter monitoring indices

Cappelaere C.H.^{1,2}, Dubois R.³, Roussel P.¹, Baumann O.², Amblard A.², Dreyfus G.¹

Laboratoire SIGMA, ESPCI ParisTech, Paris, France¹; Sorin CRM SAS, Clamart, France²; IHU LIRYC – Institut de rythmologie et de modélisation cardiaque, Bordeaux, France³

Aim: This study aimed to optimize the selection of prophylactic ICD-implantation candidates. Currently, the main criterion for implantation is a low Left Ventricular Ejection Fraction (LVEF). The specificity of this criterion, however, is relatively poor. For example, in the SCD-HeFT study, 81% of the patients did not receive therapy from their ICD over a 5-year follow-up period despite the mean LVEF of this population being 23.8% (std. 6.9%). Beyond the economic issue caused by seemingly unnecessary implantations, are the health issues due to the perioperative and postoperative complications.

Method: We designed a classifier aimed to predict, from ECG Holter recordings, whether a low-LVEF patient is likely or not to undergo ventricular arrhythmia in the next six months. Its structure capitalizes on the physiological decomposition of the arrhythmogenic factors (Coumel's triangle). A large set of ECG features was extracted from Holter recordings and sorted into three groups corresponding to the arrhythmogenic substrate, the trigger factors and the modulation factors (the autonomic nervous system). The most relevant features were selected by the random probe method for each group. Then, one neural network classifier per group was built and optimized. The final classification was performed by merging the outputs of the three networks.

Results: 186 pre-implantation 30-min Holter recordings of patients equipped with an ICD in primary prevention due to their low LVEF were used for designing and testing this classifier. 44 out of 186 patients underwent at least one ventricular arrhythmia during the six-month follow-up period.

Ten classifiers were designed and tested with ten different combinations of a training/validation set and a test set. The arrhythmia prediction performances on the ten independent test sets are NPV = 78.8% (std. 11.9%) and PPV = 27.7% (std. 15.7%).

Conclusion: Improving prophylactic ICD-implantation candidate selection by automatic classification from ECG features seems to be possible.

The Effect of the Sensor Position of the Pressure Wire Distal to a Coronary Stenosis on the Calculated Fractional Flow Reserve

Balázs Tar, Sándor Bakk, Zoltán Béres, János Sánta, Péter Polgár, Shengxian Tu, Zsolt Kőszegi*

Jósa András Teaching Hospital, Nyíregyháza
Nyíregyháza, Hungary

The determination of the fractional flow reserve can be influenced by the position of the sensor of the pressure wire distal to a coronary lesion. We aimed to achieve fluid dynamic calculation of pressure gradients restricted to the stenosis and with inclusion of the distal reference segment until the position of the pressure wire. A total of 19 de novo lesions of 17 patients were consecutively enrolled. 21 intracoronary pressures measurements were performed by Radi PressureWire™. X-ray angiographic images were recorded by AXIOM-Artis equipment. The lumen of the interrogated vessel segments was reconstructed in 3D using a dedicated software package (QAngio XA Research Edition 1.0, Medis Specials bv, Leiden). The coronary artery volumetric flow was calculated based on the velocity of the contrast material in the 3D reconstructed coronary segment. Pressure gradients were determined by fluid dynamic equations using the morphological data derived by 3D coronary angiography and contrast material velocities. The Bland-Altman analysis showed lower differences between the calculated and the measured FFR when the distal laminar resistances were also incorporated in the model compared to the calculations restricted to the lesions (mean difference: -0.05 vs. -0.09, limits: -0.11–0.02 vs. -0.16–0.01; range: 0.112 vs. 0.159). Mann-Whitney test proved significant difference between the measured and calculated values only that cases when the FFR was calculated for purely the lesions ($p=0.053$ vs. $p=0.0005$). The FFR reflects not only the pressure gradient of the stenosis, but also the laminar resistance of the poststenotic segment. Knowing the components of the detected gradients could be important for the clinical considerations of the cases near the cut of value of the FFR.

PA7

Diagrammatic Reasoning with Interactive P-V Curves

Marc Cavazza and Fred Charles

Teesside University, Middlesbrough, United Kingdom

Ventricular Pressure-Volume (P-V) curves are an important representation that helps explain cardiac physiology as well as the pathophysiology of major syndromes such as various forms of heart failure. For this reason, P-V curves are ubiquitous in physiology textbooks but also in more advanced material in cardiology and critical

care, where left ventricular behaviour is often explained through reference to a P-V curve characterising a condition. Previous work on the computerisation of P-V curves has sought to visualise them as the output of a simulation from numerical values for the main physiological parameters. While this can constitute a positive step in making P-V curves more accessible in particular to students, it misses some of the most important properties of the curves, namely the fact they support diagrammatic reasoning. This means that the curve itself should be the interface through which the characteristic elements of a syndrome are entered (for instance end-systolic elastance, telediastolic volume, end-diastolic pressure-volume relation ...), as well as the visualisation from which to draw inferences. This has led us to develop an interactive version of the P-V curve, which supports diagrammatic inference, based on user-driven modification of essential parameters of the P-V curve (Figure 1). Because diagrammatic inference cannot account for temporal adaptation of the cardio-vascular system, we have extended the diagrammatic reasoning system to incorporate qualitative simulation of adaptive mechanisms. This approach, which is based on propagating modification of physiological variables through a causal network, extends the ability of P-V curves to represent situations beyond the single-beat paradigm (for instance, preload adaptation to an increase in afterload). It is currently only implemented for short-term adaptive mechanisms. The system is able to correctly recreate all major pathophysiological syndromes from first principles (rather than explicitly encoded) supporting direct, interactive manipulation of the curve through control points, including dynamic adaptation.

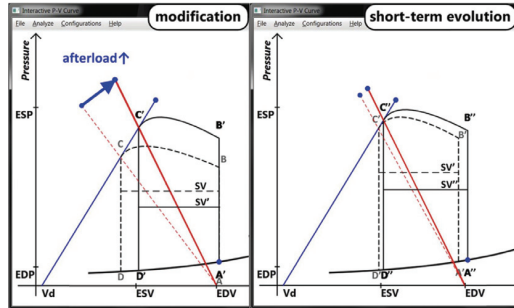


Figure 1. Results for the adaptation of a healthy heart to an increase in afterload through preload reserve.

Analysis of Seismocardiogram Capability for Prediction of Mild to Moderate Hemorrhage

Kouhyar Tavakolian*, Guy Dumont, Andrew Blaber

University of British Columbia
Burnaby, Canada

Hemorrhage is a result of significant blood loss and one of the leading causes of death on battlefields and emergency rooms. Low systolic blood pressure of less than 90 mmHg has been commonly used, clinically, to indicate hemorrhage. More recently a drop in pulse pressure has been suggested for detection of blood loss. However, it is well recognized that when the hypotension is significant it might be too late for a lifesaving intervention. Thus, there have been recent efforts towards prediction of hemorrhage using alternative methods. We believe that the seismocardiogram (SCG) has potential for providing a low-cost, portable solution for triage of hemorrhage while it is still in its mild to moderate stage (10-20% blood loss). Graded lower body negative pressure (LBNP) is an accepted experimental surrogate for hemorrhage. Thus, in this study LBNP was implemented and twelve young and healthy adults were placed in a sealed chamber where pressure was gradually lowered to -50 mmHg. The cardiac output was measured by a GE Vividi echocardiograph and blood pressure was measured using a Portapres™ device. A time feature (the period between the Q wave of ECG to the mitral valve closure point of SCG) was selected, among 34 features extracted from the SCG signal. Table 1 presents different values of this feature during LBNP alongside cardiac output and blood pressure and Table 2 lists the r^2 values for different subjects. In 11 subjects out of the twelve the percentage reduction of more than 10% in blood volume (as detected by echocardiogram, and as a sign of mild hemorrhage) is accompanied by more than 10% change in the SCG extracted feature while the corresponding pulse pressure changes are less than 10% for seven subjects. All these suggest that the SCG extracted feature is more sensitive to changes in cardiac output.

PA7

Haemodynamic Parameters for Assessment of Orthostatic Intolerance in Older People

Fernando García*, Lisa Cogan, Richard Reilly, José Millet, Raquel Cervigón

UCLM
Cuenca, Spain

Orthostatic hypotension (OH) is a frequent cause of orthostatic Intolerance (OI) and related symptoms associated with the occurrence of syncope. This study focused on examining the hemodynamic profile in older people with symptoms of OI undergoing an active stand and to investigate if their dynamic cardiovascular profile during a six-minute walk would be different to those of controls. The database included 45 participants, aged over 60 years (69.5 ± 5.1), of whom 60% were women. There were no significant differences in age and gender between symptomatic and asymptomatic participants. 46.7% ($n=21$) had symptomatic OI and 53.3% ($n=24$) did not. The participants underwent a supine to stand orthostatic test (active stand) with non-invasive beat-to-beat blood pressure monitoring using a Finometer Pro™ device. Hemodynamic parameters were registered during three phases: a pre-exercise stand lasting 3 minutes (phase 1), a six minutes walking phase (phase 2) and a post-exercise stand lasting 3 minutes (phase 3). Different hemodynamic parameters such as, HR (pulse rate derived from the pulse interval), systolic blood pressure (SBP), diastolic blood pressure (DBP) and cardiac output (CO) were extracted at each phase. Results showed differences during phases in both groups. HR differences (beats/min) in phase 1 and 2 showed statistical significance ($p=0.032$) between symptomatic OI (phase 1: 74.11 ± 14.37 vs. phase 2: 109.68 ± 15.04) and non-symptomatic OI Group (phase 1: 78.52 ± 11.70 vs. phase 2: 105.83 ± 11.47), moreover the same trend was observed in phase 2 and 3 ($p=0.016$). In addition, the combination of the variables rise/fall time -maximum/minimum amplitude in phases 2 and 3 showed opposite trends in men and women and in symptomatic and non-symptomatic OI groups in all the parameters: DIA ($p=0.005$), SYS ($p=0.006$), HR ($p=0.047$) and CO ($p=0.017$). Current methods for assessment of OH do not provide sufficient description of the haemodynamic changes produced. This study provides important information on hemodynamic parameters.

PA7

Hurst Exponent to Analysis Atrial Fibrillation Recurrence after Ablation Procedures

Raquel Cervigón*, Javier Moreno, Francisco Castells, Julián Pérez-Villacastín, José Millet

UCLM
Cuenca, Spain

With the appearance of atrial fibrillation (AF) ablation in medical practice, the managing of this arrhythmia, considered to be incurable, has changed from a strategy directed to avoid tachycardia, merely reducing heart rate, and embolism through anticoagulation, to search the cure of the disease modifying the arrhythmic substrate. The aim of this work is to improve the understanding of AF dynamics for the prediction of AF recurrence after ablation procedures. The database includes intracardiac recordings from 42 paroxysmal and persistent AF patients submitted to an ablation procedure. Four electrodes were located at the right atrium (RA) and 4 more at the left atrium (LA). All patients were monitored after ablation, and were divided in 2 groups according to AF recurrence outcome: 26 of them remained in SR (11 persistent and 15 paroxysmal AF) whereas the other 16 turned back to AF (7 persistent and 9 paroxysmal). There were no significant differences in age and gender between both groups. The Hurst Exponent has been applied in order to extract self-similarity of atrial time series. This parameter was analyzed in both groups separately. Results showed regional differences in non-recurrent AF patients. Indeed, the mean Hurst Exponent in the LA was 0.65 ± 0.16 vs. 0.72 ± 0.08 in the RA ($p=0.017$). However, in the recurrent AF group, these differences were no longer significant: 0.66 ± 0.09 in LA vs. 0.67 ± 0.10 in RA ($p=0.691$). When analyzing this parameter in paroxysmal and persistent AF groups, these regional differences were slightly more significant in the paroxysmal AF group (LA 0.69 ± 0.10 vs. RA 0.73 ± 0.07 , $p=0.045$) than in persistent AF patients (LA 0.65 ± 0.11 vs. RA 0.68 ± 0.12 , $p=0.325$). These findings show regional differences between LA and RA in non-recurrence AF patients, as well as in paroxysmal AF. This study also highlights the potential of non-linear methods such as Hurst Exponent to study AF dynamics.

PA8

Experimental Study of Arrhythmia due to Mild Therapeutic Hypothermia after Resuscitation of Cardiac Arrest

Binbin Xu*, Oriol Pont, Gabriel Laurent, Sabir Jacquir, Stéphane Binczak, Hussein Yahia

INRIA Bordeaux Sud-Ouest
Talence, France

Introduction: One of the important challenges after cardiac arrest (CA) is the neurological damage of the brain. In case of resuscitation after CA, the brain suffers the ischemia and the inflammation from reperfusion. To days, the only therapy available is the mild therapeutic hypothermia (MTH) : put the patient under 34°C - 32°C during 12-24 hours. Even though that MTH has been shown to increase the hospital survival rate, it has many adverse effects, among which the cardiac arrhythmia generation represents an important part (up to 34%). Cardiac culture in vitro provides a better spatial resolution (to cellular level) than study in vivo, which could bring some insights of the mechanism of post-hypothermia arrhythmia generation.

Method: Monolayer cardiac culture is prepared with cardiomyocytes from new-born rat (1-4 days) directly on the MEA at 37°C . The experiments consist of culture cooling (37°C - 30°C) and re-warming (30°C - 37°C). The acquired signals are then analyzed with detrended fluctuation analysis, phase space reconstruction, principle component analysis.

Results: At 35°C , Spiral waves are observed in the reconstructed activation map which is commonly considered as a sign of cardiac arrhythmia. Between 35°C - 33°C , the signals became regular. However, another transit point is found between 30°C - 33°C . At 35°C , period-doubling phenomena are observed, which can be translated as a transit point from normal state to chaos state, from the point view of nonlinear dynamics. From the reconstructed phase space, doubling-trajectories and rare tripling-trajectories are found. It implies that the general dynamics of MTH could be presented as a pitchfork bifurcation, which could explain exactly the doubling-trajectories and tripling-trajectories phenomena. These results at cellular level agreed with other clinical studies on MTH.

Conclusion: The general hypothermia therapy uses constant cooling or re-warming. Results in this study showed that a variable speed would help to reduce the rate of post-hypothermia arrhythmia.

Spectral and Nonlinear Analysis in Surgical Ventricular Fibrillation

Francisco Javier Pulido-Hidalgo, Óscar Barquero-Pérez*, Cristina Soguero-Ruiz, José Luis Rojo-Álvarez, Juan José Sánchez-Muñoz, Arcadi García-Alberola

University Rey Juan Carlos
Fuenlabrada, Spain

Background. Most studies about ventricular fibrillation (VF) in humans have attempted to analyze the first minute of its evolution. However, longer duration studies or VF complete evolution (from onset to end) have been scarcely reported. **Objective.** Our aim was to study the complete evolution of VF signal, until asystolia, in a heart surgical VF model in humans using frequency and nonlinear parameters. **Material and Methods.** We recorded ECG signals during VF from 30 patients underwent heart surgery under cardiopulmonary bypass (CPB) (Hospital Virgen de la Arrixaca in Murcia, Spain). Two types of VF can be present, before surgery (VFPre, 12 patients); and after surgery (VFPost, 18 patients). We computed dominant frequency (DF), and sample entropy (SampEn) on the first 5-sec segment and the last 5-sec segment for VFPre and VFPost. Temporal evolution of VF was analyzed before and after surgery (from VFPre[first] to VFPre[last]) (from VFPost[first] to VFPost[last]). Regarding differences between VFPre and VFPost, we compared: (1) Onset of VF in both types (VFPre[first]vs.VFPost[first]); (2) End of both VF types (VFPre[last]vs.VFPost[last]). We used nonparametric resampling statistical hypothesis test ($p < 0.05$). **Results.** Regarding temporal evolution, before surgery(VFPre) parameters decreased, DF from 2.95 ± 0.84 to 2.51 ± 0.9 , and SampEn from 0.36 ± 0.10 to 0.32 ± 0.10 (non significant). After surgery(VFPost), both parameters significantly increased; DF from 2.68 ± 0.95 to 3.50 ± 1.00 , and SampEn from 0.33 ± 0.09 to 0.37 ± 0.1 . None of the parameters were significantly different for (1) VFPre[first]vs.VFPost[first]; whereas in (2) VFPre[last]vs.VFPost[last], there were significant differences on DF (2.51 ± 0.9 vs. 0.35 ± 1.0). **Conclusions.** We found an inverse temporal evolution on each VF type, VFPre (VFPost) decreased (increased) in frequency and complexity parameters in agreement with animal models. The last 5 seconds of both types of VF were significantly different regarding DF.

PA8

Classification of inverse solutions to two dipoles

Jana Svehlikova, Michal Teplan, Milan Tysler

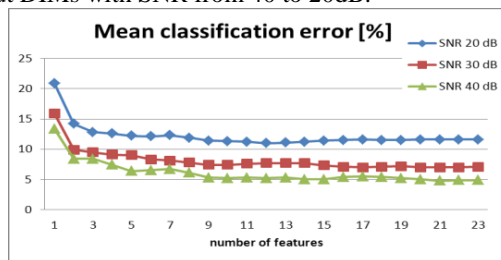
Institute of Measurement Science, SAS
Bratislava, Slovakia

Aim: The aim of the study was to identify which results of an inverse solution to two dipoles characterize the existence of two simultaneous lesions with changed repolarization.

Methods: In the simulation study difference STT integral body surface potential maps (DIMs) computed for 48 single lesions and 96 pairs of lesions were used as the input data for an inverse solution to two dipoles. Additional random noise with signal to noise ratio (SNR) 20, 30 and 40dB was applied to the input data. The inverse solution was obtained as several pairs of dipoles. Twenty three characteristics of the solution were specified and used as the features for the quadratic variant of the Fisher discriminant analysis that should distinguish the inverse solutions that correctly identify two lesions from those yielding incorrect results or corresponding to a single lesion. Resulting classification errors were computed as the mean rate of false positives, false negatives and their average.

Results: The mean localization error in cases of correct results was 1.2 ± 0.8 cm and was stable regardless of the SNR. The mean classification error decreased rapidly when the first two discriminating features were used. The optimal number of features (seven) was chosen as the number of features when the rate of false positives and false negatives were similar at each level of noise. If seven most informative features were used, the sensitivity of the double lesion identification was from 94 to 89% and the specificity from 92 to 86% for input DIMs with SNR from 40 to 20dB.

PA8



Conclusions: The inverse solution to two dipoles together with the proposed classification of obtained results yields the identification of two simultaneous lesions with the sensitivity and specificity higher than 85% for input DIMs with added noise with SNR not lower than 20dB without the need of some a-priori information about the number of lesions.

Clustering of Re-entry Close to Scar Boundaries in Ventricular Tissue during Simulated Ventricular Fibrillation

Sathyavani Malyala*, Richard Clayton

University of Sheffield
Sheffield, United Kingdom

Introduction: Scar tissue in the ventricles can act as a source of anatomical re-entry. However, the interaction of scar with complex activation during ventricular fibrillation (VF) is not well understood. In this study we investigated how simulated scars influence clustering of re-entry in simplified computational models.

Methods: VF was simulated in a 3D monodomain model. Membrane excitability was described by a 4-variable phenomenological model, fitted to human epicardial action potential shape, and modified to generate unstable re-entry. Two tissue geometries were used, a rectilinear slab (8.0 x 8.0 x 1.2 cm) representing a section through the wall of the left ventricle, and a half ellipsoid representing the left ventricle (base-apex 9.0 cm, wall thickness 1.1 cm). Both geometries incorporated orientation of fibres. Scar was represented by a cylindrical region of inexcitable but diffusively coupled tissue extending from the endocardium, with a thin layer of surviving epicardial tissue. Re-entry was initiated by imposing a single scroll wave on the tissue, and the filaments around which re-entry rotates were detected as lines of phase singularity.

Results: Initial re-entrant waves broke up resulting in complex re-entry typical of VF, with an average of 13.4 filaments for the slab and 15.5 for the ellipsoid. Filament voxels were distributed uniformly in normal tissue. Close to the scar boundary, the number of filament voxels spiked to around 5 times the mean value in normal tissue. In the surviving epicardial layer, the number of filament voxels was around one fifth of the mean. In contrast the number of epicardial phase singularities showed no spike close to the boundary.

Conclusions: During simulated VF in simplified geometry, re-entry tended to cluster close to the boundary between scar tissue and normal tissue. However, with a surviving region of epicardial tissue, clustering may not be evident on the epicardial surface.

PA8

A Machine Learning Technique Regularization of the Inverse Problem in Cardiac Electrophysiology

Nejib zemzemi*, Remi Dubois, Yves Coudiere, Olivier Bernus, Michel Haissaguerre

INRIA Bordeaux Sud Ouest
Talence, France

Aims Pulmonary veins ablation is one of the most efficient treatments of atrial fibrillation. The idea behind it is to stop the propagation of ectopic beats coming from the pulmonary vein. ElectroCardioGraphy Imaging (ECGI) provides the opportunity to reconstruct the electrical potential and activation maps on the heart surface and analyze data prior to the intervention. The mathematical problem behind the reconstruction of heart potential is known to be ill posed. In this study we propose to regularize the inverse problem with a statistically reconstructed heart potential, and we test the method on synthetically data produced using an ECG simulator.

Methods We propose to compare three methods of reconstruction: a) Statistical reconstruction based on reproducing kernel Hilbert Space (RKHS) method, b) the classical inverse problem formulation with Tikhonov regularization and c) A combination of both methods. We built a data-set of 400 couples of extracellular and body surface potentials (BSP) using our ECG simulator, each element of the data base corresponds to a different stimulus site and the BSP is measured in 264 positions on the torso. We compare the accuracy of the methods both in terms of reconstructed potential and activation maps. Results Numerical simulations show that when using the classic Tikhonov method the reconstructed electrograms signals are too much smoothed in the QRS interval this significantly affects the activation map reconstruction. We obtain a better reconstruction of activation maps using the statistical reconstruction. But as shown in previous work the magnitude of the electrograms is significantly affected. The method c) allows a better accuracy both on magnitude and stiffness of the electrical signal during the QRS interval, which provides a better reconstruction of the activation map.

PA8

Novel Potent Small Molecule Modulators of Cardiac KCa2 and KCa3.1 Channels: Potential Utility for Treating Cardiac Ischemia and Atrial Fibrillation

Aida Oliven-Viguera*, Marta Sofia Valero, Ralf Kohler

Aragon Institute of Health Sciences and ARAID, Zaragoza, E;
Cardiovascular Research Unit, Institute for Molecular Medicine,
University of Southern Denmark, Odense, DK
Zaragoza, Spain

Background: Cardiac KCa2, small-conductance Ca²⁺-activated K⁺ channels, have been proposed to be involved in atrial repolarization. Moreover, GWAS studies suggested that polymorphisms of the KCa3.2 gene are associated with lone atrial fibrillation (Ellinor et al., Nat. Genet. 2010 42(3):240-4). A related channel, KCa3.1, is expressed in the coronary artery endothelium where it enables endothelium-derived hyperpolarization-mediated vasodilation. Thus, small molecule blockers or activators of the channels could be of therapeutic utility to treat atrial fibrillation or cardiac ischemia due to CAD, respectively.

Methods and Results: Our patch-clamp screening of natural and synthetic polyphenols identified the first highly potent small molecule blocker (negative gating modulator) of KCa2.3, 13b ([3,5-bis[(3-fluoro-4-hydroxy-benzoyl)oxymethyl]phenyl)methyl 3-fluoro-4-hydroxy-benzoate), with an EC₅₀ of 241 ± 129 pM and a 58-fold selectivity over KCa3.1 (EC₅₀ 14 ± 3 nM) and with no blocking effects (at 1 μM) on other K⁺-channels like KCa1.1, cardiac hERG, or KV1.3 channels (Oliven-Viguera et al., Plos One, 2013). Moreover, we report on a novel KCa3.1 activator (positive gating modulator), SKA-31, with a 5-fold higher selectivity over other KCa that produced strong hyperpolarizing K⁺-currents (30 ± 8 pA/pF at 0 mV) in native porcine coronary endothelium and counteracted serotonin-induced coronary contraction by -50% (DMSO(Vehicle): 0.4 ± 0.1 Δg vs. SKA-31 (10 μM): 0.2 ± 0.1 Δg; P<0.05) and amplified bradykinin-induced relaxation by 110 % (Vehicle: 31 ± 5 % relaxation vs. SKA-31 (1 μM): 65 ± 6 %; P<0.01).

Conclusions: These potent novel gating modulators of cardiovascular KCa are of potential therapeutic utility to treat atrial fibrillation (KCa2.3) and cardiac ischemia (KCa3.1) and may also serve as tools to study pathological alterations of cardiac functions in animal models as well as in in-silicio modeling and ECG diagnostics.

PA8

Automatic Detection of Mitral Annulus in Echocardiography based on Prior Knowledge and Local Context

Wei Song, Wei Xu, Xin Yang*, Liping Yao, Kun Sun

Shanghai Jiao Tong University
Shanghai, China

Due to the inherent noisy, low resolution and limited imaging range of echocardiography, it is difficult to identify mitral annulus (MA) where valves end that is crucial for further segmentation, modeling and multi-modalities registration of mitral valves. This work aims to automatically detect MA hinge point combining information of intra-cardiac local context and location relationships. The method includes the following steps: (1) segment left ventricle (LV) by prior shape and local histogram fitting based Active Contour Model; (2) design the local context features for training and classification of MA hinge points; (3) utilize additive min kernel based Support Vector Machines (SVM) classifier for fast computation to obtain MA candidates; (4) estimate MA hinge points by K-means algorithm under the location constraint of LV and MA. Our method was tested on echocardiographic four chamber image sequence of 10 pediatric patients (6 boys, 4 girls, 7.6 ± 3.4 years). Compared with the manual annotations, the automatically detected MA results are reliable with reasonable accuracy, for lateral point (2.0 ± 1.9 , 1.8 ± 1.2) pixels and for septal point (2.9 ± 2.6 , 1.2 ± 1.0) pixels.

Role of 3D Echocardiography Derived Color-Coded Parametric Models of the Mitral Valve in Differential Diagnosis of Prolapse and Billowing

Karima Addetia, Lynn Weinert, Roberto M. Lang, Victor Mor-Avi

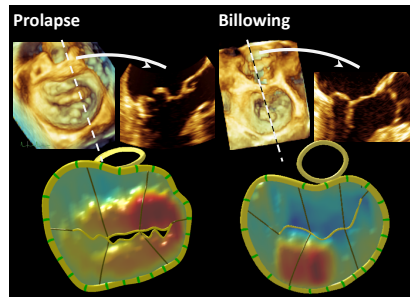
University of Chicago, Chicago, Illinois, U.S.A.

Background. Differentiation between mitral valve (MV) prolapse (MVP) and billowing (MVB) on 2D echocardiography (2DE) may be challenging. We hypothesized that color-coded models of maximal leaflet displacement from the annular plane into the atrium derived from 3D transesophageal echocardiography (TEE) would allow discrimination between these lesions.

Methods. 3D TEE imaging of the MV was performed in 52 patients with (N=40) and without (N=12) degenerative MV disease. Definitive diagnosis of MVP versus MVB was made using inspection of dynamic 3D renderings and multiple 2D cut-planes extracted from 3D datasets. MVP was defined by the leaflet free edge located on the atrial side of the annulus at end-systole. MVB was defined as systolic protrusion of the leaflet body into the left atrium with the free edge at or below the annular plane at end-systole. This was used as a reference standard to test an alternative approach, wherein the color-coded parametric models (MVQ, Philips) were inspected for integrity of the coaptation line and location of the maximally displaced portion of the leaflet. Diagnostic interpretations of these models by two independent readers were compared to the reference standard.

Results. In all cases of MVP, the color-coded parametric models depicted malcoaptation of the leaflets (disrupted coaptation line) adjacent to the prolapse and maximal leaflet displacement extending to the coaptation line. MVB was depicted by preserved leaflet apposition (intact coaptation line) with maximal displacement away from the coaptation line. The interpretation of the color-coded models took 5-9 seconds per case and resulted in good agreement with the reference technique (κ 0.82 and 0.74 for the two readers).

Conclusions. 3D color-coded parametric models provide a static display of the MV leaflet displacement and the integrity of the coaptation line, allowing differentiation between MVP and MVB, without the need to inspect multiple cut-planes. This display provides information on lesion location and extent, potentially useful for planning MV repair.



PA9

Vendor-Independent Software for Rapid Comprehensive Assessment of Changes in Left Ventricular Function During Serial Echocardiographic Studies

Gillian Murtagh, Victor Mor-Avi, Wendy Tsang, Nicole M. Bhаве, Brent DeManby, Eric Kruse, Megan Yamat, Roberto M. Lang, Jeanne M. DeCara

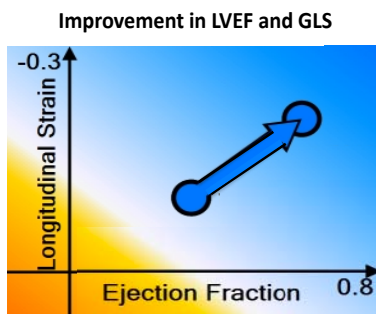
University of Chicago, Chicago, Illinois, U.S.A.

Background. Sequential evaluation of left ventricular (LV) function is critical in patients receiving potentially cardiotoxic treatments. However, identification and interpretation of the clinical significance of subtle changes in LV function from echocardiographic images is time-consuming and requires training. The aim of this study was to develop and test a new approach aimed at addressing this issue.

Methods. Dedicated semi-automated software was developed (Epsilon Imaging), which analyzes images obtained during serial examinations and provides a visual, easy-to-understand display of changes in LV ejection fraction (EF), peak systolic global longitudinal strain (GLS) or both. To test this software, 30 subjects who had 2 echocardiographic studies separated by ≥ 4 weeks were identified and their images analyzed. An expert echocardiographer reviewed EF and GLS data separately using commercial software (Philips QLab), and classified EF and/or GLS in each patient as unchanged, improved or worsened. This classification was used as a reference to test the accuracy of using a combined display of changes in EF and GLS (figure). This was performed by an inexperienced observer with and then without the dedicated software.

Results. Image analysis and interpretation were faster using the dedicated software (27 ± 5 vs 15 ± 5 minutes). The agreement with the reference was slightly better with the dedicated software (93%; kappa=0.90) than without it (90%; kappa=0.87).

Conclusions. Combined displays of changes in EF and GLS data from serial studies allows quick, easy and accurate interpretation of changes in LV function, promising to improve follow-up of patients undergoing potentially cardiotoxic treatments such as chemotherapy.



PA9

Multivariate Classification of Cardiac Autonomic Function and Echocardiographic Abnormalities

Gabriel Granåsen, Urban Wiklund

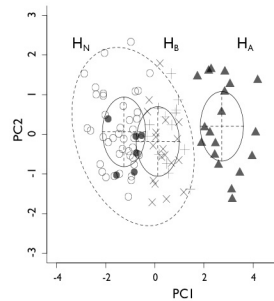
Radiation Sciences, Biomedical Engineering, Umeå University
Umeå, Sweden

Aims: Abnormalities in the function, physiology and the regulation of the heart can be diagnosed using echocardiography (ECHO) and analysis of heart rate variability (HRV). Patients with transthyretin amyloidosis often present cardiac hypertrophy and/or autonomic dysfunction. We used a novel approach to analyse the relationship between these findings, combining dimension reduction techniques and model based clustering.

Methods: Data were obtained from 39 adult patients and 62 healthy controls. HRV indices were calculated as 24-hour averages: the mean RR interval; the power of the very low-frequency, low-frequency and high-frequency components. From ECHO we used: posterior wall thickness, septal thickness, left ventricular end diastolic dimension, isovolumetric relaxation time and deceleration time. Principal component analysis was performed to model the within modality variability of each group of variables. The hierarchical Gaussian mixture modelling method, Mclust, was used to find clusters of subjects in the resulting component scores.

Results: For each modality, subjects were classified into three groups. The cluster that mainly consisted of controls was denoted as “Normal”. The most diverging cluster was denoted “Abnormal”. The “middle” cluster was denoted “Borderline”. All controls were classified as normal in ECHO, and as normal (young and middle-aged subjects) or borderline (middle-aged and old) in HRV, reflecting the well-known successive decrease in HRV with age in healthy subjects. For patients, the classification was related to the progress of disease: 36% had normal or borderline HRV and normal ECHO; 18% had abnormal HRV and normal ECHO; while 46% were classified as borderline or abnormal in both examinations.

Conclusions: The analysis successfully separated between patients with regulatory involvement but only minor structural abnormalities, and those with both structural abnormalities and severe autonomic dysfunction. The presented method can also be used to model patterns in other diseases with cardiac and autonomic involvement.



Clustering of significant HRV components

Development of Fetal Cardiac Intervals throughout 16 to 41 weeks of gestation

Faezeh Marzbanrad¹, Yoshitaka Kimura³, Kiyoe Funamoto³, Rika Sugibayashi³, Miyuki Endo³, Takuya Ito³, Marimuthu Palaniswami¹, and Ahsan H Khandoker^{1,2}

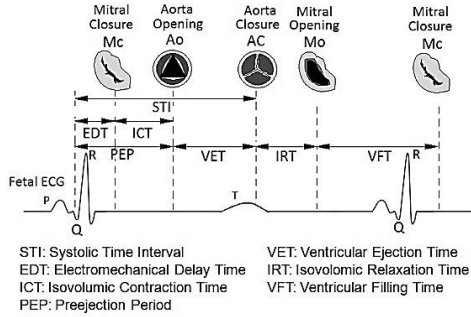
¹ The University of Melbourne, Australia

² Khalifa University, Abu Dhabi, UAE

³ Tohoku University, Sendai, Japan

In this paper a new noninvasive method is proposed for automated estimation of fetal cardiac intervals from Doppler Ultrasound (DUS) signal and their developments from early to late gestation. The proposed method is based on a combination of Wavelet analysis and hybrid support vector machines-Hidden Markov Models (SVM/HMM). Wavelet analysis is used for feature extraction by decomposing the DUS signal into a detailed component which is linked to the cardiac valve motions, i.e. opening (o) and closing (c) of the Aortic (A) and Mitral (M) valves.

The non-invasive fetal electrocardiogram (fECG) is used as a



An illustrative example of fetal cardiac intervals

The correlation between the fetal cardiac intervals (illustrated in the figure) were evaluated for 16-41 weeks of gestation and compared for three fetal age groups: 16-29 (15 fetuses), 30-35 (12 fetuses) and 36-41 (18 fetuses) weeks. Considering 16-41 weeks of gestation, significant correlations were found between EDT and STI ($r=0.5588$, $p=0.0001$); STI and PEP ($r=0.6503$, $p<0.0001$); STI and VET ($r=0.6475$, $p<0.0001$); EDT and PEP ($r=0.8729$, $p<0.0001$); IRT and VET ($r=-0.3660$, $p=0.0150$). Results also showed the changes in correlations for three age groups. For example, EDT- PEP correlation becomes more significant with increasing gestation: ($p=0.0160$ for 16-29 weeks, $p=0.0004$ for 30-35 weeks, $p<0.0001$ for 36-41 weeks). However, IRT- PEP and IRT- VET correlation were found to be significant ($p<0.01$) only for 16-29 weeks and 35-39 weeks respectively. These findings can be used as sensitive markers for evaluating the healthy development of fetal cardiac performance.

Non-Photorealistic Volume Visualization with Color Distance Gradient and Two-Level Volume Rendering

Yong Xia*, Libing Zeng, Kuanquan Wang

Harbin institute of technology
, China

Aims: Traditional approaches for rendering segmented volumetric data sets usually deliver unsatisfactory results, such as insufficient frame rate, low image quality, and intermixing artifacts. To address this problem, we proposed a novel non-photorealistic volume rendering (NPVR) technique and two-level volume rendering, based on graphics processing unit (GPU) accelerated ray casting and post-color attenuated classification.

Methods: The key idea of this work is the synthesis of 3D volume textures. Specifically, our algorithm involves three phases. • Firstly, generate a segmented heart volumetric data set from the VHP data set by mask volume. • Secondly, apply our transfer function, in which NPVR is used to enhance underlying features and color distance gradient is used for opacity design. 1>NPVR process: 1)Map voxel's color to another color space such as YUV or HIS. 2)Construct a cumulative histogram on one component. 3)Map the cumulative histogram into a piecewise linear function $F(x)$. 4)Then, every voxel in data set will be mapped to a new value by the $F(x)$. 2>Calculate color distance gradient. • Finally, we put the processed volume texture into opengl pipeline, where the two-level volume rendering is taken.

Results: Segmented heart from the Visible Human Project (VHP) data set is used for test. Through our approach we can see the structures much clearer, with only a little color distortion.

Conclusion: We strengthen color by apply a novel histogram equalization to every voxel and use color distance gradients for opacity design. This method can enhance subtle details with only a little color change which look so similar through human eyes. And we also propose a structure surface rendering based on two-level volume rendering, which proves to be effective.

PA9

QRS Delineation Algorithms Comparison and Model Fine Tuning for Automatic Clinical Classification

Antonio Casanez-Ventura, Francisco-Javier Gimeno-Blanes*, Jose-Luis Rojo-Alvarez, Jose-Maria Lopez-Ayala, Juan-Ramon Gimeno-Blanes, Arcadi Garcia-Alberola

UMH

Elche / Alicante, Spain

Background and Objective. QRS complex extraction and wave detection has been a subject of intensive scientific efforts in the last two decades. This work elaborates on different QRS delineation algorithms for diagnostic measurement. **Methods.** A subset of 150 ECGs were randomly selected from an ECG database of the inherited heart diseases unit with over 3.500 consecutive ECGs from Hospital Universitario Virgen de la Arrixaca (Murcia, Spain). Three QRS detection methods were implemented, and compared with the GE MAC 5000 ECG system Output, and with a Gold-Standard manually and carefully developed by our clinicians. The implemented methods were applied firstly to the full ECG signal, and secondly to a single averaged ECG beat calculated for each ECG lead. Ectopic beats, and beats with cross-correlation under 99,95%, were not considered for mean computation. **Results.** Better performance was obtained using averaged signals, thanks to the denoising effect. Results for QRS duration showed an error of 7.90 ± 6.83 ms for Physionet method, and $8,31 \pm 3,07$ ms for Chouhan Method. Proposed methods outperformed the ECG device output (8.63 ± 5.89 ms). Best performance was obtained using a two-step combined method. A first step using Chouhan model, provided an initial outlook of QRS onset and offset, by overcoming irregularities in real ECG. A second adjustment, using a first and second momentum threshold, provided a closer fit to Gold-Standard measurements (6.27 ± 4.77 ms). **Conclusions.** Individual methods very much rely on one single measurement that does not easily match with clinicians criteria. Chouhan method provided an accumulated risk index, but although it does not provide the right fiducial point It overcomes local singularities, where other methods failed. A two stage strategy, based on an initial rough adjustment, and a second phase driven by the fist and second momentum, provides a better match to clinicians indications.

SB1

ECG Baseline Wander Removal and Impact on Beats Morphology: A Comparative Analysis

Antonio Fasano, Valeria Villani

Università Campus Bio-Medico di Roma
Rome, Italy

Aims: This study aimed to assess the impact of different baseline wander removal techniques on ECG signal morphology. Baseline wander (BW) is a kind of noise affecting all ECGs and its removal is an unavoidable step in any processing of ECG signals. However, particular care must be paid to preserve ECG signal morphology.

Methods: High-pass filtering (HPF), median filtering (MF), adaptive filtering (AF) and wavelet adaptive filtering (WAF) – which are common techniques to BW removal – and the recent approach based on quadratic variation reduction (QVR), were compared in this study. Their performance was assessed using the two-channel ECG record mitdb/119, from the MIT-BIH Arrhythmia Database (PhysioNet), since it exhibits frequent premature ventricular complexes (PVCs) – 25% of beats are PVCs –. The first 5 minutes of this record were considered, since they are mostly free from BW, and were corrupted by different realizations of BW extracted from the record nstdb/bw from the MIT-BIH Noise Stress Test Database. The ECG record was manually segmented by an expert into: PVCs, ST segments of normal beats, and normal beats excluding the ST segment. The performance of the algorithms for BW removal was assessed by comparing the a priori known BW with the corresponding estimate by each algorithm. The (relative) estimation error was computed on the entire record, and on *each* single PVC, ST segment, and normal beat excluding the ST segment. Estimation errors were averaged over 1280 errors for PVCs and 3936 errors for normal beats and for ST segments.

Results: Mean errors are reported in the table, from left to right: mean error on entire records μ_ϵ , on ST segments μ_ϵ^{ST} , on PVCs μ_ϵ^{PVC} , and on normal beats excluding the ST segment μ_ϵ^{NB-ST} .

Conclusion: The approach based on QVR outperforms state-of-the-art algorithms in estimating BW, while preserving the morphology of all waveforms in ECG, both in normal and ectopic beats.

	μ_ϵ	μ_ϵ^{ST}	μ_ϵ^{PVC}	μ_ϵ^{NB-ST}
HPF	0.38	9.73	5.84	6.78
MF	0.68	6.66	16.87	3.72
AF	0.71	7.94	16.92	4.11
WAF	0.58	5.77	13.24	6.01
QVR	0.22	4.34	3.11	3.10

SB1

Baseline Wander Removal in ECG and AHA Recommendations

Antonio Fasano*, Valeria Villani

Università Campus Bio-Medico di Roma
Rome, Italy

Aims: To reduce artifactual distortion of the ST segment, the American Heart Association (AHA) Recommendations establish different limits for response of linear digital filters used to remove baseline wander (BW). In this work we derive a very simple single-pole digital filter that violates AHA Recommendations, but outperforms state-of-the-art algorithms for BW removal.

Methods: The starting point is our recent approach to BW removal based on quadratic variation reduction. It estimates BW by means of a linear time-variant transformation that has some optimality properties. This approach has been shown to outperform state-of-the-art algorithms on BW removal. Thus, we derive the single-pole digital filter as an asymptotic approximation of the linear time-variant transformation, and use it to filter data in both the forward and the reverse directions. Such a filter retains (approximately) the optimality properties of the original time-variant transformation, although it violates the AHA Recommendations. We carry out a comparative analysis of the filter with high-pass filtering (HPF) (compliant with AHA Recommendations), cubic spline interpolation (SPI), median filtering (MF), adaptive filtering (AF) and wavelet adaptive filtering (WAF), which are classical approaches to BW removal. The performance are assessed considering both real and synthetic ECG records and evaluating different figures of merit, in particular with regard to the distortion of the ST segment.

Results: Measuring performance in terms of average distortion of the ST segment, and setting to 1 the average distortion introduced by the single-pole filter, the average distortion introduced by the other algorithms is greater than 1 and is given by: HPF=1.4; SPI=1.3; WAF=3; AF=7.9; MF=11.4.

Conclusion: The proposed single-pole filter, even though it is not compliant with AHA Recommendations, outperforms state-of-the-art algorithms in removing BW, while preserving the ST segment. It provides insight into the way we should model BW.

SB1

Transposition of Any Lead Placement to the Standard 12 Lead ECG Configuration on a Personalized Thorax Geometry

Peter M van Dam*, Arie C Maan, Niek HJJ van der Putten, Nico Bruining, Arnold W A Dijk

Radboud University Nijmegen
Arnhem, Netherlands

Introduction: In patients with evolving acute myocardial infarction (MI) the effect of treatment through percutaneous coronary intervention (PCI) is related to the time delay between the onset of the symptoms and the reperfusion of the occluded artery. The electrocardiogram is considered to be the pivotal test for diagnosing acute MI. Contemporary ambulance equipment is able to acquire the ECG and predict the culprit artery. However, the positions of ECG electrodes on a patient in critical condition is troublesome and time consuming which needs to be optimized.

Objective: Correction of misplaced electrodes to the standard 12 lead electrode placement.

Methods: We developed an algorithm to determine the electrode position and the shape of the thorax using the coordinates generated by the KINECT camera. These data were used to correct the measured ECG to represent standard 12 lead configuration.

Study: In this study we recorded in a population of 40 healthy volunteers a standard 12 lead ECG and ECGs where some electrodes were not placed in the standard position. By using the Kinect 3D camera the exact electrode positions and also the shape of the thorax were determined. An algorithm was developed to calculate the ECGs from standard electrode positions based on the locations of the mal positioned electrodes and the shape of the thorax for each individual subject. This algorithm, derived from well known Body Surface Mapping tools was tuned on a learning population of 20 randomly chosen recording sets and tested on the ECGs from the remaining 20 volunteers. All ECGs were fed into a diagnostic program and their resulting diagnoses compared. Results and conclusions At this moment the results are analyzed. The first preliminary results show that remapping is a rewarding process and leads to an improved diagnostic value of the ECG with misplaced leads.

SB1

Hyperpolarization-activated ‘pacemaker current’ — a funny current in models of SA nodal pacemaker cells

Ronald Wilders*, Arie O Verkerk

Academic Medical Center, University of Amsterdam, Dept of Anatomy, Embryology & Physiology
Amsterdam, The Netherlands

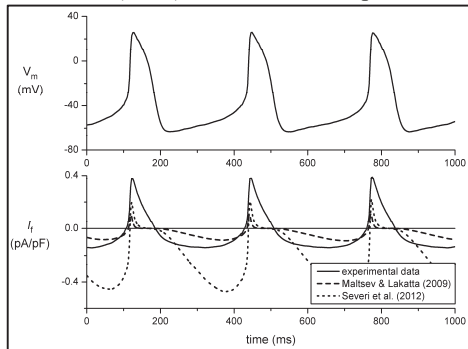
Background: A typical feature of sinoatrial (SA) node pacemaker cells is the presence of an ionic current that activates upon hyperpolarization. The role of this hyperpolarization-activated current, I_f , which is also known as the ‘funny current’ or ‘pacemaker current’, in the spontaneous pacemaker activity of SA nodal cells remains a matter of intense debate.

Aim: We aimed to characterize I_f as implemented in recent mathematical models of rabbit SA node pacemaker cells and identify any discrepancies with experimental data on I_f that we acquired over the past ten years.

Methods: We used experimentally recorded action potentials of a single isolated rabbit SA nodal pacemaker cell to reconstruct the time course of I_f according to the mathematical models of Maltsev and Lakatta (2009) and Severi *et al.* (2012).

Results: In terms of steady-state activation and fully-activated current amplitude, the model of Maltsev and Lakatta (2009) better fits our experimental

data than that of Severi *et al.* (2012), which shows a 5-fold overestimation of the resulting I_f steady-state current amplitude. With both models, the reconstructed time course of I_f shows several discrepancies with the time course based on our experimental data (Figure), largely due to the almost instantaneous deactivation of I_f at depolarized potentials in either model.



A simple and straightforward first-order Hodgkin and Huxley-type model of I_f appears sufficient to solve these discrepancies.

Conclusion: Our results explain that some investigators have successfully used computer simulations to support their view that I_f plays a fundamental role in the generation of pacemaker activity and its rate control, while others have provided computer simulation data in favor of their view that the role of I_f is limited to a modest contribution to rate control. This underscores the importance of using a model description of I_f that is properly validated against experimental data.

Accuracy of non-invasive frequency estimation using atrial fibrillation

Jorge Pedrón-Torrecilla¹, Alejandro Liberos¹, José Millet¹,
Andreu M. Climent², Maria S Guillem¹

1. Bio-ITACA, Universitat Politècnica de València, Valencia, Spain
2. Hospital General Universitario Gregorio Marañón, Madrid, Spain

Aim: Ablation procedures have become one of the most efficient treatments for termination of atrial fibrillation (AF). Prior knowledge of the region of the atria responsible of the maintenance of AF may be useful for procedure planning. The aim of this study is to evaluate the accuracy of dominant frequency (DF) maps on the epicardium computed from non-invasive recordings as a clinical tool for the identification of AF sources.

Methods: Spherical and realistic atrial models were used. Four fibrillation patterns with varying DF distributions were obtained with mathematical models. Surface potentials were computed by solving the forward problem and adding noise at signal-to-noise ratios (SNR) from 10 to 20 dB. Three AF patterns with different frequency distributions were calculated for the realistic model. For the spherical model, one AF pattern was generated with 20% of the surface activated at 21.5 Hz and 14 Hz on the other 80% of the surface.

Results: For the spherical model, RDM* between generated and inverse computed potentials was 0.56 without added noise and 1.05 with SNR=10dB. However, the RDM* of DF maps were 0.02 and 0.09, with DF errors of 0.01 ± 0.31 Hz and 0.26 ± 1.39 Hz, respectively. For the realistic model, frequency reconstruction was consistent with generated electrograms, allowing an accurate estimation of the DF distribution with a maximum RDM* of 0.19 (SNR=10dB), proving his accuracy in the highest DF location and frequency gradient detection.

Conclusion: Estimation of DF maps was consistent with the mathematical model frequency maps and has also shown to be less sensitive to noise than estimation of propagation patterns based on measured voltages and thus, more robust for detecting electrical sources during AF. This method demonstrated to be a promising tool for the non-invasive mapping of the frequency maps during AF and may help in planning ablation procedures.

SB2

Atrial Myocyte Model Parameter Optimization via Dynamic Electrophysiology Protocols and Automated Search Algorithms

Willemijn Groenendaal, Lala Tanmoy Das, Trine Krogh-Madsen, David Christini*

Weill Cornell Medical College
New York, United States

The foundation of a realistic multiscale model of atrial fibrillation is only as strong as the underlying atrial cell model. While there have been myriad advances in the improvement of cellular-level models, the identification of model parameters, such as ion-channel conductances and rate constants, remains a challenging problem. A main limitation is that such parameters are usually estimated from data recorded using standard electrophysiology voltage clamp protocols that have not been developed with model building in mind. We will describe our recent efforts to improve model parameter identification by developing and implementing novel, dynamically rich current- and voltage-clamp protocols and using the data acquired from such protocols to tune model parameters using automated computational search methods (specifically genetic algorithms). We are applying such an approach to improve the fidelity of atrial cell models and therefore multiscale human atrial modeling.

Influence Of Transmural Slow-Conduction Zones On Long-Time Behaviour Of Atrial Arrhythmia. A Numerical Study With a Human Bilayer Atrial Model

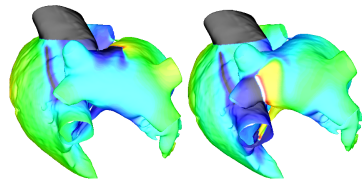
Simon Labarthe, Edward Vigmond, Yves Coudiere, Jacques Henry

Université Bordeaux Segalen, IMB - INRIA, Carmen - LIRYC
Talence, France

Aims: Two types of atrial models are usually used: surface or volume models, depending on the trade-off between the computational load and the model precision that is required for a given application. On an other hand, physiological evidence of transmural heterogeneities in the atria were documented, such as abrupt variations of the fibre structure through the thickness of the tissue, electrical dissociation or transmural reentries. Those phenomena can't be modelled by surface models. We present here a bilayer approach that enhance the usual surface models to capture the transmural heterogeneities while keeping low computational load. An example of long-time simulation is given.

Method: We used a bilayer model of the atria that included transmural heterogeneities of fibre organisation, together with a bilayer formulation of the monodomain model, and the Courtemanche's model of atrial electrophysiology. A slow conduction zone was added in one layer of the left atria, or in both, by decreasing the conductivity and the sodium channel conductance. A macro-reentry was initiated with a S1-S2 protocol. The evolution of the reentry was observed and compared to a control situation.

Results: When the slow conduction is transmural, the centre of the rotor was anchored in the slow conduction zone and became stable during a 10 seconds simulation, whereas the other simulations showed unstable rotors that disappeared after a few seconds. Furthermore, the simulations were performed with reasonable computational times (about 4 s for 1ms of simulation for a biatrial model on 6 cores). This study gave an insight of the influence of transmural fibrosis on atrial arrhythmia perpetuation. The bilayer model proved to be a good approach to investigate the effect of transmural heterogeneities with low computational times : it is a good trade-off for the study of the long-time behaviour of arrhythmia and for clinical applications.



Antero-superior view of RA and LA. Left: transmural slow conduction zone. Right: control.

SB2

Recording and Identification of Cardiac Neuron Activity in the Right Atrium Ganglionated Plexus

Siamak Salavatian*, Alain Vinet, Eric Beaumont, J Andrew Armour, Jeffrey L Ardell, Vincent Jacquemet

Montreal, Canada

BACKGROUND: There are growing evidences that imbalance in cardiac neurons activity is involved in the initiation and maintenance of atrial arrhythmias. Recent multichannel electrode array technology has enabled the simultaneous recording of multiple cardiac neurons located in ganglia on a beating heart. These signals are contaminated by the local activity of close-by atrial myocardium (atrial waveforms), possibly masking relevant neuronal activity.

AIMS: To record neuronal activity in ganglionated plexi and develop signal processing tools for identifying cardiac neuron waveforms (spikes) both outside and within atrial waveforms.

METHODS: Neuronal signals were recorded in situ for 25 min using a 16-channel unipolar linear microelectrode array (MicroProbes Inc.) inserted in the right atrium ganglionated plexus of an open-chest, anesthetized dog in sinus rhythm. An epicardial unipolar electrogram was simultaneously recorded at a nearby location to delimit the duration of proximal atrial activity (AA). Neuronal waveforms were identified outside these intervals and classified using the spike sorting and cluster analysis tools provided by the software Spike2. For each atrial beat, the close proximity of the 16 microelectrodes resulted in a very similar atrial waveform in all channels. The common atrial waveform obtained by principal component analysis of each individual beat was subtracted from the signals. Validation of AA cancellation was performed by comparing neuron spike waveforms extracted from within and outside AA.

RESULTS: Based on spike waveform classification, 18 neurons were identified. Firing rates ranged from 0.06 to 2.09 Hz (14832 spikes in total). After AA cancellation, 221 additional spikes (1.5%) were identified within AA, while AA covered 2.8% of signal duration. The correlation coefficients between matching neuronal waveforms within and outside AA were > 0.8 .

CONCLUSION: The activity of multiple cardiac neurons can be monitored in situ, even within AA. AA cancellation may provide a method to study neuronal activity during atrial arrhythmias.

Modification of Atrioventricular Node Conduction Increases RR Variability but not RR Irregularity nor Atrial Fibrillation Rate in Atrial Fibrillation Patients

Valentina DA Corino*, Fredrik Holmqvist, Luca T Mainardi, Pyotr G Platonov

Politecnico di Milano
Milano, Italy

We aimed at studying whether variability and irregularity of RR are modified by the selective A1 adenosine receptor agonist tecadenoson, the beta-blocker esmolol and/or their combination in patients with atrial fibrillation (AF). Twenty-one patients with AF were randomly assigned to either 75, 150 or 300 μg i.v. tecadenoson, administered alone and in combination with esmolol. The ECG was recorded continuously in the following 10-min phases: i) baseline1, ii) post-tecadenoson-dose1, iii) baseline2, ending at the time of the esmolol injection, iv) esmolol maintenance, v) post-tecadenoson-dose2. For every 10-min segment, heart rate (HR) and atrial fibrillatory rate (AFR) were estimated as well as variability and irregularity of RR intervals. Variability and irregularity parameters include M, SDNN, rMSSD, pNN50 and the regularity index approximate entropy, respectively. In all groups, HR decreased after tecadenoson (group taking 300 μg : 96 ± 17 vs. 87 ± 11 bpm, baseline1 vs. tecadenoson $p<0.05$; 86 ± 8 vs. 76 ± 9 bpm, baseline2 vs. tecadenoson+esmolol, $p<0.05$). Esmolol further decreased HR. The AFR was unaffected after tecadenoson. All the variability parameters were increased after tecadenoson. On the contrary, irregularity parameters did not change after tecadenoson. In conclusion, modification of AV node conduction using beta-blockade and A1-receptor blockade can increase RR variability but does not affect irregularity of RR intervals. Relative stability of RR-irregularity measures during AF supports the use of non-linear indices of RR behaviour for prediction of clinical outcome in patients with AF in large-scale trials.

SB3

Generalized Hurst Exponents as a Tool to Estimate Atrial Fibrillation Organization from the Surface ECG

M Julián¹, R Alcaraz², JJ Rieta¹

¹Biomedical Synergy, Electronic Engineering Department, Universidad Politécnica de Valencia, Spain

²Innovation in Bioengineering Research Group. University of Castilla-La Mancha, Cuenca, Spain

Atrial Fibrillation (AF) is the most common supraventricular arrhythmia found in clinical practice. The aim of the present work has been the application of the generalized Hurst Exponent of order 2, $H(2)$, to study AF organization from the surface ECG. $H(2)$ relates to the behavior of the autocorrelation function of a time series, thus measuring long-term statistical dependencies in the signal and, as a consequence, it could be used to estimate AF organization.

Since the spontaneous termination of paroxysmal AF is related to AF organization, the AF Termination Database has been analyzed. This database contains 80 ECG recordings divided into 3 groups: non-terminating (N), soon-terminating (S) and immediately-terminating (T). The atrial activity from each recording was extracted by adaptive QRST cancelation. Then, the signals were tested for nonlinearity and nonstationarity and showed a nonlinear and nonstationary behavior, thus making it advisable the use of non-linear metrics.

In order to remove noise and ventricular residua from the signals, the Main Atrial Wave (MAW) was extracted by selective band-pass filtering. $H(2)$ was computed on the last 15 seconds of the MAW as was recommended in a previous work. The MAW was obtained by a 3 Hz bandwidth selective band-pass filtering of the atrial activity centered on the Dominant Atrial Frequency (DAF). Then, the performance of $H(2)$ was compared with two established non-invasive AF organization metrics, the DAF and Sample Entropy (SampEn).

$H(2)$ yielded better classification results than DAF and SampEn (see Table 1). Moreover, statistically significant differences were found between non-terminating and terminating (S and T) groups and also between groups S and T. Therefore, $H(2)$ can be considered as a promising tool for the non-invasive study of AF organization.

Table 1. Classification accuracy of the metrics in each of the studied scenarios.

	N vs. T	N vs. S	T vs. S	N vs. (T & S)
DAF	88.3%	89.1%	59.3%	86.3%
SampEn-MAW	88.3%	89.1%	61.1%	91.3%
$H(2)$ -MAW	95.0%	93.5%	68.5%	93.8%

Spectral Analysis of Blood Pressure Variability in Atrial Fibrillation: the Effect of Tilting

Valentina DA Corino*, Federico Lombardi, Luca T Mainardi

Politecnico di Milano
Milano, Italy

During atrial fibrillation (AF), the beat-to-beat variation of blood pressure (BP) is increased because of variations in filling time and in contractility. Aim of this study was to assess changes of BP variability spectrum due to a sympathetic stimulation during a tilt-up stress test. Thirty patients (21 males, 69 ± 10 years) with AF were included in the study. Surface ECG and non-invasive beat-to-beat BP were recorded for 10 minutes at rest and during tilt (in 19 patients). During AF, R waves may not be coupled with an adequate left ventricular output to generate discrete pulses in BP and QRS can be not followed by an arterial pressure pulse. Therefore, a method which first localizes coarsely the systolic peak and then refines the position was used. The diastolic BP was also obtained. The BP series were resampled at 1Hz using cubic spline interpolation. Spectral analysis was performed using autoregressive (AR) models. The total power was decomposed into M contributions, one for each pole. The poles whose frequency was in the Low Frequency (LF, 0.03-0.15 Hz) or High Frequency (HF, 0.15-0.4 Hz) were selected. LF component power increased during tilt in both systolic and diastolic BP (rest vs. tilt: systolic BP: 6.5 ± 5.3 vs. 13.0 ± 13.4 $p < 0.05$; diastolic BP: 8.6 ± 4.5 vs. 10.9 ± 9.2 ns). HF component power also increased during tilt, and the HF peak was shifted towards lower frequency values during tilt. In conclusion, BP spectrum shows LF and HF components even in patient with AF and these components are influenced by a sympathetic stimulus, i.e., a tilt-up stress test. This finding highlights the capability of the autonomic nervous system to maintain LF and HF oscillations in BP variability even in presence of an irregular ventricular electrical and mechanical activity.

SB3

Computer-assisted Quantitative Analysis of New Interventional Treatment Methods

Giulia Paoletti*, Francesco Prati, Sebastiaan de Winter, Ronald Hamers, Nico Bruining

Erasmus MC
Rotterdam, Netherlands

Aims and methods: Coronary artery disease is being treated often by catheter based interventions such as implantation of drug-eluting stents. Recently, a new bioresorbable stent platform has been added to the treatment options. To evaluate the performance of these new methods imaging is applied including intracoronary methods. Intravascular ultrasound (IVUS) has been established for a long time and is one of the most used imaging modalities. Standard quantitative IVUS analyses methods are based on evaluation of a stack of individual cross-sectional images taken at 1s intervals of IVUS pullbacks acquired at a speed of 0.5mm/s . These methods neglect both the three-dimensional (3D) nature of the coronary vessels as well as the influence of the cardiac motion onto both the coronary artery dimensions as well as the possible IVUS catheter displacement. Over the years we developed several processing algorithms and semi-automated tools to improve the accuracy of these evaluations. Amongst them, three-dimensional reconstructions, semi-automated contour detections, retrospective ECG-gating and correction methods if accidentally different IVUS catheters or consoles have been used within longitudinal studies. The aim of this study was to apply these new analyses methods onto a study which was previously analyzed by older methods and to evaluate if this would result in a different study outcome.

Results: The most important parameters such as stent lengths and thus volumes, lumen-, stent- and vessel, were all significant different (some up to >30%) and showing standard deviations halve of those derived by the older methods. This has serious implications onto the interpretation of the performance of this new stent platform.

Conclusion: Improved image processing and computer-assisted quantitative analysis methods results in more accurate quantitative parameters allowing reducing the number of patients to be included in prospective studies and it should be considered to re-analyze previous studies analyzed by older methods.

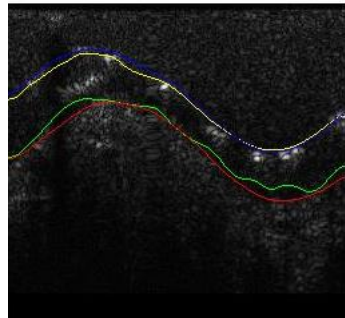
SB4

Automatic Segmentation of Intravascular Ultrasound Images based on Temporal Texture Analysis.

Adithya Gangidi¹, C. H. Chen¹, A U Coskun², Prakash Manandhar¹

University of Massachusetts Dartmouth¹, Northeastern University².

Intravascular ultrasound (IVUS) continues to be an important technique for imaging of coronary arteries and the detection of atherosclerotic disease. Since its inception, much of the efforts towards IVUS image analysis have been done using spatial information of single IVUS frame at a time. Accuracy of such approach is limited by the absence of clear boundary between lumen and arterial wall structure due to noise induced by catheter artifacts and speckle echo at high frequency. In our study we developed a novel automatic algorithm for the analysis and delineation of lumen and external elastic membrane (EEM) using both temporal and spatial variation of IVUS data. The first step of the three step algorithm accounts for noise correction by obtaining temporal Laplacian image gradient on basis of the four image neighborhood.



IVUS image comparing Lumen & EEM: Manual (Yellow and Red) vs Predicted (Blue and Green)

$$I_{g(m,n)}(t) = 5 * I_{(m,n)}(t) - [I_{(m,n)}(t+1) + I_{(m,n)}(t+2) + I_{(m,n)}(t-1) + I_{(m,n)}(t-2)]$$

In above equation $I_{(m,n)}(t+n)$ is the $(t+n)^{th}$ frame and $I_{g(m,n)}(t)$ is the gradient image obtained corresponding to frame number "t". In the second step, the resultant image is segmented into two parts using a composite measure of texture and grayscale intensity, each outlining the Lumen and EEM contour. The basis behind this step is that lumen area has coarser texture compared to the EEM, in turn characterized by finer texture. Discrete wavelet frames transform is building block of this texture demarcation. In the final step radial basis functions are used to obtain smooth contours from the radial outlines of Lumen and EEM. This algorithm is evaluated on large datasets of multi-patient (250) IVUS images (90 each) and pitted against the manually segmented contours by medical experts. It is observed that this algorithm reliably performs contour prediction with clinically appreciated limits of wall area average prediction error, well under 0.5 mm^2 , with greater than 93% overlap with actual.

IVUS Prediction Error
 Tested on 90 sets of 250 Images
 Source: BWH, Boston

Layer	Mean Error	Deviation
Lumen	0.23 mm	$\pm 0.34 \text{ mm}$
EEM	0.19 mm	$\pm 0.27 \text{ mm}$

SB4

Computer-Assisted Quantitative Evaluation of Coronary Stent Platforms by Different Intracoronary Imaging Methods

E Pociask^{1,2}, K Proniewska^{1,2} and N Bruining¹

¹ Erasmus MC, Rotterdam, Netherlands

² AGH University of Science and Technology, Krakow, Poland

Objective: Intravascular Ultrasound (IVUS) is the reference imaging method to demonstrate the anatomy of the coronary artery wall. It has led to better understanding onto the behavior of the atherosclerotic process and the effects of different treatment strategies amongst which coronary stents. However, recently optical coherence tomography (OCT), as a new intracoronary imaging tool with a much higher image resolution, has become the method of choice to evaluate new stent platforms. Due to the physical differences of IVUS (sound) and OCT (light based), stent geometry, and thus the stent struts, are markedly different visualized. The exact nature and impact of these differences onto quantitative analyses is not yet fully understood. This study investigates the differences of quantitative derived implanted stent parameters.

Methods and population: Dedicated semi-automated visualization and an adaptable quantification algorithm for OCT was applied for evaluation (Vessel Analysis, CURAD BV, Amsterdam, The Netherlands) in a series of drug-eluting stented coronary arteries in an animal model imaged by both IVUS and OCT at post-implantation (BL) and at 1 year follow-up (FUP).

Results: In absolute dimensions, within six stented coronary pig arteries, stent diameters were significantly different at BL between IVUS and OCT ($8,2\pm 1,0$ vs. $7,1\pm 0,7$ mm²), however, the delta change shows almost similar results ($2,1\pm 6,6$ vs. $3,5\pm 5,8\%$). Considering lumen area, IVUS showed smaller areas at BL and larger at FUP compared to OCT which resulted in a delta change of $-17,9\pm 13,8\%$ vs. $-29,7\pm 15,8\%$; respectively. The precision of the automated stent strut detection algorithm was at BL 82% and at FUP 67%. The number of struts detected by IVUS was 322 ± 30 and for OCT 888 ± 80 individual struts per stent.

Conclusion: OCT shows considerable more details, and quantitative differences, of implanted coronary stents as compared to IVUS. This must be taken into account when evaluating new stent platforms using both modalities.

SB4

Automatic Stent Segmentation in IOCT images Using Combined Feature Extraction techniques and Mathematical Morphology

Matheus Cardoso Moraes*, Diego Armando Cardona Cárdenas, Sérgio Shiguemi Furuie

University of São Paulo
São Paulo,, Brazil

Atherosclerosis is the cause of millions of deaths and billions of dollars in expenses worldwide. Intravascular Optical Coherence Tomography (IOCT) is a Medical Imaging Modality based on an infrared-light catheter, important for coronary investigations. Specifically, one of the IOCT applications is the investigation of neo-intima re-stenosis post stent. Therefore, segmentation is important for the re-obstruction quantification. Since IOCT provides hundreds of images in a pullback, manual or even semi-automatic segmentation procedures may become a stressful and time-consuming task. As IOCT is relatively new, few Stent segmentation works can be found in the literature, which may be the major bottleneck for improving diagnostics and speedup interventions and stent investigations. Therefore, so as to provide objective information, improving the overall procedures, automatic stent segmentation methods are necessary. Consequently, a fully automatic stent segmentation approach, based on a combination of Feature Extraction Techniques and Mathematical Morphology is presented. The Methodology has mainly two blocks: the first is a combination of Feature Extraction Techniques, which rely on a fusion of three processes; a combination of derivative information, contrast stretching process and Wavelet decompositions. The second main block is the Morphological Reconstruction, used as post-processing so as to select and improve the previous obtained information, finalizing the stent segmentation. A preliminary evaluation was performed by segmenting 160 images from pig coronaries, containing a variety of stent disposition (Figure); hence, the outcomes were comparing with their correspondent gold standards. The preliminary outcomes, resulting in values of True Positive(%) = 91.76 ± 7.94 , False Positive(%) = 8.05 ± 14.42 , False Negative (%) = 8.23 ± 7.94 . Conclusion, although the results are already good, they can be improved by finding the best combination of extracted information techniques. Therefore, future attempts will investigate the best disposition of information for better accuracy.

SB4

Cross-Entropy of Systolic Blood Pressure – Pulse Interval: Automatic Threshold and its Reliability

Tamara Čeranić, Tatjana Lončar-Turukalo*, Branislav Milovanović, Nina Japundžić-Žigon, Dragana Bajić

Faculty of Technical Sciences, University of Novi Sad, Serbia

Aims: This paper introduces a set of formulae for automatic evaluation of threshold level r_{TEOR} for which the cross-entropy of systolic blood pressure (SBP) and pulse interval (PI) (CrossEn) reaches its maximum. A mathematical method for estimating the level of consistency of entropy estimates is established as well. These two methods jointly determine a steady working point for consistent entropy estimates.

$$m=2: r_{TEOR} = T_{max}(x) + \left| -0.02 + 0.23 \cdot \sqrt{\frac{(sd_x + sd_y)}{2}} \cdot \sqrt{\frac{N}{1000}} \right| \cdot 0.1$$

$$m=3: r_{TEOR} = T_{max}(x) + \left| \left(-0.06 + 0.43 \cdot \sqrt{\frac{(sd_x + sd_y)}{2}} \right) \cdot \sqrt{\frac{N}{1000}} \right| \cdot 0.1$$

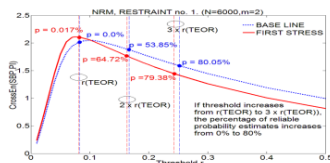
$x, y \in \{SBP, PI\}$, sd – standard deviation of differential series,
 $T_{max}(x)$ – threshold of a single series (known from literature)

Methods: The methods were applied to short signals (500 samples per subjects), recorded from healthy volunteers and to long signals (6000 samples per subjects), recorded from Wistar and Border hypertensive rats. The SBP and PI signal pairs that

passed the stationarity test were normalized and centralized, yielding 82 short and 48 long series. The error of automatic threshold in respect to its empirical true value is evaluated. The consistency of the entropy estimate is calculated as a percentage of comprising “matching template” probabilities that satisfy the criteria for statistical reliability.

Results: The relative error of automatic threshold for CrossEn(SBP,PI) and CrossEn(PI,SBP) was $2.34\% \pm 0.31$ and $1.42\% \pm 0.19$ respectively, evaluated from short time series. The corresponding relative errors for long time series were $2.37\% \pm 0.55$ and $1.85\% \pm 0.29$. For threshold values r_{TEOR} , $2Xr_{TEOR}$ and $3Xr_{TEOR}$, the percentage of probability estimates that fulfilled the criteria for statistical reliability were $5.32\% \pm 1.81$, $63.95\% \pm 3.94$ and $81.37\% \pm 2.17$ respectively for long signals, and 0% , $14.37\% \pm 2.1$ and $52.4\% \pm 2.69$ for short signals.

Conclusion: Automatic threshold for cross-entropy is of the same quality as established thresholds for single time series. The calculated percentage of statistically reliable probabilities that form a core for entropy estimates, shows that the threshold level must be shifted towards the higher values.



CrossEn estimates with percentage of statistically reliable probabilities

Prediction of Intradialytic Hypotension Based on Oxygen Saturation Variations

Claudia Perazzini*, Piergiorgio Bolasco, Luca Corazza, Michele Tramonti, Elena Mancini, Antonio Santoro, Stefano Severi

University of Bologna, Italy
Cesena, Italy

Aims. Hemodialysis (HD) sessions are often complicated by intradialytic hypotension (IDH), mainly due to the ipovolemia resulting from the insufficient refilling of fluid from the interstitial to the vascular compartment. Changes in cardiac output and tissue perfusion may be reflected in blood Oxygen content. The aim of this study was to analyze Oxygen saturation (SO₂) variations in relationship with IDH in patients with central venous vascular access. **Methods.** Ten hypotension prone patients were monitored along 3 months in standard bicarbonate HD. Systolic and diastolic arterial blood pressures (BP) were measured in pre-dialysis phase and every 30 minutes. SO₂ was continuously recorded (fc=0.2 Hz). SO₂ variations along the sessions were calculated as difference (Δ SO₂) between the SO₂ mean value in the 30 min before an hypotensive event or before the end of treatment and SO₂ mean value in the initial 30 minutes. ROC analysis was carried out to determine the predictive power of SO₂ variations in relationship with IDH. **Results.** A total number of 365 sessions were analyzed: 124 sessions were classified as “Hypo”, due to the presence of hypotensive episodes; 241 sessions were classified as “NoHypo” meaning without hypotension. Mean Δ SO₂ in Hypo sessions resulted significantly higher (absolute value) than Δ SO₂ in NoHypo sessions (respectively -7.5 ± 0.6 vs -3.6 ± 0.4 , $p < 0.001$). The decrease in systolic and diastolic BP was marked in Hypo sessions in comparison to NoHypo sessions ($p < 0.001$). ROC analysis produced a curve with AUC equal to 0.631 (CI95% 0.564-0.690); setting a threshold value equal to -7.80, sensitivity was 62% (CI95% 0.537-0.709) and specificity was 60% (CI95% 0.535-0.659). **Conclusion.** Our results suggest that SO₂ decrease can reflect hemody-namic instability and monitoring SO₂ could be useful in clinical practice to prevent IDH occurrence.

SB5

Prediction of Intradialytic Hypotension using PPG and ECG

Frida Sandberg*, Raquel Bailon, David Hernando, Pablo Laguna, Juan Pablo Martinez, Kristian Solem, Leif Sörnmo

Lund University
Lund, Sweden

Intradialytic hypotension (IDH) is the most common complication during hemodialysis; early prediction and prevention of IDH would dramatically improve the living conditions for patients with end stage renal disease. A recently published study suggests that a decrease in the envelope of the photoplethysmography (PPG) signal can be used for predicting acute symptomatic IDH. In the present study, the PPG based method is extended by introducing a patient dependent detection threshold, which involves information on heart rate variability (HRV) and heart rate turbulence (HRT) from the current dialysis session. This is motivated since several studies have found significant differences in HRV and HRT between hypotension-prone and hypotension-resistant patients. Following preprocessing, the envelope of the PPG signal is estimated by smoothing and rectification. The envelope is then normalized by the average of the envelope during the first 5 min of dialysis. The detection procedure is based on a statistical model in which the normalized envelope of the PPG signal is either unchanged (hypothesis H0) or reduced (hypothesis H1). A generalized likelihood ratio test is employed in which the reduction in envelope is first estimated using maximum likelihood estimation. The probability of H1 is conditioned on two parameters that characterize HRV and HRT of each dialysis session; these parameters are estimated from the interval series of the ECG as the mean LF/HF ratio during the initial 30 min of dialysis and the turbulence slope, respectively. Recordings from 15 patients during 38 hemodialysis sessions were used to evaluate the method. Symptomatic IDH was correctly predicted in 9 out of 14 cases, while 5 out of 24 cases were falsely predicted. The performance was better for acute symptomatic IDH, 5 out of 5 cases were correctly predicted. The present method represents a novel approach to combining information derived from ECG and PPG signals.

SB5

Heart Rate Variability Analysis for the Prediction of Hypotension during Spinal Anesthesia in Programmed Cesarean and its Relation with Fetal Cord Acid-base Equilibrium

José M Remartínez¹, Raquel Bailón², Eva Rovira¹, Juan Bolea², Pablo Laguna² and Augusto Navarro^{1,2}

¹ Hospital Universitario Miguel Servet, Zaragoza, Spain

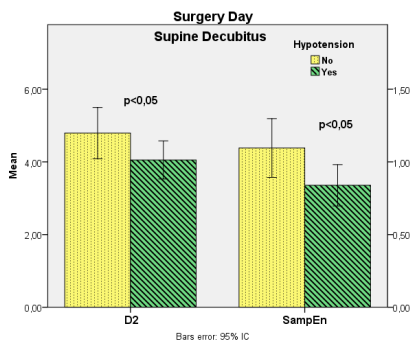
² University of Zaragoza, Zaragoza, Spain

Background: the high incidence (60%) of hypotension episodes is one of the major disadvantages of spinal anesthesia in programmed cesareans and fetal pH cord values are worse than those obtained after general anesthesia indicating fetal distress. Some heart rate variability (HRV) indices have shown ability for hypotension prediction.

Objectives: in this work we analyze linear and nonlinear HRV indices to predict hypotension during spinal anesthesia in programmed cesarean. The relationship between HRV and fetal pH cord values is also studied.

Methods: the ECG has been recorded in 35 pregnant women before the surgery and the previous day while lateral decubitus (LD), supine decubitus (SD) and recovery from seated Valsalva maneuver. Linear HRV indices included classical temporal and spectral indices. Nonlinear HRV indices included approximate and sample entropy (SampEn) and correlation dimension (D2).

Results: pregnant women who suffered hypotension (62.86%) showed higher values of arterial and venous lactic acid in cord blood ($p < 0.05$). Among all HRV indices analyzed, only SampEn and D2 were significantly different in patients who suffered hypotension from those who did not, being lower in the first group ($p < 0.05$). In patients who suffered hypotension the behavior of D2 when changing from LD to SD was opposite to those patients who did not suffer hypotension, decreasing in LD and increasing in SD. The difference in D2 value in LD with respect to SD showed highly significant difference related to hypotension ($p < 0.001$) and also correlated with venous lactic acid in fetal cord blood ($p < 0.05$).



SB5

Non-invasive Location of Re-entrant Propagation Patterns during Atrial Fibrillation

Miguel Rodrigo, Andreu M Climent, Alejandro Liberos, Jorge Pedrón-Torrecilla, José Millet, Francisco Fernández-Avilés, Felipe Ateienza, Omer Berenfeld, Maria S Guillem

Universitat Politècnica de València, València, Spain

Hospital General Universitario Gregorio Marañón, Madrid, Spain

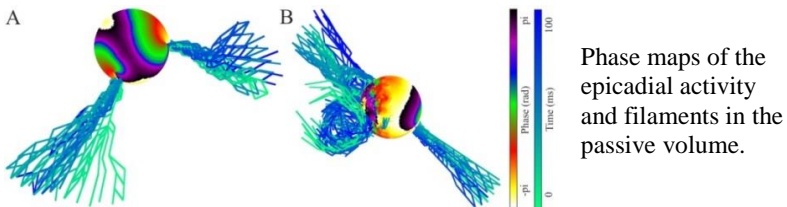
University of Michigan, Ann Arbor, MI, USA

Functional rotors have been defined as a mechanism responsible of maintenance of atrial fibrillation (AF). These re-entrant patterns can be identified in the atrial wall by locating phase singularities (PS) in the epicardial phase maps. In this study, we evaluate the potential role of body surface phase maps to non-invasively locate atrial sites that may harbor rotors. This technology could be of great interest for diagnosis and treatment of AF.

In the present study, we make use of mathematical models of atrial activity to evaluate the representation of PS in the torso and inside the passive volume. Specifically two scenarios were simulated: uniform re-entrant activity formed by two stable rotors (Panel A); and non-uniform fibrillatory activity formed by one stable rotor placed on 50% of the tissue, whereas the other 50% of the tissue contained irregular activity generated by fibrosis (Panel B). A filament was defined as a line connecting in time and space the PS detected on different layers from the epicardium to the torso.

In case (A), two stable filaments were detected in all layers. Each filament starts in an epicardial rotor and ends in a PS at torso. Case (B) shows several filaments, one arising from the main rotor and 16 from wavebreaks at the fibrotic tissue. However, only the filament from the main rotor reaches the torso and remains stable. Filaments arising at the fibrotic area cancel out with each other at increasing distances from the atria until a single filament reaches the surface with a wider meandering than that of the main rotor (0.8% of the sphere surface vs. 0.18%).

These results show that the electrical propagation pattern in the atria during AF is reflected in the electrocardiogram. Our simulations demonstrated that rotors that remained stable on the epicardium may be noninvasively detected.



MC

Computational Modelling of LQT1 in Human Induced Pluripotent Stem Cell Derived Cardiomyocytes

Michelangelo Paci*, Jari Hyttinen, Stefano Severi

Tampere University of Technology
Tampere, Finland

The production of disease-specific lines of cardiomyocytes derived from human induced pluripotent stem cells (hiPSC-CMs) opened new opportunities to study genetic cardiac disorders such as Long QT syndrome. We focus on the modelling of LQT1 in hiPSC-CMs: LQT1 is caused by the mutation of the *KCNQ1* gene, which reduces the slow delayed rectifying IKs current. Both control and LQT1 IKs formulations are based on the data published by Moretti et al.(2010), who reported an IKs reduced by 75% in LQT1 hiPSC-CMs, by characterizing peak/tail currents and the deactivation time constant. These data were integrated into our model of hiPSC-CM action potential (AP), based on the data published by Ma et al.(2011). Due to the high variability affecting hiPSC-CMs, the control APs reported by Moretti were different than those by Ma and reproduced by our model, so we tuned the maximal conductances of some membrane currents to fit our control model to Moretti's APs. The control APs showed (simulation VS experiments) (i) amplitude: 106 VS 107.8 \pm 2.1 mV, (ii) APD90: 405 VS 381.3 \pm 35.3 ms, (iii) rate of spontaneous beating: 69 VS 68.2 \pm 2.7 bpm. In simulations, LQT1 mutation induced a marked prolongation of the APD (APD90 +30%). By simulating the application of isoproterenol in the LQT1 model, the mutation effects were exacerbated (APD90 further increased by 20%) due to the impaired rate adaptation, as shown by the 13% increment of the ratio APD90/Cycle Length. Our in silico analysis confirmed that in hiPSC-CMs IKs plays a more important role in AP repolarization than in adult cardiomyocytes (e.g. a similar IKs reduction in the O'Hara-Rudy model prolonged APD90 by only 4%). This is explained in the model by a reduced repolarization reserve, in fact IKr and IK1 were reduced with respect to the adult AP in order to reproduce the control hiPSC-CMs AP features.

MC

Drug Effect Evaluation during Permanent Atrial Fibrillation using an AV-node Model

Frida Sandberg*, Valentina Corino, Sara Reinvik Ulimoen, Steve Enger, Arnljot Tveit, Luca Mainardi, Pyotr Platonov, Leif Sörnmo

Lund, Sweden

The purpose of the present study is to evaluate the effect of rate control drugs on the AV node characteristics during atrial fibrillation (AF) using a model-based approach. A statistical model of the AV nodal function is employed, defined by parameters which characterize the arrival rate of atrial impulses, the refractoriness of the fast and the slow AV-nodal pathway and the probability of atrial impulse to pass through either of the two pathways. The model parameters are estimated from consecutive 30 minutes segments of 24-h ambulatory ECG recordings. The arrival rate of atrial impulses is estimated from the atrial fibrillatory rate, whereas all other parameters are estimated from the RR interval series by means of maximum likelihood estimation. The RATAF (RATE control in Atrial Fibrillation) study database consists of recordings from 60 patients with permanent AF at baseline and on treatment with metoprolol, verapamil, diltiazem and carvedilol, respectively. A total of 283 recordings are analyzed, as 17 (5.7%) recordings were excluded due to insufficient signal quality. Out of 10590 analyzed segments, 10099 (95.5%) were considered accurately represented using by the model, i.e. the fit between the model probability density function (PDF) and an empirical PDF was >80%. The resulting model parameter estimates indicate that the refractory period of the slow pathway increased significantly during treatment with carvedilol (340+-70ms, $p<0.001$), diltiazem (350+-100ms, $p<0.001$), verapamil (350+-90ms, $p<0.001$), and metoprolol (330+-90ms, $p<0.001$) compared to baseline (260+-60ms). Also the model refractory period of the fast pathway increased significantly during treatment with carvedilol (460+-110ms, $p<0.001$), diltiazem (490+-150ms, $p<0.001$), verapamil (470+-130ms, $p<0.001$), and metoprolol (460+-110ms, $p<0.001$) compared to baseline (360+-90ms). No significant differences in model refractory periods between the tested drugs were found. The results suggest that the proposed AV-node model can correctly and non-invasively evaluate the effect of rate control drugs.

MC

Online Apnea-Bradycardia Detection using Recursive Order Estimation for Auto-regressive Models

D. Ge^{1,2}, A. Beuché^{1,2}, G. Carrault^{1,2}, P. Pladys^{1,2}, A. I. Hernández^{1,2}

¹ INSERM U1099 Rennes F35000, France

² Université de Rennes 1, LTSI, Rennes, F35000, France

Aims: This study aims to detect apnea-bradycardia episodes from preterm newborns, based on the analysis of ECG signals using an auto-regressive (AR) model. An on-line algorithm is proposed to track the AR order distribution.

Methods: The AR model for the recorded RR series is traditionally employed to compute the power spectrum density. Our objective here is to detect apnea-bradycardia episodes by abrupt changes in the model order distribution.

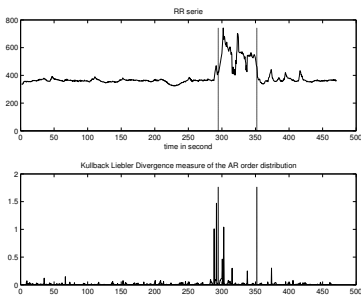


Figure 1. Apnea-bradycardia detection. The raw RR series with annotations of the AB episode is given above and the Kullback-Liebler divergence is calculated for the marginal posterior distributions for the AR model orders. Earlier than diagnosis detection is possible since the onset occurs before the RR level change.

We use the on-line Kalman filtering to track the changing coefficients of each fixed-order AR process and a Markovian model for the transition law between different model orders. We show that the marginal posterior distribution of the AR orders can be updated recursively for each newly-observed RR interval, by integrating out the normally distributed AR coefficients. The computational complexity can also be minimized to facilitate the on-line implementation of the algorithm. Compared with other detection approaches such as the Hidden Markov models (HMM), two obvious advantages are its fast learning ability (filters need only a few samples to

follow the signal dynamics) and its reduced calculation complexity.

Results: For the experiments, we used a database of apnea-bradycardia with manual annotations of RR series of 32 preterm infants suffering from frequent apnea-bradycardia. Kullback-Liebler divergences are calculated for the AR order distributions (cf Fig. 1) and a thresholding is used to trace the ROC curve of the detection. The sensitivity ($TP/(TP + FN)$) reaches 91.5% over a total of 50 episodes with perfect specificity ($TN/(FP+TN)=100\%$). Early detection is another critical quality in clinical applications and the proposed method achieves a delay of $5.08s \pm 2.90$ wrt the experts' annotations.

MC

Index

Aarts, Ronald	251	Andries, Daniela.....	254
Abächerli, Roger	40, 126, 144	Ansermino, J Mark.....	217, 279
Abbasi, Mitra	107	Antunes, Sofia.....	222, 226
Abboud, Shimon.....	128, 130	Aquilina, Michele	68
Accardo, Agostino.....	123	Arad, Marina.....	128
Addetia, Karima.....	66, 315	Aramendi, Elisabete.....	218, 219
Agostinelli, Angela	210	Arbeille, Philippe.....	208
Agten, Robin	63	Arberet, Simon	254
Aguiló, Jordi	240	Arcentales, Andres.....	216
Ajorloo, Hossein	110, 286	Arcentales, Andrés.....	31
Akematsu, Yuji.....	71	Ardell, Jeffrey L.....	328
Akhbari, Mahsa.....	50	Arenal, Ángel	157
Aktaruzzaman, M	119	Argelagos-Palau, Ariadna	127
Al-Aubaidy, Hayder.....	206	Armour, J Andrew.....	328
Albano, Amanda	209	Arsenos, Petros.....	37, 38
Alberola-López, Carlos...59, 155, 176		Arza, Adriana	240
Albertal, Mariano	164	Ashcroft, Anna	159
Alcaine Otín, Alejandro.....	181	Assanta, Nadia	271
Alcaine, Alejandro	31, 170	Atienza, Felipe	340
Alcaraz Martínez, Raúl.. 198, 199		Atsma, Douwe	140
Alcaraz, R	287, 330	Attarodi, Gholamreza	153
Alesanco, Alvaro	74	Attuel, Guillaume.....	292
Alesanco, Álvaro	7	Atyabi, Seyyed Abbas	79
Aletti, Federico	208	Augustyniak, Piotr.....	214
Allen, John	136	Auricchio, Angelo.....	235
Almeida, Rute	16, 21, 78, 241	Ayala, Guillermo	237
Alonso, Erik.....	34, 218, 219	Ayala, Unai.....	33, 34, 218
Alonso, Raúl.....	111	Babaeizadeh, Saeed.....	52
Alonso-Atienza, Felipe.....	189	Baer, Karl-Juergen	27
Altomare, Claudia .106, 227, 229		Bahrami Rad, Ali	33
Alvarez de Eulate, Maider	95	Bailón Luesma, Raquel.....	181
Álvarez, Diego.....	189	Bailón, Raquel. 31, 240, 338, 339	
Alvarez-Lacalle, Enric.....	188	Bailón-Luesma, Raquel	32
Amadori, Dino.....	68	Bajić, Dragana	61, 336
Amblard, Amel.....	302	Bakk, Sándor.....	303
Anderson, Kennet.....	29	Baldi, Mario	173, 293
Andreotti, Fernando	51	Balocchi, Rita	76
Andrés, Ana	237	Baranowski, Rafał	272
Andreu, David.....	170, 172	Barbieri, Riccardo	24, 288
		Barendse, Rogier	270

Barquero-Pérez, Óscar	6, 114, 171, 256, 266, 309
Bartolucci, Chiara .	106, 227, 229
Baselli, Giuseppe	208
Bataller, Manuel	299, 300
Bauer, Martin	298
Baumann, Oliver	302
Baumert, Mathias.....	18
Bayés-Genís, Antonio	31, 216
Beaumont, Eric	328
Behar, Joachim ..	39, 70, 80, 182, 200
Behbahani, Soroor.....	283
Benito, Salvador	273
Bennati, Marco	227
Benson, Alan.....	10
Berenfeld, Omer ...	294, 295, 340
Béres, Zoltán.....	303
Bermejo, Javier	157
Bernardes, João	78
Bernus, Olivier	312
Berruezo, Antonio	170, 172
Bertrand, Philippe B	63
Bertschia, Mattia	254
Betancur, Julián	65
Beuché, Alain.....	343
Bevilacqua, Stefano	267
Bhave, Nicole.....	223, 316
Bhuiyan, Tanveer A.....	97
Biala, Taher.....	280
Bifulco, Paolo.....	121
Billeci, Lucia	76
Binczak, Stéphane	308
Bini, Silvia.....	166
Bizopoulos, Paschalis.....	55
Blaber, Andrew.....	115, 305
Bleakley, Adam	10
Bojarnejad, Marjan.....	82
Bolasco, Piergiorgio	337
Bolea, Juan.....	4, 21, 339
Bond, Raymond	212
Bond, Raymond Robert	147, 269
Bonizzi, Pietro	102
Borkholder, David A.....	46
Bortolan, Giovanni.....	152
Boyett, Mark.....	99
Boyett, Mark R.....	224
Bragard, Jean	231, 285
Bravo, Roberto.....	6
Breen, Cathal	212
Brendle, Christian	253
Brooks, Dana.....	15
Bruining, Nico	323, 332, 334
Brüser, Christoph.....	253
Buchman, Timothy G	215
Bueno-Orovio, Alfonso	195, 232, 247
Burattini, Laura	36, 166, 210
Burrage, Kevin	232
Burton, Brett.....	15
Bustamante, John	245
Butakoff, Constantine.....	172
Buttu, Andrea	290
Cabañas, Miguel	6
Caffarel, Jennifer	251
Cai, Xue	99
Caiani, Enrico G 3, 21, 64, 69, 98,	235
Calvo, Conrado J	295
Camara, Oscar	170, 172
Caminal, Pere.....	117, 124, 216
Campillo Montes de Oca, Daniel257
Cano, Óscar.....	237
Cantalapiedra, Inma R	188
Cantalapiedra, Inmaculada R	296
Cappelaere, Charles-Henri....	302
Caravaca, Juan	299, 300
Cárdenas, Diego Armando
Cardona	335

Cardenas, Edgar.....	230	Clayton, Richard.....	107, 311
Cardona, Karen.....	13, 294	Cleland, John.....	251
Carducci, Tiziano.....	271	Clemmensen, Peter	163
Carlson, Eric.....	52	Clifford, Gari D. 39, 80, 150, 182, 200, 215, 289	
Carlyle, Jack	54	Clifford, Gari D.	70
Carmona, Neus.....	285	Climent, Andreu M194, 248, 340	
Carrasco-Sosa, Salvador113, 205		Cluitmans, Matthijs JM.....	102
Carrault, Guy	343	Cochet, Hubert	327
Casanez-Ventura, Antonio....	320	Cogan, Lisa	306
Casaseca-de-la-Higuera, Pablo	59	Cohen, Gregory.....	233
Castellanos-Domínguez, Germán.....	32, 132	Coimbra, Miguel	241
Castells, Francisco.....	307	Colantoni, Caterina.....	222, 226
Castiglioni, Paolo	131	Colloca, Roberta	200, 289
Castro, Noel Camilo.....	169	Colman, Michael Alan.....	11, 297
Castro, Simon J	11, 224	Colombo, Sebastiano.....	226
Cauwenberghs, Gert.....	145	Corazza, Luca	337
Cavazza, Marc.....	304	Cordero-Grande, Lucilio155, 176	
Cavero, Eva	74	Corino, Valentina	342
Ćeranić, Tamara.....	336	Corino, Valentina DA	329, 331
Cerutti, Sergio.....	222, 226	Corsi, Cristiana.....	68, 69, 174
Cervigón, Raquel.....	306, 307	Coskun, Ahmet Umit.....	333
Cesarelli, Mario.....	121, 123, 277	Costantino, Maria Laura	220
Charles, Fred.....	304	Couderc, Jean-Philippe ...	17, 167
Chávez, Carlos Eduardo	189	Coudiere, Yves	312
Chen, CH	333	Coudière, Yves	327
Chen, Minyi.....	259	Crescêncio, Júlio Cesar	112
Cheng, Sun.....	225	Crijns, Harry	238
Cherry, Elizabeth M	231	Croisille, Pierre.....	158
Chitiboi, Teodora	177	Cuesta, Pedro	111
Chladekova, Lenka.....	207	Cuko, Amarild	173, 293
Choletti, Sharath.....	215	Czippelova, Barbora.....	207
Christini, David	326	D'Addio, Giovanni.121, 123, 277	
Christov, Ivaylo	40, 126, 152	Dai, Ling	108
Chu, Gavin S.....	149	Dalmiani, Stefano	267
Ciaccio, Cristiano	173, 293	Daly, Jonathan	70
Citi, Luca	24, 197	Daly, Michael John.....	147
Claria, Francesc.....	124	Das, Lala Tanmoy.....	326
Clark, Elaine	163	Davoudi, Kian.....	72
		de Chazal, Philip.....	233, 260

De Felice, Alberto	123, 277	Dubois, Remi.....	312
de la Rosa, Manuel	6	Dubois, Rémi.....	292, 302
de Winter, Sebastiaan	332	Duchateau, Nicolas.....	172
DeCara, Jeanne.....	316	Dumont, Guy	305
Dedrij, Peter	63	Dumont, Guy A	217, 279
Dehkordi, Parastoo.....	217, 279	Dutta, Sara	190, 191
Del Castillo-Arrojo, Silvia	266	Echebarria, Blas	188, 296
Delgado, Victoria	140	Eftestøl, Trygve 33, 34, 175, 179,	219
della Bella, Paolo	226	Eggett, Christopher.....	178
DeManby, Brent	316	Eguzkiza, Aitor	9, 268
Demidova, Marina	35	Einax, Mario.....	298
Deo, Makarand.....	295	Elorza, Jorge.....	231, 285
Deogire, Aruna	84	Embid, Cristina.....	124
Dessi, Alessia	88	Endo, Miyuki.....	318
Dhawan, Akshay	87	Engan, Kjersti.....	33, 175, 179
Di Donato, Davide.....	129	Enger, Steve	342
Di Marco, Luigi Yuri	91	Erem, Burak	15
Di Maria, Costanzo	82, 136	Escalona, Omar Jacinto.....	169
Di Rienzo, Marco	131	Esposito, Antonio.....	222, 226
Diciotti, Stefano.....	24	Faes, Luca	30, 204
Dickhaus, Hartmut.....	44	Faini, Andrea.....	131
Didon, Jean-Philippe.....	301	Fakhri, Yama	163
Dijk, Arnold W A	323	Falcone, Denise.....	129
Dilaveris, Polychronis	37, 38	Fanelli, Andrea.....	43
Dill, Karin	223	Farolfi, Alberto.....	68
Dillenseger, Jean-Louis	67	Farré, Ramon	278
Dobrzynski, Halina	99	Fasano, Antonio....	116, 321, 322
Dokos, Socrates	105	Fatemi, Marzieh.....	48, 56
Domingo, Maria Teresa	216	Félix, Paulo.....	109, 282
Donal, Erwan	65	Fenton, Flavio H.....	231
Donati, Olivio.....	177	Fereniec, Małgorzata.....	148
Dong, Jingliang.....	1	Fernández, Carmen	237
Dorantes-Mendez, Guadalupe		Fernández-Armenta, Juan ...	170,
.....	208	172	
Dössel, Olaf.....	95, 250	Fernández-Avilés, Francisco .	340
Dovancescu, Silviu	251	Fernandez-Chimeno, Mireya	127
Dranca, Lacramioara.....	162	Ferrario, Manuela.....	208
Drexl, Johann	156	Ferrer, Ana	249
Dreyfus, Gérard	302	Festa, Pierluigi	271
Duan, Wenfeng.....	82, 178		

Figuera, Carlos	256	García-Navarro, Pilar	244
Finlay, Dewar	212	García-Vizueté, Beatriz	118
Finlay, Dewar Darren	147, 269	Garde, Ainara.....	217, 279
Fischer, Wolf-Joachim	275	Garreau, Mireille	65
Fitz-Clarke, John R	168	Gasser, T Christian	243
Fonseca, Pedro	276	Gatzoulis, Konstantinos	37, 38
Forclaz, Andrei.....	290	GE, Di	343
Forkan, Abdur Rahim		Gerlach-Hahn, Kurt.....	253
Mohammad.....	75	Ghaffari, Ali.....	79
Foster, Alice	54	Gharaviri, Ali	246
Fotiadis, Dimitrios.....	55	Giacopelli, Daniele.....	293, 297
Foussier, Jerome.....	276	Giannelli, Luigi	173, 293
Francisco, Sara.....	122	Gieraltowski, Jan.....	25, 92
Frangi, Alejandro	91	Gil Herrando, Eduardo.....	181
Frassinetti, Luca	68	Gil, Eduardo	58, 240, 278
Freed, Benjamin	223	Gimeno-Blanes, Francisco-Javier	
Frindel, Carole	158	320
Fuest, Matthias.....	62	Gimeno-Blanes, Juan-Ramon	320
Fukuoka, Yutaka	145	Giraldo, Beatriz	31
Fumero, Roberto	220	Giraldo, Beatriz F	216, 273
Funamoto, Kiyoe	318	Giuliani, Corrado.....	210
Furini, Simone.....	227	Godoy, Eduardo J.....	249
Furuie, Sérgio Shiguemi.....	335	Goette, Josef.....	180
Fusini, Laura.....	64	Gomez, Juan Fco.....	13
Gajre, Suhas.....	146	Gomis, Julio.....	230
Galbis, Antonio	237	Gomis, Pedro	117
Gale, Emma	54	Gonçalves, Hernâni.....	78
Galeotti, Loriano... 142, 211, 258		Goñi, Alfredo	162
Gangidi, Adithya	333	Gonzalez Fernandez, Rene ...	257
García, Constantino A... 109, 282		González, Iván.....	6
García, Fernando	306	Gonzalez, Rodolfo.....	230
Garcia, Irene	201	Gonzalez-Fernandez, Rene ..	137, 138, 143
Garcia, Jose.....	74	González-González, María	171
García, José.....	7	González-Otero, Digna... 34, 218, 219	
Garcia-Alberola, Arcadi.....	320	Goya-Esteban, Rebeca ..	114, 256
García-Alberola, Arcadi.... 6, 171, 256, 266, 309		Grabska-Chrzastowska, Joanna	
Garcia-Gonzalez, Miguel Angel		139
.....	127	Graff, Claus	97
García-Muñoz, José	6, 266		

Granåsen, Gabriel.....	317	Hart, George	99, 224
Grassini, Diego.....	293	Hasan, Muhammad	18
Greaves, Danielle K.....	208	Hayes, Greg.....	203
Grieten, Lars	63	Hayn, Dieter.....	85
Grigonytė, Eglė	58, 60	Hayward, Martin.....	232
Grigoriev, Roman.....	101	Hennemuth, Anja	156, 177
Groenendaal, Willemijn.....	326	Henriquez, Craig S.....	192
Grönlund, Christer	209	Henry, Jacques.....	327
Grossenbacher, Olivier	254	Hernández Alonso, Antonio.....	198, 199
Guaïta, Marc.....	124	Hernandez, Alfredo	343
Guardarrama, Ronny	257	Hernández, Alfredo I.....	65
Guardarrama-Mieres, Ronny.....	138	Hernández-Pérez, Eduardo.....	261
Guerra-Moreno, Iván.....	261	Hernando, David.....	31, 338
Guerrero, Juan F.....	299, 300	Herrera, Sergio	273
Guerrisi, Maria.....	24	Hills, Matthew	54
Guillem, María S. .	194, 248, 249, 325, 340	Himmelsbach, Tilo	51
Guillén-Mandujano, Alejandra	113, 205	Hirsbrunner, Béat	12, 100
Guldenring, Daniel.....	147, 269	Hocini, Meleze	292
Gupta, Shankar	146	Hodgson, Sam	10
Gustavsson, Sandra	209	Hoetzel, Elena.....	103
H. Lovell, Nigel.....	105	Holcomb, Mark	184
Haeberlin, Andreas.....	180	Holden, Arun.....	10
Haghpanahi, Masoumeh	46	Holmer, Mattias.....	60
Hahn, Horst.....	156, 177	Holmqvist, Fredrik	329
Haider, Syed	52	Hoog-Antink, Christoph	253
Haigney, Mark C	167	Horáček, B Milan	168
Haissaguerre, Michel....	292, 312	Hornero Sos, Fernando.....	198, 199
Halamek, Josef.....	17, 19, 236	Hoshiyama, Asagi.....	284
Halámek, Josef.....	41, 213	Hoshiyama, Masaki.....	284
Hallack Miranda Pureza, Andre	70	Hove, Leif	296
Hambly, Ethan	134	Hove-Madsen, Leif.....	188
Hamde, Satish.....	84	Hoyer, Dirk.....	22, 25
Hamers, Ronald	332	Hu, Weichih	264
Hamilton, Emily	23	Hubbard, Marjorie Letitia	192
Hanson, Ben	197, 232	Hughson, Richard L.....	208
Hargittai, Sándor	262	Hüllebrand, Markus.....	156
Harloff, Andreas	156	Hunt, Judith	18
		Hyttinen, Jari.....	341
		Illarramendi, Arantza.....	162

Imam, Mohammad Hasan	281	Jurak, Pavel	17, 236
Inthavong, Kiao.....	1	Jurák, Pavel	41, 213
Irusta, Unai	34	Jutten, Christian.....	49, 50
Ito, Kei.....	145	Kachenoura, Nadjia	223
Ito, Takuya	318	Kadkhodae, Amir	29
Ivánfai, Tamás.....	265	Kaminska, Bozena.....	72
Jacomet, Marcel	180	Kania, Michał	148
Jacquemet, Vincent	328	Kańtoch, Eliaasz	73
Jacquir, Sabir	308	Karel, Joël MH.....	102
Jafarnia Dabanloo, Nader	153, 283	Karlen, Walter.....	217, 279
Jäis, Pierre.....	327	Karmakar, Chandan 26, 125, 281	
Jäis, Pierre.....	292	Karvounis, Evaggelos	55
Jalife, José.....	294	Katz, Amos	45
Jana, Soumya	133	Kelkboom, Emile	251
Jané, Raimon	278	Keller, David.....	95
Janousek, Oto	154	Keller, Matthias W	250
Janoušek, Oto	122, 151	Kerekes, Anna.....	253
Jansen, Katrien	234	Khalaf, Kinda.....	206
Jansen, Thekla	140	Khalil, Ibrahim.....	75
Janusek, Dariusz	148	Khandoker, Ahsan..26, 125, 134, 281, 318	
Japundžić-Žigon, Nina.....	336	Khandoker, Ahsan H	206
Jarvis, Jonathan C	224	Khir, Ashraf W.....	8
Jasinski, Jamie.....	54	Khosrow-khavar, Farzad	252
Javorka, Kamil.....	207	Kimura, Yoshitaka	125, 318
Javorka, Michal.....	207	King, Susan.....	82
Jekova, Irena.....	144, 301	Klap, Tal	185
Jelinek, Herbert	26, 134, 281	Klimesh, Petr.....	213
Jelinek, Herbert F.....	206	Klinge, Annette	136
Jenei, Csaba	265	Koch, Eva	62
Jimenez Gonzalez, Daniel	257	Kodoth, Vivek.....	169
Jiménez, Juan.....	201	Kohler, Ralf	313
Jimenez-Gonzalez, Daniel.....	137	Kolarova, Jana.....	154
Johannesen, Lars ..	142, 211, 258	Kolářová, Jana.....	122, 151
Johnson, Alistair EW	182, 215, 289	Komatsu, Yuki	292
Johnson, Chris.....	15	Konrad, Niko	95
Julián, M	287, 330	Korsten, Erik.....	251
Juliá-Serdá, Gabriel.....	261	Kőszegi, Bálint.....	265
Júnior, Lourenço Gallo.....	112	Kőszegi, Zsolt	265, 303
		Koutsouris, Dimitrios	55

Kramer, Andrew A	215	Leite, A.....	120
Kramer-Johansen, Jo 33, 34,	219	Lemay, Mathieu.....	254
Krasteva, Vessela.....	144, 301	Lenk, Claudia.....	298
Krause, Rolf.....	235	Leonhardt, Steffen 183, 253,	276
Krejčířova, Lenka	19	Lewandowski, Adam.....	159
Krisciukaitis, Algimantas.....	81	Lhotska, Lenka	47
Krogh-Madsen, Trine.....	326	Li, Guojun.....	53
Kropf, Martin	85	Li, Jue	99
Kruse, Eric.....	316	Li, Lerong	259
Kugiumtzis, Dimitris.....	204	Li, Peng.....	83, 255, 274
Kuijpers, Nico HL.....	246	Li, Qiao.....	200
Kuzilek, Jakob	47	Li, Xin	149
Kvaløy, Jan T	33	Liberos, Alejandro 194, 248,	325,
Labarthe, Simon	327	340	
Lachiri, Zied.....	141	Lillo-Castellano, José María ..	118
Lado, María J	111	Lim, Chi-Wan	160
Lagae, Lieven	234	Lin, Chun-Cheng.....	264
Laguna Lasasosa, Pablo.....	181	Lindqvist, Per	209
Laguna, Pablo .. 4, 21, 31, 32,	35,	Lines, Glenn Terje	187
58, 77, 93, 164, 167, 170,	240,	Linsen, Lars	177
278, 338, 339		Lipińska, Olga.....	272
Lamata, Pablo	159	Lipponen, Jukka A.....	42
Lamberti, Claudio 66, 68, 69,	174	Liu, Changchun	255, 274
Lambiase, Pier	197, 232	Liu, Chengyu	83, 255, 274
Lang, Roberto .66, 223, 315,	316	Liu, Ming	225
Lang, Roberto M.....	3, 64, 235	Llamedo, Mariano.....	77, 164
Langley, Philip.....	82, 178, 297	Logantha, Sunil Jit.....	99
Lankveld, Theo.....	238	Lombardi, Federico.....	331
Latcu, Decebal G.....	288	Loncar-Turukalo, Tatjana.....	61
Lau, Ernest	169	Lončar-Turukalo, Tatjana.....	336
Laurent, Gabriel.....	308	Long, Xi	276
Laurin, Alexandre	115	Lopez-Ayala, Jose-Maria	320
Laws, Elaine	267	Lorenzini, Cinzia.....	68
Lázaro Plaza, Jesús.....	181	Lorenzo-Costa, Yaniesis	138
Lázaro, Jesús.....	240, 278	Lowe, Tristan	224
Lazdam, Merzaka.....	159	Lugo, Carlos	296
Lechuga-Suárez, Luis	266	Luik, Armin.....	250
Ledesma-Carbayo, María J ...	157	Lukoševičius, Arūnas.....	202, 221
Leeson, Paul.....	159	Lukoševičius, Mantas.....	57
Leinveber, Pavel	213, 236	Lunze, Katrin.....	253

Luo, Cunjin.....	96	Marsili, Davide.....	174
Lysaker, Ola Marius	186, 187	Martin, Elizabeth	212
M Climent, Andreu	325	Martín-Caballero, Carlos	118
Ma, Long.....	259	Martinez, Fernando	230
Maan, Arie C	2, 323	Martinez, Juan Pablo	338
Maass, Philipp.....	298	Martínez, Juan Pablo.....	35, 77, 164, 167, 170
Mabote, Thato.....	251	Martínez-Espronedada, Miguel ..	9, 268
Maccabelli, Giuseppe	226	Martín-Fernández, Marcos.....	59, 155, 176
Macerata, Alberto	76	Martín-González, Sofía	261
Macfarlane, Peter.....	163	Martín-Martínez, Diego	59
Macleod, Rob.....	15	Martins Rocha, Bernardo.....	103
Maestri, Roberto	121	Martín-Yebra, Alba	35, 77
Magenes, Giovanni.....	43	Martufi, Giampaolo	243
Maghooli, Keyvan	153	Marzbanrad, Faezeh	134, 318
Magjarević, Ratko.....	105	Marzo, Alberto.....	91
Magrans, Rudys	117	Matthews, Slade	134
Maier, Christoph.....	44	Mauray, Philippe	290
Maier, Julian	95	McBride, Joseph	90
Mainardi, Luca 94, 129, 289, 342		McEaney, David	169
Mainardi, Luca T	93, 329, 331	McFerrin, Brent	90
Malberg, Hagen	51	McLachlan, Craig.....	134
Malki, Guy.....	104	McNitt, Scott.....	167
Måløy, Frode	179	Melia, Umberto	124
Malyala, Sathyavani.....	311	Méndez, Arturo J	111
Man, Sumche.....	36, 166	Mendonça Costa, Caroline ...	103
Manandhar, Prakash	333	Ménétré, Sarah.....	301
Mancini, Elena	337	Menon, Carlo	252
Mangione, Maurizio	267	Meo, Marianna	288
Maniewski, Roman	148	Merino-Caviedes, Susana	155
Manis, George	37, 38	Meste, Olivier	288
Manoharan, Ganesh.....	169	Mhajna, Muhammad.....	130
Manthalkar, Ramchandra.....	146	Millet, Jose.....	325
Manzo, Alain.....	230	Millet, José...248, 295, 306, 307,	340
Marchi, Marina	267	Milovanović, Branislav.....	336
Marcotte, Christopher.....	101	Mincholé, Ana.....	190
Marinazzo, Daniele.....	30, 204	Mincholé, Ana.....	4, 191
Marisa, Thanks	180		
Marozas, Vaidotas ..	57, 202, 221		
Marques, Nuno.....	241		
Márquez, David G	282		

Mirzaee, Hanieh	156	Nelwan, Stefan	270
Misgeld, Berno	276	Neycheva, Tatyana	126
Modre-Osprian, Robert	85	Ng, G André	149, 291
Moharreri, Sadaf	110, 286	Ni, Haibo	224
Mollakazemi, Mohammad Javad	79	Niederhauser, Thomas	180
Monasterio, Violeta	167	Nielsen, Bjørn Fredrik ...	186, 187
Montalto, Alessandro	30, 204	Niknam, Sajad	56
Montano, Nicola	236	Niknami, Maryam	79
Montes de Oca-Colina, Gisela	143	Niknazar, Mohammad	49, 50
Moody, George	5	Nikolopoulos, Stavros	37, 38
Moody, George B	39	Noack, Alexander	275
Moraes, Matheus Cardoso ...	335	Noč, Marko	165
Mora-Jiménez, Inmaculada .	256, 266	Nollo, Giandomenico	30, 204
Mor-Avi, Victor	66, 174, 223, 315, 316	Novák, Miroslav	213
Moreno, Javier	307	Novakova, Marie	19, 154
Moss, Arthur J	167	Nováková, Marie	122, 151
Mostacciolo, Gaspare .	106, 229	Nugent, Chris	212
Motie Nasrabadi, Ali	283	Olde, Bo	60
Muehlsteff, Jens	183	Olejnickova, Veronika	154
Muhammad, Syamil	280	Olejníčková, Veronika ...	122, 151
Mulet-Cartaya, Margarita	137	Olivan-Viguera, Aida	313
Munoz, Laura	14	Orini, Michele	28, 197, 232
Murillo Rendón, Santiago	132	Orłowska-Baranowska, Ewa .	272
Murillo, Javier	244	Ørn, Stein	175, 179
Murray, Alan ..	82, 136, 178, 239, 242	Orozco Gutiérrez, Alvaro Angel	132
Murtagh, Gillian	316	Orozco-Duque, Andrés	245
Murzi, Bruno	271	Orsolini, Stefano	24
Nanasi, Peter P	106	Ortigosa, Nuria	237
Naranjo, Valery	175	Ortuño, Juan E	157
Naranjo-Orellana, José	114	Oster, Julien	80, 150, 200
Narasimhan, Kirthika	54	Ostojic, Vladimir	61
Navajas, Daniel	278	O'Sullivan, John	136
Navarro, Augusto	339	Otani, Niels	14
Navarro-Mesa, Juan Luis	261	Otero, Abraham	109, 282
Nayyar, Sachin	18	Ozon, Matthew	158
		Paci, Michelangelo	341
		Paggi de Almeida, Tiago	149, 291
		Palaniswami, Marimuthu	26, 125, 134, 281, 318

Palmisano, Anna	222, 226	Pioggia, Giovanni	76
Palmius, Niclas	70	Pladys, Patrick	343
Pan, Fan	82, 239, 242	Plange, Niklas	62
Pandit, Sandeep V	294	Plank, Gernot	103
Pani, Danilo	88	Platonov, Pyotr	35, 342
Paoletti, Giulia	332	Platonov, Pyotr G	329
Pappone, Alessia	173, 293	Plešinger, Filip	41
Pappone, Carlo	173, 293	Pociask, Elżbieta	334
Parati, Gianfranco	131	Podziemski, Piotr	92
Parham, Azadeh	153	Polgár, Péter	303
Pascale, Patrizio	290	Poll, Rüdiger	275
Passini, Elisa	98, 228	Pollard, Tom	54
Päßler, Sebastian	275	Pomier, Carole	292
Patel, Amit	174, 223	Pont, Oriol	135, 308
Pattichis, Constantinos	74	Potse, Mark	235
Pedrón-Torrecilla, Jorge	248,	Potter, Kristin	15
325, 340		Prassl, Anton	103
Peeters, Ralf LM	102	Prati, Francesco	332
Pelech, Nikki	10	Presedo, Jesús	109, 282
Pellegrini, Alessandro	98, 235	Proniewska, Klaudia	334
Peluffo Ordoñez, Diego Hernán		Provaznik, Ivo	154
.....	132	Provazník, Ivo	122, 151
Peñaranda, Angelina	188, 296	Pruvot, Etienne	290
Peng, Yi	20	Pueyo, Esther	4, 31, 94, 247
Pepi, Mauro	64	Pulido-Hidalgo, Francisco Javier	
Perazzini, Claudia	337	309
Pereira da Silva, Fátima Maria		Quinn, T Alexander	191
Helena Simões	112	Quintana-Morales, Pedro	261
Perez Alday, Erick Andres	297	Quintanilla, Teresa	6
Pérez, M Teresa	155	Quintanilla-Fernández, Teresa	
Pérez-David, Esther	157	266
Pérez-Villacastín, Julián	307	Quotb, Adam	292
Perlman, Or	45	Rabhi, Emna	141
Pervolaraki, Eleftheria	10	Raffo, Luigi	88
Petelczyc, Monika	272	Rahimi, Azar	196
Petrénas, Andrius	202	Ramírez Zuluaga, Liliana Patricia	
Petretta, Andrea	173, 293	132
Petrolis, Robertas	81	Ramírez, Julia	4
Piazzese, Concetta	3	Ramos-Castro, Juan	127
Pieciak, Tomasz	161	Rapalis, Andrius	221

Rauber, Martin	165	Rojo-Álvarez, José-Luis	114
Ravelo-García, Antonio Gabriel	261	Rollin, Anne.....	290
Razavipour, Fatemeh.....	48, 56	Romano, Maria	121, 277
Reilly, Richard	306	Romero Pérez, Daniel	181
Reinvik Ulimoen, Sara.....	342	Romero, Lucia	13
Reiserer, Ron	184	Ronzhina, Marina..	122, 151, 154
Remartínez, José M	339	Rosado-Muñoz, Alfredo	299, 300
Ren, Yongai	274	Rosen, Paul	15
Renevey, Philippe	254	Rossi, Giuseppe.....	267
Revilla, Ana	176	Roussel, Pierre	302
Rezaei, Shahab.....	110, 286	Rovira, Eva M.....	339
Riedl, Maik	51	Ruano Restrepo, Mario Iván.	132
Rieta Ibáñez, José Joaquín ...	198, 199	Rúa-Seoane, Juan Carlos.....	285
Rieta, JJ	287, 330	Rubio, Óscar J	7
Riveros, Fabian	243	Ruiz de Gauna, Sofía	218, 219
Rivero-Varona, Martha.....	143	Ruiz, Jesús.....	34, 218, 219
Rivet, Bertrand	49, 50	Ruiz, Puy	278
Rix, Hervé.....	148	Russell, James	218
Rizzo, Giovanna	222, 226	S. Chu, Gavin.....	291
Roberts-Thomson, Kurt	18	S. Schlindwein, Fernando	291
Robini, Marc	158	Sáenz de Pipaón, Edurne	285
Rocca, Andrea.....	68	Saiz, Javier.....	13, 230, 245, 249, 294
Rocca, Emiliano	271	Sala, Luca	106, 229
Rocchetti, Marcella.....	106	Salamero, Manel.....	124
Rocha, Ana Paula	16, 78, 241	Salavatian, Siamak	328
Rocha, AP.....	120	Salinet, João.....	291
Rodrigo, Miguel	194, 248, 340	Saltz, Joel H.....	215
Rodrigues, Rui.....	89	sameni, Reza	48
Rodríguez Rubio, Jorge.....	257	Sameni, Reza.....	56
Rodríguez, Blanca	190, 191, 195, 232, 247	Sánchez Martínez, Sergio	180
Rodríguez, Jose F	93, 94, 243, 249	Sanchez, Carlos	247
Rodríguez-Liñares, Leandro..	111	Sánchez-Muñoz, Juan José ..	171, 309
Roebuck, Aoife.....	70	Sandberg, Frida.....	60, 338, 342
Rojo-Álvarez, José Luis	6, 118, 171, 256, 266, 309	Sanders, Prashanthan.....	18
Rojo-Alvarez, Jose-Luis	320	Sandoval, Zulma	67
		Sánta, János	303
		Santamaria, Joan	124
		Santiago-Mozos, Ricardo	118

Santoro, Antonio	337	Shayegannia, Moein	72
Santos, Andrés.....	157	Shinar, Zvika.....	185
Santos, Susana.....	253	Shoemaker, Kevin J.....	208
Saoudi, Nadir	288	Siddaramu, Prakruthi.....	333
Sapp, John L.....	168	Sierra-Alonso, Edgar Felipe.....	32
Sarabia-Cachadiña, Elena	114	Signorini, Maria Gabriella	43
Sartori, Claudio	254	Silva Filho, Antônio Carlos	112
Sassi, R	119	Silva, Ikaro.....	39
Sassi, Roberto	93, 94, 129	Silva, Marta João	16
Saviano, Massimo.....	173, 293	Silva, ME	120
Savkoor, Manas	133	Simon, Antoine	65
Scarpi, Emanuela	68	Simova, Iana	40, 152
Schalij, Martin J	2	Sitges, Marta.....	172
Scheer, Peter	122	Smith, Nic.....	159
Schlebusch, Thomas	253	Soguero-Ruiz, Cristina.....	6, 171, 266, 309
Schlegel, Todd T.....	165	Solà, Josep	254
Sch lindwein, Fernando	280	Soleimani, Ali	79
Sch lindwein, Fernando S	149	Solem, Kristian.....	60, 338
Schmitt, Claus.....	250	Soltan Abady, Mohammad...250	
Schneider, Uwe.....	22, 25	Song, Wei.....	314
Schnell, Frédéric	65	Soria-Olivas, Emilio	299, 300
Scholz, Eberhard	95	Sörnmo, Leif.....	58, 60, 181, 202, 338, 342
Schotten, Ulrich.....	238, 246	Sotaquira, Miguel	3, 64
Schreier, Günter	85	Soto-Iglesias, David.....	172
Schulz, Steffen	27	Soto-Iglesias, David	170
Sebastian, Rafael	249	Souza, Regiane Máximo.....	112
Seemann, Gunnar...95, 250, 298		Sovilj, Siniša	105
Sejersten, Maria	163	Štajer, Dušan.....	165
Sepúlveda-Cano, Lina María...32		Starc, Vito	86, 165
Serrani, Marta.....	220	Stefanadis, Christodoulos.37, 38	
Serrano, Luis	9, 268	Stephenson, Robert S	224
Serrano-Balazote, Pablo	266	Stolzmann, Paul	177
Serrano-López, Antonio J.....299, 300		Stoyanov, Todor	126, 301
Severi, Stefano.....98, 106, 227, 228, 229, 337, 341		Stracina, Tibor.....	19
Sevilla, Teresa	155, 176	Strauss, David	258
Shahid, Mohammed	70	Strauss, David G.....	142, 211
Shamsollahi, Mohammad B....50		Struijk, Johannes J	97
Sharkey, Emma.....	136	Su, Yi	160

Such-Belenguer, Luís	299, 300	Toschi, Nicola.....	24
Suelze, Bart.....	63	Towers, Craig	90
Sugibayashi, Rika	318	Trajkovic, Ljiljana	74
Sullivan, Thomas.....	18	Tramonti, Michele	337
Šumbera, Josef	213	Trenor, Beatriz.....	13
Sun, Kun.....	225, 314	Tresoldi, Daniele	226
Sun, Xin.....	274	Trigo, Jesús Daniel	9, 268
Sun, Zhonghua.....	1	Tsalikakis, Dimitrios	55
Svehlikova, Jana.....	310	Tsang, Wendy	3, 316
Sweene, Cees A	36, 166	Tsuji, Masatsugu.....	71
Swenne, Cees A	2	Tu, Jiyuan	1
Szentandrassy, Norbert.....	106	Tu, Shengxian.....	303
Szilágyi, László	12, 100	Turianikova, Zuzana.....	207
Szilágyi, Sándor Miklós ...	12, 100	Tveit, Arnljot	342
Taddei, Alessandro	267, 271	Tysler, Milan	310
Taggart, Peter.....	197, 232	Ueno, Akinori.....	145
Tamboli, Roopak.....	133	Ugarte, Juan P.....	245
Tan, May-Ling	160	Ulbrich, Mark.....	183
Tan, Ru-San.....	160	Uzelac, Ilija.....	184
Tar, Balázs.....	303	Váida, Pierre	235
Tari, Zahir.....	75	Vairavan, Srinivasan.....	52
Tarroni, Giacomo	174	Valenza, Gaetano.....	24
Tartarisco, Gennaro.....	76	Valero, Marta Sofia.....	313
Tarvainen, Mika P.....	42	Vallverdu, Montserrat	124
Tassone, John L.....	8	van Dam, Peter M.....	323
Tautz, Lennart.....	177	van Dam, Teus	270
Tavakolian, Kouhyar	115, 305	van der Putten, Niek HJJ	323
Tavard, François	65	van der Velde, Enno.....	140
Teal, Paul D	203	Van Huffel, Sabine	28, 234
Télléz, Joan P	273	Vandenryt, Thijs.....	63
Teo, Soo-Kng.....	160	Vandervoort, Pieter	63
Teplan, Michal	310	Vanheusden, Frederique J....	149
ter Haar, C Cato	2	Vannier, Michael.....	223
Tessa, Carlo.....	24	Varanini, Maurizio	76
Thoelen, Ronald.....	63	Varon, Carolina	234
Thomsen, Morten B.....	97	Varona, Juan Dayron	137
Tobaldini, Eleonora.....	236	Vega, Claudia	201
Tobón, Catalina.....	245, 249, 294	Verheule, Sander	246
Tonhajzerova, Ingrid.....	207	Verkerk, Arie O	324
Torabi, Azam.....	251	Veronesi, Federico....	66, 69, 174

Vesely, Petr.....	19, 154	Wilders, Ronald	324
Vesely, Petr.....	122	Wilhelms, Mathias.....	95
Vesin, Jean-Marc	290	Williams, David	54
Vicedomini, Gabriele	173, 293	Witt, Katharina	62
Vicente, Jose.....	142, 211, 258	Woie, Leik	175, 179
Vigmond, Edward	327	Xia, Ling.....	108
Vila, Xosé	109	Xia, Yong	319
Vila, Xosé A	111	Xiong, Momiao	259
Vilaseca, Isabel	124	Xu, Binbin.....	135, 308
Villani, Valeria.....	116, 321, 322	Xu, Jingjia	196
Vinet, Alain	328	Xu, Minnan	52
Vitale, Raffaele	293	Xu, Wei	314
Vlemincx, Elke.....	28	Yahia, Hussein.....	308
Vogel, Rolf	180	Yamat, Megan.....	316
Volders, Paul GA.....	102	Yan, Chang	274
Voss, Andreas	27, 31, 62, 117, 216	Yang, Chun-Min	264
Waduud, Abdul.....	163	Yang, Xiaolin	20
Wailoo, Michael.....	280	Yang, Xin	225, 314
Wall, Samuel.....	186	Yanni-gerges, Joseph	99
Wallman, Mikael.....	195	Yao, Liping.....	225, 314
Walmsley, John.....	190	Yeo, Si-Yong	160
Walsh, Philip Richard.....	169	Yu, Linwei.....	225
Wang, John	263	Yu, Zhonghan	274
Wang, Kuanquan	96, 319	Yuan, Yongfeng.....	96
Wang, Linwei	196	Zang, Yunliang.....	108
Wang, Zhigang.....	20	Zareba, Wojciech	167
Warrick, Philip	23	Zarzoso, Vicente	288
Wartzek, Tobias.....	253	Zauneder, Sebastian.....	51
Weber, Frank M.....	298	Zaza, Antonio	106, 227, 229
Wedekind, Daniel	51	Žebrowski, Jan	25
Weinert, Lynn	315	Žebrowski, Jan, Jacek.....	272
Wessel, Niels	51	Zeemering, Stef	238
Westra, Ronald L	102	Zeman, Karel.....	213
Weyer, Sören.....	253	zemzemi, Nejib	312
Whitfield, Catherine	10	Zemzemi, Nejib.....	193
Widjaja, Devy.....	28	Zeng, Libing.....	319
Wiklund, Urban	29, 209, 317	Zeng, Xiaoping	53
Wikswow, John.....	184	Zhang, Henggui .	11, 96, 224, 297
Wilby, Mark	6	Zhao, Xiaopeng	90

Zheng, Dingchang ..82, 108, 136,
178, 239, 242, 255
Zhong, Liang160
Zhou, Xiaona.....53
Zhou, Xin.....232
Zhu, Tingting.....182

Zhu, Yi20
Zhu, Yue-Min158
Zigel, Yaniv.....45
Zink, Matthias.....183
Zlochiver, Sharon104, 295